12th EFRC CONFERENCE

August 24 – 26, 2021
Warsaw, Poland

EFRC
EUROPEAN FORUM
for RECIPROCATING
COMPRESSORS

WWW.RECIP.ORG

12th EFRC CONFERENCE

CONFERENCE SPONSORS

12th EFRC CONFERENCE
August 24 – 26, 2021, Warsaw

WWW.RECIP.ORG

12th EFRC CONFERENCE
August 24 – 26, 2021, Warsaw

COMPRESSOR AND COMPONENT DESIGN

AVAILABILITY AND REBLIABILITY

CONTENTS

12th EFRC CONFERENCE
August 24 – 26, 2021, Warsaw

DIGITALISATION AND AI

PULSATIONS AND VIBRATIONS

CONTENTS

12th EFRC CONFERENCE
August 24 – 26, 2021, Warsaw

SEALING TECHNOLOGY AND EMISSIONS

CONTENTS

12th EFRC CONFERENCE
August 24 – 26, 2021, Warsaw

CONTENTS BY CONTRIBUTOR

12th EFRC CONFERENCE
August 24 – 26, 2021, Warsaw

CONTENTS BY CONTRIBUTOR

12th EFRC CONFERENCE
August 24 – 26, 2021, Warsaw

CONTENTS BY CONTRIBUTOR

12th EFRC CONFERENCE
August 24 – 26, 2021, Warsaw

CONTENTS BY CONTRIBUTOR

12th EFRC CONFERENCE
August 24 – 26, 2021, Warsaw

STASSKOL

TNO

TU WIEN

CONTENTS BY CONTRIBUTOR

12th EFRC CONFERENCE
August 24 – 26, 2021, Warsaw

CONTENTS BY CONTRIBUTOR

EUROPEAN FORUM
for RECIPROCATING
COMPRESSORS

COMPRESSOR AND COMPONENT DESIGN

One year's successful industrial test of a new all-electric capacity control system

by:

Saillard Delphine
Air Liquide
Tavaux, France
delphine.saillard@airliquide.com

Benoni Albert, Gerhard Hölzl
HOERBIGER
Vienna, Austria
albert.benoni@hoerbiger.com
gerhard.hoelzl@hoerbiger.com

12th EFRC CONFERENCE
August 24 – 26, 2021, Warsaw

Abstract:
Capacity control of reciprocating compressors is essential for process control parameters. Common practice is to use recycle valve, variable speed control, suction valve on/off unloaders or clearance pockets to regulate compressor output. Stepless unloading systems based on electro-hydraulic actuators are the advanced approach for demanding process control leveraging high energy savings. Over the last years attractiveness of fully electrically actuated systems has increased significantly with decrease in cost of power electronics and availability of powerful processor technology. This is in line with the current industry trend of replacing fluid based actuation systems with electric ones. This development does not stop at control systems for reciprocating compressors and leads to the emergence of fully electrical control systems. Electrical actuators are considered as cost efficient, easy to handle, oil-free and low-maintenance. This paper presents the first pilot installation of a new all-electrical control system on a two stage, two cylinder process gas compressor in a technical gas plant in France. This article describes the requirements on such a system from an operator perspective and the motivation to replace the old pneumatic system. A brief overview of the process plant and details of the compressor is provided. A short overview about the working principle of the new type of all-electrically driven hybrid actuator will be given. Bullet of this paper are the efforts for conversion of existing pneumatic to the new all-electric control system from the planning phase to the commissioning in terms of mechanical, electrical and DCS implementation. This paper will close with a resume about the operators experience of the new electric system in comparison with the old pneumatic system.

by: Saillard Delphine – Air Liquide; Benoni Albert, Gerhard Hölzl – HOERBIGER

1 Introduction

Electric suction valve unloaders are starting to take over from older hydraulic and pneumatic designs in many applications as a way to provide stepless capacity control for reciprocating compressors over wide operating ranges. This paper describes the first industrial pilot test of a new all-electric hybrid actuator designed with simplicity and affordability in mind.

The year-long test took place on an air separation plant in France. The new equipment was straightforward to install, and ran without any problems. Inspection after 8000 operating hours showed that the actuators and suction valves were still in excellent condition.

We describe the plant and the compressor, the operator's reasons for replacing the existing pneumatic capacity control system, the operating principles of the new control system, and experiences with installation and operation.

As well as establishing the performance and reliability of the new actuator design, the test confirmed that the complete system is well integrated and easy to operate.

2 Operators plant

The test took place on an air separation plant in the Burgundy region of eastern France, 150 km north of Lyon. On the 200-ha site, chemicals company manufactures speciality polymers and fluorine chemicals, while other companies produce chlorine and PVC.

The air separation plant is a dedicated unit built in 1990 to supply oxygen, nitrogen and compressed air to the site. It is owned and operated by a French multinational company that provides industrial gases and services to industries including medical, chemical and electronics manufacturers.

Founded at the beginning of the twentieth century, this company is among the world's largest suppliers of industrial gases and has operations in over 80 countries.

Figure 1 shows a simplified flowsheet of the operators air separation plant. Several large rotary compressors supply air to the cryogenic air separation unit (ASU), which yields gaseous oxygen and nitrogen, and also directly to the downstream chemical plants.

The compressor we are interested in here is a two-stage vertical double-acting Neuman & Esser unit referred to as C02 (Table 1). It acts as a booster, compressing 18,000 Nm3/h of air from 5.5 to 29 bara to supply the ASU. A side stream (0–6,000 Nm3/h at 7 bar a) taken off before the second-stage inlet goes to the main site compressed air main. The driver is an electric motor and the absorbed power is close to 1.3 MW.

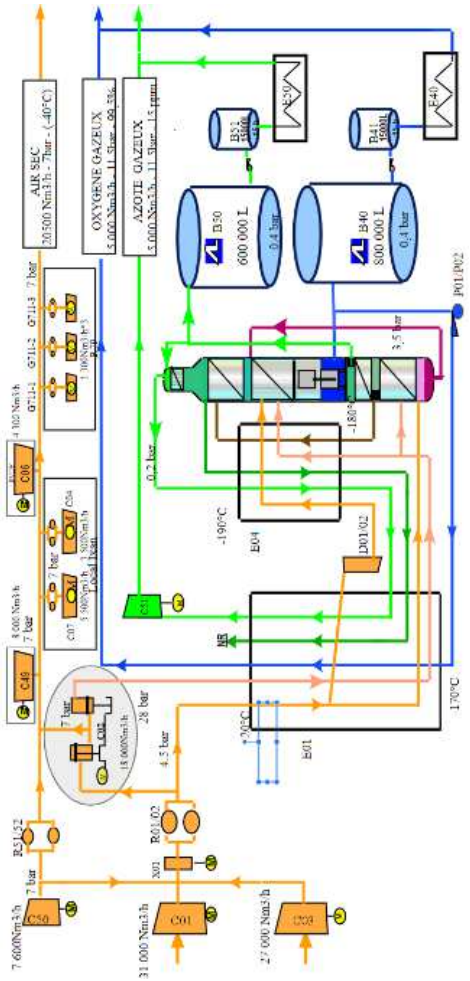

Figure 1: Simplified flowsheet of the operators air separation plant, with reciprocating compressor C02 at top left.

Neuman & Esser Type K 278.920/2 reciprocating compressor C02			
Speed: 588 rpm		Inlet	Discharge
Stage 1	Pressure [bara]	4.8–5.8	10.3–12.6
	Temperature [°C]	23	35
	Valves	6	6
	Volume [Nm³/h]	12,925–18,950	
Stage 2	Pressure [bara]	10.1–12.4	29.7–29.8
	Temperature [°C]	35	30
	Valves	4	4
	Volume [Nm³/h]	6,925–12,950	

Table 1: Operating characteristics of compressor C02.

by: Saillard Delphine – Air Liquide; Benoni Albert, Gerhard Hölzl – HOERBIGER

3 Developments in electric actuation

Almost all reciprocating compressors need some form of capacity control to enable them to match the requirements of the processes into which they fit. Traditional methods include recycle valves, variable speed control, "on/off" suction valve unloaders, and variable-volume clearance pockets. Recycle valves are wasteful of energy, while the other methods are awkward to adjust and inflexible in terms of capacity.

A better solution is suction valve unloaders with variable timing that provide stepless control over a wide range. Electro-hydraulic actuators are a proven solution here, though in the past pneumatic actuators have also been used successfully, as was the case on the operators compressor (see below).

In recent years the falling cost of power electronics and powerful digital processors has made fully electric actuators attractive. In almost all cases, electric capacity control systems now match the performance of their hydraulic counterparts, yet with lower installation costs, oil-free operation and simpler maintenance. This is in line with the industry trend of replacing fluid-based actuation systems with electric ones.

Existing electric actuators for capacity control are field-proven to be effective and reliable[1]. However, their cost – which is similar to that of the previous generation of hydraulic actuators – means they are still not fitted to every compressor that would benefit from a modern capacity control system. With this in mind, the actuators tested at this installation are of a new type that aims to suit a large proportion of real-world applications while reducing costs.

3.1 Hybrid electric actuators are self-adjusting

The new actuators are of a single-stack design that is simpler than the double-stack electric actuators developed previously. Unlike hydraulic actuators, the new electric actuators do not need to be individually sized for each valve, so spares inventories at both the operator and the manufacturer can be greatly simplified.

At the heart of the new actuator is a solenoid (Figure 2). When current flows in the coil, the resulting magnetic field pulls on an anchor plate inside the actuator. This force is transmitted to the unloader, which extends through the suction valve cover, and thence to the valve plate. The actuation force required for the operators compressor is in the upper range of what the new actuator design can achieve. In terms of both actuation force and operating speed, the new design is suitable for around 80% of the industrial recips that are currently fitted with hydraulic capacity control systems.

During the suction stroke, the force created by the solenoid pushes the suction valve open. As the compression stroke begins, the valve remains open as long as necessary to provide the required capacity, and gas flows back into the suction manifold. At the appropriate point in the cycle the control system cuts the power to the solenoid and the suction valve is allowed to close in a controlled manner.

The new actuators are compact and need no water supply or any other type of cooling. The whole electric system operates at extra-low voltage (the actuators are supplied at 60 V DC, for instance).

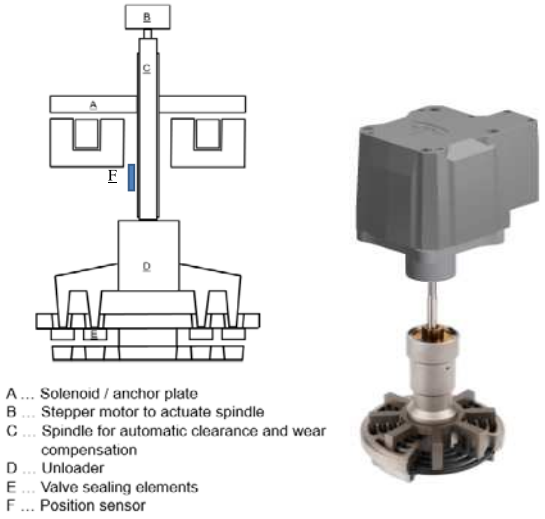

Figure 2: (Left) Cross-section showing the main components of the new electric actuator. When the solenoid is energised, the resulting magnetic force on the anchor plate holds the suction valve open against the pressure of the gas in the cylinder. (Right) External view of the actuator, unloader and valve)

With a suction valve lift of just a few millimetres and a moving mass of around 10 kg, accurate positioning of the unloader is critical to effective and safe operation. Hydraulic and pneumatic actuators require careful setting up during commissioning to make sure that the unloader is in the correct axial position. With electric actuators, on the other hand, this can be done automatically.

The electric actuators are known as "hybrid" actuators because their linear motion is provided by a combination of the solenoid referred to above and a stepper motor attached to the end of the spindle ("B" in Figure 2)[2]. As a result, they are fully self-adjusting. During startup, the stepper motor drives a

by: Saillard Delphine – Air Liquide; Benoni Albert, Gerhard Hölzl – HOERBIGER

gearbox and screw thread to position the anchor plate precisely and initialise a position sensor. During operation, the actuator monitors its range of motion on every cycle and adjusts the spindle as necessary to compensate for wear.

Another benefit of modern digital technology is that the system optionally allows secure remote access. This allows manufacturer engineers to check the system remotely for optimum maintenance and troubleshooting, and simplifies commissioning (see below).

4 The upgrade project

4.1 Existing pneumatic system

The original capacity control system on compressor C02 was of the pneumatic type, and dated from 1990 when the plant was built (Figure 3 and Figure 4). It was fitted to all ten suction valves on both stages of the compressor.

Figure 3: Compressor C02 at the operators plant. The first-stage cylinder head is at top centre. Two of the suction valve covers are visible, with their original pneumatic actuators; there are six suction and six discharge valves in total. The second-stage cylinder is behind, and the motor behind that.

The pneumatic system had operated trouble-free since it was installed, its only real drawbacks being the considerable manual adjustment required during startup after servicing, and the fact that it was not connected to the plant's main distributed control system (DCS). After nearly three decades in operation, the operator decided the time was right to replace it. Keen to see the benefits of new technology, the company offered to host the first field installation of the new electric actuator.

Figure 4: A pneumatic actuator of the type originally fitted to the operators compressor.

4.2 Scope of the project

The scope of the project included new state-of-the-art suction valves with unloaders to fit the new control system, new valve covers, the actuators themselves, and the associated control system (Figure 5).

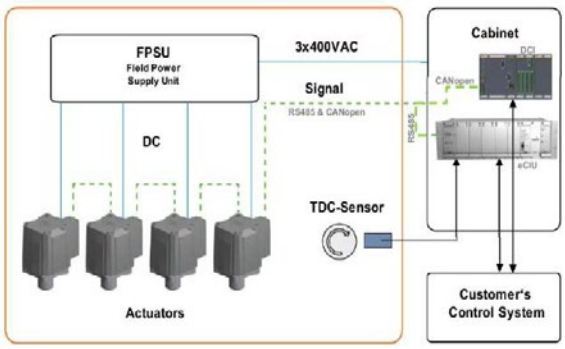

Figure 5: Control schematic showing how the actuators link to the field power supply unit, the central controller for the valve system, and the plant's main control system.

Each suction valve to be controlled is equipped with its own actuator mounted on the valve cover. The actuators receive power and digital control signals from a "field power supply unit" (FPSU). Each one can supply up to four actuators, so a large compressor may need several FPSUs. Compressor C02 has ten suction valves in total – six on the first stage and four on the second stage – and hence three FPSUs.

To synchronise the control signals sent to the actuators with the position of the piston, a TDC sensor is installed. The usual position – as at this site – is on a bracket next to the flywheel.

A standard three-phase power cable connects each FPSU to the main control cabinet, which houses the equipment that is not suitable for field installation.

by: Saillard Delphine – Air Liquide; Benoni Albert, Gerhard Hölzl – HOERBIGER

CANopen and RS485 digital signals allow the actuators to communicate with the cabinet and with each other. Compared to hydraulic systems this provides much more information about the status of the actuators, aiding remote support of the capacity control system and providing valuable feedback on the valve motion in general.

Since the control logic chosen for the original pneumatic system had worked well for many years, the new system kept the same arrangement (Figure 6).

The control strategy can be described as follows. Since compressed air can be drawn off between the stages, both stages are to be regarded as two independent compressors and so require their own controllers. The controlled variable on the first stage is the first-stage discharge pressure (PT1224). The controlled variable on the second stage is the second-stage discharge pressure (PT1236). The recycle valve (PCV) has its own pressure controller that also gets its input from PT1236, but whose setpoint is slightly higher than that of the second-stage capacity control system. The electric system therefore takes precedence in normal operation, leaving the recycle valve to handle any major deviations.

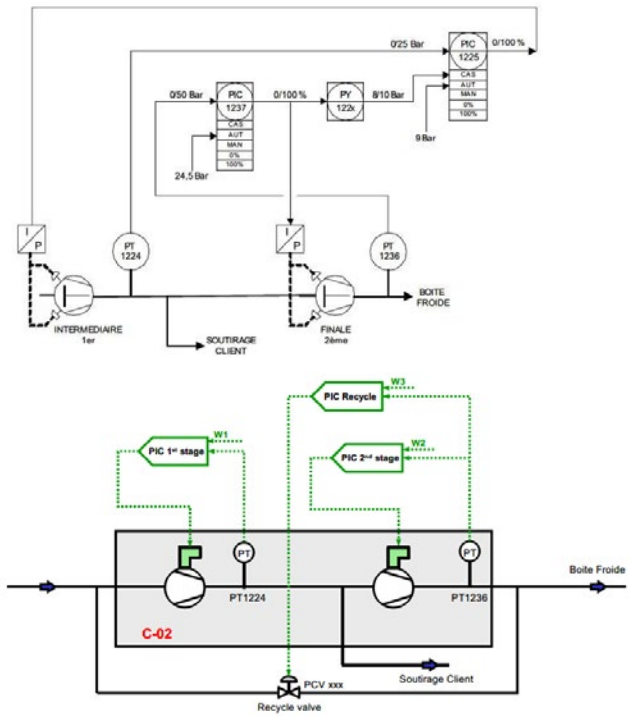

Figure 6: (top) P&ID for the original pneumatic system, and (below) the same control logic repeated for the new electric system.

4.3 Installation and commissioning

Figure 7 shows one of the actuators installed on the compressor, and the FPSUs mounted nearby.

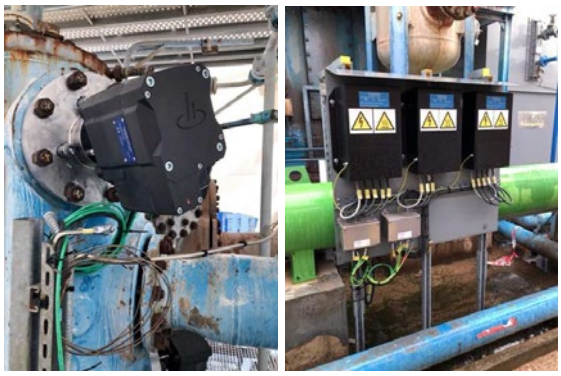

Figure 7: (Left) New electric actuator installed on a valve cover, and (right) the three FPSUs mounted alongside the compressor.

The commissioning took place in two phases and was uneventful, thanks to careful planning and excellent cooperation between operator and manufacturer. First, in September 2019 while the compressor continued to run, the main cabinet and cables were installed, and loop tests carried out. The remote access facility was a great help during the configuration and testing steps. This preparatory checking stage was key to rapid and smooth commissioning during the subsequent on-site phase.

For the second phase, in March 2020, the compressor was shut down and the new suction valves, valve covers, actuators and FPSUs were installed. Thanks to the careful advance preparation, this part of the job took just three working days.

For comparison, commissioning a capacity control system usually requires 3–5 days of site work, but it can take significantly longer if all the necessary preparation has not been done beforehand. The two-step approach with remote testing is not only quicker, but also eases the requirement for all the different disciplines (programmers, compressor experts, maintenance personnel and so on) all to be in the same place at the same time.

4.4 All good after 8000 hours

Following commissioning, the new capacity control system ran for 8000 hours with no problems. Compressor C02 was then shut down for a major overhaul, and the actuators were returned to the manufacturer for detailed inspection.

All the actuators, including their seal housings, were in excellent condition, with no noticeable wear. After routine servicing, all parts were returned to operation and the system has continued to function exactly as designed.

In March 2021 the operator decided to further integrate compressor C02 into the main DCS, which in future will be able to start and stop the compressor automatically.

From the commissioning stage onward, experience confirmed that the new system is easy to operate,

with essentially “one-button” startup and no further attention required.

5 The future is electric

This successful extended field test of a new simplified design of electric actuator matches the wider trend towards fully electric control systems, including final control elements. Compared to their hydraulic and pneumatic counterparts, electric actuators are cost-efficient, easy to handle, oil-free and low-maintenance. Simplified systems integration, with no hydraulic tubing or cooling water, means that less effort and time are needed for installation.

Compared to recycle valves, “on/off” suction valve unloaders and variable-volume clearance pockets, stepless suction valve unloading offers high turndown and energy savings large enough to provide rapid payback in many applications.

In the case of electric actuators, a further advantage is the system’s ability to calibrate itself automatically, making it much quicker to return the compressor to service after valve inspection or replacement. As the system runs, it adjusts automatically to take up any wear.

The operators air separation plant was chosen for this trial in part because the prototype actuators available at the time were not suitable for hazardous areas. Since then, EEx versions of both the actuator (II 2G Ex db eb ib mb IIC T4 Gb) and the field power supply unit (II 2G Ex db IIC T5 Gb) have been designed and certified to EN 60079-0: 2013 (“ATEX”), so the new system is suitable for refineries and other duties handling flammable gases. A second field trial has been in operation since April 2021, also in France and this time with EEx-certified equipment.

Compared to its electric predecessor the new system has the advantage of safe extra-low-voltage operation. Compared to conventional hydraulic systems it boasts simpler spares handling: with a single size of actuator suitable for a wide range of applications, operators can reduce the number of spares they need to keep. Added to the ease of installation and simplified commissioning, this all translates to lower cost of ownership.

The intelligence built into the system through the use of digital communications and a powerful central processor simplifies support and also provides valuable feedback on the state of the compressor in general. Detecting changes in valve timing or actuation force, for instance, can help to diagnose lubrication problems before they become serious enough to damage the crosshead bearing. If the system trips, it is generally for a good reason.

Perhaps 90% of reciprocating compressors in Europe and North America would already benefit from stepless capacity control, with Asia – especially China and India – not far behind. This successful trial is an encouraging step in the development of an all-electric system that is affordable, easy to set up and use, highly reliable, and offers powerful opportunities for diagnostics and integration with central plant control systems.

References

[1] McDonald, J., Dubos, A., Bosson, T., (2016): Stepless capacity control maintains efficiency of French natural gas compressor as production declines, 10th EFRC Conference, 19-27.

[2] Spiegl, B., Dolovai, P., Lindner-Silwester, T., (2012): New Concept for electrical stepless compressor capacity-control system, 8th EFRC Conference, 185-194.

Your Gas Compression Application – Reciprocating, Centrifugal, or Screw?

by:

Greg Phillippi
Technical Services
Ariel Corporation
Mount Vernon, Ohio, USA
gphillippi@arielcorp.com

Jonathan Sutter
Application Engineering
Elliott Group
Jeannette, PA, USA
jsutter@elliott-turbo.com

Tim Manthey
Process Gas Division
Aerzen USA
Coatesville, PA, USA
tmanthey@aerzenusa.com

Ben Williams
Application Engineering
Ariel Corporation
Mount Vernon, OH, USA
bwilliams@arielcorp.com

Bruce McCain
Engineering Consultant
Oxy Permian
Houston, TX, USA
bruce_mccain@oxy.com

12th EFRC CONFERENCE
August 24 – 26, 2021, Warsaw

Abstract:
This paper addresses the question of which compressor type is better suited to a given application – reciprocating, centrifugal or rotary screw - with the screw being subdivided into oil-free and oil-flooded types. The application guidelines will be addressed from the standpoint of reliability, cost, efficiency, size, and other more general application parameters such as molecular weight, compression ratio, and turndown capability. Also included in the discussion is an end-user's perspective on several non-technical issues that might impact the compressor selection for a given project. This paper was previously published for the Turbo Symposium in 2016 - see reference 7. It has been revised due to size limitations.

by: *Greg Phillippi, Ben Williams – Ariel Corporation; Tim Manthey – Aerzen USA; Jonathan Sutter – Elliott Group; Bruce McCain – Oxy Permian*

1 Introduction

Choosing the proper compressor type for an application is a critical decision. An uninformed choice will invariably lead to increased operating and maintenance costs. Selecting which compressor type to use for a specific application requires consideration of numerous parameters such as suction and discharge pressure level, gas mole weight, required flow, capital expenditure and availability. Furthermore, an understanding of how each type works, along with their specific strengths and weaknesses is essential to selecting one appropriate for a given application.

The paper provides guidelines and comparative information to be used by contractors and users to determine which of these three compressor types may be the best fit for their particular application. It is important to note that in addition to reciprocating, rotary screw, and centrifugal compressors, other compressor types are available. Among other compressor types used are rotary vane, diaphragm, liquid ring and axial.

The paper is organized into three sections. The first section includes example applications and discusses what makes one compressor type better than the others for that application. The second section provides an end-user perspective on factors that must be considered when selecting what type of compressor to use. The final section contains a reference comparison chart for use when making a compressor selection.

2 Example Applications

2.1 Introduction

This section contains three common compressor applications and discusses why a specific compressor type (listed first) is better suited for the given conditions. Also provided is information on why the other two compressor types may not be optimal for that specific application. The applications were selected to clearly show why one compressor would be the preferred selection.

2.2 Application #1 - Hydrogen Product

Gas Compressed = Pure Hydrogen
Mole weight = 2.02
K = 1.41
Suction pressure = 31 bara (450 psia)
Suction temperature = 38 °C (100 °F)
Discharge pressure = 100 bara (1450 psia)
Capacity = 70,330 Nm^3/hr (63 mmscfd)

Reciprocating Compressor – 3295 kW (4420 hp).
These conditions are typical of a hydrogen plant application. Due to the low molecular weight of hydrogen and the required discharge pressure, this is an ideal application for a reciprocating compressor.

A reciprocating compressor is a positive displacement machine and therefore the molecular weight of the gas has little impact on the ability of the unit to compress the gas. The required power, capacity and discharge pressure of this application are well within typical reciprocating compressor designs. Due to hydrogen's relatively high ratio of specific heats (K), hydrogen applications typically have low compression ratios per stage. In this case, two stages of compression are required to keep discharge temperatures within acceptable limits.

Both lubricated and non-lubricated reciprocating compressors can be used for this application. The decision depends on the process design and whether oil will cause an issue with downstream components. Most often, lubricated compressor cylinders are used.

Another consideration in hydrogen applications is that there is almost always a nitrogen run required for plant start-up in order to purge and dry the process gas system. The nitrogen operating conditions are quite different than those for hydrogen and as such the reciprocating compressor can rarely be operated at the same pressures and temperatures as the hydrogen run. That is because the valves are designed for low molecular weight gas and nitrogen is heavier, with a molecular weight of 28. If the reciprocating compressor is operated with the hydrogen valves, the time spent operating on nitrogen should be kept as short as possible since this can have a negative impact on valve life.

Centrifugal Compressor - Impractical.
Despite the inlet flow of 2620 m^3/hr (1542 acfm) being within the limitations of many centrifugal compressor designs, the low mole weight makes this an unrealistic application for a centrifugal compressor utilizing covered (shrouded) impellers. With a typical covered impeller producing 35,869 N-m/kg (12,000 ft-lb_f/lb_m) of head (reference 5), over 50 impellers would be required (assuming 85% polytropic efficiency). While multiple centrifugal units are applied quite regularly in other applications, this is clearly not a good fit when contrasted to a reciprocating compressor.

Screw Compressor - Impractical.
While there is at least one oil-flooded screw compressor available that can reach this discharge pressure, it is unlikely that it can achieve it in one stage due to slippage and heat of compression concerns. As with other applications, a multi-stage screw compressor is generally at a disadvantage compared to a multi-stage reciprocating compressor because it usually means a separate housing, driveshaft, etc. Therefore it is unlikely that this

by: *Greg Phillippi, Ben Williams – Ariel Corporation; Tim Manthey – Aerzen USA; Jonathan Sutter – Elliott Group; Bruce McCain – Oxy Permian*

would be considered a good application for a screw compressor.

2.3 Application #2 - Propylene Refrigeration

Gas Compressed = Pure Propylene
Mole weight = 42.08
K = 1.24
Suction pressure = 3.4 bara (50 psia)
Suction temperature = -15 °C (5 °F)
Capacity = 46,384 Nm^3/hr (41.55 mmscfd)
Sideload pressure = 6.9 bara (100 psia)
Sideload temperature = 7 °C (44.5 °F)
Sideload capacity =
11,600 Nm^3/hr (10.39 mmscfd)
Discharge Pressure = 17.9 bara (260 psia)

Centrifugal Compressor – 2834 kW (3800 hp).
Propylene refrigeration is commonly found in ethylene plants and natural gas processing facilities. Refrigeration usually involves the use of one or more economizers, thus the necessity of multiple stages of compression. A centrifugal compressor is ideal for this type of service due to the potential to add an intermediate process connection between two impellers. For this particular example, a single body centrifugal compressor having one impeller preceding the sideload and two impellers downstream of the sideload can meet the process requirements. The nature of the refrigeration process makes pressures at the inlet, sideload, and discharge critical. The centrifugal compressor manufacturer optimizes performance by scaling aerodynamic components, resulting in a unit capable of operating at the customer's specified conditions for all process streams within tight tolerances.

Reciprocating Compressor - Impractical.
Propylene and other heavy gases are frequently compressed with reciprocating compressors. However, in this case, due to the capacity required, the reciprocating compressor would require considerably more power than the centrifugal to meet the flow requirements. This is primarily due to the pressure drop that occurs as the gas passes through the compressor valves (or valve loss power). To lower the valve loss power the piston speed would need to be reduced and/or the flow area of the compressor valves increased. Physical size of the compressor cylinders and the flow area of the compressor valves are the practical limits for a reciprocating compressor. If the cylinder is large enough to meet the flow requirements and the valve area is large enough to reduce the valve power losses, generally the efficiency will be more comparable to the centrifugal.

Screw Compressor - 3260 kW (4370 hp).
Oil-flooded screw compressors are often used in refrigeration applications. This application could be done with an oil-flooded screw, but would require a machine that is on the larger end of size (capacity) available on the market today. The power required would be approximately 15% higher than that of the centrifugal in this case.

A screw compressor would be worth investigating if the operating parameters were to vary. Screw compressors handle changing inlet conditions very well and maintain a high efficiency across a broad range of conditions. It would be worthwhile getting a comparative sizing of a screw compressor for this application if:

- The flow varies widely
- The load changes regularly (due to changing condensing temperature or other factors)
- The gas has some contamination that could cause imbalance issues for the centrifugal

2.4 Application #3 - Flare Gas Recovery

Gas Compressed = Flare Gas
Mole weight = ~20.0, and varying
K = 1.3
Suction pressure = 1 bara (14.7 psia)
Suction temperature = 79 °C (175 °F)
Capacity = 723 Nm^3/hr (450 scfm)
Discharge Pressure = 8.9 bara (130 psia)

Screw Compressor - 97 kW (130 hp).
Flare gas recovery is a growing application due to the increasing desire to recover all energy sources, and the increasing restrictions on gas emissions and flaring. The challenge for a flare gas compressor is to be able to handle varying gas composition (mole weight) and inlet pressures as the makeup and supply of flare gas changes over time. This is one of the strong areas for a screw compressor – the positive displacement principle means that it is generally insensitive to changing inlet conditions.

It is interesting to note that if the mole weight of the flare gas varies between 10 and 30, as long as the volumetric flow rate remains constant, the brake horsepower also remains nearly constant.

Flare gas applications often need to maintain either a constant inlet pressure or a constant discharge pressure. A screw compressor is well suited to either case. For an oil-flooded screw compressor, an internal slide valve can be used for capacity control without varying the operating speed. Oil-free screw compressors are also used in this service, and in these cases a VFD or recycle line are used for capacity control.

If an oil-flooded screw compressor is used the oil will be in contact with the gas, and thus must be selected based on compatibility with the gas constituents. Oil-free screw compressors are less

by: *Greg Phillippi, Ben Williams – Ariel Corporation; Tim Manthey – Aerzen USA; Jonathan Sutter – Elliott Group; Bruce McCain – Oxy Permian*

susceptible to issues related to gas composition, and as long as the gas is above the dew point (as is true most of the time with oil-free screw compressors), there is little risk to the materials of the compressor.

Reciprocating Compressor - Impractical.
The challenge for a reciprocating compressor in this application is the varying molecular weight. Although reciprocating compressors can compress a wide variety of gas molecular weights, in order to achieve the required reliability. The compressor valves are configured based on the operating conditions and the gas molecular weight. Since the gas composition varies in flare gas service, it can be difficult to configure the valves to meet the entire range. The valves can never be "optimized". In cases where reciprocating compressors are used in flare gas service, the valves are typically configured for the lower mole weight gases.

Centrifugal Compressor - Impractical.
In considering the use of a centrifugal compressor, the first problematic attribute is the low flow rate of 934 m^3/hr (550 acfm). Due to the size of the flow passages in the centrifugal compressor the efficiency will suffer. Secondly, the ratio of specific heats, K, coupled with the lower efficiency will require at least one intercooler. Although there are centrifugal compressors that accommodate connections for up to two process-intercoolers on a single casing, the number of impellers required to reach the final discharge pressure at the lower mole weight of 10 will require multiple compressor bodies (due to rotor dynamics). Finally, there is the large mole weight variation between the operating cases. In theory, a recycle loop could be added after the process-intercooler (every four to six impellers) which would allow recycle flow to be added to each section of compression, thereby counter acting the effect of volume ratio mismatch, however the overall system efficiency and amount of equipment (multiple compressors and an intercooler) would quickly lead one to investigate another type of compressor.

3 An End-User's Perspective on Compressor Selection

3.1 Introduction

The comments expressed in this section primarily come from an upstream end user's perspective, but certainly can apply to any oil and gas industry application. As discussed so far in this paper, there can be multiple compression solutions for a single application. The end user has to balance technical and non-technical requirements in order to finalize on a particular selection. Non-technical requirements such as familiarity with the machine, delivery, costs, maintenance frequency, parts availability, quality, and operability can make or break the project. The ability of the compressor selection to handle off design operation (including startup and shutdown) has to be considered. Oversight of these nuances can have consequences, some not becoming apparent until the equipment is installed.

It should be recognized that while technical requirements are critical for long term reliable service, the engineer may find himself having to select a machine that is best for the project and not so much the application. The project always has technical constraints, but also commercial and schedule considerations to take into account. Also important are items such as availability of replacement parts, craft skills available for maintenance, repair facility options, staffing, and automation. Ultimately, the end user has to make a technical compromise to select the best machine the project can bear that will be delivered and installed in the promised time, without exceeding the budget. Everything about machinery selection can be lumped into one of these three categories: Quality, Delivery, and Price.

As simple as it may sound, this entire process begins with having a thorough understanding of the project requirements. Input from operations personnel provides insight to operational deviations. For example, 95% of the time a gas gathering service may carry an tolerable amount of liquids entrained in the gas, but the other 5% of the time (18 days per year) the amount of liquids is beyond the capacity of the scrubbing system. This additional liquid loading could be due to low ambient temperature, high winds, well treating chemicals, pigging of the pipeline, etc. If a reciprocating compressor is applied here, the user may not be able to replace compressor valves as fast as they fail, or scrubber high level alarms won't clear. Considering a centrifugal compressor with a water wash system, the end user may exhaust their water supply, or the system freezes. Alternatively a screw compressor is installed in a gathering service where a new well is tied in with a composition very different than the existing system. This can cause significant lube problems. In all cases, for one reason or another, the compressors won't run reliably. There may not be an easy solution for each of these problems every time, but the project staff should understand "off design" conditions and practical future expectations. The operations team must be involved when deciding how to handle off design issues that have occurred in the past.

3.2 Reciprocating Compressors

The upstream sector uses a large number of reciprocating compressors. One of the reasons is the high degree of flexibility. Reciprocating compressors can be very forgiving for a wide range of operating conditions, so long as those conditions

by: *Greg Phillippi, Ben Williams – Ariel Corporation; Tim Manthey – Aerzen USA; Jonathan Sutter – Elliott Group; Bruce McCain – Oxy Permian*

are taken into account during the early phases of the project.

Many installations are unmanned, either initially or converted to unmanned. The degree of potential automation must be taken into account. If it's reasonable to believe it will eventually be unmanned, then one should design it as such.

One of the biggest problems users of reciprocating compressors deal with is the change of seasons. The first freeze of the year, or a late freeze in the spring, causes problems if the interstage coolers have manual louvers configured for warmer ambient conditions, and/or have constant speed fans. One successful option is to have automated louvers with variable speed fans on temperature control. This latter option is more costly to implement, but successful in avoiding condensation (water or hydrocarbon) that can carry over into the compressor causing downtime if it gets past the scrubber. Conversely, blowing sand can cause problems with automated louvers.

Reciprocating compressors can handle a large range of conditions with the proper design. Reciprocating compressors generate gas pulsations at harmonics of running speed. These pulsations can couple mechanically with piping, fittings, vessels, nozzles, and if coincident with mechanical natural frequencies can amplify significantly causing component failures. There are two schools of thought on this topic: vibration control, and pulsation control.

Vibration control seeks to hold components in place with clamps and supports, and design components such that mechanical natural frequencies (MNF) have adequate separation margin from excitations (mechanical and acoustic). Pulsation control minimizes amplitude of pulsation and filters out frequencies above a specific value. In reality, both are important. Predominate mechanical excitations on reciprocating compression generally occur at 1X and 2X running speed frequencies due to the reciprocating masses (pistons, crossheads, etc.), while pulsations occur at all harmonics (1X, 2X, 3X, 4X, etc.). Predicting MNF is not an exact science and has significant error, depending on stiffness of components, manufacturing, assembly, etc.

3.3 Centrifugal Compressors

A typical upstream gathering application can be a rather difficult service as the gas is generally wet and can have a significant range of composition and pressure as the field matures over time. The quantity of hydrogen sulfide (H_2S) and carbon dioxide (CO_2) may increase which increases both corrosiveness and mole weight. An accelerated drilling program may increase flow and pressure. Well chemicals can increase liquid handling requirements and add components to the gas stream that reacts with heat of compression causing fouling on impellers, balance lines, and cooler tubes. Neglecting these issues with a centrifugal compressor (or any other for that matter) can cause significant operational difficulties. What should one consider when looking at a centrifugal compressor for a particular application?

Understanding gas composition, specifically mole weight, is critical when considering centrifugal compressors. If the mole weight has a large range, centrifugal compressors may not be the best choice. As mole weight decreases for a given operating point, speed has to increase (along with power requirements) to maintain mass flow and discharge pressure.

It is imperative to understand what it is the compressor will be compressing. Look at other equipment that may already be installed in the same service. For example, if the same service utilizes a reciprocating compressor, is there any contaminant build-up on the compressor valves? Regardless of what a gas analysis says, these contaminates should be understood and taken into account. If installing centrifugal, screw, and/or reciprocating compression in parallel or in series, consideration should be given to acoustic interaction between the machines.

Understand what degree of gas conditioning is needed: scrubbers, coalescing filters, etc., and how they will be maintained. If little to no gas conditioning is to be installed in a typical gathering service, there could be significant operational impact to a centrifugal machine. Gas conditioning is critical to reliable operation in dirty gas services.

Understand requirements for compressor washing, both volume and frequency. If water will be used, there will be cleanliness requirements. Does the facility have the capability of making that water, will facilities be constructed, or will the wash water be trucked in? The volume and frequency of the wash should also be discussed with the compressor manufacturer to ensure erosion throughout the gas path does not occur. Along with the wash system, injection nozzles must be installed. Installation of wash nozzles is recommended, even if not needed during the early stages of operation due to unknowns with field maturity, well chemical program and drilling program. As this will be part of the compressor fabrication, wash nozzles should be specified early in the project.

Make sure the inside of the centrifugal machine (wetted parts) is designed for the range of composition, including off design operations like pigging, well work, and the addition of new wells. Be very cautious of applying coatings to impeller wheels as there is difficulty in getting a spray coating deep inside an impeller. Also, be aware of potential damage to coatings due to abrasives from

by: *Greg Phillippi, Ben Williams – Ariel Corporation; Tim Manthey – Aerzen USA; Jonathan Sutter – Elliott Group; Bruce McCain – Oxy Permian*

the gas stream. Ultimately, a better solution is to ensure the metallurgy of the wetted parts is suitable for everything the gas could potentially contain. These discussions should be had early with the compressor manufacturer.

3.4 Screw Compressors

Oil-flooded screw compressors are often considered for applications with low suction pressure and a relatively clean gas, especially when a small footprint is desired. Flooded screw compressors are often selected over dry screw machines when a large compression ratio and single casing is needed. High compression ratio, and resulting high heat, requires a synthetic lubricant be used to seal the clearance and provide cooling. Dry screw compressors operating at higher temperatures may need special casing metallurgy. However, dry screw compressors are more suitable for dirty gas services, high water content, or has other properties that would contaminate the oil of a flooded screw.

For oil-flooded screws, accurate gas composition is critical so the correct lubricant can be selected. If the gas composition changes before or after startup, this must be addressed immediately to minimize risk of lubricant carryover and/or impact to machinery health. Oil-flooded screw compressors in upstream oil and gas service typically utilize a synthetic oil. In some services, the large expenditure for synthetic oil may be offset by lower frequency of oil replacement. Oil usage and costs should be taken into account when performing life cycle cost analysis: both initial fill and subsequent oil replacement. Some end users have been guilty of only looking at unit cost (per gallon) comparisons of synthetic and mineral oils. Synthetic oil unit costs may be higher, but the entire operation must be looked at. Mineral oil may breakdown faster, resulting in a significantly higher volume of mineral oil being used. The end user should also be aware that this premature breakdown could result in more maintenance for the compressor. For these reasons, detailed discussions should be had with the screw compressor manufacturer and operations personnel during the selection process.

3.5 Driver Considerations

Many projects do not consider drivers until after compressor selection has been completed, which can cause delays and unnecessary rework if there is a driver requirement that limits compressor selection. Some decisions are easy - no electric power is available, the user has a preference towards a certain driver type (“we only install gas engines”), or one wishes to avoid the major issue of regulatory permitting that accompanies the use gas turbines or gas engine drivers.

3.5.1 Electric Motors

Electric motors, whether induction or synchronous, are a good selection for all the discussed compressor types and have lower maintenance costs, reduced downtime, and improved efficiency when compared to gas turbines and gas engines. Electric motors are generally more accepted in unmanned facilities due to their simplicity and reliability. The choice between induction and synchronous motors takes power factor and the power grid into account.

Recognizing that an electric motor will need an electric power supply is clear, but often this is where the forethought ends. The end user should ask themselves the following:

- Is the power supply already at site? If not, when will it be available?
- Will there be sufficient power available to support startup, not just normal operation? Startup philosophy needs to be discussed very early in the project.
- Is the power “clean” or “dirty”? Power with harmonic issues can cause torsional problems that can be detrimental to any machine.
- Is the proposed location of the installation at the end of the grid? Other customers, even residential locations, can be negatively impacted by the project which can cause public relations issues.

3.5.2 Gas Turbines

If the site has primarily gas turbines in service, and the plan is to install a gas turbine driver, reciprocating compressors may not be the best choice. Some end users have done it, and many have proposed it, but there are significant challenges to overcome such as gear box design and ensuring torsional integrity. Screw compressors would also typically require a speed decreasing gearbox, which can be integral to the oil-free screw compressor and supplied as a single unit from some manufacturers. A centrifugal compressor is commonly paired with a gas turbine driver. Care should be taken to understand impact of conditions such as ambient heat, air contaminants from salt spray or fog, blowing dust, and fuel quality. Whether in the fuel, air, or wash water, chlorides and H_2S can have a significant impact on time between hot-section-overhaul of the gas turbine.

3.5.3 Gas Engines

Screw and reciprocating compressors are generally paired with gas engine drivers. Utilization of gas engines requires a good understanding of fuel gas composition. Many engines have fuel gas heating value limits, ethane limits, dew point requirements,

by: *Greg Phillippi, Ben Williams – Ariel Corporation; Tim Manthey – Aerzen USA; Jonathan Sutter – Elliott Group; Bruce McCain – Oxy Permian*

and H_2S limits. When having the torsional analysis performed, assure that the system can handle failure of a power cylinder. Also, assure the torsional damper is sized correctly for the full range of expected operation. Compressor turndown should take into account that engine drivers can experience poor operation when in an unloaded state. Both gas turbines and gas engines may have significant de-rates that apply due to site conditions such as elevation, gas composition and ambient temperature.

Similar to the electric motor, consideration must extend past the existence of the energy source. There may be a fuel gas source, but not all gas is the same. If planning to install a gas turbine or engine, consider the following.

- What gas (i.e. composition) will be used for fuel?
- Is the gas source a pipeline or a well head? If the latter, has sufficient conditioning been taken into account?
- Is sufficient gas available for "blowing the line" from the sales gas line to the machinery without negatively impacting other users? Sufficient velocity is needed to clean the piping.
- Have sufficient plans been made for pigging the gas supply line (typical for gathering system gas)?
- If there is H_2S present in the gas, have the correct modifications been made to the engine to allow for it? If installing a gas turbine, have the economics taken into account the performance and life degradation for operation with H_2S?

3.5.4 Steam Turbines

If selecting a steam turbine driver, a centrifugal compressor is the predominant choice since centrifugal compressors typically operate in the same speed range as steam turbines (2,500 to 20,000 rpm), thus a gearbox would not be required. Screw compressors do operate in this speed range, but not as typically as centrifugal units. Many screw compressors and virtually all reciprocating compressors would need a speed reducing gearbox. The increased complexity of the installation by installing gearboxes and controlling torsional related issues may make this option both technically and commercially unattractive.

4 Compressor Selection Criteria

4.1 Introduction

The Natural Gas Processor Suppliers Association (NGPSA) publishes an Engineering Data Book (reference 1) and included in the book is a chart (Figure 1) showing the range of application for several different types of compressors. Applications which fit inside the regions defined by the various lines signify the application fits that machine. As depicted in the chart there is a fair amount of overlap involving reciprocating, screw, and centrifugal compressors. Determining which type of compressor is a best fit for a specific application requires an understanding of how these compressors operate and the tradeoffs associated with a particular selection.

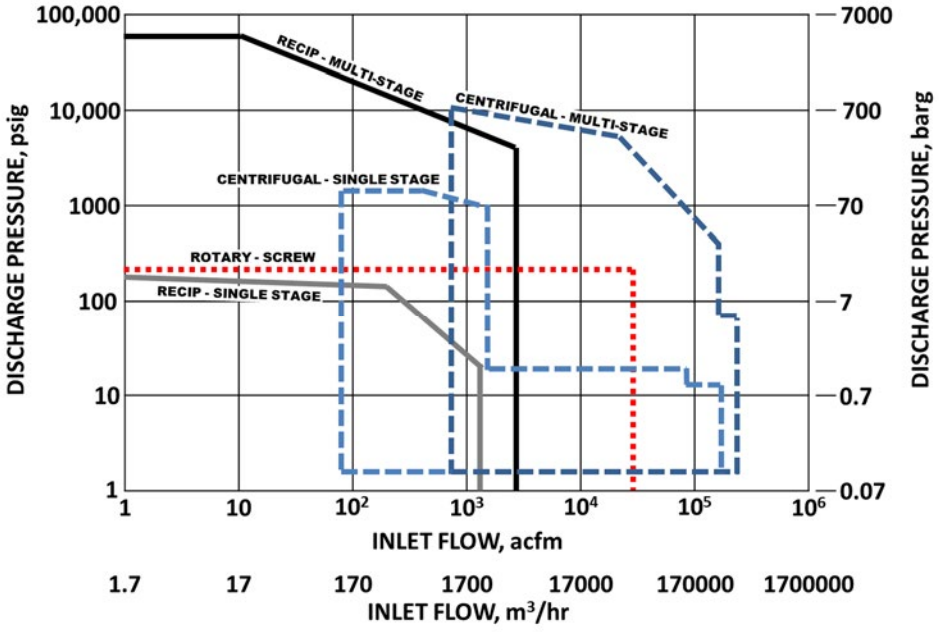

***Figure 1**: Compressor type based on discharge pressure and flow (NGPSA, ref. 1)*

by: *Greg Phillippi, Ben Williams – Ariel Corporation; Tim Manthey – Aerzen USA; Jonathan Sutter – Elliott Group; Bruce McCain – Oxy Permian*

Note: The following table is strictly a guideline and is based on the opinions and experience of the authors. When determining which compressor is best suited for an application, it will be necessary to consider multiple criteria. A ranking value of 1 is considered superior within this table. Eleven criteria have been selected to compare the three compressor types. The possible list of criteria could be almost endless and will vary with each application type.

Topic	Reciprocating	Centrifugal	Rotary Screw	
			Oil-Free	Oil-Flooded
High Mole Weight (> 25)	Gas mole weight has no direct bearing on the reciprocating compressor's ability to compress gas. However, high mole weight gases can impact the ability of the compressor valves to function properly. Ensure proper lubricating oil selected.	Compression of a high mole weight gas is an ideal application for centrifugal compressors.	A dry screw will compress gas regardless of mole weight. The mole weight of course impacts machine limits, but there is virtually no mole weight that is inherently unsuitable for a dry screw.	Gases with a mole weight >50 (heavier hydrocarbons) do not readily separate from the oil and can dilute it.
Ranking	**3**	**1**	**2**	**4**
Low Mole Weight (< 6)	Gas molecular weight has no direct bearing on the reciprocating compressor's ability to compress gas. With proper valve selection, low mole weight gases are easy to compress with a recip. This is an ideal application.	Similar to the compression of high mole weight gases, low mole weight gases are suited for centrifugal compressors when a high flow is desired.	Good at low differential pressures. At higher differential pressures, the slippage leads to inefficiency and high discharge temperatures.	Ideal since injected oil closes internal clearances.
Ranking	**1**	**2**	**4**	**3**
Wet Gas	Every effort should be made to prevent liquids from entering the compressor cylinder and compression chamber. Liquids can cause compressor valve failures and can dilute lubrication.	A centrifugal compressor can be used in a wet gas application if the size and quantity of any liquid droplets are very small, and process gas temperature limits can be met.	Generally not a problem. If droplets are expected to enter a dry screw, stainless steel should be considered to prevent erosion.	Can be done, but the discharge temperature should be kept >-7 °C (20 °F) over dew point to prevent dilution of oil by condensation.
Ranking	**2**	**2**	**1**	**4**
Dirty Gas	Solids in the gas stream can cause premature wear of sealing components thus leading to reliability issues. Gas with significant entrained solids should be filtered.	Depending on size and quantity, particulates and liquid droplets can have a significant erosion effect due to the high gas velocity within the machine. Performance will suffer due to the particulates' effect on aero components.	Small particles will pass through a dry screw without issue. Larger particles can cause scoring on rotors and casing.	Particles are not much of an issue unless they dilute or otherwise change the oil properties. Dirt will be caught in filters before the oil returns to the compressor.
Ranking	**3**	**4**	**1**	**2**

by: *Greg Phillippi, Ben Williams – Ariel Corporation; Tim Manthey – Aerzen USA; Jonathan Sutter – Elliott Group; Bruce McCain – Oxy Permian*

Topic	Reciprocating	Centrifugal	Rotary Screw	
			Oil-Free	Oil-Flooded
Low Suction Pressure (< 0.34 bar, 5 psig) **(high flow)** **Ranking**	A recip can compress gas from a low suction pressure but can be relatively expensive. Low pressure typically means multiple large cylinders which increases cost. **3**	Suction pressures slightly above atmospheric are typical for some centrifugal applications. Sub-atmospheric conditions also can be accommodated. **1**	Ideal for a screw, which can also be used for vacuum applications. **2**	
High Suction Pressure (> 34.5 bar, 500 psig) **Ranking**	No issues at all for a recip. **1**	A high suction pressure is within the mechanical design limitations. **1**	Few screws are suitable for this operating pressure. Due to internal compression, suction pressures this high must be treated with great care. **3**	
High Discharge Pressure (> 207 bar, 3000 psig) **Ranking**	No issues at all for a recip. **1**	Discharge pressures up to 1034 bar (15,000 psig) can be accommodated. These high pressures would necessitate a vertically split casing. **2**	Screw compressors cannot reach this pressure. **3**	
Capacity Control (Turndown) **Ranking**	Many capacity control devices are available including suction valve unloaders and devices that add fixed clearance. Speed variation, suction throttling and recycle can also be used. **1**	Since head and flow are directly related, methods of control such as suction throttling, speed variation, or adjustable inlet guide vanes are employed to achieve flexibility. Ultimately, surge and stonewall, will establish the limits of operation. **3**	Turndown via speed control is possible but limited, especially if maintaining a constant discharge pressure. **4**	With a capacity slide and sometimes a vi slide, an oil-flooded screw is specifically designed for varied operating cases without need for recycle or speed variation. **2**
Changes in Gas Properties **Ranking**	The reciprocating compressor easily handles changes in gas properties. **1**	The amount of head that a centrifugal compressor stage can impart is highly dependent on mole weight, geometry, flow, and speed. With the geometry fixed, variations in mole weight can only be accommodated to a limited degree. **3**	The screw compressor easily handles changes in gas properties. **1**	The screw compressor easily handles changes in gas properties. Ensure lubricating oil is suitable for changes in gas properties. **1**

by: *Greg Phillippi, Ben Williams – Ariel Corporation; Tim Manthey – Aerzen USA; Jonathan Sutter – Elliott Group; Bruce McCain – Oxy Permian*

Topic	Reciprocating	Centrifugal	Rotary Screw	
			Oil-Free	Oil-Flooded
Capital Cost	Capital cost of a reciprocating compressor system is dependent on the gas composition, customer specifications and the application.	The capital investment for a low flow application can be quite high relative to other compressor types. In contrast, savings can be realized when the application requires large flows.	An oil-free screw compressor for process gas will almost always be higher in capital cost than an oil-flooded for the same duty, mainly due to internal seals and the seal support systems.	Can be quite reasonable with base materials and design, mainly because there is no need for internal seals, and thus no external seal gas system.
Ranking	**2**	**4**	**3**	**1**
Life Cycle Cost	A reciprocating compressor has more wear parts than centrifugal or rotary screw compressors. Wear part replacement is typically required every one to three years.	Due to the low number of moving parts, constant loading, and low vibration, it is common for centrifugal compressors to be in continuous service for seven years or more.	Very few wearing parts. Five years between overhauls is normal; often longer. Wear is prevented indefinitely if the oil and sealing medium quality are properly maintained. Overhaul consists of bearings and seals if needed. Overhaul cost is <10% of new machine cost, generally <3% of complete package cost.	
Ranking	**4**	**1**	**3**	**2**

5 Conclusions

The Compressor Selection Criteria table will provide perspective on the ideal compressor type for a single characteristic of an application but by no means will the table provide the solution to an application. Additionally, the comparisons within the table are general and may not be representative of a particular manufacturer's special feature or design. Careful consideration of all of the application characteristics and working with the equipment manufacturers is the best way to ensure the right equipment is being utilized.

6 References

1. ***NGPSA Engineering Data Book***, Volume 1 Revised 10th Edition 1994. Compiled and edited in co-operation with the Gas Processors Association. Copyright 1987 Gas Processors Association.

2. Phillippi, Greg; ***Basic Thermodynamics of Reciprocating Compression***, short course presented at the 2005 Gas Machinery Conference, October 2005, http://www.gmrc.org/index-title.php?year=2005

3. Paluselli DA, ***Basic Aerodynamics of Centrifugal Compressor***, Elliott Co., Jeannette, PA.

4. Brown, Royce N., ***Compressors – Selection and Sizing***, Gulf Publishing Company, 1986

5. Gresh, Theodore M., ***Compressor Performance – Aerodynamics for the User***, Butterworth-Heinemann, 2001

6. Smith, Donald R., ***Pulsation, Vibration, and Noise Issues with Wet and Dry Screw Compressors***, Proceedings of the 40th Turbomachinery Symposium, 2011

7. This paper first published and presented as: Phillippi, Greg; Sutter, Jonathan; Manthey, Tim; Williams, Ben; McCain, Bruce (2016). ***Your Gas Compression Application - Reciprocating, Centrifugal, or Screw?***, Turbomachinery Laboratories, Texas A&M Engineering Experiment Station, http://hdl.handle.net/1969.1/159808

Baker Hughes

Large Reciprocating Compressor Modules A new integrated design process to minimize all risks related to this challenging application

by:

Simone Bassani, Riccardo Bagagli*, Marco Passeri, Leonardo Sapuppo
BH Nuovo Pignone
Via Felice Matteucci, 2 – 50127 Florence, Italy
Simone.Bassani bakerhughes.com, Riccardo.Bagagli@bakerhughes.com,
Marco.Passeri@bakerhughes.com, Leonardo Sapuppo @bakerhughes.com

12th EFRC CONFERENCE
August 24 – 26, 2021, Warsaw

Abstract:
Hydrogen compression is one of the key areas of refinery processes where the application of reciprocating compressors is required. Recent refinery investments trend is to maximize the plant size reducing as much as possible the time between the investment decision and the plant start-up. With such target in mind compressor OEMs are required to develop capability not only to design and manufacture large reciprocating compressors but also to design and produce larger packages (modules) to simplify and shorten the installation activities.
This paper provides a deep description of the design process developed by BH Nuovo Pignone to support the new market demand to supply a large reciprocating compressor fully packaged, here named modules. Package applications with large reciprocating compressors have been seen in this industry for several years, however those were typically limited to the bare compressor while the process components like pressure pulsation dampeners 6 and auxiliary systems were installed on foundation block. The new developed reciprocating module design capabilities allow BH Nuovo Pignone to supply large reciprocating compressors fully packaged integrating on the skid all key process gas equipment, auxiliary components as well as control panels and instrumentation racks so that the field installation activities are minimized, see Figure 1.

by: Simone Bassani, Riccardo Bagagli*, Marco Passeri, Leonardo Sapuppo – BH Nuovo Pignone

1 Introduction

A reciprocating compressor is one of the most common rotating machines installed in thousands of worldwide refineries. History of reciprocating compressors is very old; it is needed to look back more than a hundred years to find the first application of this machine type; that is for sure due to its simple design principles and also to its vast flexibility. Despite its age, reciprocating compressors are still largely applied in the refinery world, especially for services where the gas to be treated is extremely light, like pure hydrogen or mixtures with hydrogen as the main component. In those applications, even if the large flow is required, the efficiency and flexibility of the reciprocating compressor make it the preferred solution, winning the competition with the more advanced centrifugal compressor types.

The refinery application of large reciprocating compressors for hydrogen services is typically made through low-speed machines designed in accordance to API 618 [1]; low-speed units are preferred compared to the high-speed ones because of the heavy-duty service of the refinery which requires high availability and also strong reliability; users and manufacturers, following their experience and design capabilities, have proven the low-speed reciprocating compressors are the best choice for that application; however, the large size of new refineries generated new challenges for the design of reciprocating compressor applications. Easy to understand that the increase of refinery capacity has driven the request for an increase of applied reciprocating compressor size; together with a reduction of the "time to plant start-up" after investment decision seems fundamental to make sure to get the expected return of investment. Those two key basic requirements have put a lot of challenges on compressor manufacturer side when designing the overall solution; large compressor size, has historically driven long delivery time and installation time, so how to answer to this market needs is the purpose of this article which specifically focus on the path followed by Baker Hughes through the Nuovo Pignone reciprocating compressor product line.

While huge reciprocating compressors are part of the referenced Nuovo Pignone portfolio for a long time, with potential capabilities to build machines up to 30-35 Mega Watt of power, the challenge is now to design a solution enabling a minimal installation time using such machine sizes. The decision has been to explore a fully packaged large unit accommodating on the package all main equipment, those in the past typically installed directly on foundation because of the size and the difficulties to control the vibration level of the overall system, machine and devices around it. A package for that purpose becomes really large and could be considered a module. Many challenges to designing that solution have been listed, and particular focus has been dedicated to identifying risks associated with each one and actions to be put in place to mitigate them:

a. Large modules are difficult to be transported when assembled; a dedicated plan is needed to identify the right place to make the assembly and from where the module can be shipped to site

b. The large reciprocating compressor must have well balanced reciprocating masses; to limit as much as possible the dynamic loads generated during operation, which typically responsible for vibrations and fatigue failures of machine, equipment and piping around the machine

c. Complex steel structures need to be designed to arrange the module layout; such structures shall be stiff enough to avoid vibration issues when the compressor is in operation.

d. Module needs to be designed to prevent maintenance issues; basic ergonomic rules have to be respected while minimizing the impact on the overall module size. This requirement could be against item b.

Risks related to the item (a) can be easily mitigated working with the client to define the proper shipping plan when potential yards where the module can be assembled have been identified.

Item (b) is for sure more critical when the compressor has to be installed on top of a steel structure like a module instead of a traditional foundation installation; however, techniques to balance a reciprocating machine are well known so risks associated with this item can be mitigated applying such techniques, minimizing both the dynamic forces and moments generated by the compressor.

Item (c) in combination with item (d) generates the more challenging risk to be mitigated, the risk of having a complex module structure with vibration problems discovered after plant start-up. To make sure this risk is adequately reduced, the engineering team of OEM with dynamic vibration specialist shall follow a design methodology capable to predict in a reliable way the stress and vibration behaviour of the overall module considering all possible operating scenarios of it defined in combination with Client, who knows better how the system will be used. This design methodology can be developed by OEM that have a in house experience on pulsation and vibration control techniques/tools [3,4,6,8,9,10,11,12] and field validated assumptions, this is the key focus of this article.

by: Simone Bassani, Riccardo Bagagli*, Marco Passeri, Leonardo Sapuppo – BH Nuovo Pignone

2 Triggers and Trade-off analysis to select Skid VS Foundation based

The market for large Reciprocating Compressors as aforesaid traditionally has been a foundation-based approach, the compressor is delivered partially assembled with the loose auxiliaries' items to be mounted at the final end-user site. There are some well-known advantages in this approach, one is related to the larger area available to install all the equipment's that improve plant ergonomics, smooth erection, maintenance and operation, the other advantage is related to unbalance forces and couples, dynamic loads containment that in a big reciprocating compressor may reach high magnitude, in such cases the vibrations levels can be managed thanks to the stiffness design of the foundations and the direct connection of the crankcase, distance piece and cylinder supports to the foundations.

Trigger	Weight on specific project	
	Skid	Foundations
Safety risk related to all additional site activities required for foundation base	negligible or NO impact	low/medium/high
Skilled workmanship availability for Recip installation on site	negligible or NO impact	low/medium/high
site activities **costs** for installation of all loose parts and F2F	negligible or NO impact	low/medium/high
Complexity due to remote area installation or country where workmanship maybe difficult to be available and at high cost or environment conditions could delay the project milestones	negligible or NO impact	low/medium/high
Defined **timing** for compressor start up, no delay or uncertainty related to site commissioning activities so no potential LDs versus final customer	negligible or NO impact	low/medium/high
Loose materials/parts **logistic issues management**	negligible or NO impact	low/medium/high
Loop checks to be performed on site	negligible or NO impact	low/medium/high
Fit-up issues related to unproper **alignment activities**	negligible or NO impact	low/medium/high
Functional tests on subsystems as stepless recycle system performed on completed package prior shipment	negligible or NO impact	low/medium/high
Cleanliness issues related to site activities i.e. lube console circuit already connected to compressor in the skid	negligible or NO impact	low/medium/high
Interfaces issues due to wrong assembly or complexity related to project	negligible or NO impact	low/medium/high
Vibration issues on large auxiliaries equipments and/or main baseplate	low/medium/high	low/medium/high
Unbalanced Forces and Couples magnitude	low/medium/high	low/medium/high
Skid **Grouting** execution, material, enviromental and workmanship ev.	low/medium/high	negligible or NO impact
Additional costs to sustain for compressor OEM related to skid erection	low/medium/high	negligible or NO impact
Additional OEM **timing** (5-7 months) for skid erection	low/medium/high	negligible or NO impact
Large skid/module **transportation** constraints	low/medium/high	negligible or NO impact
Selected **Recip Packager with yards** close to sea	low/medium/high	negligible or NO impact
Availability of OEM proven experience with Single Lift solution design and **module handling**	low/medium/high	negligible or NO impact
Availability of OEM with **Proven experience** on full skid solution referenced **on field**	low/medium/high	negligible or NO impact
Availability of OEM with **Digital design process** capable to perform **fast feasibility assessement** in bid stage of large RC fully or partially on skid	low/medium/high	negligible or NO impact

Figure 2 – Decision-making triggers

The decision on the approach shall be taken considering several triggers, as shown in *Figure 2* that depending on a specific project may have a different specific weight. In this rapidly changing market, the drivers for the success of a project may vary. The tight schedule, skilled workmanship availability, the country of installation, contractual terms or liquidated damages may profoundly influence the material requisition and/or the commissioning start-up plan, in these scenarios the traditional approach maybe not the best choice, all the projects stages impacted from the decision of selecting skid vs foundation based solution shall be taken in account in a trade-off analysis (see Figure 2) a proper weigh/impact shall be assigned and then project by project there will be a sum of factors to drive the final decision that will be based on a full picture assessment.

Some projects even requiring a large Compressors maybe not very critical from vibrational and/or plant complexity point of view while at the same time may have a short delivery timing for the Client, in such case or any other where one or more triggers may have a high impact in the project success then shall be performed a trade-off analysis.

The final rate for the project recently suggested in most of the cases a skid solution for the rating on timing, costs and Health & Safety is at the same time technically feasible and robust, triggers maybe more, the table resume some of the most commons discussed in several bids and that in our experience have driven the decision.

Finally, the choice of a skid solution imply for the Client to rely on an OEM capable to deliver on modules, promptly support in the bid stage to allow a fast trade-off analysis enabling the right decision and solid reference-based experience, the availability on the market of such OEM or with a mixed rate of these characteristics is part of the trade-off analysis itself and will have a relevant weight in the Client decision making process

3 Digitalized Design Process and Reference-based approach

As mentioned in the previous chapter, the OEM needs to rely on a strong project reference fleet, proven on the field that ensures alignment and consistency with the following consequent steps:

a) design assumptions

b) construction process

c) site assembly procedures

d) field measurements and feedback

Since early 2000 Compressor OEM started to Digitalize and Evolve the design process leveraging on the increasing computational capabilities of FEM software and the large server farms availability in the Florence campus, developing year over year refined and detailed Models of compressors and related auxiliaries [3,8,9] commonly employed in the projects. The rough models developed in early 2000 are very detailed thanks to the employment of super elements and predefined libraries of standard parts that accelerate execution especially the pre-processing stage while computational timing is basically driven from the server capacity that in Florence campus is well oversized having to fulfil a greater multi-product demand.

by: Simone Bassani, Riccardo Bagagli*, Marco Passeri, Leonardo Sapuppo – BH Nuovo Pignone

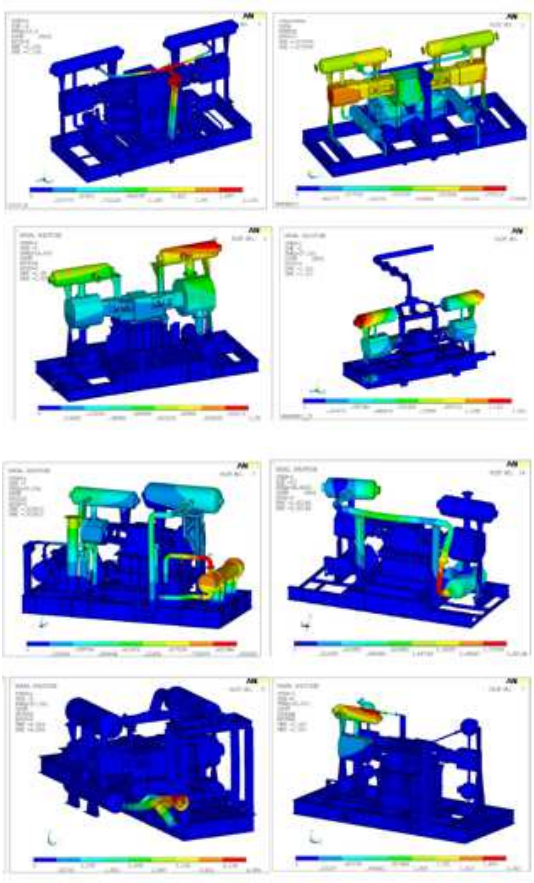

Figure 3 - Cylinder manifold benchmark

In the last 20 years, several units delivered as single lift solution with all the equipment mounted on skid have been processed through step a) b) c) and d) with positive results validating and allowing a continuous improvement process in the accuracy of the vibration evaluation and mitigation, several references with mixed combinations of equipment arrangement have been validate on the field as showed in *Figure 3* and are considered as benchmark. The 4-step execution model has been employed for almost all the compressor sizes, from single to multiple bays (from 2 to at least 4 throws) and increasing the gas loads showing up in the practice that the approach can be scalable.

Figure 4 - single lift solution

In Figure 4 is showed a compressor of medium size (type 4HE 4m x 12m, 90 tons) packaged with all auxiliaries including pressure vessel in a single lift solution, the motor has been supplied on a separate skid with reference pins that allow for a precise assembly at the site and for a fit-up test with compressor skid before delivery (Figure 5), the market is showing interest for solutions that minimize like in this case activities or unplanned events during installation.

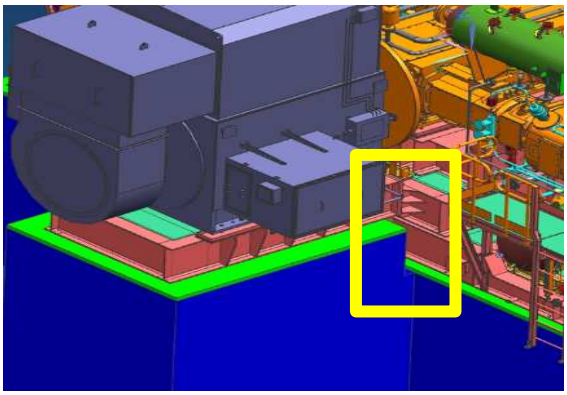

Figure 5 – Zoom on reference connection between the compressor and motor skid

As shown in the below picture, following the same rigorous process has been scaled up to the larger sizes of the compressor, more than 10 years ago the four throws large compressor (up to 130 tons load per throw) has been delivered to the site with crankcase and distance piece installed on a baseplate. In that project having large suction and discharge vessels, there was not been advantages to realize a single lift solution for the expected vibration level of very large vessels on the baseplate and for the costs in the trasportation for a single lift solution; however the most critical parts concerning unbalanced force and couples have been on skid base installed and had proven to work fine along these years confirming that assumption, construction and assembly procedure are repeatable and scalable to a larger size. In case such this, even if a single lift solution may create issues in the overall dimension for transportation, separate modules to be assembled at the site could minimize the effort of the client at commissioning stage, a similar approach has been useful in other projects to perform a fit-up test at the packager premises prior shipping in a kind of Lego approach; the motor for example that is typically shipped loose and directly grouted on its foundation block while in some cases the end-user has requested to be skid mounted, pre-assembled and fit-up tested with the compressor skid. This could be a redundancy, so in the execution, it has been useful to verify interfaces and discover potential interfaces mismatch.

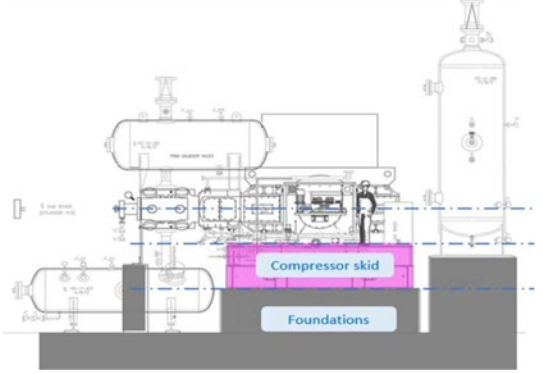

by: Simone Bassani, Riccardo Bagagli*, Marco Passeri, Leonardo Sapuppo – BH Nuovo Pignone

Figure 6 - design with the frame on skid only

The consistency in assumption, construction and assembly means having a structured quality system to ensure along these years through procedures and process the repeatability of these steps, for example in step a) repeatability on how to perform the calculations including FEM software employed, calculation process and boundary conditions set up, design engineers procedure for pre-processing and post-processing is fundamental as well as a defined design flow process where all the tuning options for the dynamic response [3,8,9,11,12] of the skid are well balanced and optimized see Figure 7.

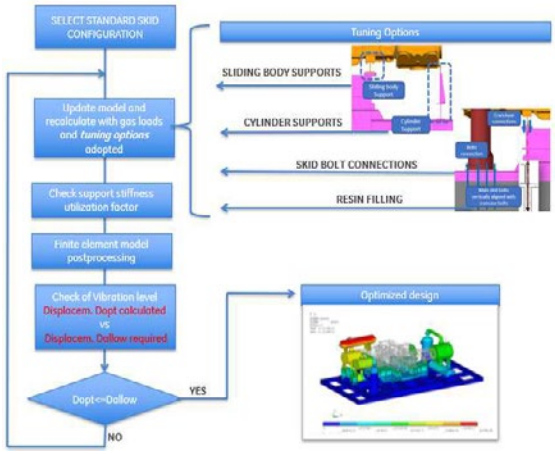

Figure 7 - design flow process for structural response optimizing utilization factor of several tuning options

In step b) the baseplate layout shall be the same for each frame, the supporting point and its locations during construction are defined according to a design standard, welding procedures and welding details are according to a standard and didn't change varying the manufacturer in the supply chain, in step c) the grouting procedures developed in the field during the years are fundamental to ensure the compressor operating at the vibration level estimated, because poor grouting may results in a different real constraint condition that reducing the supporting areas lead to higher vibration amplitude and different mechanical modal shapes compared to the estimated (see Figure 8).

Figure 8 - Unsupported Areas due to poor grouting under the skid

When the sizes start to increase significantly, then greater attention shall be paid in step b) and c), where the criticalities are essentially related to 4 aspects:

1. Preliminary dynamic assessment
2. Construction mode Transition from skid to module
3. Lifting and transportation special requirements
4. Special grouting procedure to be performed on-site

Increasing the size, it is necessary to analyze aspect 1) to determine the feasibility of a single lift solution or multi-module; a large vessel or high unbalance loads may be an issue later in the execution if not analyzed and addressed since the first draft layout, this preliminary rough analysis identify all mitigation actions at early stage of the project or in the bid stage.

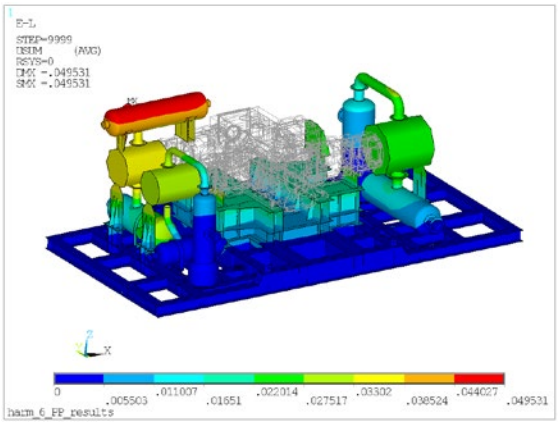

Figure 9 - cylinder manifold preliminary study, all-on-skid design

As previously described there is a process [3,8,9] with well-defined libraries for compressor parts and auxiliaries that enable the Design Engineer during the bid stage to rapidly verify the suitability of the preliminary solution with the project loads conditions and process variability, the FEM analysis is performed according to API 618 [1] requirements, the results are showed both in a resuming table reporting stress and vibration value for each harmonic (see Figures 9 and 10), the same analysis can be summarized in a plot showing the most critical points and how they are placed respect to the

by: Simone Bassani, Riccardo Bagagli, Marco Passeri, Leonardo Sapuppo – BH Nuovo Pignone*

allowable limits according to the API 618 [1] or to the values that end-user has defined as critical for a specific application. When the dimensions are going over 6m x 12m, and the overall weight is estimated to be greater than 180 tons we are starting to deal with a kind of module execution and aspect 2) change the scenario from the construction point of view, it is necessary to identify a yard close as much as possible to a ship delivery point that shall be equipped with all the facilities and qualified personnel to handle the erection and logistic of large carpentry and machinery.

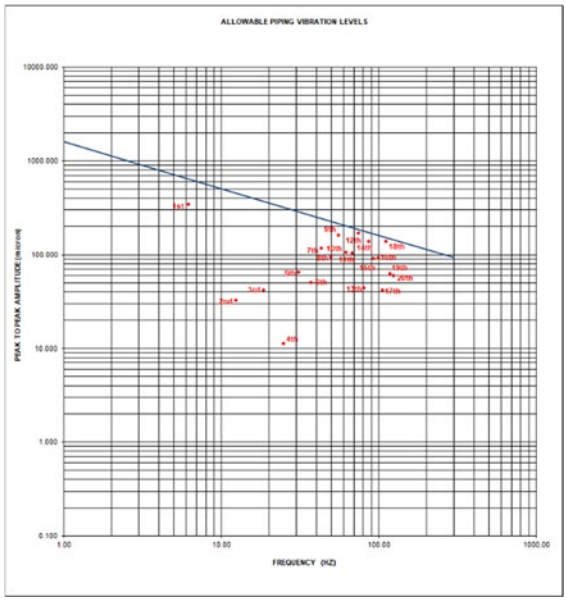

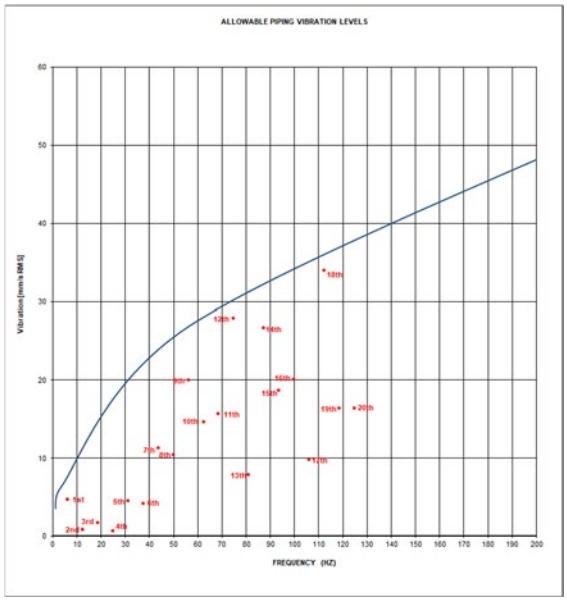

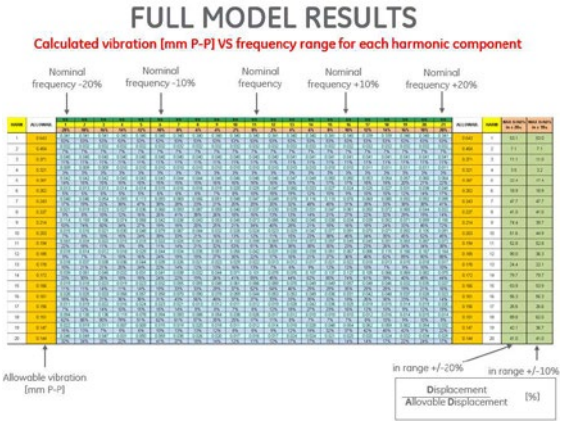

Figure 10 - analysis of vibrations after preliminary study, all-on-skid design

When the module is extensive, EPC could request an additional verification that is to verify the vibrations amplitude limits for baseplate (see API 618 5th edition par 7.5.4.14 vibration limits). This verification requires a vibration frequency less than or equal to 10 Hz, a maximum displacement of 100 µm 0 – peak (4 mil 0-peak) (0.008 in peak-to-peak); for a vibration frequency greater than 10 Hz, a maximum velocity of 4.5 mm/s RMS (0.175 in/s RMS).

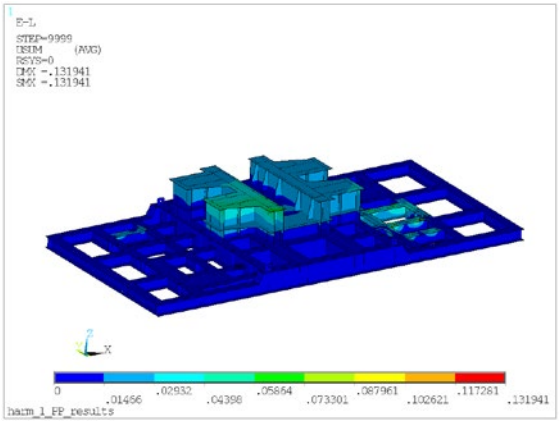

by: Simone Bassani, Riccardo Bagagli*, Marco Passeri, Leonardo Sapuppo – BH Nuovo Pignone

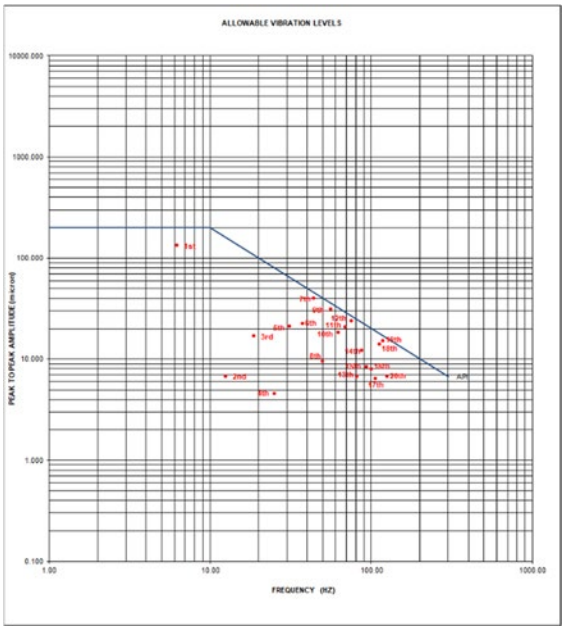

Figure 11 - analysis of vibrations after preliminary study, of skid baseplate design

Once the module is built, it becomes critical the aspect 3), good practices in the design of the lifting points will ensure smooth lifting while containing the overall side dimensions, a full 3D model is mandatory to assess with precision the position of the centre of gravity, an accurate measure of the weight and how it is distributed.

During the execution, when 30% of 3D model review is jointly released between OEM and EPC the more considerable weight are almost defined and placed on the module, on this basis will be identified the anchor points locations that optimize the module stability and balancing during lifting, any variation in weight and its distribution raising during the 60% and 90% 3D model review will be prior managed monitoring centre of gravity at each significant difference introduced on the skid by modifications of equipment, added instrumentation, walkway or any other item change may come for project needs. Increasing the size of the skid even the grouting become a critical part of the project and according to 4) that shall be treated with the involvement and the commitment of a resin manufacturer that will lead the activities on the field and acting as a reviewer at the 30% 3D model review declaring all the necessary features needed in the large baseplate to allow a proper pouring and to reach each internal part and avoiding vacuum or un-grout large areas.

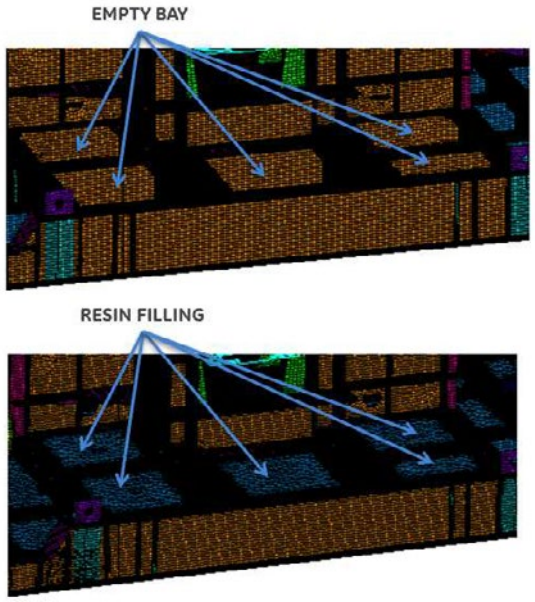

Figure 12 – FEM model of baseplate resin filling

Depending on the resin characteristic and the installation site the requests on the baseplate may change, if a resin filling of the baseplate is required then a minimal bay area shall be sized, including venting holes diameter and related spacing, pouring holes, the gap with concrete for a specific area and so on, for these reasons is mandatory the involvement of a resin manufacturer since the early phases of the project execution, here criticalities are such only if not managed with the proper timing and awareness. Increasing the size of the Compressor and the associated gas loads it may be beneficial increase the mass and damping of the baseplate, the baseplate can be designed to be totally filled by a specific resin (see Figure 12) where the filling is included in the FEM model to assess the potential relative improvement. The resin filling is a process that can be applied after the successful completion of grouting which require its visual inspection trough baseplates holes to check that there are no void between baseplate and ground. The baseplate filling is an additional process (e.g. in case of need) to further control vibration amplitude at the more energetic harmonics (1°-7° harmonic) which typically are associated to the gas loads and have highers order of magnitude respect to the other dynamic load components as highlighted in Figure 13, the gas loads content by harmonic is basically distributed within the first 7 harmonics depending on the capacity system installed. The approach of baseplate filling successfully applied in the past has also been tought to be used in a large module, where the crankcase itself has been already successfully operated in the field with baseplate limited to the compressor footprint (see Figure 6). These field results on the large frame together with the results on smaller packages lead to extend the positive references to the solution with a large frame inclusive of the dampers on the skid as confirmed by calculation (Figure 9, Figure 11 - analysis of

by: Simone Bassani, Riccardo Bagagli*, Marco Passeri, Leonardo Sapuppo – BH Nuovo Pignone

vibrations after preliminary study, of skid baseplate design)

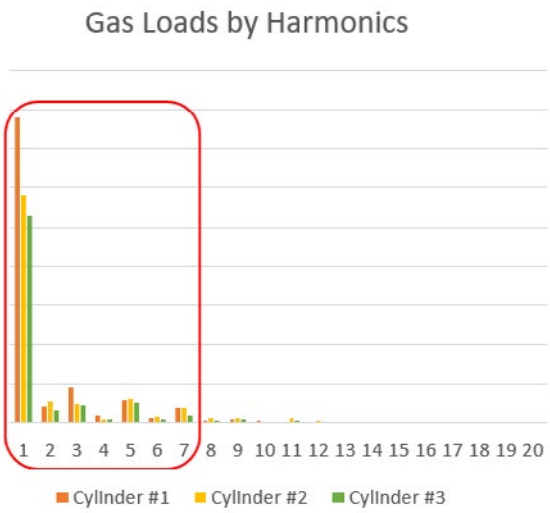

Figure 13 – Typical gas load magnitude composition by harmonic

Analyzing the dynamic response of the module for a specific point over the crankcase, as showed in Figure 14, all the loads acting on the skid are considered, and the magnitude of displacements is reported by harmonic content; two evident conclusions can be done, one is that the highest reduction of amplitude is clearly within the first 9 harmonics where the most significant energetic responses are 1°, 5° and 9° (see red bars in Figure 14) the second is that running the same analysis with the introduction of the resin filling in the baseplate, according to Figure 12, it can be clearly noticed the beneficial effects within first 9 harmonics, see blue bars in Figure 14 (-30% for 1° harmonics and up to -90 % for 5° and 6° harmonics). It can be noticed that in this specific analysis, there are also some increments at higher harmonics (10°, 11° and 12°) but relatively small in percentage and for low energy content harmonics.

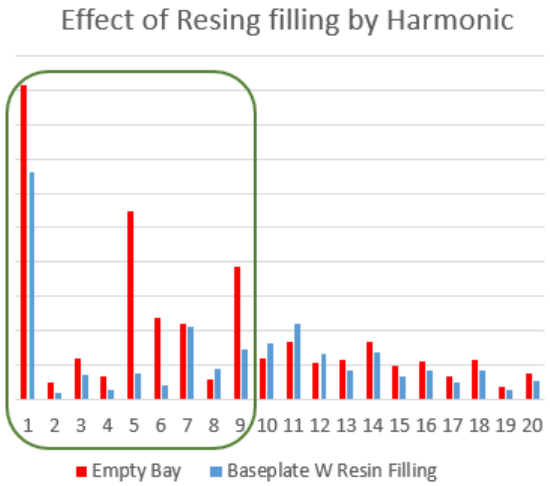

Figure 14 – Effect of resing filling by harmonics

4 Functional Test and loop check on the assembled module

As mentioned in the previous chapter, it is fundamental for the EPC to minimize site activities, commissioning, skilled personnel at the site, unplanned events and for this essential requirement it necessary to organize a dedicate test plan on the full module assembled before shipping the compressor. Most process-related testing needs to be postponed on the machine assembled on-site, both because it's unpractical to reproduce on the test bench the process conditions and, even in this case, the possibility to replicate actual process dynamic behaviour is questionable. On the other hand, an accurate testing strategy allows checking in the assembly shop most of the machinery monitoring and auxiliary systems. Also, the interaction among systems is a critical aspect, to be assessed as part of the functional test by simulation of unit start-up, run and shutdown.

The list of systems to be considered for extensive functional testing on skid depends on the assembly configuration, but can be summarized with the following:

- Gas recovery from packings and distance piece
- Nitrogen buffering (when applicable)
- Capacity control (by recycling valves, step unloader or step-less reflux)
- Crank mechanism lubrication
- Cylinder and packing lubrication (when necessary)
- Cylinder and packing cooling
- Machinery monitoring
- Starting sequence

by: Simone Bassani, Riccardo Bagagli*, Marco Passeri, Leonardo Sapuppo – BH Nuovo Pignone

4.1. Preliminary activities

In the proposed approach, the functional test is intended to give feedback on adequate interaction among instrumentation, equipment and loops inside the sub-system and different subsystems. For this reason, individual systems shall be tested with relevant specific procedures before the functional testing, and the preliminary activity shall include

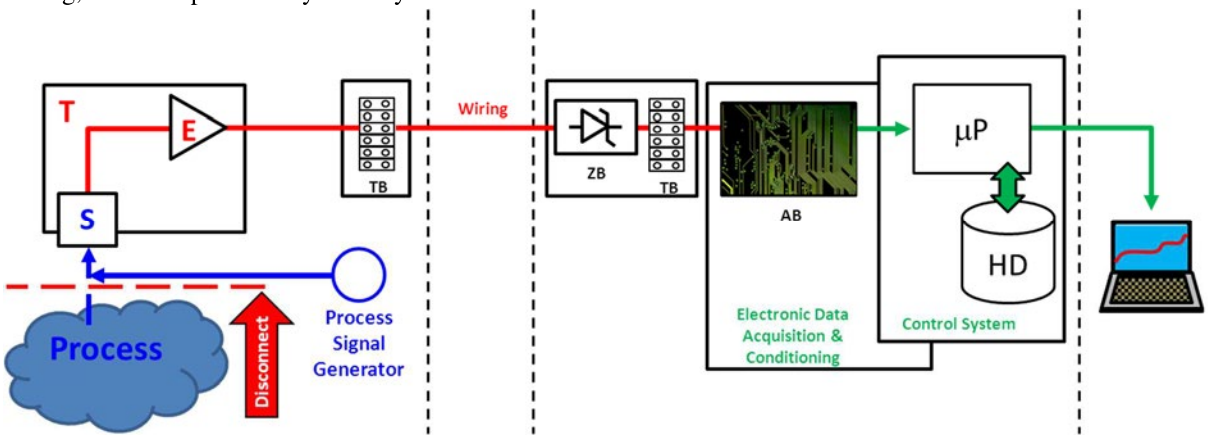

Figure 15 - loop check overview

package assembly completeness and consistency checks and loop checks, to be done before starting the overall functional test.

Assembly checks shall include:

- Mechanical assembly of the crankcase and cylinders
- Pipe systems assembly
- Oil system flushing and test filling
- Electrical instrumental assembly
- Dedicated assembly checks for pre-assembled systems (gauge boards, lubricators…)

4.2. Loop check

The loop check is a much more standardized activity, with different possible configurations depending on the available loop elements during the check. To properly fit with the functional test scope, the most extended configuration shall be available, inclusive of Unit Control Panel, or simulator, terminal boxes and interconnecting cabling. The specification shall include dedicated procedures for the different type of signals:

- Analog Input
  - Pressure Transmitter
  - Temperature Transmitter
  - Level Transmitter
  - Flow Transmitter
  - Seismic Transmitter
  - No Contact Transmitter
  - A system with End of Line Resistor
  - Position Transmitter
- Digital Input
- Analog Output
- Digital Output

Test typology shall be selected in a propaedeutic way for the following functional test. A process signal generator will ensure a higher level of completeness of the check, catching potential assembly mistakes that would otherwise be detected later in the overall functional test.

4.3. Functional test

Most activities in the proposed approach will replicate the typical individual test procedure already foreseen for each system on the final assembled package. Some single testing won't be possible, and as well useful, to replicate on the assembled unit; on the other hand, the assembled systems give the possibility to check reactions from sensors that wouldn't be otherwise possible to be tested before the unit commissioning on site. Here below are presented some highlights on proposed additional testing on the fully assembled units and criticalities for specific systems.

- Gas recovery from packings and nitrogen buffering. After connecting the buffering system to dry air in the range of site utility, all pressure and packing flow readings can be recorded. Since compressor type packings can be subject to high bias without compromising the effectiveness of buffering, the check will be done to confirm individual indicator reaction only. At the same time, air flowing from packings to the distance pieces and vent recovery lines will be detected by flow transmitters giving valuable average data on expected leakage during operations. The system shall be flushed with nitrogen or inert gas after the testing.

- Frame lubrication, cooling and machinery monitoring. After the repetition of conventional individual system testing, the frame heater will be activated, sending warm lube oil to the crank mechanism. This will allow having feedback on the correct operation from temperature sensors in the frame machinery monitoring. An equivalent strategy will allow checking packing temperature monitoring

by: Simone Bassani, Riccardo Bagagli*, Marco Passeri, Leonardo Sapuppo – BH Nuovo Pignone

after activating the cooling system heater. Other probes typically challenging to be checked before commissioning are valve cover temperature elements. The sensor reaction can be safely initiated after packaging completion by contact with instant cold packs (water and ammonium nitrate). As an alternative, R 12 or equivalent fluid-based ice-spray can be used. This will avoid uncontrolled cooling (or warming) techniques potentially exceeding the material design range.

- Starting sequence and stop. Besides (or in parallel) to the functional test system-by-system based, a starting sequence will be simulated collecting all the data from sensors. This will allow the collection of sensor readings during the sequence, with relevant consistency check, and simulation of all the interlocks correctly working on the wired UCP.

It's clear that UCP/simulator availability and its configuration plays a crucial role in this kind of activity (with the design software and proper overrides, or with a testing version developed for the functional test). Installation/wiring on the testing shop may represent an additional and potentially huge wiring activity on the execution schedule. This is an aspect enhancing the benefit for a design inclusive of junction boxes with remote input/output embedded systems, also called Smart Junction Boxes: the simple datalink (optic fibre or Modbus) interconnection will hugely facilitate testing setup, both with the UCP or with a simulator, reducing the need for time and skilled personnel in the same way it does during erection on site.

6 Conclusion

The increasing adoption of advanced calculation suite together with customized digitization processes are encouraging the adoption of increasing power large Reciprocating Compressor modularized solution, employing large frame with load capability up to over 130 tons per throw and a final single lift solution including lube oil console in a total weight of approximately 200 tons in a 6 X 14 X 5 meters (width X length X height) overall dimensions. The criticality linked to a reliable dynamic structural design to ensure smooth operation has historically limited the adoption of the skid for the big compressor in favour of a foundation-based solution, the paper explained how after evaluating project triggers trade-off the technical challenge can be managed with a pre-study performed in the feeding stage where the feasibility can be assessed in advance optimizing the structural design through several tuning options, the process can be fast iterated several times, thanks to servers infrastructure, OEM components libraries modelled and tuning capabilities based on a solid reference validated on the field [3,8,9]. The repeatability of the process is guaranteed thanks to a robust quality system that ensure and monitor adoptions of a defined process, tools, qualified designers and strong partnership along the supply chain, availability of yard where perform assembly and functional tests as described in detail. The EPC can be involved in all the stages of the design and construction processes, especially in the final functional tests on the completed module where the OEM can optimize client requests prior shipping.

7 Nomenclature

EPC= Engineering, Procurement & Construction
OEM= Original Equipment Manufacturer
UCP= Unit Control Panel
FEM = Finite Element Model
R 12 = Fluid Refrigerant (highly versatile)
% 3D model = % of finalization of the three dimensional model

8 Acknowledgements

The authors wish to thank Baker Hughes Nuovo Pignone, for permission to publish the information reported in this paper.

9 References

[1] API 618 STD 5th edition, Reciprocating Compressor for Petroleum, Chemical and Gas Industry services American Petroleum Institute.

[2] ASME - Boiler and Pressure Vessel Code, sect. VIII DIV. 2 2001, The American Society of Mechanical Engineers.

[3] Passeri M., Generosi S.: Cylinder Manifold forced, 7th Conference of the EFRC October 21th / 22th, 2010, Florence, Italy

[4] Giacomelli E., Passeri M., Giusti S., Zagli F., Generosi S.: Modelling of Pressure Pulsations for Reciprocating Compressors and Interaction with Mechanical System, Proceedings of ESDA, Eng. System Design and Analysis, 19-22 July, 2004, Manchester, UK, The American Society of Mechanical Engineers.

[5] Giacomelli E., Passeri M., Romiti M., Generosi S.: Forced Response of cylinder manifold for Reciprocating Compressors applications, proceedings of ESDA 2006: Eng. Sys. Design Analysis 4-7 July 2006

[6] Giacomelli E., Passeri M., Battagli P., Euzzor M.: Pressure Vessel Design for Reciprocating Compressors Applied in Refinery and Petrochemical Plants - PVP2005-71292, Proceedings of PVP conference 2005, Pressure Vessel and Piping July 17-21, 2005, Denver, Colorado, USA The American Society of Mechanical Engineers.

by: Simone Bassani, Riccardo Bagagli, Marco Passeri, Leonardo Sapuppo – BH Nuovo Pignone*

[7] Passeri M., Generosi S., Bagagli R., Carmelo M.: Preliminary piping sizing and pressure pulsation evaluation, Proceedings of ASME PVP 2014 Pressure Vessels & Piping Conference PVP 2014 July 20-24, 2014, Anaheim, California, USA

[8] Passeri M, Bagagli R, Carmelo M.: Compressor general arrangement design guided by cylinder manifold forced response, Proceedings of ASME PVP 2015 Pressure Vessels & Piping Conference PVP 2015 July 19-23, 2015, Boston, Massachusetts, USA

[9] Passeri M., Bagagli R., "Cylinder Manifold automation". 10th European Forum for Reciprocating Compressors 2016, Düsseldorf - Germany

[10] Passeri M., Rossi C., Ferrari G., Guerrini L., Mazzoli M., Melis S., "Pulsation optimization by dynamic variable orifice & Recips starting phase selection". 11th European Forum for Reciprocating Compressors 2018, September 13th / 14th, 2018, Madrid

[11] A. Eijk: Cost-effective and detailed Modelling of Compressor Manifold Vibrations, ASME Pressure Vessels and Piping Conference 21-26 July, 1996, Montreal, Canada

[12] A. Eijk: Economic benefits of CAD models for compressor manifold vibration analysis according to API 618, 3rd EFRC Conference 27-28 March, 2003, Vienna

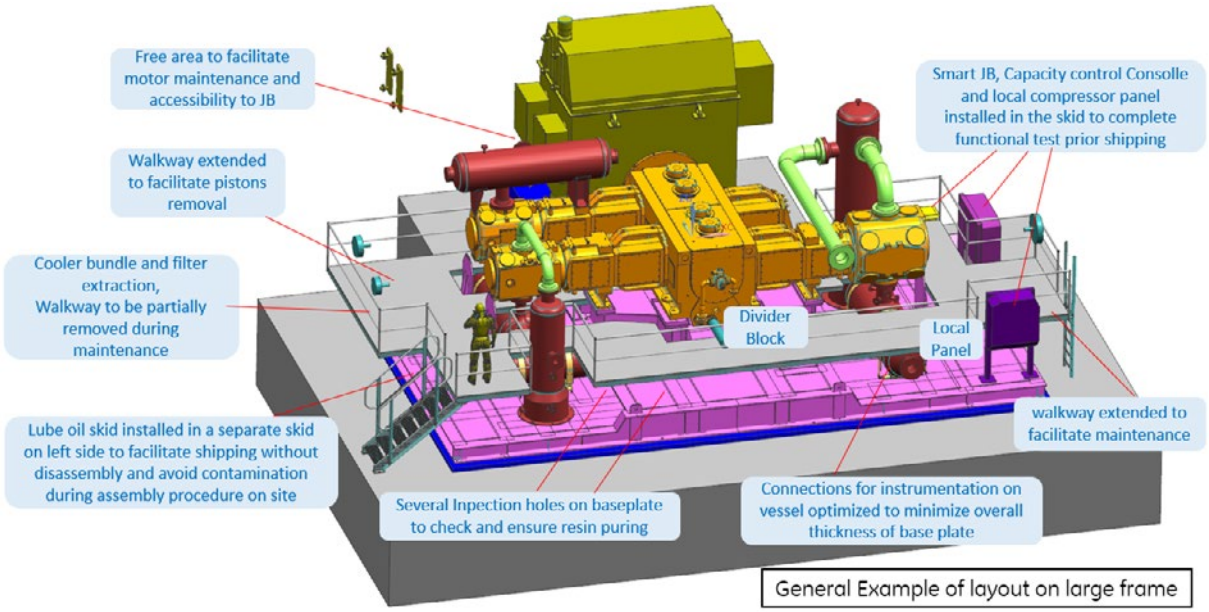

Figure 1 - skid design with a big frame, dampers, gauge board and oil console. Off-skid motor

The main technical barrier to overcome to design and build a reliable fully packaged large reciprocating compressor solution, is to avoid vibration issues that may heavily affect the plant availability and reliability with potential implications in creating hazardous scenarios. Since large reciprocating compressors typically have high gas loads, potentially high unbalanced forces and torques, moving mass and static parts that are very high in conjunction with a big overall foot-print of the module, the design challenge is tremendous and to succeed it need a large experience and the availability of tailored and integrated design tools is required.

ITW Performance Polymers

Innovative Remediation Techniques to Compressor Foundation Systems

by:

Christopher Matthews-Ewald
Industrial Application Engineer
ITW Performance Polymers
Cary, North Carolina
U.S.A.
cewald@itwpp.com

12th EFRC CONFERENCE
August 24 – 26, 2021, Warsaw

Abstract:
When reviewing the major threats to reciprocating compressor performance reliability, substandard maintenance practices and loss of operating efficiency have profound negative impacts on the total life cycle costs - driving down overall profitability. Considering that the majority of maintenance budgets are spent on a minority of equipment1, it is imperative to correctly diagnose and remediate issues before they lead to equipment breakdown and unintended stops in production. This paper will highlight some common threats to operational efficiency in reciprocating compressors, with a specific focus on the foundation system. Through the presentation of multiple case histories, innovative approaches will be shown that can help all personnel focused on proper maintenance and reliability best practices to effectively identify the root causes of poor performance and paths to successfully remediate and improve operating reliability.

by: Christopher Matthews-Ewald – ITW Performance Polymers

1 Introduction

Due to the critical role that reciprocating compressors play in industrial environments, it is clear why so much attention is paid to reliability and efficiency of these critical pieces of dynamic equipment. With a thorough understanding of the economic factors that influence the asset profitability that is influenced by these machines, this focus is justified. This paper will show the importance of operational efficiency and how threats to this critical metric will affect total life cycle costs, and in turn overall profitability. With a specific focus on the foundation system, examples will be shown of innovative remediations implement to address deficiencies that led to increases in reliability and efficiency. Through effective collaboration between foundation experts and equipment manufacturers, long term solutions were provided to restore foundation integrity that will last for decades to come.

2 Effects of Poor Compressor Reliability

Poor equipment reliability has a direct negative impact on the overall profitability of an asset. Especially with compressors, the increased expenditures due to misalignment directly impacts the bottom line[1]. With power consumption accounting for as much as 90% of the total life cycle costs[3] or total cost of ownership, of dynamic mechanical equipment, maintaining precise alignment to maximize operational efficiency is critical to the desire to increase profitability.

The most effective methods of mitigating threats to overall compressor reliability come from design for the entire design environment and performing regular maintenance before costly failures occur. It is more profitable to invest incrementally and perform needed regular maintenance prior to a failure that necessitates the shutdown of equipment and an emergency repair[4].

In looking specifically at the effects resulting from the foundation system, a thorough understanding of the potential operating environment, including environmental exposures and operational requirements, will help to ensure that machinery operators more efficiently and with less potential degradation to wearable components. With a proper execution of a predictive maintenance program, including regular checking of the anchor bolts for proper tensioning, the foundation system can continue to accomplish its functions for extended lengths of time. It is not unheard-of for a foundation system to be in constant operation and without degradation after 40 years of constant operation.

3 Foundation Design for Compressor Reliability

For the perspective of this paper, a foundation system includes the following items:

- Dynamic Equipment
- Base Plate of Dynamic Equipment
- Anchor Bolts
- Load Transfer Medium
- Foundation
- Sub Foundation/Concrete Mat
- Sub-surface/Soil

Please see Figure 1 for more details on the foundation system.

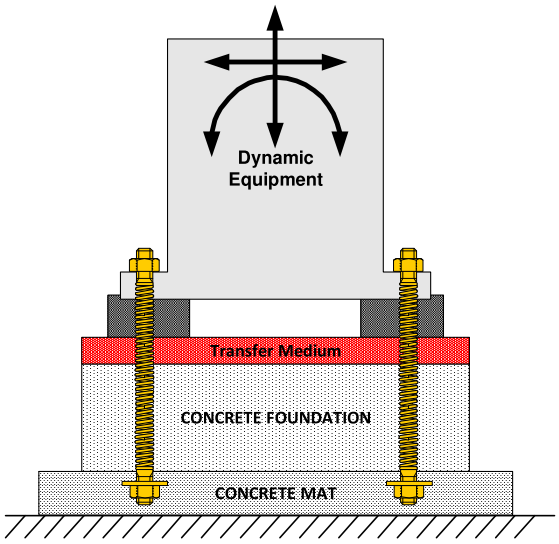

Figure 1: Foundation System for Dynamic Equipment

An effective foundation system design for a reciprocating compressor will achieve the following functions:

1. Keep equipment in position
2. Mitigate forces due to equipment operation
3. Prevent Foundation Degradation[5]

To be able to effectively accomplish these functions over long periods of time, it is imperative that initial design and installation of the foundation system fully considers the potential environmental and operation conditions which the system will be exposed[6]. By taking the time to fully understand and consider these factors in the up-front design, operational efficiency will be increased, resulting in reduced need for future remediation and increased overall asset profitability.

After a foundation system has been installed, regular inspection and maintenance of the system should be a core aspect of any maintenance plan. For the foundation system, it is key to perform regular reviews for any potential breaks within the system. This includes monitoring of the anchor bolt tensions, evaluation of the condition of control

by: Christopher Matthews-Ewald – ITW Performance Polymers

joints, and proper treatment of any cracks or breaks that develop over time. These are just some of the key aspects that will contribute to increased longevity of the foundation system.

The following case histories will show identification of deficiencies within the foundation system, and steps that were taken to complete remediation. In each of these examples, a regular maintenance schedule that included inspection would have allowed the asset owners to identify and diagnose the underlying root causes before they became larger concerns. Early detection and treatments lead to reduced remediation, meaning less direct expenditure and greater profitability of the asset.

4 Case History – Equipment Removal and Foundation Rework

A major operator of a petrochemical facility was experiencing ongoing performance and mechanical problems with a critical, one-stage, 4-cylinder reciprocating process gas compressor. The asset owner contracted the original equipment manufacturer (OEM), which partnered with a regional team of foundation experts. Through the innovative collaboration of all parties, the remediation work was identified and performed to bring a non-operating asset back into service and increase the operational efficiency.

4.1 Previous Installation

The compressor was originally installed in 1978. When installed originally, the foundation was mounted on a cementious grout. Over time, the vibrations resulting from the operation of the compressor steadily increased. This resulted in extensive mechanical damage to the compressor, as well as damage to the foundation system. Initial efforts were made to ensure the proper tensioning of the anchor bolts, but the bolts kept relaxing over time. The vibrations eventually increased to the point that the equipment could no longer be operated due safety concerns.

4.2 Problem Identification and Proposed Solution

As part of the overall overhaul of the equipment, the first step was to evaluate the state of the anchor bolts and identify all areas in need of overhaul. All anchor bolts were tensioned to the recommended load, and the alignment was checked. From this review, it was determined that only the piston loaded areas would need remediation.

4.3 Removal of Previous Transfer Medium

After determining the scope of the intervention, the compressor was removed from the remainder of the foundation system. The compressor was being overhauled off-site, and this allowed full access to the remaining portion of the foundation system. Removal of the existing sole plates and the damaged cementious grout was performed. Please see Figure 2**,** Figure 3**, &** Figure 4 for detail on the initial condition and removal of the previously installed transfer medium.

Figure 2: Removal of Existing Cementious Grout

Figure 3: Degradation of Existing Cementious Grout under Support Rails

by: Christopher Matthews-Ewald – ITW Performance Polymers

Figure 4: Surface of Concrete after removal of Cementious Grout and Support Rails

This step also included removal of the anchor bolts using a core drill. Core drilling was performed using a 6" OD core drill bit and were drilled down to a depth of 1000 mm, to accommodate the new bolts with a length of 950 mm. Please see Figure 5 & Figure 6 for details on the removal process of the anchor bolts and the foundation after core drilling was completed.

Figure 5: Core Drilling Damaged Anchor Bolts

Figure 6: Foundation After Damaged Anchor Bolts Removed

A total of 4 support rails and 16 damaged bolts were removed under the compressor. The core drilling of the anchor bolts also allowed access for further inspection of the cracks within the concrete foundation, as well as the overall integrity of the concrete block.

4.4 Reinstallation of Compressor

After delivery of the new anchor bolts was completed, the final portion of the foundation overhaul could be completed. The new anchor bolts were Class 8.8 per ISO 898-1. After ensuring that the anchor bolts were cleaned, the compressor was aligned, and the anchor bolts were hung into the newly drilled anchor bolt pockets. Formwork was constructed to allow filling of the mounting area. The mounting area under the compressor support rails were filled with a superior epoxy grout, as recommended and installed by the regional foundation expert team. Please see Figure 7 & Figure 8 for preparation and pouring of the epoxy grout under the compressor.

Figure 7: Formwork for Mounting Support Rails on Epoxy Grout

by: Christopher Matthews-Ewald – ITW Performance Polymers

Figure 8: Superior Epoxy Grout Installed Under Compressor Support Rails

After sufficient time had elapsed, as advised per the recommendations of the epoxy grout manufacturer, the formwork was removed, the removable alignment devices were backed out, and the anchor bolts were properly tensioned per the recommendations of the OEM. Please see Figure 9 for a view of the final mounting of the compressor.

Figure 9: Final View of Compressor Support Rails on Superior Epoxy Grout

4.5 Follow Up

A follow up visit was conducted approximately 1 year after the initial installation. At that time, the anchor bolts were observed to be maintaining the proper tension without concern and the compressor was reported to have been operating very well. There were no concerns with excessive vibrations or wear to the mechanical components of the compressor.

Through a successful collaboration between the asset owner, original equipment manufacturer, and a foundation expert, a solution was designed and effectively installed to return a compressor with a history of poor performance back into service.

5 Case History – In-situ Anchor Bolt Remediation

An operator at a large petrochemical facility in Western Canada had experienced on-going difficulties with being able to achieve proper anchor bolt tension for a critical piece of dynamic rotating equipment. The asset owner partnered with a regional team of foundation experts for review of the anchor bolts and proposed solutions. An innovative solution was proposed and implemented to replace the anchor bolts without requiring the removal of the equipment. The reduction in associated downtime minimized the amount of time that the process had to be offline, directly leading to greater profitability.

5.1 Previous Installation

The equipment was originally installed approximately three decades prior to the decision to perform the remediation. Epoxy grout was used in the initial installation and maintained its integrity. The epoxy grout encapsulated the entire top of concrete foundation block, which extended beyond the footprint of the steel baseplate approximately 300 mm (Please see Figure 10). Due to the exposure of the foundation system to the harsh environmental elements, including extreme temperature changes, edge lifting occurred within the concrete below the bond line with the epoxy grout (Please see Figure 11).

Figure 10: Original Equipment Installation

Figure 11: Edge Lifting on Foundation

by: Christopher Matthews-Ewald – ITW Performance Polymers

In the course of regular maintenance inspections, it was identified that the anchor bolts were unable to achieve designed tension. The remediation was not performed for many years due to budgetary constraints and not wanting to take the equipment off-line. The lack of proper anchor bolt tension resulted in high vibrations during equipment operation.

5.2 Problem Identification and Proposed Solution

The asset owner decided to investigate opportunities to achieve proper anchor loading of the fan without the downtime associated with removal and entire foundation rehabilitation.

Since the original concrete foundation extended significantly beyond the footprint of the equipment baseplate, a solution was proposed to use a custom fabricated baseplate extension to house new anchor bolt assemblies. New anchor bolt pockets would be core drilled into the concrete foundation using industry accepted best practices with epoxy grout.

5.3 Remediation Process

The first step was to core drill new anchor bolt pockets through the epoxy grout and into the concrete foundation. The new pockets were approximately 300 mm into the existing concrete foundation. Please see Figure 12 showing the core drilling operation.

Figure 12: Core Drilling New Anchor Bolt Pockets

After adding the anchor bolt pockets, hand-held pneumatic chipping guns were used to remove as much of the existing epoxy grout as possible. This was performed to the extent possible by the reach of tooling and kept in place most of the original epoxy grout under the center of the equipment. This also allowed the equipment alignment to be maintained without requiring temporary supports. Existing epoxy grout and underlying concrete were removed until clean and sound concrete was reached and prepared per best practices for installation of a superior epoxy grout. Additionally, the edges and corners of the foundation were chamfered to help minimize the potential for edge lifting to occur in the future. Please see Figure 13 showing the surface preparation of the concrete foundation and Figure 14 showing the new anchor bolt pockets outside of the original base frame.

Figure 13: In-Process of Removal of Existing Epoxy Grout and Underlying Concrete

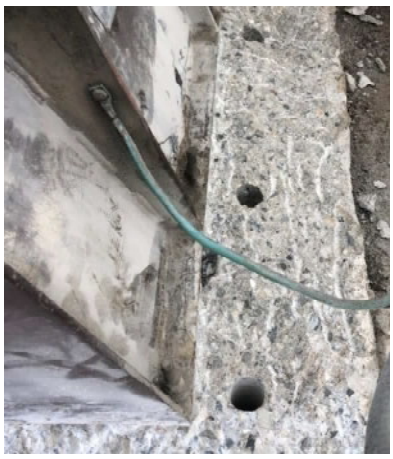

Figure 14: New Anchor Bolt Pockets in Properly Prepared Concrete Surface

After the surfaces were properly prepared, the formerly used anchor bolts were cut flush with the existing baseplate. In this position, they could not be tensioned and would reduce confusion for future maintenance activities. The newly manufactured baseplate extension was welded to the existing baseplate, as shown in Figure 15.

by: Christopher Matthews-Ewald – ITW Performance Polymers

Figure 15: Baseplate Extension Welded to Existing Baseplate

New ASTM A193 B7 anchor bolts were installed in the baseplate extension and hung in the anchor bolt pockets. It was ensured that the new anchor bolts featured recommend free-stretch length, as shown in Figure 16. The original bolts did not have this free-stretch length, and it is thought that this is the primary reason why the bolts failed prematurely.

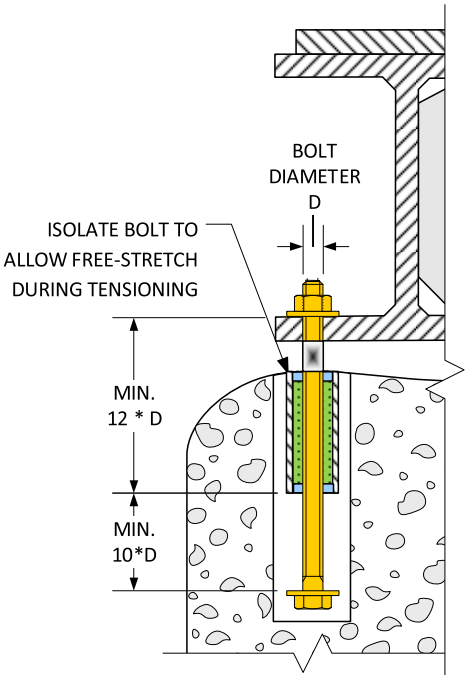

Figure 16: Proper Anchor Bolting Configuration

A superior quality epoxy grout was poured in the anchor bolt pockets and under the baseplate. The entire original epoxy grout cap was encapsulated within the new, superior epoxy grout cap. Control joints were used to segment the pour and allow for expansion and contraction of the epoxy grout due to thermal changes.

Figure 17: Superior Epoxy Grout Installed in New Anchor Bolt Pockets and Under Baseplate and Baseplate Extension

After sufficient time had elapsed, as advised per the epoxy grout manufacturer, the formwork was removed, and the anchor bolts were properly tensioned.

Figure 18: Final View of the Equipment Remediation

5.4 Follow Up

After the remediation was performed, the observed vibrations during equipment operation are minimal and greatly reduced from the original situation. The anchor bolt tension has been maintained. The entire remediation resulted the equipment being offline for only three days and resulted in a significant improvement in operational efficiency.

by: Christopher Matthews-Ewald – ITW Performance Polymers

6 Conclusion

Proper understanding of the foundation system of rotating equipment is an important aspect of overall reliability and operational efficiency. When there are deficiencies in this system, it is imperative to quickly identify and remediate these problems before they cause more catastrophic and expensive failures. By forming true partnerships with local foundation experts to properly diagnose the root causes of the problems, innovative solutions can be designed and effectively implemented, leading to great improvements in operational efficiency and a reduction in total costs. This directly results in greater asset profitability.

7 Acknowledgements

The author would like to acknowledge the invaluable contributions by the following experts to the content of this paper:

- Jesús Vilchis, Sintemar, Managing Director of Latin America, Mexico City, Mexico - jvf@sintemar.com
- Jason Bierbach, Chinook Industrial Ltd., Technical Sales Representative, Calgary, Alberta, Canada - jason.bierbach@chinook.ca
- Timothy Barrington, ITW Performance Polymers, Regional Sales Manager, Overland Park, Kansas, United States – tbarrington@itwpp.com

References

[1] Bloch, Heinz P. (2011). Pump Wisdom. Hoboken, New Jersey: John Wiley & Sons.

[2] Bloch, Heinz P. (2012, April). Pump Alignment Saves Power. *Hydrocarbon Processing*. Retrieved from: http://www.heinzbloch.com/docs/HB_Tech_Paper_24.pdf.

[3] Frenning, L., et al., 2001, *Pump Life Cycle Costs: A Guide to LCC Analysis for Pumping Systems*, Hydraulic Institute and Europump, Parsippany, New Jersey.

[4] Sondalini, Mike. *What is the connection between equipment risk and equipment reliability and how does it affect your maintenance strategy selection?*. Retrieved from Lifetime Reliability Solutions website:https://www.lifetime-reliability.com/cms/free-articles/reliability-improvement/only-path-to-reliability-excellence/link-between-risk-and-reliability/.

[5] Kuly, James A. (2010, October). *Best Practices in Compressor Mounting*. Paper presented at the 7th Conference of the European Forum on Reciprocating Compressors, Florence, Italy.

[6] ACI 351.3R-04 "Foundations for Dynamic Equipment", Reported by ACI Committee 351, James P. Lee, Chair and Yelena S. Gold, Secretary.

ELECTROLYZERS and COMPRESSORS Optimizing the H_2 VALUE CHAIN

COMPRESSORS
The H_2 Experts

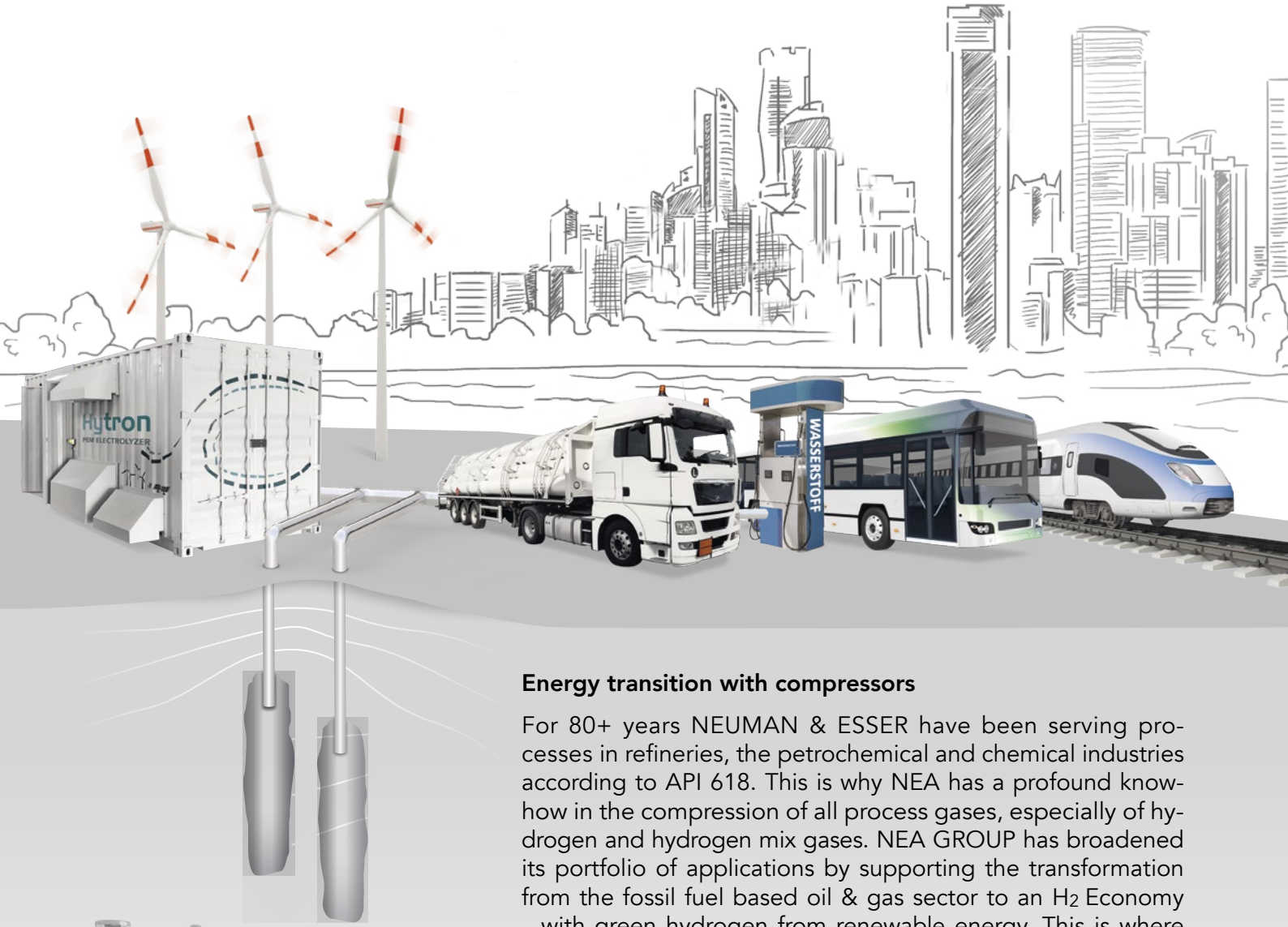

Energy transition with compressors

For 80+ years NEUMAN & ESSER have been serving processes in refineries, the petrochemical and chemical industries according to API 618. This is why NEA has a profound know-how in the compression of all process gases, especially of hydrogen and hydrogen mix gases. NEA GROUP has broadened its portfolio of applications by supporting the transformation from the fossil fuel based oil & gas sector to an H_2 Economy with green hydrogen from renewable energy. This is where the proven compressor technologies from NEA and HOFER come into play. The conversion of the energy system with Power to Gas needs energy-efficient piston and diaphragm compressors. They are the perfect match to ensure both the flexibility of demand and energy security with green gases.

NEUMAN & ESSER: Agile. Solution. Experts.

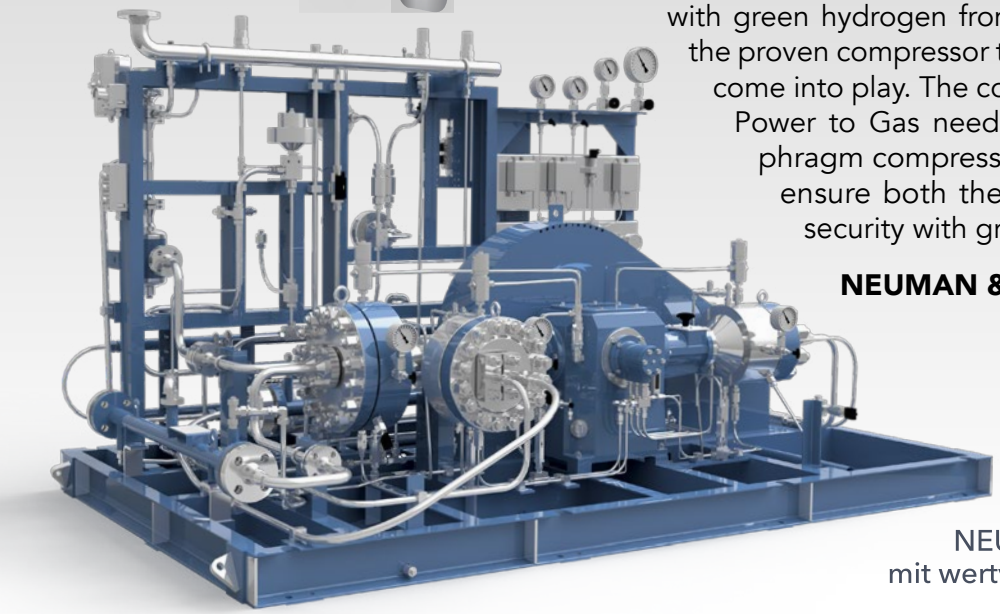

Lesen Sie den
NEUMAN & ESSER Blog
mit wertvollen Informationen
neuman-esser.com

Accurate load limit determination of reciprocating compressor components

by:

Gerhard Knop, Dr. Klaus Hoff
Central Division of Technology
Neuman & Esser GmbH & Co. KG
Übach-Palenberg, Germany
gerhard.knop@neuman-esser.de, klaus.hoff@neuman-esser.de

12th EFRC CONFERENCE
August 24 – 26, 2021, Warsaw

Abstract:
If you compare old and modern reciprocating compressors, the main difference is their size. Considering an equivalent job (flow rate and pressure build-up), recent compressors are designed much smaller than their older counterparts were. This might imply that newer recips go closer to the limits and are therefore more susceptible to overloading. However, this is not the case. The explanation to this is in the accuracy of the strength evaluation methods, which have much improved. Today's compressors provide equalized load capacities of all main components whereas old compressors may have one component which is close to the limit, representing a bottle neck, and other components much oversized. The latter define the compressor size and mass.
This paper takes a closer look at the methods used for fatigue strength quantification. This discipline is quite special compared to other fields of technology, as it is entirely empirical. Everything needs to be found by testing or comparison to similar structures for which load limits are known. Moreover, it can be observed that the fatigue strength at the critical locations is mostly little and sometimes not at all related to the material strength properties. This is driven by heavy stress concentration and fretting fatigue effects. All this makes load limit definition quite a challenge.
The most successful approach is to set up a calculation model and apply it to the investigated design as well as to comparable existing designs for which the limits are known. The calculated local load quantities consisting of stress, stress gradients, slip and contact pressure can then be used in a comparative manner. This approach requires a big database of strength investigations. The bigger this collection is, the more accurate the load limits can be defined.

by: Gerhard Knop, Dr. Klaus Hoff – Neuman & Esser GmbH & Co. KG

1 Introduction

In compressor design, load limit evaluation is a central task of designers and requires good understanding of the methods used in this field.

Deviating from traditional ways of setting up introductions, this foreword just lists the main messages of this paper. These statements are discussed in more detail afterwards.

Statement I: 'Modern reciprocating compressors are much smaller than their older counterparts. Nevertheless, their safety in terms of overloading is higher.'

Statement II: 'If the effort invested for evaluating fatigue strength does not match the effort of the preceding Finite Element Analysis (FEA), the value of the entire work is to be questioned.'

Statement III: 'It can be observed that the fatigue strength *at the critical locations* is mostly little and sometimes not at all related to the selected steel grade.'

Statement IV: 'Fatigue strength can finally not be calculated but only tested.'

Statement V: 'Only by using a large data base of part strength information, proper strength evaluation can be carried out'.

2 Statement I

'Modern reciprocating compressors are much smaller than their older counterparts. Nevertheless, their safety in terms of overloading is higher.'

If you compare old and current compressor designs, you will find that the main difference is the size. Today, the same job (flow rate and pressure build-up) can be done with much smaller machines than decades ago, without loss of reliability. This dimensional reduction has been mainly achieved by using state of the art calculation possibilities like FEA to find local part-loads (stresses and other load parameters), but much more by a better understanding of the properties and effects which mainly define the compressor-part strength.

One of the most important tasks of compressor designers is the dimensioning of the parts. Only if the designer manages to balance the strength utilization of the main compressor components, he or she will end up with an appropriately small machine without compromising reliability. It seems that this job is done better than in the past because the reputation of reciprocating compressors, which is closely linked to the number of failures, has much improved [1].

The challenge is in the accuracy of global and local part load quantification and (even more challenging) the strength. High accuracy allows balancing the strength utilization of the compressor components resulting in adequately sized machines.

3 Statement II

'If the effort invested for evaluating fatigue strength does not match the effort of the preceding Finite Element Analysis (FEA), the value of the entire work is to be questioned.'

The process of part dimensioning starts with the quantification of global loads which include

- compression gas forces
- mass inertial forces
- gas inertial effects inside and outside the compression chambers
- uneven pressure distribution across the piston
- torsional crank shaft vibrations that feed back to the piston rod
- mechanical cylinder vibrations

These loads can be called 'global', 'external' or 'outer loads' as they are acting somewhere at the boundaries of the respective parts.

In a second step, these global loads are converted into local part-loads. Local loads could comprise

- Stress
- Stress gradients
- Strain
- Contact pressure
- oscillatory micro slippage of two contacting part faces
- fretting fatigue damage load parameters
- further load parameters

The conversion from global into local loads is usually carried out by applying Finite Element Analysis (FEA). These resulting local part-loads are finally to be compared to fatigue strength limits.

Note: For the purpose of fighting against widespread misunderstandings, it is once more emphasized at this point that FEA yields no strength but just local load magnitudes!

The third and last step evaluates the fatigue strength in order to compare with the local part loads. This task is described in the next statements, but it can be already said that it requires at least the same effort as the FEA simulation.

However, when reviewing publications, it seems to come rather as an exception than as a rule that this effort is actually taken. The FEA part is always carried out comprehensively and detailed whereas finding load *limits* often misses such a comprehensive approach and restricts on merely

by: Gerhard Knop, Dr. Klaus Hoff – Neuman & Esser GmbH & Co. KG

using material strength properties or in a somewhat better way derives part strength from the material strength considering surface roughness, mean stress and other effects. The following statements will show the insufficiencies of this approach *at the critical locations* of the compressor parts. Those locations require more attention.

Summarizing, there might be a discrepancy between the effort taken for load quantification and load limit quantification. However, one quantity cannot really live without the other. Equal accuracy is required for both.

4 Statement III [16]

'It can be observed that the fatigue strength *at the critical locations* is mostly little and sometimes not at all related to the selected steel grade.'

In order to understand the method of fatigue strength evaluation, the difference between material strength and part strength is to be explained.

Material fatigue strength:

'Material fatigue strength' refers to the fatigue strength figures which depend only on material properties. They have been gained by respective tests (load cycle tests) on uniaxial loaded, small, smooth-surface, notch-free, friction-free, specimens. All parameters that may have an effect on the fatigues strength except the material properties have been eliminated in these tests.

Part fatigue strength:

'Part fatigue strength' refers to the fatigue strength of the actual compressor part at the respective location, including all the influences that have been excluded in the material tests.

Note: This paper focuses on fatigue strength since experience and general understanding of this subject clearly show that for reciprocating compressor parts static strength is of almost no significance. When failures occur, they are always caused by fatigue and hardly by static overload.

Critical locations of compressor parts are usually affected by either fretting fatigue or stress concentration. Both effects create a fatigue part strength which is no longer proportional to the material fatigue strength. In extreme cases, the influence of the selected steel grade is negligible. Every material grade (low-grade steel and high-grade steel) provides about the same fatigue part strength.

4.1 Fretting fatigue

Experimental tests [2,3,4,5,6,7] show that the material strength can be significantly reduced by micro slip of two contacting faces. This issue occurs with every assembled compressor part and cannot be avoided in principle. Hence, it must be considered as the most important effect on fatigue and a good knowledge on this matter is required to establish accurate compressor-rod load limits.

The small end bore of the connecting rod is used as an example to describe fretting fatigue.

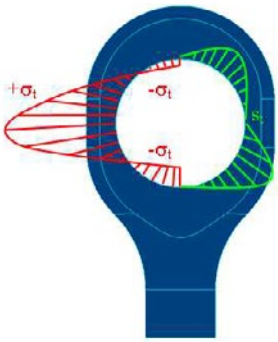

Fig. 1: Tangential bulk stress σ_t (red) and slip s (green) in a connecting rod bore [8]

The above figure shows tangential slip between the bushing and the connecting rod bore (in green color). Its magnitude depends on the location around the circumference. The amount of slip is one parameter out of several at the face-to-face contact that can enormously reduce fatigue strength, however in a different way than firstly expected.

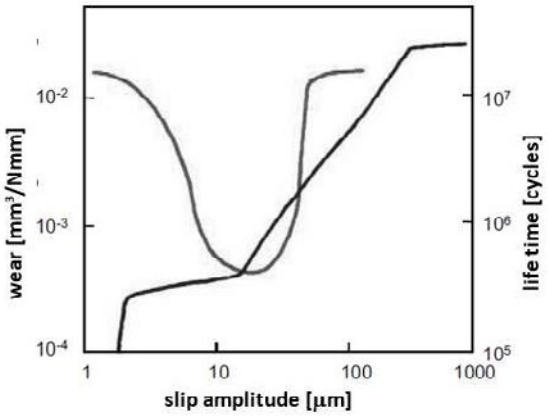

Fig. 2: Lifetime vs. slip (U-shaped curve) and wear of a surface exposed to fretting [2]. Note that the numbers given here are not general and give only a representation in quality.

It is interesting to find that not the locations subjected to large slip but those subjected to low slip provide the lowest fatigue strength (Fig. 2). This was already described by Vingsbo and Söderberg [2] in 1988 and confirmed by many others (e.g. [3]) later. The diagram gives rise to define two failure mechanisms:

Fretting fatigue: In the low-slip region, cracks would be initiated which can propagate if the tangential bulk stress level around the crack is high enough. These locations can typically be not noticed beforehand (e.g. by a regular inspection) as the small slip creates no visible surface damage or even corrosion.

by: Gerhard Knop, Dr. Klaus Hoff – Neuman & Esser GmbH & Co. KG

Fretting wear: In the high slip region, a surface damage and corrosion can be observed. Continuous large slip would create material loss of the contacting faces. Experiments yielded however no crack propagation or fractures. This is interpreted in a way that any newly initiated crack is worn away at the presence of the large slip.

From both observations it can be concluded that obvious surface 'damages' are not critical in terms of fatigue and clean surfaces on the other hand are no proof that there is no danger of fatigue fracture. It must be however noted, that in real parts, normally both surface 'damages' are close together with a gradual transition.

Coming back to our assembly example, the small end connecting rod, no location around the bore provides enough slip to produce wear. Fretting wear is normally no issue with connecting rods. The critical zones in terms of fretting fatigue are near the areas of the highest bulk stress. Other regions may also produce initial cracks by fretting but these would stop propagating after a certain crack depth, when the crack tip is out of the range of the fretting influence (in terms of depth) and – at the same time – only low tangential bulk stress is present. For more details, refer to the work by Naumann and Knop [8]. The intention of this paper is just to give an idea about the amount of strength loss one typically has to expect with fretting.

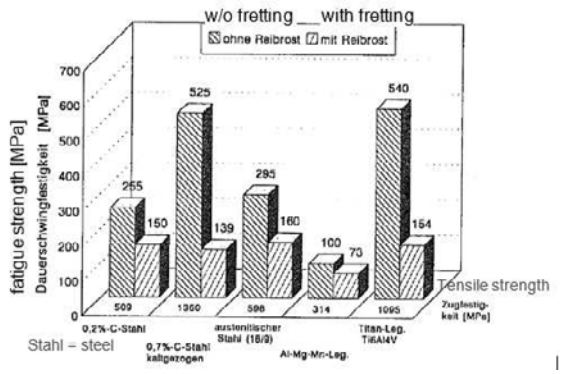

Fig. 3: Fatigue limits of different materials with and without fretting [7]

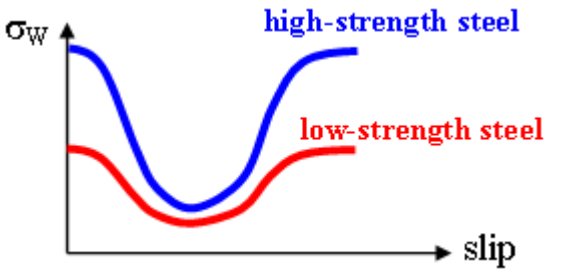

Fig. 4: Comparison of the Söderberg U-curve (Fig. 2) for different material grades [8]

Figures 3 and 4 give an impression about the loss in fatigue strength. It turns out that high-strength steels can lose strength by a factor of 2 or 3 (in cases, even much more), whereas low-strength steels lose only little strength. Exposed to fretting, both material groups approach about the same fatigue level!

The figures above clearly show the need to include the fretting fatigue aspect into the strength evaluation. The most well-known approach is probably the FFDP parameter (fretting fatigue damage parameter) or Ruiz criterion [4].

$$FFDP = \sigma_t \cdot \tau \cdot s$$

σ_t = tangential stress
τ = shear stress
s = slip

For a certain shear stress and FFDP, the Ruiz equation above yields the qualitative hyperbolic relation

$$\sigma_{t-admissible} = \sigma_W \sim \frac{1}{s}$$

(σ_W = fatigue strength in Fig. 4)

which is reflecting the decreasing branch of the curve in Fig. 2 and Fig. 4.

4.2 Stress concentration by geometrical notches

The next important design feature, which creates a possible weak location of compressor parts, is the notch (like a fillet or a radius). This section does not address the generally known aspect of stress concentration at which the local stress is increased compared to the nominal stress (force per area or moment per second moment of area), but the fatigue strength loss of different materials at such areas.

Considering approved approaches as given in [9], it turns out that in the presence of notches, high-strength metals loose much more strength than low-strength metals.

by: Gerhard Knop, Dr. Klaus Hoff – Neuman & Esser GmbH & Co. KG

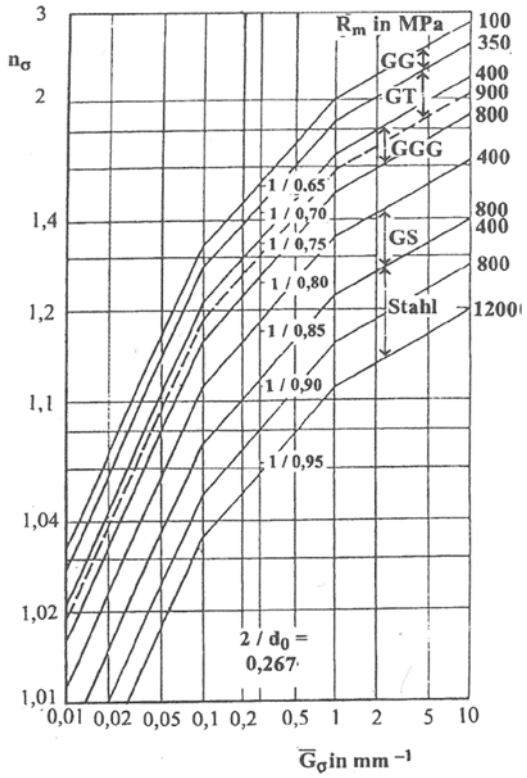

Fig. 5: Notch influence n_σ versus normalized stress gradient G_σ [9] 'Stahl' = 'steel', GG = grey cast iron, GGG = nodular cast iron, GS = cast steel

The symbols in figure 5 represent the following:
$n_\sigma = K_t / K_f$ High n_σ numbers mean low strength reduction by stress concentration
K_t = stress concentration factor = ratio local stress to nominal stress (only dependent on geometry and load kind) (could be a result of a FEA)
K_f = fatigue notch factor = ratio of unnotched fatigue strength to the fatigue strength of the notched part. (dependent on K_t, stress gradient and material)
G_σ = normalized stress gradient = $1/\sigma_a \cdot d\sigma_a/ds$
σ_a = stress amplitude on and along the surface
$d\sigma_a/ds$ = stress gradient normal to the surface
R_m = material tensile strength

Other parameters like surface roughness show a similar material dependence on fatigue strength:

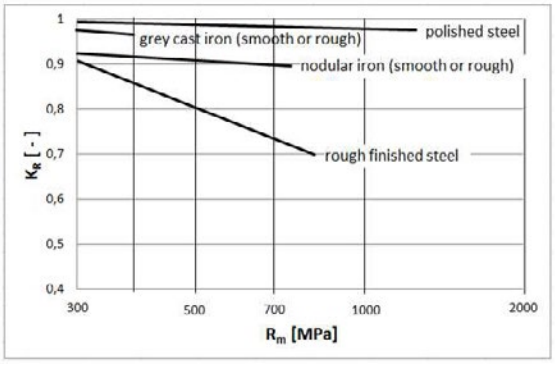

Fig. 6: Surface roughness influence; simplified illustration of [9, Fig. 4.3.4]

Symbols:

K_R = surface roughness factor ($K_R = 1 \rightarrow$ no influence, $K_R < 1 \rightarrow$ loss of strength)

R_m = material tensile strength

The above figure shows that
- high-strength steels are sensitive to rough surfaces, they only maintain their high material strength, if the surface is very smooth
- low-strength materials (as grey cast iron or nodular iron) are insensitive to rough surfaces, their fatigue strength is low anyway and will not go significantly further down with increasing roughness

There is a further aspect to be looked at in this context: The surface roughness only creates a significant effect at notch free locations. This non-proportional relation can be represented by the following equation [9]:

$$K_{WK} \sim \frac{1}{n_\sigma} \cdot \left(1 + \frac{1}{\widetilde{K}_f} \cdot \left(\frac{1}{K_R} - 1\right)\right) \cdot \ldots$$

(Parameters as in Fig. 5 and 6)

High K_{WK} means much loss of material strength

Low K_{WK} means little loss of material strength

The equation looks a bit confusing at first glance but finally means the following:

If no notch is present ($K_f = 1$), the surface roughness factor K_R is fully effective.

If the notch is very sharp (K_f = large), the surface roughness factor K_R has no influence.

As a summary it can be said that, same as with fretting, the part strength of notched locations is much less dependent on the material than assumed by just looking at the pure material strength numbers.

4.3 A special load situation – High mean stress, low amplitude

A special load situation is present at all threaded connections. Due to the high stress concentration, often combined with high preload, it is normal that the local stress levels exceed the elastic limit. The material is yielding at the thread teeth. This is mostly the case and nothing to worry about. Its implication is that this precludes the use of the "classical" stress-based fatigue strength evaluation methods.

Instead, strain-based approaches can be used as described in [11], [13], [14] and other publications.

by: Gerhard Knop, Dr. Klaus Hoff – Neuman & Esser GmbH & Co. KG

The interesting and attractive feature of such strain-based approaches in highly notched areas is that the part strength seems to be the same as the material strength, independent of any other effect like surface roughness or part dimension. It must be noted however that this material strength is not reflected by the well-known stress-based quantities like ultimate tensile strength or yield strength. Instead, other strength parameters are used like the SWT-parameter (Smith-Watson-Topper):

$$P_{SWT} = \sqrt{\sigma_o \cdot \varepsilon_a \cdot E} \quad \text{using} \quad \sigma_o = \sigma_m + \sigma_a$$

$$\text{and } \varepsilon_a = \frac{\sigma_a}{E} + \left(\frac{\sigma_a}{K'}\right)^{\frac{1}{n'}}$$

σ = stress, ε = strain

Indexes: o = maximum, m = mean, a = amplitude

E, K', n' = parameters of the Ramberg-Osgood relation, K', n' describing plasticity behavior, E = Young's modulus

Other common methods are the Brown-Miller and Findley approaches with or without the strain component as described in [12]. The motivation to erase the strain component in these approaches is driven by the circumstance that parts, which survive very high cycle fatigue, are usually loaded in the elastic range.

For preloaded threads this can be however different (as with bolts). These threads are loaded beyond the elastic range and require respective approaches.

A good approach for such applications should also cover the empirical finding that the fatigue strength of highly preloaded, sharply notched parts (like bolts) is almost independent of the steel grade used. High-strength steel bolts show the same fatigue limits as low-strength steel bolts. This is experimentally verified in many publications like VDI 2230 [15].

When considering simple bolts one can also come back to the nominal stress approaches since there is probably no other machine part so extensively and comprehensively tested like the bolt. VDI 2230 gives the following expression.

$$\sigma_{ASV} = 0{,}85 \cdot \left(\frac{150}{d} + 45\right)$$

σ_{ASV} = allowable bolt fatigue nominal stress amplitude in MPa

d = bolt diameter in mm

The fatigue strength depends only on the bolt diameter, not on the material!

Frithjof Marten [11] could show that the empirical VDI 2230 equation, when made dimensionless, almost perfectly reflects the reciprocal of the fatigue notch factor, obtained by FEA and applying the notch influence factor of Fig. 5. It shows the same strength decline with diameter due to increasing stress concentration and decreasing stress gradients (refer to Fig. 7). This finding once more gives a strong indication of the independence of the mean stress and of most material strength numbers on the bolt fatigue strength.

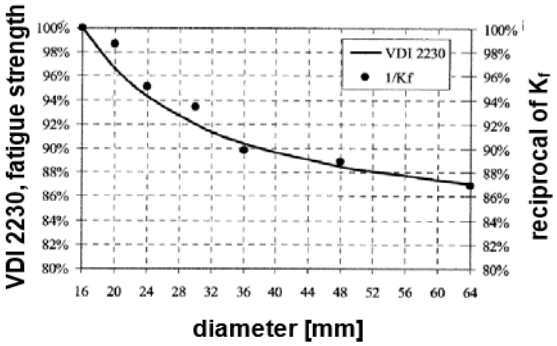

Fig. 7: Correlation of fatigue strength and reciprocal of fatigue notch factor K_f [11, p. 74-76]

To summarize: The fatigue strength of bolts and other threaded parts is almost not dependent on the material characteristic of the steel grade used.

4.4 Conclusion on Material vs. Part Strength

Looking once more at the effects described in the previous sections, it can be noticed that whenever deviations from the ideal conditions at material cycle tests (uniaxial load, smooth and un-notched geometry, small dimension, no contact forces) are present for real compressor parts (which is always the case at the critical locations), the fatigue load capacity of high-strength steel is much more reduced than with low-strength steel.

It looks like especially with contacting part faces of assemblies or geometrical notches, the fatigue part-strength seems to approach the same low level, with only little or even no dependence on the steel grade.

The significance of material strength is often much overrated.

by: Gerhard Knop, Dr. Klaus Hoff – Neuman & Esser GmbH & Co. KG

5 Statement IV

'Fatigue strength can finally not be calculated but only tested.'

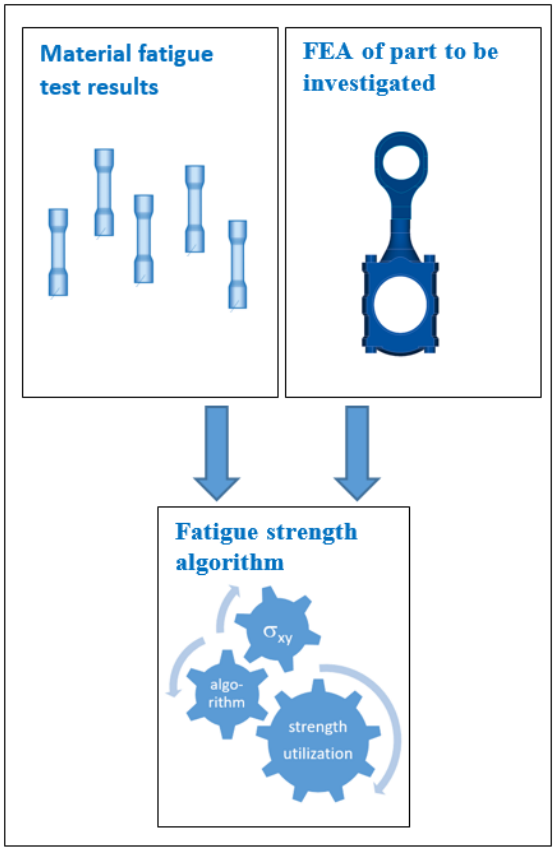

Fig. 8 Strength evaluation by comparing to strength numbers derived from material strength

Fig. 8 illustrated the method of deriving fatigue strength utilization from empirical material strength numbers. A FEA of the part to be investigated is run and the resulting local load (stress etc.), together with the material strength properties is used in an algorithm that considers further empirically quantified effects like those of mean stress, stress gradients and surface roughness to get the strength utilization.

The previous statement however shows how much the part fatigue strength can deviate from the material fatigue strength. At sharp notches or contacting surfaces, only a very week connection of both remains. That makes the derivation of the part fatigue strength from material strength properties inaccurate or even impossible.

So, how to resolve the issue?

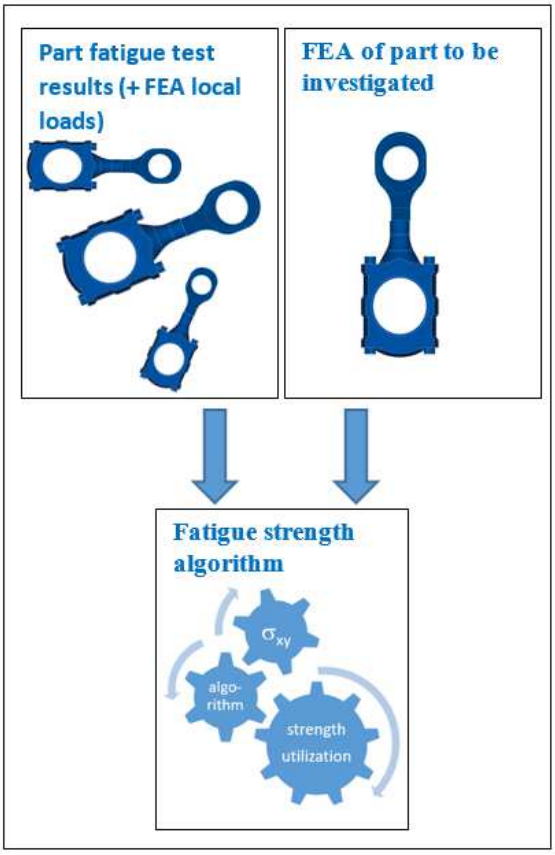

Fig. 9 Strength evaluation by comparing the strength utilization of the part to be investigated with those of equivalent parts of which field experience is given.

The much more superior method derives fatigue strength numbers from equivalent parts rather than from material strength numbers.

Same as for the material fatigue strength numbers, tests are required. Material load cycle test results can be easily found in literature and standards and there is no need to repeat those tests. But test results of individual parts are hardly available in literature (apart from some common machine elements like e.g. bolts). Therefore, there is no other way than carrying out one's own tests. These could be load cycle tests of the respective part in a laboratory or (more common) using the experience of long running compressors for which the load levels are known.

Fig. 9 illustrates the method. A FEA case study of a set of parts of the same kind is carried out that produces the local loads at the respective locations. These parts can deviate to some extent in terms of geometry and other properties. The same FEA is done for the part to be investigated.

The remaining deviations of all parts (tested parts and part to be investigated) require some calculation algorithm. Such algorithm is individually set up for the respective part location and includes all relevant loads (stress, stress gradients, contact pressures, contact slippage …) and strength weakening effects (mean stress, size …). Important is that all these

by: Gerhard Knop, Dr. Klaus Hoff – Neuman & Esser GmbH & Co. KG

quantities should deviate not too much between the parts of the comparison.

Both methods described (Fig. 8 and Fig. 9) finally compare fatigue strength test results of a set of specimens with the results of a strength calculation algorithm for the given local load coming from FEA. The main difference is, the compared parts in the method described in Fig. 9 are very similar, whereas the comparison in the method described in Fig. 8 is done with very unlike parts (material test specimen vs. real part). This dissimilarity makes the difference in terms of accuracy.

Coming back to the statement, there is actually a certain amount of calculation required but in total the greatest share of the task is in empirics. Without these empirics, no proper strength evaluation could be carried out. The next statement builds on this fact.

6 Statement V

'Only by using a large data base of part strength information, proper strength evaluation can be carried out'.

Taking the conclusions of the last statement, it is obvious that only the availability of many test results (laboratory tests and/or field experience) allows good strength evaluation. Usually there are not many laboratory tests carried out and the main source of information are long running existing compressors (field experiences). From those however, there are not many that actually experienced failures (negative test results) but survived their operation time without fatigue issues (positive test results).

The negative-test-result cases need to be selected carefully because fractures could also be caused by out of spec operation. Negative-test-result cases can only be used after a comprehensive root cause analysis which proves the global load to be as expected and not amplified for example by liquid hammers.

Positive-test-result cases represent the great majority of test cases. Of those compressors however, only few have been operated near their strength limits. The success of comparing to compressors with positive-test-results is finally based on quantity. If hundreds of cases are given the highest loaded ones can be selected for the strength investigation.

There are also locations on compressor parts that have never seen a fracture (a negative test result) but they can still be used to define load limits. Then the load limit might be much on the safe side (or perhaps not – you do not know), but if this respective location of the part does not cause over-dimensioning the compressor, it can be accepted. Typically, such compressor-part locations do not belong to the critical bottle-neck locations.

In summary, it can be concluded that the success of obtaining load limits from field experience is based on the quantity of given cases. It applies: 'One test is no test'.

7 Conclusion

It could be shown, that for the critical compressor part locations, the load capacity can be best derived from real parts. This way is much superior to methods that are based on material strength properties, because fatigue strength *of the critical locations* is only secondarily related to material strength numbers.

Since strength can finally not be calculated but only tested, the most accurate way is to make use of a collection of given strength levels of existing compressors.

Precondition of a successful and accurate load limit definition is a sufficiently large data base of such field experience.

References

[1] EFRC R&D project on Compressor Reliability Survey, 2010

[2] Vingsbo, Söderberg: On fretting maps. Wear, 1988, 126 (2), 131-147.

[3] Rabb, Hautala, Lehtovaara, Fretting Fatigue in Diesel Engineering, Paper No. 76, CIMAC Congress 2007, Vienna

[4] Merrit, Zhu, The Prediction of Connecting Rod Fretting and Fretting Initiated Fatigue Fractures, SAE International 2004

[5] Madge, Leen, McColl, Shipway, Contact-evolution based prediction of fretting fatigue life: Effect of slip amplitude, Wear 262 (2007) 1159-1170

[6] Forschungsvereinigung Verbrennungskraftmaschinen FVV,
-Auslegungsrichtlinie Reibkorrosion,Heft 984 -2013
-Reibkorrosion, Heft 1097 -2016
-Reibkorrosion/fretting Corrosion III, 1201|2020

[7] Issler, Ruoß, Häfele, Festigkeitslehre – Grundlagen, Springer Verlag 1997

[8] Naumann, Knop, A Review on the Methods of Load and Strength Evaluation of Connecting Rods, EFRC 2010, Florence

[9] FKM-Guideline, Analytical Strength Assessment, 6th edition 2012, VDMA Verlag

[10] Radaj, Vormwald, Ermüdungsfestigkeit, Springer 2007

[11] Frithjof Marten, Zur Ermüdungsfestigkeit hochfester großer Schrauben, Diss., Gottfried Wilhelm Leibniz Universität Hannover, 2009

by: Gerhard Knop, Dr. Klaus Hoff – Neuman & Esser GmbH & Co. KG

[12] Winkler, Holt, Vallance, Concerning the Synergy of Stress and Strain-based Methods in Modern Metal Fatigue Analysis

[13] Traversari, Rossi, Faretra, Nonlinear multi-axial fatigue analysis of a threaded crosshead to piston rod connection of a reciprocating compressor using the Brown-Miller algorithm, EFRC 2012, Düsseldorf

[14] R. Schneider, Örtliche Bewertung der Schwingfestigkeit von Gewindeverbindungen, Diss., Technische Universität Darmstadt, 2011

[15] VDI 2230, Systematic calculation of highly stressed bolted joints, Part 1, 2014

[16] Knop, Hoff: A closer Look at Rod Load Definitions and Rod Load Limitations of Reciprocating Compressors, GMC Conference Oct 2015, Austin, Texas

EUROPEAN FORUM
for RECIPROCATING
COMPRESSORS

AVAILABILITY AND REBLIABILITY

- **Stay safe**
- **Keep running**
- **Get better**

Efficient solutions to lower emissions:

- Purge systems
- Control systems
- Lubrication systems
- Valves
- Check valves
- High performance piston
- Rings & packings
- Workshop repair
- Field Service

HOERBIGER

HOERBIGER

Maximizing run-time and predicting performance of compressor pistons

by:

Andreas Brandl, John Ladd, Cory Bulloch
HOERBIGER Service Inc.
12206 West Fairmont Pkwy
La Porte, TX 77571, USA
andreas.brandl@hoerbiger.com

12th EFRC CONFERENCE
August 24 – 26, 2021, Warsaw

Abstract:
Cylinder rings (piston rings and rider rings) are often cause for unplanned shut downs and subsequent high costs due to repair and potentially lost production. The piston ring leakage influences the main performance indicators of compressors such as reliability (high piston ring leakage increases the risk of rider bands activating), capacity (20% and higher capacity losses due to poor piston and ring design have been observed) and discharge temperature (in certain applications the discharge temperature can exceed API and alarm limits if piston ring leakage is excessive). A new design process has been developed to optimize reciprocating compressor pistons. During this process, the blow-by trend over time is calculated for a given application and the performance defining piston paramters, such as number of piston rings, piston ring location, piston ring design, piston to cylinder clearance, rider band width and rider band design, are optimized to yield the minimum blo-by for maxium rider band life. The first pistons that have been engineered using this process were installed 2015. This lecture presents the details of two installations and explains the changes from the existing to the new design, shows the result of the ring inspection and quantifies the wear rate and compares the measured wear and compressor operating parameters to the prediction of the model that was used during the design and engineering phase.

by: Andreas Brandl, John Ladd, Cory Bulloch – HOERBIGER Service Inc.

1 Introduction

The most critical components on reciprocating compressors with respect to reliability are compressor valves, cylinder rings and pistons and compressor packings. Cylinder rings are responsible for about 20% of all unplanned compressor outages (2nd most frequent cause after valve related problems). In an attempt to take cylinder rings off the list of most critical components and to make reciprocating compressors more reliable the problem of cylinder ring failures has been tackled within the last 5 years. A model has been developed that predicts piston performance[1]. The model indicates reliability weaknesses and allows for optimization of the piston design during the engineering and design phase. The core of this piston analysis is blow-by prediction for any given run-time and evaluation of the impact of a certain amount of blow-by on discharge temperatures, capacity losses and reliability of the piston assembly. The study[1] gives the details of the piston analysis, explains the mathematical model and gives some examples. It suggests that the model should be applied in the engineering and design phase for every critical application in order to minimize the risk of cylinder rings being the reliability bottle-neck due to an insufficient piston design.

The first case study explains the details of piston related run-time increase. It compares the temperature trends of a non-lubricated Ethylene recycle compressor with the results of the piston performance model. The second case study features the performance improvements on a lubricated Hydrogen recycle compressor in a refinery process. The MTBF (mean time before failure) bottle-neck was piston ring wear and ring breakages. Redesigned piston and rider rings have been inspected after a certain run time. The model assumptions are compared to measurements on the rings in order to validate the approach and optimize the model.

2 The piston performance model

In order to evaluate the impact of blow-by on compressor performance, the gas leakage path across the piston rings on a compressor piston has to be considered. Each piston ring is modelled as an orifice with a defined leakage area. The effective orifice area depends on piston-liner clearance, end gap width of the piston rings and ring style. If, for example, the radial wear of the piston rings is 1mm at a piston-liner clearance of 1mm, the effective orifice area for an straight cut ring with a discharge coefficient of 0.65 is 2π x 1mm x 1mm x 0.65 = 4.1mm^2. Due to the radial wear of the piston rings, the end gap opens over time (see Figure 1, Figure 2 and Figure 3) and the blow-by and subsequent compressor performance changes accordingly. Wear coefficients can be estimated based test rig results, or similar services or can be found from existing, worn piston rings and rider bands for the specific application. Under the assumption of identical wear coefficient on piston rings and rider bands, the piston can be optimized to yield the best performance (blow-by) for maximum life (rider band wear or rod drop). This leakage area increases as material wears off of the running face of the ring

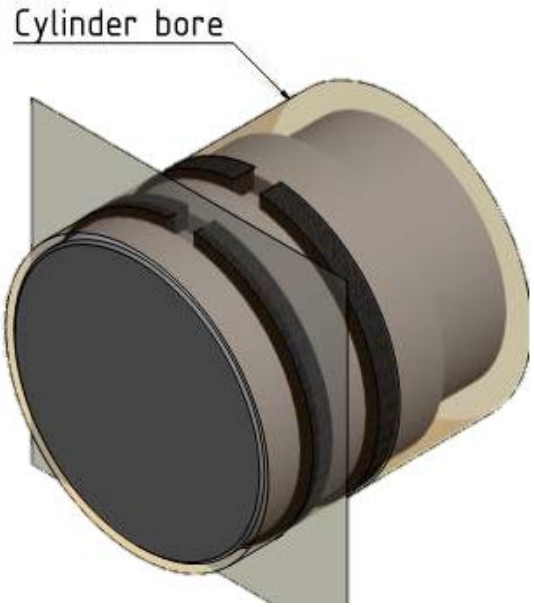

Figure 1: Piston ring in piston ring groove.

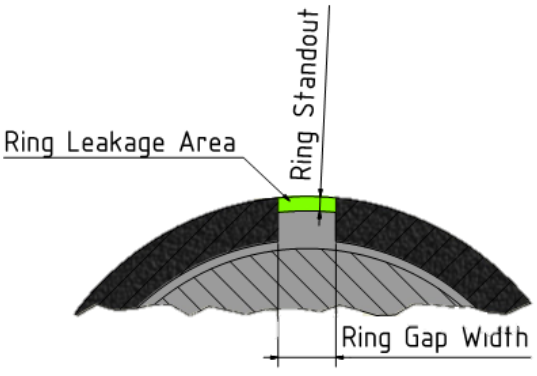

Figure 2: Leakage gap on a straight cut piston ring.

by: Andreas Brandl, John Ladd, Cory Bulloch – HOERBIGER Service Inc.

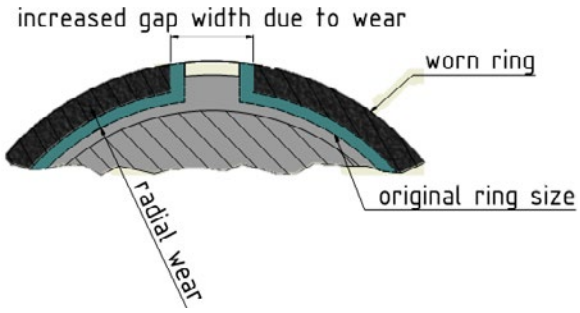

Figure 3: Worn piston ring.

The piston that is illustrated in Figure 4 has two angle cut rider rings with face and side relief grooves and four angle cut pressure balanced piston rings. Figure 5 and Table 1 show an illustration of corresponding model that is used to determine the piston ring leakage for given operating conditions.

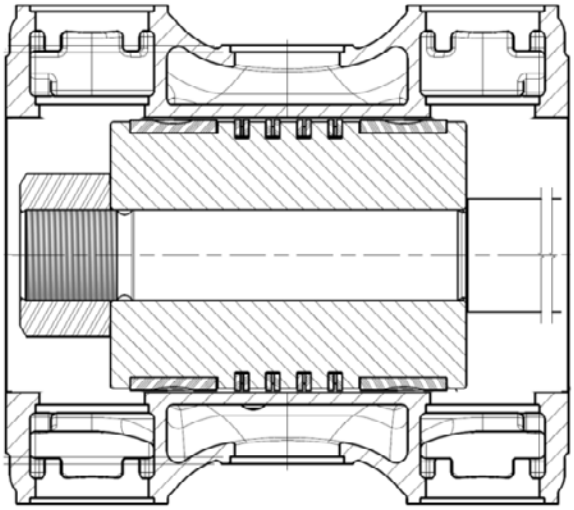

Figure 4: Piston with two rider bands and four pressure balanced piston rings.

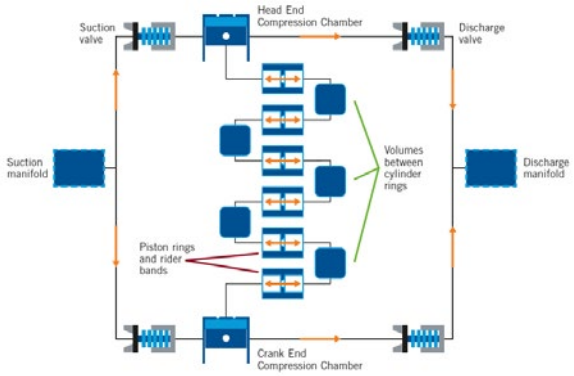

Figure 5: Corresponding piston performance model.

Table 1: Components in piston performance model.

	Ambiancee.g. Suction and discharge conditions
	Suction or discharge valve
	Compression chamber (HE or CE)
	Piston ring or rider ring
	Volume in between the piston rings

If, for example, the piston performance model predicts a rider band life of five years and corresponding blow-by capacity losses of 35% at a discharge temperature increase of 20°C, the piston is likely not optimized (35% blow-by losses and 20°C temperature increase is excessive in most applications). In such a case the piston-liner clearance can be reduced (resulting in a shorter rider band life and a recuction in blow-by) or a piston ring can be added by decreasing the rider band width. If, on the contrary, the estimated rider band life is two years and the corresponding blow-by 2%, the piston is not optimized either (Two year rider band life may not be enough and capacity losses of up to 10% may be acceptable). Increasing the piston-liner clearance or adding a rider band (at a reduced number of piston rings) will lead towards a more ideal design with respect to run-time and performance. For any given application with a certain maximum allowed capacity loss or temperature increase, the ideal piston can be found by applying the piston performance model and optimizing the performance defining parameters of the piston.

3 Case study: Non-Lubricated Ethylene Recycle Compressor

The recycle compressor in this case study is used in an Ethylene Oxide production plant. Low pressure Ethylene gas mixture (45% Ethylene, 23% Methane, 22% Carbon Dioxide and the rest Oxygen) is compressed in two stages from 14psig to 255psig. The compressor had to be shut down due to rider band wear every 4-6 months. Particle contamination

by: Andreas Brandl, John Ladd, Cory Bulloch – HOERBIGER Service Inc.

was one known factor that lead to accelerated wear on the cylinder rings. This study focuses on the two 2nd stage pistons. The relevant parameters of this compressor and the 2nd stage cylinders are given in Table 2. Both pistons have two outboard piston rings and two shrunk on rider bands in one common groove in the middle of the piston. Figure 6 and Figure 7 give an assembly drawing of the original and upgraded design respectively. Table 3 and Table 4 compare the performance relevant paramters of the two designs. The piston performance model indicated that piston wear and and subsequent blow-by was the bottle neck in this application. Increasing the number of piston rings by 50% with the use of pressure balanced rings while increasing the rider band width and increasing the piston-liner gap yielded the best run-time and performance results. Two upgraded pistons were installed in May 2018 with the intent of maximizing the run-time. After 18 months (13,000 hours and life-time increase of a factor of three) the two pistons were inspected and repaired.

Table 2: Relevant parameters of the Ethylene recycle compressor.

Compressor Parameter	Value
Cylinder Lubrication Type	Non-Lube
Speed [rpm]	440
Bore [in / mm]	10 / 254
Stroke [in / mm]	9 / 228.6
Avg. piston speed [ft/min / m/s]	659 / 3.35
Rod dia [in / mm]	2.5 / 63.5
Isentropic exponent [-]	1.25
Molecular mass [kg/mol]	25.8
Suction pressure [psig, barg]	65 / 4.48
Discharge pressure [psig, barg]	255 / 17.6
Liner Material	Grey cast iron

Figure 8 shows the broken piston rings found on the NE (north east) piston. Figure 9 is a picture of the cracked rider bands of the NE cylinder. Figure 10 shows the piston rings on the SW (south west) cylinder. The rings from that cylinder are heavily worn but mostly undamaged. One rider band from the SW piston is cracked as well (Figure 11) while the 2nd rider band of this cylinder is undamaged. Figure 12 shows that, as expected, the wear is similar on all piston rings and is on average 6.2mm radially.

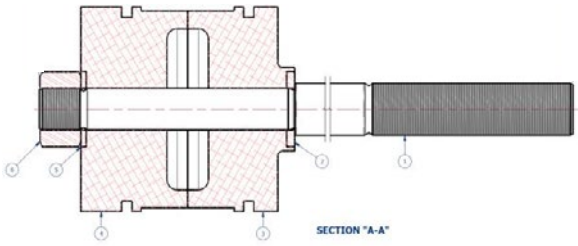

Figure 6: Original piston design.

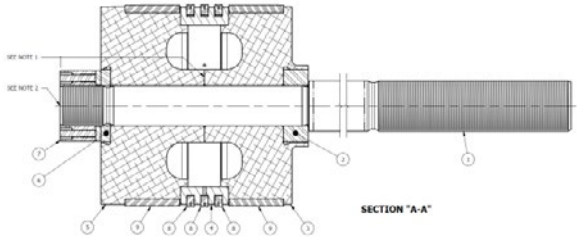

Figure 7: Upgraded piston design.

Table 3: Relevant parameters of the original piston.
[1)]Overtravel is the length of the rider band that travels beyond the recess of the cylinder or liner.

Relevant Piston Parameters	Initial
Piston OD [in / mm]	9.822 / 249.5
Piston – liner clearance [in / mm]	0.089 / 2.2
Rider ring width [in / mm]	2 x 2.25 / 57.15
Rider contact pressure [psi / bar]	3 / 0.21
Overtravel[1)] [in / mm / %]	0 / 0 / 0
Number of piston rings	2
Piston ring design	Angle cut
Rider band design	Shrunk-on

This wear results in a wear coefficient of 0.147 µm/(bar m/s hr). The wear coefficient is the ratio of the measured radial wear and the product of average piston speed, time and space averaged contact pressure of the ring and run time. The wear on the

by: Andreas Brandl, John Ladd, Cory Bulloch – HOERBIGER Service Inc.

rider bands is not as uniform. Figure 13 shows the wear measurements on the rider bands and reveals that the rider bands that are broken, show a much higher wear than the rider band that was undamaged.

Table 4: Relevant parameters of the upgraded piston.

Relevant Piston Parameters	Upgraded
Piston OD [in / mm]	9.8 / 248.9
Piston – liner clearance [in / mm]	0.1 / 2.54
Rider ring width [in / mm]	2 x 2.75 / 69.9
Rider contact pressure [psi / bar]	2.5 / 0.17
Overtravel [in / mm / %]	0.656 / 16.7 / 24
Number of piston rings	3
Piston ring design	Pressure balanced
Rider band design	Shrunk-on

Ring activation after breakage and the subsequent higher contact pressure and wear rate explains the heavier wear on the broken riders. The undamaged ring shows a uniform wear all around the circumference which indicates that the rider band rotated during operation. The wear rate of the rider bands is calculated from this single ring since it is the only rider band that has not seen additional contact loading due to gas pressure. At an average wear of 0.26mm on this unbroken ring the wear coefficient becomes 0.101 µm/(bar m/s hr) and is only 69% of the wear coefficient of the piston rings (see Table 5 for a comparison of contact pressure and wear coefficient on piston rings and rider bands). This indicates that the wear coefficient on the rider band is slightly lower than the wear coefficient on the piston rings which is in line with observations on other piston ring inspections not detailed in this paper. Figure 14 and Figure 15 show the rod drop on both cylinders. The rod drop on the cylinder with the undamaged rider (SW cylinder) is far lower than on the cylinder with the cracked riders. This is in line with the wear measurements on the rider bands. The rider band wear is very low in the beginning and then increases rapidly as the riders crack and start to get activated.

Table 5: Contact pressure, wear and wear coefficient of SW cylinder piston ring and uncracked rider band. The wear coefficient is calculated taking into account the pressure balancing groove of the piston ring and the fact that rider band rotated during operation.

Component	Piston Ring	Rider
Avg contact pressure [bar]	0.873	0.176
Avg. wear [mm]	6.1	0.26
Wear coeff. [µm/(bar m/s hr)	0.147	0.101

Figure 8: Broken piston rings on the NE (north east) cylinder.

Figure 9: Both solid, shrunk-on rider bands on the NE cylinder were cracked.

Figure 10: Piston rings on the SW (south west) cylinder came back heavily worn but mostly intact.

by: Andreas Brandl, John Ladd, Cory Bulloch – HOERBIGER Service Inc.

Figure 11: One rider band on the SW cylinder was cracked, the other one was worn but mostly undamaged.

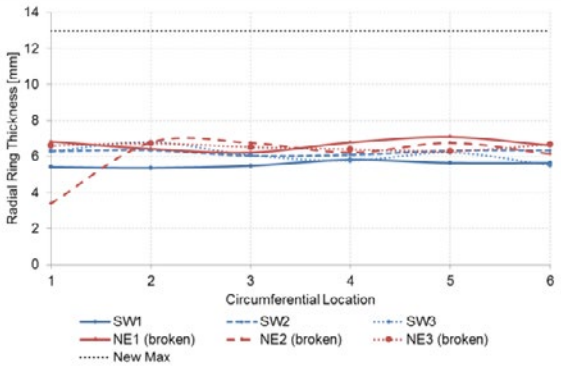

Figure 12: Radial wear on all six piston rings is comparable. Average wear is 6.2mm (wear coefficient of 0.147 µm/(bar m/s hr)).

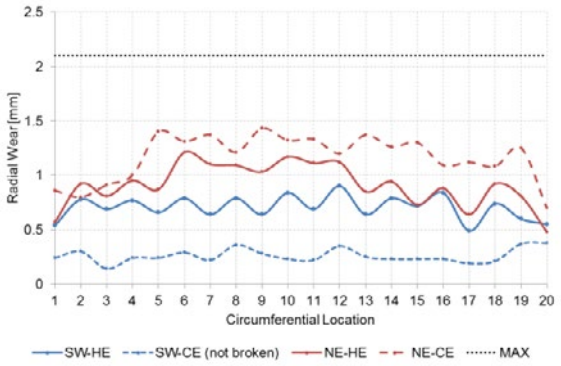

Figure 13: Rider band (middle of the ring) wear showing that the rider that was not broken had the lowest amount of wear indicating that the rest of the rider bands were activated once the crack developed.

The wear coefficient for piston rings that was developed from ring wear measurements, is applied to calculate capacity loss and discharge temperature increase. Figure 16 gives the expected capacity decrease from the piston performance model over time due to piston ring wear. For any given run-time shown on the secondary y-axis the expected effective piston ring flow area can be found. This effective flow area yields the expected capacity losses (primary y-axis) after the considered run-time. Figure 17 shows the expected discharge temperature over time due to blow-by. The discharge temperature starts at 129°C and rises steadily up to 145°C after 18 months (16°C temperature increase).

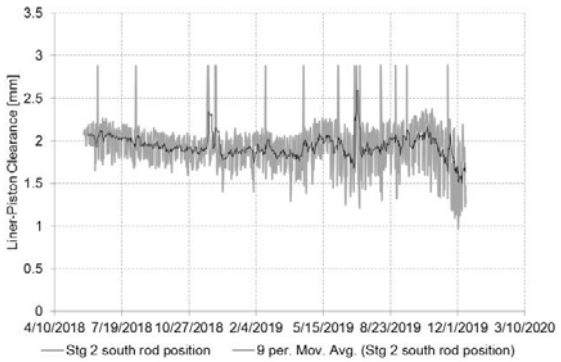

Figure 14: Piston to liner clearance on the SW cylinder.

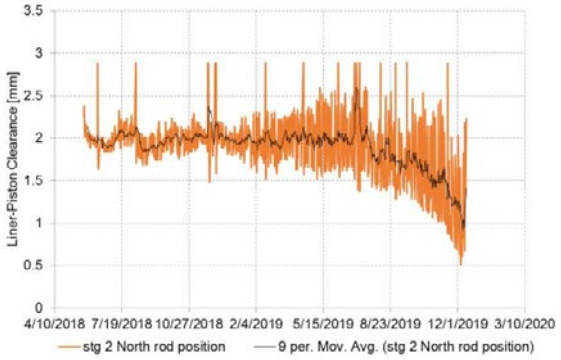

Figure 15: Piston to liner clearance on the NE cylinder.

The discharge gas measurement at the compressor shows a discharge temperature of 130°C right after start-up in May 2018 and 140°C before shutdown in December 2019 which corresponds to a temperature rise of 10°C (see Figure 18) It seems that the blow-by model overpredicts the temperature increase. A closer look at Figure 18 reveals though, that the suction temperature varies by about 5°C between summer and winter time. The compressor started in May 2018

by: Andreas Brandl, John Ladd, Cory Bulloch – HOERBIGER Service Inc.

(at a high suction temperature of 26°C) and was stopped in December 2019 (at a low suction temperature of 21°C). Taking the suction temperature trend into account the real discharge temperature increase is actually higher and results in a better match with the model (5°C suction higher suction temperature results in 7°C higher discharge temperature of 147°C). The suction pressure trend, Figure 19, shows some waviness but the values at start-up and shutdown are very similar. The discharge pressure trend is stable and hence no further temperature correction is required. This case study demonstrates that piston performance and the impacts on the operation of the compressor are well predictable. The wear coefficient on the rider band is slightly lower than on the piston ring which is in line with previous observations and can be taken into accout for future piston optimization projects.

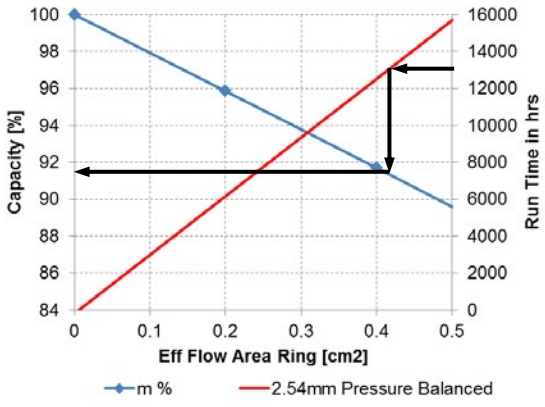

Figure 16: Capacity losses over time with a wear coefficient of 0.147 µm/(bar m/s hr).

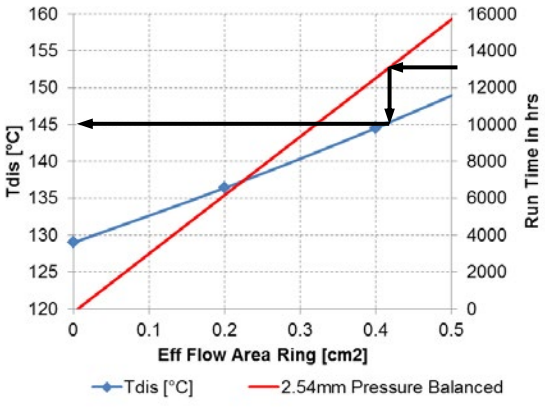

Figure 17: Discharge temperature over time with a wear coefficient of 0.147 µm/(bar m/s hr).

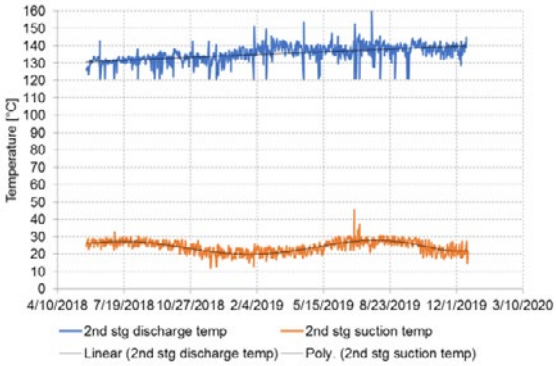

Figure 18: DCS data of suction temperature and discharge temperature. The suction temperature shows summer / winter variations. The discharge temperature shows a steady upward trend due to piston ring blow-by.

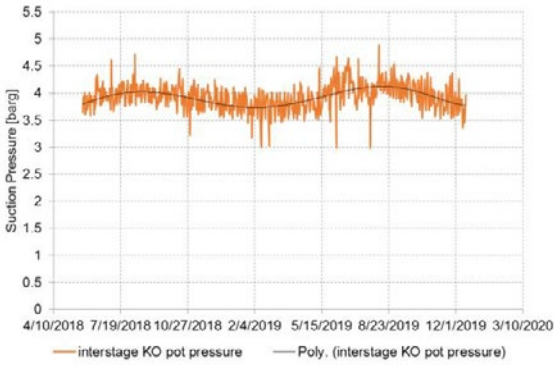

Figure 19: DCS data of the suction pressure trend. Suction pressure at start-up and shut-down are close to 3.7barg.

4 Case study: Lubricated ULSG Hydrogen Recycle Compressor

Recycle compressors are used in a variety of refinery application including catalytic reforming, hydrocracking and hydrotreating. The ULSG (ultra low sulfur gasoline) compressor is feeding hydrogen-rich recycle gas to the reactor, where suflur compounds from the feedstock are decomposed to form hydrocarbon and hydrogen sulfide amongst various other compounds. The reactor effluent flows through a series of gas-liquid separators and the separated and cleaned gas flows back to the recycle compressor. Recycle gas is often contaminated and sludge and viscous material tends to accumulate on various components such as valves (Figure 20) and

by: Andreas Brandl, John Ladd, Cory Bulloch – HOERBIGER Service Inc.

pistons (Figure 21), often making it a challenging application.

Figure 20: Sludge build up on the compressor valves on a USLG recycle compressor.

Table 6: Relevant paramters of the ULSG recycle compressor.

Compressor Parameter	Value
Cylinder Lubrication Type	Full Lube
Speed [rpm]	440
Bore [in / mm]	12.5 / 317.5
Stroke [in / mm]	10 / 254
Avg. piston speed [m/s / ft/min]	3.7 / 728
Rod dia [in / mm]	2 / 50.8
Isentropic exponent [-]	1.38
Molecular mass [kg/mol]	3.67
Suction pressure [psig, barg]	200 / 13.8
Discharge pressure [psig, barg]	311 / 21.4
Liner Material	Grey cast iron
Uninterrupted running length of the liner [in / mm]	14.5 / 368.3
Lube rate for two cylinders and two packings [pint/day]	4.5

Initial situation: The maximum run time of the compressor (see compressor data in Table 6) is 8 months due to cylinder ring related problems. The production unit is on a 5 year turnaround and the frequent outages due compressor related issues are costly as there is no stand-by compressor available. Usually the machine has to be brought down due to loss of capacity, but high discharge temperature has been the reason for shutdown as well. These operational problems are often accompanied by vibration, knocking and audible noise such as squeaking and rubbing. Figure 22 to Figure 25 show typical failure modes of the piston and its rings, including breakages and heavy wear. The black, viscous material on the rings contains iron suflide particles and is a contributor to this high wear situation.

Figure 21: Piston after removal from cylinder in March 2018: Piston rings show signs of heavy wear and are broken into pieces. One rider band is broken as well. Particles trapped in viscous material on the piston of a recycle compressor can act similar to a lapping compound.

Figure 22: Rider band showing signs of extrusion (which indicates heavy blow-by) and breakages.

In order to evaluate the piston design a piston performance analysis was performed, considering a constant wear coefficient on piston rings and rider bands. By the time the rider bands have worn away (1.64mm rider band stand-off), the expected radial wear on the piston rings is 7.35mm. At a radial thickness of 15.9mm this equals 46% of the radial thickness. Figure 25 and Figure 26 show the discharge temperature trend and capacity trend over time due to blow-by. The compression ratio in this

by: Andreas Brandl, John Ladd, Cory Bulloch – HOERBIGER Service Inc.

application is only 1.5 which means that the increase of the discharge temperature is not a big concern. The main problem reported from the field was capacity losses. Figure 26 shows that the expected capacity losses due to blow-by at the end of the rider band life is 8%. The radial wear on the piston rings at that point is 7.35mm.

Figure 23: Piston with a broken rider band.

Figure 24: Piston rings with reduced radial thickness after the run indicating a heavy wear situation.

The risk of ring breakages at that amount of wear is substantial due to the reduced radial thickness as well as the potentially high impacts of the rings due to the available space in the groove. It is suspected that the piston ring breakages (as seen in Figure 21) contribute to further capacity losses. The damages on the rider bands as seen in Figure 21, Figure 22 and Figure 23 can be attributed to installation related problems. The piston is a single piece and the solid rider band has to be stretched substantially while installing it over the long shoulder of the piston. Although the required stretch of 6.7% is within the limits of the material, the ring can be damaged depending on the method used to install the ring. The circumferential cracks in particular indicate installation related problems. In order to mitigate these issues (piston ring blow-by, ring breakages and rider band breakages) a piston re-design was suggested. The overtravel (travel of the rider band past the recess or the valve ports in the liner) on the original design is substantial and could not be increased any further.

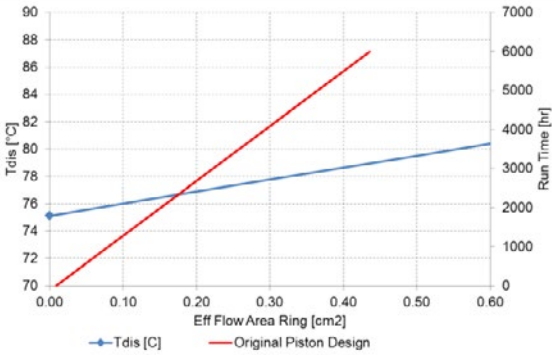

Figure 25: Temperature increase over time until the end of the rider life. Original piston design.

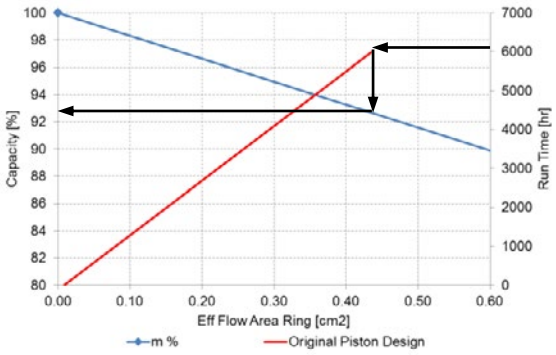

Figure 26: Capacity losses over time up to end of rider life with the original piston design.

Table 7: Relevant parameters of original piston.

Relevant Piston Parameters	Original design
Piston OD [in / mm]	12.34 / 313.4
Piston – liner clearance [in / mm]	0.08 / 2.0
Rider ring width [in / mm]	2 x 3 / 76.2
Rider contact pressure [psi / bar]	4.9 / 0.34

by: Andreas Brandl, John Ladd, Cory Bulloch – HOERBIGER Service Inc.

Overtravel [in / mm / %]	1.8 / 45.7 / 60.5
Number of piston rings	2
Piston ring design	Angle cut

The space on the piston is limited, so the number of piston rings could not be increased either. The piston ring was changed to a pressure balanced design and Figure 27 shows that a three piece piston was designed to facilitate rider band installation and mitigate the risk of rider band damage (see Figure 28 for a picture of the piston). Table 7 lists the relevant piston parameters of the initial design and Table 8 gives the data of the upgraded design. The upgraded pistons have been installed in two cylinders in March 2019. The machine was brought down after 10 months of run time due to a unit outage and the piston and piston rings were inspected and analyzed. Figure 29 shows the piston ring wear of the four piston rings (two pistons with two piston rings each).

Table 8: Relevant parameters of upgrade piston.

Relevant Piston Parameters	Upgraded design
Piston OD [in / mm]	12.359 / 313.9
Piston – liner clearance [in / mm]	0.70 / 1.78
Rider ring width [in / mm]	2 x 3 / 76.2
Rider contact pressure [psi / bar]	4.9 / 0.34
Overtravel [in / mm / %]	1.8 / 45.7 / 60.5
Number of piston rings	2
Piston ring design	Angle cut / pressure balanced

The average radial wear on the piston rings is 2.25mm which represents 37% of the available wear thickness of the pressure balancing groove Extrapolation yields a life time of 26 months whic represents a life-time increase of a factor of three The measured wear coefficient on the piston rings is thus 0.108 µm / (bar m/s hr). The rider band wear is shown in Figure 30 with an average wear of 0.27mm which results in a wear coefficient of 0.0291 µm/(bar m/s hr), see Table 9 for an overview of measured wear coefficients.

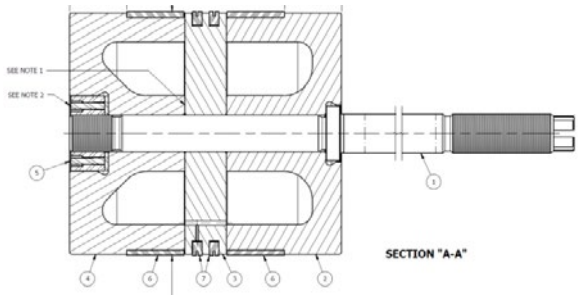

Figure 27: Assembly drawing of the optimized piston.

This indicates that the wear coefficient of the rider band is only 27% of the wear coefficient measured on the piston rings. One possible explanation is that the wear coefficient in lubricated appliations is lower at lower contact pressures. Hutchings[2] shows that the wear coefficient drops significantly as the oil film thickness increases.

Figure 28: Picture of the newly manufactured piston.

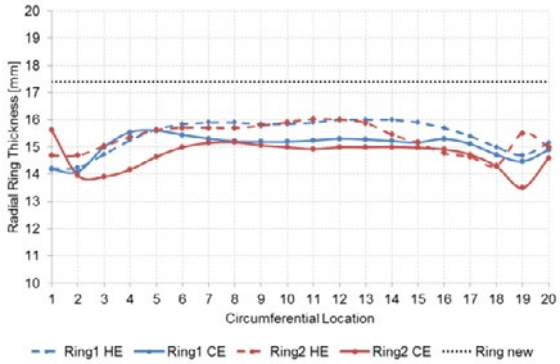

Figure 29: Radial ring thickness after 10 months of run-time with an average wear of 2.25mm resulting in a wear coefficient of 0.108 µm/(bar m/s hr).

by: Andreas Brandl, John Ladd, Cory Bulloch – HOERBIGER Service Inc.

Bayer[3] shows that lower contact pressures lead to higher oil film thicknesses which could explain the lower wear rate on the rider bands. One other potential reason for low wear coefficients on the rider band (compared to the piston rings) is the lubrication set-up on this cylinder with only one single lubrication port at the bottom of the cylinder. This means that the rider band, which takes the load of the piston at the bottom of the cylinder is well lubricated while the piston rings may not get a sufficient amount of oil on the top side of the cylinder leading to a higher wear.

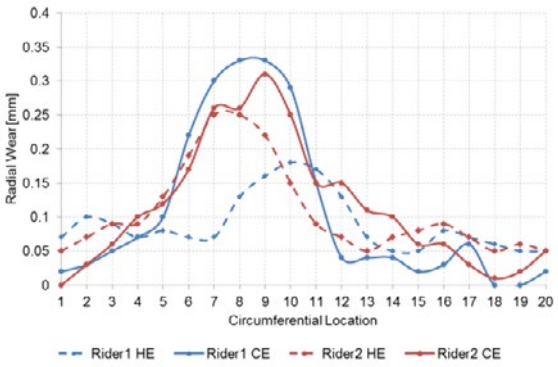

Figure 30: Radial wear of four inspected rider bands (two pistons with two rider bands each) with an average wear of 0.27mm and a resulting wear coefficient of 0.029 µm/(bar m/s hr)

Table 9: Contact pressure and wear coefficient of piston ring and rider band.

Component	Piston Ring	Rider
Avg. contact pressure [bar]	0.765	0.341
Avg. wear [mm]	2.25	0.27
Wear coefficient [µm/(bar m/s hr)	0.108	0.029

5 Conclusion

Blow-by calculation and piston performance prediction has evolved to a fundamental part of the piston design process. The piston parameters that are relevant for the reliability of the cylinder rings can be optimized and run-times can be extended by a factor of two or more in most cases when compared to an existing piston that had been designed using conventional methods without performance optimization. The DCS data and monitoring system data of a 1.5 year run on a non-lube application verifies the piston performance model and its performance prediction. The measured temperature trend matches the model results. The assumption of a similar wear coefficient on piston ring and rider band is not too far off in the case of a non-lube application (measured wear coefficient on rider band is 69% of the wear coefficient on the piston rings). The presented non-lube case and previous analyses suggest that the rider band wear coefficient is slightly lower than the piston ring wear coefficient. Maintaining the assumption of identical wear coefficients in the design phase provides some saftey margin against piston to liner contact. It is suggested to use the same wear coefficient on piston rings and rider bands for non-lube machines to avoid the risk of capital damage of the cylinder. The case study on the lubricated machine indicates that a lubrication port on the bottom of the cylinder leads to accelerated piston ring wear compared to the wear on the rider bands (The rider band wear coefficient is only 26% of the wear coefficient on the piston rings in this case). This case study also shows that the causes for ring breakages can be identified and mitigated. Piston ring breakages are often wear related and can be avoided by reducing wear rate or increasing the available wear thickness on the piston ring. Broken shrunk on rider bands are often caused by damaging the rider band during the installation. A multi-piece piston is a reliable way of eliminating the risk of installation related rider band damages.

References

[1] Brandl, A.; Ladd, J.; Hermonat, B.; 2018, “High reliability pistons for reciprocating compressors with validated performance modelling”, 47th Turbomachinery & 34th Pump Symposia, Houston, TX.

[2] Hutchings, I.M., 1992, “Tribology: Friction and wear of engineering matrials”, Edward Arnold, Great Britain, 273 pp.

[3] Bayer, R.G., 1994, “Mechanical Wear Prediction and Prevention”, Marcel Dekker, USA, 687 pp.

Fabrication of test bench for reciprocating compressors valve and choosing proper valve leakage testing procedure according to experimental results.

by:

Fouladivanda Mojtaba, Sadeghi Vahid, Momeni Omid
Engineering and Technical Departments
Iran Chemical Industries Investment Company
Esfahan, Iran
m.fouladivanda@iciiclab.com
mojtaba.f.vanda@gmail.com

12th EFRC CONFERENCE
August 24 – 26, 2021, Warsaw

Abstract:
In this experimental research, three different methods were investigated for a reciprocating compressor valve test. The first one is liquid testing. Second is measuring valve leakage by airflow quantity. The last method is the pressure drop method at a specific time. All of these procedures are used to measure leakage for different types of valves. The valves which investigated in this experiment are Low pressure- High flow valves, which usually are using for recycling compressors and High pressure- low flow, which generally is using for make-up compressors. These valves have different designs and internals. For valve leakage testing, a test bench was designed and fabricated. The measuring test circuit includes a pressure gauge, pressure regulator, flow meter, filling, and isolating valves.
For each type of valves, one new valve examined, and results are used as a reference. Results for different valves, including different pressure and flow, were measured and depicted in various plots and tables. In conclusion, the best method for each type of valves will be chosen and by choosing best repair and leaking test methods, reliability and efficiency of reciprocating compressors will increase, also by using these repair and test procedures, it will be possible to prevent operational problems and downtime of compressor related to valve failure which is the most common reason of compressors downtime.

by: Fouladivanda Mojtaba, Sadeghi Vahid, Momeni Omid – Iran Chemical Industries Investment Company

1. Introduction

Reciprocating compressors are the most widely used type of compressor found in industrial applications. It is a crucial machine in gas transmission pipelines, petrochemical plants, and refineries, due to a high-pressure ratio achievement. One of the critical components of reciprocating compressors is self-acting valves, which have a profound impact on the reciprocating compressors' efficiency. The most demanded attributes for these valves include perfect sealing when closed, rapid opening, sustained high flow area when open, fast, timely closing, tolerable impact with no bounce, tolerance to the maximum temperature, and low flow resistance of entire flow path[1].

Several experimental and theoretical studies have done, which shows a direct correlation of efficiency and compressor's valves. When a valve begins to exhibit signs of leakage, compressor efficiency will decrease. Gartmann[2] stated that the ideal compression cycle of a reciprocating compressor is affected directly by valve losses, which lower the adiabatic efficiency of the machine. In an experimental study, Noall and Couch[3] investigated six different compressor valves from five manufacturers and indicated that reciprocating compressor's efficiency is directly related to the performance of suction and discharge valves. Furthermore, they found that the suction valve's losses were approximately twice as high as the discharge valve losses. Foreman[4] in his research stated that companies' most concerning issue for reciprocating compressors is valve reliability because primary maintenance and operational expenditure of reciprocating compressors are valve repairs and associated unscheduled downtime.

According to Leonard's[5] studies, 36% of the cases where the compressor needs to be shut down, and 50% of total repair costs are related to the valve faults. Bialek and Bielawski[6] established a study on hydrogen reciprocating compressors fault analysis based on post-repair documentation of compressors maintained according to their service life, and using technical diagnostics applied to 21 compressors, covering the last 20 years. They estimated failure risk by the "R" indicator is based on the number of failures, material cost factor, repair work cost factor, cost factor arising from wear margin loss, and cost factor arising from difficulties in identifying a failure. Failure risk calculation in this research shows that suction and discharge valves failures are the most concerning failure, among other failure causes.

One compressor's valve manufacturer[7] , divided valve failures into two significant categories, environmental and mechanical. Environmental causes are those elements in the valve environment that can lead to valve failures, such as corrosive contaminants, foreign material, liquid slugs, or improper lubrication. Mechanical causes are valve failures that result from high cycle fatigue and abnormal mechanical motion of the valve, caused by high valve lift, valve operation at off-design conditions, valve flutter, pulsations, or spring failure.

Gas leakage in the incomplete sealing of valves may considerably affect the volumetric and isentropic efficiencies of compressors. It has been observed that leakage can significantly reduce the efficiency of compressors. The effect of gas leakage on the compressor efficiency shown in this paper is significant enough to justify a more detailed analysis of the phenomenon with the inclusion of other aspects, such as slip flow regime, surface finishing, and valve misalignment[8]. Chaykosky[9] stated that when the operating conditions significantly deviate from the ideal case, the valve design reliability is not necessarily ensured. Also, he indicated that the most common cause of plate or spring failure is valve operation at off-design conditions. In designing a valve to work reliably without failure, a range of operating conditions is assumed. The design, however, is optimized for a single set of operating pressures, temperatures, speed, cylinder clearance, gas molecular weight, lubrication rate, and pulsation level.

According to Soedel studies[10] , the excessive impact stress of the compressor valve plate against the lift limiter and the valve seat is one of the main reasons for the valve failure. The impact of stress is related to the valve impact velocity. Wang Yu et al.[11] established calculations to understand maximum impact speed for various lift values. These study results indicate that the maximum impact speed has a direct relation with the valve lift. Thus, they suggested that the lift should not be designed very large, and if the requirement of allowable stress could be satisfied, the valve plate should be as thin as possible. A significant lift may result in a flutter. The reason was that hydrogen is the small molecular weight gas with a high sound speed, and it is susceptible to flow areas. A big lift may contribute to high impact speed, large inclined angle, and flutter, all of which would bring along excessive impact stress and finally lead to valve failure. Moreover, they showed that when inclined motion happened, the maximum inclined angle would grow almost linearly as the lift increased, which would increase the impact stress.

Pan et al.[12] established a mathematical model to calculate the inclined motion of a plate valve and analyzed the influence of the inclined motion on the reliability of the plate valve. Besides, the solid particle, deposited on the surfaces of the valve seat and the lift limiter, could cause the stress

by: Fouladivanda Mojtaba, Sadeghi Vahid, Momeni Omid – Iran Chemical Industries Investment Company

concentration when the valve plate impacted against them and increase the impact stress.

In other technical reports[13], one of the valve manufacturers declared that valve losses for a typical (1 to 4 MW) reciprocating compressors operating in refineries are about 3 to 10 percent. So we can conclude that by improving valve internals and sealing, it is possible to improve efficiency and energy saving for reciprocating compressors.

All the researches as mentioned above, and experimental tests have shown that the most critical component of reciprocating compressors are suction and discharge valves that proper operation of these valves guarantee the efficiency of compressors, on the other hands, these valves malfunction can impose unscheduled downtime and lead to loss of profits of companies. Also, these works mentioned several problems related to the valves which have a profound impact on the life of these crucial reciprocating compressors components. Today's competitive economy forces companies for continuous production and more capacity, so every second count and is so important. Continuous monitoring is the key to managing valve health in reciprocating compressors. By continuously monitoring the vibration and temperatures on the valve cover, a rate of degradation can be established, allowing the maintenance engineers to predict the ideal time to schedule a valve replacement. Regardless of the compressor operation point, valves utilize internal springs with fixed stiffness and dampening to control the motion of the valve elements.

Two types of reciprocating compressors are using in some petrochemical industries: Make-up compressors and recycle compressors with a variety of working pressure and delivery gas flow. These differences in operation point need different valve designs. Besides, choosing proper repair and test procedures for the compressor's valves is crucial. In this experimental research, three different test procedures were investigated and examined to select the best way for a valve test. Then some pilot test rig was built, and after reviewing test results and importance of test procedure, one particular test bench was fabricated for all valves. Also, the best repair procedure for these valves was chosen. Furthermore, for monitoring the proper valve operation, periodic vibration, and temperature measurement on the valve cover performed.

2. Self- acting valve elements

For a better understanding of this study, it is necessary to know the main elements of self- acting valves. These main components are:

- Seat: the main body of the valve, which withstands the differential pressure of the stage when the valve is closed; it also distributes the gas flow to the shutters.
- Shutter: This component can have various shapes (ring, plate, poppet), and in addition to withstanding the differential pressure of stage, it must ensure the gas seal.
- Counter seat: This part of the valve limits the lift of the shutters. It also contains the springs.
- Springs: This element acts on the shutter, determining valve closing

Cyclic mechanical and thermal loads which cause fatigue wear, excessive cylinder lubrication, contamination from upstream, lack of sufficient filtration, condenses existence in stages are the most common cause of valves failure. These failures are shutter breakage, spring breakage, seat hammering- in and distortion, seat breakage, etc.

Grinding or machining distorted elements, replacement of worn or broken parts are the most common and recommended procedures for restoring valves. After the restoration of valves, to ensure the correct sealing, these valves should have subjected to a suitable leakage test. While the compressor is in service and shutter sealing face and seat not sealed sufficiently at the close position of the valve, part of compressed gas will backflow through valves, and it can cause recirculation of hot gas into the compressor's stage, and it will cause the rise in temperature. It will lead to increase the wear rate of compressor internals and finally compressor shut-down. So choosing a proper leakage test method has tremendous importance. To be ensured of valve health, the best test method should apply to gain the best result from compressor operation and minimizing energy loss and down-time.

In the next section, governing equations for the leaking valve and three different test methods for valves will be explained. After that, various valves with different designs have been tested, so the pros and cons of these procedures will be investigated.

3. Equations for leaking valve

The continuity equation for the compressor stage as a control volume expresses as[14]:

$$\dot{m} = \dot{m}_s + \dot{m}_d + \dot{m}_{leak\text{-}s} + \dot{m}_{leak\text{-}d} + \dot{m}_{leak\text{-}PR}, \quad (1)$$

Where $\dot{m}$ is the mass flow and s, d, leak-s, leak-d, leak-PR suffix are representing suction valve, discharge valve, suction valve leakage, discharge valve leakage, and piston ring leakage, respectively.

The mass flow rate through a leaking valve can be simulated as the flow taking place across an orifice having an area equal to leaking area that this flow depends upon the leaking area and pressure difference across the valve:

by: Fouladivanda Mojtaba, Sadeghi Vahid, Momeni Omid – Iran Chemical Industries Investment Company

$\dot{m}$= Cd. A_o. $\sqrt{\frac{2\rho.\Delta P}{1-\beta^4}}$, (2)

where Cd denotes the discharge valve coefficient, ρ is gas density, β is the square root of the ratio of orifice area to the inlet area of the valve, $\sqrt{Ao/Ai}$, ΔP denotes pressure difference across the orifice.

A_o, Leaking area across the valve plate can be express as[15]:

A_o= πDb y_{max} X/100, (3)

Where the term πDb y_{max} is the area of flow if the healthy valve would have been fully open, and X denotes the amount of leakage in terms of the maximum area of flow through a healthy valve. By replacing "ye" as the equivalent valve lift with $_{max}$ X/100 which the valve is assumed to remain open throughout the cycle resulting in the area of orifice equal to the leaking area and eq. (3) will be express as:

A_o= πDb ye, (4)

If the discharge valve leak, the leaking area of the valve can be expressed as:

A_o= π Db_d y_{maxd} Xd/100

= πDb $_d$ ye_d, IF $y_d(t) \leq ye_d$, (5)

And

A_o= πDb $_d$ $y_d(t)$, If $y_d(t) > ye_d$, (6)

Db is equivalent diameter, y is valve lift, y_{max} maximum valve lift, and t represents time.

4. Leakage test procedures

4.1 Liquid test

One of the traditional ways for checking the sealing of ring-type and plate-type valves, which mostly preferred for metal ring valves, is executing the liquid test. This simple test shall be carried out by filling the valve seat with a liquid having a low specific weight.[16] Light viscosity fluids like Kerosene and Varsol should be employed in this leakage test procedure. Two minutes after filling, the amount of liquid still being in the seat must be at least equal to half the initial amount of liquid. The advantage of this procedure is that is easy and simple. Still, the fluid will exert preload to the sealing element toward its opening lift, and it can lead to faulty test especially for the valves which use non-metallic sealing parts, which require less spring stiffness.

4.2 Leaked flow measurement

In this test procedure, leaked airflow through the closed valve subjecting to a set air pressure will be measured utilizing flow meter[17]. This test method is so accurate because it can simulate the compressor stage conditions and accurately shows the amount of leaked air through the closed valve and has none of the previous method limits. Figure.1 shows the schematic of this test method[17].

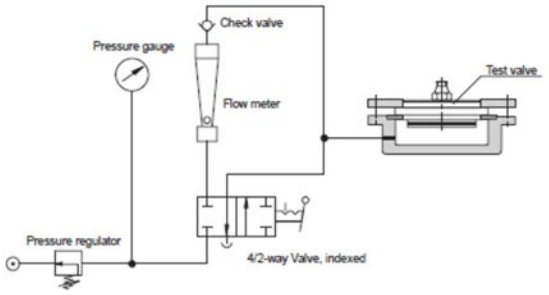

Figure.1. Schematic of the leaked flow measurement method.

4.3 Pressure drop measurement

In this method, the valve will be mounted in the test rig and subjected to specific air pressure. At the same time, the volume of test rig vessel filled with air, pressure drop will be measured. The acceptable time for pressure drop will be chosen according to the parameters such as the volume of the vessel, valve size, and specified test pressure.

This test is more preferred to the liquid test because it simulates the compressor stage condition, and it is more reliable. Still, for every valve size and every valve type, the parameter as mentioned above, test conditions will be changed.

5. Test results

In this experimental research, for different types of valves, three above mentioned test methods applied. These valves types are using for two different types of Hydrogen service compressors:

- Low Pressure, High Flow recycle compressor. (type 1)
- High Pressure, Low flow Make-up compressor. (type 2)

Table1. Valve details.

Compressor type	Differential pressure	Diameter	Valve lift
Type 1	1,03 bar	215 mm	1.5 mm
Type 2	17,24 bar	95 mm	1.8 mm

As mentioned in the table.1, make-up compressors have more differential pressure across the valve in comparison to recycle compressors. In the first step, all the valves were disassembled, and every component of the valve checked accurately. All the seat faces cleaned and visually inspected, springs height compared to the new one. If the sign of hammering- in or other distortion on the sealing face of seat observed, first it should be restored by finish- grinding, hand lapping, or machining.

by: Fouladivanda Mojtaba, Sadeghi Vahid, Momeni Omid – Iran Chemical Industries Investment Company

All the valves were liquid tested by using kerosene according to the procedure mentioned above. All the valves passed this test successfully.

In the next step, to ensure liquid test results for repaired valves, for each type of valves, as figure 2 shows, one pilot test rig manufactured by using two flanges and welded up two caps at two sides of flanges, so one test enclosure built up. Then inside of this enclosure machined to the size of the valve. For sealing of the valve inside the enclosure, two O-rings were used. Two mentioned valves subjected to the stage pressure, then supply has been shut-off. The results were impressive. Valve "type 1" pressure drop rate was slight while for valve "type 2" showed different results, and pressure suddenly dropped to zero.

Figure 2: Pilot Test Bench for each type of valves.

These results showed that valve type 2 has no proper sealing in the closed position and is not repaired well enough to be prepared to mount on the cylinder. This problem will show itself when the operator wants to pressurize the cylinder, but the valve leakage will drop the stage pressure, and the compressor start-up will be impossible.
To know the accurate value of leaked air through valve "type 1", the leaked air measured employing flowmeter. The results of the test for the suction and discharge valve of type 1 are shown in figure 3. To understand the allowable leakage values, a new valve is tested too. Results indicate that, in this kind of valves, new and repaired valves show the same values. This will ensure that this valve is ready to operate well.
In continue, for approaching to better sealing in the valve type 2, the seat has been machined on a center lathe with very low feed, and the plates were lapped using 1200 emery paper on the flat surface like glass carefully, then after assembly, this valve subjected to the different air pressure from 0.5 bar to 20 bar using the pilot test bench and results shown in figure 4. This range for the test was chosen according to the operating pressure of the valve.

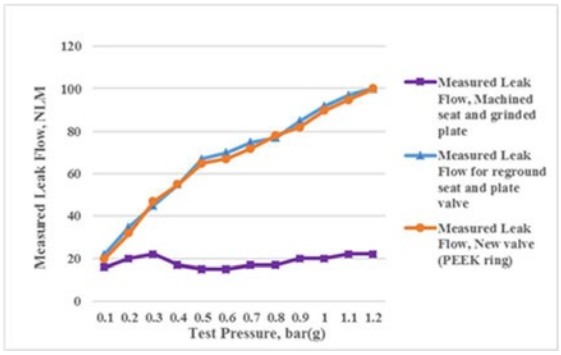

(a)

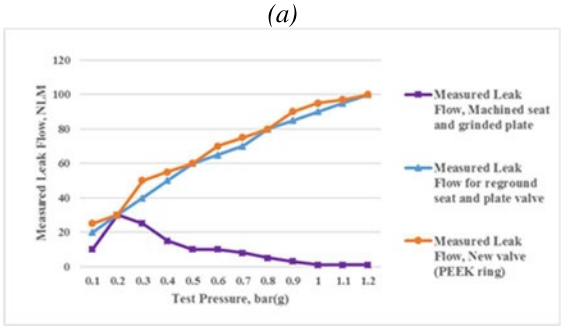

(b)

Figure 3: Test results for (a) Suction valve, (b) Discharge Valve (Low Pressure- High Flow Recycle Compressor), ΔP= 1,03 bar

As results reveal, by this secondary repairs, measuring the leaked flow was possible because of better sealing for valve type 2. To have a reference for this test, two new valves manufactured by two different valve manufacturers tested at different test pressures. These results also are shown in figure 4 and table2.

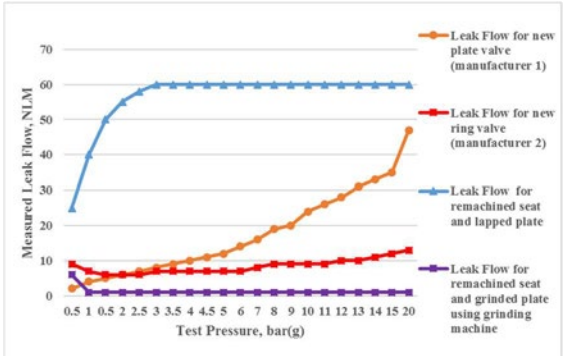

Figure 4:Test results For Discharge Valve (High Pressure- Low Flow Make-up Compressor) ΔP=17,24 bar.

by: Fouladivanda Mojtaba, Sadeghi Vahid, Momeni Omid – Iran Chemical Industries Investment Company

Table 2: Test results For discharge valve (high pressure- low flow make-up compressor) ΔP=17,24 bar.

Test Pressure, bar(g)	Leak Flow for new plate valve (manufacturer 1), NLM	Leak Flow for new ring valve (manufacturer 2), NLM	Leak Flow for remachined seat and lapped plate, NLM	Leak Flow for remachined seat and grinded plate using grinding machine, NLM
0.5	2	9	25	6
1	4	7	40	1
0.5	5	6	50	1
2	6	6	55	1
2.5	7	6	58	1
3	8	7	60	1
3.5	9	7	60	1
4	10	7	60	1
4.5	11	7	60	1
5	12	7	60	1
6	14	7	60	1
7	16	8	60	1
8	19	9	60	1
9	20	9	60	1
10	24	9	60	1
11	26	9	60	1
12	28	10	60	1
13	31	10	60	1
14	33	11	60	1
15	35	12	60	1
20	47	13	60	1

These results indicate that from 0.5 to 3 bar test pressure, two new valves are shown the nearly same amount of leakage through the closed valve, seven normal liters per minute. After that point, the new valve from the second manufacturer shows the increasing trend to 47 NLM. For this repaired valve, flow leakage measurements for the pressures test more than 3 bar, indicate that this value is 60 NLM constantly, six times more than the results for valve manufacturer 2.

To get to the best results, machining using a surface grinding machine have done on the seat of the valve (figure 5). All the machining has to be done in the allowable range to prevent an increase in valve lift. An increase in valve lift will cause valve failure or, in the worst condition, will lead to valve breakage. After grinding of sealing surfaces and ensuring the flatness of the sealing parts, these valves were reassembled. Also, all the springs replaced even if visually did not show any defect.

After restoration, valve type 2 subjected to the different test pressures from 0.5 to 20 bar, and surprisingly, results showed that after the test pressure point of 0.5 bar, which shows 6 NLM, other results showed 1 NLM leakage. These test results indicate that valve sealing is perfect and is better in comparison to the new valves. This valve shows approximately 60 NLM less leakage in comparison to the previously repaired valve.

In pursuance of best results for valves type 1, these valves disassembled again and seat and plates of these two valves, suction and discharge valve, using surface grinding machine finished. All springs replaced, and these valves reassembled. These valves tested using the 3rd test method again. These results illustrated in figure 3 and table 3.

As predicted, results were impressive. Less leakage in comparison to new valves for both repaired valves. It is necessary to mention that new tested valves are PEEK material ring-type valve while repaired valves are plate type valves which need more preload to seal well; however, results indicate that it is possible to get better sealing from plate type valves by better sealing surface finishing. By testing various valve types, we can choose the proper testing method according to each valve type results.

Table 3: Test results for (a) suction valve, (b) discharge valve (low pressure- high flow recycle compressor), ΔP=1,03 bar.

(a)

Test Pressure, bar(g)	Measured Leak Flow, New valve (PEEK ring), NLM	Measured Leak Flow for reground seat and plate valve, NLM	Measured Leak Flow, Machined seat and grinded plate, NLM
0.1	20	22	16
0.2	32	35	20
0.3	47	45	22
0.4	55	55	17
0.5	65	67	15
0.6	67	70	15
0.7	72	75	17
0.8	78	77	17
0.9	82	85	20
1	90	92	20
1.1	95	97	22
1.2	100	100	22

(b)

Test Pressure, bar(g)	Measured Leak Flow, New valve (PEEK ring), NLM	Measured Leak Flow for reground seat and plate valve, NLM	Measured Leak Flow, Machined seat and grinded plate, NLM
0.1	25	20	10
0.2	30	30	30
0.3	50	40	25
0.4	55	50	15
0.5	60	60	10
0.6	70	65	10
0.7	75	70	8
0.8	80	80	5
0.9	90	85	3
1	95	90	1
1.1	97	95	1
1.2	100	100	1

To fabricate a test bench for different valve sizes, one particular enclosure designed and machined as figure 6. This design suitable for different valve sizes, which mounted on compressors at the site plant.

It has been connected to air supply with a regulator to set the test pressure. This enclosure up and down parts will clamp together, and one flowmeter, which can measure the flow range of 0 to 100 NLM, will indicate the flow leak through the closed valve.

by: Fouladivanda Mojtaba, Sadeghi Vahid, Momeni Omid – Iran Chemical Industries Investment Company

Figure 5: Using a surface grinding machine to get better flatness for sealing elements

It is also possible to measure the pressure drop by shutting off air supply using a 4/2 way valve. This fabricated device has been connected to the control table, and conditions of the test will be quickly applied. (figure 1)

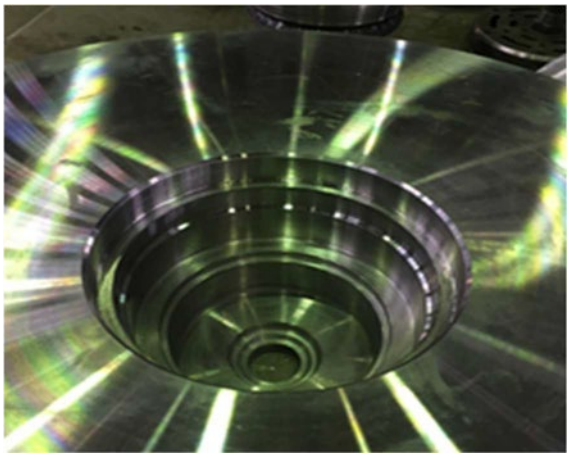

Figure 6: Particular test bench design

For more quality assurance and get a reliable valve, the valves mentioned above, were tested again by the pressure drop method. Figure 7 and 8 indicate pressure drop through time.
To better understand the characteristics of valves were undergone this test, a more extensive pressure range was chosen for high flow valves. Figures 7 and 8 illustrate that for both types of valves, machined seats and grinded rings were taken more time for a pressure drop to zero bar(g), which indicates less leakage. On the other hand, grounded seats and rings which not machined were taken less time for a pressure drop to zero bar(g), and it was leaked more than others. Two last test methods, pressure drop, and leaked flow measurement, indicated almost the same results, and by this means, can conclude that these two test methods, which simulate the conditions as they exist in a cylinder, are preferred to liquid test.

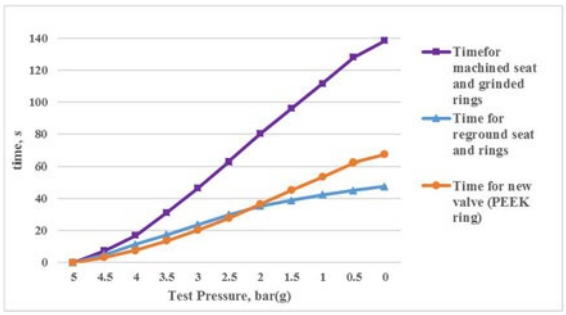

Figure 7: Pressure vs. time graph for discharge valve (low pressure- high flow recycle compressor), ΔP= 1,03 bar.

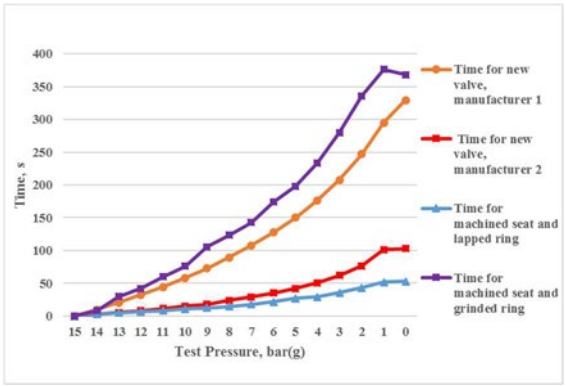

Figure 8: Pressure vs. time graph for the discharge valve (high pressure- low flow make-up compressor) ΔP=17,24 bar.

Table 4: Pressure drop test results for discharge valve (low pressure- high flow recycle compressor), ΔP=1,03 bar.

Test Pressure, bar(g)	New valve (PEEK ring), s	Reground seat and rings, s	Machined seat and grinded rings, s
5	0	0	0
4.5	3.31	5	7.5
4	7.61	11.45	17
3.5	13.71	17.45	31.3
3	20.3	23.75	46.5
2.5	27.78	29.85	63.1
2	36.68	35.35	80.4
1.5	45.33	38.95	96.2
1	53.71	42.35	111.85
0.5	62.33	45.15	128.3
0	67.43	47.59	138.6

by: Fouladivanda Mojtaba, Sadeghi Vahid, Momeni Omid – Iran Chemical Industries Investment Company

Table 5: Pressure drop test results for the discharge valve (high pressure- low flow make-up compressor) ΔP=17,24 bar.

Test Pressure , bar(g)	New valve manufacturer 1 (ring), s	New valve, manufacturer 2 (plate), s	Machined seat and lapped ring, s	Machined seat and grinded ring, s
15	0	0	0	0
14	9.75	2.64	3.12	8.03
13	20.57	5.39	4.71	29.83
12	32.24	8	6.56	42.15
11	44.36	11.3	8.25	59.58
10	58.47	14.95	10.65	75.9
9	72.8	17.8	12.73	105.78
8	89.45	23.61	14.67	123.54
7	107.5	29.11	18	142.45
6	127.41	34.85	21.71	173.79
5	150.44	42.05	27.17	198.34
4	176.66	50.92	29.04	233.87
3	207.93	61.77	35.52	279.75
2	247.07	76.69	43.15	335.65
1	295.14	101.47	51.85	376.35
0	329.2	102.77	52.95	368.21

6 Valve monitoring

One of the conditions monitoring ways to monitor reciprocating compressors' valves is vibration measurement on the valve cover. Vibration analysis and temperature measurement simultaneously are powerful tools to monitor valve health. To analyze the vibration, it is necessary to get data in the time domain and frequency domain (acceleration).

In this study, two valves mounted on two same compressors on the same stage monitored. Valve “A”, the valve which repaired and tested by the liquid test procedure, and passed this test. Valve “B”, the valve which repaired and tested by the leak flow measurement and has been shown the best results, above mentioned valve type 2, which test results have shown that sealing of this valve in the closed position is perfect.
Figure 9 indicates time signals, and figure 10 indicates frequency signals measured on the valve cover after 2000 hours of work time. These time signals, repeated every 0.1225 seconds, which shows that these valves have been cycled 8.16 times every second and 490 cycles per minute, which indicates compressor rotational speed. Time signals indicate that valve “A" has a bigger burst with more amplitude, and valve impacts for valve “A" are higher.

It means that higher vibration while this valve is trying to push the gas through. Figure 10, also confirms that frequencies amplitude for valve "A" is higher. Valve "A" has less 300 hours in comparison to valve "B". The repair procedure applied for valve "B" ensures the parallel collisions of the valve plate and the seat. So the valve plate has better motion.

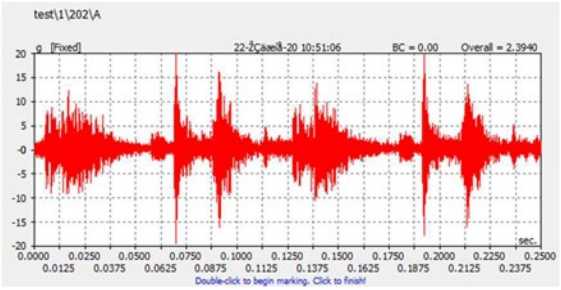

Valve A

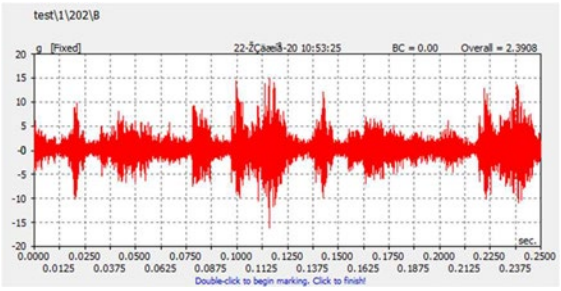

Valve B

Figure 9: Time-domain signals after 2300 hours of work time for valve A and 2000 hours of work time for valve B.

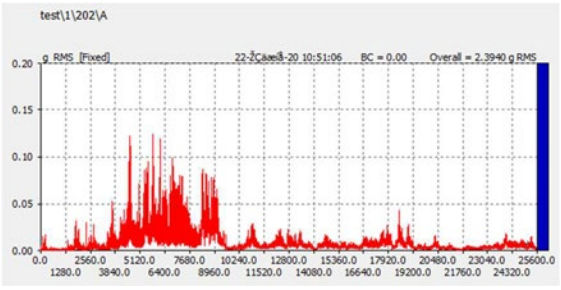

Valve A

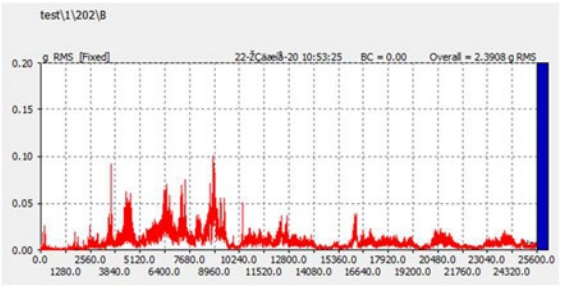

Valve B

Figure 10: Frequency signals after 2300 hours of work time for valve A and 2000 hours of work time for valve B.

Non-parallel impact of the plate or impact with higher speed causes higher amplitude in vibration, leading to lower valve lifetime and finally fracture. At non-parallel impact, large local peak values of the tangential tensions are generated because of the so-called Dynamic Stress Concentration Effect. This effect occurs when the propagation speed of

by: Fouladivanda Mojtaba, Sadeghi Vahid, Momeni Omid – Iran Chemical Industries Investment Company

the contact front equals the speed of the elasticity waves, which induces a robust increasing tension peak leading to radial cracks[18]. These results in a rocking motion with several rebounds because some kinetic energy recovery during a collision[19].

7 Conclusion

The main purpose of this study is to achieve the best procedures to repair and test the valves of the reciprocating compressor to flow efficient and reliable in service. In this research, reciprocating compressors valves failure causes and main elements investigated and then three different procedures for valve leakage testing introduced. At the next stage, a different type of valves has been undergone various repair procedures and test methods. For validating the results, test results of new valves used as a reference. Results indicate that for High-flow Low-pressure valves, reground of seat and lapping of plate surface without replacement of spring, which visually checked and had no problem can get the results the same as a new valve. Preferred test to get these results are liquid leakage testing. Also, it was shown that it is possible to improve the flatness of sealing parts by using the grinding machine. This repair procedure ensures parallel sealing surface and better valve sealing at the closed position and better plate motion.

On the other hand, it was concluded that using the liquid testing procedure is not reliable for High-pressure Low flow valves. The best test for this type of compressor is leaked flow measurement. To implement this test procedure, one test bench fabricated. Two different repair procedures applied for this type of valves:

- machining of the seat using center lathe and lapping of the valve rings.
- machining of seat and valve rings using grinding machine and replacement of springs.

The first procedure of valve repair gives approximately acceptable results, while the second repair method is preferred and gave the best test results even better than new valves. Second repair method may lead to some problems:

- It is such a time-consuming repair procedure and needs more human resources. Sometimes it can be the main problem for continuous processes that need compressors in service continuously, and there is limited time for compressor repair.
- This repair procedure can be applied to the sealing elements just for limited times because it will increase valve lift and can lead to severe problems for the valve and compressor.

The valves which restored according to the first repair procedure and tested by measurement of leaked flow or pressure drop time, are approximately suitable to mount on the compressor. But if company policies are the implementation of the best repair and test procedure to get more reliable and more efficient compressors, the best repair method is the machining of seat and valve plates using grinding machine and replacement of springs, and best test method is leaked flow measurement or pressure drop method for valves, which simulate cylinder condition. Besides, by measuring vibration on the valve cover, it was shown that these procedures give better valves in operation.

by: Fouladivanda Mojtaba, Sadeghi Vahid, Momeni Omid – Iran Chemical Industries Investment Company

References

[1] Deffenbaugh, D.M., Brun, K., Harris, R.E., Harrell, J.P., Mckee, R.J., Moore, J.J., Svedeman, S.J., Smalley, A.J., Broerman, E.B., Hart, R.A., Nored, M.G., Gernentz, R.S., & Siebenaler, S.P. (2005): Advanced Reciprocating Compression Technology (ARCT).

[2] Gartmann, H., (1970): De Laval Engineering Handbook, Compiled by the engineering staff of De Laval Turbine, Inc., McGraw-Hill Book Company, New York.

[3] Noall, M. and Couch, W., (2003): Performance and Endurance Tests of Six Mainline Compressor Valves in Natural Gas Compression Service, Gas Machinery Conference Paper.

[4] Foreman, S. (2002): Compressor valves and unloaders for reciprocating compressors-an OEM's perspective. Dresser-Rand Literature.

[5] Leonard, S. M. (1996): Increase reliability of reciprocating hydrogen compressors. Hydrocarbon Processing, 75, 67–74.

[6] Białek, P., and Bielawski, P. J. (2018): Failure analysis of refinery hydrogen reciprocating compressors. Diagnostyka, 19(1), 83-92.

[7] Hoerbiger Bulletin, HCA 8200-86: How and Why Compressor Valves Fail, Hoerbiger Corporation of America, Inc.

[8] Silva, Leandro R. and Deschamps, Cesar J., (2012): Modeling of Gas Leakage through Compressor Valves, International Compressor Engineering Conference.

[9] Chaykosky, S., (2002): Resolution of a Compressor Valve Failure: A Case Study, Dresser-Rand Literature.

[10] Soedel W.(1974): On dynamic stresses in compressor valve reeds or plates during co-linear impact on valve seats. In: Proceedings of the international compressor engineering conference, Purdue, USA.

[11] Wang Yu, X. Dianbo, F. Jianmei, P. Xueyuan, (2010): Research on sealing performance and self-acting valve reliability in high-pressure oil-free hydrogen compressors for hydrogen refueling stations, international journal of hydrogen energy 35, 8063 – 8070

[12] Pan SL, Lin M, Shu PC. (1995): A study of leaning motion of plate valves of reciprocating compressors. Chem Eng Machin China, 22, 272–6.

[13] Hoerbiger REE (Reliability, Efficient, Environmentally Sound) Audit Report for Iran Chemical Industries Investment Company. (ELAB) (2015): Esfahan, Iran.

[14] Guerra, Christopher, (2013): "Condition monitoring of reciprocating compressor valves using analytical and data-driven methodologies", Thesis. Rochester Institute of Technology.

[15] Manepatil, Smita S. and Tiwari, Ashesh, (2006): Fault Diagnosis of Reciprocating Compressor Using Pressure Pulsations. International Compressor Engineering Conference. Paper 1819.

[16] GEPS Oil& Gas, Nuovo Pignone manual for reciprocating compressors, 1st volume, 109-05-N00-0A.

[17] Practical Leakage Testing of Compressor Valves, Hoerbiger Ventil Werke GMBH.

[18] Böswirth, L., (2000): Strömung und Ventilplattenbewegung in Kolbenverdichterventilen, Eigenverlag, Vienna.

[19] Habing, R. (2005): Flow and plate motion in compressor valves.

BORSIG

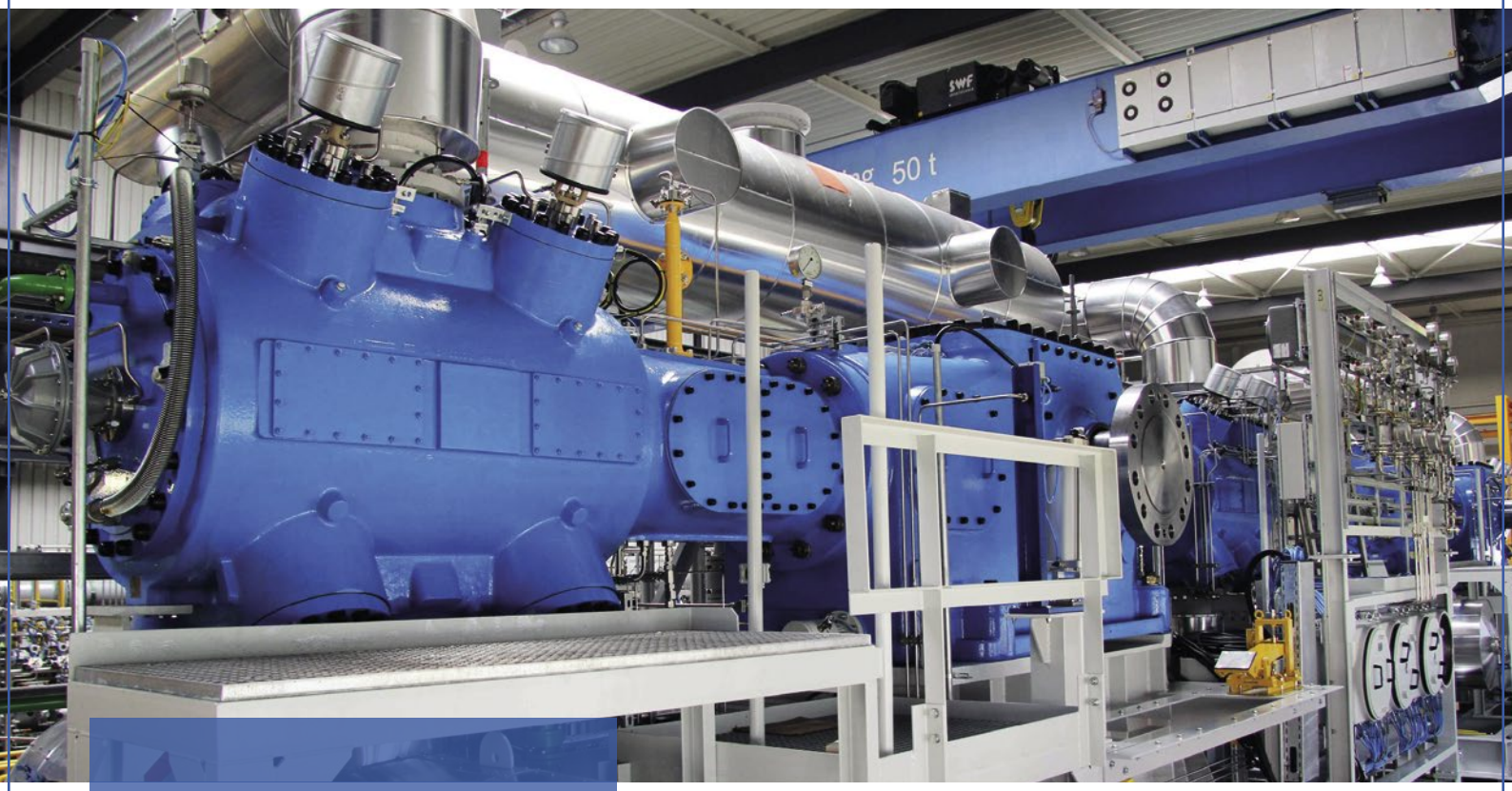

PROCESS GAS COMPRESSORS

API 618
Reciprocating Compressors

API 617 & 672
Integrally Geared Centrifugal Compressors

We, at BORSIG ZM Compression GmbH, design and manufacture tailored compressors for innovative process gas compression solutions.

BORSIG ZM Compression GmbH

↘ To learn more, please visit
www.borsig.de/zm

wood.

A Case Study on Modernising the Maintenance Management of Reciprocating Gas Compressors

by:

EUR ING **Kenneth Burns**, BEng MSc, CEng
Site Mechanical Technical Authority
Wood
Teesside, United Kingdom
Kenneth.burns@woodplc.com

Ramin Rahnama, MSc, PEng
Consultant Engineer
Wood
Glasgow, United Kingdom
ramin.rahnama@woodplc.com

12th EFRC CONFERENCE
August 24 – 26, 2021, Warsaw

Abstract:
Control and computing systems such as condition monitoring eventually become obsolete and unsupported. This is especially prevalent in aging assets. As spares and repairs become less available, the operations team will recognise the risk this poses to reliable operations. During an obsolescence project, it is easy to overlook the real design purpose of the obsolete system. Therefore, providing a replacement, modern equivalent without a full review of the systems intended design function can mean that a like-for-like swap may be impracticable, unsuitable, or impossible. Multi-discipline teams must review these systems and ensure a suitable solution is engineered and specified to remove the risk to reliable operations. Considering a replacement may need to incorporate change because of developing technology. The change brings a secondary benefit; new technology that can also help modernise the way the equipment is maintained. The benefits of a smarter maintenance approach will often have more significant gains than reducing the risk of plant failures. As most modern equipment provides masses of data, it is now more prevalent for users to understand and use that data in a sustainable, beneficial, and profitable way.
This paper details how the CATS gas terminal moved from a time-based maintenance strategy to a predictive maintenance strategy for reciprocating gas compressors. This change in strategy requires an educated leap from time-based maintenance through the learnings of condition-based maintenance to what is a predictive maintenance strategy.

by: Kenneth Burns, Ramin Rahnama – Wood

1 Introduction

The Central Area Transmission System (CATS) is a natural gas gathering, transportation & processing system located on the United Kingdom Continental Shelf (UKCS) spanning from the central North Sea to the North East of England. It is a critically important piece of utility infrastructure and in 2020 delivered over 9 billion cubic metres of gas to UK markets.

To process the gas, CATS uses fractionation to separate some of the heavier constituents and pump them separately to end-users in Teesside. The lightest components of the hydrocarbon liquids (Methane and Ethane) are removed from the stabiliser by a boiling process known as distillation. These components are still a considerable percentage of the incoming gas and are recovered for distribution into the National Transmission System. From distillation processing, the gas pressure is now lower than the export pressure and needs to be compressed for distribution. The CATS site has four type 1MW 2HE/1 reciprocating compressors. They are 17,000kg single stage, two throws, balanced-opposed piston machines capable of compressing gas from 24 Bar g to 77 Bar g. The machines have valve unloaders to allow 25%, 50%, 75% and 100% duty.

The compressors will typically receive 24 Bar g gas from the stabiliser consisting of 74% Methane, 19% Ethane, 3.5% Carbon Dioxide and 2.5% Propane. Gas will be compressed to the National Grid backpressure of between 55 to 70 Bar g and comingle with the other gas entering the National Transmission System.

2 Maintenance Strategies

2.1 Types of Maintenance

The following three types of maintenance are all preventative maintenance actions, mentioned throughout this paper. The following guidelines will help us understand the differences.

2.1.1 Time-based Maintenance

Time-Based Maintenance refers to replacing or renewing an item to restore its reliability at a fixed time, interval, or usage regardless of its condition. The purpose of Time-Based Maintenance is to protect systems against a failure assuming that it is age-related. The part may have had numerous similar failures and a predictable Mean Time Between Failure (MTBF). This maintenance objective is to intervene before it happens again.

2.1.2 Condition-based Maintenance

Most failure modes are not age-related. However, most failure modes do give some warning that they are in the process of occurring or are about to occur. If evidence can show that something is in the early stages of failure, it may be possible to take action to prevent it from failing and avoid the consequences of failure. Condition Based Maintenance (CBM) as a strategy looks for physical evidence that a failure is occurring or is about to occur. Condition monitoring systems can detect the early onset of common failure types and show an indication of potential failures. (Steinkamp, 2011). Thinking of CBM in this way shows its broader applications outside condition monitoring techniques often only associated with rotating equipment. (Hupjé, 2019)

2.1.3 Predictive Maintenance

Up until recently when people spoke about Predictive Maintenance, this was usually as a synonym for Condition Based Maintenance. However, with the advent of Artificial Intelligence, much lower costs of equipment sensors (Industrial Internet of Things) and machine learning there is a difference appearing between Predictive Maintenance and Condition Based Maintenance. (Hupjé, 2019)

CATS terminal used to engage a specialist contractor to visit the site and provide snapshot Pressure/Volume and Vibration Analysis studies on various machines, including reciprocating compressors. The contractor may have picked up early warning signs of failures and can be considered condition-based monitoring. A predictive maintenance scheme has similarities in sensor positions, but there is a difference in how it functions. The continuous logging of data and relying on precise formulas within the software to alert users to early onset of failures is the step change. The continuous self-assessment of data using artificial intelligent algorithms is another differentiator.

2.2 CATS Maintenance Strategy

The CATS compressors were commissioned in 1998 with a Bently Nevada 3300 condition monitoring system. This system is now obsolete and spares are unsupported leaving the safe and reliable operation of the CATS compressors at risk. The Bently Nevada 3300 is a basic system and compliant with earlier API 618 standards.

While utilising the Bently Nevada 3300 condition monitoring system, it was necessary to perform time-based preventative

by: Kenneth Burns, Ramin Rahnama – Wood

maintenance routines on the compressors. Without enough information from the Bently Nevada 3300 to understand the condition of parts within the machine, OEM scheduled maintenance and inspection activities were continuously being performed.

The site strategy for maintaining the compressor availability was to complete a minor service every four years, to inspect components which would indicate a major service is required but also replace wear components in the cylinders.

A minor service consists of a large quantity of long lead and expensive spares, scaffolding and lifting operations, specialist contractor support for both labour and the overhaul of large compressor components.

Historically CATS terminal has not observed major failures on its machinery from process excursions or fatigue of parts. Some failures were attributed to poor quality of spares overhaul. The terminal has followed OEM recommendations for time-based maintenance. This paper will explore options for moving away from time-based maintenance routines by collecting “big data” on the machines and utilising a predictive maintenance strategy.

The expected benefits from a predictive maintenance strategy, in comparison to time-based, are:

- Increased machine availability
- Reduced demand for site resources
- Reduced maintenance completion times (due to specific tasks)
- Reduced overall maintenance cost/machine upkeep
- Ability to accurately monitor machine condition

3 Procedure for Replacing an obsolete monitoring system

In order to replace an obsolete system with an updated one, the following steps were carried out:

1- Review of machine operating signatures and component failure modes

2- Selecting an up-to-date system that is suitable for the machine characteristics and user requirements

3- Update the maintenance strategy to reflect how the use of big data and algorithms can help manage the equipment

4- Implementing the changes by installing the equipment, but also embedding its use into the common working practices on site.

3.1 Review of failure modes

A fundamental part of the project is to understand the failure modes and machine characteristics, where noise, heat & movement will be picked up for internal events under normal operation and then again during a failure. Basic characteristics of machine failures are:

a) Long term – wear related
b) Sudden (Eike Drewes, 2008)

Both failure types can be monitored and maintained. Wear related types occur after the useable life of a part has elapsed. If worn parts are not replaced, machine damage will occur. An example is rider rings wearing down enough, so the piston starts to scratch the cylinder liner.

Sudden failures occur without any prior notification. The whole failure takes minutes or in some cases, seconds to progress to the point of damage. So, the quicker the machine can be stopped in these instances the limited amount of damage will occur. An example is a piston rod failing after a liquid slug, as the machine continues to move the part of the rod still attached to the crosshead colliding into the snapped piece of rod carrying the disconnected piston.

Each failure will have unique signatures which will be represented by changes and attributes within crank case velocity, crosshead accelerations, rod displacement, cylinder accelerations and cylinder pressure name a few. Each component reacts in a phase, plane, or position and this will reflect where a sensor will be mounted on the machine.

Some examples of failure modes that are mitigated with trip signals and condition monitoring warnings associated with the crank case are foundation instability, out of balance, damaged bearings, crank fractures, broken counterbalance bolts. Example of failure modes associated with the crosshead are crosshead shoe looseness, crosshead pin looseness, excessive clearances from little end wear, crosshead nut failure, crosshead failure. Some examples of failure modes associated with the piston rod could be excessive wider band wear or failure, cylinder liner movement, rod fractures.

by: Kenneth Burns, Ramin Rahnama – Wood

A full review is required to understand all failure modes and their effects, symptoms, and potential alarm levels.

3.2 Selecting a new monitoring system

Once the types of signatures of failure modes are understood along with their relevant position on the machine, the user needs to understand the compatibility and suitability of sensors. Appropriate sensors need to be selected to properly measure the critical parameters. It is best practice to prepare a component failure mode table and ensure all failure modes are covered by various sensors.

For example, a vibration will be monitored on the crank case, the crosshead, and the cylinder, but all three sensor types will be different. Heavy undulating frequencies from the main crank are best detected by a velometer to pick up the low frequency changes in inertia. The crosshead will pick up middling frequencies from the sliding motion of the crosshead shoes and the quick clearance knocks during rod load reversal. The cylinder vibration will show as high frequency accelerations caused by high pressure gases leaking to low pressure areas. While selecting the sensors it's important to understand crosstalk and any filtration of signals to focus on the components being monitored.

It's not only accelerations that will be monitored. The temperature of valve covers, pressures in cylinders and position of rods should also be tracked to provide feedback for performance and condition assessment, and in some cases safety trip functions.

The proximity probe will need to be positioned within a calibrated range. The correct rod material and coating should also be specified for accurate readings of the proximity probes. The pressure transducers should be set for the correct range to cover the full operating range of pressures.

It is important to note the condition monitoring systems that are usually used for rotating machinery would not apply to reciprocating compressors. Reciprocating machines operate at lower running speeds (compared to rotating machinery). Also, valve events and rod load reversal happen within one evolution. Therefore, the vibration signatures and characteristics vary during one revolution. Historic condition monitoring technology could not sample signals quickly enough to differentiate problems to normal vibrations (M.Wenisch 2011).

Once the technical requirements for various failure modes are fully understood, the commercial process to pick a new comprehensive monitoring system starts. 'Invitation to tender' documents should clearly explain the technical requirements. The commercial process may require a few rounds of clarifications with the potential tenderers. The site team should be prepared to adjust the plans if the technical requirements cannot be met by condition monitoring providers, or there are practical challenges in implementing all the requirements. The initial commercial offerings also may reveal the cost of the project does not match the allocated budget. The technical team need to work closely with the commercial team to ensure the technical specifications are met within the budget.

3.3 Review and update of the maintenance strategy

All four machines have been overhauled several times since their commissioning in 1996 and 1997. The most recent overhauls were completed in 2017 and 2018, where a detailed analysis of parts was completed. The frequency of overhauls was previously extended from 24,000 hours to 48,000 hours from inspections completed in 2011 and 2012.

All the inspection reports form evidence that the wear parts and areas of concern for failures were not providing indicators that they require intervention. This includes Rider bands, piston rings, cylinder liner, packing, crosshead slide, crosshead shoes and little end bearings. The OEM guidance for overhauls recommends a minor service (piston rod assembly & cylinder maintenance) every 12,000 hours and major service (addition of rod bushings, main bearings, and crosshead shoes) every 24,000. The frequency intervals were subsequently extended by the site team to a minor service every 48,000 hours. However, a machine running for extended run periods could hide indicators that would warn of impending catastrophic failure. The operational risk is that the machine may arrive at a failure mode before an extended duration preventative maintenance routine was completed.

The clearances obtained within overhauls completed prior to this project are consistent with those obtained six to eight years ago, proving the machine tribology is being maintained accurately to minimise any bearing wear. A complex condition monitoring system with integrated algorithms and machine parameters can review the vibration, pressure, temperature, and proximity probes data to look for changes or safety limit excursions. The system will then warn of impending failures and provide detailed analysis to the user running diagnostics.

by: Kenneth Burns, Ramin Rahnama – Wood

The condition monitoring system supplier provided a detailed commissioning schedule advising that all trip values would be baseline, factory standard. This pre-setting of the safety trips to OEM recommendations or supplier experience would help avoid spurious trips of the machines while collecting running data. The supplier recommended at least 3 months of running if the machines operated at all load settings during this period. Once the machines had run online, on load for a duration in various operating modes, the trip settings were changed to the expert threshold settings. These settings follow normal running data closely allowing algorithms to pick up subtle changes and early failure detection and safety trips.

3.4 Implementing the changes

Throughout the project it was important to regularly engage the site leadership team, maintenance team, planning team and operators. There was a need to convince peers that although a previously developed well-practiced time-based maintenance strategy was being performed appropriately, but this didn't mean it could be further improved. The move from a very easy to understand strategy to one which would be driven by site or remote experts needed examples of learnings from other sites to be widely accepted.

The effort in implementing the new system lies heavily with the instrument, electrical and communications fraternity. Understanding the network topology and construction needs a multi-discipline team of experts to ensure it interfaces with the important site apparatus such as machine PLC and plant DCS.

Commissioning of the equipment is not instantaneous, there needs to be significant running history to understand the unique signatures of the machine. Initial trip values and any warnings or alerts are set to manufacturers standards, code standards or the OEM guidelines for the machine. However, over time these trips, warning levels and thresholds should be set on trend data, on all operating modes, over at least 3 months. The best safety systems are ones that are sensitive to changes but also avoid spurious trips. It is important to agree the voting logic and/or the algorithms involved in checking that machine events are genuine problems before sending the dreaded trip signal. False alarms can be minimised by using the following pre-conditions:

a) Threshold violations in at least 'X' number of segments; checking if a violation occurs at the same angle of revolution to indicate a specific error such as crosshead shoe looseness. This will ignore people working nearby, creating excess noise/vibration.
b) Threshold violations in at least 'Y' number of consecutive revolutions; strongly indicates a genuine fault as interference would need to match the compressor speed.
c) Threshold violations in 'Z' number of various segments; in case of unique problems for example broken rods hitting the crankcase. (Burns 2019)

The reciprocating compressors in CATS are operating at a relatively constant operating conditions, hence finding the set points can be slightly easier. To set alarm parameters for compressor with more wide range of operations, more advanced artificial intelligence techniques could be used.

The energy industry has a hard and long-standing opinion on new and novel equipment, which is not to pursue it and suppliers must prove use in the field for long periods of time, sometimes decades, by which point the system is obsolete. It's important that industry recognises that someone needs to be the first and with this comes some pressure and risk. Safety will always be the top priority and all the risk should be calculated and methodical way. It was important to define the testing which included offline compatibility tests with mimic PLC and DCS machines.

The concerted effort of additional testing and quality assurance holds did not leave the project free from problems. The new hardware and software tested in laboratory conditions arrived with firmware and electronics issues. These issues did not affect the safety system but hampered the long-term trend data and subsequent diagnostics. This challenge was suitably worked through with the supplier and required a small amount of commissioning rework and card changeouts in the field (Burns, 2019).

4 Conclusions

By capturing quality and comprehensive data on machine condition, it is not optimal to continue any time-based maintenance. To avoid unnecessary costs of overhauls or the unfortunate possibility of damaging machines through unnecessary invasive work, an online condition monitoring system should dictate any intervention requirement. Using a condition monitoring system which has been designed for the specific equipment class provides an accurate prediction of the machines condition allowing the site to operate equipment under a predictive maintenance strategy.

by: Kenneth Burns, Ramin Rahnama – Wood

Involving all stakeholders was important in successful delivery of the project. It is only possible to deliver real value to the business from such a project if it is set up correctly and well managed. It is essential to recognise the multi-discipline input to these types of projects and set clear objectives.

A project to install online condition monitoring equipment will require the following items:

- Comprehensive knowledge of the machine.
- Knowledge of condition monitoring techniques.
- Instrumentation knowledge.
- Comprehensive knowledge of current market options for condition monitoring.
- Understanding of the site operations & maintenance practices and procedures.
- Understanding of the site planning processes.
- Overview of operational spend on the machines.
- Access to site personnel, knowledge, and group competence.
- Influencing the site maintenance strategy.

This project successfully achieved:

- An increase in the level of protection for the reciprocating compressor units
- A change from time-based maintenance to predictive maintenance strategy
- A reduction in maintenance spend over the life of the asset
- An increase in availability due to a decrease in invasive work and targeted maintenance.

5 Future Work

The additional information gathered by the machines is more than enough to extend its uses for safety and maintenance planning. It's now possible to accurately represent individual machine's reliability and availability to respond to complex problems promptly and remove bad actors. It's also possible to review the machine overall efficiency and consider using it to provide analysis of possible efficiency savings realising projects such as:

- Tribology status and oil suitability
- Valve efficiency
- Packing efficiency

6 References

Burns, K., 2019, Modernising the maintenance management of reciprocating gas compressor with use of an online condition monitoring system, dissertation for Master of Science, Brunel University London

Eike Drewes, P. S. G. G., 2008. *Improving safety protection of reciprocating compressors.* The Hague, Institute of Mechanical Engineers.

Hupjé, E., 2019. Road to Reliability. [Online] Available at: https://www.roadtoreliability.com [Accessed 20 September 2019]

M.Wenisch, L. W., 2011. Special Requirements for monitoring and machinery protection systems on reciprocating compressors. s.l., IMechE

Steinkamp, C., 2011. Monitoring and Protection: Best practices for reciprocating compressors. The Hague, IMechE.

EUROPEAN FORUM
for RECIPROCATING
COMPRESSORS

DIGITALISATION AND AI

Bently Nevada
a Baker Hughes business

What´s going on with my recip? How uncommon failure modes get detected.

by:

Gaia Rossi
Senior Application and Solution Architect, Italy
gaia.rossi@bakerhughes.com

Thorsten Bickmann
Senior Technical Leader for Recips, Germany
thorsten.bickmann@bakerhughes.com

Fayyaz Qureshi
Technical Leader for Recips, UAE
fayyaz.qureshi@bakerhughes.com

Bently Nevada, a Baker Hughes business

12th EFRC CONFERENCE
August 24 – 26, 2021, Warsaw

Abstract:
According to the EFRC Compressor Reliability Survey, the primary causes for reciprocating compressor unscheduled shutdowns include faults at valves, pressure packing, process problems, piston rings, rider bands and unloaders.
Modern condition monitoring technologies provide key information to pinpoint to malfunctions at those components and enable effective operating and maintenance decisions.
This paper describes several case studies where condition monitoring information helped in identifying piston rings failure progression, loose and leaking valves, stepless unloader problems, hyper compressor valve malfunction and process related issues. More case studies highlight the significance of horizontal rod position measurement and dynamic analysis in detecting uncommon failure modes, such as partition packing failure, uneven crosshead wear and microscopic cracks, which typically get identified only during major inspections.
Those cases show the importance of adding specific instrumentation to standard safety measurements, not only to assess performance, but also to promptly identify developing issues.
Rapid return on investment from monitoring systems adoption is achieved when maintenance strategy moves from preventive to predictive providing the ability to operate in a more reliable and predictable way and extend the period between outages.

by: Gaia Rossi, Thorsten Bickmann, Fayyaz Qureshi – Bently Nevada, a Baker Hughes business

1 Objectives of a condition monitoring system

Reciprocating compressors, being the lifeline of most mid-stream, downstream and petrochemical facilities, are well known for their flexibility but simultaneously notorious for unanticipated expensive downtimes and catastrophic failures. To avoid such incidents and production loss, OEMs and operators have set strict timelines on routine checks and overhauls based on operating hours following preventive maintenance strategy. These periodic inspections are expensive, due to resources required in scheduling and execution and the inventory built-up to have all spares available onsite, causing extensive overheads.

At the same time, the priorities in oil and gas industry include improving safety, reliability and availability and require operators to install an online condition monitoring system to ensure safe operation and prevent catastrophic failures.

The adoption of such systems also enables the implementation of a condition-based maintenance program to perform focused maintenance just on the specific components that need it, while minimizing downtime. Operators want to detect gas leaking and failures in the running gear at an early stage.

Additionally, an online condition monitoring system allows to visualize key parameters as indicated cylinder pressure and synchronized vibration, to provide the full picture of compressor health and performance during critical phases as commissioning or post overhaul.

2 Machine faults, which are detectable by a Condition Monitoring System

A compressor reliability survey has already been carried out by Dresser-Rand approximately 15 years ago and was published in an EFRC R&D project including a Compressor Reliability Survey [1] (in European Forum for Reciprocating Compressors e. V.). In this survey 217 questionnaires were distributed worldwide and 62 were returned (response quota of 28.6%). The results of this survey are summarized in Figure 1, which illustrates the reciprocating compressor systems and components identified to result in unscheduled shutdowns. According to the results, eight systems and component areas are responsible for nearly 94% of all unscheduled shutdowns of reciprocating compressors. One interesting result was the ranking of the cylinder lubrication system as one of the top eight problem areas. This was determined to be significant as the reliability of the systems can directly affect the reliability of three other components also ranked among the top eight problem areas: pressure packings (#2), piston rings (#4) and rider bands (#5).

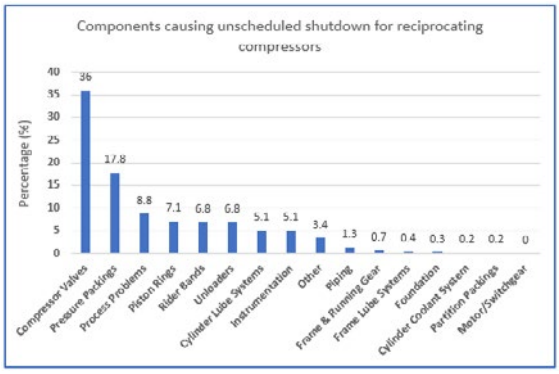

Figure 1: Components causing unscheduled shut-down on reciprocating compressor [1]

As shown in the figure above, valve failures are the most common issue on reciprocating compressors, and they contribute to most of the maintenance cost.

Online access to the internal pressure measurement for each compressor cylinder enables continuous monitoring of compression cycles, compression ratios, peak rod loads, and rod reversal. This provides valuable information on the condition of suction valves, discharge valves, piston rings, packing glands, piston & piston rod connection and crosshead pin. In addition, the functionality of capacity control devices, such as unloaders, clearance pockets and stepless control systems can be analysed.

From a diagnostic standpoint, dynamic cylinder pressure measurement provides great value. The ability to correlate events in the crosshead acceleration waveform with events in the pressure, rod load curve and crosshead vertical force is essential. This enables efficient decision making, regarding the parts that need to be replaced.

An indicated cylinder pressure versus crank angle plot provides a quick reference to identify leakages/failures on valves from the very outset. Valve cover temperatures start showing increasing trend once the valve leakage becomes severe.

2.1 Valve leakages

On a six-throw compressor unit, high frequency accelerations were noticed in the crosshead vibration versus crank angle plot (Figure 2). These high frequency components appeared when the crank end (CE) suction valve was closed, and gas flow was producing a high frequency sound (“hiss”), which was captured by the crosshead accelerometer across the same throw [2]. The cylinder dynamic pressure versus crank angle plot on CE chamber also showed a deviation between actual and ideal pressure curves, i.e. actual pressure was rising slower than expected, which signified the presence of gas leaking into low pressure areas (either gas leakage through suction valve into suction bottle, or gas leakage through pressure packing).

by: Gaia Rossi, Thorsten Bickmann, Fayyaz Qureshi – Bently Nevada, a Baker Hughes business

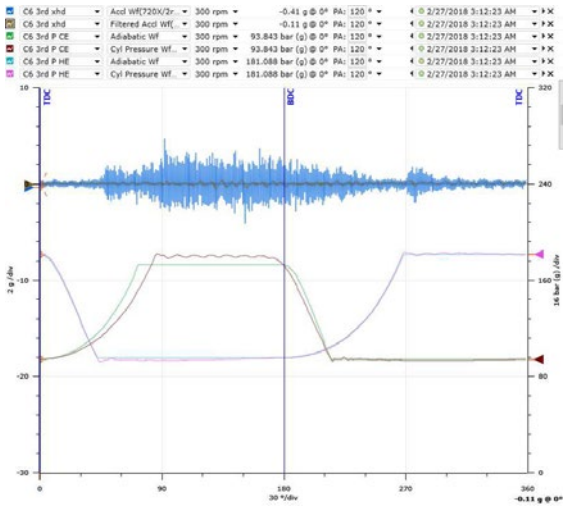

Figure 2: High frequency leakage sound captured by crosshead accelerometer, when CE suction valve is closed. Dynamic pressures confirm CE suction valve leak additionally

The suction valve cover temperatures were checked too, and the temperature of suction valve on crank end was found significantly higher than that at the head end. Thus, a packing leak can be excluded. Maintenance teams were advised to check the suction valve on CE and the valve cage was found broken, causing severe leakage.

2.2 Valve failure detection at a Hyper Compressor

Health monitoring of suction and discharge valves at a hyper compressor can be easily achieved by acceleration measurements at each cylinder.

The normal occurring impulses generated by valve opening and closing are plotted for one revolution in the next figure.

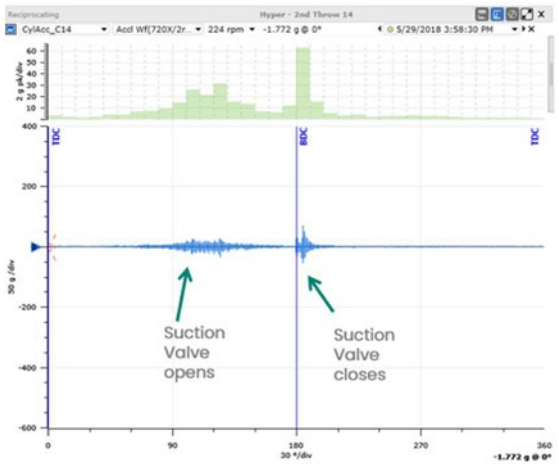

Figure 3: Typical impulses measured at the valve of a hyper compressor in good condition

In this example the valve spring broke and the measured acceleration changed drastically in amplitude and signature.

The broken spring lead to strong opening and closing impacts of the suction valve, which also lead to a saturated acceleration waveform (Figure 4).

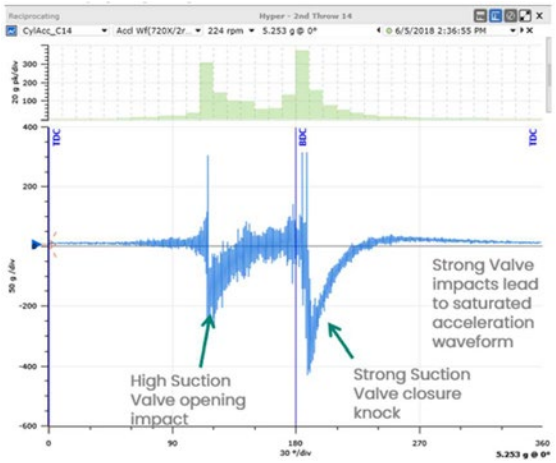

Figure 4: Impulses measured at the valve of a hyper compressor in bad condition

The banded waterfall diagram shows the developing trend of the vibration over the time (Figure 5).

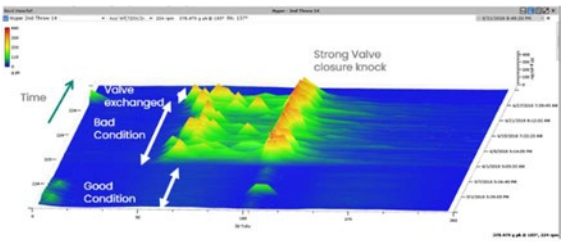

Figure 5: Waterfall diagram of cylinder vibration measured at the valve of a hyper compressor over time

3 Significance of Horizontal Piston Rod Vibration Monitoring

Experiences have shown that having a single sensor installed vertically across pressure packing, cannot provide comprehensive information about movement of piston rod throughout the revolution. Thus, several primary malfunctions cannot be detected due to the absence of a horizontal rod position probe, until these cause secondary expensive failures triggering high frame (crankcase and crosshead) vibration; a few of these malfunctions will be shown in the following subsections.

The forces caused by gas compression and the inertial forces caused by the running gear movement are in line with crankshaft main bearing axis, for which frame vibration sensors are installed to detect any abnormalities.
Any abnormal crosshead movement in vertical direction and impacts generated by looseness are picked up by a vibration sensor installed vertically on top of the crosshead casing. But if there is no monitoring at the horizontal direction of the piston

by: Gaia Rossi, Thorsten Bickmann, Fayyaz Qureshi – Bently Nevada, a Baker Hughes business

rod, then an abnormal horizontal movement in the running gear cannot be captured.

Piston rod peak-to-peak vibration has proven to be an early and the only indicator of developing cracks in the piston rod. On the other hand, crankcase and crosshead vibration increase significantly, only when the piston rod is already disconnected.
Having said that, piston rod flexing/bending significantly depends upon the location and axis of the crack. Perpendicular cracks will show up as high piston rod vibration in vertical axis and can be picked up by vertical rod position probes as mentioned in API 670. However, lateral cracks will show up as increasing horizontal piston rod vibration, which can only be picked up by a horizontal piston rod position sensor.

Failure modes such as partition packing failure, uneven crosshead wear and microscopic cracks at the piston rod, which are usually identified during major inspections can be determined during machine operation by analysing dynamic data of the condition monitoring software.

3.1 Running gear misalignment is leading to uneven crosshead wear

The alignment of motor and crankshaft of a reciprocating compressor train is part of the preventive maintenance check. To ensure that any severe misalignment is captured during operation, vibration sensors are installed on motor bearings and compressor crankcase and alarm/trip is set to save machines from severe damages and expensive repairs.

The vertical alignment ofthe running gear (connecting rod, crosshead, piston rod and piston), is typically monitored by crosshead vibration sensors installed vertically on top of crosshead guide. Vertical rod drop/position proximity sensors are installed at the pressure packing flange to detect any abnormal vertical movement of the piston rod and alarm/trip when parameters exceed pre-configured setpoints.
However, if there is any abnormal horizontal movement of the piston rod in the horizontal plane, the only sensor/measurement that can detect this variance would be a horizontal rod position sensor. The following case study shows how an online monitoring system can detect a misalignment in the running gear which historically could only be witnessed during a machine overhaul.

On a Diesel HydroTreating Unit in a refinery, 3 trains of 4-cylinder recycle/makeup gas compressors (2 running, 1 standby) are used to raise pressure from 26 barg to 85 barg for makeup in two stages and to raise pressure from 54 barg to 85 barg for recycle. These machines are equipped with an online condition monitoring and protection system and a resident engineer is available onsite for system management.
The machines are monitored for motor bearing vibration, crankcase vibration, crosshead vibration, vertical and horizontal piston rod position and peak-to-peak vibration, cylinder chamber pressure monitoring, rod load analysis and performance monitoring and keyphasor probe with multi-event wheel for accurate crank angle reference.

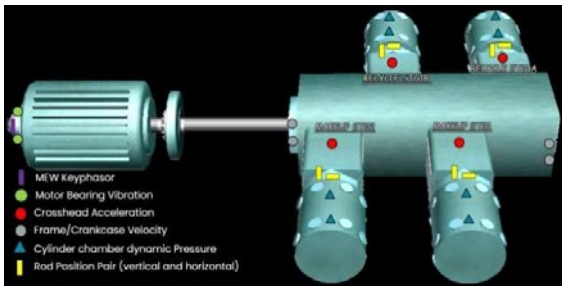

Figure 6: Sensor Layout

In March 2019, the peak-to-peak piston rod vibration in horizontal direction increased gradually from a nominal value of 200µm pp to 500µm pp (where alarm was set at 400µm pp).

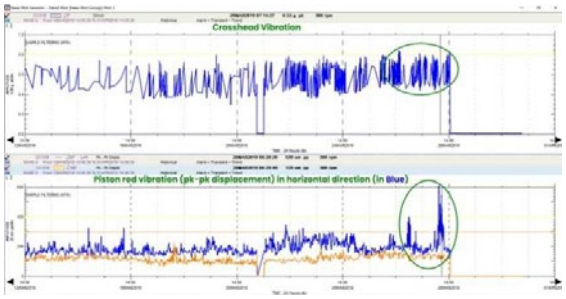

Figure 7: Crosshead vibration trend (top) and peak-peak displacement trend in horizontal and vertical direction (bottom)

Since the actual movement was in horizontal direction only, no apparent change was observed in vertical piston rod vibration and/or crosshead vibration since crosshead vibration sensor is installed vertically, as shown below in Figure 8.

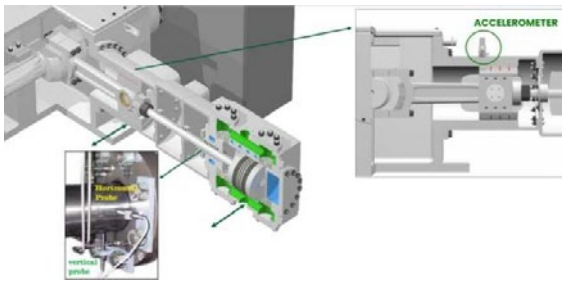

Figure 8: Crosshead vibration sensor mounting

The horizontal movement can happen either because of horizontal movement of piston inside cylinder, or because of unusual horizontal movement of the crosshead within its guide. The piston can move horizontally if there is any load change or piston rings get damaged and broken particles get trapped on the sides of piston causing horizontal movemement.
When referred to the second dynamic cylinder

by: Gaia Rossi, Thorsten Bickmann, Fayyaz Qureshi – Bently Nevada, a Baker Hughes business

pressure vs. crank angle plot in Figure 9, both head end (HE) and crank end (CE) chambers are fully loaded, confirming no/partial load changes. The ideal (adiabatic) and actual pressure plots are mostly coinciding (CE shows slight suction valve/pressure packing leak) confirming that there is no piston ring failure (in case of failure there would be a crossover between adiabatic and actual curves).

Hence it was concluded that there was an unsual horizontal movement of the crosshead within its guide, also evident from the bottom plot in Figure 9, showing the horizontal piston rod displacement fluctuating throughout the revolution and from rod position plot in Figure 10, showing the piston rod movement to be primarily horizontal and fluctuating.

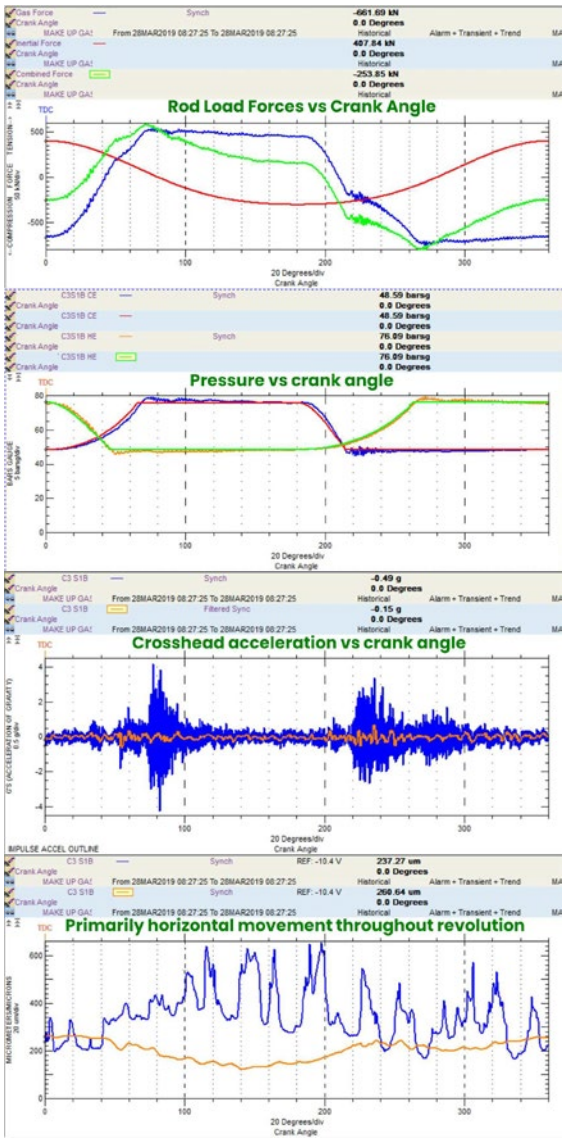

Figure 9: Dynamic plots in crank angle domain

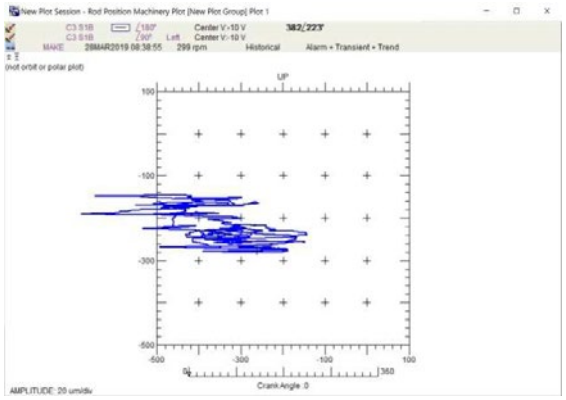

Figure 10: Rod Position plot showing horizontal and fluctuating movement

The maintenance team was asked to inspect the crosshead on cylinder 3 and to check the running gear alignment across the connecting rod and the piston rod connections on either end. During a physical inspection, the crosshead bottom shoe to guide clearances were measured as shown in Figure 11. The clearance should ideally be zero but significant clearances of around 5 mils were measured towards the frame end.

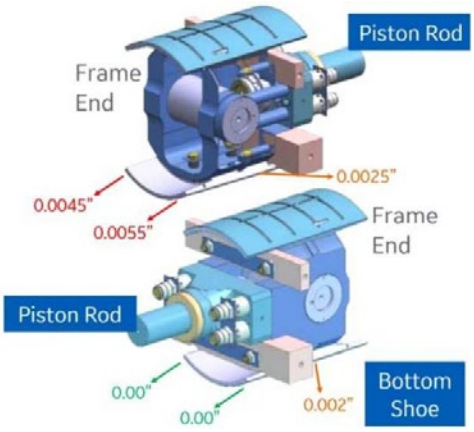

Figure 11: Measured clearances on crosshead, displayed measurements are in inches

After performing further run out checks and after verifying the connections, it was observed that the connecting rod was not properly aligned, because of an offset between the crosshead pin and bushings. This was causing the unusual horizontal movement and resulted in uneven crosshead wear. Early detection of this unusual failure mode from a non-conventional parameter (piston rod vibration peak-peak displacement) and the advised decision of performing condition-based maintenance (CBM) instead of waiting for time-based overhaul window saved the machine from expensive repairs and extended downtime.

3.2 Loose partition packing

The machine operator carried out a 16,000 hours major overhaul in the presence of the OEM, to ensure all procedures and checklists were followed thoroughly; however, the possibility of human error can never be completely eliminated.

by: Gaia Rossi, Thorsten Bickmann, Fayyaz Qureshi – Bently Nevada, a Baker Hughes business

It was reported to the machinery diagnostics resident engineer that within 10 minutes of machine startup, the rod position magnitude changed by over 1000 µm and the horizontal piston rod vibration increased drastically. The customer requested to review the data and to evaluate whether the machine could be kept running, suspecting this to be an instrumentation issue. The machinery diagnostics engineer advised to shutdown the machine to avoid further damage.

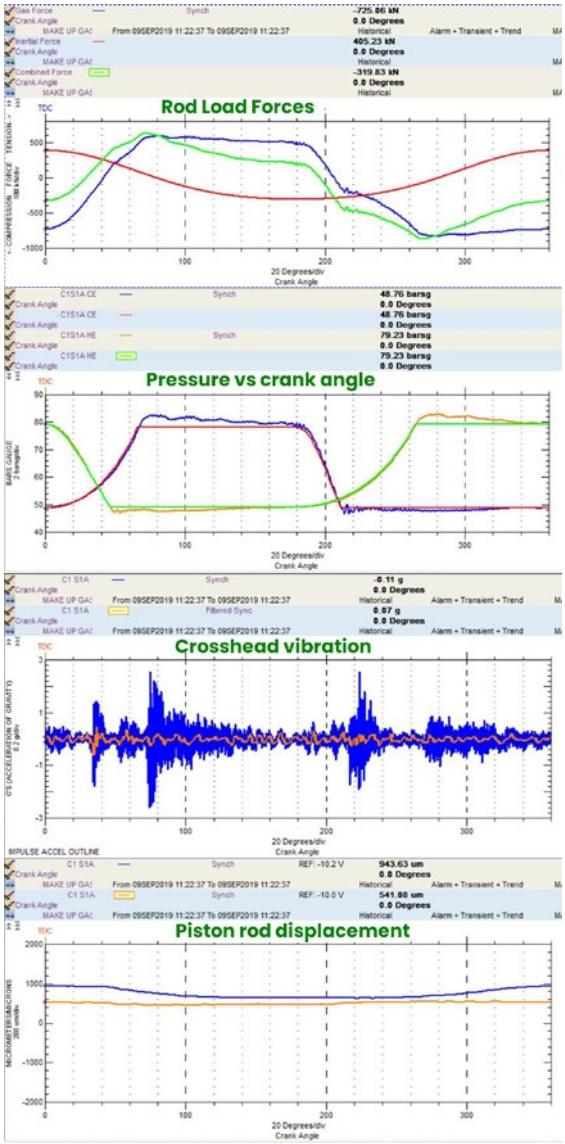

Figure 12: Dynamic sample upon starting compressor @ 11:22am

The machine was restarted around 11:22 am and all parameters seemed to be fine, as shown below in Figure 12. The top rod load forces plot showed adequate rod load reversal; combined rod load forces of 600kN in tension and 800kN in compression were well within rated values of 1300kN and 1500kN respectively. The third part of the figure, the crosshead vibration vs. crank angle plot displayed no significant impacts in the filtered waveform, which confirmed no mechanical looseness in the running gear. The dynamic pressures curves in the second part of the plot were aligned perfectly with the adiabatic (ideal) plots confirming an healthy cylinder trim (valves, pressure packing, rings) condition. The piston rod vibration and displacement were normal and within the limits in the bottom piston rod displacement vs. crank angle plot.

The horizontal piston rod peak-to-peak vibration started to increase, and within 9 minutes the peak-to-peak displacement in horizontal direction reached over 1000 µm, as shown in the bottom right quadrant in Figure 13. All other plots showed the same condition as before: no developing mechanical looseness in the running gear and no apparent issues in the cylinder trim.

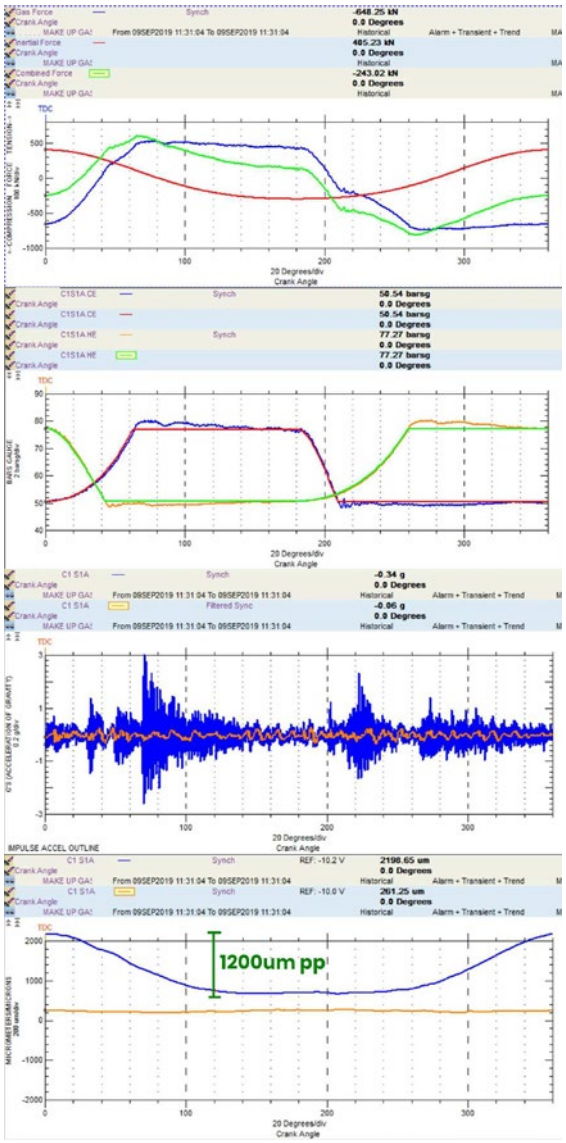

Figure 13: Dynamic sample @ 11:31am (9 minutes after starting up)

The piston rod position magnitude increased from 700µm to 2800µm; the position angle (direction of movement) was primarily horizontally left, i.e. 270 degrees, when viewed from the crankshaft towards the cylinder as shown in Figure 14. This movement was suspected to be caused by a force acting in horizontal direction. Since the compression

by: Gaia Rossi, Thorsten Bickmann, Fayyaz Qureshi – Bently Nevada, a Baker Hughes business

chambers were loaded and no piston ring leak showed up, that lead to the confirmation that no piston ring loose pieces caused the horizontal movement of piston.

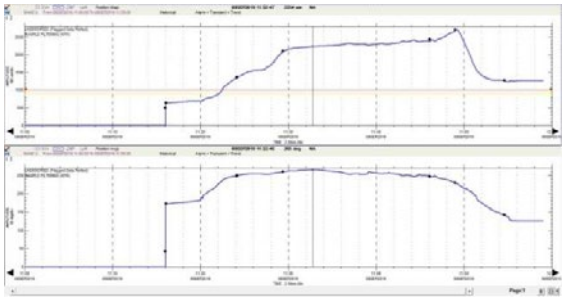

Figure 14: Rod Position Magnitude (top) and Position Angle Trend (bottom)

The horizontal probe was installed 90 degrees left for this cylinder. Due to the significant movement of the piston rod in horizontal left direction, the gap voltage decreased (as shown in Figure 15).

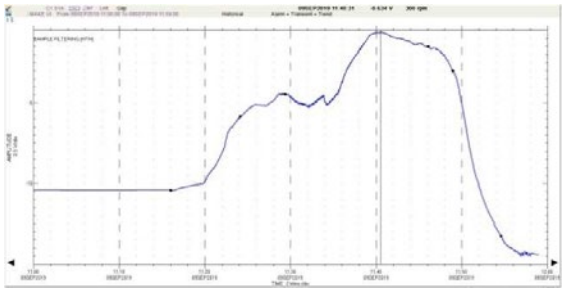

Figure 15: Horizontal probe gap voltage trend over time

The blue plot in Figure 16 represents the piston rod position and movement when the machine was started. The orange plot shows the piston rod trajectory over one revolution when the piston rod was forced to move horizontally left.

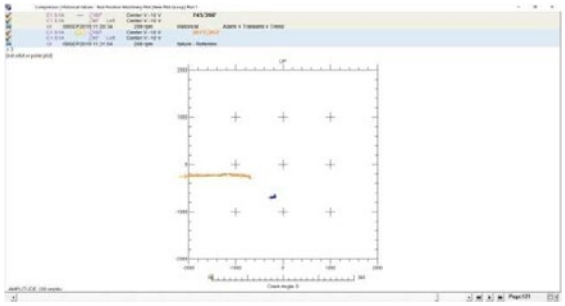

Figure 16: Rod Position Plot (blue – normal & orange – failure)

Upon opening the inspection windows, the partition packing tie rods were found loose, thus forcing piston rod to move horizontally left and to hit the probe, damaging tip completely. The pictures in Figure 17 show the rubbed piston rod and the damaged partition packing.

Upon careful data analysis, informed decision was made to safely shut the machine down, avoiding secondary expensive repairs and extended downtime.

Figure 17: rubbed piston rod and damaged partition packing

3.3 Piston rod failure

To meet a hydrocracker capacity requirement, three out of four make-up gas compressors have to be operational. All machines are monitored with a proactive condition monitoring and protection system comprising of crankcase vibration, crosshead vibration, piston rod position and vibration (vertical and horizontal), cylinder chamber dynamic pressure measurement,, rod load analysis and performance monitoring and multi-event wheel keyphasor for accurate crank angle reference.

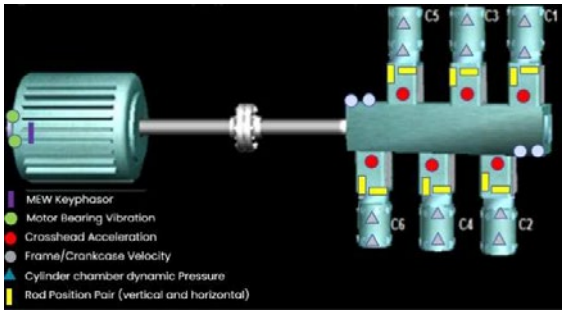

Figure 18: Sensor Layout

One morning, the crankcase vibration of one of the six-throw make-up gas compressors suddenly increased from a nominal 3mm/s pk to 41mm/s pk within a second and tripped the machine. The magnitude was higher for the velocity sensors installed near the pump end (NDE) of the compressor. However the amplitude at the sensors on the driving end was also higher than alarm setpoints (Figure 19).

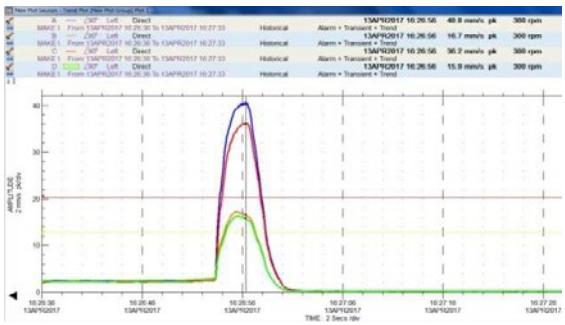

Figure 19: Crankcase vibration trend

by: Gaia Rossi, Thorsten Bickmann, Fayyaz Qureshi – Bently Nevada, a Baker Hughes business

The crosshead acceleration trends were checked, and it was noticed that throw 2 (closer to pump end) crosshead vibration went highest compared to the rest; the amplitude increased from a nominal 0.8g pk to 24g pk in 3 seconds which confirmed that the failure has happened in throw 2.

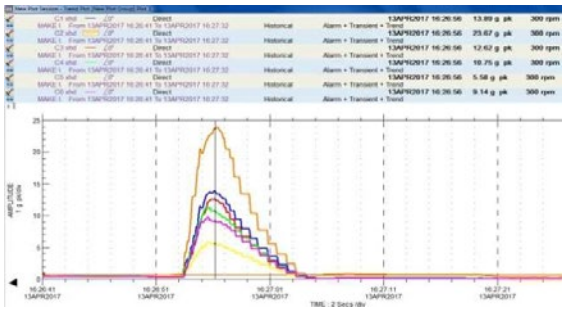

Figure 20: Crosshead vibration trend of all six throws

The impact happened when the disconnected piston rod hit the freely hanging piston inside the cylinder as shown below in Figures 21 and 22 (in crosshead orange filtered waveform). It is interesting to note that API 670 (5th Edition) recommended shutdown parameters (crankcase and crosshead vibration) were not sufficient to save the machine from piston rod failure.

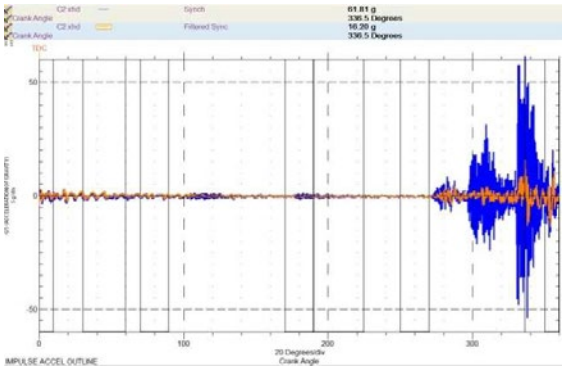

Figure 21: Throw 2 crosshead vibration filtered acceleration (orange) at point of suspected piston rod failure

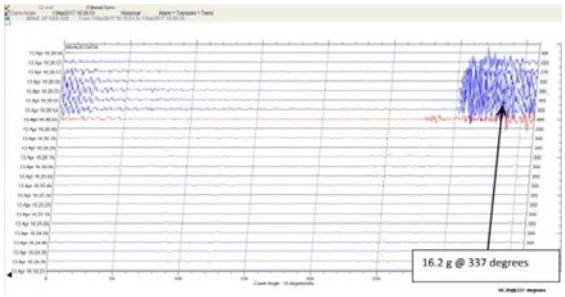

Figure 22: Throw 2 waterfall of crosshead filtered acceleration, cursor (red) at point of suspected piston rod failure

The only parameters that showed a gradual change over time were rod position magnitude and peak-to-peak displacement (piston rod vibration). In Figure 23, the green rod position waveform shows a smaller position magnitude close to the bore center. Nine minutes before the failure, it can be noticed that even the rod flexing (piston rod vibration) in vertical and horizontal axis both was nominal. However, just before the failure (blue waveform), the rod flexing increased significantly in the horizontal direction. It is suspected that the crack in piston rod was lateral and not perpendicular, which would have caused the vertical piston rod vibration to increase.

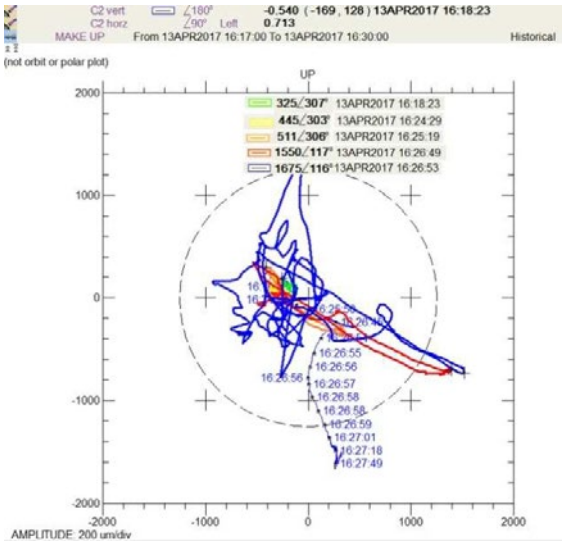

Figure 23: Cylinder 2 Piston Rod waveforms manually overlaid on bore centerline plot

The peak-to-peak displacement trends (Figure 24) in both vertical and horizontal directions confirmed that the machine could have been safely shut down two minutes prior to the piston rod breakage, if a careful alarm at 400µm peak-peak and automatic trip setpoints at 650 µm peak-peak would have been configured. Expensive repairs on crosshead as a secondary damage could have been avoided.

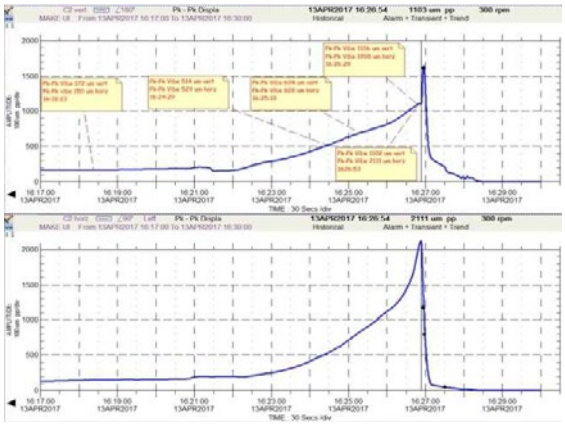

Figure 24: Trend of piston rod peak-peak displacement, throw 2 (top: vertical, bottom: horizontal)

API recommendations have matured over the years; in 2007, API 618 (5th Ed.) only recommended crankcase/frame vibration as automatic shutdown parameters and then in 2014, due to several case studies/lessons learnt across the globe, API 670 (5th

by: Gaia Rossi, Thorsten Bickmann, Fayyaz Qureshi – Bently Nevada, a Baker Hughes business

Ed.) added crosshead vibration also as a shutdown parameter. The journey continues as operators and condition monitoring solutions vendors partner together in identifying unconventional failure modes on reciprocating compressors with some novel useful parameters like piston rod vibration and understand the behavior of these intricated machines better through extensive data analysis and domain knowledge.

3.4 Piston ring failure

The crosshead vibration at stage 2A of a four-throw hydrogen compressor increased beyond 4g pk (alarm setpoint was 2g pk).

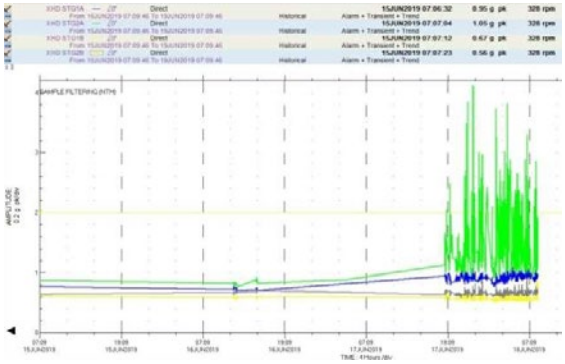

Figure 25: Crosshead vibration trend

Simultaneously, the piston rod vibration increased above the configured setpoints of 500µm pp in both vertical and horizontal directions, as shown in the next figure.

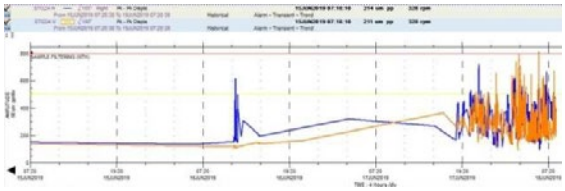

Figure 26: Trend stage 2A piston rod peak-peak displacement (blue: horizontal, orange: vertical)

On the other hand, the crankcase vibration did show a very slight increase with variations, but still was much lower than the configured setpoint. This proves the fact that crankcase vibration alone may not be sufficient for machine protection.

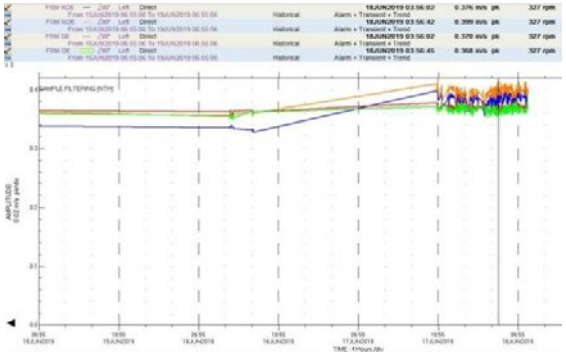

Figure 27: Crankcase vibration trend

Dynamic data in Figure 28 was referred for further investigation into the root cause of this high crosshead and piston rod vibration. Crossover in the HE pressure curves (adiabatic and actual) in the second part of the plot delineated a piston ring failure (crossover should also show up in CE pressure curve, however the discharge valve leakage masked that, due to the severe leaking). High-3-2000 Hz filtered crosshead vibration (orange waveform in third part of the plot) confirmed vibration generated by mechanical impacts, which can be due to broken particles of piston rings coming underneath the piston. Changes in piston rod displacement (bottom plot of Figure 28) show that the piston lifted up due to piston ring pieces getting trapped on the sides of the piston.

by: Gaia Rossi, Thorsten Bickmann, Fayyaz Qureshi – Bently Nevada, a Baker Hughes business

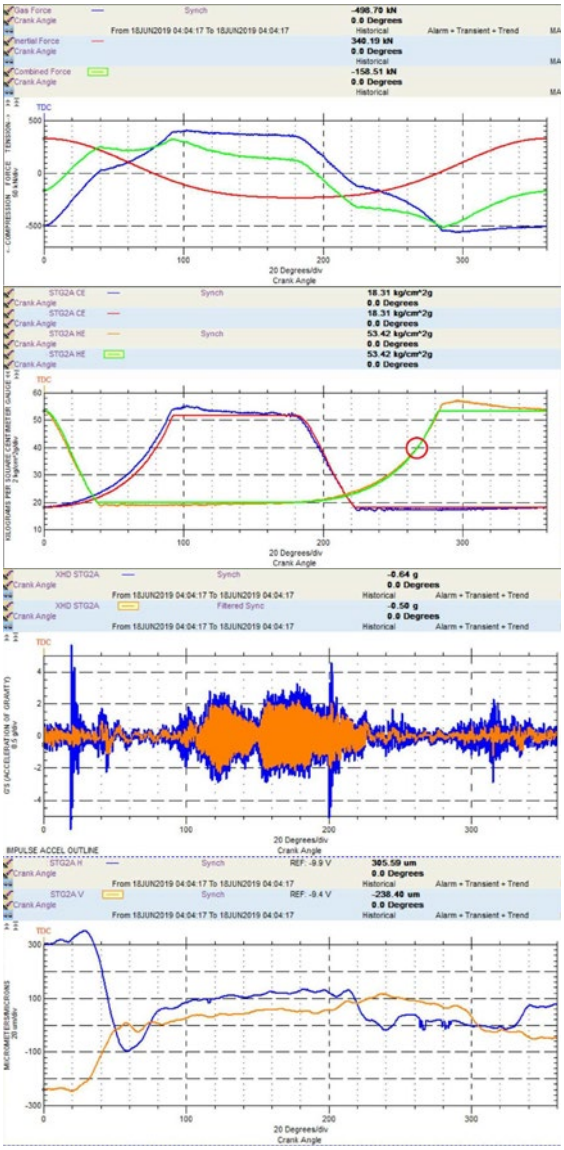

Figure 28: Dynamic sample for Stage 2A

Inspections showed that the piston rings were found broken as shown in Figure 29. Thus, the condition monitoring system was able to identify and pinpoint to failures as soon as they happened. The machine was shut down safely and that saved from expensive secondary failure(s) and extended downtime.

Figure 29: Broken piston rings

6 Conclusion

In addition to crankcase and crosshead vibration as recommended shutdown parameters by API standards, piston rod peak to peak displacement provides vital information about the running gear health and, being a very reliable and stable parameter, it can be made part of the trip logic, to ensure comprehensive protection. A careful study of compressor baseline data at different operating conditions may help define optimal setpoints to save machines from impending primary and secondary failures. The review of dynamic data supports the identification of developing faults from the very outset by pinpointing the failing components and by determining severity. With this help, machine shutdowns can be scheduled efficiently with minimal spare inventory.

References

[1] EFRC R&D project on Compressor Reliability Survey (2010)

[2] Fayyaz Qureshi, Thorsten Bickmann (2018): Online Condition Monitoring System identifies developing faults in reciprocating compressors at the very outset, ADIPEC

Valve Data Acquisition throughout the Life Cycle

by:

M. Schiavone, A. Raggi, A. Giampà, G. Ballerini
Dott. Ing. Mario COZZANI s.r.l.
Arcola (SP), Italy
info@cozzani.com

12th EFRC CONFERENCE
August 24 – 26, 2021, Warsaw

Abstract:
Nowadays the industry driving requirements are focusing on running costs reduction, energy saving, and predictive maintenance. The energy and Oil & Gas industries are called to react promptly with cutting edge technologies and the best competencies. In this scenario the data management (acquisition, processing, security and storage) is the corner stone of the actual industrial revolution.
This article describes the real experiences about the advantages brought by the mobile data acquisition systems for reciprocating compressors, and in particular how these can verify and improve the valve performance. The article shows examples at different stages of the compressor life cycle, from the development to the commissioning, and from the performance improvement to the generation of data for digital-twin models. Cases of experimental activities for NPI (New Product Introduction) compressors before the entry into market, as well as activities carried out on working plants -from stand-alone plants to complex petrol-chemical plants- are also introduced to show the opportunities brought by the data-acquisition systems. The article gives also an insight of possible developments of this technology. The cases presented in this article demonstrate how the valve OEM can create values for both compressor OEMs and compressor End-Users by transforming data acquisition into improvements of either the valve or the compressor performance itself.

by: M. Schiavone, A. Raggi, A. Giampà, G. Ballerini – Dott. Ing. Mario COZZANI s.r.l.

1 Introduction

The activities of product development and service related to reciprocating compressor valves are the keys to enhance the performance and the profitability of a plant, because these can improve multiple areas of interest such as performance improvement, service cost reduction, and energy efficiency.

The Total Cost of Ownership (TCO) is often not fully controlled throughout the lifecycle. The service costs, such as spare part costs, man hours and non-planned service stops can exceed forecasted budgets of spare part costs. At the same time the opportunities for upgrades and improvements which may reduce operational costs are often overlooked.

In a business where the growing complexity of the regulations together with the raise of costs may threaten the profitability of the compressor End-Users, the main challenges focus on how to improve processes and how make each plant more efficient, both in the short and in the long term.

In this business context, IoT technologies has grown fast over the last years, also reaching several application fields, including industrial applications. This growth has been possible thanks to the generation and processing of Big Data generated by the products or systems on field. The data acquired give a better understanding of the behaviour on field, and they allow a continuous improvement of the Digital Twins of products and systems.

IoT technology is spreading quickly within the industrial applications by creating the Industrial IoT which is at the heart of Industry 4.0. The combination of the integration of production processes (made possible by the interconnection of multiple devices, systems and software that allows the acquisition of data and information) together with the availability of devices designed for industrial and harsh environments (such as high temperatures, ATEX, etc.) allow the introduction of Industrial IoT technologies in complex systems and industrial plants.

The mobile Data Acquisition System for reciprocating compressor valves developed by Dott. Ing. Mario Cozzani s.r.l. fits in the context described. In particular it allows both the cost optimisation and the growth of knowledge available to product engineers and also to the maintenance engineers of the plant.

2 The challenges of mobile acquisition systems for reciprocating compressor valves.

The compressor valves play a significant role in the overall reliability of reciprocating compressors and of the plants in which the compressors are working. For this reason, the data acquisition about the valve behaviour is helpful for a more precise tuning and validation of valve simulation software. Furthermore, the information and knowledge built on valve data acquisition allows the End-user plant managers to deploy efficient and tailored maintenance plans and actions.

The advantages of data acquisition are not limited to the maintenance. Nowadays the reciprocating compressor energy consumption can be reduced with the adoption of the new generation of profiled valve type. In these cases, it is required to compare the compressor before and after the valve type change in order to have an accurate assessment of the achieved energy saving. To do so, only an acquisition system designed for valve data acquisition can assess the valve contribution within the compressor operating envelope. The acquisition system here described allows the acquisition of pressure losses of the valve and the corresponding housing, by reading pressures upstream and downstream of the valves.

2.1 The reciprocating compressor valve data acquisition system developed

The Data Acquisition System developed by the Company (in short CDAS) is a mobile device developed specifically for Reciprocating Compressor Valves (see *Figure 1*).

The system hardware is composed by an acquisition box onto which connectors and sensors are connected to.

The acquisition box has both voltage channels and current channels, and these are suitable for several physical quantities such as temperature and pressure, acceleration, etc. The box can be easily moved and carried to the plant, even as a piece of flight luggage.

The acquisition box can be interfaced to multiple sensors and transmitters, such as Top Dead Centre (TDC) Acquisition sensor, pressure transmitters, temperature transmitters, accelerometers and wattmeter. The TDC sensor -shown in *Figure 2*- allows the detection of the crankshaft position and speed. Pressure transmitters can be placed in different position inside the compressor, and near the valves: these allow the measurement of both average pressures and instantaneous pressure variations (see *Figure 3*).

by: M. Schiavone, A. Raggi, A. Giampà, G. Ballerini – Dott. Ing. Mario COZZANI s.r.l.

Figure 1: CDAS installed on a reciprocating compressor

Figure 2: TDC Sensor

Figure 3: Pressure transmitters and Kiene valves.

By interfacing the data acquisition system with a wattmeter it is possible to get tension, current and active power. It is then possible to synchronize the electrical quantities related to the motor with the mechanical quantities of the rest of the compressor.

Figure 4: Wattmeter interfaced to the CDAS.

The hardware is connected to a workstation with an internal-developed software. The software performs the analysis of the working conditions of the valves and of their performances.

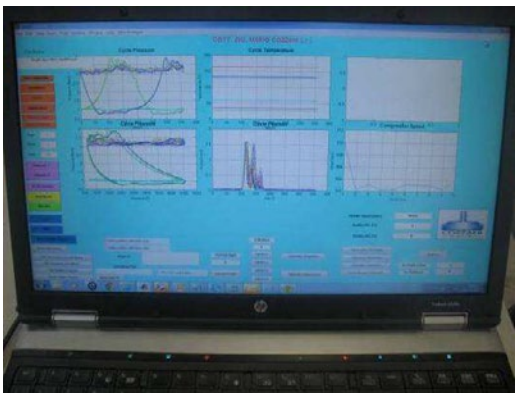

Figure 5: Workstation screen with a page of the CDAS software

The compressor geometry can also be imported into the software to determine the exact position of each piston.

The software allows a fast data elaboration and it generates several charts as the PV diagrams, pressure trends, temperatures, accelerations with respect to time or crank angle. Pressure losses, power losses due to valves, indicated power and opening and closing angles of the valves are also calculated and reported. The CDAS software allows the comparison of different acquisitions in order to compare the trends of the valve performance over time.

Periodic data sampling allows comparison of performance data over the compressor history, and the End-User can be ensured the performance are maintained over time, as well as show anomalies and faults of the compressor or of the valves.

2.2 Cloud and remote connectivity.

The CDAS software can be operated remotely via the Company Cloud. This functionality brings

by: M. Schiavone, A. Raggi, A. Giampà, G. Ballerini – Dott. Ing. Mario COZZANI s.r.l.

several advantages such as time saving, cost saving, and easy deployment of the service. The remote functionality and the use of a proprietary cloud are mandatory to carry out periodic data acquisitions and predictive maintenance of the system.

The connectivity managed by the CDAS is designed to keep separated the End-User network, from the Company Cloud network. The connectivity can be granted either via WAN, PSTN (Public Switched Telephone Network – for fixed line), Wifi, or UMTS.

The Cloud embeds the cybersecurity and high availability principles. The high availability is reached by redundant storages, networks and connections.

3 Examples of CDAS application.

This section describes some cases that show how the reciprocating compressor valve data acquisition is useful in every stage of the compressor lifecycle. In particular cases related to compressor design and validation, commissioning, operation, and performance optimisation will be shown.

The first challenge is compressor cylinders are rarely designed to enable data acquisition, and accesses to cage and cylinder are not available. In these cases, the CDAS is integrated with specific devices for sensors installation.

It is worth mentioning the valve is interfaced with the compression chamber on one side, and with upstream or downstream piping on the other side (depending if it is a suction valve or a discharge valve). For a precise data acquisition, it is very important to fit the transmitters and sensors in order to minimize the position effects on the variable which is measured, or to take it into account during the data elaboration. As an example of pressure acquisition on a test compressor *Figure 6* and *Figure 7* show the pressure loss of the pocket below a discharge valve. This pressure loss (difference between green and red lines in *Figure 7*) sums up the 20% of the overall pressure loss (area between red and blue lines in *Figure 7*).

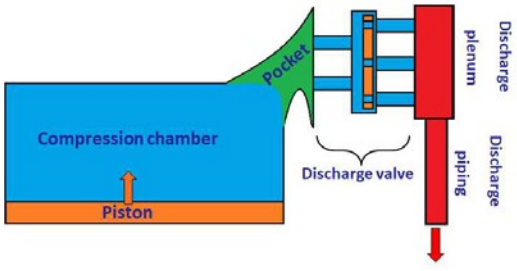

Figure 6: Compressor scheme with main volumes and domains.

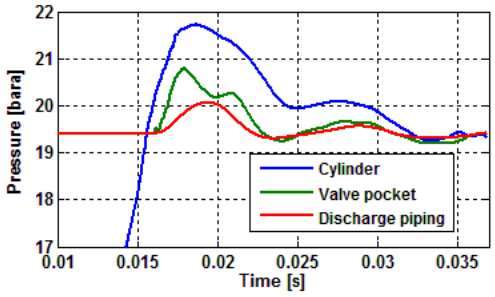

Figure 7: Pressure trend measured on a discharge valve.

3.1 Data Acquisition for Product Development

During the compressor development -especially for compressor series- it is useful to validate the valve behaviour on compressor prototypes. The first objective is to verify the actual performances against the design point performances, initially predicted by the valve OEM. The measured performances take into account some details which are unknown during the design phase, such as the geometries upstream and downstream of the valve. Another objective is to evaluate design modifications to improve compressor performance or valve reliability.

3.1.1 Piping and valve lift optimisation

Compressor power:	10kW
Number of stages:	2
Working gas:	Air
Country of installation:	Italy(prototype); WW(series)

Table 1. Compressor and setup information.

For a 10kW prototype compressor a data acquisition campaign has been carried out to validate the valve behaviour and to identify possible improvements of the valves.

For this air compressor the pressure losses due to the air pocket can be neglected, since the valves are perfectly aligned to the cylinder.

As shown in Figure 8, a significant pressure loss over the suction valve and one pulsation on the discharge valve are identified. The discharge valve loss is instead acceptable.

by: M. Schiavone, A. Raggi, A. Giampà, G. Ballerini – Dott. Ing. Mario COZZANI s.r.l.

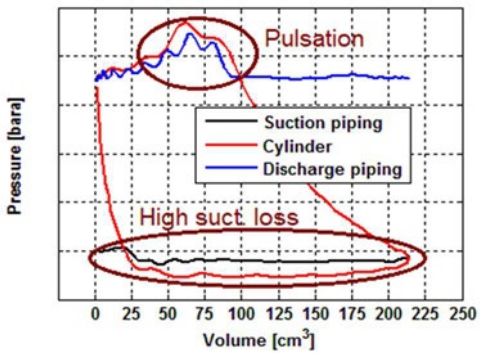

Figure 8: Losses and pulsations detected during the acquisitions

Based on the data collected, the passage area of the suction valve has been increased conveniently. The pressure pulsation has been notified to the compressor OEM, since it is not related to the valve.

As a result of that, the compressor OEM has identified some changes to apply to the discharge duct geometry in order to increase the gas passage area.

The new architecture has been tested with a long-run test and the improvements have been validated and monitored with periodic checks.

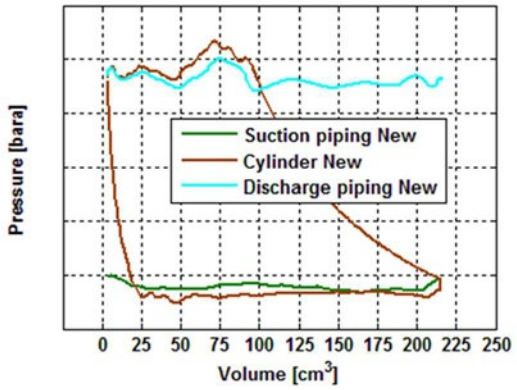

Figure 9: Pressure-volume chart from readings on the compressor after the modifications.

As shown in Figure 9 the pressure losses on the suction end have been decreased of about 40%, and the overpressure on the discharge end has been reduced.

3.2 Data Acquisition for Commissioning

This section describes the importance of a data acquisition system CDAS during commissioning.

3.2.1 Stepless capacity control system

The case here described is about commissioning of a stepless capacity control system installed on a 1.4MW compressor.

Compressor power:	1400 kW
Number of stages:	2
Working gas:	CO2+CO+H2S
Country of installation:	China

Table 2. Compressor and setup information.

The stepless capacity control system acts on suction valves by keeping these open at every compressor cycle allowing a backflow, for a period of time which is related to the capacity or pressure required. The stepless capacity control system changes the compressor PV cycle depending the condition requested. In order to verify the correct functioning of the system, the pressures have to be measured and to do so a CDAS is installed on the compressor. The analysis of the PV diagrams at different conditions allowed to confirm the correct functioning of the capacity control system and to confirm the capacity could be controlled precisely.

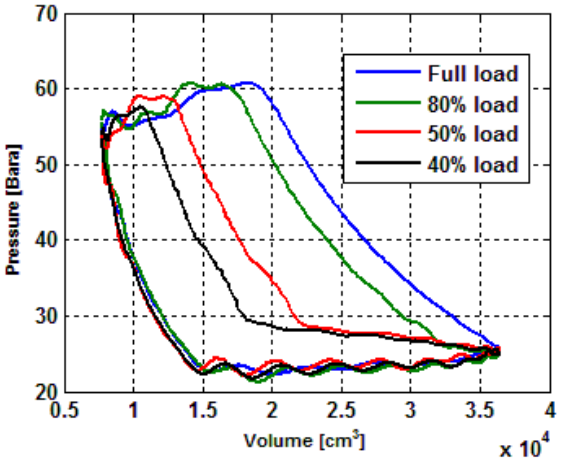

Figure 10: Cylinder pressure at different load conditions

3.3 Data Acquisition for Root Cause Analysis

Data Acquisition Systems are often key to identify valve issues in a quick and precise way. In particular, the acquisitions help to identify the right corrective actions, instead of working by multiple attempts. This section shows how the CDAS allowed to troubleshoot some Root Case Analysis (RCA) and to identify and verify the corresponding solutions.

by: M. Schiavone, A. Raggi, A. Giampà, G. Ballerini – Dott. Ing. Mario COZZANI s.r.l.

3.3.1 Valve closure delay

Compressor power:	350kW
Number of stages:	5
Working gas:	CH4
Country of installation:	Uzbekistan

Table 3. Compressor and setup information.

The case described is about a series of compressors for which valve sealing elements were observed to wear too early with respect to the target life.

Based on data gathered on field, the wear was observed not across the whole fleet, but only on certain compressors, without a clear pattern or commonality.

From the observation and analysis of the worn parts it was deducted the cause to be the sticking of the sealing elements due to the high lubrication of the compressors. An alternative valve type has been installed in order to avoid any sticking effects even with particular lubrication conditions.

In order to verify the solution effectiveness Field Service Engineers carried out compressor data acquisition. As the compressor was not compatible with sensors and transmitters, special valves with integrated sensor interface and new cages have been made.

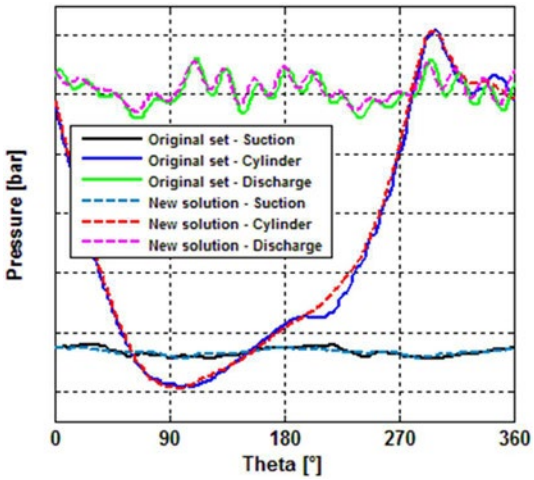

Figure 11: The pressure readings with initial and new valve sets.

By analysing the data collected it has been possible to detect the suction valve had a closing delay. The sticking effect led to a delay of the compression cycle with respect to the inversion of the piston stroke. The result is a not negligible backflow through the valve and a heavy impact of the sealing element onto the valve seat. The data readings of the new solution showed the issues were no longer present.

The corrective action together with the data acquisition not only enabled to recover the valve life but it could prove the valve life of the new solution could guarantee an extension of the maintenance interval for the whole compressor fleet, with significant cost benefits for the End-User.

3.3.2 Piping loss

Compressor power:	355kW
Number of stages:	4
Working gas:	CH4
Country of installation:	China

Table 4. Compressor and setup information.

For a CH4 compressor in China the End-User requested a valve performance check since the engine power consumption were resulting higher than the nominal values.

The Service Team carried out power consumption measurements and all stages have been fitted with sensors to detect pressure losses due to the valves.

The data collected showed the engine power consumption was near to the maximum allowed. Some minor issues to the geometry have been identified both upstream and downstream of the valve. In addition to that, the main focus was pointed to the third stage. In the third stage a non-negligible pulsation was recorded in the piping downstream the valve, as shown in Figure 12.

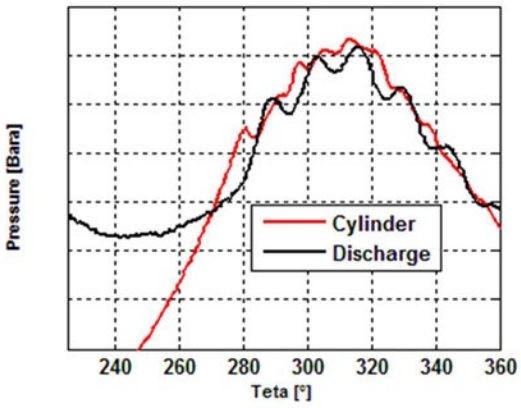

Figure 12: 3rd stage discharge pressure trend

By considering that the discharge valve pressure loss (pocket included) can be obtained by subtracting the two pressure readings it can be noted that this loss is negligible with respect to the amplitude of the pulsation determined by the interface geometries.

After sharing the knowledge based on the data readings with the compressor OEM it resulted the third stage discharge piping was undersized to deliver the nominal capacity, and it generated overpressures and a corresponding engine absorbed power increase.

by: M. Schiavone, A. Raggi, A. Giampà, G. Ballerini – Dott. Ing. Mario COZZANI s.r.l.

3.3.3 Resonance

Compressor	Same as **Fehler! Verweisquelle konnte nicht gefunden werden.**

Table 5. Compressor and setup information.

For an entire compressor fleet, the Compressor End User operates beyond the compressor specification without noticing the valve manufacturer

As a result of that, the valve Mean Time Between Maintenance (MTBM) resulted to be shorter than the MTBM of the compressor.

In order to assess the cause of the valve shorter life, an acquisition campaign has been carried out. Measurements have been taken with the compressor running both at the nominal speed and at the new speed at which failures occurred.

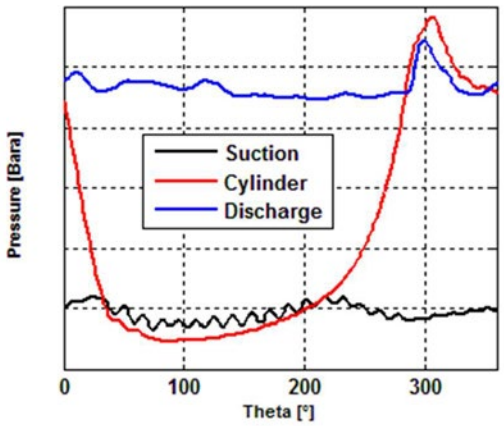

Figure 13: Pressure readings at nominal conditions.

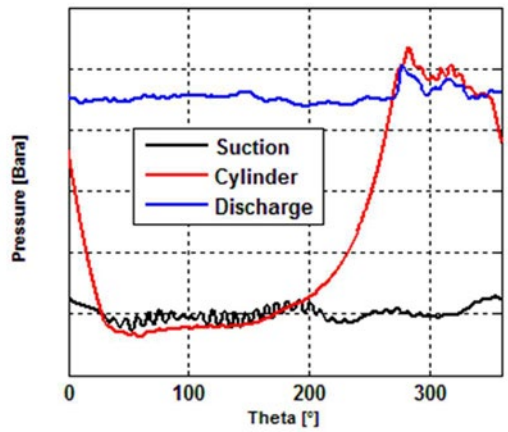

Figure 14: Pressure reading at speed outside the nominal values.

When the compressor is working at design conditions (*Figure 14*) the readings are as expected. Whereas at conditions different to the design point, high frequency pulsations raise at low speeds both in the suction duct and in the discharge duct. These pulsations did propagate also inside the cylinder.

To better address this phenomenon special valves and cylinder heads have been made to detect also the sealing element motion and impact speeds. All recorded variables had to be synchronized to have a consistent set of variables.

Within the design speed range both motion and impact speeds are acceptable. Beyond the design range the motion is characterized by high number of oscillations and resonance phenomena can be observed (see Figure 15), because some valve internals matched the compressor frequency when the compressor operates beyond the specification limits)

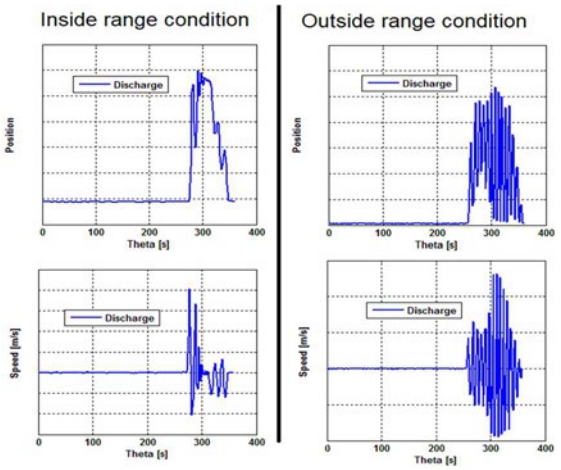

Figure 15: Position and speed charts recorded for both design point and new working point.

The knowledge built from the analysis enabled to identify a new valve design optimised for low compressor speeds (new working point) which avoids resonance. The new solution has been validated by carrying out a new campaign of data acquisition. The last readings confirmed the vibration disappeared at the new design point, as shown in Figure 16.

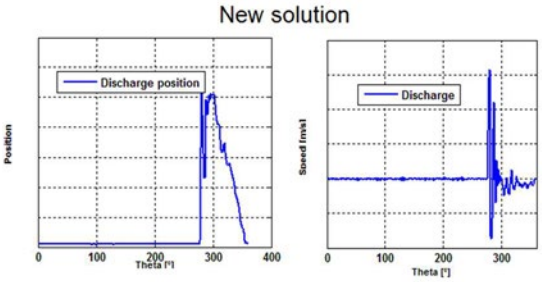

Figure 16: Speed and position of the sealing element at the new valve solution, at low speed design point.

by: M. Schiavone, A. Raggi, A. Giampà, G. Ballerini – Dott. Ing. Mario COZZANI s.r.l.

3.4 Data Acquisition for Optimisations and Improvements

The Data Acquisition System can be used to support validation strategies of product optimisation as well as improving the product Digital Twin, by comparing the design performance to the real working conditions.

3.4.1 Life increase (case one)

This section shows how the Data Acquisition System has been used in order to optimise the valve reliability of a compressor which reported discharge valve sealing failures following some plant layout changes and change of operating conditions.

Compressor power:	225kW
Number of stages:	2
Working gas:	Air
Country of installation:	Japan

Table 6. Compressor and setup information.

In order to increase the reliability and life of the valve, a new valve characterized by reduced lift has been identified as alternative solution. The effectiveness of this solution has been verified by fitting the compressor of the data acquisition system and instrumentation to detect suction pressure inside the cylinder and discharge pressure of the first stage.

The variables have been recorded from both the original solution and from the new solution proposed.

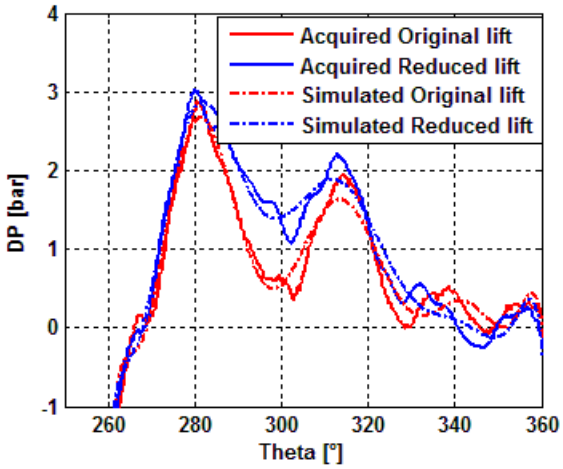

Figure 17: Delta pressure across the original valve and new valve.

By comparing the variables, it has been possible to confirm the pressure loss increment by using the new solution was acceptable and it was aligned to the values assumed during the design phase as shown. The analysis confirmed the new valve was suitable for that application, and satisfies the reliability requirement.

3.4.2 Life increase (case two)

The valve optimisation described in the previous section led to an increase of reliability in most of the compressors of the fleet, with some exceptions. For some compressors the failures were still observed before of the planned maintenance interval.

Compressor	Same as 3.4.1
Country of installation:	Japan-France

Table 7. Compressor and setup information.

A new measurement campaign has then been organized. In addition to pressure transmitters, accelerometers have been fitted to the compressor. The combined configuration of sensors allows a more precise detection of the valve sealing element motion. The data analysis has identified significant impacts after the ideal discharge valve closure time. This phenomenon of closing delay could also be observed by the cylinder pressure trend.

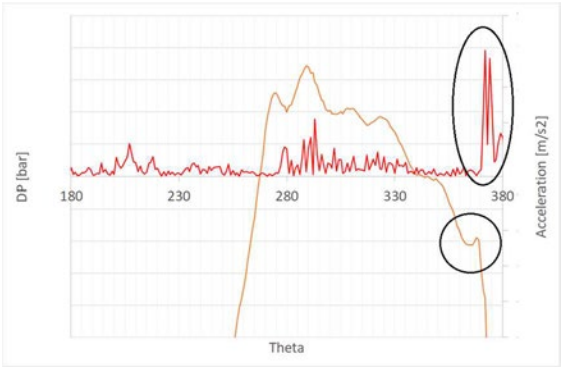

Figure 18: Pressure delta and accelerations. The closure time and impact are highlighted in the chart.

The valve internals have been modified in order to eliminate the closure time delay. The final solution adopted on these compressor types includes also passage area reduction (described before), spring load optimisation, minor layout changes of the plant, and -at last- updated compressor operating conditions. The new solution has been verified by repeating the measurements on the compressor and by observing no more fluctuations due to the impact. The overall result has been confirmed by the performance of compressors installed worldwide.

by: M. Schiavone, A. Raggi, A. Giampà, G. Ballerini – Dott. Ing. Mario COZZANI s.r.l.

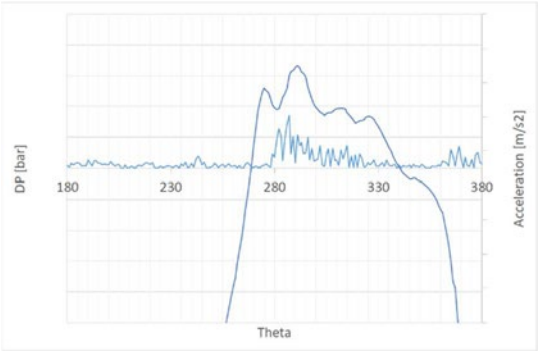

Figure 19: Data acquisition chart of the latest solution.

3.4.3 Performance increase

An End-User detected high compressor power consumption to the maximum allowed. For this reason, the End-User asked for a new set of valves which is optimised for that machine in order to obtain lower consumptions.

Compressor power:	300kW
Number of stages:	1
Working gas:	Air
Country of installation:	Italy

Table 8. Compressor and setup information.

Before of offering a more performing valve set than the one on field, the cause of the higher consumption has been investigated by equipping the compressor with a CDAS with pressure transmitters. The measures are reported in Figure 20.

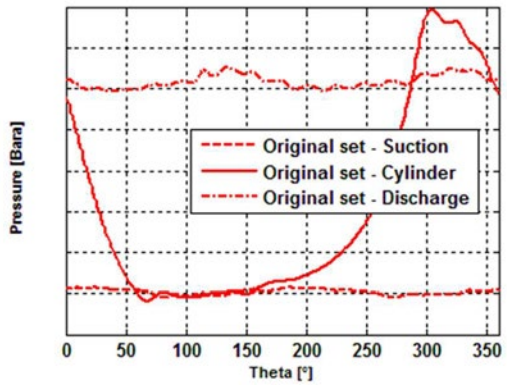

Figure 20: Pressure data reading on the compressor with the original valve set.

From pressure versus crank angle chart it is evident how the pressure losses of the suction side are negligible with respect to the discharge pressure losses. Based on this information a set of high efficiency valves -with shaped valve sealing elements- has been identified as new set of discharge valves.

After the installation and entry into service of the high efficiency valve set, the next data acquisition showed a significant reduction of losses. The compressor efficiency gain due to the introduction of the high efficiency valve was sufficient to lower enough the compressor energy consumption sufficiently below the maximum allowed.

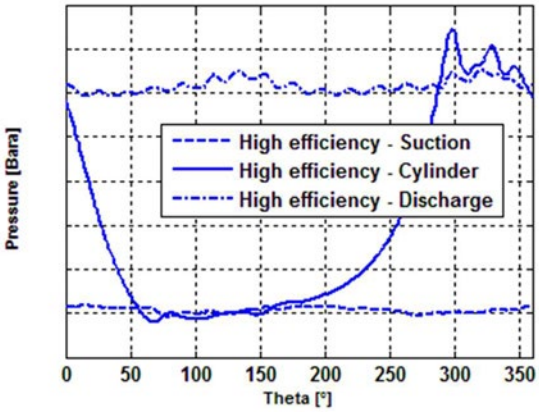

Figure 21: Pressure chart of the high efficiency valve solution.

4 Data Acquisition for Customised Maintenance and Digital Twin.

The mobile data acquisition system for valves is able to log the measurements carried out on different compressors and devices. This allows the Service Engineering departments of both the End-Users, Compressor OEM, and the Valve OEM to design customized maintenance plans. The extension of the MTBM can be defined based on the real working conditions, which gives cost saving to the End-User and clear and precise operating conditions to the Valve Manufacturer.

In addition to that, the Data Acquisition System allows the Valve Manufacturer Dott. Ing. Mario Cozzani s.r.l. to improve the Digital Twins of its products by comparing data against models. In particular numerical tools used in Engineering for valve design can be improved continuously, and simulations of the valve performance as well as internal part dynamic can be thoroughly validated.

5 Conclusions

This article shows the applications of a mobile data acquisition system for compressor valves, in particular the Data Acquisition System developed by Dott. Ing. Mario Cozzani s.r.l..

After a first description to the system and introducing the Cloud data management and the remote connectivity, the corresponding cost and operational advantages have been presented. The system offers advantages to the End-Users in terms of accuracy of the analysis which allows precise root cause investigation; the cloud based architecture minimizes all the activities in the plant, both in terms of the number of Service Engineers

by: M. Schiavone, A. Raggi, A. Giampà, G. Ballerini – Dott. Ing. Mario COZZANI s.r.l.

involved, and also in terms of fast response, tailored planned activities on-site, and reliability ad validation of the solutions proposed.

Several real cases have been reported to describe how the Data Acquisition System supports the valve and compressor lifecycle, starting from the product development, to commissioning, up to the optimisation of products in service.

The availability of a mobile Data Acquisition System designed for reciprocating compressor valves allows the development and the introduction into service of more performing and more reliable products by optimizing them to the real working conditions and integrating valves and the specific compressor. The described Industrial IoT system related to compressor valves allows collecting Big Data to be used for Digital Twin optimization.

The remote connectivity is also possible: after the first on site setup phase, measurement campaigns extended over time without any operator on site are also possible. Cozzani engineering or compressor OEM or End-users can analyse the valve and compressor performance, and issue custom maintenance plans base on End-User needs and real working conditions.

References

1 – API Standard 618 “Reciprocating Compressors for Petroleum, Chemical and Gas Industry Services”
2 – Workshop “Compressor Control", 5th EFRC-Conference 2007 Prague
3 – F. Manfrone, A. Raggi “Analysis of the Movements of the Valve Sealing Elements”, 8th EFRC-Conference 2012, Dusseldorf
4 – M. Schiavone, A. Raggi, A. Giampà “The challenge of Industry 4.0 applied to a stepless capacity regulation system”, 11th EFRC Conference, Madrid
5 – “Condition Monitoring” Design and Operation of Reciprocating Compressors - 2nd EFRC Training Workshop 2015
6 – "Monitoring Wear" EFRC Training Workshop "Lubrication and Wear" 13 September, 2016
7 – "Condition Monitoring for reciprocating compressors - Block I CM Basics & Block II Standards /Performance/Big Data" 3rd EFRC Training Workshop 2017

ऑयल इंडिया लिमिटेड
(भारत सरकार का उद्यम)
Oil India Limited
(A Government of India Enterprise)

Introduction of Electronic Control Panels in Reciprocating Gas Compressor packages

by:

Baruah Prateek
Gas Management Services Department
Oil India Limited
Duliajan, Assam, India
prateek_baruah@oilindia.in

12th EFRC CONFERENCE
August 24 – 26, 2021, Warsaw

Abstract:
Oil India Limited (OIL) is a premier Indian national oil company engaged in the business of exploration, development and production of crude oil, natural gas and LPG under the aegis of Govt. of India. The roots of OIL date back to 1889 when its parent company Burmah Oil Company Ltd, UK discovered oil for the first time in Asia in the extreme north east corner of India in a place called Digboi situated in the state of Assam. OIL is also a pioneer in the utilisation of field gas for crude oil production. OIL has been using reciprocating compressors for compression of low pressure field gas for flare reduction and also "Gas Lift Gas" for artificial gas lift wells for crude oil production since 1970s. We take pride in maintaining 126 numbers of gas compressor packages placed in 19 Gas Compressor Stations spread across an area of 1400 Square KMs in the state of Assam. OIL started its gas business with integral slow speed compressors, subsequently moving on to high speed separable compressors with either electric motors or gas engines as prime movers. The journey has seen various compressor makes and models serving the desired purpose for the company. The frequent sale and purchase of gas compressor frames has been mastered by OIL through innovation and liaisoning to develop foreign as well as indigenous alternative vendors. The basic mechanical design philosophy of reciprocating compressors has not been changed in the last few decades but the monitoring and control systems have undergone a sea change in the same period. From microprocessor based SLC to proprietary PLC and to specialised control systems, all of which are specifically made to cater to gas compressor packages. The challenges and overcoming the same to achieve successful execution has led to acceptability, availability and maintainability. Despite our 5 decade long legacy in gas compressor packages, we moved ahead with induction of digital technology in control panels since 2013 only. However, we are now rushing in the path of digitalization with 23 numbers of new gas compressor packages commissioned till date with state of the art electronic control panels and such advanced packages make up almost one fifth of our arsenal. My paper will highlight the challenges (both technical and statutory), technical details and performance and also advantages and benefits of introduction of such new technology in reciprocating gas compressor packages vis-à-vis our company's business.

by: Baruah Prateek, Oil India Limited

1. Introduction

Oil India Limited[1] (mentioned as OIL from here onwards) is one of the only two national petroleum E&P companies of Republic of India. OIL produces crude oil, natural gas and Liquefied Petroleum Gas (LPG) and has extended its business to Wind and Solar energy sectors in recent times. The company's primary operational area is around its FHQ situated in Duliajan City in the state of Assam in the North Eastern region of India.

The natural gas, coming in from petroleum rich fields of upper Assam, is received in Gas Compressor Stations (GCS) located in different parts in and around the FHQ of the company. The Gas is received in two pressure ranges viz. 1.5 – 2.2 Kg/CM^2 (termed as LP Gas) and 14 – 16 kg/ CM^2 (termed as HP Gas).

Currently every GCS has reciprocating gas compressor packages (also termed as "package" or "Unit" in this paper) performing two different duties with either an engine or a motor as prime mover. The Low Pressure Booster (LPB) compressor's duty is to compress the LP Gas from 1.5 – 2.2 Kg/CM^2 to 14 – 16 Kg/CM^2 range. Another reciprocating compressor termed as Gas Lift (GL) compressor compresses a part of HP Gas from 14 – 16 Kg/CM^2 to a pressure range of 85 – 90 Kg/CM^2. This highly pressurised gas termed as "Gas Lift Gas" is sent to oil wells equipped with Artificial Gas Lift technology. The remaining part of HP Gas is utilised to maintain the natural gas distribution grid pressure in the range of 14 – 16 Kg/CM^2. This distribution grid connects all the 19 nos. of GCSs of the company (Ref. Abstract) which helps to maintain the GL compressors' suction pressure to individual GCSs, gas pressure to OIL's in-house LPG plant at Duliajan and also to downstream industries in upper Assam.

Gas Management Services (GMS) Department of OIL works relentlessly to minimise the downtime of gas compressor packages for smooth running of the company's business.

It is a constant endeavour of OIL to keep looking for advanced equipment, procedures and services to minimise downtime of its reciprocating gas compressor packages and enhance their reliability, efficiency and life.

The Control Panel of a gas compressor package or any rotating equipment is the heart of the package, which imparts reliability, safety and troubleshooting functions to the package. The technology of the reciprocating compressors has not changed too much over the last few decades other than - materials of construction, operating speed and valve construction/design. However, due to the global digital revolution, the control panel design changed rapidly from pneumatic relay based control panels with pneumatic field instruments to online microprocessor based digital technology capable of remote monitoring and trending methodology for preventive maintenance solutions.

To keep up with the global scenario and also to obtain possible parameters for troubleshooting and preventive maintenance, the upgradation of the control system became a necessity.

OIL introduced reciprocating gas compressors for the already mentioned reasons since the 1970s. The journey has seen OIL introduce low speed integral compressors initially and moving on to separable high speed compressors from the early 1980s.

OIL currently possesses 126 nos. of high speed separable reciprocating gas compressor packages (118 nos. gas engine driven and 08 nos. electric motor driven) with compressors of reputed makes from around the globe.

As OIL's business grew, the constraints of using pneumatic control panels appeared more glaring (Ref. Section 2). OIL needed to increase the number of reciprocating compressors based on business demands and the upgradation of Instrument Panel technology in the incoming new compressor packages became a necessity for increasing reliability, availability, safety and better troubleshooting. The solution came in the form of ELECTRONIC CONTROL PANELS.

by: Baruah Prateek, Oil India Limited

2. Reasons and Challenges (Why and how the Electronic Control Panels were introduced)

2.1 Advantages of Electronic Panels against Pneumatic Panels

2.1.1 Availability of more parameters

The MMI screen embedded in the control panel (Ref. Figure 14 and 15) displays many more important parameters of a running gas compressor package, rendering it highly advantageous for the operator than "the pneumatic panels currently in use in OIL's reciprocating gas compressor packages". (Referred to as "pneumatic panels" from here on)

Figure 1: Recycle percentage display

Ref. Figure 1, the display of recycle percentage provides the operator with a clear picture of the current load condition of the Unit, thereby helping the operator to run the Unit at different load conditions as per requirement. Such an advantage is not available in pneumatic panels.

Ref. Figure 2, the display of compressor main bearing temperatures ("Bearing DE" and "Bearing NDE") is an advantage that helps the maintenance crew to monitor the condition of the bearings and experienced personnel can pre-emptively take corrective measures to prevent damage to bearings and compressor internals. Unavailability of such a parameter in pneumatic panels had always been a bane for the maintenance group.

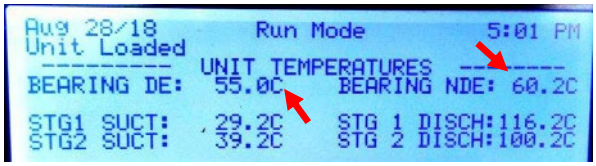

Figure 2: Bearing DE and NDE display

2.1.2 Advantage air? Or the lack of it!

Pneumatic panels require quality air with sustained pressure. This raises the need for air compressor infrastructure and associated operation & maintenance of the same. OIL already possesses air compressor infrastructure in all of its GCSs spending a sizeable amount of money in maintaining the same. The electronic panel on the other hand uses wires; hence requirements associated with air pressure are greatly eliminated. (The only air requirement in our compressor packages with electronic panels are - air required to keep the Engine fuel shut off valve open, functioning of Engine Governor and Compressor Recycle Valve apart from occasional Engine Starting Air requirement. This eliminated the need of additional air compressors for continued running of the new packages.) The electrical power supply infrastructure is already in place in all our GCSs. Hence the additional requirement was a mere extension of power to the panels and conversion of available 230V AC supply to 24V DC. The Switched Mode Power Supply (SMPS) that came integrated with the electronic panels' housings do this job (Ref. Figure 14). Hence, the 23 nos. of new packages installed with Electronic Panels did not require any air compression capacity enhancement in any of the GCSs.

2.1.3 No Lag!

Pneumatic panels suffer from unwanted response delay, especially when components being actuated with compressed air are at a significant distance. Reciprocating gas compressors at OIL's GCSs are exposed to fluctuation of suction and delivery pressures due to various reasons like simultaneous opening or closing of Time Cycle Controllers at Gas Lift Oil Wells, Well servicing activities like scrapping etc. We needed faster response from instrument panels to cater to varying pressure and load conditions. Electronic panels' functions are instantaneous and hence better equipped for such circumstances. It was, therefore, one of the primary reasons for going ahead with electronic panels. Ref. Figure 3, all important parameters like Engine Starting Air Pressure (START AIR), Fuel Gas Pressure to Engine (FUEL GAS) etc. are available without any lag.

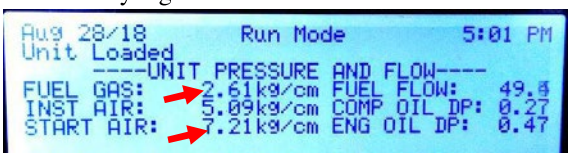

Figure 3: Display of parameters without lag

2.1.4 Accuracy and Alarm!

As pneumatic systems are powered by the force provided by compressed air, their operation is dependent on the volume of the compressed air. As the volume of air may change when compressed or when it undergoes a temperature change, the supply of air to the system may not be accurate, causing a decrease in the overall accuracy of the system. Electronic panels, devoid of such inherent problems, provide greater accuracy. All the critical parameters displayed in the MMI screen (Ref. Figure 4 displaying a few of the parameters) give a clear picture of the package's health and skilled personnel can anticipate forthcoming troubles and plan pre-emptive corrective measures accordingly.

In addition, prior to an eventual trip due to any parameter going beyond set limits, the corresponding parameter's alarm mode is displayed. (Ref. Figures 5 and 6, further elaborated during the presentation). Corrective measures may be scheduled while the Unit is still running and

by: Baruah Prateek, Oil India Limited

significant reduction of downtime is possible when one is armed with such information.

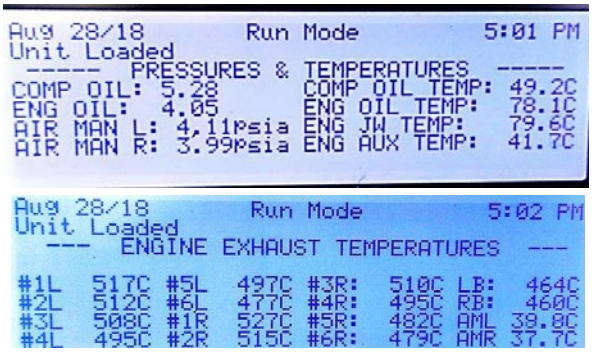

Figure 4: Accurate Critical parameters

Figure 5: Compressor running with alarm (1)

Figure 6: Compressor running with alarm (2)

2.1.5 Calibration: time is money!

Calibration of pneumatic instruments and switches is done in a designated lab of OIL's Instrumentation department located centrally in OIL's FHQ at Duliajan. The vastness of our operational area (mentioned in the abstract above) makes the process of calibration of pneumatic panels extremely time consuming with intertwined financial overheads, avoidable compressor downtime and production losses. Electronic panels being used by us provide the opportunity of password protected on-site setting changes, thereby allowing the flexibility to run the compressor packages as per site requirements. (Ref. Figure 7-A & B displaying a few of the settings).

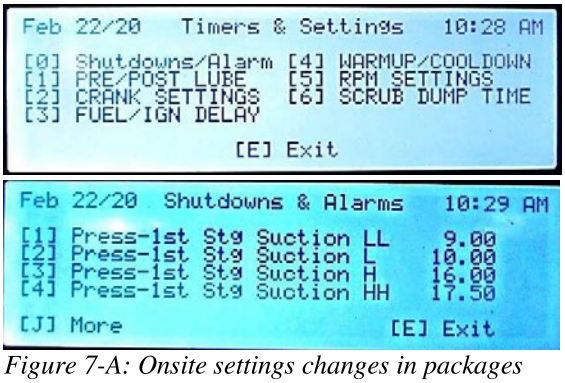

Figure 7-A: Onsite settings changes in packages

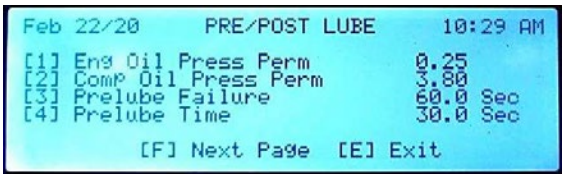

Figure 7: Onsite settings changes in packages

2.1.6 Growing electronics market

Growing market and availability of electronic spares is an added advantage that prompted OIL to switch to electronic panels.

2.1.7 Trip ambiguity

Pneumatic Panels in reciprocating gas compressor packages of OIL are equipped to display shut down flags in the event of shut down of a package pointing to the corresponding reason (Ref. Figure 8, further elaborated during presentation of the paper).

Figure 8: An example of Unit trip reason ambiguity in our pneumatic panels

However, after the shutdown of the package, due to decrease in the value of parameters like Engine Lube Oil Pressure, Compressor Lube Oil Pressure, Engine Water Flow and Compressor Lube Flow, the corresponding shut down flags of these parameters also may get displayed even when the Unit trips due to other reason and displays that corresponding other flag as well. Sometimes, the package may get tripped due to Engine or Compressor Lube Oil Pressure drop itself and these flags may pop up as shut down cause even then. As such, the trip reason mostly remains ambiguous unless any operator or maintenance crew witnesses the entire shut down event. Such a shortcoming creates confusion and almost always delays troubleshooting. On the other hand, Electronic panels show history of the unit via the History menu (Ref. Figure 9). The "First In Shutdowns" lists all the shutdowns encountered (Ref. Figure 10), The "Event History" notes down all the critical

by: Baruah Prateek, Oil India Limited

events like start, alarms and shutdowns and "Captured Data" takes a screenshot of the package parameters every 10 minutes. The available data may be accessed, downloaded and analysed for prompt and accurate preventive / breakdown / condition based / proactive maintenance of the package, thus helping to reduce Unit downtime.

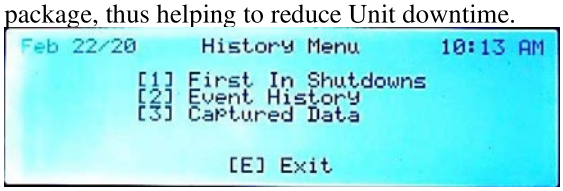

Figure 9: History Menu

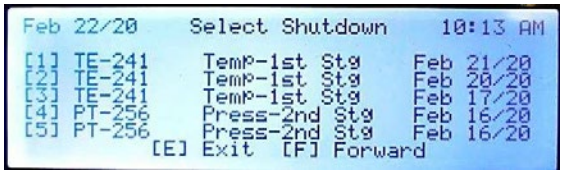

Figure 10: History of Shutdowns

Figure 11: Event History

Figure 12: Captured Data

2.2 Challenges galore!

2.2.1 The challenge of obtaining statutory approval

OIL's exploration and production activities are governed by Government of India's Mines Act 1952[2] whose provisions are laid down as per Oil Mines Regulations 1984[3] with its latest version declared in 2017. The statutory authority overseeing adherence to these regulations in industries governed by Mines Act across India is known as the Director General of Mines Safety (DGMS). Any electronic/ electrical appliance installed in designated Hazardous Area[3] needs to be approved by DGMS authorities. The process of obtaining the approval takes time which includes liaising with both the vendor as well as with the DGMS authorities. For OIL, the job in hand was to obtain an electronic control panel meeting the laid down safety norms.

In this regard, OIL took up the challenge from the beginning. During the first phase of procurement i.e. 10 nos. engine driven reciprocating gas compressor packages in 2009, OIL specified the need of field trial and DGMS approval certification of electronic control panels to prospective bidders in the tender stage itself. The selected vendor sent 1 no. of their electronic control panels for DGMS accredited lab testing and subsequent field trial in one of OIL's installations in 2011. The field trial was conducted for six months, during which DGMS authorities visited the site and gave their favourable comments. The successful approval process also helped in the ensuing procurement of an additional 13 nos. gas compressor packages which came equipped with already approved (by DGMS) electronic control panels. As of today, all the 23 nos. packages commissioned in between 2013 – 2018 in different GCSs of OIL are running successfully.

In addition, OIL also required corresponding electronic field instruments to comply with statutory safety norms. Hence, OIL took up the matter with all the reputed vendors around the globe for the additional approval of the field instruments viz. Pressure Transducers, Temperature Sensors, Pressure Switches, Differential Pressure Switches, Temperature Switches, No-Flow switches etc. Eventually, the process of field trial of those field instruments was carried out on the same unit where the control panel was also being tested. After lots of efforts of senior officials of OIL, the field trial was successful and the DGMS approval was obtained.

2.2.2 Challenge to arrange Quality Power and emergency back up

Co-ordinated efforts of all concerned sections and departments especially electrical department of OIL helped arrange the requisite power to the panels (Ref. Figure 14). The emergency backup is provided from the integrated battery panel (Ref. Figures 16 and 17)

2.2.3 The Human Challenge

Any industry, introducing new equipment or a system in its operation, faces its biggest hurdle while acclimatising its workforce to the new operating scenario. Operation, maintenance and instrumentation crew as well as concerned engineers of the company, were given extensive hands on training at all the electronic panel installation sites to acquaint them with the new panels. (Ref. Figure 13)

Figure 13: Onsite hands on training

by: Baruah Prateek, Oil India Limited

3. Technical Details of panel

3.1.1 Adaptability

The panels are compressor specific modular units fully-configurable to large or small compressors, screw or reciprocating compressors having either gas engine or electric prime movers.

3.1.2 No Programming shackles

Licensed programs are not required to communicate with the Control Panel. Any computer operating system based relevant "free to use" software may be used for settings configuration, programming and data downloading.

3.1.3 Retrofittable

The panels are ideal for both new and retrofit packages eliminating the need for an entire new package for installation of the panel. This also gives us the opportunity to replace older pneumatic panels with electronic ones in the future. However, the retrofitting has not been done in old Units yet.

3.1.4 Wide connectivity options, Industrial Internet of Things (IIoT) and security considerations:

Panel connectivity options include Local Area Network (LAN), Distributed Control System (DCS) and Ethernet. These electronic panels have built-in RS232 and RS485/422 ports. All that is needed to communicate with the system is a simple terminal program (examples withheld due to brand name constraints). The panels can be linked to a SCADA (Supervisory Control and Data Acquisition) system by using the Modbus Protocol. The transmission medium can be direct, modem, FM transmitter, MSat satellite, or any other comparable method. The recent SCADA system implemented by GMS Department in 70 nos. of installations of OIL can also be connected to our electronic control panels for data acquisition.

As far as security is concerned, IIoT usually has 3 potential hack points, viz. Cloud storage, network and the devices themselves. The data obtained from the panels are not yet stored into any cloud platform and also the network connectivity of the panels to remotely obtain real time data is not yet established. However, data stored in the panel can be obtained or altered as already mentioned in section 3.1.2. While carrying out such activities, adequately protected devices equipped with state of the art anti-malware programs are used to avoid data loss or data-theft. OIL also has a robust data security policy which guides all the network traffic within the company as well as for all types of communications with the outside world. A glimpse of the company's data security policy is available in the relevant webpage[4] in our company's website. The company's data security policy shall address the IIoT related security concerns whenever we decide to connect the panels remotely to networks or cloud storage.

3.1.5 OEM Reliability

Panels are built around a proprietary, PLC-Style Controller. The controller and all Input / Output (I/O) circuit boards are built by the OEM themselves.

3.1.6 Power Supply Requirement

Panels are fed with 230 V AC Power supply which is already available in our company's installations and a switched-mode power supply (SMPS) inbuilt in the panel circuitry converts it to 24 V DC which is the requirement of both panel and field instruments. (Ref. Figure 14). In the event of power failure, a battery pack provides emergency power back up for a duration of 4 hours. The batteries are recharged as the Units keep running. It is noteworthy that, the battery pack was installed on the skid itself which minimised the requirement of long cables and voltage drop inconveniences. (Ref. Figure 16 and 17).

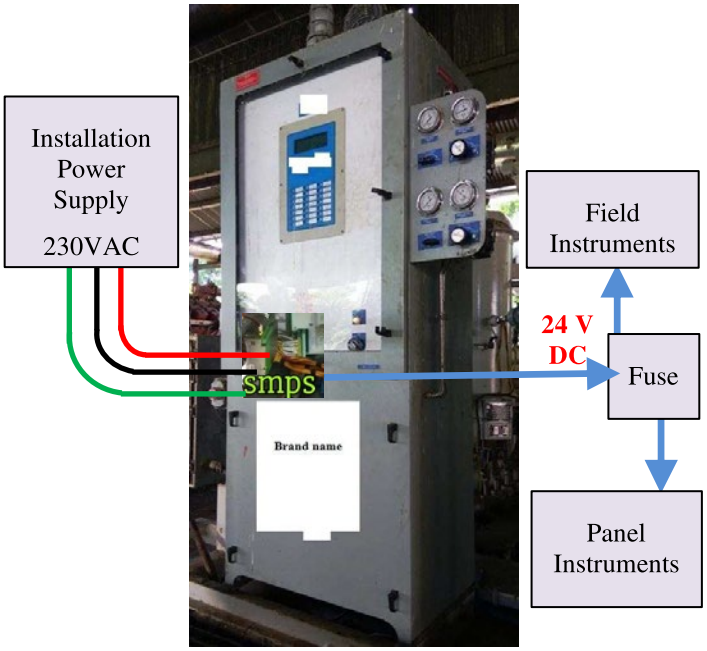

Figure 14: Power requirement and arrangement.(For SMPS, Ref. Figure 21, Sl. No. 5)

Figure 15: MMI Display Panel

by: Baruah Prateek, Oil India Limited

Figure 16: Panel housing with Battery Pack

Figure 17: Layout of Electronic Panel's Battery Pack (Cover opened and zoomed)

3.1.7 Capability:

Ref. Figures 18, 19, 20, 21, 22, 23 and 24, our electronic control panels monitor temperatures, pressures, levels and other signals, through smart analog and discrete (digital) Input/Output (I/O) boards. The system can handle a maximum of 192 I/Os. A digital I/O board has been detailed in Figure 22. Each analog board contains 16 channels and each digital board contains 12 channels that can be individually configured to accept different input types. Also 4 nos. PID loops can be configured in these panels. Currently only one of those PID loops (signal to the recycle valve for loading and unloading of the packages) is in use (Ref. Figure 1 and 23).

Various types of Inputs (to the Panel) possible are :

a) 4 to 20 mA (Example: From Pressure Transmitter, In-built Passive Sensor powered by 24V DC)

b) 0.5 to 4.5 V (Example: Manifold Air Pressure (MAP), In-built Passive Sensor powered by 24V DC). (Ref. Figure 18 (A & B))

c) Thermocouple Type J and K (Active Sensors, No power required, converts temperature to mV)

d) Resistive temperature devices (RTDs), (Also active sensor, coverts Temperature to resistance, **Ω**)

e) Discrete i.e. Digital signals from switches

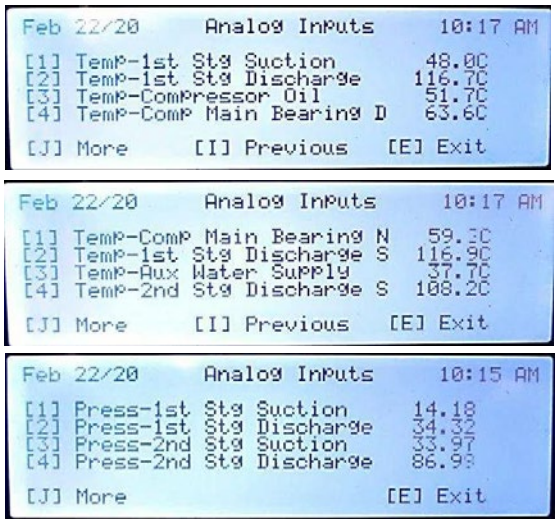

Figure 18 (A) : Analog Inputs in MMI display

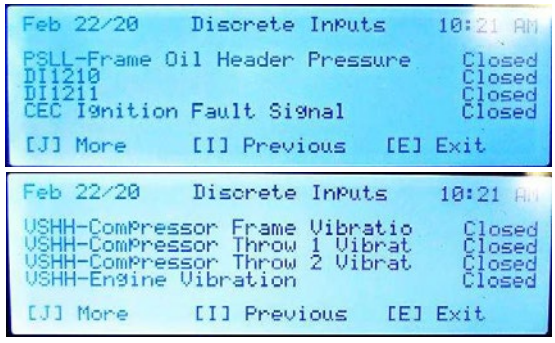

Figure 18 (B): A few Digital (Discrete) inputs showing in MMI Display

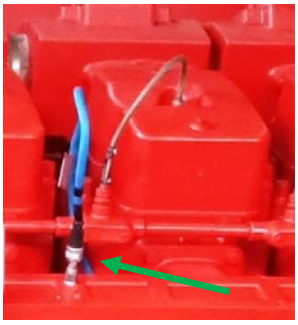

Figure 19: MAP Sensor

Figure 20: L.H.S: Digital Switch (to send inputs to digital boards), R.H.S: Pressure transmitter (to send inputs to Analog boards)

by: Baruah Prateek, Oil India Limited

3.1.7.1 The advantage with opportunity:

The availability of such a plethora of communication modes also open up the possibility for us to integrate independent third party monitoring systems for even more advanced data acquisition from the compressor packages to increase the reliability of the packages. (Also Ref. Section 3.1.4). OIL is already in the process of acquisition of such state of the art monitoring systems and continuously looks to upgrade to newer technology in that front.

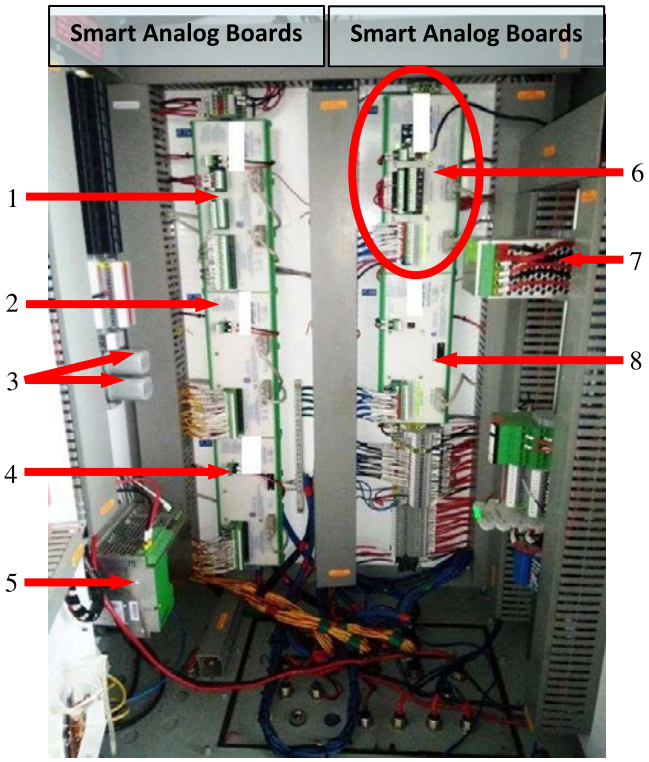

Figure 21: Layout of Electronic Panel's I/O Boards, 1. I/O Smart Analog Board [For Pressure, 14 Nos. 4-20mA & 2 Nos. 0.5-4.5 V] 2. I/P Only Smart Analog Board [For Temperature, Max 16 Nos. Output: Bypass Control] 3. Relay, 4. I/P Only Smart Analog Board [For Cylinder Exhaust Temperature, K type thermo couple, max. 16 Nos.], 5. SMPS (Ref. Figure 14) 6. I/O Digital Board [Input from digital switches, 12 Nos., Ref. Figure 22], 7. DC-UPS for battery charging (Ref. Figure 17), 8. Input Only Digital Board [8 Nos. Inputs].

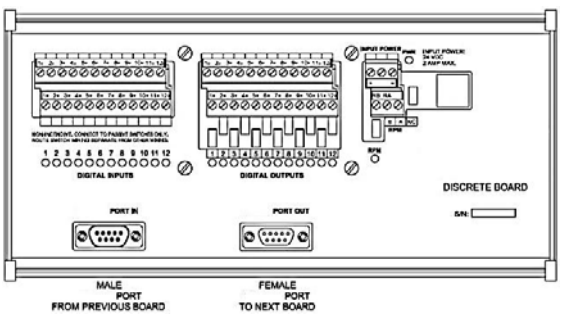

*Figure 22: Overview of Digital Input Output Board (**Inputs** : EMERGENCY STOP, REMOTE EMERGENCY STOP, 1ST Stg Suction Pressure, 1st Stg Discharge Pressure, 1st Stg Scrubber Level, 2nd Stg Scrubber Level, Lube Oil No Flow, 2nd Stg Discharge Pressure, Engine Jacket Water Level, Auxiliary Water Level, Engine Oil Level, Compressor Oil Level), **Outputs** : Ignition Module Powering Via Ignition Relay, Engine Fuel Signal To Solenoid Valve, Crank Signal To Solenoid Valve, Compressor Pre Lube Signal To Solenoid Valve, Engine Pre Lube Signal To Solenoid Valve, Panel Light-Alarm, Panel Light-Fault, Panel Horn)*

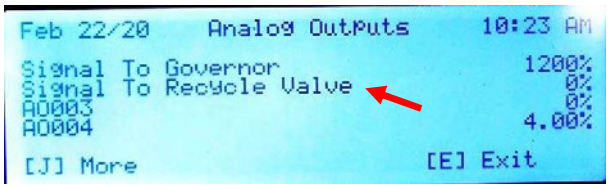

Figure 23: Analog Output Display in MMI

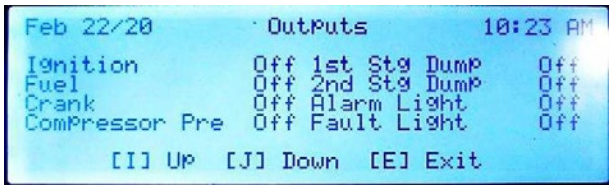

Figure 24: A few of the Digital Output Display in MMI

3.1.8 Explosion Protection :

These panels are Canadian Standards Association (CSA) certified for use in Class I, Division 2[5], Group C and D areas[6]. Based on this certification, DGMS provided the approval after lab testing and field trials under its watch. The same has been detailed in Section 2.2.1, which covers the methods and challeges faced during the approval process. These panels also conform to Atex directive 94/9/EC[7] (Latest Atex directive 2014/34/EU will be desirable by us for electronic panels that may come in the future). The harmonised European standards[8] that apply to these products are IEC 60079-0-6:2011, IEC 60079-10-1:2015, IEC 60079-14:2013, IEC 60079-15-4:2010 and most importantly IEC 60079-11-6:2011 (Equipment Protection by Intrinsic Safety). This renders the panels "instrinsically safe" and hence do not need explosion-proof enclosures as well as maintenance-intensive purging systems. (To be further elaborated during presentation of the paper).

4. Benefits:

Since introduction of electronic control panels in our company in 2013, we have been benefited in the following ways till the end of 2019 (Ref. Table 1- 6):

Table 1: Comparison of number of instrument control panel breakdown related reports resulting in Compressor downtime (Period: 2013 – 2019)

Instrument Panel Type	Number of Reports
All Instrument Panel Reports	921
All minus Electronic Panel Reports	839
Electronic Panel Reports	82

by: Baruah Prateek, Oil India Limited

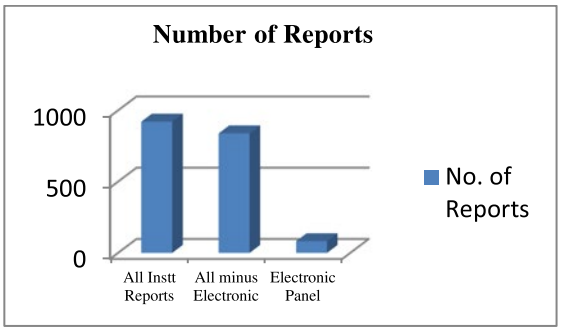

Table 2: Spares cost comparison while attending reports resulting in Compressor downtime (Period : 2013 – 2019)

Instrument Panel Type	Spares Cost (Million INR)
All Instrument Panel Reports	21.97
All minus Electronic Panel Reports	19.03
Electronic Panel Reports	2.93

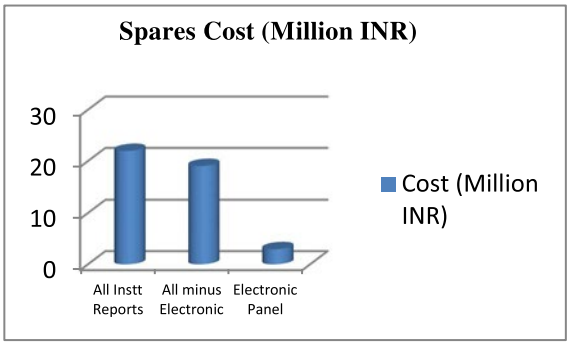

Table 3: Period Comparison: No. of Instrumentation Reports resulting in Compressor downtime

Period	No. of Instrumentation Reports
2005 - 2012	1963
2013 - 2019	921

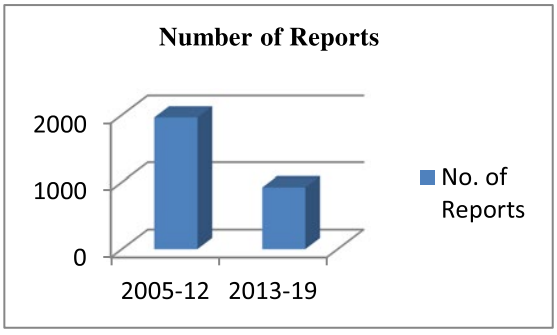

Table 4: Period Comparison vis-a-vis spares cost for Instrumentation Reports resulting in Compressor downtime

Period	Spares Cost (Million INR)
2005 - 2012	14.23
2013 - 2019	21.97

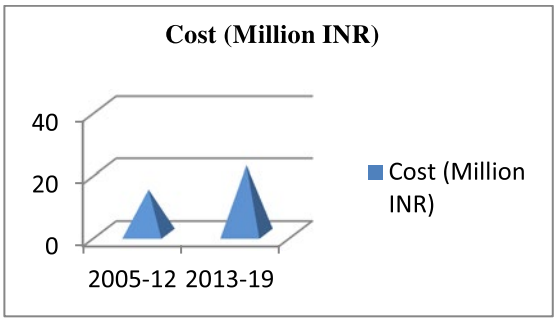

Table 4-A: Period Comparison vis-a-vis average spares cost per Unit for Instrumentation Reports resulting in Compressor downtime:

Period	Spares Cost (Average Per Unit in Million INR)
2005 - 2012	0.138
2013 - 2019	0.174

Table 4-B: Period Comparison vis-a-vis average spares cost per Unit with Pneumatic Panel vs Electronic Panel for Instrumentation Reports resulting in Compressor downtime:

Period	Pneumatic Panel Spares Cost (Average Per Unit in Million INR)	Electronic Panel Spares Cost (Average Per Unit in Million INR)
2005 - 2012	0.138	Not Applicable
2013 - 2019	0.184	0.127

Ref. Table 4, the increase in cost of instrument spares in between 2013 – 2019 compared to 2005 – 2012 is due to the following factors:

1. Gradual increase in number of Gas Compressor Units

2. Initial teething problems of Electronic Control Panel equipped packages with our existing infrastructure

3. Major breakdown problems of ageing pneumatic panels involving high cost of resurrection.

4. Revival of a few long Shutdown Gas Compressor Units requiring complete overhaul of pneumatic instrumentation panels with significant cost of overhaul.

However, from Table 4-B it is evident that, during the period of 2013- 2019, the average per Unit cost for electronic panels is significantly less the pneumatic panels.

Digging deeper into these comparisons, if we consider a period of 2018 - 2019, when all the 23 nos. of reciprocating compressor packages with electronic control panels were up and running and 10 of them had already served the business for 4-5

by: Baruah Prateek, Oil India Limited

years, then another picture is depicted. Let us see what is in store in this period:

Table 5: Comparison of number of instrument control panel reports resulting in Compressor downtime (Period: 2018 – 2019)

Instrument Panel Type	Number of Reports
All Instrument Panel Reports	312
All minus Electronic Panel Reports	278
Electronic Panel Reports	34

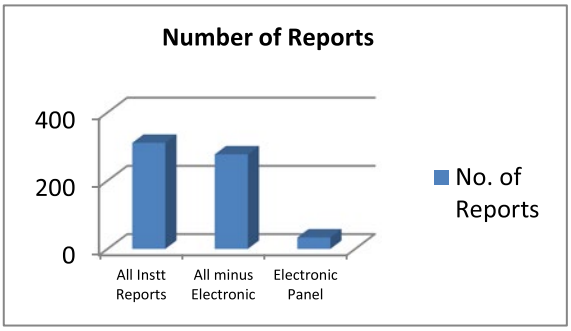

Table 6: Spares cost comparison while attending reports resulting in Compressor downtime (Period: 2018 – 2019)

Instrument Panel Type	Spares Cost (Million INR)
All Instrument Panel Reports	11.14
All minus Electronic Panel Reports	8.80
Electronic Panel Reports	2.34

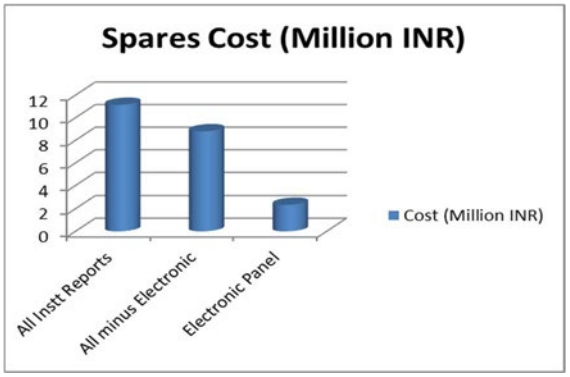

4.1 Benefits in Nominal Working Condition of the Plant:

The gas compressor packages installed with the electronic control panels come equipped with Low Suction Bypass Control for LPB compressors and High Delivery Bypass Control for GL compressors. Due to various operational reasons, whenever, the suction pressure of any LPB unit drops below a set value or the delivery pressure of GL unit rises above a desired value, then, based on PID (Proportional, Integral and Derivative) logic, the electronic panels send prompt and accurate signals to bypass the Unit from fully loaded condition to desired partial load conditions. This arrangement helps in auto-adjustment of load conditions of the compressors based on plant parameters, thereby improving the overall the plant functioning.

5. Conclusion

The above mentioned tabular and corresponding graphical representations clearly depict that, during the period of 2013 – 2019, Electronic Control Panels constitute only 8.9 % in terms of number of reports (Ref. Table 1) and 13.3 % in terms of spares cost (Ref. Table 2) as far as Instrument Panel Reports are concerned. Whereas, in the more recent past, i.e. during 2018 – 2019, the corresponding figures are 10.89 % in terms of number of reports (Ref. Table 5) and 21 % in terms of spares cost (Ref. Table 6). Table 4-B also makes it evident that the Cost/Unit in case of electronic panels is almost 31 percent less than its pneumatic counterparts. It is highly noteworthy that, not just in terms of spares cost, the reduction of number of reports in far flung installations have helped to reduce company's vehicle mileage, reduction of man hours, manpower remuneration / overtime expenditure and most importantly aided in sustaining production apart from reduction of avoidable gas flaring in those installations. The bottom line is - introduction of Electronic Control Panels in Engine Driven Reciprocating Gas Compressor Packages of Oil India Limited have significantly improved the reliability of the packages and this is always the sole aim of any reciprocating compressor maintenance group.

6. Acknowledgements

The author sincerely thanks Mr. Malay Kumar Das, Chief General Manager and H.O.D – GMS Dept (OIL) and Compressor Maintenance Section (GMS) for their invaluable guidance and help throughout this endeavour.

References:

1. https://www.oil-india.com/
2. http://www.dgms.gov.in/writereaddata/UploadFile/Mines%20Act,%201952.pdf
3. http://www.dgms.gov.in/writereaddata/UploadFile/Oil_Mines_Regulations-1984.pdf
4. https://www.oil-india.com/Web_Policies.aspx
5. https://www.csagroupuk.org/services/ex-product-certification-approvals/csa-north-american/definition-for-hazardous-locations-product-certification-in-north-america/
6. https://www.grainger.com/content/qt-hazardous-locations-124
7. https://ec.europa.eu/growth/sectors/mechanical-engineering/atex_en
8. https://www.iecex.com/publications/standards/

TNO innovation for life

Pulsation Damper Optimization with AI

by:

Jonah Poort, Can Tümer, Pejman Shoeibi Omrani
TNO, Heat Transfer and Fluid Dynamics
Delft, The Netherlands
jonah.poort@tno.nl; can.tumer@tno.nl; pejman.shoeibiomrani@tno.nl

12th EFRC CONFERENCE
August 24 – 26, 2021, Warsaw

Abstract:
Design of pulsation dampers in a reciprocating compressor system is critical from a pulsation or vibration risk mitigation perspective. An inadequate damper design may lead to high vibration levels and, eventually, to failures of the field piping and/or the compressor. Accordingly, requirements of a suitable pulsation damper design are covered in prevalent standards, such as the API 618 Std.
The common damper design workflow usually consists of two steps: (1) analytical (or rule-of-thumb) estimations of damper size based on relevant parameters (required flowrate, pressure ratio and gas properties), and, (2) final damper design, aided by established pulsation analysis software that complies with the requirements from API 618 Standard. The latter step is iterative with a lead time that is heavily dependent on the results of the former. Additionally, obtaining a decent damper size estimate in the first step is challenging (or impossible) for complicated cases where, for instance, a large range of capacity control options, gas compositions or process conditions needs to be evaluated.
This paper presents a machine learning approach which aims to combine the computational efficiency of the first step and the accuracy of the second, leading to shorter lead times and lower costs for damper design evaluations. The method involves the use of acoustic performance data from a large array of pulsation analysis calculations, a feature analysis that discusses the most influential features (or parameters) for the acoustic performance of a damper, and selection of an appropriate machine learning model that predicts resulting line or cylinder connection pulsation levels with a given dampers design.

by: Jonah Poort, Can Tümer, Pejman Shoeibi Omrani – TNO, Heat Transfer and Fluid Dynamics

1 Introduction

Reciprocating compressors, due to their non-continuous way of operation, generate high pressure pulsation levels. Pulsation dampers are commonly used to limit the transmission of these high pulsations into the field piping. If properly designed, a pulsation damper provides enough transmission loss such that the resulting shaking forces (and, subsequently, the vibration levels) in the system do not lead to failures. Although commonly done, pulsation damper design is not a trivial task;

- Acoustic performance of a damper is influenced by the spectral content of the generated pressure pulsations, which is a function of cylinder internals, valve properties, process conditions, gas compositions, capacity control options, etc.

- Bigger may not always be better for a pulsation damper. For instance, achieving the same damper volume with an increased length may lead to internal acoustic resonances. Under resonance conditions, transmitted pulsations to the field piping are amplified (by *orders*), degrading a damper's acoustic performance. As costs of a damper rise rapidly with increasing diameters, a trade-off has to be sought between manufacturing costs and acoustic performance.

- Dimensioning the cylinder connection is also not a straightforward task. During compressor design, the cylinder connection (nozzle) is usually kept longer to improve the manoeuvrability during maintenance periods. However, longer cylinder connections may also be susceptible to resonances similar to dampers. Additionally, a resonance in the cylinder connection also affects valve behaviour and may lead to an even more pronounced pulsation source.[1]

As such, finding the optimal damper design for any given pulsation source can be a slow process, requiring iteration over a multitude of damper sizes and repeated time-consuming acoustic response calculations until a design is found that satisfies the API 618 Standard.[2] Machine learning methods could significantly improve the computational efficiency of this process by replacing the relatively slow physics based numerical calculation methods with faster data-driven alternatives such as artificial neural networks (ANN) or support vector machines (SVM). This type of approach has previously been successfully implemented in a wide variety of applications.[3,4,5,6]

In this study, ANN were applied to represent the acoustic response within a reciprocating compressor/damper system. Neural networks were trained to predict pressure pulsation levels at the line connection of the damper as well as the cylinder connection flange. A data set of 100,800 acoustic simulations, generated using the TNO numerical pulsation simulation software Pulsim[7], was used for training the neural networks. The neural networks use (a minimal number of) input features that are causally connected to the acoustic properties in a given damper check system. When tested against the available data (all 100,800 cases), the trained model was found to perform with a *mean* absolute relative error of around 2 to 5.5% until the 8th harmonic. Furthermore, in order to confirm the logic of the trained models, a feature analysis was conducted to determine to what extent each of input feature contributed to the predictability of the neural networks. Lastly, the trained ANN models were also evaluated against actual case studies and were seen to perform reasonably well.

To the authors' best knowledge, the presented work is the first application of an artificial neural network on a pulsation damper check problem and the conducted acoustic feature derivation, in the way described in section 3.1, can be considered a novelty.

Section 2 briefly covers the working principles behind artificial neural networks. In section 3, algorithm development and methods used to train the different neural networks are explained. Results of the computational experiments are reported and discussed in section 4. Finally, conclusions on the current work and recommendations for future work are provided in section 5.

2 Artificial Neural Networks

An artificial neural network consists of a network of interconnected nodes called **neurons**, which are separated into multiple mutually exclusive layers (see Figure 1). Neurons in the first layer are part of the **input layer**, and are referred to as input neurons, or simply inputs, while neurons in the last layer are part of the **output layer** and called the outputs, all other layers in the network are called **hidden layers**. A neural network can have any number of hidden layers with a minimum of one.[8] Every neuron in a layer is connected to every neuron in the layer before it (unless it is an input neuron), and every neuron after it (unless it is an output neuron). These connections are shown as lines in Figure 1.

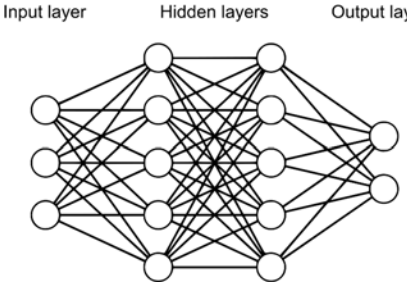

Figure 1: Schematic representation of a feedforward artificial neural network with two hidden layers containing five hidden neurons each, three input neurons, and two output neurons.

by: Jonah Poort, Can Tümer, Pejman Shoeibi Omrani – TNO, Heat Transfer and Fluid Dynamics

Every connection between node i in one layer and node j in the subsequent layer has a corresponding **weight** w_{ij} that determines the "strength" of the connection. In addition, the neurons themselves also have a corresponding "strength" called their activation A_j. For the input neurons, the activation corresponds to the input values to the problem. The input activation is propagated through the connections between the input layer and first hidden layer to the neurons in the next layer, which will each have their own activation value based on the values of the inputs and the weights of the connections. Weights can be positively-valued, increasing the activation of the next neuron, or negatively-valued, decreasing the activation of the subsequent neuron. The activation of the first hidden layer is similarly propagated to the next hidden layer through the connections between both layers. The final hidden layer propagates its activation values to the output layer; the activation of the output neurons corresponds to the output of the entire network. A network in which activation propagates in a single direction from input layer to output layer is referred as a feedforward network.[8]

In addition to weights, a neural network also contains so-called **biases**. Every neuron (apart from input neurons) has a corresponding bias, a constant valued parameter that is added to the activation of a neuron before an **activation function** is applied. The activation function determines the actual activation value of a neuron based on its bias and the activation propagated from the neurons in the previous layer. In mathematical terms, a neurons activation is calculated as follows:[8]

$$A_j = f_a\left(b_j + \sum_{i=1}^{n} A_i w_{ij}\right) \qquad (1)$$

where A_j is the activation of the current neuron j, b_j is its corresponding bias, A_i is the activation of neuron i in the previous layer, and w_{ij} is the value of the weight of the connection between the current neuron j and neuron i in the previous layer. It should be noted that both the values of bias and weight can be any real value, positive, negative, or zero. Each layer can have a different type of activation function $f_a(...)$. While the output layer often has no activation function applied to it, the activation function in the hidden layers should always be a non-linear function (and is usually kept the same for all hidden layers in the network). Without the introduction of non-linearities through the hidden layer activation function, a neural network can only model linear relationships, severely limiting its usefulness. Often used activation functions include the sigmoid function, hyperbolic tangent, and rectified linear unit (ReLU).[8]

Equation (1) shows that the output of a neural network depends entirely on its inputs, weights and biases; by properly tuning these weights and biases, any desired output can be realized for any given input. Given enough input-output combinations, weights and biases of a network can be tuned in such a way that they can emulate the underlying relationship that maps input to output (if one exists), and provide the correct output for all valid inputs in the problem domain. This is a mathematically proven concept called the universal approximation theorem of artificial neural networks.[9,10]

While it has been proven that an artificial neural network can approximate any continuous multi-variate non-linear function to an arbitrary degree of accuracy given enough neurons in the hidden layer, finding the weight and bias values that achieve this is far from trivial, and is done in a process called **training**. As the output of a network is a function of inputs, weights and biases, an optimization algorithm can be used to minimize the error between the desired output of the network and its actual output by tweaking the values of the weights and biases. This error is often referred to as the network's **loss**, and is determined by a loss function, which is the objective function of the optimization algorithm. Common loss functions are mean absolute error (MAE) and mean squared error (MSE).[11]

During training, a network is made to predict the output values for a large set of inputs with known outputs, and an optimization algorithm is used to determine the changes required to the weight and bias values in order to decrease the overall loss value determined by the difference between the *true* output values and the predicted output values.[8] Every step in which the network predicts output values, is given a loss value, and its weights and biases are updated, is called an **epoch**. The training process is repeated until either a desired loss value is achieved, or a maximum number of epochs is reached. In general, when more input-output examples are available to be used in the training process, a higher accuracy of the final network can be achieved.[11]

Once the "optimal" weights and biases of a network have been found, predicting outputs using the neural network has a computational burden based entirely on the size of the network and the type of activation function used; as these parameters will not change after training, the burden will remain fixed.

In the remainder of this document (and as is common in machine learning literature) inputs to the neural networks will be referred to as **features**, while outputs will be referred as **labels**.

3 Methodology

3.1 Data and Derived Features

Defining an "operational envelope" for a regression model (e.g. ANN) is challenging, especially when the variable space is as large as the design space of a common reciprocating compressor. Introducing this entire variable space (flow passage dimensions, process conditions, gas properties etc.) as features in an ANN would likely lead to a complex network, that is very computationally costly to train. Even if

by: Jonah Poort, Can Tümer, Pejman Shoeibi Omrani – TNO, Heat Transfer and Fluid Dynamics

one can afford to train such a model, it would be difficult to interpret the workings of this "black box" model and to have confidence in it. Deriving a reduced feature space can help alleviate both of these issues. The aim of this section is to highlight quantities that define the acoustic response of a compressor/damper system and to determine their respective mathematical definitions as features for the ANN model. In this way, all acoustically relevant quantities in a compressor/system (from gas compositions to flow passage sizes) can be projected to the features of the ANN model. Furthermore, if appropriately normalized, the derived features could be used to extend beyond the range of the dataset that is used to train the model.

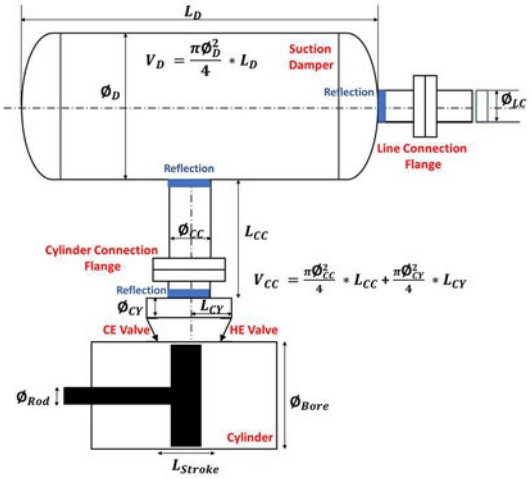

Figure 2: Relevant dimensions in a compressor damper system.

A sketch of a compressor/damper system can be seen in Figure 2. The interaction of the following quantities determine the acoustic response of a compressor/damper system:

- **Pulsation Source**: The mass flowrate that is generated by the cylinder (Q), illustrated in Figure 3 as a time series, is the generator of pressure pulsations in a recip. compressor. Coupled with characteristic specific acoustic impedance, i.e. gas density (ρ) and speed of sound (c), one can approximate the acoustic pressure that a compressor generates at the cylinder passage with:

$$\tilde{P} \propto \rho\, c\, \frac{Q}{A_{CY}} \propto \rho\, c\, u_{CY} \qquad (2)$$

where, A_{CY} is the cross-sectional area of the cylinder passages downstream the valves. In order to facilitate the analysis, $\frac{Q}{A_{CY}}$ is simplified to u_{CY}; time-averaged flow velocity during suction/discharge events. To describe the pulsation source amplitude, ρ, c and u_{CY} are chosen as features for the ANN models, while normalized in the range seen in Table 1.

The overall mass flowrate (Q) can be calculated via volumetric efficiency (η), the swept volume (SV) and the compressor speed (RPM).

$$Q = \eta * \rho * SV * \frac{RPM}{60} \qquad (3)$$

$$\eta \propto \left[1 - CV * \left(P_R^{1/\gamma} - 1\right)\right] \qquad (4)$$

Neglecting any leakages, volumetric efficiency (η) is a function of the relative clearance volume (CV), pressure ratio (P_R) and the gas' polytropic exponent (γ). For values above ~50%, volumetric efficiency is negatively proportional with the sudden rise identified in Figure 3. Since the extent of this "climb" is a major contributor to pulsation amplitudes at multiples of the compressor speed, volumetric efficiency (η) is selected as a feature to help characterize the frequency content of the pulsation source. The used capacity control scheme also has considerable effect on the frequency content of a pulsation source. A reciprocating compressor operating at 100% load gives dominant pulsation levels at even multiples of the compressor speed, whereas with valve lifting, dominant pulsation frequencies shift to odd multiples. Accordingly, a categorical variable, f_2, is identified as a feature indicating whether the compressor is functioning at 100% load or a part load (e.g. single acting crank end).

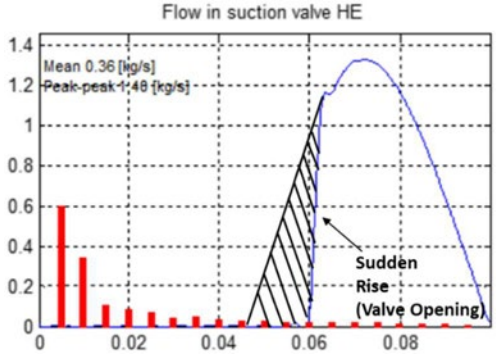

Figure 3: A *suction flow pulse (blue) and the loss of efficiency (black, hatched)*[1]*. Y-axis denotes the flow pulsation levels (in kg/s) and X-axis refers to time (one crank revolution) for the blue line.*

- **Volumes (Acoustic Compliance)**:

Volumes of both the damper and the cylinder connection contribute to the system's acoustic compliance. Instead of using these volume definitions as features in ANN, it is beneficial to normalize them against a meaningful quantity; an estimate of the required damper volume (V) that reduces the residual pressure pulsations at the line connection to the API piping allowable pulsation levels (e.g. $\tilde{P}_{API,1}$, line connection allowable level at the 1st harmonic of the compressor speed). (V) can be derived using electro-acoustic analogy, with the help of acoustic impedance ($|Z|$) of a volume connected to an infinitely-long pipe (with area A_{LC}).[7]

$$|Z| = \frac{c}{\sqrt{{A_{LC}}^2 + \left(2\pi \frac{RPM}{60}\right)^2 \frac{V^2}{c^2}}} \propto \frac{Q}{\tilde{P}_{API,1}} \qquad (5)$$

by: Jonah Poort, Can Tümer, Pejman Shoeibi Omrani – TNO, Heat Transfer and Fluid Dynamics

$$V \propto \frac{c}{2\pi\frac{RPM}{60}} \cdot \sqrt{c^2 \cdot \left(\frac{Q}{\tilde{P}_{API,1}}\right)^2 - {A_{LC}}^2} \qquad (6)$$

$$\tilde{P}_{API,n} = \sqrt{\frac{c}{350}} * \frac{400}{\sqrt{P * \emptyset_{LC} * n * \frac{RPM}{60}}} \qquad (7)$$

API allowable piping pulsation level ($\tilde{P}_{API,n}$) at a given harmonic (n) can be calculated with equation (7), where P is the static pressure (in bar) and $\emptyset_{LC}$ is the line connection inner diameter (in mm). In equations (5) and (6), mean mass flowrate (Q) is used instead of peak-to-peak to simplify the definition of the flow pulse. The following two features, normalized volumes of damper (f_3) and cylinder connection (f_4), are used as input in the ANN.

$$f_3 = \frac{V_D}{V}, \qquad f_4 = \frac{V_{CC}}{V} \qquad (8)$$

- **Resonances:**

  For a compressor/damper system, acoustic resonances mostly occur in either the pulsation damper and/or the cylinder connection (between compressor valves and pulsation damper). Both resonance conditions can be calculated analytically as a function of the acoustic wavelength (λ). Best results with ANN were obtained by identifying "the closest distance to resonance mode" as features for each harmonic (n) individually. Distance to resonance patterns can be described by half-wavelength and quarter-wavelength patterns for the damper ($f_{5,n}$) and for the cylinder connection ($f_{6,n}$) respectively. In Figure 4, the behaviour of these two features is illustrated.

$$\lambda_n = \frac{c}{\frac{RPM}{60} * n} \mid n \in \mathbb{N} \qquad (9)$$

$$f_{5,n} = \min\left(\left|\frac{L_D}{k * \frac{\lambda_n}{2}} - \frac{k}{2}\right|\right) \mid k \in \mathbb{N} \qquad (10)$$

$$f_{6,n} = \min\left(\left|\frac{L_{CC} + L_{CY}}{(2k-1) * \frac{\lambda_n}{4}} - \frac{2k-1}{4}\right|\right) \mid k \in \mathbb{N} \qquad (11)$$

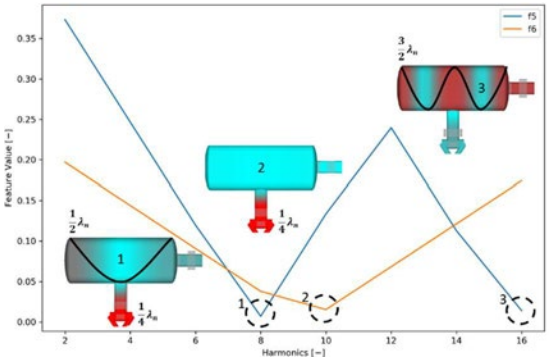

Figure 4: $f_{5,n}$ and $f_{6,n}$ as a function of harmonics. A value of zero indicates resonance condition.

- **Reflection Coefficients:**

  The acoustic energy that is generated at the compressor cylinder (valves) travels through the system as pressure waves. There are three main acoustic reflectors in a compressor/damper system; diameter change between cylinder flow passages and cylinder connection piping (f_7), diameter change between the cylinder connection piping and pulsation damper (f_8), and diameter change between pulsation damper and line connection (f_9). Reflection coefficients at these three points can be estimated by;

$$f_7 = \frac{{\emptyset_{CY}}^2 - {\emptyset_{CC}}^2}{{\emptyset_{CY}}^2 + {\emptyset_{CC}}^2} \qquad (12)$$

$$f_8 = \frac{{\emptyset_{CC}}^2 - {\emptyset_{D}}^2}{{\emptyset_{CC}}^2 + {\emptyset_{D}}^2} \qquad (13)$$

$$f_9 = \frac{{\emptyset_{D}}^2 - {\emptyset_{LC}}^2}{{\emptyset_{D}}^2 + {\emptyset_{LC}}^2} \qquad (14)$$

In order to sufficiently cover the defined features with data points, the following (100,800) suction side "damper check" cases (see illustration on Figure 5) were modelled and simulated with Pulsim;

- Design flowrates ranging from 1 kg/s to 5 kg/s are considered in the analysis. Depending on these design flowrates, the compressor cylinder, compressor/valve flow passages and cylinder/line connection nozzles were sized to comply with a limit on dynamic pressure (a rule of thumb value of 500 Pa) during the modelling of each data point. Due to the large effect of cylinder connection diameter on acoustic response, 2 additional cylinder connection diameters (50% smaller and larger) are also included in the dataset.
- Two pressure ratios were considered, 2.5 (10 bara to 25 bara), and 3 (20 bara to 60 bara).
- The following capacity control measures were investigated; compressor speeds ranging from 240 RPM to 600 RPM (in 4 steps), in combination with valve lifting at the head end (single acting crank end, SACE) as well as regular 100% (full load).
- Three different clearance volumes were explored; 10%, 20%, and 30%.
- For each case, a "sufficient damper volume" (V) is estimated as per equation (6) and 5 different damper volumes are covered at 10%, 50%, 100%, 150% and 300% of this volume. On top of the damper volume, different damper aspect ratios (diameter divided by length) are also investigated in 4 steps, ranging from 2 to 5. The chosen damper geometry is symmetric with line connection on the cap and cylinder connection in the middle.
- 7 different gas compositions, included in the current analysis, were pure methane, pure

by: Jonah Poort, Can Tümer, Pejman Shoeibi Omrani – TNO, Heat Transfer and Fluid Dynamics

nitrogen, pure hydrogen, Dutch grid gas, and three admixtures of grid gas with hydrogen (10%, 20%, and 30%). Hence, covered molecular weights range from 2 to 28 g/mol.

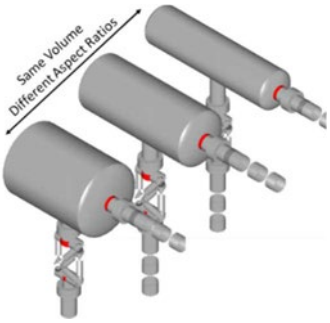

Figure 5: Aspect ratio changes for a given volume.

Resulting feature distributions within the dataset are plotted from Figure 6 to Figure 8, and their statistical identifiers are listed in Table 1. The generated dataset contains predominantly non-resonant values at the first harmonic $f_{5,1}$ and $f_{6,1}$; high mean values, relatively high kurtosis and negative skewness. As frequency increases, however, distributions favour resonance conditions considerably more, as suggested by the drop in mean values and kurtosis. This trend is expected (and welcomed), as wave-lengths at the first few harmonics are usually too large to fit into damper or cylinder connection dimensions of currently operating reciprocating compressors. Furthermore, absolute reflection coefficients at inlet (f_8) and outlet (f_9) of the damper shows a mean value of approximately 0.75, suggesting that on average, damper diameter is 3 times as large as line or cylinder connection diameters in the analysed dataset.

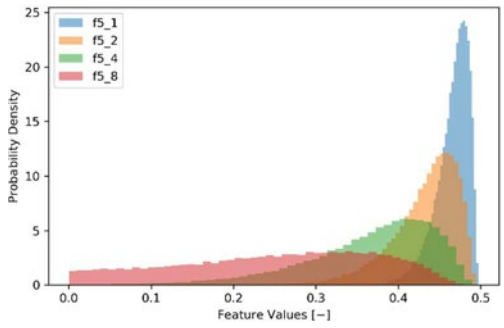

Figure 6: Probability density distribution of resonance feature $f_{5,n}$.

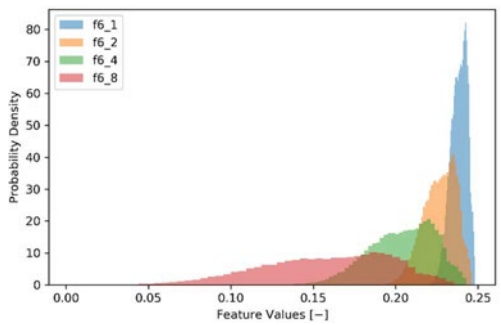

Figure 7: Probability density distribution of resonance feature $f_{6,n}$.

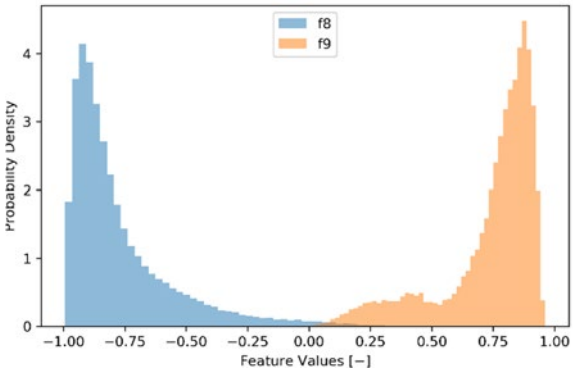

Figure 8: Probability density distribution of reflection features f_8 and f_9.

Table 1 – Statistical identifiers of the resulting feature distributions.

	Min. - Max.	Mean (μ)	Std. Dev. (σ)	Skew (γ)	Kurtosis (β_2)
η	0.60 - 0.91	0.77	0.10	-0.22	-1.14
ρ	0.80- 22.36	9.42	5.51	0.50	0.05
c	355 - 1341	568.66	318.65	1.95	1.94
u_{CY}	0.93 - 100.2	13.03	16.04	2.87	10.74
f_2	0.00 – 1.00	0.50	0.50	0.00	-2.00
f_3	0.04 - 3.34	0.83	0.76	1.34	1.26
f_4	0.00 - 0.14	0.03	0.02	1.37	1.61
$f_{5,1}$	0.36 - 0.50	0.47	0.02	-1.13	1.42
		…			
$f_{5,8}$	0.00 - 0.48	0.25	0.12	-0.29	-0.92
		…			
$f_{6,1}$	0.22 - 0.25	0.24	0.00	-0.44	-0.33
		…			
$f_{6,8}$	0.00 - 0.24	0.16	0.04	-0.44	-0.33
		…			
f_7	-0.64 - 0.33	-0.19	0.40	0.36	-1.55
f_8	-0.99 - 0.00	-0.77	0.20	1.89	3.89
f_9	0.01 - 0.96	0.74	0.20	-1.50	1.46

For each data point (viz. damper check case), the following 17 quantities are extracted and used as labels in the ANN:

- $\tilde{P}_{LC,n}$: Pressure pulsation amplitude (in Pa peak-to-peak) at the line connection for the 1st to 16th harmonics (n).
- $\tilde{P}_{CC}$: Overall pressure pulsation level amplitude (in Pa peak-to-peak) at the cylinder connection flange.

The complex interplay between the derived features and labels are visible in Figure 9, where so-called Pearson correlation coefficients are plotted between the derived features and the line connection pulsation levels at 4 dominant harmonics in a full load operating system. Here, a negative value

by: Jonah Poort, Can Tümer, Pejman Shoeibi Omrani – TNO, Heat Transfer and Fluid Dynamics

indicates a negative correlation between the feature and label and a positive value indicates the opposite. Clear relationships exist for almost all features except the speed of sound (c) and harmonic dependent features that describe resonance conditions ($f_{5,n}$ and $f_{6,n}$, denoted as f_5* and f_6* in Figure 9, respectively). Considering equations (2), (10) and (11), the shift of the correlation coefficient to negative values at higher frequencies (lower values for f_5 and f_6) imply stronger influence of resonance conditions as opposed to the pulsation source. The presented positive correlation coefficient values for f_5 and f_6 suggest that a majority of the dataset consists of non-resonant conditions, as illustrated in Figure 6 and Figure 7. The fact that f_6 is smaller than f_5 can be attributed to the relatively higher amplification of pulsation levels during a cylinder connection resonance, as explained in Section 1.

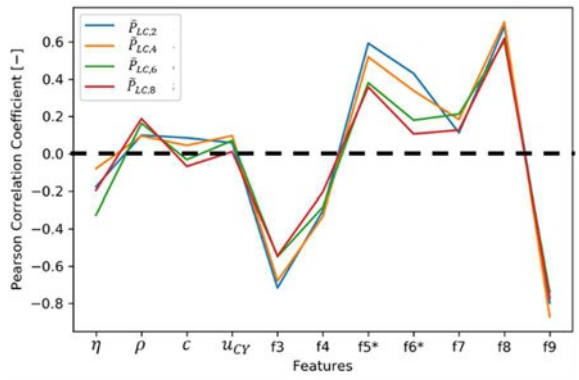

Figure 9: Correlation between used features and line connection pulsation levels, for full load cases.

In order to standardize the data whilst training the networks and to avoid introducing any bias based on the absolute values of the features, all features were scaled to the interval [0, 1] before training.

3.2 ANN Model Definition and Training

Initially, it was decided to predict all labels for all harmonics with one single network using the entire dataset at once. This decision was made in order to streamline the process of training the ANN and the trial of different hyperparameter combinations. However, initial results indicated that splitting the resonance related features ($f_{5,n}, f_{6,n}$) and training individual neural networks for each harmonic (n) could potentially increase accuracy, as well as reduce the complexity of the networks.

Furthermore, the cylinder connection pulsation levels were not found to be sensitive to $f_{5,n}$, and therefore, the damper resonance related features ($f_{5,n}$) were omitted for the prediction of the cylinder connection pulsation level.

An overview of features and labels for each trained ANN is listed in Table 2.

Table 2 – ANN and their labels and features.

# ANN	Label	Features
1	$\tilde{P}_{LC,1}$	$\eta, \rho, c, u_{CY}, f_2, f_3, f_4$ $f_{5,1}, f_{6,1}, f_7, f_8, f_9$
2	$\tilde{P}_{LC,2}$	$\eta, \rho, c, u_{CY}, f_2, f_3, f_4,$ $f_{5,2}, f_{6,2}, f_7, f_8, f_9$
...		
17	$\tilde{P}_{CC}$	$\eta, \rho, c, u_{CY}, f_2, f_3, f_4$ $f_{6,1}, \dots, f_{6,16}, f_7, f_8, f_9$

The Python neural network library Keras (version 2.3) was used with Tensorflow backend during the analysis. Out of the generated (100,800) data points, 80% were used in the training and the rest were used for testing. A brief manual hyperparameter analysis was conducted to find the optimal settings of the learning algorithm;

- Optimization algorithms, *rmsprop*, *adam*, *adagrad* and *adamax* were explored and *adam* with *amsgrad* option was found to be the best performing.
- Learning rates of 0.001 to 0.1 were evaluated and a learning rate of 0.001 was found optimal.
- Satisfactory results were obtained with 3 hidden layers and 250 neurons for each layer. The use of fewer layers were seen to rapidly degrade the regression performance (R^2) and a higher number of layers were not chosen to avoid overfitting, albeit at the cost of the R^2 value.
- *ReLU* was used as the activation function.
- Number of epochs were set to 1000 and an early stopping criterion (*patience* of 25 epochs) was used to avoid overfitting.

With these presented settings, the training of the model took no more than approximately 10 minute for each individual ANN on a PC with Intel i7 CPU, with no GPU acceleration.

4 Results and Discussion

In Figure 10, the regression performance of the neural networks can be seen as a function of all available data points. An R^2 value of at least 0.963 (at the 16th harmonic) was achieved for all trained ANN. The R^2 value was found to reach as high as 0.999 in the prediction of the line connection pulsation levels ($\tilde{P}_{LC,n}$) at the 1st and 2nd harmonics. At the second harmonic, the predictions have a *mean* absolute relative error of 2% and a *maximum* absolute relative error of 15%. The R^2 value is seen to drop at higher orders of the compressor speed, however, *mean* absolute relative error does not go beyond 6% for the first 8 harmonics. Upon closer inspection, all identified cases with highest *maximum* absolute relative errors have derived features which lie at the edges of the feature spaces

by: Jonah Poort, Can Tümer, Pejman Shoeibi Omrani – TNO, Heat Transfer and Fluid Dynamics

and are cases with resonances in the damper and/or the cylinder connection.

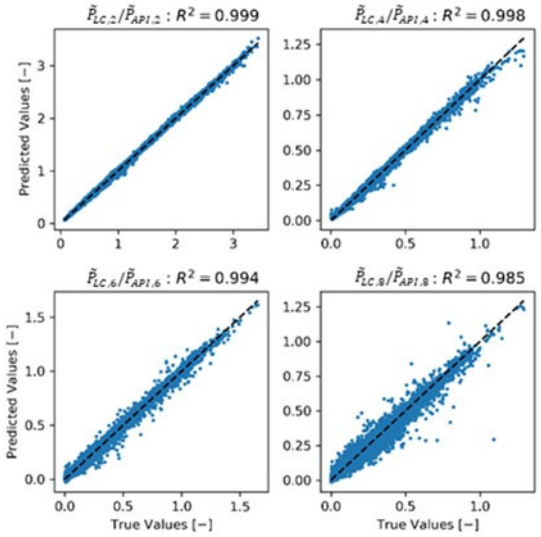

Figure 10: True vs. predicted values normalized by API piping allowable levels (blue) and ideal regression (black dashed) for harmonics 2 to 8.

The prediction for the pulsation levels at the compressor flange show an R^2 value of 0.98. The *mean* absolute relative error was 4.5%; however, a *maximum* absolute relative error of around 40% was reached for a case with *multiple* resonant frequencies at the cylinder connection (a nitrogen duty at the highest considered speed of 600 RPM). The limited coverage of the cylinder nozzle resonance feature space in the training dataset (see f_6 in Figure 7) is thought to be the reason of the poor performance of the ANN for the case with maximum absolute relative error.

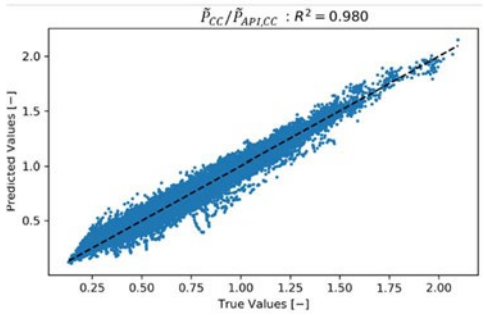

Figure 11: Scatter plot (blue) of true vs. predicted values (normalized by API compressor flange allowable levels) and ideal regression (black dashed) in a full load compressor.

Next, a feature analysis was done in order to gain insight into which features contribute the most to the predictions made by a machine learning model. Feature analysis is often used to verify the trustworthiness of a model by comparing whether the features that are considered important or unimportant by the model are in line with what would be expected from a physical perspective.

The feature importance method used in this study is a relatively straight-forward global "variance importance analysis"[12] method that estimates the relative importance per input. This is done by going through each input feature, creating a new dataset in which the current feature is varied by stratified sampling while all other features are kept constant. The predictions on the new dataset are compared to predictions on the original dataset that contains no changes. The difference between the new predictions and original predictions is, then, used to determine the relative importance of the current feature; a larger difference in output predictions indicating a larger relative importance. The results of the feature analysis is presented in Figure 12 for both the 2nd and 8th harmonics. Intuitively, while going from the 2nd to the 8th harmonic, the emphasis is seen to shift from pulsation source and damper capacitance (f_3, f_4) to resonance conditions (f_5, f_6) and reflection coefficients (f_7, f_8, f_9). The reduction in f_5 with the 8th harmonic implies that the predictions are not as sensitive to resonances in the damper. This could be attributed to either the relatively less frequent occurrence of a cylinder connection resonance as compared to a damper resonance (see Figure 6 and Figure 7) and/or to the higher severity of a cylinder connection resonance, as explained in Section 1.

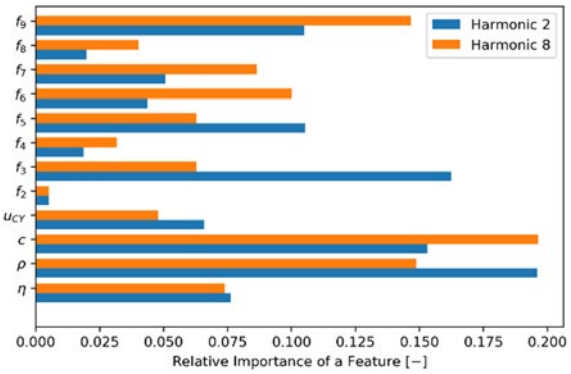

Figure 12: Changes in feature importance at higher orders of the compressor speed.

Two additional cases, outside the presented dataset (of 100,800 artificially created cases), were used to further test the trained model, outside of its "comfort zone". These cases are introduced in Figure 13 and

Figure *15*. Design flowrates and pressure ratios of both of these compressors are outside the range of the training dataset. Additionally, the first case has a slightly higher suction pressure than what was considered within the training data set.

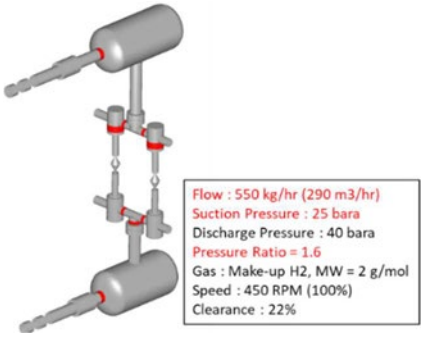

Figure 13: Make-up gas (H_2) compressor test case.

by: Jonah Poort, Can Tümer, Pejman Shoeibi Omrani – TNO, Heat Transfer and Fluid Dynamics

In Figure 14, the predicted pulsation levels at the suction side line connection and the compressor flange are compared with the true values. It is seen that the pulsation levels were overpredicted by around 10% for the 2nd harmonic at the line connection and 5-10% for the overall pulsation level at the compressor flange. These values comply with the reported *maximum* absolute relative errors from testing against training data, i.e., 15% at 2nd harmonic.

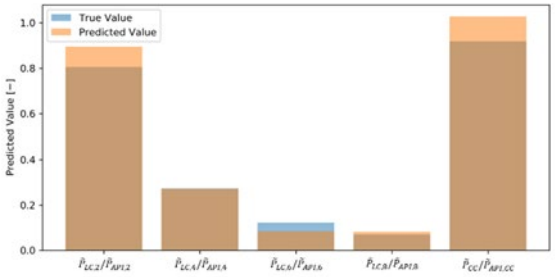

Figure 14: Predicted (orange) vs true (blue) values at the nominal speed of sound.

The results of the second test case can be found in Figure 16, in the form of a sensitivity analysis for the speed of sound. With this case, one can take a critical look at the trained ANN's ability to capture changes in the acoustic response as a function of the speed of sound. Performing a speed of sound sweep is a common technique, where the aim is to evaluate the performance of the damper also for slight changes in process conditions and/or gas compositions. A side goal of this case is to also identify any possible indication of overfitting. If the trained model has overfitted its data points, then continuous trends as seen for the 2nd harmonic cannot be captured well.

From Figure 16, it can be concluded that the predictions of pulsation levels capture the changes as a function of speed of sound reasonably well. At the 2nd and 4th harmonics, a *maximum* relative error of around only 5% is reached. At the 8th harmonic (plotted in blue), however, the overall trend is captured but not the "nuances"; the ANN is too simple to represent the climb of the 8th harmonic line connection pulsation level between -20% to -5%.

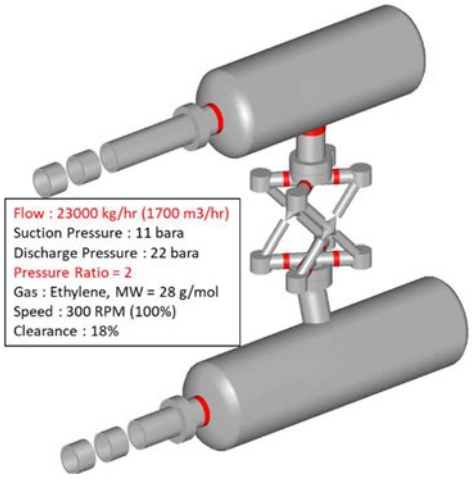

Figure 15: Ethylene compressor test case.

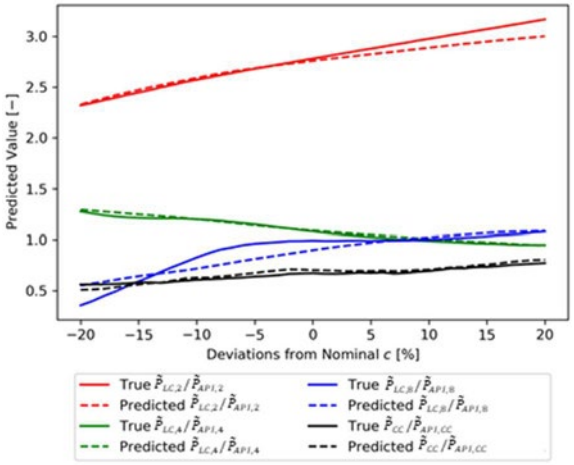

Figure 16: Predicted (dashed) vs true (solid) values from a speed of sound sweep around the nominal value, at 0%.

A final comparison between acoustic simulations and ANN predictions can be made on computational speed. The creation of the training dataset (100,800 points) took the TNO High Performance Cluster (Intel Xeon CPU's, parallelized to around 80 cores at a given time) around a week to calculate. In comparison, while plotting Figure 10 and Figure 11, predictions were made on the same (entire) dataset under 10 seconds on a machine with an Intel i7 CPU.

5 Conclusions and Outlook

From an acoustic perspective, pulsation damper design is a critical step in the protection of a reciprocating compressor system. Currently, pulsation damper (optimization) is done through the evaluation of manually drafted designs with a trial and error approach. The iterative nature of this process requires time consuming acoustic response calculations and usually results in long lead times.

In this paper, artificial neural networks (ANN) were applied to represent the acoustic response within a reciprocating compressor/damper system. The conclusions of the study are as follows:

- Due to the large variable space that is a characteristic of reciprocating compressors, a thorough analysis of ANN features is necessary. Hence, a bare minimum set of features were derived that describe the acoustic response of the compressor/damper system. This reduced dimensionality helps increase the validity range, the computational speed and the interpretability of the used ANN. At later stages, it was found that regression errors are more pronounced at higher harmonics. The current set of defined features does consider a representation of the acoustic resistance, that generates acoustic damping, with (ρ) and (u_{CY}), but does not take into account the spatial distribution of those resistances which play a large role in the damping at higher order modes/frequencies.

by: Jonah Poort, Can Tümer, Pejman Shoeibi Omrani – TNO, Heat Transfer and Fluid Dynamics

- A large range (100,800 data points) of acoustic simulations were performed to generate training data for the ANN. These data points were chosen to cover a wide range of design features (from design flowrates to gas properties and damper geometries) and can be considered representative of a considerable portion of the current class of reciprocating compressor systems. A more comprehensive dataset may include more complicated damper geometries with asymmetric and/or multiple cylinder connections and internals, as illustrated in Figure 17.

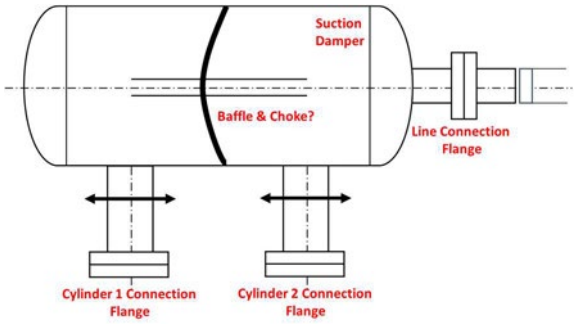

Figure 17: A complicated pulsation damper design.

- The ANN model shows good convergence when tested against its own training and test data. Especially at lower harmonics of the compressor speed, R^2 values reach above 0.99. The accuracy was found to decay with increasing orders of the compressor speed with a lowest computed R^2 value of 0.96, at the 16th harmonic of the compressor speed. This degradation of performance can be associated to the limited occurrence of resonant conditions at the cylinder connection for the data set and/or the inadequate coverage of acoustic damping in the derived features.
- A feature analysis was conducted to verify the interpretability of the ANN ("Can we open the black box?"). The designed ANN was found to capture the shift in importance from pulsation source to resonance conditions when increasing orders of the compressor speed.
- Tested against two real use cases, the developed ANN performed reasonably well. In both cases, the *maximum* absolute relative error was found to reach not more than 10% at relevant harmonics. For the second test case, predictions also captured the evolution of pressure pulsation levels within a speed of sound sweep.
- As expected, from a computational speed perspective, ANN runs orders faster compared to an acoustic simulation.

The point of departure of this work was to check the feasibility of replacing physical (acoustic) models with computationally efficient ANN without compromising on accuracy. The developed ANN delivered promising results with respect to both of these considerations. However, more extended testing (and scrutiny) is needed to develop insight/confidence in before it can be considered for operational use.

References

[1] Van Lier, L., & Smeulers, J. (2018). Identification and mitigation of Cylinder Gas Passage Pulsations. 11th EFRC Conference Proceedings, 128–138.

[2] API Standard (2007), API 618 Reciprocating Compressors for Petroleum, Chemical, and Gas Industry Services. 5th Ed.

[3] Krasnopolsky, V.M; Chalikov, D.V; Tolman, H.L. (2002): A Neural Network Technique to Improve Computational Efficiency of Numerical Oceanic Models. Ocean Model., Vol 4, 363–83.

[4] Poort, J.P; Ramdin, M; Van Kranendonk, J; Vlugt. T.J.H. (2019): Solving Vapor-Liquid Flash Problems Using Artificial Neural Networks. Fluid Ph. Equilibria, Vol 490, 39–47.

[5] Wang, S; Fan K; Luo N; Cao Y; Wu F; You L; Zhang C; Heller K.A. (2019): Massive Computational Acceleration by Using Neural Networks to Emulate Mechanism-Based Biological Models. Nat. Commun., Vol 10 (4354), 1–9.

[6] Breen, P.G; Foley C.N; Boekholt T; Zwart S.P. (2019): Newton vs the Machine: Solving the Chaotic Three-Body Problem Using Deep Neural Networks. arXiv.

[7] Van Bokhorst, E.; Korst, H. J.; Smeulers, J.P.M. (1995). PULSIM3, a program for the design and optimization of pulsation dampers and pipe systems. Euro noise'95

[8] Bishop, C.M. (2006): Pattern Recognition and Machine Learning. Springer Science+Business Media, New York.

[9] Cybenko, G. (1989): Approximation by Superpositions of a Sigmoidal Function. Math. Control, Signals Syst., Vol 2 (4), 303–14.

[10] Hornik, K. (1991): Approximation Capabilities of Multilayer Feedforward Networks. Neural Networks, Vol 4 (2), 251–57.

[11] Géron, A. (2017): Hands-On Machine Learning with Scikit-Learn and TensorFlow. O'Reilly Media.

[12] Wei, P; Lu Z; Song J. (2015): Variable importance analysis: A comprehensive review. Reliab. Eng. Syst. Safe., Vol 142, 399-432.

TNO innovation for life

Big Data Anomaly Detection Methods for Reciprocating Compressors

by:

Can Tümer, Jonah Poort, Pejman Shoeibi Omrani
TNO, Heat Transfer and Fluid Dynamics
Delft, The Netherlands
can.tumer@tno.nl; jonah.poort@tno.nl; pejman.shoeibiomrani@tno.nl

12th EFRC CONFERENCE
August 24 – 26, 2021, Warsaw

Abstract:
An anomaly is a part of a dataset which differs significantly from the remainder or expected patterns within a dataset. Since anomalies are often (simply) associated with spikes in a dataset, industry standards of anomaly detection are usually based on heuristics such as if-then threshold statements (e.g. if pressure > threshold value, then notify operator). These methods heavily rely on the experience of system designers/operators and may have one or more of the following limitations: if a certain situation has never been identified in advance, or if a systems behaviour is too complex, threshold values can be hard or impossible to define. In addition, regular behaviour may change over time, requiring rules to adapt. If the systems operational flexibility is large, it is cumbersome to define the "normal" for each case.
The advent of data-driven algorithms (data analytics, machine learning, and deep learning) addresses the above mentioned challenges in a number of ways. Firstly, unsupervised learning techniques such as clustering and principle component analysis reduce dimensionality of datasets and assist downstream anomaly detection algorithms, as well as operators, in the form of decision support. (semi-)Supervised learning algorithms continuously detect more complex and non-linear anomalies in the data with (a limited) input from experts/operators.
In this paper, an inventory of both standard and modern anomaly detection methods is presented. The reviewed methods are associated to detection challenges from the reciprocating compressor industry and are assessed based on accuracy/precision of anomaly detection and their feasibility (for either online detection or offline detection/troubleshooting).

by: Can Tümer, Jonah Poort, Pejman Shoeibi Omrani – TNO, Heat Transfer and Fluid Dynamics

1 Introduction

Anomalies are defined as parts of a dataset which differ significantly from the remainder of the dataset or expected behaviour/patterns within the data. In the reciprocating compressor industry, anomalies (for instance, increasing crosshead vibrations) are often associated with the degrading performance of faulty components (for instance, loose bolts or nuts). If undetected, such faults can in-time lead to equipment failures, which in turn can result in economic damage.

It is, therefore, of paramount importance to be able to quickly and reliably detect component faults based on available sensor data, both for monitoring (early warning) and diagnostics (root-cause analysis) purposes. While modern compressor systems are equipped with many sensors, their data are often insufficiently leveraged. The industry standard is human-defined rule-based anomaly detection systems. This approach may fail to capture anomalous behaviour, if appropriate rules are not pre-defined, and may struggle to distinguish between normal and abnormal behaviours in a system with large operational flexibility.

On the other hand, "smarter" data-driven methods such as advanced data analytics, machine learning, or deep learning can effectively utilize available data by learning from it and associating different patterns in the data with (specific) faults and present a more robust approach for the anomaly detection of complicated systems.

This paper consists of a literature survey on different data-driven anomaly detection approaches and their application to the reciprocating industry, as illustrated by examples and references to industry articles. The ultimate goal of this survey is to highlight the current state-of-the-art in reciprocating compressor anomaly detection techniques, as well as identifying gaps and new opportunities in the application of the identified techniques to the industry, with emphasis on machine learning methods. This manuscript is organized as follows: in Section 2 the basic concepts related to anomaly detection are given. Section 3 covers the non-machine learning approaches to anomaly detections such as heuristics and statistics, while Section 4 describes more advanced machine learning and deep learning methods. Finally, conclusions on the survey and future outlooks are given in Section 5.

2 Anomaly detection basics

An anomaly (or outlier) is a part of a dataset which differs significantly from the remainder of the data set or does not fit within expected behaviour.[1] Anomaly detection is the science of finding and isolating the anomalies in a dataset.

2.1 Anomaly types

Anomalies are often associated with peaks or spikes in the data, or show up as trends that do not follow what is expected from regular behaviour. In addition, anomalies may also appear as fluctuations or frequency changes within a data set. These types of anomalies are based on abnormal patterns rather than abnormal values, and their subtlety may prove to be harder to spot at first sight. Anomalies can be classified in three categories:[1]

- **Point anomalies**. A single data instance that differs significantly from the remainder of the data set, i.e. a spike. Statistical outliers or measurement errors are typical examples.

- **Contextual anomalies**. Values within a data set that are only anomalous due to the context in which they occur. For example, it is normal for a thermometer in an oven to record temperatures of 120 °C, but not if the thermostat was set to 180 °C.

- **Collective anomalies**. Values themselves are not aberrant, but the order or amount/frequency in which they appear is, e.g. an individual buying one bag of fertilizer is normal, but a person buying a few thousand bags is strange.

In general, the occurrence of an anomaly does not imply the occurrence of a problem or fault. While a fault is almost always an anomaly, an anomaly is not always a fault. Changes in piston rod drop readings (anomaly) could be due to piston rider ring wear (fault) and/or thermal load changes inside a cylinder (during normal operation). Hence, fault detection is much more complex than pure anomaly detection, oftentimes requiring human (expert) supervision, or additional algorithms which can differentiate between statistical anomalies (resulting from randomness), expected/planned, or fault induced anomalies.

2.2 Features and labels

In the following sections, the terms "feature" and "label" are used frequently, especially in the context of machine learning. It was therefore judged apt to introduce them to avoid future confusion. When talking about a set of data from which a predictive model is derived, the word "feature" is used to describe any of the inputs to the model, while "label" is used to refer to the output the model is intended to predict. A complete dataset thus consists of both features and labels. For example, in the reciprocating industry it is common to use statistical measures such as mean, kurtosis, skewness, etc. derived from vibrational data (features) to predict a specific type of compressor fault such as valve leakages, piston settling, or loose components (labels).

by: Can Tümer, Jonah Poort, Pejman Shoeibi Omrani – TNO, Heat Transfer and Fluid Dynamics

3 Non-machine learning approaches

3.1 Heuristics

Heuristic anomaly detection methods, also called static rules, are mostly based on experience and insights of experts in the relevant field. An expert, or preferably a group of experts, uses the knowledge gained working with the system of interest to construct a list of potential anomalies and how they could be spotted within relevant data sets. This expert knowledge can then be codified into an if-then algorithm, i.e. if piston rod drop is higher than 1000 µm, then warn the operator. Additionally, fuzzy logic[2] can be used to relax the discrete nature of threshold values into different regions of magnitude in order to better estimate the severity of the anomaly. Such an approach can be greatly helped by defining an anomaly score and asking an expert to define threshold regions above which outliers become problematic.[3]

Heuristic based approaches are useful in fault detection as the experts can also identify which faults lead to which anomalies, or which anomalies indicate which types of faults. On the other hand, there is a possibility that certain situations have not occurred before and will, therefore, not be spotted in time because they are not part of the expert knowledge base (the "unknown unknown" problems). In addition, what is considered regular behaviour can change over time[3], a phenomenon called concept drift. This means that the heuristic rules must continuously be updated, which is resource and time intensive. Lastly, data patterns might already be too complex to be codified into simplistic if-then statements.

An example from the reciprocating compressor industry is piston ring wear detection with piston rod drop measurements. In case of systems with large cylinders (for instance, hydrogen compressors), the piston rod drop can be largely influenced by the static deflections of the piston due to changing cylinder thermal loads. This makes definitions of thresholds in the machine protection system difficult or even unfeasible if the system is required to function within a large operational envelope (e.g. underground gas storage).

3.2 Statistical methods

3.2.1 Statistical measures

Outliers in a data set can be determined by comparing the values of all individual data points to a number of statistical measures of the data set as a whole. Examples include the z-score (a data point's distance to the mean value of the dataset in terms of standard deviations of the data set), the median and MAD (median of all absolute deviations) as replacements for the mean in determining the z-score (Rousseeuw & Hubert, 2017).[4] Other statistical methods include the Q-value/statistic[5], and Hotelling's T^2-statistic[6], which have been used extensively in the compressor industry.

In (Ahmed, Baqqar, Gu, & Ball, 2012)[7], four common valve faults (leaky discharge valves, suction valve leakage, a leaky intercooler, and a loose drive belt) were detected based on both the T^2-statistic and Q-statistic derived from vibrational data. Statistical features were extracted from vibration data obtained from a two-stage reciprocating compressor. The features included peak factor, RMS, crest factor, shape factor, and others. In the paper, they conclude that based on different feature combinations, different types of faults were easier to detect than others. Unfortunately, it is not made entirely clear which features are best for which fault. In addition, it is mentioned that the Q-statistics performs best, but no concrete accuracy scores were mentioned.

Furthermore, (Pichler, Schrems, Buchegger, Huschenbett, & Pichler, 2011)[8] also used vibrational data to classify valve failures, although their methods were based on the statistical similarity between spectrograms derived from the vibration signals. The used similarity measure is based on a norm defined in the vector space of the spectrograms which can be interpreted as a residual that decreases in value as two spectrograms are more alike. With this residual a distance metric is established and used to compare two spectrograms, if the distance between two spectrograms is less than a specified threshold, they are considered to correspond to the same behaviour. This threshold is determined based on the "logistic classification rule", for more information on what this entails the reader is referred to the article itself (Pichler et al., 2011)[8] and (Webb, 2002)[9]. The spectrograms were obtained from vibration data from a two-stage reciprocating compressor. Two faults were seeded by creating a fissure in a valve, and breaking part of a valve. According to the authors, all faults could be correctly identified, and most notably, the fault threshold determined for one valve type could be extrapolated to others, a very useful result.

3.2.2 Correlation methods

Anomalies in time series data can be detected by the use of correlation coefficients, such as Pearson's r coefficient. A measured signal can be correlated to a signal of known normal behaviour. If the measured signal contains considerable deviations from regular behaviour, it will be noticeable in the changes of correlation coefficient. It is often the case that correlations change more abruptly when anomalies occur.[10] When multi-variate time series data is available, it is also possible to correlate a signal to one or more others in order to detect anomalous behaviour in one signal by changes in other signals.[10]

An example from the reciprocating compressor industry is the active use of correlation analysis (or pattern recognition through correlation analysis) for

by: Can Tümer, Jonah Poort, Pejman Shoeibi Omrani – TNO, Heat Transfer and Fluid Dynamics

the purpose of detecting deviations in PV plots between "normal" and "faulty" machines. Here, PV plots (or temperature measurements at the valves) are used to detect non-ideally operating (leaking) valves or pressure packings due to the distinct patterns[11], as can be seen in Figure 1, that emerge during suction or discharge strokes.

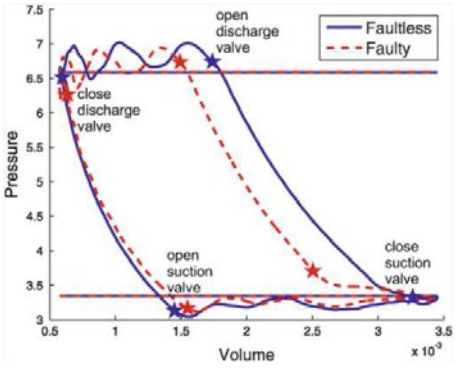

Figure 1 : PV measurements (pressure in bar and volume in m³) of a faultless (in blue) and a leaking (faulty, marked in red) discharge valve. Leaking discharge valve delays expansion to suction pressure.

4 Machine learning approaches

The use of machine learning for anomaly detection facilitates the handling of complicated cases for which the expected anomalies are too convoluted to be described by even an expert user (viz. "leave it to the algorithm"). These complicated cases might require treatment of complex components (such as valves) or reciprocating compressor systems with a large operational flexibility where definitions of normal and abnormal change dynamically.

The machine learning approach generally revolves around using "intelligent" learning algorithms to find general structures and relations in, or between, data sets, and isolating data points that deviate from these norms. There are numerous different machine learning approaches applied to anomaly detection, and almost as many ways to classify them. In this section, machine learning approaches are classified based on their learning methods: supervised or unsupervised.

Supervised machine learning algorithms learn relationships based on data sets that contain only labelled data, meaning that for every data sample (feature combination), it is known whether it belongs to a class of regular behaviour or anomalous behaviour. The goal of supervised machine learning is to find the appropriate relationship that maps features (inputs) to labels (outputs). Unsupervised methods learn from data sets where no labels are present, and only features are available. The goal is to find relationships between data points or patterns in the data so that data points that fall outside these relationships or patterns could be classified as anomalous. The difference between supervised and unsupervised learning methods is depicted in Figure 2. In addition, semi-supervised algorithms learn from data sets in which the majority contains only features, but a small set of labelled instances are present. Semi-supervised algorithms are often combinations of supervised and unsupervised methods, which support each other in order to get a more accurate model than would be possible to achieve using either method alone. In this paper, semi-supervised methods will not be covered separately, but will be mentioned where relevant.

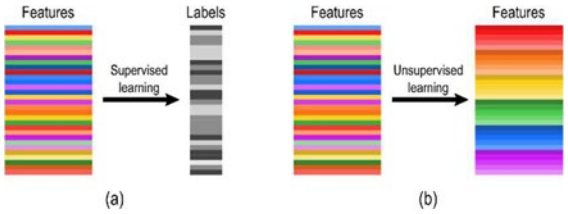

Figure 2: Difference between supervised (a), and unsupervised learning (b). Supervised learning aims to relate features (inputs) to their corresponding labels (output). In unsupervised learning, no labels are present, and the process aims to order, cluster or find patterns in features.

The main bulk of this section will cover different applications of machine learning, ordered per subsection by the type of learning methods. In these subsections, references will be made to algorithms that can be used for the different applications. In order to provide some background to the reader, a number of often used machine learning algorithms will be briefly explained in the next subsection.

4.1 Basic machine learning algorithms

4.1.1 Support vector machines

A support vector machine (SVM) is a supervised learner often used for classification. The principle behind a regular supervised SVM is that a dataset whose classes are not linearly separable in its original feature space is transformed onto a higher-dimensional space in which different classes are linearly separable by some hyperplane[12], as illustrated in Figure 3. Mapping from the original feature space to the hyper-space is done based on a predefined kernel function.[12] The labelled data set is used to find the linear hyperplane with the largest separation margin, i.e. the plane that classifies the most instances correctly and is equidistant from the furthest data points in each class.[12]

The main benefit of SVM is their simplicity; requiring the definition of only few parameters in order to determine their optimal accuracy. On the other hand, SVM can be slow to tune, and do not provide any posterior probabilities (in a classification problem it would return the predicted class of a sample, but not how certain the model is about this).[12]

(Pichler et al., 2013)[11] used SVM to detect broken compressor valves from pV diagrams, this is further described in Section 4.2.1.

by: Can Tümer, Jonah Poort, Pejman Shoeibi Omrani – TNO, Heat Transfer and Fluid Dynamics

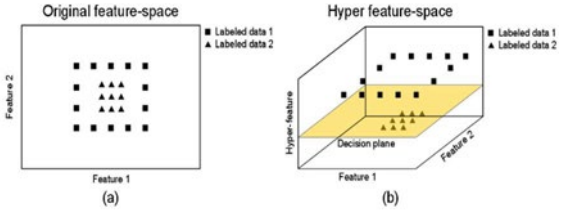

Figure 3: Illustration of how a Support Vector Machine determines its decision boundary. In the original view (a), there is no clear linear class boundary (i.e. one cannot draw a single straight line that separates all squares from all tringles). By transforming the data into a hyper-dimension, SVM can find a linear "decision plane" that does separate both classes linearly (b).

4.1.2 Artificial neural networks

Artificial neural networks (ANN) are a group of mathematical methods that can be used to construct an input-output relation between features and their corresponding labels.[12] An ANN consists of a connected network whose nodes (neurons) are divided into subsequent layers; the first is called the input layer, the last the output layer, and all layers in between are called hidden layers (see Figure 4).

Each neuron in the network has a corresponding value called its activation. Similarly, the connections between the neurons in the network all have a corresponding value called their weight. The activation of the neurons in the first layer are determined by the inputs given to the network. Information propagates through the network, starting from the input layer, by multiplying the activations of the neurons in one layer with the weights of the connections to the neurons in next layer, adding the results up at each neuron in the next layer, and applying a non-linear activation function. This process is repeated through each layer until the last one is reached, the activation in the last layer is the output of the network. Figure 4 schematically shows this procedure.

By finding the right values for each weight in the system, any desired output can be achieved for any given input.[13] Likewise, given a data set of features and corresponding labels, there exists a set of weight values that links each feature combination to its corresponding label with minimal error, making it possible to use ANN to model complex non-linear relationships based on data alone. Finding the optimal set of weights that leads to the best performing network is a non-trivial task and is done in a process called training; more details on this process can be found in (Bishop, 2006).[12]

The ANN described above and depicted in Figure 4 is typically referred to as a "vanilla" ANN or MLP (Multi-Layer Perceptron). When an ANN has more than one hidden layer, it is generally referred to as a "deep" neural network. Deep neural networks can typically achieve much higher accuracies than MLPs, at the cost of model explainability. Examples of specific types of deep neural networks include the Long Short-Term Memory network (used for predicting data-sequences), the convolutional neural network (used for image-recognition), and the autoencoder (see Section 4.1.5). In addition to these, many other types of neural networks exist, all of which are variation on the basic MLP type.

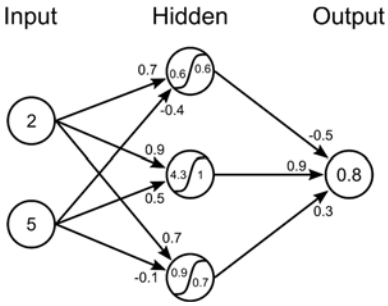

Figure 4: Illustration of a simple Multi-Layer Perceptron type artificial neural network with two inputs, one hidden layer with three neurons, and one output. Weights and activation values are given to show how the output is derived from the input. The hidden activation function is the sigmoid function (Bishop, 2006).

While ANN have a lot of parameters that need to be specified in order to find the optimal network, and their inner workings can be difficult to explain, the flexibility and performance that can be achieved with them make them one of the most used machine learning techniques.

4.1.3 Decision trees

In a decision tree, the feature space is cut into separate regions by linear boundaries such that a tree-like structure is created.[12] Figure 5 shows an example of a simple tree. The end-points of the tree (called leaves) will have a corresponding label associated with it, while each branching point represents a split in the feature space. A new feature combination can be related to one of the labels by traversing the tree from the top down, at every branching point either the left or right path is taken based on the feature value and decision boundary at the branching point, when a leaf is reached the label corresponding to that leaf is given to the feature combination in question.

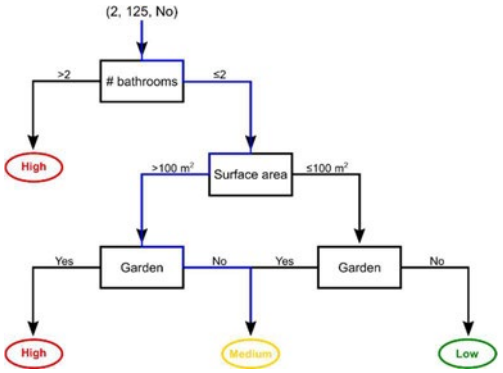

Figure 5: Schematic illustration of a decision tree, used to classify houses into different price ranges.

by: Can Tümer, Jonah Poort, Pejman Shoeibi Omrani – TNO, Heat Transfer and Fluid Dynamics

When using machine learning, the optimal decision boundaries are determined based on a dataset containing known combinations of features and corresponding labels. Using this data, decision boundaries are determined such that the number of incorrectly classified instances is minimized, while keeping the complexity of the resulting tree to a minimum. In a sense, decision tree are similar to heuristic rule-based systems, but where the if-then rules are automatically generated from data instead by a human expert.

The biggest advantage of decision trees is their explainability, as it is easy to see why and how a given data point is classified. On the other hand, the tree structures can grow very large, decreasing their interpretability. In addition, if poorly designed, decision trees can be unstable, meaning that a small change to the dataset of features and labels can lead to a completely different tree structure.

4.1.4 k-Nearest neighbours

The (k-)nearest neighbour algorithm is a simple algorithm that relates features to their corresponding label based on similarity to other known feature-label combinations.[12] Unlike the previously discussed algorithms, the dataset of example features and labels is not used to tune parameters and construct a model to be used later for evaluating new data points. Instead, the data is used as a direct comparison to the new data point. The feature combination of the new point is compared to the feature combinations in the dataset and the most similar combinations, called the nearest neighbours, are used to determine the label of the new data point. The number of neighbours (k) that is used to determine the label can significantly influence the outcome of the model and is the main parameter that needs to be optimized when using the k-nearest neighbour algorithm.

Figure 6 shows a schematic representation of the k-nearest neighbour algorithm used to determine whether a new data point (grey circle) is part of the group of red triangles or green squares. When only one neighbour is considered (k = 1), the closest point to the circle is taken as the only indicator of the group to which the circle belongs. In this case this is a red triangle so the circle is classified as also being one. However, when the number of nearest neighbours is increased (k = 5), it becomes clear that there are much more green squares that are close to the circle, and it should likely be classified as a green square.

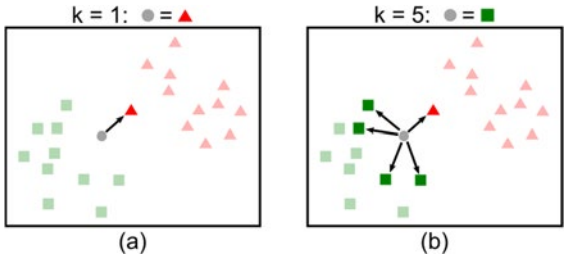

Figure 6: Schematic representation of a k-nearest neighbour algorithm. When k is equal to 1 (a), the grey circle is (incorrectly) classified as a red triangle, while when k is 5 (b) it is (correctly) classified as a green square.

Simplicity is the main advantage of using the k-nearest neighbour algorithm, as it only compares features to each other and no model has to be constructed. Furthermore, the only parameter that has to be specified is the number of neighbours to evaluate. This also makes it a good algorithm to use when not enough data is available to construct a proper model using other techniques. On the other hand, choosing the optimal number of neighbours to consider can be difficult, and an improper choice can lead to large errors. Furthermore, since the algorithm compares a new data point to all example data points, it can be slow to compute when the example dataset becomes very large.

4.1.5 Autoencoders

An autoencoder is a type of neural network that transforms a given input vector to an output vector (typically of lower dimension), and transforms the output back to the original input vector while minimizing the difference between original and reproduced input vectors.[14] An autoencoder generally consists of two components, the encoder, and the decoder. The encoder is responsible for encoding the original data set into a more compact, less complex encoding while keeping the loss of information to a minimum. The decoder is responsible for retrieving the original data set back from the encoding while minimizing the error between the original and reconstructed data set. A schematic representation of an autoencoder is shown in Figure 7. Since the encoding and decoding is often achieved using multiple neural network layers, autoencoders are a typical example of a deep learning model.

An autoencoder can be used for anomaly detection by only training it on regular data instances. The main assumption is that after training, whenever the autoencoder encounters irregular data, the reconstruction error will be significantly higher than for regular data.[15]

by: Can Tümer, Jonah Poort, Pejman Shoeibi Omrani – TNO, Heat Transfer and Fluid Dynamics

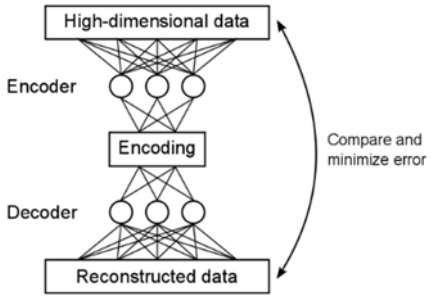

Figure 7: Schematic illustration of an autoencoder. The autoencoder is made up of two neural networks, the encoder and decoder. Encoder reduces high-dimensional data to a more compact encoding, while decoder reconstructs the original data from the encoding. Reconstructed and original data are compared and the difference is minimized until a desired reconstruction quality is achieved.

4.2 Supervised methods

In supervised machine learning, the data used for training, validation and testing purposes is in its entirety made up of labelled instances.[12] This means that for every input (feature combination), there is a corresponding known output (label). The goal of supervised learning is to generate a model that reflects the correct relationship between features and corresponding labels[16], and can generalize to new unknown feature-label combinations.

In the field of anomaly detection, a supervised learning data set is one for which it is known whether a given data instance is considered regular or anomalous. Depending on whether the labels for anomalous data are discrete or continuous, the problem could be considered as a classification or regression, respectively.

4.2.1 Classification

Given a set of labelled data divided into at least two classes, one for regular and one for anomalous samples, a machine learning algorithm (e.g. ANN, SVM) can be used to distinguish between the two label classes based on their feature values.[12] Specific anomalies could then be isolated by subdividing the class of irregular instances.

The classification approach has been widely investigated in the reciprocating compressor industry, and is a very popular method for fault detection. Many studies have investigated the use of primarily SVM and ANN for classifying different types of failure modes.

For example, (Keerqinhu et al., 2016)[17] combined principal component analysis (PCA, see Section 4.3.2) with a SVM to a large dataset to classify different faults such as broken suction valve reeds, suction valve leakages, broken exhaust valve reeds, exhaust valve leakages, and piston-rod settling. Main results from this study are shown in Figure 8, showing accuracy scores for each fault type for different attempts. Each attempt consisted of a model that was trained and scored on a different subset of the total dataset. As seen, accuracy can vary significantly, especially for piston-rod settling, but scores of at least 90% can reliably be achieved.

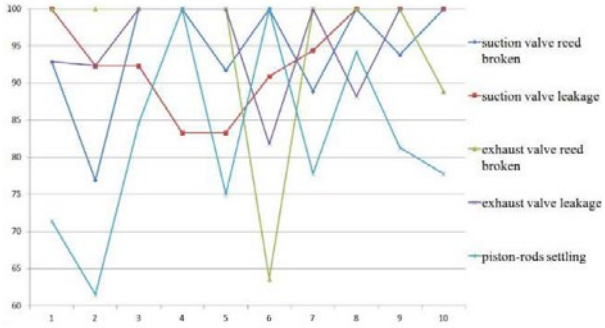

Figure 8: Classification accuracy for different compressor faults from (Keerqinhu et al., 2016).[17] Y-axis shows fault prediction accuracy for different attempts, where each attempt has different training and testing data.

Other studies, with applications of SVM to similar problems in reciprocating compressors, managed to achieve similar accuracies of over 96% when based on pV diagram data[11] or vibrational spectrograms.[18] (Pichler et al., 2013)[11] especially show quite distinct classification regions (see Figure 9) when using features extracted from pV diagrams.

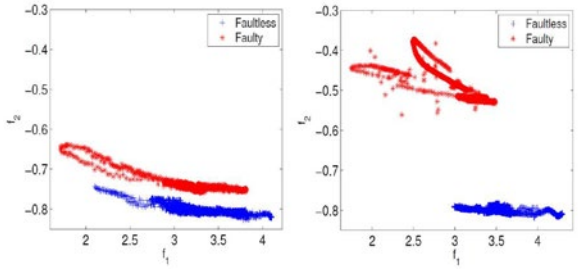

Figure 9: Features extracted from a pV diagram. From (Pichler et al., 2013).[11]

A specific type of neural network called the probabilistic neural network was used by (Ahmed, Gu, & Ball, 2011)[19] to classify different fault behaviours based on cylinder head vibration data in both time- and frequency-domains. Different features were extracted for both domains, for time they were (among others) peak factor, entropy, skewness, kurtosis, and variance, while for the frequency domain these were the amplitudes of different harmonics. In the study, they investigated which feature combinations resulted in the highest accuracies, the findings are shown in Table 1 and Table 2. As can be seen data from the frequency-domain outperformed the best network trained on time-domain data with 96% versus 93%. It was also concluded that for the frequency domain, the inclusion of more features always led to better results, while for time-domain features the best accuracy was achieved using only three features (RMS, variance, and kurtosis), indicating that sometimes using more features can actually overcomplicate the classification process.

by: Can Tümer, Jonah Poort, Pejman Shoeibi Omrani – TNO, Heat Transfer and Fluid Dynamics

Table 1: Classification accuracy results based on time-domain features from (Ahmed et al., 2011)[19]

Total of combination	Number of input features	Features name	Correct rate
36	2	Variance, Kurtosis	80.55%
84	3	RMS, Variance, Kurtosis	93.05%
126	4	RMS, Peak factor, Variance, Kurtosis	91.66%
126	5	RMS, UB, Entropy, Variance, Kurtosis	91.66%
84	6	RMS, Peak factor, UB, Entropy, Variance, Kurtosis	91.66%
36	7	RMS, Peak factor, LB, UB, Entropy, Variance, Kurtosis	88.89%
9	8	RMS, Peak factor, LB, UB, Entropy, Variance, Kurtosis, Range	88.89%
1	9	RMS, Peak factor, LB, UB, Entropy, Variance, Skewness, Kurtosis, Range	83.33%

Table 2: Classification accuracy results based on frequency-domain features from (Ahmed et al., 2011)[19]

Number of input features in the frequency domain	Correct rate
10	81.81%
20	87.88%
30	93.94%
48	95.45%
65	95.50%

(Liu, Duan, Yuan, Wang, & Zhoa, 2019)[20] have used a denoising autoencoder to distinguish between normal condition and three different failure modes of a reciprocating compressor by combining unsupervised and supervised learning methods. Using an autoencoder, features were extracted from vibration signals in an unsupervised manner. Once the feature extraction was successful, a supervised neural network classification layer was used to classify the extracted feature combinations into different condition classes. Vibration data was obtained from a four cylinder natural gas reciprocating compressor. Four different conditions were considered: normal behaviour and three faults including spring failure, valve fracture, and valve wear. Figure 10 shows an example waveform for each of the four conditions. The feature extraction autoencoder was trained on the raw vibration signals and signals to which different levels of noise were added. As such, the model was able to learn to extract the right features even under noisy circumstances. Results from the feature extraction are shown in Figure 11. As can be seen, the four conditions are easily separable when no noise is added to the input data. However, as the amount of noise increased, separation between the regions became less pronounced, and overlap started to occur (especially between the two valve-related faults). These effects are reflected in the classification scores, which, although they were always good, decreased from 100% for the noiseless case to 92% for the case with the highest amount of added noise.

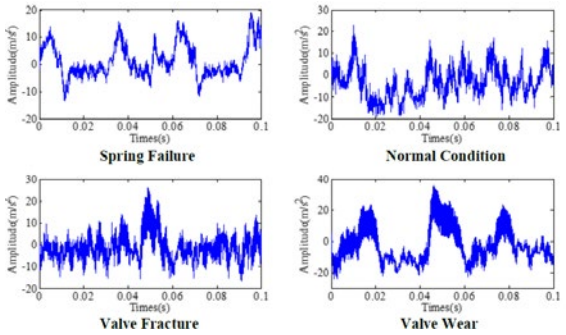

Figure 10: Acceleration waveform examples for each condition considered in (Liu et al., 2019).[20]

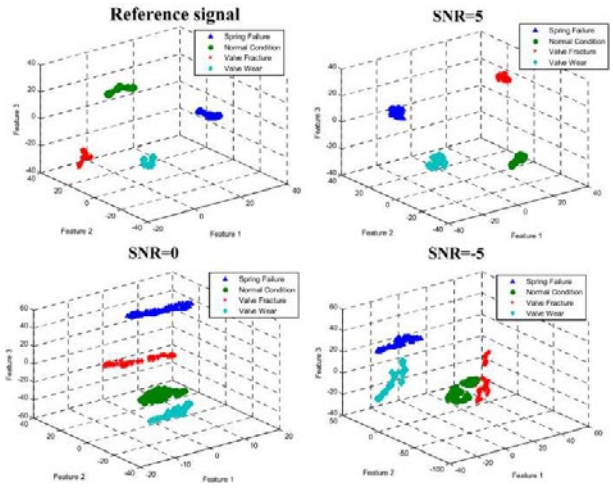

Figure 11: Feature space extracted by the denoising autoencoder from (Liu et al., 2019).[20] The considered four different conditions (normal, spring failure, valve fracture, and valve wear) are clearly separable (to three features) when noise is absent in original input data. With increasing amount of noise, conditions begin showing overlap.

4.2.2 Regression

Based on a data set containing only regular instances, a machine learning algorithm can be trained with the purpose of predicting expected data trends.[12] In this case known labels in the supervised data set are continuous values instead of classes, but many of the same algorithm types can be used.

If a model is trained to predict regular behaviour, any points in a data set that deviate by more than a predetermined margin from this prediction can be flagged as anomalies. It is important that the prediction can take expected future changing behaviour into account, or it might incorrectly flag the expected change as an anomaly itself. This approach is not exclusive to machine learning methods, and could be based on physical models as well. The wide use of theoretic pV curves as a basis of reference for judging measured pV curves can be given as an example.

4.3 Unsupervised methods

Unsupervised learning is done based on unlabelled data sets, meaning that the features themselves are the only known information.[12] The general goal of

by: Can Tümer, Jonah Poort, Pejman Shoeibi Omrani – TNO, Heat Transfer and Fluid Dynamics

unsupervised learning is to find structures or relations within the feature data set[16], as opposed to finding relations between features and labels.

Unsupervised data sets are prevalent due to the fact that anomalies are usually very rare, or it is too costly or time-consuming to manually label them. This leads to data sets for which no clear "regular vs. anomalous" labels can be defined. As unsupervised methods lack labelled data, it can also be difficult to determine how well the system is working until it is put into practice.

4.3.1 Clustering

Given a set of unlabelled data, a machine learning algorithm is used to group the data instances into clusters of features that show similarities.[12] Any data point that does not fit into any of the clusters can be classified as anomalous, a concept shown in Figure 12. Once clusters' boundaries are identified, an anomaly can be classified based on its distance to the nearest cluster centre, if it is above a predefined threshold, it is labelled an anomaly.

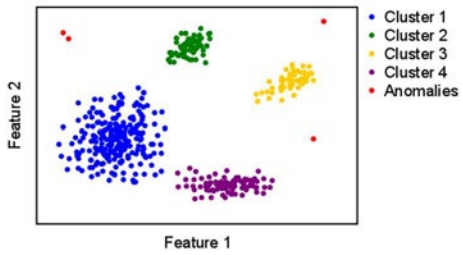

Figure 12: Schematic illustration of clustering based anomaly detection. Based on the given features, the algorithm finds clusters of similar data points (blue, green, yellow, purple points). Feature combinations that do not fit into any of these clusters, are flagged as anomalies (red points).

The number of clusters is oftentimes not known or disputable, and determining it is one of the more difficult aspects of clustering. Unsupervised clustering is less suited for spotting collective anomalies, as it can only spot data instances that do not fall into one of the clusters, and not whether the number or order of cluster appearances is expected, i.e. if one type of anomaly occurs somewhat frequently it can start to form its own cluster, without a label to ascribe to this cluster, it might not stand out as anomalous anymore.

However, unsupervised learning algorithms could be used as a starting point to identify clusters, which can later be labelled for (semi-) supervised learning, decreasing the amount of data points that would require (manual) labelling. This approach is also known as generative modelling, and is illustrated in Figure 13. Generative Models (GM) generally try to determine the joint probability of feature x and label y, i.e. determine $p(x, y)$[21], this sets them apart from *discriminative* models, whose aim is to find the conditional probability $p(y|x)$. GM are often used for classification or clustering by using the found probability $p(x, y)$ to define a decision boundary between classes or clusters. GM can be seen as an unlabelled clustering algorithm, supported by a limited number of labelled instances, used to improve or verify boundaries, or as a classification algorithm, based on labelled data, where unlabelled data is used to obtain a better indication of decision boundaries.

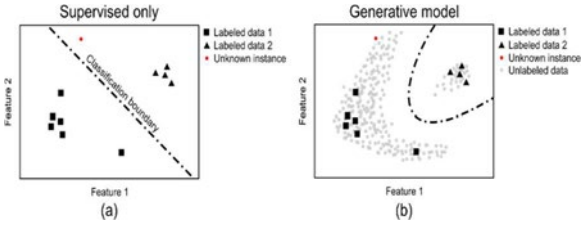

Figure 13: An example of a classification problem solved using only supervised learning (a), and solved using a generative model that uses a combination of labelled and unlabelled data (b). In the first case, the unknown point shown in red would have been (incorrectly) classified as class 2 (triangles), while for the second case, for which the classification boundary has been updated based on the clusters found in the unlabelled data, it would be correctly classified as class 1 (squares).

4.3.2 Dimensionality reduction

As the name implies, dimensionality reduction is used to decrease the size (number of features) of a large, multivariate dataset to one with a lower dimensionality while trying to lose as little information as possible.[12] Methods for dimensionality reduction include the autoencoder and principle component analysis. The latter is not always considered a machine learning approach.

The main assumption behind using dimensionality reduction methods for anomaly detection is that when the raw dataset is reduced, any anomaly will "appear significantly different"[1] from the rest of the data set. The reason for this is that since an anomaly does not 'fit in' with the remainder of the data, it cannot be reduced as effectively in the same manner as the regular data, and thus will stand out.

These methods are also often used as a pre-processing step and combined with a classifier to distinguish between different types of anomalies and regular data in the reciprocating compressor industry, for example in (Ahmed et al., 2012)[7], (Keerqinhu et al., 2016)[17], and (Qi et al., 2018).[22]

4.4 Transfer learning

Transfer learning can be used for supervised, unsupervised, and semi-supervised learning, as well as different ML algorithm types such as ANN and SVM.[23] The main idea behind the technique is that a problem, for which no to very little labelled data is available, can be approximated by a related problem for which extensive labelled datasets do exist.[24] The model is first trained on the labelled data of the related problem and the resulting set of parameters (or a selection/subset of the parameters)

by: Can Tümer, Jonah Poort, Pejman Shoeibi Omrani – TNO, Heat Transfer and Fluid Dynamics

is transferred to the original problem. If limited labelled data is available for the original problem, it could be used to adapt parameters to better fit the original problem.

For anomaly detection, transfer learning could be used in the same way when two similar problems exist, where one has an extensively labelled data set, and the other has no labelled data. A model can be trained in a supervised manner on the labelled data, and part of the model (for example the weights of some of the layers in a deep neural network) could be transferred to a model, used to make predictions on the problem with the unlabelled data set.

5 Conclusions and Outlook

Anomaly detection is defined as finding anomalous data points or patterns in a data set. This paper contains a brief literature study on the subject of anomaly detection with a specific focus on existing (and possible) applications for the reciprocating compressor industry. Following can be concluded:

- Three different approaches for the detection of anomalies were identified: heuristic (rule-based detection), statistics based methods, and machine learning based methods. The latter is further divided into three categories, based on the availability of labels in the training and testing data sets, namely supervised, unsupervised and semi-supervised learning.
- Heuristic, and statistics based methods form the backbone of the currently deployed monitoring systems. These methods rely on expert knowledge for defining rules that capture anomalous behaviours in a reciprocating compressor system and may perform ineffectively for complex components or systems. Use of machine learning may offer breathing space for these complicated cases.
- Surveyed papers with machine learning applications report correct rates above 90% for detecting a variety of anomalies that can be expected in a reciprocating compressor system.
- It is seen that a vast majority of the reported applications employ supervised learning which requires labels to be present in the used dataset. It is often the case in the industry, however, that labels are not present (or are scarce) in the measurement histories of systems. Albeit their absence in the surveyed papers, the use of unsupervised or semi-supervised learning based techniques may, thus, be more suitable for handling the already available datasets.
- Despite showing satisfactory performance, surveyed models may suffer a significant loss of performance in real life settings, where they are asked to work outside their training domain. Instead of providing even more training data, transfer learning may offer a more accessible solution to help deal with any novel scenarios that might occur in real life.
- To the authors best knowledge, k-nearest neighbour and decision tree algorithms have seen little application in the reciprocating compressor industry thus far. The authors still see opportunities for the potential implementation of decision tree methods due to their inherent interpretability, which can aid greatly in the fault analysis process.

6 Acknowledgement

Authors thank the EFRC for supporting this work and approving to present a summary in this paper.

References

[1] Chandola, V; Banerjee, A; Kumar, V. (2009): Anomaly Detection: A Survey. ACM Comput. Survey, Vol. 41 (3).

[2] Novák, V; Perfilieva, I. (2013): The Principles of Fuzzy Logic: Its Mathematical and Computational Aspects. Lectures on Soft Computing and Fuzzy Logic, 189–237.

[3] Chalapathy, R; Chawla, S. (2019): Deep Learning for Anomaly Detection: A Survey, 1–50.

[4] Rousseeuw, P. J; Hubert, M. (2017): Anomaly detection by robust statistics. ArXiv E-Prints.

[5] Storey, J.D. (2003): The positive false discovery rate: a Bayesian interpretation and the q-value. Annal. Statist., Vol. 31 (6), 2013-2035.

[6] Hotelling, H. (1931) The Generalization of Student's Ratio. Ann. Math. Statist., Vol. 2 (3), 360-378.

[7] Ahmed, M; Baqqar, M; Gu, F; Ball, A. D. (2012): Fault Detection and Diagnosis using Principal Component Analysis of Vibration Data from a Reciprocating Compressor. International Conference on Control at Huddersfield, U.K.

[8] Pichler, K; Schrems, A; Buchegger, T; Huschenbett, M; Pichler, M. (2011): Fault Detection in Reciprocating Compressor Valves for Steady-State Load Conditions. 2011 IEEE International Symposium on Signal Processing and Information Technology (ISSPIT) at Bilbao, Spain.

[9] Webb, A. (2002). Statistical Pattern Recognition. John Wiley & Sons, New York.

[10] Zhao, P; Kurihara, M; Tanaka, J; Noda, T; Chikuma, S; Suzuki, T. (2017): Advanced correlation-based anomaly detection method for predictive maintenance. 2017 IEEE International Conference on Prognostics and Health Management (ICPHM) at Dallas, U.S.A.

[11] Pichler, K; Lughofer, E; Pichler, M; Buchegger, T; Klement, E; Huschenbett, M. (2013): Detecting

Broken Reciprocating Compressor Valves in the pV Diagram. 2013 IEEE/ASME International Conference on Advanced Intelligent Mechatronics at Wollongong, Australia.

[12] Bishop, C.M. (2006): Pattern Recognition and Machine Learning. Springer Science+Business Media, New York.

[13] Hornik, K. (1991): Approximation Capabilities of Multilayer Feedforward Networks. Neural Networks, Vol. 4 (2), 251–57.

[14] Baldi, P. (2012): Autoencoders, Unsupervised Learning, and Deep Architectures. JMLR: Workshops and Conference Proceedings.

[15] Borghesi, A; Bartolini, A; Lombardi, M; Milano, M; Benini, L. (2018): Anomaly Detection using Autoencoders in High Performance Computing Systems. arXiv.

[16] Chapelle, O; Schölkopf, B; Zien, A. (2006): Semi-Supervised Learning. The MIT Press, Cambridge, Massachusetts, U.S.A.

[17] Keerqinhu, Qi G; Tsai, W; Hong, Y; Wang, W; Hou, G; Zhu, Z. (2016): Fault-Diagnosis for Reciprocating Compressors Using Big Data. 2016 IEEE Second International Conference on Big Data Computing Service and Applications at Oxford, U.K.

[18] Pichler, K; Lughofer, E; Pichler, M; Buchegger, T; Peter, E; Huschenbett, M. (2016): Fault detection in reciprocating compressor valves under varying load conditions. Mech. Syst. Signal Pr., Vol. 70–71, 104–119.

[19] Ahmed, M; Gu, F; Ball, A. (2011): Feature Selection and Fault Classification of Reciprocating Compressors using a Genetic Algorithm and a Probabilistic Neural Network. Journal of Physics: Conference Series, Vol. 305 (1).

[20] Liu, Y; Duan, L; Yuan, Z; Wang, N; Zhoa, J. (2019): An Intelligent Fault Diagnosis Method for Reciprocating Compressors Based on LMD and SDAE. Sensors, Vol. 19 (5).

[21] Kingma, D.P; Rezende, D.J; Mohamed, S; Welling, M. (2014): Semi-Supervised Learning with Deep Generative Models. arXiv.

[22] Qi, G; Zhu, Z; Erqinhu, K; Chen, Y; Chai, Y; Sun, J. (2018): Fault-diagnosis for reciprocating compressors using big data and machine learning. Simulation Modelling Practice and Theory, Vol. 80, 104–127.

[23] Weiss, K; Khoshgoftaar, T.M; Wang, D. (2017): A survey of transfer learning. Journal of Big Data, Vol. 3 (9).

[24] Weiss, K; Khoshgoftaar, T.M; Wang, D. (2017): A survey of transfer learning. Journal of Big Data, Vol. 3 (9).

EUROPEAN FORUM
for RECIPROCATING
COMPRESSORS

PULSATIONS AND VIBRATIONS

Validation of Pressure Pulsation and Vibration Analyses in a Reciprocating Compressor for Design Optimization

by:

Cappelli Leonardo
C.S.T. S.r.l., Florence, Italy
leonardo.cappelli@cstfirenze.com

Fusi Andrea
C.S.T. S.r.l., Florence, Italy
andrea.fusi@cstfirenze.com

Sacco Marco
C.S.T. S.r.l., Florence, Italy
marco.sacco@cstfirenze.com

Mazzoleni Thomas
SIAD Macchine Impianti S.p.A.
Bergamo, Italy
thomas_mazzoleni@siad.eu

12th EFRC CONFERENCE
August 24 – 26, 2021, Warsaw

Abstract:
Pressure pulsations are one of the main issues in reciprocating compressors applications. They can generate high pulsation induced shaking forces leading to high vibrations on compression plant elements such as piping, dampers, coolers, small branches and shaking forces, which can even lead to fatigue failures. In addition, pulsations can affect the reliability and life of compressor valves. For this reason, pressure pulsation prediction according to API 618 standard is a fundamental step in reciprocating compressor plant design. The present work shows the comparison between design simulation, carried out through a dedicated proprietary multi-physics software, and the results of a dedicated test on the plant (2 stages, 800 kW compressor for Oil&Gas application) performed together with the OEM. The test was fitted with dynamic pressure and vibration measurements in a series of key points on the cylinders and dampers. The simulation is solved in the time domain, using a one-dimensional CFD model for piping, dampers and plenums, and a lumped model for the cylinders. The flow dynamics in the ducts relies on conservation equations (mass, momentum and energy) using the Lax-Wendroff method to obtain numerical solutions (based on finite differences, second-order accuracy in space and time) for internal points and the method of characteristics for external points. If compared with simulations based on acoustic theory, this method provides a better accuracy because it can take into account cylinder-plant mutual interaction, the non-linear effects of viscosity, the heat exchange and the real behaviour of valves. On the other hand, this method requires a large amount of input data. Therefore, a comprehensive consistency between test and simulation can be difficult to achieve, due to possible measurement interferences and to lack of information regarding the actual setup. In this paper, the methods to overcome possible discrepancies are shown in detail.
Furthermore, a study to reduce pulsations in the most critical condition was carried out and the effect on pulsations of alternative capacity control techniques (reverse flow and additional clearance) was also investigated. Finally, a tuning with vibration measurement was used to show the correct setting of the model. The work constitutes an important lesson learned that allowed the OEM to better evaluate and optimize the effectiveness of efficient countermeasures to reduce pulsations, as pulsation dampers and pipe and support geometries.

by: Cappelli Leonardo, Sacco Marco, Fusi Andrea – C.S.T. S.r.l.; Mazzoleni Thomas – SIAD Macchine Impianti S.p.A.

1 Introduction

Reciprocating compressors are cyclic machines and the generation of pressure pulsations is one of their main issues. Each cylinder is equipped with suction and discharge valves, acting like check valves; they stay open for a small part of the cycle and thus generate flow and pressure pulsations propagating in the lines through the piping and the auxiliary equipment at the speed of sound.
Unless carefully analyzed, pressure pulsations can have several negative effects on a compressor: they can cause change in performance, reduction of valve availability, and errors in flow measurement. But primarily, designers have to take care of pulsations because they cause shaking forces in the plant, at all points where there is a discontinuity, with consequent vibration of piping and equipment and potential fatigue failures.
In order to reduce pulsations amplitude, damping volumes and orifices are commonly used. General advices for sizing these devices can be found in [1].
API 618 standard provides procedures to predict and control pressure pulsations and vibrations under certain limits, by means of Pulsation Analysis and Mechanical Analysis [1].
The Pulsation Analysis can be performed by means of the Acoustic Wave Equation or by means of numerical methods for Navier-Stokes equations. For more detailed review on fluid equations see [3].
The Acoustic Wave Equation consists in linear equations, which can be solved in frequency domain with a relatively low computational effort but can introduce uncertainty in the results, since they neglect the non-linear terms of the Navier-Stokes equations.
Numerical methods for Navier-Stokes equations can be solved in time domain, taking into account viscosity, heat exchange, mean flow and gas compressibility [4].
After the Pulsation Analysis a Mechanical Analysis is performed, having as input the gas and inertia forces of the compressor and the shaking forces acting on the piping and on the pulsation dampers, obtained with the former analysis.
Furthermore, a study to reduce pulsations in the most critical condition was carried out and the effect on pulsations of alternative capacity control techniques (reverse flow and additional clearance) was also investigated.

2 Case Study: Measurements & Simulation

2.1 Measurements

The compressor (see Figure 1) is a horizontal balanced-opposed model with four double-acting cylinders; compression takes place in two intercooled stages. Two equal cylinders (90° phased) are dedicated to each stage with common suction and discharge dampers. Table 1 shows the main compressor data.

Table 1: Main Compressor Data

Shaft speed	490	RPM	Suction Pressure	2.89	bar-a
Motor nominal power	800	kW	Discharge Pressure	19.89	bar-a
Cylinders phasing	90	°	1° Stage compression ratio	2.56	-
Processed gas	Air	-	2° Stage compression ratio	3.06	-

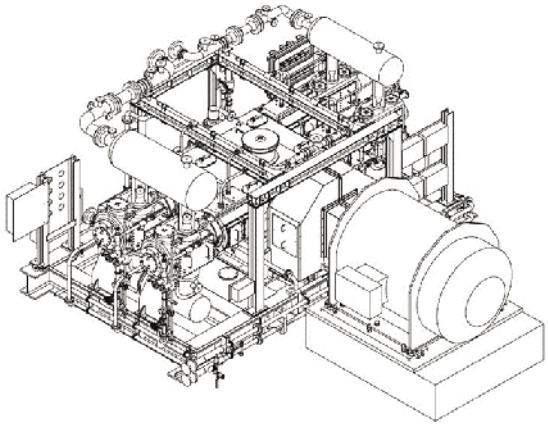

Figure 1: Compression skid

2.1.1 Pulsation Measurements

There are twenty pressure measurement points: eight in the cylinders (two for each cylinder) and twelve in the piping (one for each cylinder flange and one for each line side volume bottle connection). These points allow API pulsation requirements check.
The measurement chain includes a piezoresistive transducer, probe assembly and analyser.
The pulsation analysis performed during the design phase was repeated for the actual test conditions after the measurements, in order to get a good comparison between the model and the measurements. Figure 2 shows the analyser used for the test campaign.

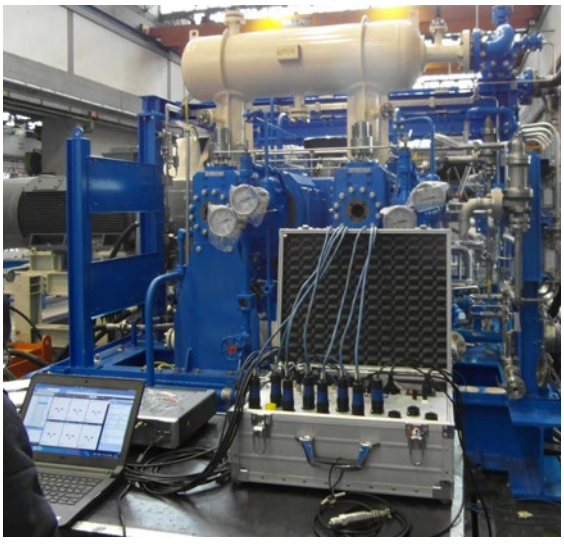

by: Cappelli Leonardo, Sacco Marco, Fusi Andrea – C.S.T. S.r.l.; Mazzoleni Thomas – SIAD Macchine Impianti S.p.A.

Figure 2: Analyser

2.1.2 Vibration Measurements

Vibration measurements have been carried out on cylinders, dampers and piping most significant points by means of an accelerometer (Figure 3).

Figure 3: Accelerometer for vibration diagnostic

2.2 Modelling and simulation

2.2.1 Acoustical analysis

The model used to simulate the plant was developed by CST, based on the multi-physics software AmeSim.

Figs. 4, 5, 6 and 7 show the main elements of the model and the related connections; respectively:

- the double-acting cylinder, with the piston chamber and piston, driven by the crank-mechanism (to be connected to suction and discharge valves),
- the suction/discharge cylinder valves: check valves connected to the plenum and to the cylinder, comprehensive of the dynamic of the shutter (the moving element of the valve) considering springs, mass, and damping.
- the suction and discharge cylinder plena, connecting the valves of the head and crank ends (HE and CE) to the related volume bottle (in the case shown, each cylinder has just one suction and one discharge valve for each end, therefore only two suction and two discharge valves in total),
- the pulsation damper (which is commonly a volume bottle) modelled like a header connecting the cylinder HE and CE plenum and the pipeline.

Plenum and damper complex geometries are modelled as a sequence of mono-dimensional pipes.

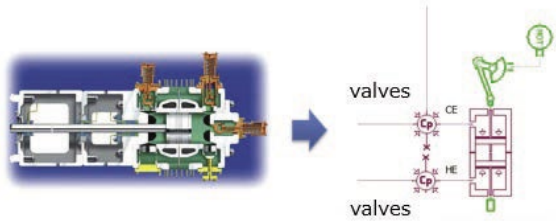

Figure 4: Double Acting Cylinder

Figure 5: Cylinder Valve

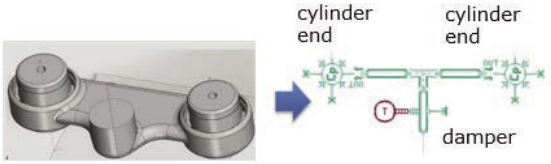

Figure 6: Cylinder Plenum

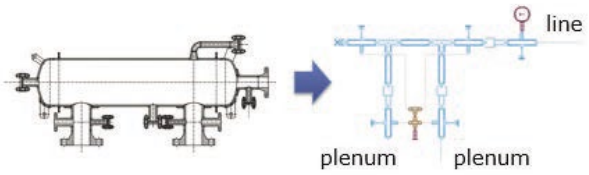

Figure 7: Pulsation Damper

The simulation is solved in the time domain; several cycles are computed starting from initial conditions up to steady-state: only the last 80 cycles were considered for the post-process.
The test was performed on a closed circuit equipped with a throttling valve and an additional off-skid damper between final discharge and first stage suction.
The boundaries of the model consist in two anechoic endings, positioned up- and down-stream the throttling valve.
The model consists of mono-dimensional CFD models for piping, dampers and plenums, and a lumped parameters model for cylinders (variable volume chambers generating the flow pulses). The flow dynamics in the ducts relies on conservation equations (mass, momentum and energy) solved with finite differences using the Lax-Wendroff Method (second-order accuracy in space and time) for internal points and the Method of Characteristics for external points. If compared with simulations based on acoustic wave equation, this method provides a better accuracy because it can take into account cylinder-plant mutual interaction, the non-linear effects of viscosity, the heat exchange and the real behavior of valves.

2.2.2 Mechanical analysis

The finite elements model of the compressor unit includes:

by: Cappelli Leonardo, Sacco Marco, Fusi Andrea – C.S.T. S.r.l.; Mazzoleni Thomas – SIAD Macchine Impianti S.p.A.

- 1st and 2nd stages suction and discharge cylinders,
- Distance pieces,
- Compressor frame including crossheads slides,
- 1st and 2nd stages suction and discharge dampers,
- Suction and discharge piping,
- Support structure.

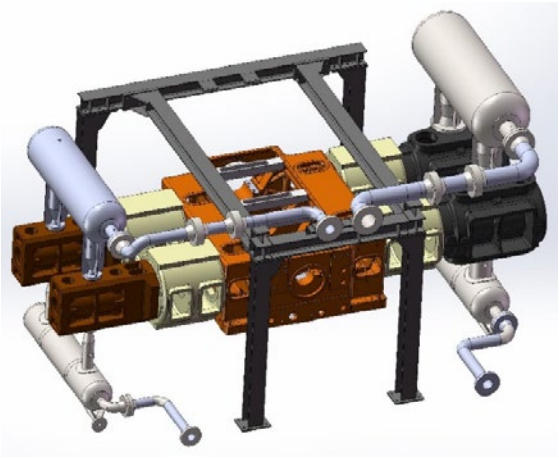

Figure 8: 3D model

The forced mechanical response analysis has been set up imposing dynamic forces on the 3d model. Dynamic loads have been considered on cylinders, crossheads slides and main bearings houses, in order to take into account gas forces and inertia, whilst the shaking forces (direction, amplitude, frequency and phase) computed with the previous acoustical simulation have been imposed on piping and dampers. Spectra of dynamic gas and inertia loads can be seen in Figures 9 and 10.

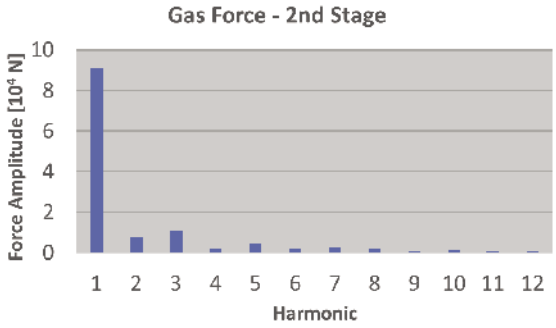

Figure 9: 2nd stage cylinder gas dynamic loads

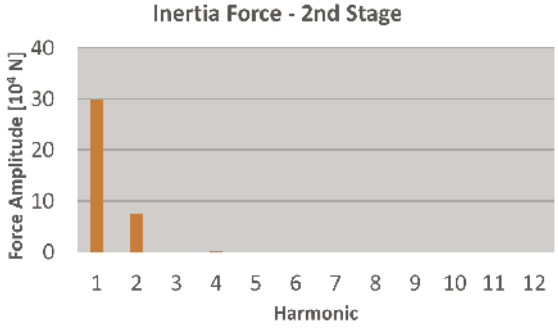

Figure 10: 2nd stage inertia dynamic loads

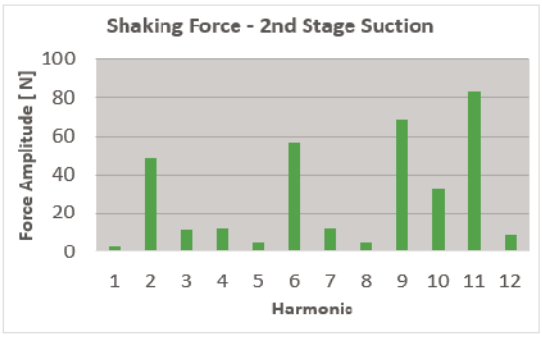

Figure 11: 2nd Stage Suction Damper shaking forces

3 Analysis of results

3.1 Results of Pulsation Analysis

A correct calculation should consider many precautions. Here we want to point out that a good analysis of the field data could require reduction techniques to take into account phenomena affecting the measurement.

3.1.1 Resonance in pressure transmitter connection

Figure 12 shows the PV-cycle of the CE of one of the 2nd stage cylinders, with the calculated and measured (unfiltered) PV-cycle.

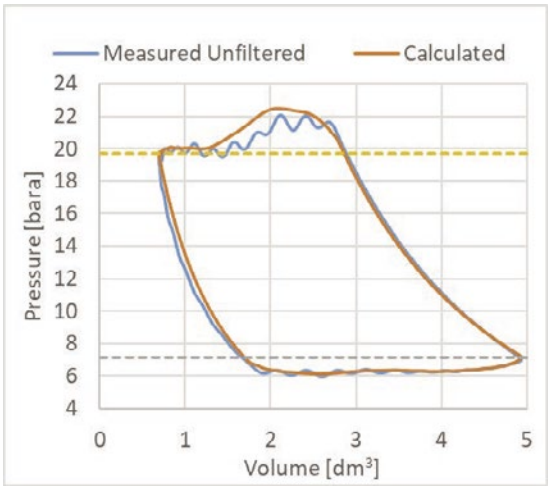

Figure 12: PV-cycle 2nd Stage Cylinder CE – measured unfiltered vs. calculated

Anomalous oscillations at high frequency can be noticed in the measured cycle, but not in the calculated one. The cause of these oscillations was found in the acoustic resonance occurring in the internal connection of the probes. In fact, according to the acoustic theory, this connection can be schematized as an Open-Closed pipe, the length of which is related to a 1st natural frequency of approx. 350 Hz (as shown in Table 2).

by: Cappelli Leonardo, Sacco Marco, Fusi Andrea – C.S.T. S.r.l.; Mazzoleni Thomas – SIAD Macchine Impianti S.p.A.

Table 2: Acoustic resonance in probe connection

Harmonic order	Frequency Hz	O-C pipe resonant length m
37	302.17	0.331
...	...	...
46	375.76	0.266

After filtering the measured pressure in order to eliminate the above-mentioned effect, the PV-cycle shown in Figure 13 is obtained, showing better consistency with the calculated one.

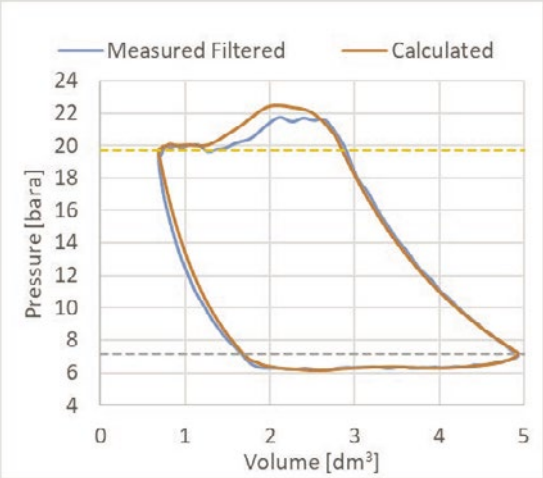

Figure 13: PV-cycle 2nd Stage Cylinder CE – measured filtered vs. calculated

3.1.2 Electrical noise (50 Hz)

The bar chart in Figure 14 shows the calculated and measured peak-to-peak pulsation amplitude for the 6th harmonic at the twelve piping measuring points. The blue bars refer to the measured values obtained with a first post-process method, performing the Fast Fourier Transformation (FFT) on each cycle and then making the average, with a frequency resolution of 8.16 Hz. The green bars show the measured values obtained with a second post-process method, performing the FFT on the entire data sample with a frequency resolution of 0.1 Hz.

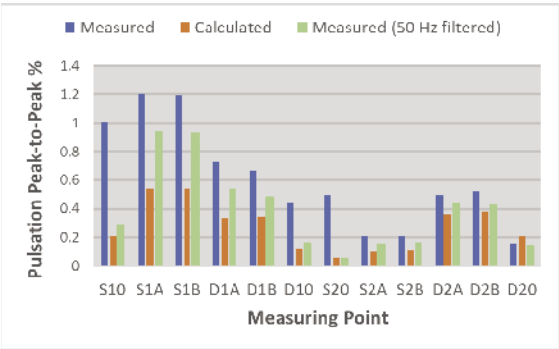

Figure 14: Pulsation amplitude in the measuring points: 6th Harmonic

The difference between measured values post-processed with the first method and the calculated ones is due to the presence of interference coming from the electrical measurement apparatus (50 Hz). The noise was not distinguished from the 6th harmonic in the first method, but clearly identified with the second one (see also Figure 15 showing the spectrum obtained from the measurements post-processed with higher resolution).

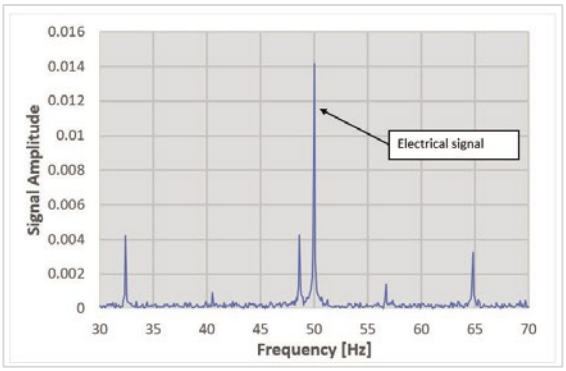

Figure 15: Measured pulsation amplitude spectrum

As can be seen the higher resolution, which makes it possible to distinguish the electrical noise contribution from the pulsation, allows us to get results much closer to the calculated values.

3.1.3 Heat exchanger modelling improvement

The heat exchanger response, in terms of pulsation transmission, is strongly dependent on its pressure drop (other than its internal geometry); so, it must be correctly taken into account. The bar chart in Figure 16 shows a comparison between the spectrum of the pulsation downstream the heat exchanger, calculated on the basis of the actual pressure loss (green bars) and of the value resulting from data sheets (red bars). It can be noted the big difference between the two simulations.

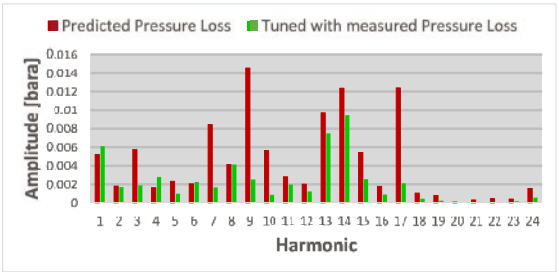

Figure 16: Effect of heat exchanger model on pulsation

Concluding the analysis of the results of the case study, we can see bar charts of calculated and measured pulsation values (peak-to peak percentage for each harmonic) at the 1st Stage Suction Damper nozzle line side (Figure 17). The measured values are in accordance with the calculated ones.

by: Cappelli Leonardo, Sacco Marco, Fusi Andrea – C.S.T. S.r.l.; Mazzoleni Thomas – SIAD Macchine Impianti S.p.A.

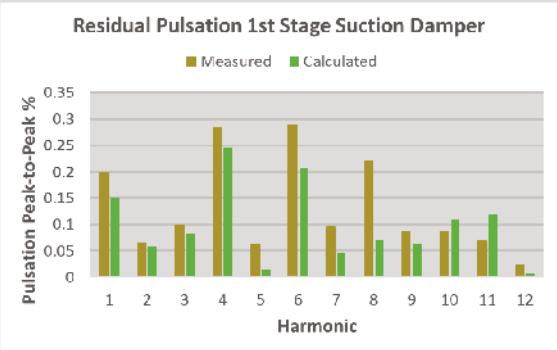

Figure 17: Residual Pulsation @ 1st Stage Suction Damper Nozzle (line side)

3.2 Results of Mechanical Analysis

The mechanical simulation results in terms of vibration velocity have been compared with the vibration measurements. The results of this benchmark have been summarized in Table 3.

Table 3: Vibration velocity values benchmark

VIBRATION VELOCITY BENCHMARK		
Component	Measurements	Simulation
	Vres [mm/s]	
1st Stage Cylinder	3.9	3.1
2nd Stage Cylinder	9.0	6.9
1st Stage Suction Damper	6.7	6.2
1st Stage Discharge Damper	3.6	2.5
2nd Stage Suction Damper	10.8	8.2
2nd Stage Discharge Damper	3.8	4.1

As it can be seen, there is a good match between the vibration velocity values found with the dynamic simulation and the measured values. More specifically, the estimated values are found to be on average lower than those found during measurements. This trend can be due to relative movement which may occur in actual foundation bolts tightening. In the simulation the two components are forced not to have relative movement instead, as it would happen for an ideal bolting. Spectra of measured and calculated vibration velocity for 1st stage cylinder are shown in figures 18, 19, 20.

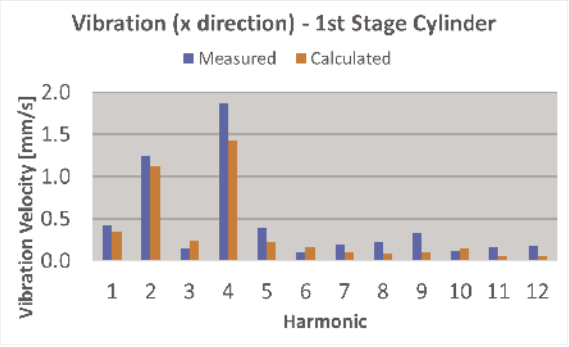

Figure 18: 1st stage cylinder vibration in compressor shaft axis direction (x)

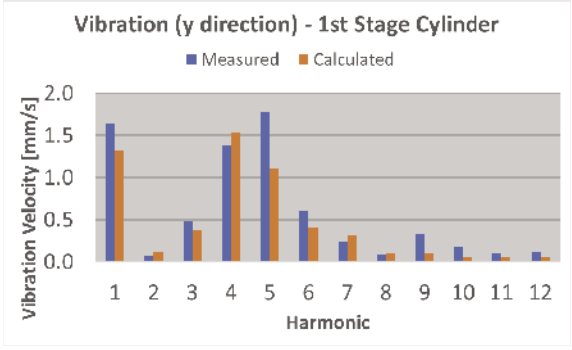

Figure 19: 1st stage cylinder vibration in vertical direction (y)

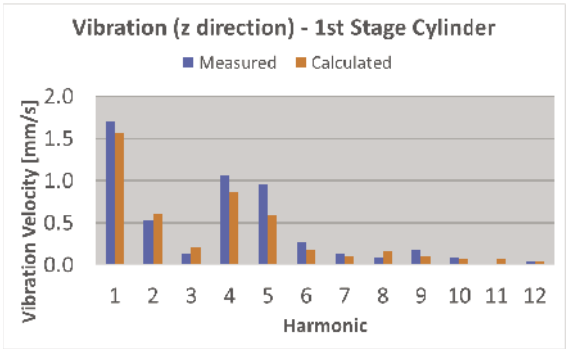

Figure 20: 1st stage cylinder vibration in cylinder axis direction (z)

4 Comparison of Capacity Control Techniques

The capacity control system has a significant effect on the pulsation generated by the compressor, since reduced capacity operation very often generates more critical conditions than at full load, producing a higher pulsation amplitude and/or changing the damper sizing harmonic order. The bar chart in Figure 21 compares the residual pulsation calculated at line side nozzle of the 1st stage suction damper at full load (100% capacity with all four cylinder ends acting – grey bars) and at 50% load obtained in two different ways:

- 50% with unloaded cylinder ends (only the two CE acting – red bars)
- 50% with reverse flow devices acting on all suction cylinder valves (yellow bars).

With unloaded ends, the 1st harmonic is dramatically higher than at full load and represents the sizing condition for the suction damper. In fact, considering API 618 Design Approach 2 pulsation level limit, the full load condition would not require a damper, while 50% load (by means of unloading effects) requires a 200-litre damper.

by: Cappelli Leonardo, Sacco Marco, Fusi Andrea – C.S.T. S.r.l.; Mazzoleni Thomas – SIAD Macchine Impianti S.p.A.

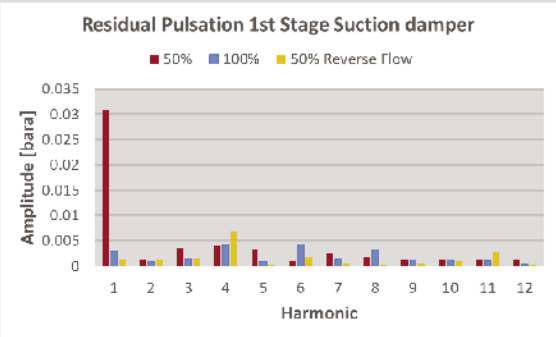

Figure 21: Residual Pulsation @ 1° Stage Suction Damper Nozzle line side

With a reverse flow control system, the harmonic content of the significant frequencies is similar to the full load one, and the 1st harmonic is much smaller; consequently, the damper volume can be much smaller, thus resulting in less costs and less oscillating mass, therefore higher vibration frequency for the cylinder header.
Another way to control the capacity is to use additional clearance pockets on the HE of the cylinders. The diagrams in figs. 22 and 23 show respectively the volume required for 1st stage suction and discharge volume bottles vs load condition with the three different systems. Unloading ends is the most critical situation for both suction and discharge volume bottles.

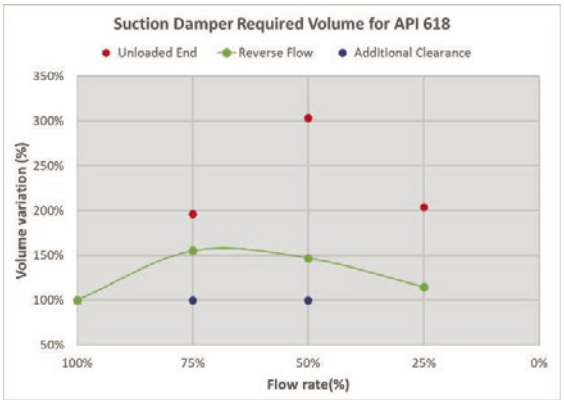

Figure 22: Volume required for suction damper according to API 618 preliminary sizing

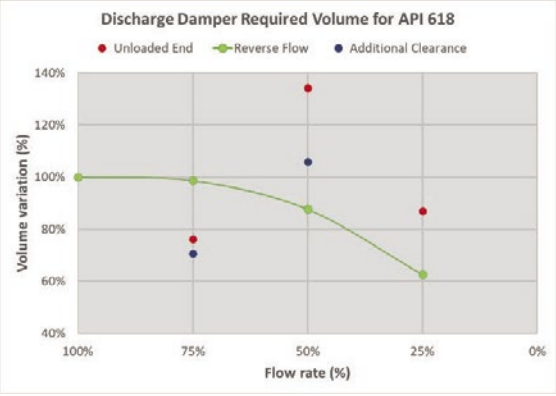

Figure 23: Volume required for discharge damper according to API 618 preliminary sizing

5 Conclusions

The model used for Pulsation Analysis can get the best accuracy, but on the other hand, it is elaborate and requires a large amount of input data. Therefore, the information regarding the actual setup has to be clear and complete. Moreover, API acceptance criteria provide limit for pulsation amplitude at each pulsation damper connection line side and the limit is function of the frequency, so several measurement points are to be taken and all the values have to be carefully post-processed with FFT to get the pulsation spectra. All these values can be affected by interferences which complicate the possibilities to achieve a comprehensive consistency between test and simulation.
The work constitutes an important lesson learned allowing the OEM to correctly analyze the pulsation values measured on field, to better evaluate and optimize the effectiveness of the countermeasures to be taken in order to reduce pulsations and consequent vibrations (i.e. pulsation dampers, pipe geometries and supports).
In particular, some reduction techniques are shown, which must be used in Pulsation Analysis to take into account phenomena affecting the model/measurement:

- resonances in the sensor duct
- electrical noise superimposed to the pulsation signal

It has also been shown the big influence of the capacity control system selected on the volume of dampers required.

References

[1] Almasi A. (2009) Pulsation Suppression Device Design for Reciprocating Compressor, World Academy of Science, Engineering and Technology 31 2009.

[2] Atkins K.E., Pyle A.S., Tison J.D. (2004) Understanding the Pulsation & Vibration Control Concepts in the New API 618 Fifth Edition, Gas Machinery Conference 2004, Albuquerque, New Mexico.

[3] Tweten D., Nored M., Brun K. (2008) "The Physics of Pulsations", Gas Machinery Conference 2008.

[4] Cappelli L., "Numerical Modelling and Experimental Validation of Dynamic Interaction of Reciprocating Compressor and Plant", master's degree thesis, Università degli Studi di Firenze, 2017-2018, supervisors G. Ferrara, A. Fusi, M. Sacco.

Sauer Compressors

Reduction of Vibration – Modal testing of a reciprocating compressor, theoretical background and practical testing

by:

Heumesser, Thomas
CTO
J.P. Sauer & Sohn Maschinenbau GmbH
Kiel, Germany
thomas.heumesser@sauercompressors.de

Marks, Ferdinand
Engineering
J.P. Sauer & Sohn Maschinenbau GmbH
Kiel, Germany
ferdinand.marks@sauercompressors.de

12th EFRC CONFERENCE
August 24 – 26, 2021, Warsaw

Abstract:
In order to understand the vibration behaviour of a system, there are various test procedures that can be applied. Typically, an operational vibration analysis is carried out as first step to gain an impression of the entire unit. Afterwards, further investigations, such as a modal analysis, can be performed to examine the system in more details.
This article presents both procedures to analyse the vibration behaviour of a high pressure compressor. The main aim of improving this compressor is to reduce structure-borne noise and resulting vibrations in order to increase the safety of the technical staff and the machine itself. In addition also the reliability of the unit increases, which causes further advantages for the customer and the supplier.
In order to identify the structures which need improvement, an operational vibration analysis was carried out. Significant vibration frequencies of the whole unit can be identified. Subsequently, an experimental modal analysis of the main components of the compressor has been performed. The results show the natural frequencies and the associated motion of the individual structures in the overall system. The combination of both methods helps the user to understand the vibration pattern of such a machine and to identify the components excited with the resonant frequency at defined speeds.

by: Thomas Heumesser, Ferdinand Marks – J.P. Sauer & Sohn Maschinenbau GmbH

1 Introduction

Increased structure-borne noise levels of a system can pose a risk to the environment and to the machine itself. In addition to interactions with the place of installation, the person in this environment may also be injured. Furthermore, the service life of machine parts can be reduced if the system is incorrectly designed, resulting in locally high vibrations. Therefore it is necessary to know the structural behaviour of the whole system and of selected parts.

There are various methods that can be applied to record and understand the structural dynamic properties of a system. In principle, these methods can be divided into numerical and experimental procedures. The numerical methods include, for example, FEM (finite element method) analysis, in which components or entire systems are represented by means of a substitute model and the desired quantities (natural frequency, natural vibration mode shape, modal mass and modal damping) can be calculated with selected approach functions. In contrast to this, in an experimental approach, the structural behaviour is determined by using sensors to record measured values and then interpreting the data. In this investigation the experimental methods of modal analysis and frequency analysis are applied to understand the vibration problem.

The high pressure compressor series are the most powerful and largest machines in the company´s family. Since their release in 2009, many units and customer-specific systems, such as container systems, have already been built and delivered. The reciprocating compressor with a maximum pressure of up to 500 bar is mainly used in industry.

In this working environment it is important to ensure acceptable vibration levels for man and machine. To decouple the machine from the working environment during operation, the compressor and the motor are elastically mounted. Several rubber buffers are installed for this purpose, which are mounted on a base frame. The base frame is intended to stiffen the entire machine and help to reduce the vibrations transmitted to the outside. The main problem that arises here is that the vibrations transmitted to the environment are too high (acceleration level about L_{ai} = 100 dB above the shock mounts[*]). In addition, some components vibrate very strongly during operation, so that breakages occur on pipes at their joints after a certain running time. The aim of this investigation is to identify the causes of the vibrations and to develop specific suggestions for improvement.

2 Dynamic analysis

2.1 Theoretical background of the structural dynamic

Machine and structural vibrations always occur in connection with moving components and/or moving media. Thus, there are a certain number of excitations that lead to vibrations or structure-borne noise.

Typical triggers for excitations by flowing media in and on machines are air and water flows. Turbulence, which is always generated depending on the flow velocity, is the decisive factor for the interaction with the component. Turbulence occurs when hitting obstacles, such as the flow around bodies, or through friction, such as on pipe walls. In the case of machine vibrations, these turbulence excitations are usually less energetic than excitation by moving components, so that they only have a supplementary effect on smaller machines.

The characteristic vibration pattern of a machine is accordingly determined by the moving components. In the case of reciprocating compressors there are mainly two types of excitation by moving parts which lead to vibrations of the machine, if the gas forces in the cylinder are properly balanced and reduced. These are excitations caused by imbalances of rotating parts and by unbalanced inertia forces and moments of inertia in the drive train.

Inertia forces occur at uneven movements of masses. The inertial forces are generated by two movement categories. One is the oscillating mass force $F_{m,osc}$, which is generated by an oscillating movement, and the other is the rotating mass force $F_{m,rot}$, also known as centrifugal force and is caused by a rotational movement. Figure 1 shows the different types of movement. The shown piston moves back and forth on a line between top and bottom dead centre. Thus it has an oscillating movement and thus an oscillating inertia force. The rotary motion of the crankshaft results in a rotating inertia force. The connecting rod in turn has both types of movement, so that both a rotating and an oscillating inertia force results. If several crank mechanisms are used for compression, moments of inertia are generated due to the shift around the zero point. [1]

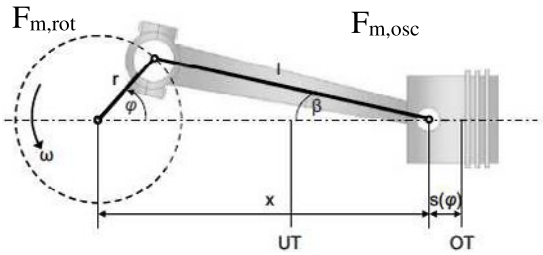

Figure 1: Schematic representation of the movement of a crank mechanism

[*] $L_{ai} = 20 * \log\left(\frac{a_i}{a_o}\right), a_0 = 1 * 10^{-5}\ m/s^2$

by: Thomas Heumesser, Ferdinand Marks – J.P. Sauer & Sohn Maschinenbau GmbH

Imbalances, on the other hand, result from an eccentricity of the centre of mass in relation to the axis of rotation of a component. A typical component here is the flywheel.

In addition the vibration can be occurred due to pulsation-induced forces. By displacing the gas, an alternating pressure is created, which leads to so-called aeropulsive noises. The displacement can be caused by pulsating flow processes. In this case, a defined volume of gas is periodically released and sucked in again. As a result, pressure differences are built up with the immediate surroundings as a result of pressure equalisation processes. These pressure fluctuations are passed on via the gas and transmitted to the components, which are excited with the frequency of the pulsation. In addition, these pulsations strike fixed boundaries which reduce the flow speed. Since the gas can be regarded as a moving mass, forces and thus vibrations are also transferred to the components.

Based on the speeds of the individual rotating parts, typical excitation frequencies can be recorded and assigned to each. In practice, a frequency analysis is carried out for this purpose.

The aim of frequency analysis is to map the vibrational signature of a system in operation. Depending on the measuring point placed on the object to be examined, different conclusions can be drawn from the measurement. For example, measurements on pipelines are more likely to detect pulsations than if the sensor is placed on the foundation of a unit. For this purpose, recorded measured values are displayed, for example, in an acceleration frequency diagram. In this way, significant peaks can be identified with the associated frequency, so that conclusions can be drawn about the system in question.

Frequency analysis can be used to map the entire behaviour of the machine during operation. In addition, it is possible to easily identify the exciting frequencies and assign them to the cause. However, if conspicuous peaks occur in a multiple of the excitation frequency, it is difficult to interpret. This is where modal analysis may come into effect.

Every subsystem that is installed has a large number of natural frequencies. The natural frequency is the frequency where a vibrating system oscillates after a one-time excitation such as a hammer blow (see chapter 2.3). The system always oscillates at characteristic natural frequencies of first and higher order. If the natural frequency of a component in the installed state is very close to an excitation frequency, so-called resonance occurs. A frequency analysis can only detect that structures have to be excited at a certain frequency, but it will not be possible to detect which structures are excited. Modal analysis is used for this purpose.

In contrast to frequency analysis, modal analysis is carried out on machines that are not in operation. Here a response signal is measured, which was triggered by a previously defined introduction pulse. The input as well as the output signal of several sensors is measured at different points. Thus, movements of individual points can be recorded and combined together until a movement image of the entire system is obtained. From this result the movement frequency of individual subsystems can be derived. [2]

2.2 Vibration measurements and spectrum analysis

In a frequency analysis or operating vibration analysis, single- or triaxial accelerometers are usually installed at selected measuring points to measure the resulting accelerations of parts while the machine is running. An acceleration-time curve is recorded, which serves as the basis for further evaluation. With the help of an FFT analysis (Fast-Fourier-Transform) the time-discrete signal can be decomposed into its frequency components and thus analysed. For a better understanding and to simplify the comparison, the acceleration values are converted into acceleration levels with the pseudo unit dB.

The acceleration levels are now displayed above the frequency, whereby a differentiation can be made between broadband and narrowband analyses. In a broadband analysis, the standard frequency range according EN ISO 266 from 31.5 Hz to 20 kHz can be divided logarithmically into octaves and third octaves. In this process, the acceleration values of several frequencies are combined into one value. The choice which frequencies are combined is determined by the centre frequency. A calculation then makes it possible to determine the upper and lower limits, the corner frequencies. The resulting frequency range is called a band. All frequencies that lie outside a band are removed by a specific filter and are not included in the post processing.

In a narrow-band analysis, on the other hand, the frequencies are plotted linearly, which allows a more precise observation. The frequency steps, for example df = 1 Hz, which are to be displayed can be set by the user.

In practice, both evaluation methods are used. The broadband analysis offers the possibility to quickly make a statement about the vibrational behaviour of a machine. The logarithmic display provides an overview and allows direct detection of abnormalities, as the display is very clear and compressed to a few frequency bands. However, if you want to go into more detail, narrowband analysis should be used. By mapping individual frequencies, it is possible to identify exactly where the issue is. This makes it possible to make targeted improvements and thus change the vibration image of a machine. [3]

by: Thomas Heumesser, Ferdinand Marks – J.P. Sauer & Sohn Maschinenbau GmbH

2.3 Measurement of Frequency Response Functions

Modal analysis is a process involving testing components or structures with the objective of obtaining a mathematical description of their dynamic or vibration behaviour. The mathematical description can be determined numerically or experimentally, whereby only the experimental consideration is explained here.

In the experimental approach, a defined excitation is applied to the test object and both the input and the response level are measured. The aim is to determine the so-called FRF (Frequency Response Function), which is used to determine the typical modal quantities (natural frequency, natural vibration mode shape, modal mass and modal damping) of a system. Figure 2 shows the theoretical scheme of such a determination.

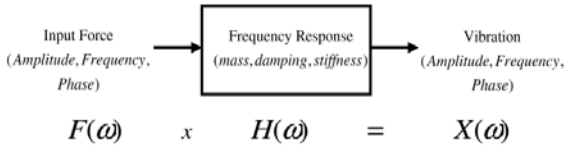

Figure 2: Theoretical scheme of the FRF (Frequency Response Function) determination

It can be seen that the input force F(ω) multiplied by the frequency response H(ω) equals the output vibration X(ω). The output vibration can be measured as acceleration, which in turn can be converted into a displacement. This results in the following relationship:

$$H(\omega) = \frac{X(\omega)}{F(\omega)} = \frac{output}{input}, (1)$$

The mathematical relationship between the transfer function and the actual behaviour of the machine is the equation of motion. The result of the equation of motion and the determined frequency response should be the same. This relation helps to match the mathematical model.

Different methods can be used for excitation. It is possible to excite the system with a shaker at a certain frequency or to apply a transient input by means of a hammer blow or sudden release from a deformed position which results in broadband excitation. It is important that all installed subsystems receive sufficient excitation so that a meaningful response can be measured.

In this study, the excitation was carried out by hammer blow to generate a broadband excitation. Also, the method of moving the sensors while keeping the excitation position constant was used. This method was chosen because only a limited number of sensors are available to record the accelerations. The procedure is such that one first defines at which positions of the machine the sensors should be placed. Then a suitable excitation point is selected so that all subsystems are sufficiently excited. The measurement is carried out in such a way that several impacts are carried out per considered measuring point, so that an average value can be formed. Then the sensors are replaced and a new excitation is generated on the machine. Thus, with each further measurement the overall picture of the machine is built up. The mathematical calculation of the natural vibration quantities is carried out by the measuring system used and as a result provides a narrow band analysis as well as the qualitative representation of the movement in the individual measuring points represented in the model. [4]

3 The high pressure compressor series

3.1 General information

The machine under investigation is a reciprocating compressor of the high pressure series, which are mainly used for industrial purposes. A general structure of such a machine is shown in Figure 3. The shown compressor has the dimensions 2700 x 1600 x 1650 mm and weighs about 4000 kg.

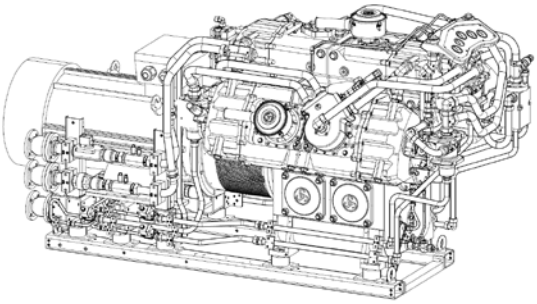

Figure 3: Drawing of the tested high pressure compressor

With a shaft power of up to 250 kW, the performance area of the machines extends from 10 to 500 bar final pressure and a volume flow ranges from 200 to 800 m³/h. Various gases (air, nitrogen, helium, argon, hydrogen and natural gas) can be compressed. The high pressure series is designed as a modular system, so that basically two superstructures can be selected. Depending on the crankcase, four or six compression cylinders can be installed, whereby one to five compressor stages can be realized. Figure 3 shows six compressor cylinders. The pistons can be selected and installed from seven variants with a diameter range from 22 mm to 195 mm to achieve the required final pressure. In order to meet customer requirements, the high pressure compressor series can be built as atmospheric or as gas tight booster versions up to 20 bar suction pressure.

3.2 Details of the tested compressor

Figure 3 and Figure 4 show drawings of the compressor under investigation. As already mentioned, it can be seen that six compression cylinders are installed in a W-arrangement. This compressor has a total of four compressor stages, which means that three stages act as air inlet stages. These are marked with 1.1, 1.2 and 1.3 in Figure 4

by: Thomas Heumesser, Ferdinand Marks – J.P. Sauer & Sohn Maschinenbau GmbH

and shown in light yellow. The numbering corresponds to the sequence of compression. With such an arrangement a final pressure of 420 bar and a volume flow of 580 m³/h can be achieved. The machine is operated at speeds of 1500 and 1800 rpm.

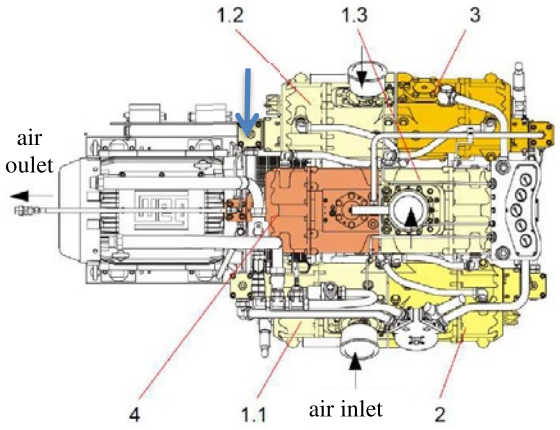

Figure 4: Compressor stages of the high pressure compressor

A sectional view of the crankcase including the crankshaft can be seen in Figure 5. In order to guarantee the compressor sequence, a double cranked crankshaft (1) is provided. This means that three piston rods (2) are installed per crank, whereby the adjacent piston rods have an angular offset of 180°. The individual piston rods and pistons are designed to have identical weights, regardless of their final pressure. In combination with the counterweights (3) installed, the inertial forces and moments are kept low.

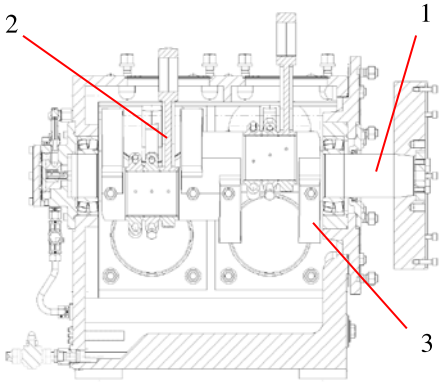

Figure 5: Sectional view of the crankshaft

4 Applied vibration analysis

4.1 Applied frequency analysis

As already discussed in theory, frequency analysis can be used to determine the vibrational behaviour of a machine. For this purpose, five triaxial accelerometers were mounted on both sides of the compressor above the elastic mounting, in order to evaluate the vibration behaviour of the entire machine. Figure 6 shows the base frame and the elastic mounting that were used. The measuring points where the sensors were mounted are located directly above the buffers.

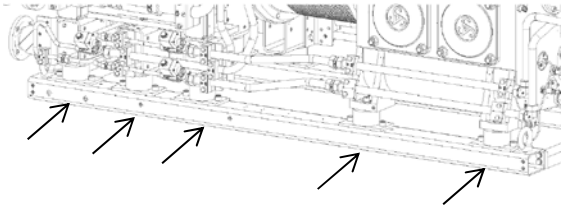

Figure 6: Base frame, resilient mounting and measurement points

In order to define the measurement results, the operating conditions must be established. In this case a final pressure of 400 bars was maintained and both possible speeds of 1500 and 1800 rpm were run. Since short disturbances can occur during a measurement, a measuring time of 30 s was set, so that these were not significant.

The results are displayed in a frequency range from 8 Hz to 20 kHz. In order to measure this bandwidth the Nyquist-Shannon sampling theorem must be observed. The theorem states that the sampling frequency must be at least twice as high as the highest frequency component present in the time signal. The sampling rate for this measurement is 51200 s/sec (samples per second) therefore the theorem is taken into account. To ensure that higher frequencies do not interfere with the signal, the anti-aliasing filter is also used. This filter is a low-pass filter that only allows signals below a certain frequency to pass. [3]

After carrying out the measurement, several diagrams were created in post processing, also to compare the different speeds. In order not to show all directions and measuring points individually, the energetic average of the values was calculated for each frequency and shown in the third octave band (see Figure 7) and in the narrowband (see Figure 8). The energetic average is calculated as followed, whereas N is the number of measurement points and $L_{a,i}$ is the sound acceleration level at every measurement point in dB:

$$L_{a\ aver.} = 10 * \log\left(\frac{1}{N}\sum_{i=1}^{N} 10^{0.1*L_{a,i}}\right), (2)$$

The red curve in Figure 7 shows the measured values recorded at 1500 rpm and the green curve shows the higher speed of 1800 rpm. “Average all” means that each measurement point in each direction was taken into account when calculating the energetic average. Ten measuring points and three directions, totally thirty values, are taken into account.

This view only shows the centre frequencies of a range and several values are combined. The higher the centre frequency rises, the more values are combined. Therefore the biggest differences in the individual measurements can be detected up to about 400 Hz.

by: Thomas Heumesser, Ferdinand Marks – J.P. Sauer & Sohn Maschinenbau GmbH

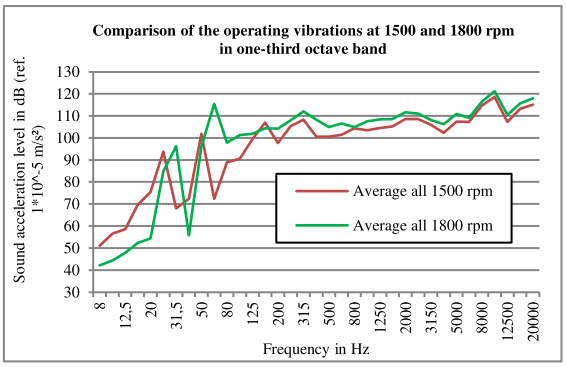

Figure 7: Operating vibrations in third of octave

First of all, the red curve is observed, which shows two significant peaks in this range up to 400 Hz. These peaks are at 25 Hz with an acceleration level of 94 dB and at 50 Hz with a value of 102 dB. If the compressor speed is converted to frequency by dividing it by sixty, these peaks can be clearly explained:

$$f_{exc1} = \frac{1500\ min^{-1}}{60\ s * min^{-1}} = 25\ Hz, (3)$$

The excitation frequency is assigned to the speed of the drive train in the frequency analysis as 1st order at 25 Hz and as 2nd order at 50 Hz. Mechanically, this depends on several factors. For example, due to residual imbalances in components, centrifugal forces act on the bearings, which are transferred from shaft rotation to the crankcase and thus cause the machine to vibrate. Typical components that show a residual imbalance are the flywheel and the crankshaft.

A further reason for excitation are unbalanced mass forces and moments caused by the oscillating movement of the pistons, the rotating movement of the crankshaft and the superimposition of both components in the movement of the connecting rods. Rotating inertial forces can be compensated by attaching a counterweight at the crank shaft. The counterweight must be calculated in such a way that the centre of gravity of the overall arrangement lies in the axis of rotation. This has been realized with this machine, as shown in Figure 5. When compensating the oscillating inertia force, this conversion can only be partially adapted. Due to the rhythmic dependence on the crankshaft rotation in the 1st order, this inertial force can be completely compensated by counterweights on the crankshaft. In contrast, the 2nd order inertia force can only be balanced by arranging several shafts with counterweights. Moments of inertia are created around the centre of gravity of the compressor by the interaction of several cylinders through the movement of the individual pistons, for example when one piston moves up and the other moves down simultaneously. Mass moments can be eliminated by an appropriate number and arrangement of the cylinders.

The third factor that leads to vibrations is the irregularity of the machine. Gas and inertia forces generate the torque that is effective at the crank pin of each cylinder. Since these forces change constantly in a reciprocating compressor, in accordance with the non-uniformity of the crank drive as a function of the crank angle, there are also fluctuations in the torque and angular velocity of the crankshaft. This non-uniformity can be compensated by means of a flywheel.

In practice, vibrations cannot be prevented totally, only minimized. The resulting structure-borne noise is transmitted via the crankcase to all installed systems and parts, which may also start to vibrate. If a natural frequency of a subsystem is in the 1st order or a multiple of the excitation frequency, the occurring vibrations can be amplified even further.

When looking at the green graph in Figure 7, the second high peak is striking. Here, a centre frequency of 63 Hz is present. When comparing the rotational frequency at 1800 rpm with this peak, the correlation can be seen again:

$$f_{exc2} = \frac{1800\ min^{-1}}{60\ s * min^{-1}} = 30\ Hz, (4)$$

Again the 1st and 2nd order of the rotational frequency can be determined as excitation frequency. However, since 63 Hz does not correspond exactly to the rotational frequency, a narrow-band analysis has been carried out, as shown in Figure 8. Here it can be clearly seen that these formed peaks are the rotational frequency of the compressor of 30 and 60 Hz.

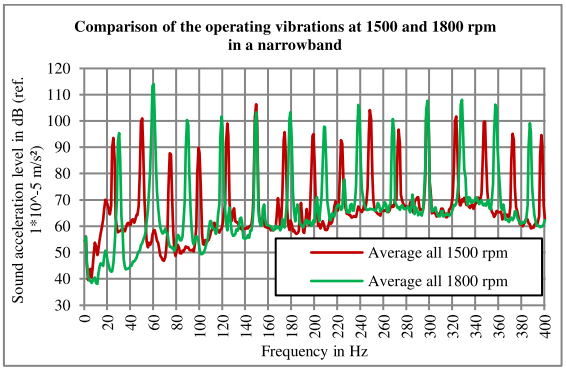

Figure 8: Operating vibrations in narrowband

If the high and the low rotational frequency are compared, the shift of the peaks in the lower frequency range can be attributed to the 5 Hz difference in the rotational frequency. This can also be clearly seen in the narrow band analysis, which is carried out up to 400 Hz. It is also clear that the recorded peaks in the narrow band are always a multiple of the rotational frequency. This is therefore the decisive excitation.

What cannot be explained by the different speeds is the jump in the respective second order. In general it can be said that the level of the green and red graphs over all frequencies is equal. The only noticeable deviation is at 50 and 60 Hz. Here a difference in the vibration acceleration level of about 15 dB is seen. Also the level at 60 Hz is very

by: Thomas Heumesser, Ferdinand Marks – J.P. Sauer & Sohn Maschinenbau GmbH

high at 115 dB. This may indicate an existing natural frequency of a system, which can only be checked by a modal analysis.

However, before dealing with the modal analysis, the frequency range above 400 Hz shall be considered. There is an approximately constant level of vibration acceleration between 100 and 110 dB at both speeds.

At this area, overlays of different mechanisms prevail, which excite the periphery to vibrate. It is very difficult to name single causes for the occurring levels. For example, the rattling of valves occurs while the compressed gas leaves the compressor stage. These components are excited by the turbulent flow around the obstacle, as occurs in concentric valves by the plate springs.

Another excitation is the turbulent flow in the pipes. Due to turbulences at the pipe wall, the pipe is excited and starts to vibrate, which is also transferred to adjacent parts.

4.2 Applied modal analysis

This modal analysis is performed on the basis of the frequency analysis of the compressor. The natural frequencies of the subsystems determined by the modal analysis are compared with the excitation frequencies as well as the measured results of the frequency analysis to find any consistencies. The natural frequencies were examined in the frequency range from 0 to 500 Hz.

In order to understand the behaviour of the entire machine, 223 measuring points were specified. With such a large number of measuring points not only the main structure of the system can be mapped but also the periphery, such as pipes, filter dampers and oil filters, can be measured. When it is about the vibration behaviour of the machine itself, these components matter only a minor role. Therefore a system reduced to the main components was chosen. Figure 9 shows the variant with 98 measuring points including all the main components of the compressor. The yellow points represent one measuring point each, so that the compressor in the model is very similar to the physical modal. On the model the electric motor is shown on the left side and the compressor with the compressor cylinders on the right side. The white placed arrow represents the excitation point, as it can be seen again in blue in Figure 4. In order to better illustrate the movement of the individual measuring points to each other, points can be connected with lines. In this way an overall picture is created from the recorded movement of each individual point and the movement of entire assemblies can be detected. The recorded movements are always frequency-dependent, so that it is possible to detect where natural frequencies are present.

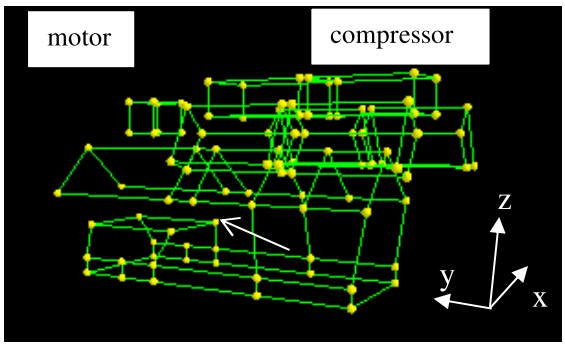

Figure 9: Geometric model of the compressor with 98 measuring points

In order to be able to detect natural frequencies, the recorded FRFs are mapped into a narrow-band analysis (see Figure 10). The frequency is shown on the abscissa in Hz and the amplitude of the FRF in m/s²/N on the ordinate. If there is an accumulation of peaks at a certain frequency, this could indicate a natural frequency. To verify this, the phase angle is also mapped (see Figure 11). At a given natural frequency there is a phase shift, which indicates a standing wave.

Figure 10 shows the FRFs determined from 1 to 30 Hz. The figure starts with 1 Hz because the sensor is overdriven below this value. Each line shown is a measured point of the model. Several peaks can already be seen here

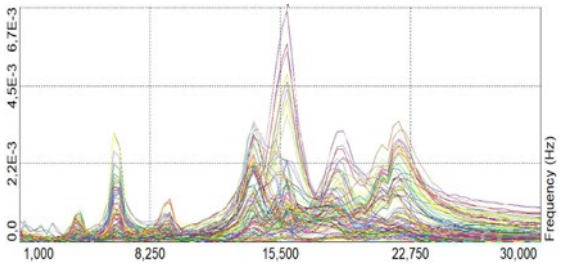

Figure 10: FRF determined in the frequency range from 1 to 30 Hz

The phase shift mentioned above is shown as an example in Figure 11. The abscissa of the diagram shows the frequency from 1 to 30 Hz and the ordinate the phase from -180 to 180°. Accordingly, the middle of the ordinate of the diagram has a value of 0°. To clearly show a phase shift, a red box is inserted at 9.3 Hz. It can be seen that there is a rather steep phase shift from 180 to 0° in the upper half and from 0 to -180° in the lower half.

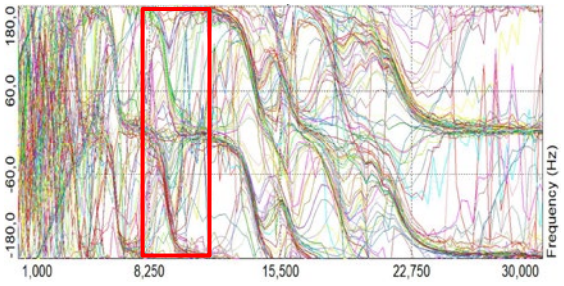

Figure 11: Phase shift at 9.3 Hz

by: Thomas Heumesser, Ferdinand Marks – J.P. Sauer & Sohn Maschinenbau GmbH

By looking at both diagrams together, the system natural frequencies can be determined. In addition, the circle-fit method can be used to specifically determine the natural frequency and the loss factor, i.e. the ability of a material to damp vibrations. The natural frequencies, as well as the loss factor and the corresponding movements are listed in Table 1. The movement can be determined by means of the displacement amplitudes determined by the measurement software, which are then mapped in the model seen in Figure 9.

Table 1: Determined natural frequencies from 1 to 30 Hz

no.	natural frequency (Hz)	loss factor	movement
1.	4.0	0.053	translatory z
2.	6.2	0.045	translatory y
3.	9.3	0.057	translatory x
4.	14.0	0.059	rotatory
5.	15.9	0.093	rotatory
6.	19.0	0.048	rotatory
7.	22.1	0.073	rotatory

Looking at the results of the modal analysis, the low natural frequencies can be clearly assigned to the elastic mounting used. This can be recognized by the fact that the system oscillates as a whole and in phase. This means that all measuring points above the mounting move with similar amplitudes and in the same direction. This type of movement is also called rigid body movement. Elastic mountings installed in this way have six relevant natural frequencies. These are three translational in x, y and z direction and three rotational around the respective axis. The rotatory natural frequencies are usually higher than the translatory ones. In the compressor series, the rubber buffers are designed in such a way that the vertical natural frequency, which can be measured here, is about 5 Hz. The reason for this is that the buffers are soft enough to ensure sufficient insulation between the compressor and the environment. These natural frequencies of the rubber buffers are not critical at the given speeds of 1500 and 1800 rpm and are outside the excitation. However, as the modal analysis shows, the highest rotational natural frequency is at 22.1 Hz. At an excitation frequency of 25 Hz this frequency is still excited, as can be seen in Figure 8. If the compressor is run at even slower speeds, it must be ensured that the rubber buffers are adjusted accordingly, otherwise there is a risk that the lower natural frequencies will also be in the range of the excitation frequency.

The frequency range from 30 to 100 Hz is shown in Figure 12. Again, clear peaks which can be identified as natural frequencies can be seen. The diagram of the phase angles has been omitted here due to lack of clarity.

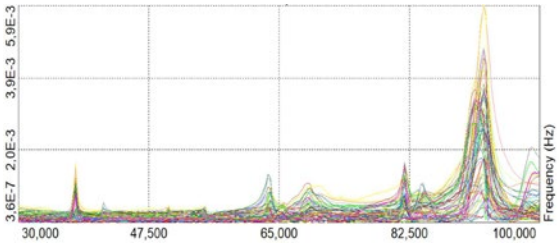

Figure 12: FRF determined in the frequency range from 30 to 100 Hz

Again, the determined natural frequencies are listed in Table 2. The movement is omitted here because there is no rigid body movement.

Table 2: Determined natural frequencies from 30 to 100 Hz

no.	natural frequency (Hz)	loss factor
8.	37.7	0.023
9.	63.8	0.011
10.	68.8	0.029
11.	81.9	0.039
12.	92.4	0.024
13.	99.0	0.022

The first natural frequency worth mentioning is 63.8 Hz. It has already been explained that the increase at 60 Hz compared to 50 Hz is probably due to a natural frequency. This can now be proved by means of modal analysis. 63.8 Hz is very close to the 2nd order excitation frequency at 1800 rpm which causes the system to oscillate. The consequences can be clearly measured. Looking at the movement of the system, it can be seen that tilting occurs. The point about which the tilting occurs is the coupling between the motor and the compressor. An exaggerated representation of the movement shows the tilting around the coupling (see Figure 13). The white cross is intended to show the initial state to illustrate the tilting.

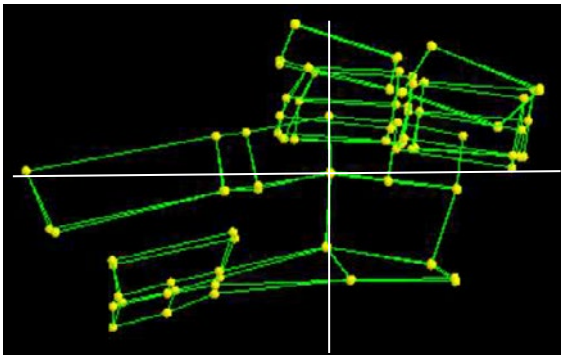

Figure 13: Movement of the system at 63.8 Hz

The second frequency, which is to be examined more closely, is 92.4 Hz, because in the operating vibration analysis an increased peak is shown in the green curve compared to the red curve at 90 Hz. At this frequency the compressor itself is rigid and shows little movement. This is different in the

by: Thomas Heumesser, Ferdinand Marks – J.P. Sauer & Sohn Maschinenbau GmbH

motor area (red box in Figure 14). In this case, there is a torsional movement of the base frame and the intermediate frame on which the motor is mounted. This shows that both frames are not stiff enough.

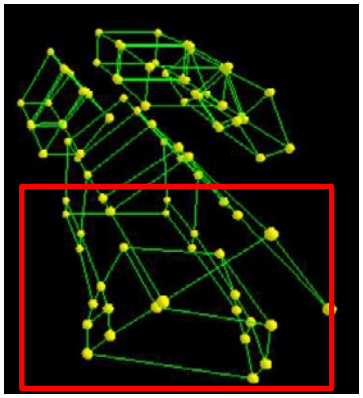

Figure 14: Movement of the motor area at 92.4 Hz

When examining higher frequencies, it is becoming increasingly difficult to identify clear system natural frequencies. The reason is that signal noise makes the recorded values unclear, which means that no clear peaks can be identified. This is illustrated in Figure 15, where the frequency range from 100 to 300 Hz is shown.

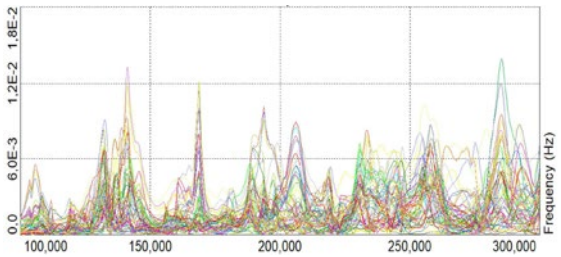

Figure 15: FRF determined in the frequency range from 100 to 300 Hz

In contrast to the frequency ranges considered so far, the problem of noise can already be identified in this consideration. Furthermore, it should be added that mainly natural frequencies of single components and not of subsystems are present. This can also be detected in narrowband and third-octave band analysis. There are no clear peaks, but the level remains at one level. The natural frequencies present in this frequency range under consideration are shown in Table 3.

Table 3: Determined natural frequencies from 100 to 300 Hz

no.	natural frequency (Hz)	loss factor
14.	132.3	0.023
15.	141,3	0.015
16.	169,3	0.013
17.	189,3	0.017
18.	254,9	0.006

The natural frequency to be considered here cannot be detected in the operating vibration analysis, but it can explain the already mentioned problem of broken pipes. It can be seen that compressor stage 4 vibrates strongly at 189.3 Hz. This also causes the attached pipes to vibrate during operation until fatigue fracture occurs. The fourth compressor stage is highlighted in red in Figure 16. The component exhibits rotation about the z-axis, while the other components are rigid.

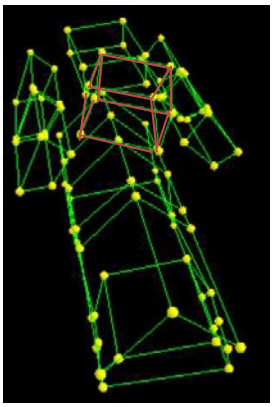

Figure 16: Movement of the compressor stage 4 at 189.3 Hz

Despite the high number of peaks, there are only a few clearly identifiable natural frequencies in the frequency range from 300 to 500 Hz (see Figure 17).

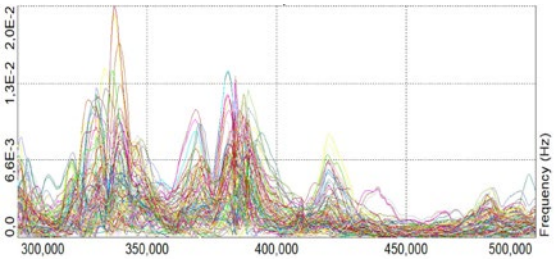

Figure 17: FRF determined in the frequency range from 300 to 500 Hz

The existing frequencies are listed in Table 4.

Table 4: Determined natural frequencies from 300 to 500 Hz

no.	natural frequency (Hz)	loss factor
19.	320.9	0.013
20.	339.9	0.014
21.	387.5	0.017
22.	419.6	0.010

One natural frequency should be considered in this range. Matching the operating vibration analysis, where the compressor has a slightly elevated peak at 315 Hz in the one-third octave band and more precisely at 322 Hz (1500 rpm) and 328 Hz (1800 rpm) in the narrow band, a natural frequency of 320.9 Hz is present. Here again the motor with the intermediate frame is the vibrating component. Unlike before, however, at this frequency there is a

by: Thomas Heumesser, Ferdinand Marks – J.P. Sauer & Sohn Maschinenbau GmbH

movement in opposite phase. The motor and the intermediate frame rotate around the y-axis with the opposite direction of rotation of the components.

Finally, it must be considered that the modal analysis results should always be viewed with caution. There is always a reduced substitute model which only represents reality to a certain extent. Often, the results of the modal analysis are used to describe problems which are caused by something entirely different.

5 Review of results

The investigation has shown that the compressor unit shows conspicuously high acceleration levels at some frequencies during operation. The excitation frequency is known due to the two specified speeds which made it possible to search specifically for relevant natural frequencies. Thus it could be determined that there are mainly three problems. First of all, the elastic mounting should be emphasized. In vertical direction it is correctly designed with a natural frequency of 4 Hz, but the rotational natural frequencies up to 22 Hz were disregarded. This can lead to problems with resonances at even lower speeds.

The next point to be considered is the base frame consisting of two hollow profiles on which the entire unit is mounted. It is too soft, which can be recognized by the low natural frequencies beginning at 63.8 Hz. In order to be able to absorb the transmitting energy of the compressor unit without deforming, the base frame must be stiffened, thereby shifting the natural frequencies into higher frequency ranges. For this purpose, either stiffening elements such as cross sections can be used, or the shape of the sections must be changed to, for example, solid sections.

Also the intermediate frame between the motor and the elastic mounting needs strengthening, as the modal analysis has shown. The fact that natural frequencies of the motor-intermediate frame system are excited causes the intermediate frame to deform. As a result the structure should also be detuned by changing the profile or stiffening.

The last points to mention are the individual components such as the compressor cylinder units. These often vibrate in response to a movement of the entire system with a counter movement, which places a load on attached pipes. Here, an additional support can be considered to limit the movement.

In general it can be said that the excitation cannot be reduced by adjusting the system. It can only be ensured that the excitation is not amplified by natural frequencies.

Therefore, the stiffening of the base frame and the intermediate frame should be carried out first. Then it is advisable to carry out a new vibration analysis. Here the periphery and suitable mounting concepts can also be considered.

6 Conclusion

The aim of this study was to analyse the vibration behaviour of a compressor with six compressor cylinders, driven by an electric motor, and to propose improvements. In order to implement this, an operating vibration analysis was first carried out. Based on this analysis it could be determined how the system behaves during operation. Since the compressor only runs at two fixed speeds, a very good impression of the behaviour was gained.

In the operating vibration analysis, local accelerations of the machine are recorded using fixed sensors. These can then be converted into levels and plotted over the frequency band. In this way it can be detected at which frequency strong vibrations are present and which dynamic effects can be responsible for them. If conspicuous peaks are present in the evaluation of the operating vibration analysis, this can indicate resonances in the system. A modal analysis is carried out to verify the results. For this purpose, a broadband signal in the form of a hammer blow is applied to the test object and the response of the system is measured in the form of acceleration. A measurement software can use these recorded values to determine the transmission behaviour of the system and calculate the modal quantities (natural frequency, natural vibration mode shape, modal mass and modal damping). In this way, it is possible to determine the natural frequencies of the individual structures and it can be shown how these components move. With only two fixed excitation frequencies, it can be clearly seen how the structure must be changed to avoid resonances and thus increased vibrations.

The modal analysis clearly shows the vibration not perceived by the eye and thus supports the designer in the decision-making process. Components that were previously considered uncritical for the designer can thus become conspicuous. In this analysis, these were the base frame and the intermediate frame, which are each too soft for such a large moving mass. Thus, a vibration analysis supports the targeted design improvement of the system in order to reduce the vibration behaviour.

7 Update

The modal analysis performed previously found a natural frequency at 63.8 Hz where the compressor and motor tilt around the coupling between the two components. Therefore, two profiles made of solid material have been initially added to the construction to which both the compressor and the motor were directly connected. The profiles were then connected to the mounts. The vibration behaviour of the entire unit including these profiles is shown in Figure 18. To ensure consistency of the measured values, the average of all directions and measuring points was also evaluated here. Only the higher speed of 1800 rpm is shown here, since the

by: Thomas Heumesser, Ferdinand Marks – J.P. Sauer & Sohn Maschinenbau GmbH

subjectively perceptible and also measurable vibration was higher than at 1500 rpm.

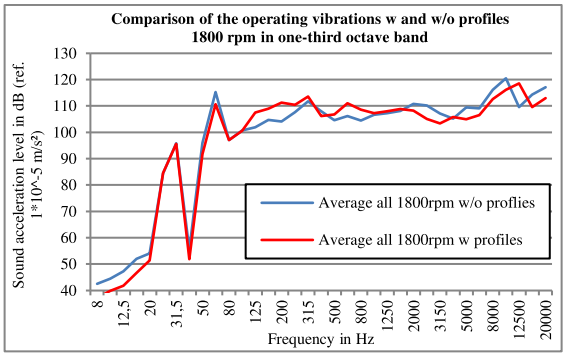

Figure 18: Operating vibrations of the entire unit with profiles

Due to the stiffening of the system by additionally installed profiles, an improvement of the vibrations in the 2nd order by 5 dB can already be detected. This improvement is consistent with the results of the modal analysis.

After reviewing all the data and further investigation on the compressor itself, a new conclusion was revealed. In order to find the cause of the broken pipes, the operating vibration analysis was carried out with measuring points on each of the cylinder units. In the following observations, the additionally added profiles remained assembled. The results of the measurement are shown in Figure 19.

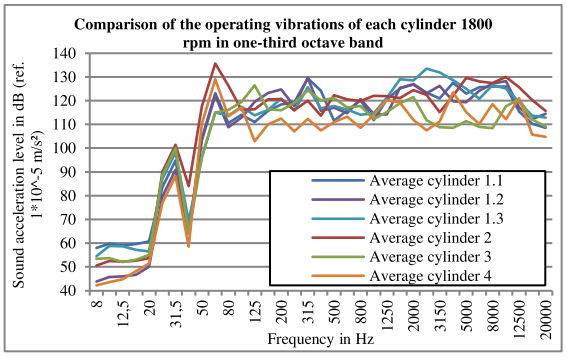

Figure 19: Operating vibrations of each cylinder in third of octave

The measurement shows that both cylinder unit 2 as well as cylinder unit 4 exhibit increased vibrations at 60 Hz with acceleration levels of 135 and 129 dB in contrast to the other units. These increased vibrations at 60 Hz could also be detected in the measurement above the mounting (see Figure 7 and Figure 18), which is why further consideration was focused on this frequency.

Accordingly, the movement from the previously performed modal analysis at 63.8 Hz was considered again and it was decided to remove the intermediate housing connecting the motor and the compressor. This is to detune the present system and show the relationship between motor and compressor motion. Subsequently, an operating vibration analysis was first performed, as seen in Figure 20.

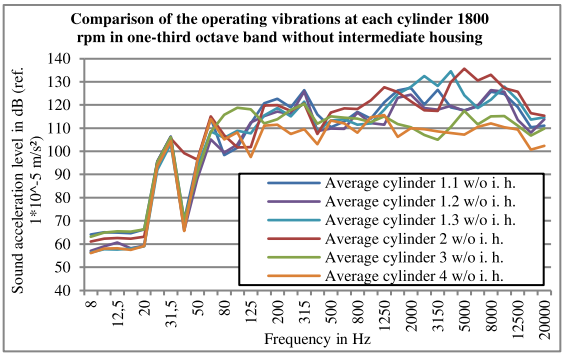

Figure 20: Operating vibrations of each cylinder in third of octave without the intermediate housing

By removing the intermediate housing the acceleration levels at 60 Hz were significantly lowered to 115 and 113 dB for cylinder unit 2 and 4. In addition, the vibrations of some cylinder units could also be reduced.

One aspect that is negatively noticeable with this adjustment is that the 1st order vibrations at 30 Hz increase by 16 dB from 88 to 104 dB for cylinder unit 4 and by 5 dB from 99 to 104 dB for cylinder unit 2. The other cylinder units also show an increase in vibrations.

In order to find the reasons for this behaviour again a modal analysis were carried out. The modal shown in Figure 9 was reduced to only the motor, compressor and foundation, to see the movement and the natural frequencies of those components. As an additional measuring point, the motor shaft, the coupling and the crankshaft of the compressor were measured to detect the transmission of vibrations at these components.

First the determined 2nd order shall be examined. The previously determined natural frequency of 63.8 Hz could be raised to 69.1 Hz by removing the intermediate housing. As a result, the natural frequency is further away from the excitation frequency of the system. In addition, a different vibration behaviour is apparent, which can be seen in Figure 21.

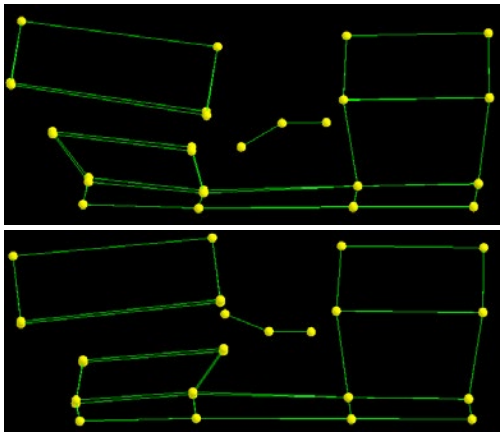

Figure 21: Movement of the system at 69.1 Hz

by: Thomas Heumesser, Ferdinand Marks – J.P. Sauer & Sohn Maschinenbau GmbH

The tilting around the coupling is still present, but is now only based on a movement of the motor and the motor frame. The compressor remains quite rigid at this frequency. There is also no vibration transmission via the coupling. In addition, it can be seen that the base frame deforms less, which can be attributed to the additional profiles used. This may indicate that the vibrations at the cylinder units may be a counter-movement to the motor movement, with the vibrations being transmitted via the intermediate housing. The motor still performs the tilting motion, but has an increased number of degrees of freedom of movement due to the removed intermediate housing, allowing it to vibrate freely.

Now the 1st order can be considered. The modal analysis has shown a new natural frequency of the system at 29.6 Hz, where mainly the motor performs a rotational movement around the y-axis, as it can be seen in Figure 22.

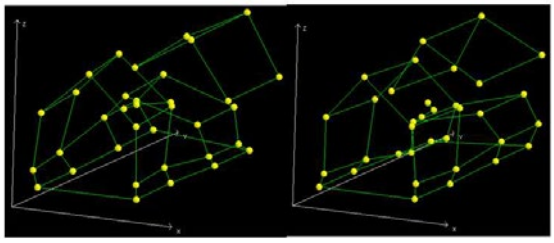

Figure 22: Movement of the system at 29.6 Hz

A comparison of this motion with the operating vibration analysis shows that indeed the motor has increased vibrations. Figure 23 shows the evaluation of four measuring points. Here, measuring points 1 & 4 are located above the mounting of the compressor and measuring points 2 & 3 above the mounting of the motor. The respective measuring points of the components are summarized for the sake of clarity. Shown are the acceleration levels with and without intermediate housing.

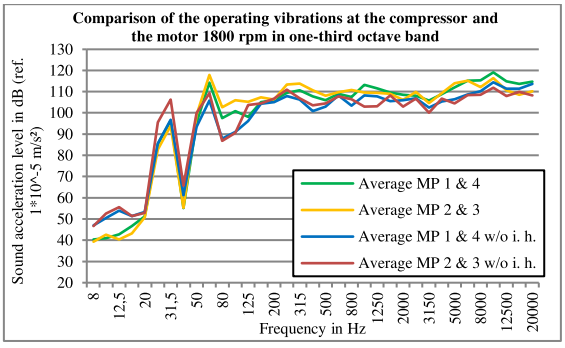

Figure 23: Operating vibrations of the motor and the compressor w and w/o the intermediate housing

When comparing the 1st order, it is noticeable that only the measuring point at the motor shows increased vibrations when considering the system without intermediate housing compared to the system with intermediate housing. The compressor, on the other hand, remains at the same vibration level. This reflects the results of the modal analysis well.

In contrast, when looking at the 2nd order, it can be seen that both the motor and the compressor have reduced vibrations without an intermediate housing.

The first and further investigations on the system have shown that the vibrations caused on the compressor are caused by the movement of the motor and are transmitted via the intermediate housing. By inserting a stiffening profile, the vibrations of the entire system could already be reduced specifically in the 2nd order, but the vibrations of the cylinder units remained increased. Thus, an adjustment of the compressor-motor connection should be made. Due to the strong detuning of the system by removing the intermediate housing, it has become clear that the cylinder units are also excited to vibrate by the movement of the motor.

Also, the investigation without the intermediate housing has shown that any change to the system can improve some aspects but worsen others, so either a compromise must be made or further research must be done. Nevertheless, it can be said that with the help of the operating vibration and modal analysis, the critical points of the system can be identified and now adjusted in a targeted manner.

---

[1] Eifler, W., et al. (2009): Küttner Kolbenmaschinen, GWV Fachverlag GmbH, Wiesbaden, Germany

[2] Fallen M., Henn, H., Sinambari R. (2008): Ingenieurakustik, GWV Fachverlag GmbH, Wiesbaden, Germany

[3] Angert R., Kollmann F.G., Schlösser T.F. (2006): Praktische Maschinenakustik, Springer-Verlag Berlin, Heidelberg, Germany

[4] Ewins, D.J. (2000): Modal Testing: Theory, Practice and Application. Research Studies Press Ltd., Philadelphia, USA

COMPRESSOR TECH2

DEDICATED TO GAS COMPRESSION PRODUCTS AND APPLICATIONS

The world leader in gas compression news and information, covering products, systems, services and technologies.

www.compressortech2.com **www.ctssnet.net**

FREE MAGAZINE SUBSCRIPTIONS
AVAILABLE FROM **www.khl.com**

khl
www.khl.com

TNO innovation for life

Mechanical optimization methodology for reciprocating compressor systems

by:

Leonard van Lier, Paul Egberts, Can Tümer
TNO, Department of Heat Transfer and Fluid Dynamics
Delft, The Netherlands
leonard.vanlier@tno.nl

12th EFRC CONFERENCE
August 24 – 26, 2021, Warsaw

Abstract:
A comprehensive and robust design approach for reciprocating compressor systems is stipulated in the API 618 standard. In addition to the acoustic design (aiming at minimizing pulsation and shaking forces), also the mechanical design must be validated and optimized. The optimization of the pipe support locations is commonly done based on expert judgement. This ad-hoc approach is time-consuming and sometimes the optimal layout is not found.
In this paper, an optimization methodology is presented, aiming to reduce the time needed for mechanical optimization and to enhance the confidence that the optimal solution is found. It is the authors opinion that these optimization techniques provide a valuable extension of the toolbox of the pulsation and vibration consultant, saving engineering time and resulting in a more robust system.

by: Leonard van Lier, Paul Egberts, Can Tümer – TNO, Department of Heat Transfer and Fluid Dynamics

1 Introduction

For reciprocating compressor systems, the design evaluation with respect to pulsations and vibrations is contained in the API 618 standard. API 618 prescribes a systematic and step-wise approach to minimize risk on pulsation and vibration issues during the design of the compressor and the pipe system. The most elaborate design approach is the design approach 3, which contains an optimization of the system with respect to the gas pulsations (often called 'acoustic study'). This first step aims to limit the transfer of the pulsation source toward the rest of the system. It typically contains optimization of pulsations dampers, optimal restriction orifice plates and changes to the piping, for example by shortening dead-leg side branches and local diameter expansions. In the next step ('mechanical study'), the vibration response of the mechanical system is optimized, that aims to mitigate harmful symptoms, such as high vibrations on main lines, vibration response of Small Branch Connections and avoidance of high cyclic stresses.

In case of very simple, non-critical systems the mechanical analysis may be restricted to a simple pipe support span evaluation. Here, no detailed mechanical simulations are done. Instead, tabular data based on analytical models are used, that dictate maximum distances between pipe supports, for given line size and compressor speed. Though conceptually simple and convenient, the major drawback is that it must be used in a conservative manner. Hence, an excessive number of extra pipe supports would be required. If the strict application of the maximum support span is relaxed, details such as coincidence of acoustic shaking force frequencies (higher orders!) and mechanical resonances may occur, leading to integrity issues. Note that the API 674 standard for plunger pumps dictates such a pipe span approach. To the authors experience, this simplified approach has major practical inconvenience to both the pulsation consultant as the end user. Instead, the design approach 3 in the API 618 standard is preferred.

In design approach 3, the mechanical study is typically split into two steps. The first evaluation is the check of the separation margin. API 618 proposes a separation margin criterion in section 7.9.4.2.5.3.2:

a) The minimum mechanical natural frequency of any compressor or pipe system element shall be designed to be greater than 2.4 times maximum rated speed.

b) The predicted mechanical natural frequencies shall be designed to be separated from significant excitation frequencies by at least 20%.

The first criterion a) is a very robust guideline to achieve a stiff layout. Indeed, for normal operation of reciprocating compressor, the 1st and 2nd order generally contain sufficient energy to cause severe vibration issue, in case the acoustic shaking force frequency coincides with a mechanical resonance frequency. The criterion ensures a 20% margin of the lowest mechanical resonance frequency to the 2nd order of the compressor speed. Generally it is desired that this criterion is met in all circumstances. However, the criterion originates from the large (petro-chemical) heavy-duty service machines with low compressor speeds. For high-speed compressors, the criterion a) may be strict. For example, a 1200 rpm compressor requires that all mechanical resonances of the pipe system are in excess of 48 Hz, which demands an unrealistically stiff pipe system.

Criterion b) can be interpreted in a more broad sense (viz. what is "significant excitation"?). Judgement on the shaking force amplitude is required, since complete separation within 20% is not feasible. For the higher orders ($i > 3$) the 'forbidden' frequency bandwidths start overlapping, see Figure 1. However, in most compressor systems, the pulsation spectrum of the source has a specific harmonic signature. That is, certain orders will have relatively large amplitude, while others are much weaker. An example is the double-acting cylinder (dominated by 2nd order) or a single-acting cylinder (dominated by 1st order). In case of stepless reverse flow systems, the 2nd order, but also higher even orders (4th 6th) will be present on the pulsation signal. In addition to the frequency distribution of the source, the acoustic response of the system strongly determines the dominant frequencies in the shaking forces. For example, in a closed side branch, such as a relief line, specific acoustic resonances (e.g. ¼λ, ¾λ standing waves) will amplify specific harmonic components of the source. Manual application of a separation criterion for the higher orders may require a substantial analysis and automatic detection of the dominant orders will be valuable.

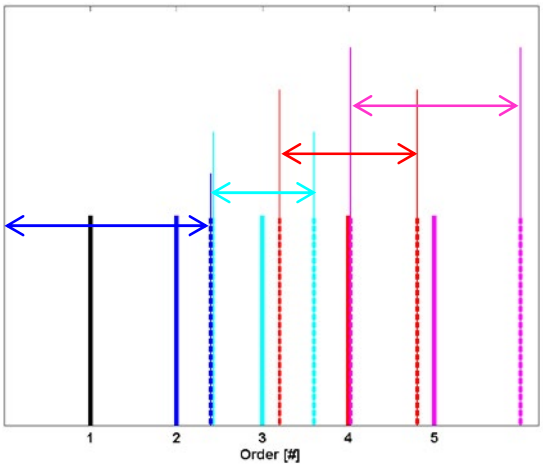

Figure 1. Separation margins stipulated by API 618, overlapping frequency bands at higher orders.

by: Leonard van Lier, Paul Egberts, Can Tümer – TNO, Department of Heat Transfer and Fluid Dynamics

Using the separation criteria, an initial optimization of the pipe system is made, usually by applying extra supports on parts where inadmissible flexibility is observed.

As a next step in the mechanical analysis, the harmonic response study is performed. Here, the pulsation-induced shaking forces are applied to the pipe system (acting on elbows, tees, reducers, closed valves etcetera). The correct force frequency, orientation, phase of each component shall be used. Generally, the worst-case conditions, yielding the largest shaking force amplitudes are selected for the mechanical analysis, to ensure a conservative design evaluation. The vibration levels and cyclic stresses are computed and compared with allowable levels in (for example) API 618.

It is the author's experience that a strict adherence to the separation criterion yields a relatively stiff piping layout. As a consequence, in general little issues are found during the mechanical response analysis and the analysis effort is limited, as no (or little) design optimization steps are required.

The effort during the mechanical response analysis is in many projects a critical concern. For example, a large number of engineering hours may be required for constructing a sufficiently detailed and realistic Finite-Element model. Collecting information on for example pipe supporting structures, and valve / actuator weights may be elaborate. Note: this detailed information may not be available at all during the time of the pulsation study; in such case essential simplifications may be needed often accompanied by sensitivity study on the input parameters. In addition to the construction of reliable simulation models, also the optimization process itself may be time-consuming. Most often, exceeding of vibration limits will be encountered (which will generally be the case, even if the pulsation levels comply with the pulsation limits in API 618). To reduce the calculated vibrations and cyclic stresses, extra supports are required. These are generally placed by hand, based on the engineer's experience. This is done for each critical section in the system. After some iterations, ultimately, an optimal layout with extra supports results in satisfactory vibration and cyclic stress levels. Now, this optimal layout is shared with the piping constructor, responsible for the engineering of the piping system (this is often a different company, and often not a direct subcontractor of the pulsation consultant's firm). The optimal layout with extra supports will be judged on practical feasibility. For example, extra pipe supports usually require a robust steel structure nearby, to be mounted to, Absence of stiff structures often eliminate the options to place extra pipe supports. In general, the position of the pipe supports is (slightly) modified during the feasibility check than the optimal support location. The next verification is if the extra pipe supports do not lead to issues with static stress. The optimization of a mechanical system with respect to dynamic stress (preferably as stiff as possible) and static stress (preferably as flexible as possible) requires a delicate compromise. This compromise generally requires extensive discussion and various iteration steps between different parties in the project.

A final aspect of mechanical optimization that is worth mentioning, is the sometimes 'counter-intuitive' or even capricious effect of adding pipe supports. Both in numerical investigations as in practical (ad-hoc) attempts to reduce vibrations with extra supports, sometimes an adverse effect is observed: adding an extra support may increase the vibration level, in the critical area and/or in other parts in the vicinity of the critical area [1]. For this, a robust optimization approach would be of large benefit.

As a consequence of the impact of engineering effort and project lead time, it may be tempting to do the optimization of the pipe support with 'large leaps'. Instead of a fine-tuning approach and gradually working toward a efficient solution, the optimization is done in a conservative approach, resulting in many additional pipe supports. Also, once an acceptable solution is found, the optimization process may be stopped without further investigation if more efficient solutions may exist.

In section 2 of this paper, the purpose of the investigation is discussed. Section 3 highlights the fundamental background of the optimization techniques applied. In sections 4, 5 and 6 the results of the optimization methods are presented, for different cases. In sections 7 and 8 the conclusions and outlook for future work are discussed, respectively.

by: Leonard van Lier, Paul Egberts, Can Tümer – TNO, Department of Heat Transfer and Fluid Dynamics

2 Objective of the investigation

TNO's experience with the effort and robustness of the mechanical response analysis is the main trigger of this investigation. The purpose of the investigation is to explore methodologies to improve the efficiency of mechanical optimization of pipe systems ('the system is optimized with limited engineering effort') and verification of the robustness of the method ('the optimum solution is reached').

Ultimately, these optimization techniques shall be made available to the pulsation consultant by implementation into practical design and simulation tools.

Numerical optimization techniques, already adopted in other branches of science and engineering ([2],[3]) are investigated for this specific purpose.

The scope of this optimization methodology will be limited to supports in the pipe system. It does not address the mechanical layout of the compressor (cylinder or pulsation damper supports). Moreover, as a first step, the support modelling was chosen to be simplified as follows: each pipe support is represented with 3 fixed translational degrees of freedom. The rotational degrees of freedom loose. Effects of underlying steel structure (supporting beams) was not considered. However, during optimization of a pipe system, commonly the need for extra pipe supports will be handled as a first step. The design of underlying steel structures is usually a next step, during more detailed engineering.

3 Numerical Optimization

3.1 Structure of the optimization tool

The optimization methods that are presented in this paper are applied to TNO's simulation software tool. The simulation tool is GUI-based and contains a project model file that is generated based on input from the user. This project model file contains all relevant input data, such as compressor properties and design, operational conditions and the layout of the pipe system. The GUI steers various solvers, such as the acoustic solver (to calculate the pulsations sources and the propagation of pulsations inside pipe system) and the mechanical solver (to calculate vibrations, cyclic stresses and dynamic support loads).

The optimizer directly communicates with the simulation tool, in an iterative procedure to update the simulation models, based on the simulation results.

To solve the optimization problems the Dakota framework [6] is applied, which facilitates the use of several optimizers.

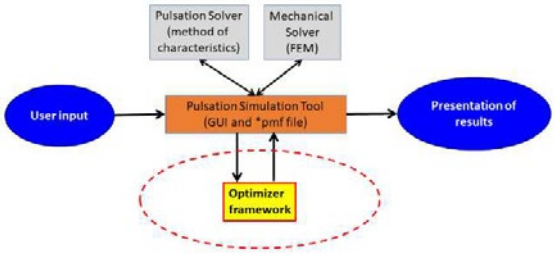

Figure 2. Coupling of Tools.

3.2 Optimization problems

The three optimization problems, referred to as P1, P2 and P3, considered in this paper can be described as finding support locations that

P1: Maximizes the first mechanical natural frequency (MNF).

P2: Minimizes the number of MNFs in predefined frequency ranges according to separation margin criteria.

P3: Minimizes the maximum total vibration velocity along the pipe system.

The number n of supports is taken fixed and is thus not part of the optimization problem. The optimization variables are the support locations. To treat these variables as continuous variables, pipe trajectories of the pipe system are identified in advance that can be parametrized by a continuous parameter. Such pipe trajectory can be drawn without lifting a pencil and without tracing a pipe twice. To each such pipe trajectory a number of supports can be assigned. The support locations will be optimized constrained to the associated pipe trajectory.

Introducing the objective function J (e.g. the maximum total vibration velocity for problem P3) that is to be optimized and denoting the n support locations by $x_1, x_2, \dots, x_n$, the optimization problem can be stated as

$$\min_{\substack{x=(x_1,x_2,\dots,x_n) \\ x\in\Omega}} J(x) \qquad (1)$$

in which $\Omega \subset \mathbb{R}^n$ defines all constraints for the support locations including upper and lower bounds and linear inequality constraints.

Without loss of generality the optimization problems can all be written as a minimization problem since maximizing J is equivalent to minimizing $-J$.

The ordering of supports is retained during the optimization process through linear inequality constraints of the form $x_{i-1} < x_i$. This improves the optimization efficiency as the solution space of support locations is reduced because swapping of support locations cannot occur.

by: Leonard van Lier, Paul Egberts, Can Tümer – TNO, Department of Heat Transfer and Fluid Dynamics

3.3 Solution methods

The optimization problems P1 and P3 are continuous optimization problems as the variables (support locations) are continuous and the objective function is continuously depending on the variables whereas problem P2 is a discontinuous optimization problem because the objective function has discrete values as it counts the occurrence of MNFs in given frequency bands.

Problem P1 is solved with a gradient-based optimization technique (initial attempts using a parametrization of a support location in terms of a (discrete) pipe identifier and a (continuous) local position parameter combined with a mixed-integer non-linear optimization approach appeared to be much less efficient). This is a method that exploits the gradient of the objective function J with respect to the support locations $x_1, x_2, \ldots, x_n$, to iteratively improve the support locations. These gradients are calculated through finite differences.

The discontinuous problem P2 is solved by a genetic algorithm [4] which is a gradient free optimization technique. This technique uses principles from genetics and natural selection. It starts with initializing a population of (encoded) potential solutions and improves iteratively the population through biologically inspired operations as inheritance, selection, crossover and mutation, to obtain an overall better fitness quantified by the objective function values. A strength of a genetic algorithm is that it explores the variable space globally and thereby avoiding getting stuck in a local optimum. A downside however is that the method is computationally expensive.

For problem P3, it was found that it was solved efficiently with a pattern search optimization technique [5] which is an iterative method that evaluate so-called trial points around the best solution so far. The trial points are chosen according to a pattern and the objective function is evaluated at the trial points. A trial point will be accepted as next iterate if it has the best improved objective function value among all trials.

4 Optimization of modal analysis

An obvious first step in the optimization method is the modal analysis. This has as main advantages that the method is relatively fast (low computational requirements) and that the interpretation of the result is rather straightforward. The key parameter used for the objective function is the lowest mechanical natural frequency (MNF). This MNF is an indication of the stiffness of the system: the higher the MNF the stiffer the system. This objective function has also a direct relation with the separation margin criterion stipulated in API 618.

The value and applicability of this initial optimization step is an interesting aspect. This optimization aims at the overall stiffest possible system, with a minimum number of extra pipe supports. For applications with a stochastic loading, the stiffest layout generally results in the lowest mechanical vibrations. An example is mechanical excitation caused by turbulent flow or a multiphase flow in the mist or annular flow regime. However, this is not necessarily true for reciprocating compressor systems. The pulsation-induced shaking forces caused by a reciprocating compressor provide the loading on the mechanical structure (forced response). The shaking forces are dominated by multiple orders of the compressor speed. The individual amplitude of the frequency components depends on the properties of the compressor, the operational conditions and the piping layout. For example, orders that coincide with acoustic resonances, such as standing waves, will be strongly amplified and hence strongly present in the shaking force spectrum. Moreover, the orientation of the pulsation-induced shaking forces is in the axial direction of the pipe sections. Thus, the shaking forces of the piping are not a stochastic distribution that demand an overall stiffness of the piping system. Rather, a specific stiffness is required with a specific orientation and for specific frequencies. In extreme (but not unrealistic) cases, it may be that a stiffer layout suffers from higher vibration levels, because the frequencies of the shaking forces and the mechanical resonances are placed closer together.

4.1 Maximizing first MNF

The first optimization step (P1) is achieving the stiffest possible system. Thus the objective function is associated with the first MNF. The optimizer target is to maximize the value of the first MNF. The approach is demonstrated for a simple flex-loop system, see Figure 3. Such configuration is rather uncommon for reciprocating compressor systems, but will be applied for example on subsea templates where large displacement of wellheads must be accommodated. In its original application, the flex-loop is only supported (with rigid anchor points) at the wellhead connection and at the connection to the subsea transport header. The connections can be considered rigid (anchor points, fixing all translations and rotations). The flexibility of the layout is reflected in the lowest MNF of 1.4 Hz. This case serves as a good starting point for optimizing the stiffness by introducing extra supports. This was done in a systematic way. First with 1 extra support on 1 prescribed pipe section (the optimizer to determine the best location). Next, the optimizer was given the freedom to locate the extra support on a collection of pipes. The complexity was gradually increased by allowing multiple extra supports to be chosen at a multitude of pipe sections.

by: Leonard van Lier, Paul Egberts, Can Tümer – TNO, Department of Heat Transfer and Fluid Dynamics

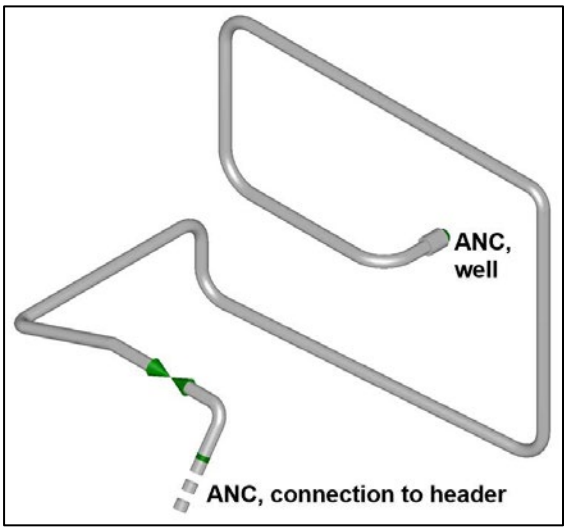

Figure 3. Test model, Flex-loop example.

A typical iteration process of the optimizer is shown in Figure 4. The overall optimization finds its way relatively easily toward the global optimum. In this exercise a gradient-based optimizer is used. The optimizer algorithm makes at some iterations a too large update of the variables leading to a lower objective function, these large steps are then reduced using a backtracking line search algorithm.

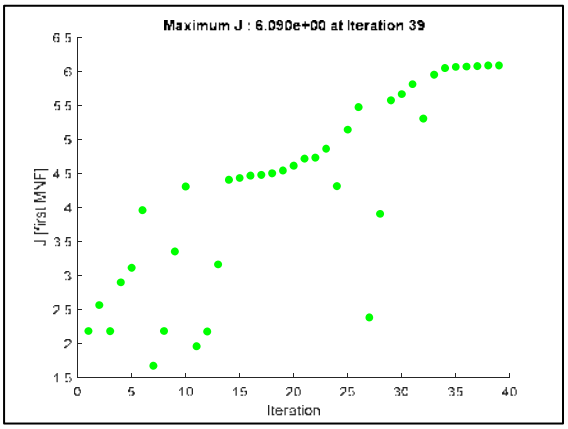

Figure 4. Convergence of the objective function J (first MNF [Hz]) to optimum. Flex-loop example with 3 extra supports.

The layout was optimized with increasing number of extra pipe supports; first with 1 support (optimized for the optimal location) next with 2 supports etcetera. As expected the structure becomes increasingly stiff when more supports are applied. The advantage of the systematic optimization is obvious: first, the optimizer determines the most efficient disposition of supports which saves considerable amount of time and manhours. Next, the optimizer indicates the additional effect of adding extra supports. In the example shown in Figure 5, it is clear that adding a 6th support, hardly adds to the overall stiffness. Depending on the stiffness requirements, Figure 5 immediately conveys the number of extra supports required.

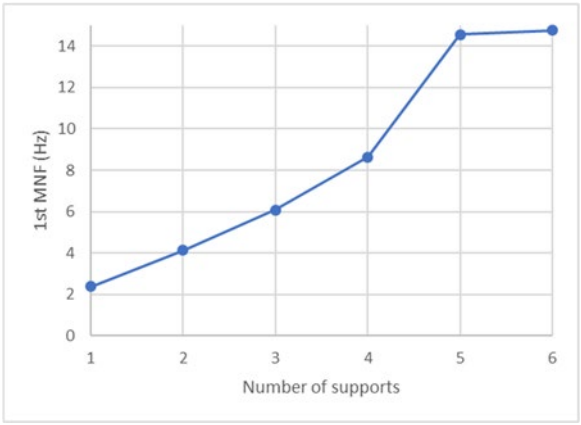

Figure 5. Maximized 1st MNF for different number of supports. Flex-loop example.

4.2 API 618: Separation margin criterion

As a next step, the optimization method for the modal analysis is applied to the separation criterion in API 618 (problem P2). To this purpose, a more realistic model is used, see Figure 6. The model is still simplified, but contains some of the essential features of a discharge system. It is a simple, single cylinder compressor outlet, including the pulsation dampers, a large outlet vessel and a relief line. The mechanical boundary conditions were chosen in accordance with normal pulsation studies (stiff cylinders, stiff outlet vessel, supporting layout beyond the closed PSV).

Five supports in the model that are subject to the optimization, labelled 620, 630, 640, 690 and 700. Again, these supports are 'free' to be moved along the pipe sections.

The optimization problem considered for this example shall minimize the occurrence of MNF's in frequency bands according to the separation margin criterion. For reasons of efficiency of the optimization, linear constraints are imposed on the variables to remain the initial ordering so to avoid equivalent solutions.

A compressor speed of 480 rpm is used as a typical value.

Now, the objective function is not related to the lowest MNF, but to the number of mechanical modes found in the 'forbidden' zones. The amount of mechanical modes in the forbidden zones shall be minimized (ideally to zero). Note that in contrast to the optimization problem discussed in the previous section, the objective function takes only discrete values making the use of a gradient-based optimizer not feasible. Instead a genetic algorithm is used.

by: Leonard van Lier, Paul Egberts, Can Tümer – TNO, Department of Heat Transfer and Fluid Dynamics

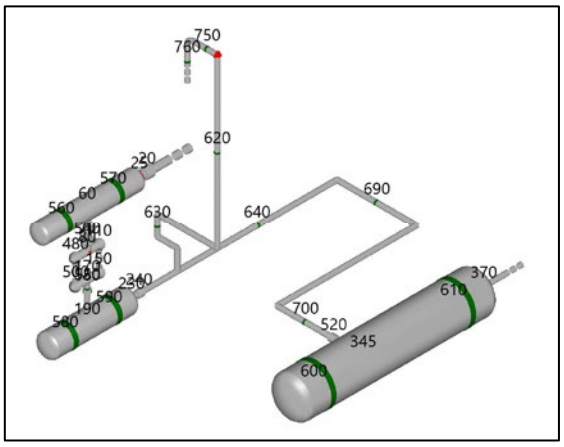

Figure 6. Test model, compressor pipe system example.

For example 1, the first separation criterion in API 618 is used (separation up to 2.4 times the fundamental frequency), in combination with an assumed "significant" excitation at the 4th order. This assumption is not uncommon for a double-acting reciprocating compressor operating at a significant pressure ratio.

Applying the typical 20% separation bandwidths yields the following 'forbidden' frequency zones:

$[0,\ 1.2 \times 2 \times \frac{rpm}{60}]$ and

$[0.8 \times 4 \times \frac{rpm}{60},\ 1.2 \times 4 \times \frac{rpm}{60}]$

Ideally there shall be no MNFs located within these forbidden zones. If that cannot be practically reached with the number of extra supports, then at least the amount of violations shall be minimized. The results of the genetic algorithm optimizer are shown in Figure 7. The initial distributions of the pipe support results in a gross violation of the separation required. During the first function evaluations, the layout has 4-9 MNFs that are located inside the forbidden zones. From the optimization process it becomes clear that the initial population of variables improves to much better fit population (i.e. lower objective function values) in a few hundred of function evaluations. The observed scattering of objective function values is inherent to a genetic algorithm due to randomness of the mutation and crossover operators. After a number of iterations, the situation improves to 1-4 MNFs in the forbidden zones. Complete separation is, even for this simple system, not feasible. This suggests that in realistic system, the separation margin requirements in API 618 are only indicative and of limited practical use for a full endorsement of the mechanical design. The ultimate qualification of the mechanical design then cannot be provided by the separation margin analysis only, but shall be provided by the subsequent harmonic response analysis.

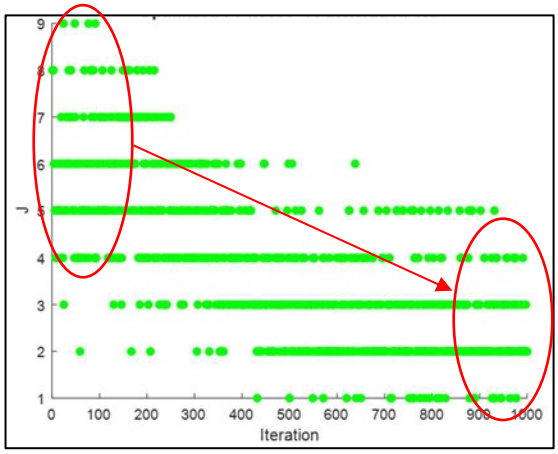

Figure 7. Example 1: number of violations (MNF's in forbidden zones), as the optimizer iterates.

For example 2, the common separation limit is used (separation up to 2.4 times the fundamental frequency), in combination with an assumed "significant" excitation at the 6th order. This assumption is not uncommon in case of acoustic resonances (for example in the relief line), and/or in case of stepless reverse flow capacity control systems that tend to put emphasis on the higher (even) orders of the compressor speed.

Applying the typical 20% separation bandwidths yields the following 'forbidden' frequency zones:

$[0,\ 1.2 \times 2 \times \frac{rpm}{60}]$ and

$[0.8 \times 6 \times \frac{rpm}{60},\ 1.2 \times 6 \times \frac{rpm}{60}]$

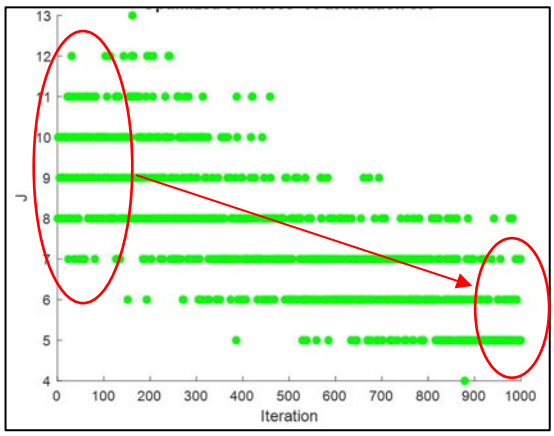

Figure 8. Example 2: number of violations (MNF's in forbidden zones), as the optimizer iterates.

Again, the initial distributions of the pipe support results in a violation of the separation required. Due to the increased frequency range, it is even more difficult to find support realizations that are completely separated from the higher orders. Complete separation appears to be not feasible. The optimizer does demonstrate this point clearly, which will save time-consuming attempts to achieve a fully separated system with a limited number of pipe supports. This observation is the trigger to the next step in the mechanical optimization: the harmonic response analysis.

by: Leonard van Lier, Paul Egberts, Can Tümer – TNO, Department of Heat Transfer and Fluid Dynamics

Note that in the separation margin analysis discussed above, the violations of the forbidden zones are 'unweighted'. Information on the relative amplitude of the shaking forces is not used. The force amplitudes (for the different harmonics) could be added as a feature to the objective function, which will result in a more 'intelligent' optimization of the pipe supports, mainly avoiding coincidences with critical zones that are really relevant. However, instead the authors propose the (equivalent but more complete) final step to the optimization for the harmonic response analysis.

5 Optimization of forced harmonic response analysis

For problem P3, the same simplified compressor model was used. Now a pulsation analysis was done on this model, in such a way that the 2nd and 6th order are clearly present in the acoustics (pulsations and shaking forces). The pulsation levels, compared to the limits in API 618, are illustrated below.

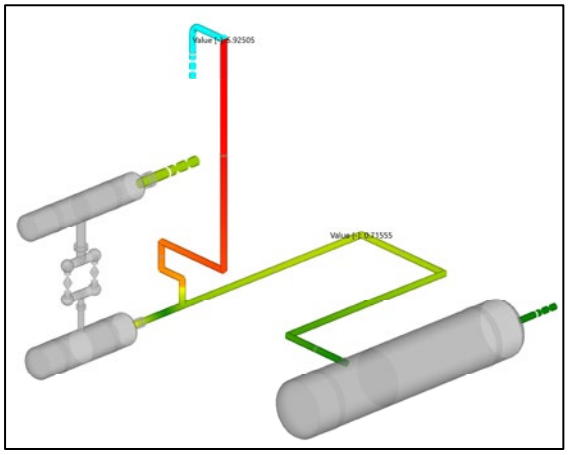

Figure 9. Pulsation levels, at 2nd harmonic, compared with API 618.

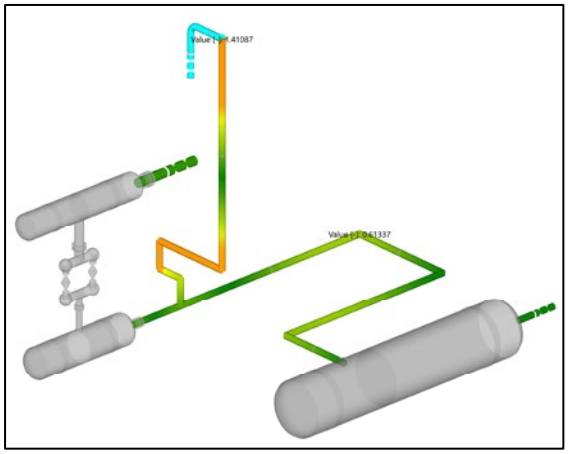

Figure 10. Pulsation levels, at 6th harmonic, compared with API 618.

The pulsation analysis provides powerful insight into the relevant areas and frequencies, by inspecting the shaking force amplitudes and frequencies. This information allows for an efficient execution of the optimization step P2 (section 4).

Now, the forced response mechanical analysis is performed as described in section 1. Response calculations are performed for a large range of conditions that may occur within the realistic operating envelope of the compressor. The calculations provide the maximum vibration levels (velocities, displacement, acceleration) and the maximum cyclic stresses. Also related information such as dynamic loads on the pipe supports is computed, relevant for the practical design of the pipe support types and the supporting structures.

The vibration amplitude in case of the initial (default) supporting layout is well in excess of the vibration limits normally used. The maximum vibration velocity is > 250 mm/s peak-peak (triggered by the 6th harmonic).

The maximum vibration velocity amplitude is used as a basis for the objective function. The optimizer aims at achieving the best pipe support distribution, which yields the lowest vibration velocity amplitude. In this relatively simple case, this is done for the global vibration velocity. For more complex systems, this should preferably be done for a localized critical area.

The result of the optimization is shown in Figure 11. The optimization process seems rather erratic, but after 80 iterations, the optimizer robustly converges to a support layout with low vibration levels. Although the optimization problem is a continuous problem and could be handled by a gradient-based optimiser, it was found to be efficiently solved by a pattern search optimizer which is a gradient free optimization technique. As in the previous problem (P2) linear constraints are added to avoid supports crossing each other during the optimization process.

This result appeared surprising at first instance. The expectation was that due to the much larger computation effort (harmonic response calculations are much more demanding than modal analysis calculations) and the large number of degrees of freedom, this case could lead to unstable convergence and/or excessive computational restrictions. However, it appeared that the weight of the critical shaking forces is such that it enhances the convergence to an optimum support distribution.

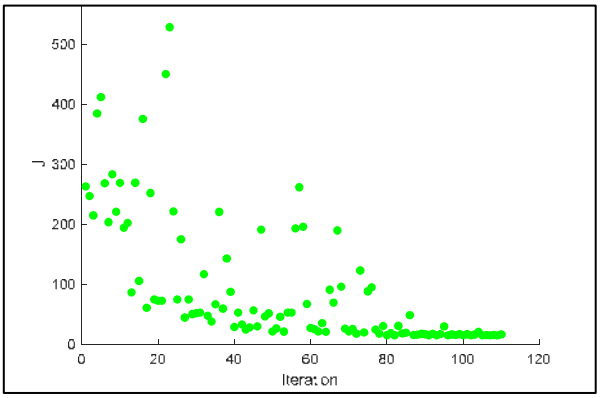

by: Leonard van Lier, Paul Egberts, Can Tümer – TNO, Department of Heat Transfer and Fluid Dynamics

Figure 11. Convergence to optimum of the objective function J (maximum vibration velocity [mm/s]) for forced harmonic response analysis.

6 Comparison of optimized cases

The various optimization steps described in sections 4 (modal analysis) and 5 (harmonic response analysis) are now evaluated and compared for the final performance (vibration levels). In other words, how do the support layouts that were optimized with modal analysis perform compared to the support layout optimized with harmonic response analysis?

The vibration levels in the optimized model using the modal analysis ('maximum first MNF') are still very high. Apparently the stiffest overall layout is not the best to achieve minimum vibration levels. The maximum vibration levels are >400 mm/s peak-peak.

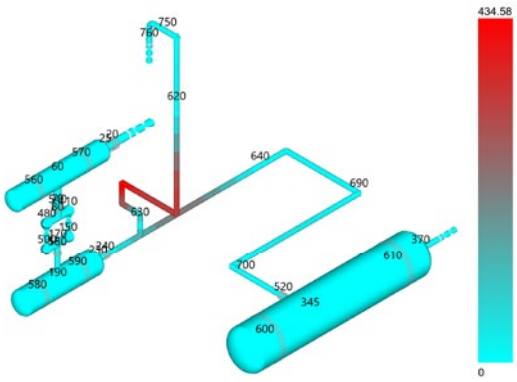

Figure 12. Vibration levels for support layout, optimized for maximum first MNF.

The vibration levels in the optimized model using the modal analysis ('minimum MNFs in the forbidden zone for 2nd and 4th order') are still high. The 6th order vibrations (which were not considered in the optimization of the pipe supports) are still well above the allowable level. The maximum vibration levels are >220 mm/s peak-peak. An interesting feature of the optimization is the placement of two supports very closely together. The close placement suppresses both the translations and the rotational flexibility. Thus, this is an indication that a rotational-restraint pipe support is very effective to minimize vibrations and a powerful, practical hint to the pulsation consultant. This example may demand a fixed point (or a rigid, double-clamped pipe support).

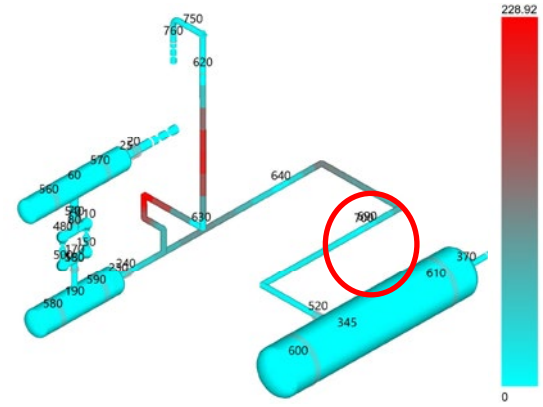

Figure 13. Vibration levels for support layout, optimized for minimum #MNF in forbidden zones for 2nd and 4th order.

The vibration levels in the optimized model using the modal analysis ('minimum MNFs in the forbidden zone for 2nd and 6th order') are considerably lower. Now, the vibrations due to the 6th order shaking forces are effectively suppressed. The maximum vibration levels is 72 mm/s peak-peak.

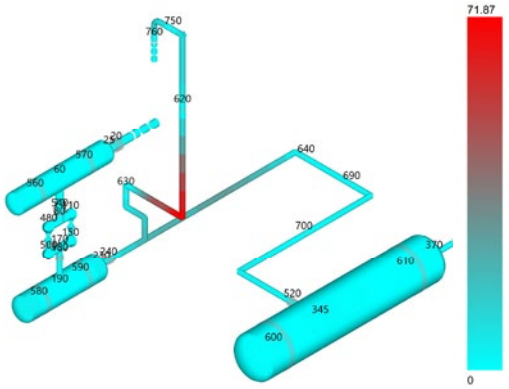

Figure 14. Vibration levels for support layout, optimized for minimum #MNF in forbidden zones for 2nd and 6th order.

Finally the vibration levels in the optimized layout using harmonic response analysis are indeed the lowest: 15 mm/s peak-peak. This confirms that this 'direct' optimization approach is the most effective.

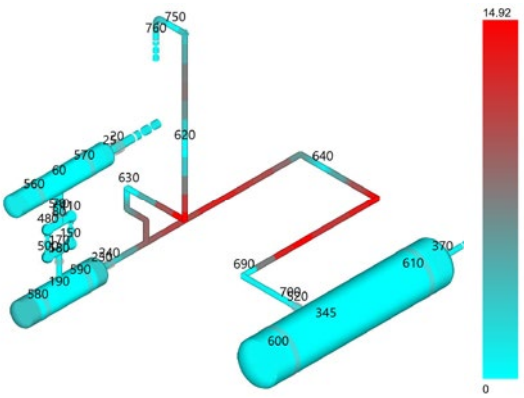

by: Leonard van Lier, Paul Egberts, Can Tümer – TNO, Department of Heat Transfer and Fluid Dynamics

Figure 15. Vibration levels for support layout, optimized for minimum vibration amplitude.

7 Conclusions

Based on the investigations presented in this paper, the following conclusions are drawn:

- In normal engineering practice, the optimization of pipe supporting layout of pipe systems is generally done by hand, based on experience.
- Though this usually results in satisfactory performance, the process is time-consuming and a thorough study if the chosen layout is optimal is not performed.
- Various methods of optimization are presented, applied to modal analysis (aiming at the stiffest overall system; aiming at maximum separation for specific orders of the compressor speed) and to harmonic response analysis (minimizing the vibration amplitude).
- For the specific case of minimizing the pulsation-induced vibrations of a reciprocating compressor, the direct optimization of harmonic response leads to the most effective pipe supporting layout.
- Handling effort and numerical expenses of the optimization appear to be within reasonable limits.
- Optimization speed could be improved by combining various steps. For example, by using an optimal supporting layout based on modal analysis, as initial guess for the harmonic response optimization.
- The optimization tools provide practical guidance for the specific supporting layout; for example cases where rotation-stiff supports may be more effective.
- The optimization method presented in this paper is considered a valuable tool to enhance efficiency and robustness during the engineering process. However, as for every automatic solving computational analysis, the results must be managed with care and by skilled people who can critically evaluate them.

8 Outlook

Research on this optimization topic is still ongoing. Ideas for further improvement include the separation margin optimization: the 'forbidden' zones could be chosen automatically using the results of the pulsation analysis (viz. "what are the really critical bands and how are these distributed spatially over the system?"). It is expected that this will increase the efficiency of the optimization.

Sensitivity analysis on the optimization approach is recommended, to ensure confidence that the optimization yields the global optimum and that the results does not depend critically on the choice of the initial guess.

In addition to optimization of pipe supports, also activities are deployed to other relevant optimization steps in the design. One example is the optimization of restriction orifice plates, to suppress pulsation levels. Another example is the optimization of the design of complex pulsation dampers (multi-chamber dampers with choke tubes and other internals are challenging examples).

The ultimate goal would be to include these optimization toolboxes into the simulation software and make them available to the benefit of the pulsation engineering consultants. This will enable an efficiency improvement during the design process, and to shorten lead times and improve chances on success during trouble-shooting.

9 Acknowledgment

The authors wish to dedicate this paper to the memory of Mr. Bert Egas, one of the pioneers and founding fathers of the Pulsim group at TNO. During his 45 year service at TNO, Bert optimized by his great experience countless numbers of process installations. With his positive and enthusiastic attitude he helped generations of colleagues and clients to appreciate the features of pulsations and vibrations in reciprocating compressors systems.

10 References

[1] Eijk, A., Pereboom, H., Fröbel J., Application of a Constrained Layer Damping to Reduce Pipe Vibrations of a Reciprocating Compressor System, 11th EFRC Conference 2018, Madrid.

[2] Ghisu, T., Parks, G.T., Jarrett, J.P., Clarkson, P.J., 2011. Robust design optimization of gas turbine compression systems. Journal of Propulsion and Power 27, 282{295. doi:10.2514/1.48965

[3] Rozvany, G.I.N., 2009. A critical review of established methods of structural topology optimization. Structural and Multidisciplinary Optimization 37, 217{237. URL:

https://doi.org/10.1007/s00158 007-0217-0, doi:10.1007/s00158-007-0217-0.
[4] Haupt R.L. and Haupt S. E., Practical Genetic Algorithms, Wiley, 2004
[5] Gray G. A. and Kolda T. G.. Algorithm 856: APPSPACK 4.0: Asynchronous parallel pattern search for derivative-free optimization. ACM Transactions on Mathematical Software, 32(3):485–507, September 2006.
[6] Adams, B., Bauman, L., Bohnho_, W., Dalbey, K., Ebeida, M., Eddy, J., Eldred, M., Hough, P., Hu, K., Jakeman, J., Stephens, J., Swiler, L., Vigil, D., Wildey, T., . Dakota, A Multilevel Parallel Object-Oriented Framework for Design Optimization, Parameter Estimation, Uncertainty Quantification, and Sensitivity Analysis: Version 6.10 User's Manual. Sandia Technical Report SAND2014-4633 Unlimited Release, July 2014, Updated May 15, 2019.

Wrocław University
of Science and Technology

The impact of system parameters on reactive damper transmission loss characteristics – experimental and simulation approach

by:

Warzyńska Urszula, Siwulski Tomasz
Wrocław University of Science and Technology, Department of Technical Systems Operation and Maintenance
Wrocław, Poland
urszula.warzynska@pwr.edu.pl

12th EFRC CONFERENCE
August 24 – 26, 2021, Warsaw

Abstract:
The article discusses the influence of operating parameters (flow, pressure) and system impedance (end boundary condition) on pressure pulsation attenuation. The research is based on pulsation measurements performed with the use of pressure transducers in a dedicated test stand equipped with a reciprocating compressor, reactive pulsation dampers and simple piping installation. Furthermore, the adequacy of previously described mathematical models of transmission loss characteristics is discussed in relation to the modeling of variable operating parameters of the system. In the paper, numerical simulation results are compared with measurements for selected cases. The obtained results of simulation research, as well as experimental tests, may be a valuable base for an improved simulation method of damper selection for specific system requirements.

by: *Warzyńska Urszula, Siwulski Tomasz –Wrocław University of Science and Technology*

1 Introduction

The common method employed to obtain experimental transmission loss characteristics of a reactive pulsation damper is to perform acoustic measurements with the use of a broad-frequency noise source and an array of microphones. Conventional approaches to measuring damper transmission loss characteristics include either the decomposition method or the transfer matrix method [1].

The decomposition method is based on the use of a two-microphone technique with the assumption of anechoic termination of the tube [2,3,4,5,6]. It was originally used to measure acoustic properties such as absorption coefficient and surface impedance of absorbing materials [7]. Damper transmission loss is defined as an acoustical power level difference between incident and transmitted waves. In the decomposition method, the transmission loss function is obtained by decomposing sound pressure into incident and reflected waves. After the wave is decomposed, the sound power of the input wave may be calculated. The transmitted sound power can be easily obtained by measuring the sound pressure at the outlet. The major drawback of the method is the need to provide an anechoic termination (e.g. by using high absorbing material), which may not be easy especially for low frequency measurements. The schematic of a setup using the decomposition theory is presented in figure 1.

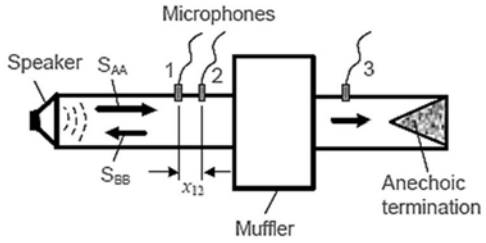

Figure 1: Measurement setup for the decomposition method [1]

The second approach to obtain damper transmission loss characteristics employs the two-source method [8] and the two-load method. These methods are based on the four-pole transfer matrix description of a damper and do not require an anechoic termination. The transfer matrix approach assumes that each acoustic element may be described by four parameters, which enable relating the pressure and velocity at the inlet to that at the outlet [9,10].

In the two-source method, the sound source is placed in two configurations in a system and four microphones are used in order to obtain the four parameters of a damper transfer matrix, as shown in figure 2.

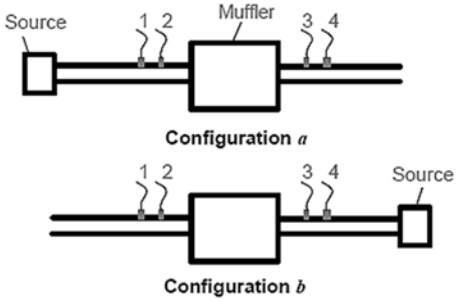

Figure 2: Setup of measurement with the use of two-source method [1]

A similar approach to define a four-pole damper matrix is the two-load method, which assumes that instead of moving the sound source to the other end, the same result may be obtained by changing the end condition. The two loads may be acquired with two tubes of different length or by inserting an absorbing material into one of the tubes. Changing the end condition effectively changes the impedance at the system termination. The schematic of a measurement setup with the use of the two-load method is shown in figure 3.

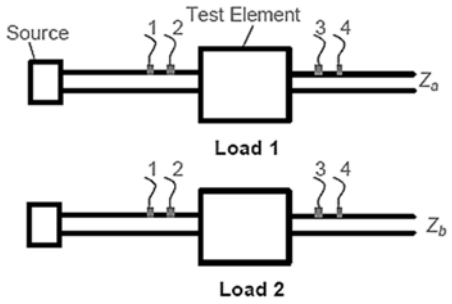

Figure 3: Measurement setup for the two-load method [11]

Another method for measuring damper transmission loss assumes the usage of PU probes instead of microphones. A PU probe can measure both sound pressure and particle velocity, as a particle velocity sensor and a miniature microphone are placed close together. The particle velocity measurement principle is based on the detection of the temperature difference between two heated wires. A damper transmission loss may be calculated using the transfer matrix approach and by measuring particle velocity at the inlet and at the outlet. In recent years the method was applied to acoustic measurements, such as the determination of absorption coefficients. The transmission loss measured with the PU method agrees well with the result measured with the conventional four-pole method and with the FEM result in the frequency range within the applicability of plane wave theory [11].

The described methods have been frequently used to verify numerical models of reactive dampers characteristics, both in 1D models based on plane wave theory and 3D models solved with boundary or finite element methods [12]. Nevertheless, most research describing the usage of these methods does

by: *Warzyńska Urszula, Siwulski Tomasz –Wrocław University of Science and Technology*

not involve a real piping system with a pulsation excitation induced by a compressor. Therefore, their applicability is limited to laboratory tests.

For many years, the measurements of real attenuation of gas pulsation in a reciprocating compressor piping system were also made, mostly by consultancy companies. Some of the researchers also undertook this subject and used pressure transducers to measure the dynamic pressure component during the flow of a working medium [13, 14]. In this research, the source of pulsations was a piston compressor, and the system was terminated with an air tank. The research concerned a system with a volume-choke-volume filter and with a Helmholtz resonator.

Although transmission loss characteristics of common-type dampers obtained even with the use of an uncomplicated 1D approach are generally in good agreement with the measurements, the situation changes significantly when an actual damper is installed in the system. The influence of the compressor operating parameters and the impedance of the system, etc. lead to a radical modification of damper characteristics, and thus in many cases, the damper attenuation efficiency may be insufficient.

2 Experimental approach

2.1 Test stand

The test stand for experimental research on the impact of operating parameters on the characteristics of pressure pulsation dampers comprised a single piston air compressor together with an electric motor and an inverter to control the rotational speed, as well as a pulsation damper. The piston compressor operated in the range of 1000 – 2000 rpm at a nominal pressure of 8-10 bar. The volumetric flow at 8 bar pressure and at a nominal speed of 1500 rpm was 125 l/min. Air was used as the working medium in the system. Dynamically variable pressure was measured with a system consisting of two industrial pressure transducers along with a signal processing and recording system. The first pressure transducer was mounted on the discharge side of the compressor at the inlet of the damper, while the second pressure transducer was placed at the outlet of the damper. The line termination was closed-end and a choke valve at the end of the line was mounted on a tee. Therefore, the wave reflection at the end of the installation should not depend on the size of the orifice between the valve seat and the needle. In the system, the suction and discharge temperatures of the compressor were measured in order to assure the same temperature for each test. The ambient temperature for each test and the suction and discharge temperatures at the beginning of each measurement were 23°C in order to obtain the same velocity of sound for each case, which ensures that the resonance frequencies do not change in the system depending on sound velocity. The test stand and a schematic of measurement points are depicted in figure 4.

Figure 4: Test stand for determining the change of damper transmission loss characteristics under different operating parameters

Experimental tests of pressure pulsation were carried out using different configurations of the damper. This required constructing a damper with exchangeable internal attenuating elements according to an original design. The required volume of the chamber damper was calculated following the Helmholtz resonator theory, by considering the lowest operating speed of the compressor. Based on the minimum required volume, general dimensions of the damper were calculated: internal diameter D=200mm, and chamber internal length L=650mm. The API 618 formulas for surge volumes do not apply to such small compressors (minimum volume should not be less than 0.03m^3) and generated too minimized dimensions of a damper. The chamber damper (figure 5) was constructed as a cylinder with two demountable flanges with removable internal elements: two sleeves (1) positioning an internal baffle with a choke tube (2) or a single baffle (3) and internal tubes (4) mounted into a flange. The internal elements may be mounted in different configurations and the elements in the set have different lengths and diameters.

by: *Warzyńska Urszula, Siwulski Tomasz –Wrocław University of Science and Technology*

Figure 5: Chamber damper with different internal attenuation elements

For the current study, three configurations of the damper were assumed:

- a single chamber damper without internal elements,
- a damper with a choke tube, whose length was equal to half of the chamber length L4=325mm and whose internal diameter was equal to the internal diameter of the connecting pipe d=24mm (figure 6),
- a damper with an internal baffle and a choke tube with a length and a diameter identical to those in the second configuration (figure 7).

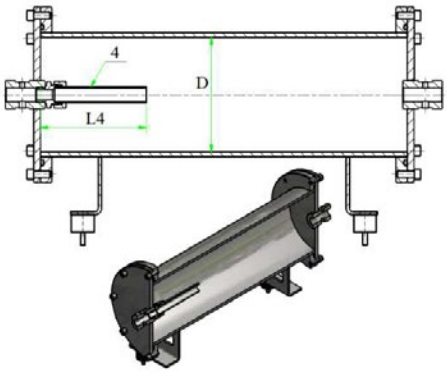

Figure 6: Chamber damper with a choke tube used in the tests

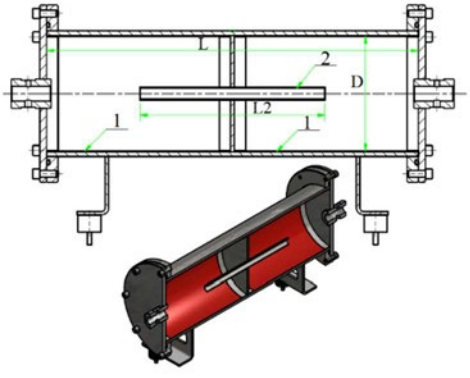

Figure 7: Chamber damper with internal baffle and choke tube used in the tests

The tests were carried out for three rotational speeds of the compressor: 1000rpm, 1500rpm and 2000rpm generating different flows of gas and with the assumption of different system impedances (opened and partially closed choke valve at the end of the line) defining changes of pressure in the system. The static pressure in the system depended on the flow resistance: in the case of a fully opened valve the static pressure resulted from the local loss and varied with the flow change, while in the case of a partially closed valve the static pressure was set to 5 bar for each measurement. The measurement cases and operational parameters are listed in table 1. In the following descriptions, the three damper designs are referred to shortly in the following manner: single chamber damper = Chamber, a damper with internal choke tube = Tube, a damper with internal baffle and choke tube = Filter.

Table 1: Measurement cases and operational parameters

LC	Damper type	End condition	Rotational speed n [rpm]	Static pressure p [bar]
1	Chamber	Fully opened choke valve (OV)	1000	1.53
2			1500	2.30
3			2000	2.93
4	Tube		1000	1.57
5			1500	2.35
6			2000	2.87
7	Filter		1000	1.50
8			1500	2.27
9			2000	2.90
10	Chamber	Partially closed choke valve (CV)	1000	5.00
11			1500	
12			2000	
13	Tube		1000	
14			1500	
15			2000	
16	Filter		1000	
17			1500	
18			2000	

2.2 Measurement results

The following figures show the selected results of experimental tests for measured pressure pulsations in the system. In figures 8-10, pressure-time series (one wave period) are presented for the three damper designs: the chamber damper, the damper with a tube and the filter, and for three rotational speeds: 1000, 1500 and 2000rpm in the unloaded system (with the choke valve open). The analysis of the results has shown that each tested damper design ensures high damping ratio of pressure pulsations for all rotational speeds. The time-course graphs also show that the higher the compressor speed, the higher the static pressure in the system, which phenomenon is due to an increase in the local flow resistance (the pressure drop in the system increases with the square of the gas flow velocity). The static pressure in the installation also depends on the type of the damper design: the acoustic filter generates the smallest pressure drops for 1000 and 1500rpm rotational speeds, while in the case of the 2000rpm the lowest static pressure value occurred in the system with the tube damper.

by: *Warzyńska Urszula, Siwulski Tomasz –Wrocław University of Science and Technology*

The higher the gas flow rate, the greater the pressure pulsation amplitudes. It may be explained by the fact that the shape of the compressor flow pulse is “sharper” because of shorter discharge valve opening time which leads to pulses with higher amplitude and harmonics.

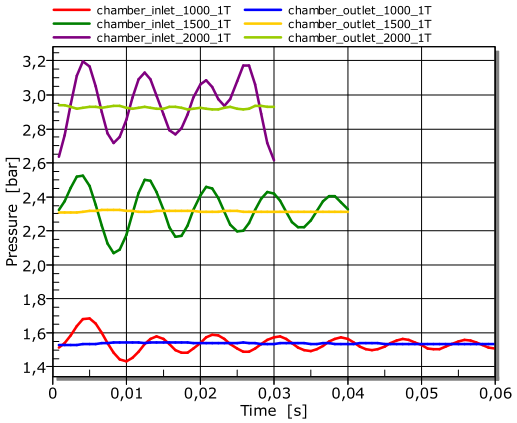

Figure 8: Time history of pressure in one period – Chamber, OV, n: 1000, 1500, 2000rpm

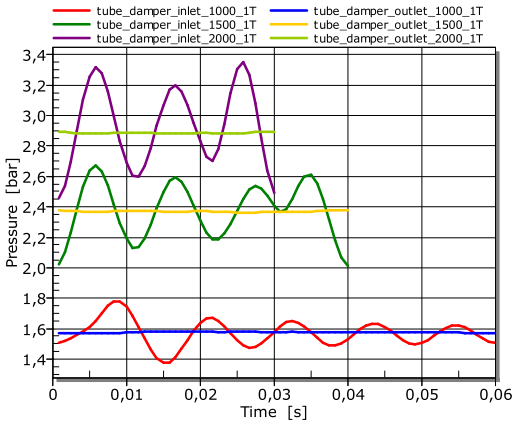

Figure 9: Time history of pressure in one period – Tube, OV, n: 1000, 1500, 2000rpm

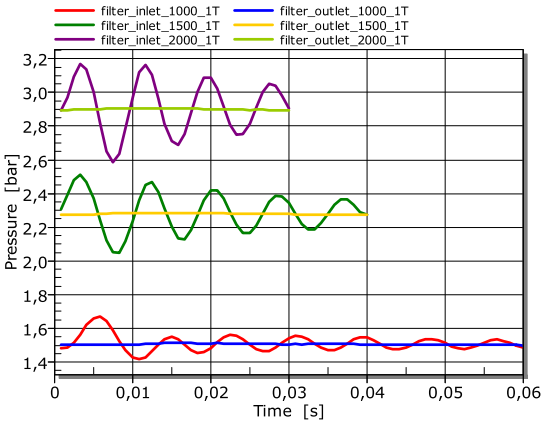

Figure 10: Time history of pressure in one period – Filter, OV, n: 1000, 1500, 2000rpm

In order to better illustrate the magnitude of pressure pulsations, further analysis of the results was carried out based on the amplitude-frequency characteristics. Figures 11-13 compile graphs of pressure pulsation amplitudes depending on the frequency for three damper designs, for three rotational speeds of 1000, 1500 and 2000rpm in an unloaded system (with opened choke valve). Because the inlet amplitudes are much higher than the outlet (all the outlet peaks are lower than API 618 limit value for pipes), in the graphs the API limit values for compressor flanges are also shown.

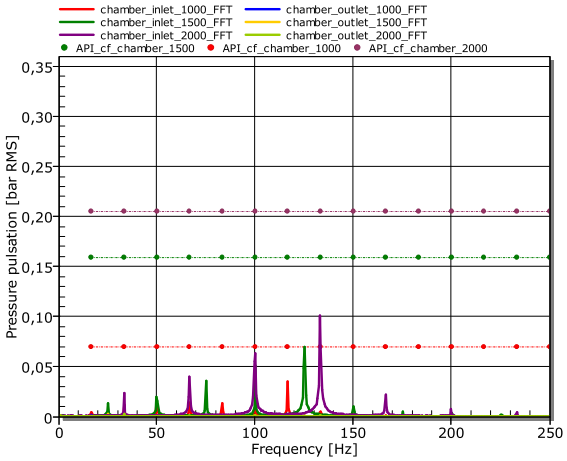

Figure 11: Frequency spectra – Chamber, OV, n:1000, 1500, 2000rpm

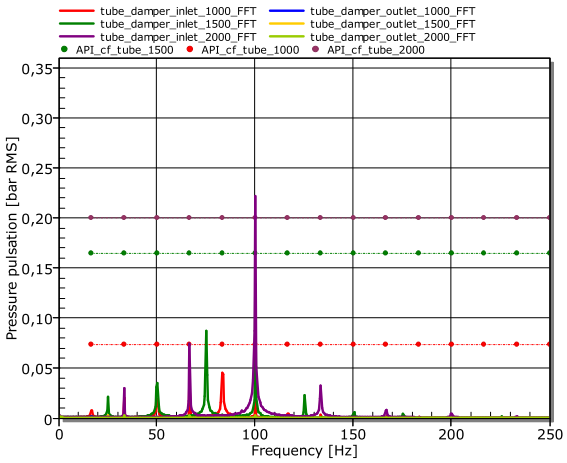

Figure 12: Frequency spectra – Tube, OV, n:1000, 1500, 2000rpm

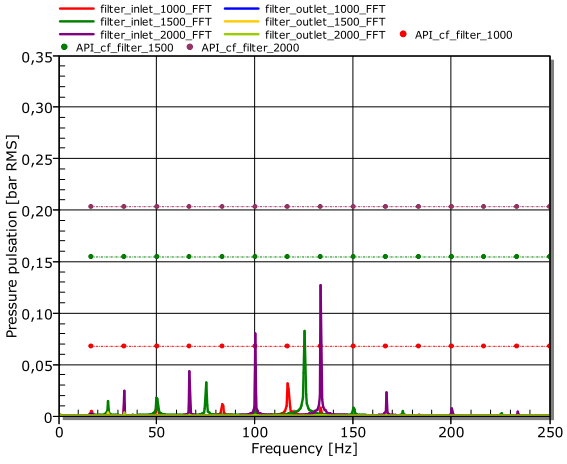

Figure 13: Frequency spectra – Filter, OV, n:1000, 1500, 2000rpm

by: *Warzyńska Urszula, Siwulski Tomasz –Wrocław University of Science and Technology*

In the analyzed measurement cases, the amplitudes of pulsations at the inlet of a damper can be observed to increase together with the increasing rotational speed of the compressor. The limit value according to API 618 for compressor flanges is exceeded only in the case of the tube damper for the highest rotational speed. For a single piston compressor, the pulsation amplitude of the first harmonic component of the excitation resulting from the rotational speed is dominant. Depending on the damper design, different pulsation frequency is dominant at the inlet, which indicates wave reflection and additional amplifications of higher harmonics.

In the second series of measurements, the analyses focused on the effect of system load (with a partially closed choke valve maintaining static pressure in the installation at 5 bar) on pressure pulsation values. Figures 14-16 show pressure pulsation amplitudes depending on the frequency for three damper designs, for three rotational speeds of 1000, 1500 and 2000rpm in a loaded system (with a partially closed choke valve).

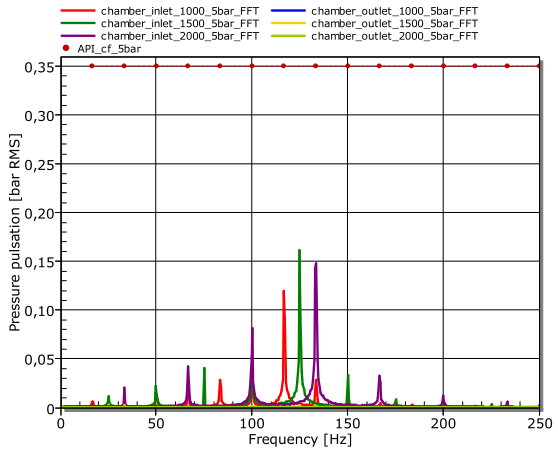

Figure 14: Frequency spectra – Chamber, CV, n:1000, 1500, 2000rpm

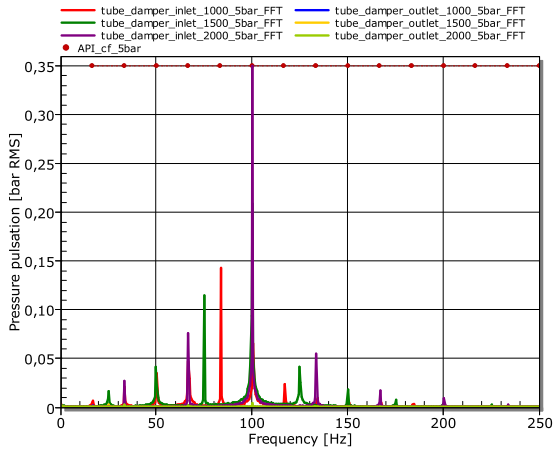

Figure 15: Frequency spectra – Tube, CV, n:1000, 1500, 2000rpm

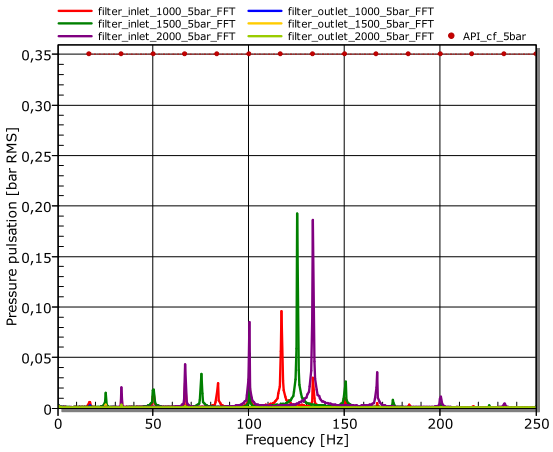

Figure 16: Frequency spectra – Filter, CV, n:1000, 1500, 2000rpm

The analysis of the results indicates a significant increase in the pulsation amplitudes of the higher harmonics at higher compressor rotational speeds. This fact suggests that inserting a damper into the system causes the reflection and interference of pulsation waves, resulting in pressure pulsation at the inlet higher than it would result from the operation of the excitation source, i.e. the piston compressor. Pressure pulsation amplitudes are attenuated at the outlet of the damper (for each analyzed design) to allowed values.

3 Simulation approach

3.1 Analysis setup

The currently available and used mathematical models for the selection of a proper damper in a compressor installation were described in the previous publication[15]. There are three main models which enable the selection of general dimensions for a damper and the determination of theoretical transmission loss characteristics: analytical formulas for initial damper sizing (Helmholtz model or recommendations of API 618[16]), numerical simulations based on plane wave theory in 2D (wave equations solved in the frequency or time domain with the use of the transfer matrix approach or the method of characteristics) and 3D simulations based on a Helmholtz equation solved by means of the finite element or boundary element method (FEM, BEM). Full CFD simulations coupling the medium flow with the acoustics field are still not commonly used due to high computational costs.

In the current study, the theoretical transmission loss characteristics of the dampers were determined with the use of the 3D Helmholtz equation calculated with FEM. In the FEM-based 3D acoustic simulation, the fluid momentum (Navier-Stokes) equations and continuity equations are simplified to obtain the acoustic wave equation using the assumptions that the fluid is compressible (density changes due to pressure variations) and no mean flow of the fluid is taken into consideration.

by: *Warzyńska Urszula, Siwulski Tomasz –Wrocław University of Science and Technology*

Viscous dissipation is allowed for using the Stokes hypothesis (the lossy wave equation). The wave equation is reduced to the inhomogeneous Helmholtz equation and the finite element formulation is obtained from a testing wave using the Galerkin procedure. In harmonic response analyses, the following equation is solved for pure acoustic problems:

$$(-\omega^2[M_a] + j\omega[C_a] + [K_a])\{p\} = \{f_F\} \qquad (1)$$

where:
$[M_a]$ – acoustic fluid mass matrix,
$[C_a]$ – acoustic fluid damping matrix,
$[K_a]$ – acoustic stiffness matrix,
$\{f_F\}$ – acoustic fluid load vector.

Normal surface velocity (inhomogeneous Neumann condition) was applied as an inlet boundary condition. At the inlet and at the outlet ports, the radiation boundary condition was set (Robin boundary condition), which enables to model an anechoic termination.

The finite element grid was applied to each damper geometry with the use of identical mesh parameters (figure 17). The medium was air at 23°C, in which the sound velocity was equal to 348 m/s.

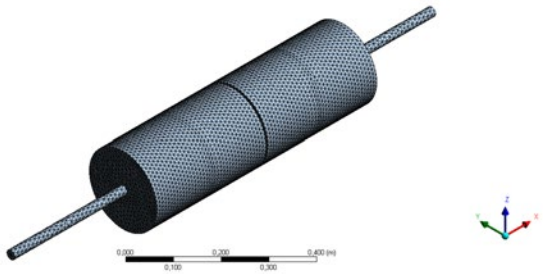

Figure 17: Finite element grid of the damper

4 Comparison of simulations and measurements results

The comparison of the simulation and measurement results was based on the determination of the transmission loss characteristics function, which describes the decrease of the acoustic signal power between the inlet and the outlet of the pulsation damper and is typically determined from the ratio of pressure pulsation amplitudes at the damper inlet and outlet for a given harmonic of the signal. For the purpose of determining the transmission loss function, Fourier transforms were prepared from pressure time signals measured with pressure transducers in order to determine the amplitude of pulsations in the frequency domain. The transmission loss function can be then calculated from the formula:

$$TL = 20 \cdot log \frac{P_0}{P_L} \, [dB] \qquad (2)$$

where: P_0 and P_L are the Fourier transforms of the pressure-time histories of the incident and the transmitted waves respectively.

A TL graph is normally determined by using a frequency sweep of the excitation source with a speaker. In the research a different approach was used. The TL characteristics were obtained individually for each compressor speed by FFT of the damper inlet measured signal divided by FFT of the damper outlet measured signal.

If the amplitude of the pulsation at the outlet is much greater than the amplitude of the pulsation at the inlet, the transmission loss function reaches the minimum, which indicates the damper resonance – amplification of the pulsation in a given frequency. The maximum of a transmission loss function determines the highest attenuation for a given frequency.

Figures 18–20 show the transmission loss characteristics obtained from both the measurement and the simulation approach. In each graph, the measurement results include three rotational speeds of the compressor in the system with opened choke valve at the end.

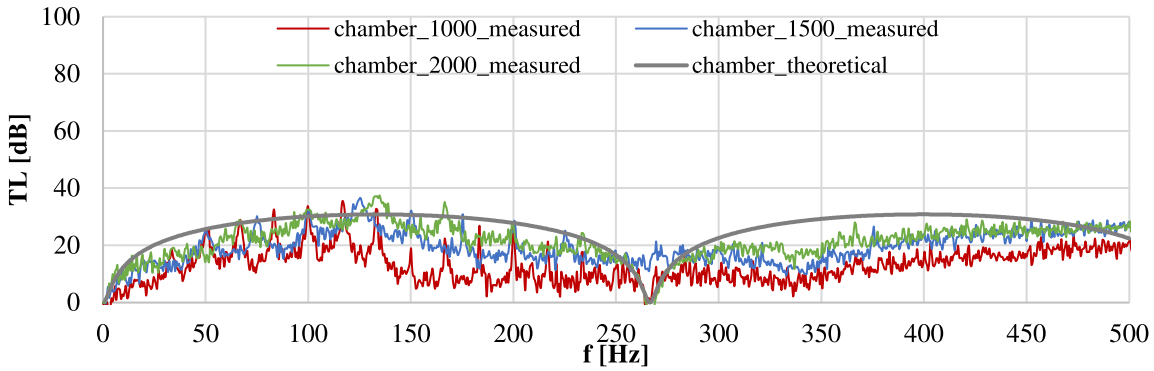

Figure 18: Transmission loss characteristics of a chamber damper obtained from simulations and measurements for rotational speeds of 1000, 1500 and 2000rpm in the system with opened valve termination

by: *Warzyńska Urszula, Siwulski Tomasz –Wrocław University of Science and Technology*

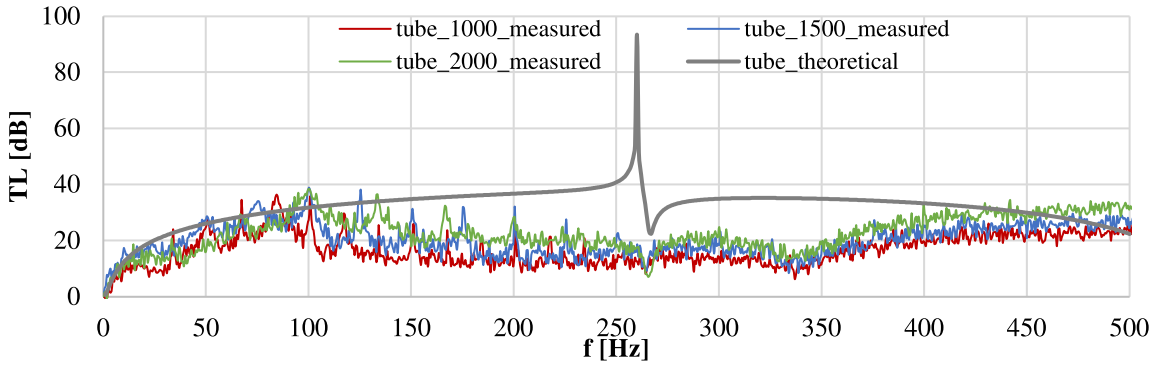

Figure 19: Transmission loss characteristics of a damper with an internal tube obtained from simulations and measurements for rotational speeds of 1000, 1500 and 2000rpm in the system with opened valve termination

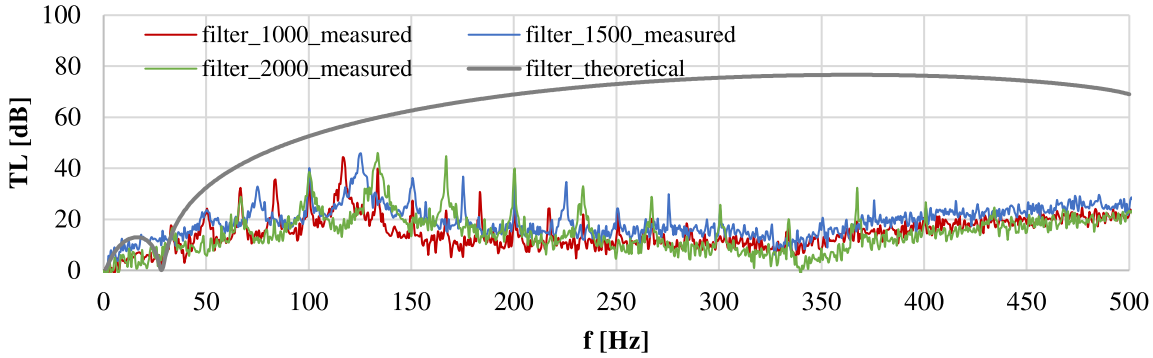

Figure 20: Transmission loss characteristics of a damper with an internal baffle and choke tube obtained from simulations and measurements for rotational speeds of 1000, 1500 and 2000rpm in the system with opened valve termination

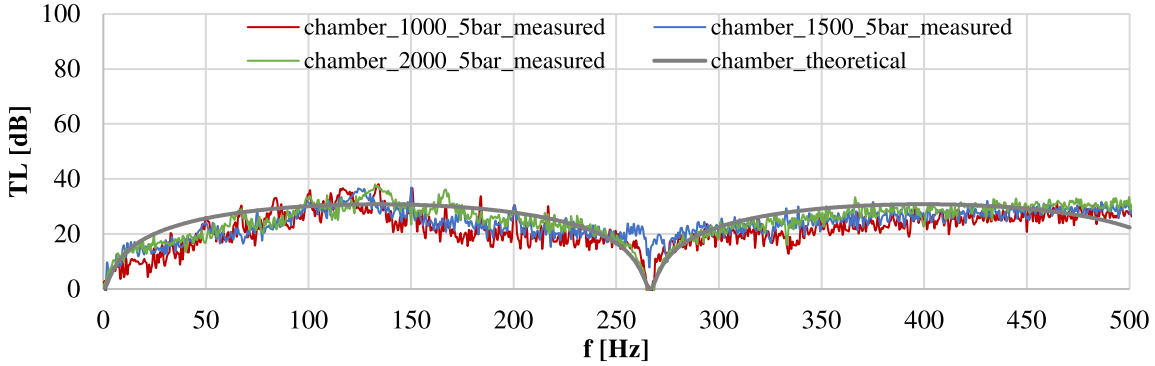

Figure 21: Transmission loss characteristics of a chamber damper obtained from simulations and measurements for rotational speeds of 1000, 1500 and 2000rpm in the system with 5bar load

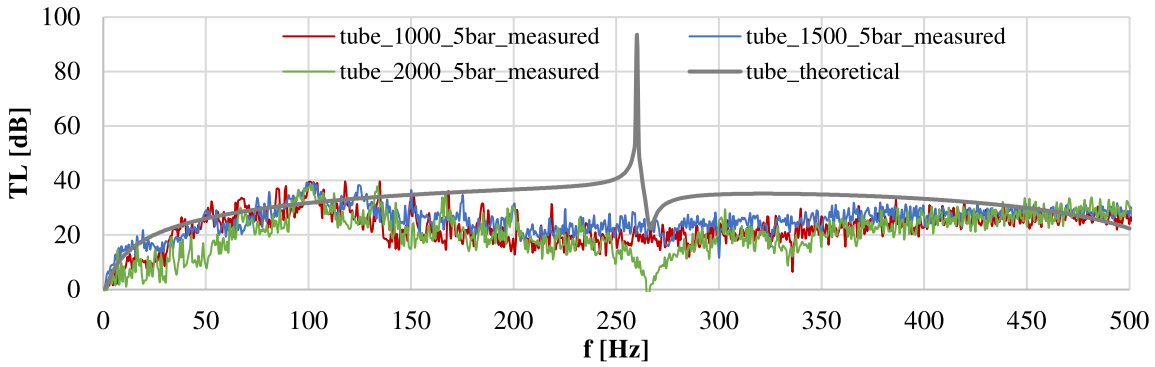

Figure 22: Transmission loss characteristics of a damper with an internal tube obtained from simulations and measurements for rotational speeds of 1000, 1500 and 2000rpm in the system with 5 bar load

by: *Warzyńska Urszula, Siwulski Tomasz –Wrocław University of Science and Technology*

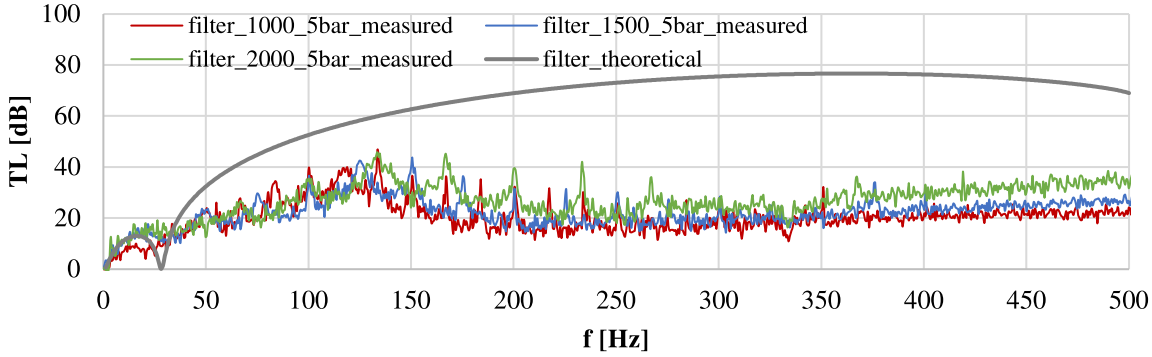

Figure 23: Transmission loss characteristics of a damper with an internal baffle and choke tube obtained from simulations and measurements for rotational speeds of 1000, 1500 and 2000rpm in the system with 5 bar load

The comparative analysis of the transmission loss characteristics determined by means of the simulation and the measurement methods indicates the best agreement of results in the case of a chamber damper and significant discrepancies in the characteristics for dampers with internal attenuating elements.

The measured transmission loss characteristics of the chamber damper (figure 18) show damper resonance to be 267Hz at 1000 and 2000rpm, which result is consistent with the theoretical characteristics. However, the resonance is not observed for the rotational speed of 1500rpm. For the lowest rotational speed, the attenuation values are smaller than the theory would suggest. Very good agreement of the results between the measurements and the simulation may be seen for the chamber damper in the system with 5bar load (figure 21).

In the case of the tube damper (figure 19), good agreement between the measurement results and the theoretical characteristics is observed in the frequency range up to 100Hz, but above this value the transmission loss characteristics in actual conditions acquire half of the theoretical values. The damper resonance is clearly visible for all three speeds, and in this design it is 265Hz. In the system with pressure load (figure 22), the damper resonance occurred only at 2000rpm.

The measured and the theoretical transmission loss characteristics of the damper with an internal baffle and a choke tube (figure 20) show convergence of results for damper resonance at 29Hz for 1000 and 2000rpm, while no resonance is observed for 1500rpm. According to the theoretical characteristics, this damper design should provide attenuation in the range from 29Hz to 500Hz, while actual characteristics show additional resonances resulting from wave reflection in the frequency range 317 – 340Hz. The measured characteristics of the filter (figure 23) in the system with the 5bar load indicate no resonances in the analyzed frequency range.

The proposed method of measuring the transmission loss characteristics is obviously not a method for verifying theoretical models, as the already known and above described acoustic measurement methods with anechoic termination are sufficient. The purpose of the research was to analyze the effect of system operating conditions on actual transmission loss characteristics. As can be seen from the presented measurement data, amplifying the pulsation amplitudes at the system inlet may be significantly influenced already by the damper design, even before the geometry of the piping system is considered as a factor. Moreover, the reflection of the wave in the system behind the pulsation damper can affect the formation of additional acoustic resonances, which do not result from the characteristics of the damper itself and are not visible in the transmission loss functions determined by simulation methods.

5 Conclusion

The article investigated the problem of determining the transmission loss characteristics of passive pressure pulsation dampers, with consideration to the actual operating parameters of the system. The geometrical parameters of the installation and the operating conditions have a significant impact on the change in the transmission loss characteristics. The current methods for selecting pressure pulsation dampers used in actual compressor installations involve simulations with a reflection terminations line that replaces the actual pipe system and take into account the majority of possible combinations of operating parameters according to API 618 guidelines. This has been, to date, the most reasonable method. Nevertheless, simulations carried out with the use of acoustic-based solvers not always allow using complex boundary conditions, such as a partially closed choke valve, valve gap geometry, etc. It is, however, possible by the use of time-domain solvers (e.g. based on the method of characteristics). The presented measurement results indicate that a slightly modified static pressure caused by the change of the size of the choke valve

by: *Warzyńska Urszula, Siwulski Tomasz –Wrocław University of Science and Technology*

orifice significantly influenced the pulsation amplitudes, while the length of the outlet line was unchanged in each test case and so was the speed of sound (pressure variation range did not noticeably affect the speed of sound value). Test results suggest that changes in transmission loss characteristics are not only due to the phenomenon of wave reflection, but also depend on the volume of compressed gas in the system that creates a kind of energy accumulator. It seems reasonable to attempt to describe the phenomenon of pressure pulsation not only using acoustic models, but full energy models also taking into account gas pressure energy.

6 Acknowledgements

Calculations have been carried out using resources provided by Wroclaw Centre for Networking and Supercomputing (http://wcss.pl), grant No. 223.

References

[1] Tao, Z. and Seybert, A.F. (2003): A review of current techniques for measuring muffler transmission loss, SAE Technical Paper 2003-01-1653.

[2] Chung, J.Y. and Blaser, D.A. (1980): Transfer function method of measuring in-duct acoustic properties, I: Theory, J. Acoust. Soc. Am, 68, 907-913.

[3] Chung, J.Y. and Blaser, D.A. (1980): Transfer function method of measuring in-duct acoustic properties, II: Experiment, J. Acoust. Soc. Am, 68, 914-921.

[4] Seybert, A.F. and Ross, D.F. (1977): Experimental determination of acoustic properties using a two microphone random excitation technique, J. Acoust. Soc. Am., 61, 1362-1370.

[5] Seybert, A.F. (1988): Two-sensor methods for the measurement of sound intensity and acoustic properties in ducts, J. Acoust. Soc. Am, 83, 2233-2239.

[6] Selamet, A., Radavich, P.M. (1997): The effect of length on the acoustic attenuation performance of concentric expansion chambers: an analytical, computational and experimental investigation. Journal of Sound and Vibration. 201, 4, pp. 407–426.

[7] ASTM standard, E1050-19, Standard test method for impedance and absorption of acoustical material using a tube, two microphones and a digital frequency analysis system.

[8] Munjal, M.L., Doige A.G. (1990): Theory of a two source-location method for direct experimental evaluation of the four-pole parameters of an aeroacoustic element, Journal of Sound and Vibration, 141(2), 323-333.

[9] Munjal, M.L. (2014): Acoustics of Ducts and Mufflers, John Wiley & Sons.

[10] Soedel W. (2007): Sound and vibrations of positive displacement compressors. CRC Press.

[11] Yan, L., Jiang, W. (2013): A simple method for measuring muffler transmission loss with PU probes, Proceedings of the ASME 2013 International Mechanical Engineering Congress and Exposition IMECE2013.

[12] Kadam, P., Kim, J. (2007): Experimental formulation of four poles of three-dimensional cavities and its application. Journal of Sound and Vibration 307 pp. 578–590.

[13] Liu B., Feng J., Wang Z., Peng X. (2012): Attenuation of gas pulsation in a reciprocating compressor piping system by using a volume-choke-volume filter. Journal of Vibration and Acoustics, Vol. 134.

[14] Jia,, X., Liu, B., Feng, J. and Peng, X. (2014): Attenuation of Gas Pulsation in the Valve Chamber of a Reciprocating Compressor Using the Helmholtz Resonator. Journal of Vibration and Acoustics. 136, 5.

[15] Warzyńska, U., Kollek, W. (2018): Modelling of transmission loss characteristics of reactive pulsation dampers. In: Herbert Steinrück (ed.) 11th EFRC Conference 2018, pp. 198-205. EFRC, European Forum for Reciprocating Compressors, Wien.

[16] API STD 618 Reciprocating Compressors for Petroleum, Chemical, and Gas Industry Services, Fifth Edition, 2007, Errata 1 2009, Errata 2 2010. American Petroleum Institute.

A LIFETIME EXPERIENCE IN RECIPROCATING COMPRESSORS

Since 1977 we have been repairing foundations, installing new machinery, aligning, and regrouting all kinds of **reciprocating** and **rotating machinery**.

Do you want to have a reliable installation? **Start with the foundation!**

Noise and **vibration** indicate issues that can affect a machine's reliability, such as imbalanced parts, and can even cause machines to fail through their own damaging effects. As the **only epoxy grout manufacturer** with its own engineering and contracting arm, Alphatec Engineering is uniquely placed to give you the best combination of products and services, together with our commitment to quality reflected with our ISO 9001 certification.

Epoxy Grout Manufacturing

Anchor Bolt Replacement

4,000+ CONTRACTS

ALPHATEC grouting specialists

57 COUNTRIES

Epoxy Resin Injection

Foundation Repair

GROUTING SPECIALISTS

At Alphatec Engineering we have different procedure of repairing critical machinery foundations, and the best technique of application of our polymer products.

Our main products are epoxy resin based grouts with inert fillers for stiffness and heat resistance, which we use to repair cracked or damaged foundations and to install new machinery following the **OEM** and **API RP** 686 recommendations.

End-user	Location	Equipment type (No) - Output	Condition	Service description
Fluxys-LNG Terminal	Belgium	BOG IHI Compressors 32HF-4N-CM (4) – 6 MW	New	Epoxy grouting 4 Compressors & Auxiliaries
BayernOil GmbH	Germany	Worthington BDC gas compressor - 410 kW	1967	Full regrout & foundation repair
Caltex Petrochem Corp	New Zealand	Cooper V-275 GWMK - 3.8 MW	82/06	Engine/compressor regrout & foundation repair
ExxonMobil Chemicals	Belgium	Ingersoll-Rand primary compressor - 3.25 MW	1975	Foundation and anchor bolt repair
Gujarat State Fertiliser	India	Kobe LM-6 recip-compressor - 5.6 MW	Existing	Regrout & pressure injection foundation repair
Incitec Pivot Fertilisers	Australia	Dresser-Rand HHE recip compressor - 4.0 MW	Existing	Foundation repair, re-alignment & regrout
MFGT	Hungary	SYCC/Burckhardt 6-cylinder compressor - 2.9 MW	New	Engine & compressor epoxy grouted
Petkim Izmir	Turkey	Nuovo Pignone primary & hyper compressor - 2.65 MW	1985	Foundation repair, realignment & regrout
Petrochemical Industries	Kuwait	I-R HHE compressors (3)	Existing	Regrout & pressure injection foundation repair
Petronas Melaka	Malaysia	Dresser-Rand HHE gas compressors (3) - 3.8 MW	1998	Regrout & realignment
Petroplus Cressier	France	Thomassen 1MC1 gas compressor - 480 kW	1964	Foundation repair, encapsulation & full regrout
Repsol Puertollano	Spain	Nuovo-Pignone 6PH/2 hyper compressor - 4.5 MW	1974	Regrout & pressure injection foundation repair
Santa Fe Energy	Indonesia	Waukesha/Ariel compressors (5)	New	Align machines, supply & install epoxy grout
Shell Refinery	Singapore	Thomassen recip compressor - 3.0 MW	1981	Pressure injection foundation repair
Total La Mede	France	Ingersoll-Rand recip compressor - 1.69 MW	1992	Regrout & pressure injection foundation repair

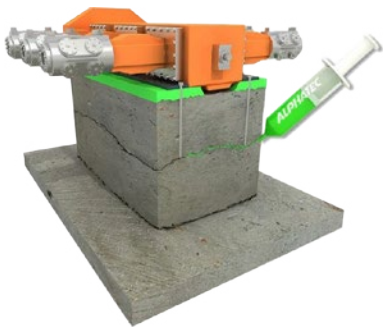

Follow us:

(+34) 961 45 15 99

info@alphatec-engineering.com

www.alphatec-engineering.com

Feasibility Study of a Novel Toroidal Damper Concept for Improved High Frequency Pulsation Control

by:

André Eijk, Javier Fatou Gómez, Olaf Vijlbrief
TNO
Delft, The Netherlands
andre.eijk@tno.nl
javier.fatougomez@tno.nl
olaf.vijlbrief@tno.nl

Cyril Wentzel
Wentzel Dynamics
Den Haag, The Netherlands
cyril@wentzeldynamics.com

12th EFRC CONFERENCE
August 24 – 26, 2021, Warsaw

Abstract:
Modern day compressor installations pose challenges for pulsation and vibration control. Classical pulsation dampers, with e.g. a cylindrical shape, are extensively used with and without internals to obtain desired Transmission Loss (TL) characteristics throughout the operational range. A trend is the increase of frequencies of interest due to higher compressor speeds that become more and more difficult to attenuate, both acoustically and mechanically. This paper reports on an ongoing study that was carried out for the EFRC R&D group to assess the possibilities of an alternative damper concept to obtain favourable TL for a large frequency range. It was found in an earlier project that a class of toroidal shaped damper volumes could be both structurally efficient, avoid shaking forces on the damper and have good TL at higher frequencies. Following these initial explorations, experiments were carried out including the effects of overpressure and continuous gas flow to investigate whether the anticipated behaviour computed with simplified models could be confirmed. A direct comparison was made to the TL of a more conventional cylindrical damper with favourable connecting pipe configuration. The design and manufacture of the test hardware is described as well as the tests in a state-of-the art acoustic test facility of TNO, presenting TL over the relevant frequency range. It was found that for the chosen ‚Perforated Hub'-type of Toroidal damper (PHT), the presence of a gas flow causes a large drop in the TL performance. In a second iteration, another sub-type of toroidal damper, the Open Throat Toroid (OTT) damper" was tested to investigate if this loss of TL could be avoided. The exercise was supported by the application of advanced numerical flow computations, giving more insight into the flow features that contributed to the observed loss of TL. This concerns both detailed flow computations of the choke-cavity connection in the time domain and an intermediate resolution aero acoustic method.

by: André Eijk, Javier Fatou Gómez, Olaf Vijlbrief – TNO; Cyril Wentzel – Wentzel Dynamics

1 Introduction

An intrinsic feature of a reciprocating compressor is that it generates pulsations which can be mitigated by the application of pulsation dampers. The acoustic performance of pulsation dampers shall be large enough to meet the requirements as stipulated in the API Standard 618[1]. There is a trend that the sizes, powers and speeds of reciprocating compressors increase. The consequence is that the size of pulsation dampers can be large and heavy, leading to an exceeding of mechanical restraints such as the size and mass. It is shown from experience that it becomes more difficult to mitigate the mechanical vibrations of pulsation dampers and piping for higher frequencies (> 50 Hz). This requires very stiff and large structures to support pulsation dampers and the attached piping which is not always feasible due to space limitations and required structure stiffness at elevated levels. This is especially challenging for offshore applications.
It was concluded in a previous project carried out for the R&D group of the EFRC that a novel class of toroidal shaped dampers might offer substantial improvements over classical types of dampers, e.g. cylindrical shaped, in mitigating pulsations.
The acoustic performance of a pulsation damper to mitigate pressure pulsations is defined by the Transmission Loss (TL). The higher the TL of a system it has, the better it will perform in terms of pressure mitigation. TL is defined as the ratio between the applied pressure pulsations at the inlet and outlet of the pulsation damper with an anechoic termination at the outlet as follows:

$$TL = 20\log\left(\frac{P_{in}}{P_{out}}\right)\ [dB] \quad (1)$$

with P_{in} the incident field (average pressure pulsation at the inlet), and P_{out} the pressure pulsation at the outlet.

The potential benefits of a toroid damper would be an increased TL for higher frequencies, a more compact construction with less weight, and even negligible pulsation forces on the pulsation damper. This will lead to an increase of the mechanical integrity of the compressors due to lower mechanical vibrations of e.g. the compressor manifold.

The toroid dampers might also be very beneficial for systems with a stepless flow control system because these systems generate in general pulsations with higher frequencies especially at the suction side.
Hydrogen applications require in general larger sized pulsation dampers due to a lower acoustic performance caused by the high speed of sound. It is expected that more and larger size hydrogen reciprocating compressors are required in the near future caused by upscaling of refineries[2]. Besides that, it is also expected that centrifugal compressors will be replaced by large reciprocating compressors serving as transport compressors if hydrogen will be the new energy carrier of an energy transition.

This paper will explain the design, manufacturing and testing of the Perforated Hub Toroid (PHT) damper and the Open Throat Toroid (OTT) damper. The results of the toroid dampers have been compared with the results of a cylindrical damper with the same volume, serving as the "reference" damper. The testing has been done in a TNO facility dedicated for this type of measurements using well established procedures and hardware allowing also pressure and flow to be applied during testing over a broad range of frequencies.

The results of the PHT and OTT damper showed that the mean static flow has a large effect on the TL which is hardly present for the cylindrical damper. This effect was also described by Selamet[3] and turns out to be very pronounced for the toroid dampers, especially for the PHT type. An explanation of this effect is given using aero-acoustic theory and detailed Computation Fluid Calculations (CFD).

2 Design, manufacturing and measurements of the cylindrical and PHT dampers

2.1 Design of the research dampers

The reference damper for comparing the results of the toroidal damper was a classical cylindrical damper with opposing nozzles at the cylindrical wall as shown in Figure 1. The opposing nozzle layout has a much better acoustic performance than the "in-line" type with nozzles at both end caps. The PHT damper has been designed aiming for a frequency range between 50 and 150 Hz. This is achieved by variation of the hub and choke parameters as shown in Figure 2, while fixing the overall size to a practical value. The model boundary conditions are anechoic (reflection free) terminations at the inlet and outlet.

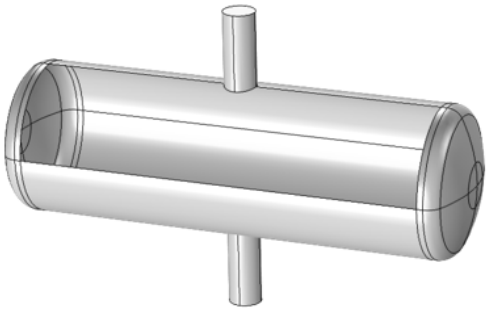

Figure 1 Cylindrical damper

by: André Eijk, Javier Fatou Gómez, Olaf Vijlbrief – TNO; Cyril Wentzel – Wentzel Dynamics

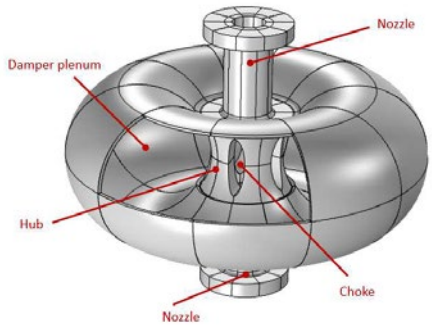

Figure 2 Perforated Hub Toroid damper

The results of the TL calculations without a mean static flow are shown in Figure 3. It is clear that the TL for the PHT damper is much larger (grey area) in the target frequency range between 50 and 150 Hz than that of the classical cylindrical damper. This could be achieved by creating a Helmholtz frequency near 100 Hz between the hub and damper volume by a proper design of the hub geometry.

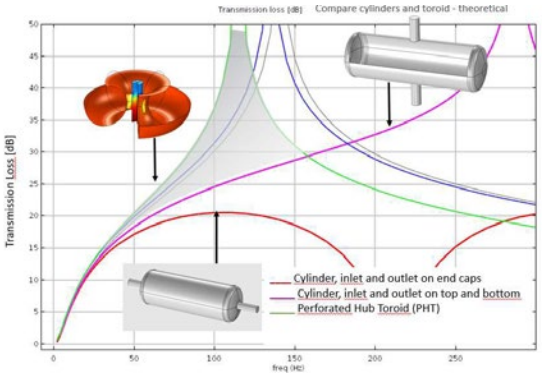

Figure 3 Computed TL of the cylindrical and PHT damper for a zero (static) flow condition

The effectiveness of the computational approach in studying the complex interactions of the flow field with the acoustics of Helmholtz resonators were also demonstrated by Selamet[3]. The results of his study are shown in Figure 4 for a zero-flow situation and for two different Mach numbers, i.e. flow velocities.

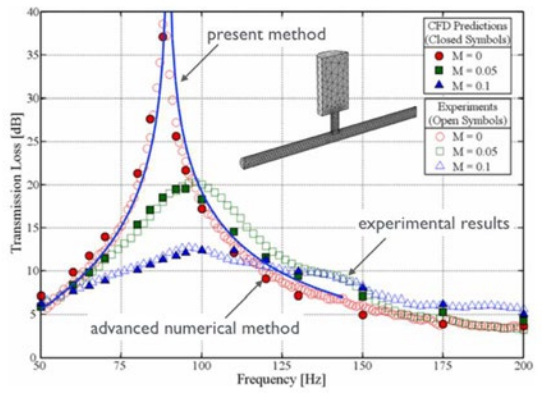

Figure 4 Experimental and predicted results of the effect of grazing flow on the transmission losses[3]; literature results and our result (blue line) for zero flow. M=0.1 corresponds to 34 m/s inflow velocity.

The authors have also investigated a similar approach by using multi-physics software (COMSOL[4]) to analyse the combined effect of flow and acoustics for the PHT configuration for flow velocities of 7.5 and 15 m/s and the results are shown in Figure 5. It is seen that the same effect as investigated by Selamet[3] is calculated but the effect is more pronounced, especially for the higher velocity of 15 m/s in a frequency range between 85 and 150 Hz. One of the explanations could be that the geometries are different: a cylindrical choke versus an elliptic choke in a multi-choke configuration with a single cavity. A further investigation of this effect is explained in detail in section 2.4.

It should be mentioned that the aero acoustic method is not yet a validated design tool. Given the large but uncertain flow effect, the experimental work reveals its actual magnitude, enabling both validation of the tool and explanation of phenomena particular to the design concept.

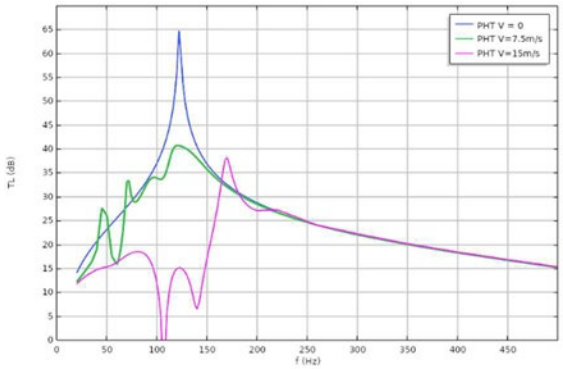

Figure 5 Computed TL for the PHT damper with a static flow of v=7.5 and 15 m/s

2.2 Manufacturing

The toroidal damper hardware is more difficult to commission than a straightforward cylindrical vessel. There was a significant challenge to stay within a low manufacturing budget while simultaneously allowing overpressure and learning something about the manufacturing feasibility of the toroidal concept as well.

The chosen approach of using sheet metal fabrication yielded useful hardware with a not overly detrimental anomaly in the final shape. Figure 6 shows the hub as machined from solid steel. The damper shell was made from pre-shaped sheet metal which only required a final forming step in the centre part. The closing weld to the hub element could not be heavily loaded and the final (hydro-) forming step could therefore not take place. Nevertheless, notwithstanding deviations from the nominal shape, the test hardware was considered to be fit for purpose for the experiments. The volume was measured by weighing with water fill.

by: André Eijk, Javier Fatou Gómez, Olaf Vijlbrief – TNO; Cyril Wentzel – Wentzel Dynamics

Figure 6 Hub detail

2.3 Measurements

2.3.1 Test setup and test method

The TL was measured in the flow/acoustic laboratory of TNO in Delft and the setup as used is shown in Figure 7. The flows and pressures are controlled and kept constant by a flow (FCV) and pressure control (PCV) valve. The flow is delivered by a screw compressor and to ensure a pulsation free inlet flow of the test section, a buffer vessel upstream the flow control valve is installed(not shown in picture). The damper is mounted in the middle section (orange part) and on both sides of the damper an anechoic termination device is placed which acts as a silencer with a very low reflection coefficient.

A speaker is used to generate a pure sine wave. The two-load method has been used which means that the same measurements are carried out at least two times but with different boundary conditions. The results of the two measurements are then combined to extract the transmission loss of the silencer. With this method the influence of the up-and downstream system is eliminated, and the actual isolated performance of the test section can be extracted.

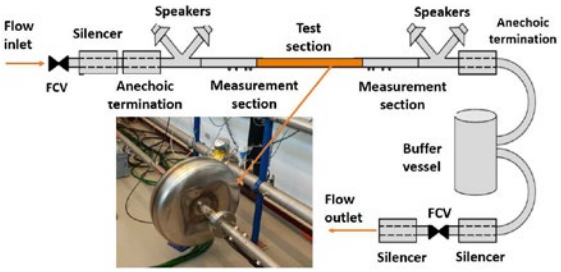

Figure 7 TNO's measurement test rig

2.3.2 Comparison of calculated and measured results

The first measurements have been carried out for the cylindrical and PHT damper for zero-flow and for a mean static flow of 15 m/s, both for atmospheric conditions (1 bara) and for a pressure of 4 bara.

The results for the zero-flow condition at atmospheric pressure is shown in Figure 8. It is clear that the calculated results match the measurements very well for the PHT damper. For the cylindrical damper, the maximum measured TL at approximately 350 Hz is lower than the calculated value and the peak has shifted a bit to a higher frequency.

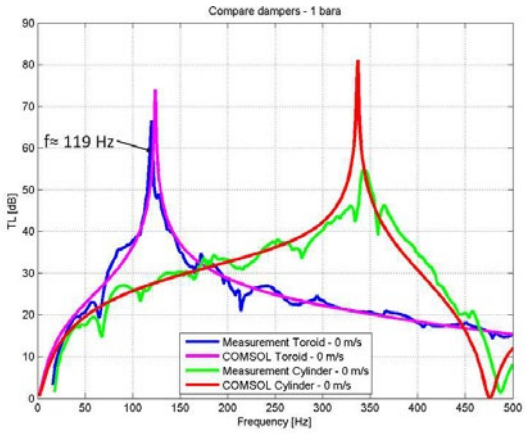

Figure 8 TL for zero-flow conditions for the PHT and cylindrical damper @ 1bara

A comparison of the results for a flow of 15 m/s of the PHT and cylindrical damper is shown in Figure 9. It is seen from Figure 8 and Figure 9 that the TL for the cylindrical damper is hardly reduced with a mean static flow. As compared to the conventional Helmholtz configuration[3], the reduction in TL is much stronger for the PHT damper , especially at 115 Hz and in the frequency range between 57 and 65 Hz. The TL for the PHT is even lower than that of the flow-insensitive cylindrical damper for almost the complete frequency range.

The results for a pressure of 4 bara are not shown in this paper but the measurements showed in general that the TL is reduced for the higher pressure.

Comparison of the *measured* and calculated (shown in Figure 5) results for the PHT for a flow of 15 m/s shows a roughly similar pattern. However, the calculated TL drop is even stronger for a mean static flow velocity of 15 m/s than the measured values in the frequency range between 85 and 150 Hz.

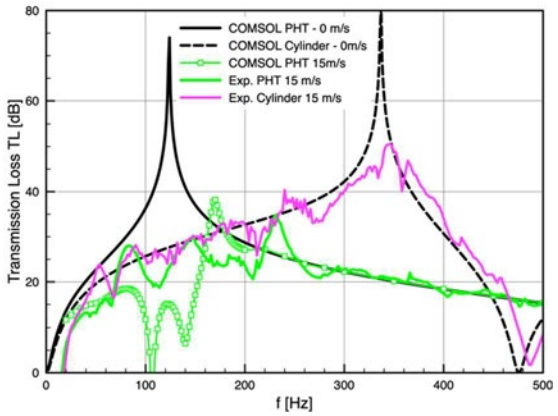

Figure 9 Measured TL for a stationary flow of 15 m/s for the PHT and cylindrical damper (@1 bara)

It was expected that the decrease in TL would depend on the flow velocity, but in a complex manner, so to investigate this relation, additional measurements were carried out for different flows

by: André Eijk, Javier Fatou Gómez, Olaf Vijlbrief – TNO; Cyril Wentzel – Wentzel Dynamics

for a pressure of 1 bara. The results are shown in Figure 10.

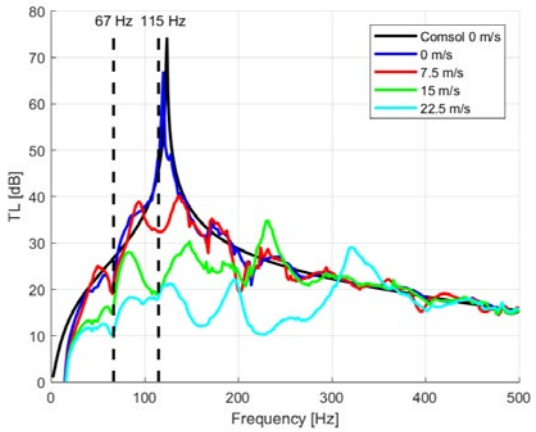

Figure 10 Measured TL for different stationary flows for the PHT damper (@1 bara)

One of the possible causes for the sudden drop in TL for a frequency around 67 Hz and 115 Hz, can be related to grazing flow over the choke of the hub. An example of grazing flow is shown in Figure 11. The side branch, named "choke" in the PHT damper, will cause flow vortices, named Flow Induced Pulsations (FIP's). In general, these very local, unsteady and complex flow phenomena have an effect on the TL. Philips[5] observed that the acoustic resistance of the choke increases linearly with flow velocity. Besides that, Anderson[6] also noted a linear increase in the fundamental resonance frequency of a side branch Helmholtz resonator. Through experiments and semi-empirical predictions, Hersh et al.[7] demonstrated that the Helmholtz resonator exhibits a linear increase in acoustic resistance and a diminishing reactance with grazing flow, leading to a lower TL. Additional detailed CFD calculations and measurements have been carried out to confirm the hypothesis of the drop in TL caused by FIP's in the choke, see for an explanation in the next section.

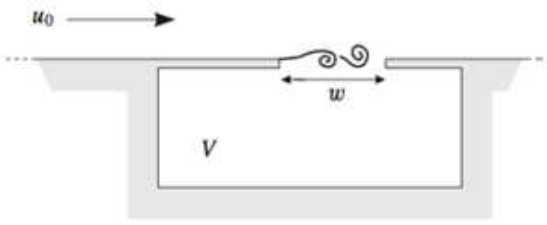

Figure 11 Example of a grazing flow leading to Flow Induced Pulsations (FIP's)

2.4 Detailed investigation to the cause for the drop in PHT performance

2.4.1 Introduction

The combined calculation of the acoustics including the steady state flow field as presented in section 2.1 has predicted a drop in TL performance. This was also confirmed by measurements as shown in Figure 9 and Figure 10.

To understand the cause for the PHT performance drop in TL under flow conditions, and to be able to better answer the feasibility question, the following mutually related questions had to be answered:

- What are the dominant phenomena affecting the TL drop of the PHT?
- How can it be prevented by design under known conditions of velocity and mean static flow?
- What alternative designs, e.g. an Open Throat Toroidal (OTT) damper, may minimize the impact of flow?

One hypothesis was that a Flow Induced Pulsation (FIP) in the choke was one of the possible causes. The investigation to answer these questions, involves additional measurements of the PHT for more flow velocities and a more detailed time domain CFD analysis of the flow in and near the choke.

Moreover, consideration of the effect of the shear flow characteristics as accessible by the aero-acoustic analysis will help explaining the observed behaviour.

In addition, experiments on a new damper with open throat (OTT) would quickly confirm whether indeed the difficulties could be easily circumvented. This latter option seems to be a pragmatic approach to the feasibility assessment.

2.4.2 Detailed Computation Fluid Dynamic (CFD) analysis of the choke-duct geometry

It was assumed that the cause of the lower TL performance at flow conditions is related to a local FIP phenomenon in the choke. For that reason, the model could be restricted to one of the five chokes including a part of the duct and Figure 12 shows the simplified geometry. The mesh consisted in slightly below 2 million grid cells, with hexahedrals in as many regions as possible and tetrahedrals in the rest, performing a T-rex meshing analysis using the Pointwise software. The case study was simulated using a Reynolds-Averaged Navier-Stokes (RANS) $k-\omega$ SST turbulence model, in both steady-state and transient simulations with ANSYS Fluent.

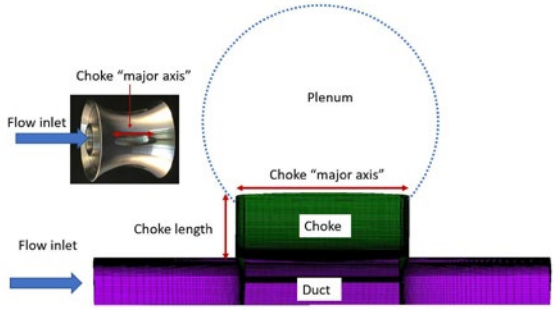

Figure 12 Model for CFD calculations

The first calculation was a steady state situation with a closed choke end. The flow configuration is very similar to the well-known *lid-driven* cavity flow, where a shear layer is formed in the open side of a

by: André Eijk, Javier Fatou Gómez, Olaf Vijlbrief – TNO; Cyril Wentzel – Wentzel Dynamics

cavity due to a flow moving in the horizontal direction.

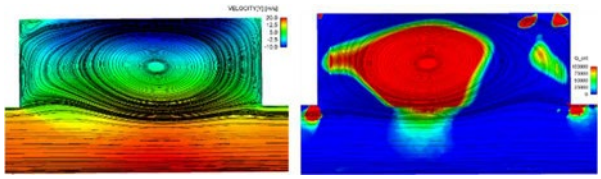

Figure 13 Streamwise velocity and Q-criterion for the steady state case

The left picture of Figure 13 represents the local velocity in the choke. The vortex which is formed in the corner of the transition between the hub (duct) and the choke is shown in this picture. It occupies the cavity and only some small secondary vortex structures can be seen close to the connection with the plenum (left top) and in the corner close to the outflow region of the duct. In the right picture the so-called Q-criterion is shown which represents the local balance between shear strain rate and vorticity magnitude as described by Hunt, *et al*[8] and Jeong *et al*[9]. This criterion can be used to visualise vortex structures, and confirms the analysis made by looking at the streamlines and velocity components in the left picture, with barely any major vortex structures observed.

The second calculation which has been carried out is a transient (time domain) calculation of which the results are shown in Figure 14. This picture shows a snapshot taken at a certain time step. The main vortex varied slightly in location and shape, but not significantly for many other vortex structures to develop, except in the top left corner, with recirculating flow as expected and also shown in the steady state calculation.

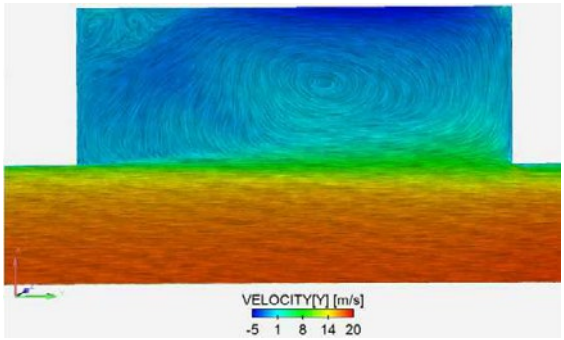

Figure 14 Velocity distribution in the mean flow direction at a certain time step in the choke and duct

Detailed CFD results are very valuable in explaining the root cause of the dynamic flow phenomenon field. Nevertheless, analytical aeroacoustics calculations can provide also qualitative information about what is expected. In this case, using the results as a rough guide for the interpretation of the CFD simulation, analytical calculations were performed and then compared with a frequency analysis of the transient CFD calculations.

The frequency of the vortex at the edge of the choke can be estimated as follows:

$$f_{vortex} = Sr\ \frac{U_0}{D}\ [Hz], (2)$$

with Sr the Strouhal number, U_0 the mean static flow velocity, and D the choke diameter (in this case the major axis of the elliptical shaped choke, see also Figure 12). The calculations show that for a flow velocity of $U_0 = 15\ m/s$, the frequency of the vortex shedding is ≈57-65 Hz.

The vortex frequency is based on a Strouhal number estimated using the velocity profile along the mean flow path of the time domain CFD results to calculate the propagation time due to vortex shedding towards the opposite edge.

These numbers show that for this value of the mean flow velocity of 15 m/s there is potentially a strong interaction between the PHT damper and the vortex shedding near 67 Hz.

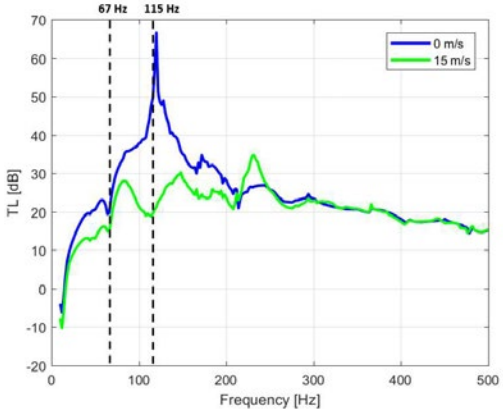

Figure 15 Experimental results of PHT damper for zero-flow and v=15 m/s (@1bara)

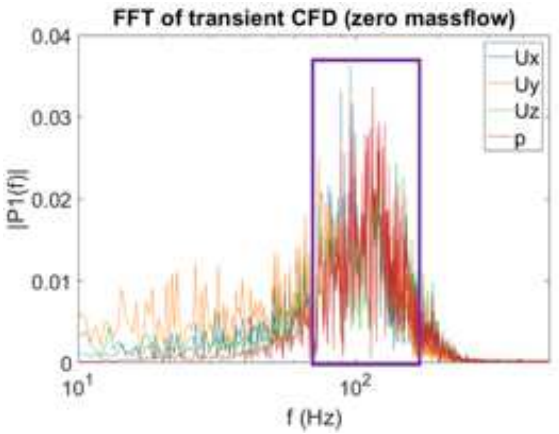

Figure 16 Frequency spectrum CFD analysis (box from 90-120 Hz)

Figure 15 shows the measurement results for zero-flow and for a flow of 15 m/s and Figure 16 shows the FFT analysis of the transient CFD calculation. A clear peak is predicted around 115 Hz for the pressure, and also there is an intense activity in the 90-120 Hz range. This is precisely the interval where the experiments showed a strong degradation of

by: André Eijk, Javier Fatou Gómez, Olaf Vijlbrief – TNO; Cyril Wentzel – Wentzel Dynamics

performance in the transmission loss. The hypothesis is that there are two different and interacting phenomena:

- Vortex shedding with a frequency *dependent* on the mean static flow velocity.
- Acoustic resonance between the choke and plenum around 67 Hz *independent* of the mean static flow velocity (for the case tested).

In the transmission loss curve, two dips are observed. The first one, around 60 Hz, happens for both no-flow and flow conditions, and while it is not entirely clear what its cause is, it seems to be related to the hub-choke geometry. The biggest performance degradation happens around 90-120 Hz for $U_0 = 15\ m/s$, and based on the results of the FFT, it seems to be correlated with the vortex shedding. This last effect causes a larger reduction in Transmission Loss.

In the experimental results, a degradation in performance was seen at multiples of around 60 Hz. In the previous section, it has been shown that the first mode of the vortex shedding could occur at around this frequency for $U_0 = 15\ m/s$. As this frequency scales linearly with the mean static flow velocity and the three original speeds tested in the experiments $U_0 = \{7.5, 15, 22.5\}\ m/s$, these peaks could correspond to the first, second and third harmonic of the vortex shedding.

To test this hypothesis, two additional velocities, $U_0 = \{10, 20\}\ m/s$ were tested and the results (not shown) did indeed confirm the hypothesis.

2.4.3 Explanations based on aero-acoustic analysis

Two complex phenomena are included in the aero-acoustic analysis: sound propagation under velocity gradients and the effects of turbulence. These effects are mainly embedded in a stationary *shear layer* as an approximation to the real flow.

We may compare the results of the aero-acoustic analysis as presented under the design section to the experimental results as shown in figure 5 for the calculations, figure 10. The 7.5 m/s TL as modelled and experimental characteristic around 60 Hz show very corresponding features, but remarkably for zero-flow condition these features seem *also* to be present while being fully *absent* in the computation. Around 120 Hz, the peak in TL level seems to be captured reasonably well, but the frequency of the peaks are shifted.

The 15 m/s computed TL curve does not show the features around 60 Hz at all which is again remarkable. The computed reduction in TL around 120 Hz is so much lower than the experiment that the responsible mechanism is probably overrepresented in the model.

It should at this point be emphasised that comparison of analysis results to experiments should not only include the acoustic performance, but also measurements of the flow field in the choke-duct itself. Both the flow patterns and the turbulence quantities seem indispensable for an adequate assessment of the model.

2.4.4 CFD and aero-acoustic analysis based conclusions

The general conclusions which can be drawn from the detailed choke-duct CFD calculations are:

- Two phenomena are occurring: an acoustical resonance between the choke and plenum *independent of the mean flow velocity* and a vortex shedding *dependent on the flow speed.*
- The Fast Fourier Transform (FFT) of the CFD flow variables shows modes in a frequency range between 90 and 120 Hz range in which also a TL degradation has been measured. It is therefore believed that CFD can thus predict at least qualitative results for different configurations/geometries of a pulsation damper.
- The results of 1) a detailed CFD (stationary and time dependent), 2) aero acoustic calculation, and 3) experiments match reasonably well qualitatively.
- With the current PHT geometry which includes a choke, one of the two phenomena, the acoustical resonance between the choke and plenum, could be partially mitigated by decoupling the effects, but not the other, the vortex shedding itself. Decoupling both effects seems to occur when testing at $U_0 = 10\ m/s$. However, the reduction in transmission loss is still unavoidably present in other frequency ranges corresponding to the different harmonics of the vortex shedding frequency. Results at $U_0 = 20\ m/s$ were less conclusive and would require additional analysis.

3. Open Throat Toroid (OTT) damper

3.1 Introduction

It was shown that the reduction in TL for mean stationary flow conditions is associated with dynamic flow features (FIP's) around the perforated hub.

It is believed that the TL of the PHT damper could be improved by a different geometry of design details, e.g. a larger number of smaller cylindrical chokes.

A damper without discrete chokes could also mitigate higher frequency pulsations, shown by the blue curve in Figure 3. It would not suffer from the intense and turbulent shear layer separating the main flow from the cavity, nor the FIP related phenomena. For that reason, is was investigated whether the adoption of an Open Throat Toroid (OTT) damper, without the hub ('internal parts') would be a good alternative. This concept with simpler in-line single

by: André Eijk, Javier Fatou Gómez, Olaf Vijlbrief – TNO; Cyril Wentzel – Wentzel Dynamics

cavity toroidal design could be the basis for an improved damper, but for pressurisation it requires additional structure which should not interfere with the acoustic performance. Consequently, a generic OTT damper was manufactured and tested without a requirement for pressurisation.

The advantage of the PHT damper is that the frequency of the maximum TL peak can be optimised in an easy way by "tuning" the geometry details of the choke. This is however, more difficult for the OTT damper due to fewer design parameters and the maximum peak for the OTT damper is mainly determined by the volume of the damper, the throat length and diameter. To achieve the TL peak at the same frequency of the PHT, a larger volume would be required. However, for comparison reasons the damper volume is kept roughly the same as for the PHT for this project.

There was also the choice to either apply gentle rounding of the entry and outflow corners or to apply sharp edges. This will affect the flow field especially due to any divergence in the entry flow. Sharp edges were rejected for this stage of the investigation, aiming at velocity reduction in the throat section. The final construction is shown in Figure 17.

Figure 17 Photo of the OTT damper

3.2 Application of the aero-acoustic method

Because of cylinder symmetry, a 2D model calculation is carried out.

The TL as computed for one nominal OTT design is shown in Figure 18 for zero-flow and for a flow velocity of 7.5 m/s and 15 m/s. The curves show that the maximum TL of this OTT is much larger than that of the PHT, especially for the higher frequencies, keeping in mind the shift in frequency of the TL peak for the OTT damper to higher frequencies.

It is further shown that there is a much-reduced influence of the flow velocity relative to the PHT configuration. This is indeed confirmed by measurements as shown in the next section for a similar as-manufactured OTT geometry.

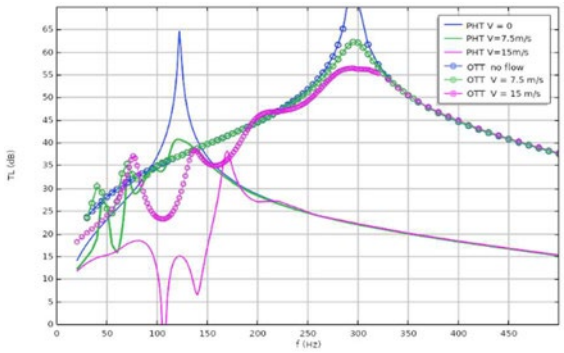

Figure 18 Calculated TL for PHT and nominal OTT damper for zero-flow and for v=7.5 and v=15 m/s

3.3 Measurement results

The as-manufactured OTT damper has somewhat different geometry than the nominal one used in the computation. Only the zero-flow case was recalculated (compare the dashed and dotted curves in Figure 19); the TL curves for this "OTT-1" were measured for the zero-flow condition and for flow velocities of 7.5 m/s, 15 m/s and for a higher flow velocity of 22.5 m/s. From the results, shown in

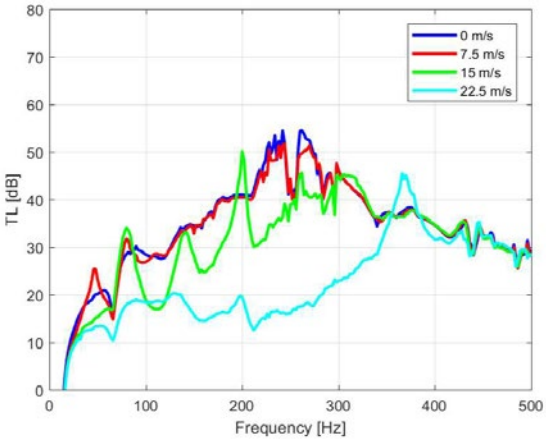

Figure 19, the following observations were made:

- As expected, the TL is in general lower for higher flow velocities.
- According to the results of the acoustic calculations as shown in Figure 18, a peak in TL performance was expected for the zero-flow condition at approximately 250 Hz with a higher value than that of the PHT. However, there is a narrow dip in TL for that specific frequency, for zero-flow and for a flow of 7.5 m/s. This could not be explained yet in this feasibility study and more detailed investigation is necessary to find the cause.
- The TL for the zero-flow condition is approximately the same as for a flow of 7.5 m/s for almost the complete investigated frequency, including the dip for 250 Hz which is also remarkable.
- From all measurements (not shown in this paper), it is shown that the TL for the OTT damper is larger than that of the PHT damper for the higher flow velocities of 15 m/s and 22.5 m/s. However,

by: André Eijk, Javier Fatou Gómez, Olaf Vijlbrief – TNO; Cyril Wentzel – Wentzel Dynamics

the TL of the PHT damper is larger than that of the OTT damper for a frequency range of 82-150 Hz for the low flow velocity of 7.5 m/s.

– The TL of the OTT damper is also larger than that of the cylindrical damper for the largest part of the investigated frequency range for all lower flow velocities except for frequencies between 300-400 Hz for nearly all measured flow velocities.

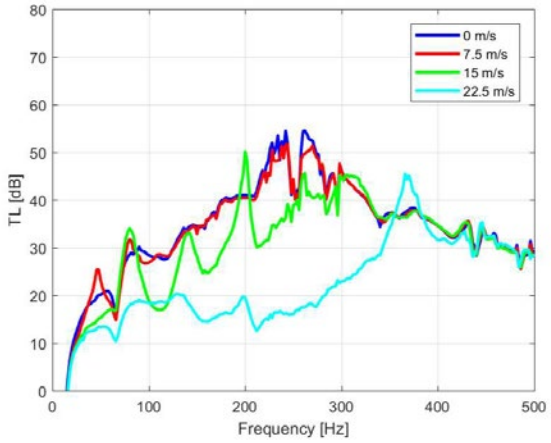

Figure 19 Measured TL for OTT-1 damper for zero-flow and for v=7.5 and v=15 m/s (@1bara)

3.4 Comparison of experimental results to computed results

Whereas significant flow phenomenon effects could be calculated as shown in section 3.2 and Figure 18, it appeared that these effects were much dependent on the type of damper (PHT or OTT). A first step towards validation is obtained by comparing these effects to experimental results.

Figure 20 shows the comparison of the calculated TL for zero-flow for OTT-1 (grey dotted line) with the measurement results. This allows a comparison to the relative features of the OTT flow effect calculation in Figure 18.

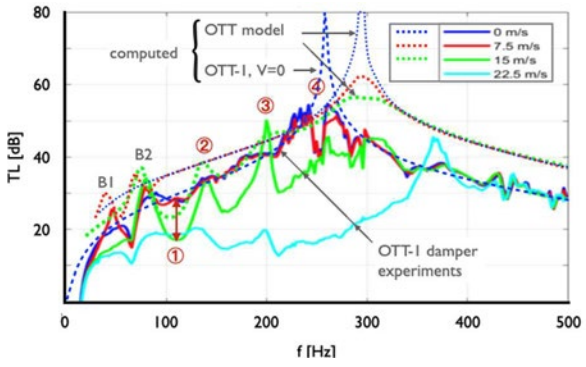

Figure 20 Comparison of experimental to computed results for zero-flow, plus 7.5, 15 and 22.5 m/s (compare to Figure 18); "OTT" should be interpreted as OTT-1 (as-manufactured) geometry.

We can observe the following features, corresponding to the encircled numbers in Figure 20. We see that for zero and low-flow of 7.5 m/s (blue and red curve), the approximation by the models is quite accurate up to a frequency of approximately 240 Hz. For these low-flow velocities, the deviations are similar with two blunt peaks near 50 and 80 Hz, marked with B1 and B2. Only when a certain value of the flow velocity is exceeded, the deviations become more significant, especially between 80 and 200 Hz.
Proceeding from B2 to higher frequencies, the computed peak at (2) (green curve for 15 m/s) has a similar topology and magnitude as well. The peak at (3) also corresponds but is much more pronounced for the 15 m/s experiment.

The general features around the main resonance peak at approximately 260 Hz (4) do correspond on the flanks, but a persistent difference at the peak itself shows a local dip rather than a peak. The difference between the peak and the dip is approximately 40 dB which is extremely large, 40 dB is a factor of 100 in pressure ratio at the inlet and outlet. This feature seems to widen for higher flow velocities.

To the right of the maximum peak, the computation shows no big flow effects, corresponding to the experimental results even for high velocities beyond 400 Hz. There is thus a remarkable agreement between the numerical method and the experiments for the zero and low-flow velocities. However, for higher flow velocities, which are common in reciprocating compressor systems, the differences become larger, especially near the peak of the TL curve.

Not all complex features seem to be captured with the calculations and full explanation is lacking, especially the occurrence of an inverted main peak around 250 Hz. More detailed investigation is necessary to find the root cause.

4 Conclusions and recommendations

Modern day compressor installations pose challenges for pulsation and vibration control. Classical pulsation dampers, with e.g. a cylindrical shape, are extensively used with and without internals to obtain desired Transmission Loss (TL) characteristics throughout the operational range. A trend is the increase of frequencies of interest due to higher compressor speeds and it becomes more challenging to attenuate the pulsations and vibrations for higher frequencies. A feasibility study was carried out for the research group of the EFRC to explore different geometries of pulsation dampers resulting in a higher TL for higher frequencies in comparison with the classical cylindrical damper.

As first novel candidate, the Perforated Toroid Throat (PHT) concept has been investigated because it is easier to optimise this type of damper in

by: André Eijk, Javier Fatou Gómez, Olaf Vijlbrief – TNO; Cyril Wentzel – Wentzel Dynamics

achieving the largest TL for the frequency of interest. Acoustic calculations were carried out for zero-flow conditions and the results from measurements showed excellent agreement. Thus, it was confirmed that the TL of the PHT damper was much higher than that of the cylindrical damper.

The damper was also tested for several mean static flow velocities and it appeared that the damper was very sensitive to flow. This effect was so strong that the high TL values for zero-flow conditions completely vanished and reversed, especially for the higher flow velocities and at the frequency where the peak was calculated. A detailed Computation Fluid Dynamics (CFD) calculation in the time domain showed that a Flow Induced Pulsation (FIP) in the choke was part of the cause of the reduction in TL. Besides that, the mean stationary flow condition was included in advanced aero-acoustic calculations to investigate if this effect could also be predicted. The analysis captured features of the TL curves reasonably well for the zero and low-flow velocities. The sensitivity to flow, together with the necessity to capture the flow field well, implies that detailed (and validated) flow calculations are required in the optimization process of these type of dampers.

As it was shown that the chokes of the PHT damper cause the loss in TL for flow conditions, the flow effect has been investigated for an Open Throat Toroid (OTT) damper concept as well.

The results confirm that the maximum measured TL of the OTT is much larger than that of the PHT, especially for the higher frequencies, keeping in mind the shift in frequency of the peak in TL for the OTT damper to higher frequencies.

It is further shown by aero acoustic computations that a much-reduced influence of the mean static flow velocity for the OTT damper relative to the PHT configuration could be expected. This was also confirmed by measurements. State of the art multi physics methods allow to include the effect of stationary flow in a TL calculation, but this approach is subject to all the difficulties inherent in aerodynamic approximations of reality, such as Reynolds and separation effects. Nevertheless, a remarkable agreement between the numerical method and experiments was found for the zero and low-flow velocities. However, for higher flow velocities, which are common in reciprocating compressor systems, the differences become larger, especially at the peak of the TL. The dip in the peak could not be explained yet during the course of this feasibility project.

Despite that not all complex features seem to be captured with the calculations, for both the PHT and OTT damper, these damper concepts seem to be interesting candidates for mitigating pulsations for higher frequencies in comparison with the classical cylindrical dampers.

Although not investigated yet, the other benefits of a toroid damper would be a more compact construction with less weight and negligible pulsation forces on the pulsation damper, increasing the mechanical integrity of the compressor due to lower mechanical vibrations.

Since flow features determine the pulsation damper effectiveness and design of the toroidal shaped dampers, additional research into the toroidal building block could be directed at details which *affect* flow. Recommendations are given to the EFRC R&D group to be able to achieve accurate prediction and optimization methods for this type of dampers.

5 Acknowledgements

The authors would like to thank the R&D sponsors of the EFRC for their permission to publish the results of this project.

References

[1]API Standard 618 “Reciprocating Compressors for Petroleum, Chemical, and Gas Industry Services”, 5th edition 2007

[2]N. Albers, L. van Lier, M. van der Biezen; “Engineering approach for world’s largest hydrogen compression system”, 11th EFRC conference, September 13 – 14, 2018, Madrid

[3]E. Selamet et al, “Effect of Flow on Helmholtz Resonator Acoustics: A Three-Dimensional Computational Study vs. Experiments”; SAE paper 2011-01-1521

[4]COMSOL version 5.3a

[5]Philips, B, “Effects of high-wave amplitude and mean flow on a Helmholtz resonator,” NASA Technical Memorandum NASA TM X-1582, 1968.

[6]Anderson, J. S., “The effect of an air flow on a single side branch Helmholtz resonator in a circular duct,” Journal of Sound and Vibration, 52(3):423-431, 1977.

[7]Hersh, S., Walker, B., and Bucka, M., “Effect of grazing flow on the acoustic impedance of Helmholtz resonators consisting of single and clustered orifices,” AIAA 11th Fluid and Plasma Dynamics Conference, Seattle, WA, AIAA Paper 78-1124, 1978

[8]Hunt, J., Wray, A., & Moin, P. (1988). Eddies, stream, and convergence zones in turbulent flows. Center for Turbulence Research Report CTR-S88, 193.

[8]J.Jeong, & F.Hussain. (1995). On the identification of a vortex. Journal of Fluid Mechanics, 69-94

Improved plant reliability due to acoustical and vibrational optimisation

by:

Dr.-Ing. Patrick Tetenborg, Dr.-Ing. Johann Lenz
Department Machine Dynamics
KÖTTER Consulting Engineers GmbH & Co. KG
Rheine, Germany
p.tetenborg@koetter-consulting.com

12th EFRC CONFERENCE
August 24 – 26, 2021, Warsaw

Abstract:
Due to their working principle reciprocating compressors can be used in a wide range of operating conditions. This high variability makes it necessary to check the connected piping system for dynamic loads in detail. Critical dynamic loads occur due to oscillating mass forces and high pressure pulsation forces.
Usually these dynamic loads are checked by a theoretical pulsation and structural response study during the engineering phase. These studies protect the plant from critical dynamic material stress. Nevertheless, as a consequence of uncertainties of these studies it is very common that some obvious local vibration hot spots occur during the commissioning. These local hot spots may decrease the reliability of the plant. Thus, the operator does always focus on preventive action against unwanted dynamic loads on several piping sections, plant components or the connected instrumentation.
A well-functioning option for reducing increased dynamic loads is to perform an acoustic and vibration-related optimization of a system. The approach for a measurement based metrological and theoretical investigation is presented in this paper. In addition to the procedure short-term mitigation measures are also described to ensure that the plant runs smoothly.

by: Dr.-Ing. Patrick Tetenborg, Dr.-Ing. Johann Lenz – KÖTTER Consulting Engineers GmbH & Co. KG

1 Introduction

A well working procedure to optimise the vibrational behaviour of a reciprocating compressor plant is described in this article. The optimisation is focused on the piping system and the close environment of the compressor. The procedure consists of several phases. The need for these phases is explained on the basis of the physics that cause critical vibrations and pulsations.

2 Physical principles

Compared to turbomachinery the operation of reciprocating compressors always leads to higher dynamic loads on the system. These loads should be as low as possible to ensure a high reliability and safety standard.

Figure 1 shows the main mechanisms that might cause unwanted dynamic loads. The possible reasons for high vibrations at a compressor system are too high initial forces or amplification mechanisms.

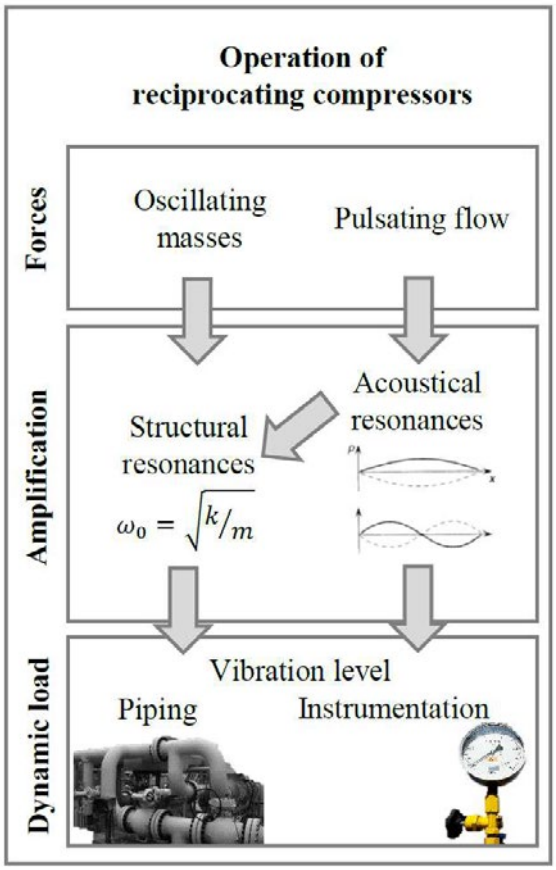

Figure 1: Cause and effect chains for elevated vibrations in reciprocating compressor systems.

Usually it is not possible to mitigate the initial forces of an already running reciprocating compressor. Thus, the more common way to improve the dynamic situation on site is the improvement of possible amplification mechanisms.

To investigate amplification mechanisms in detail, it is helpful to divide them in two different types: acoustical and structural resonances.

Acoustical resonances occur when the discharge frequency of the compressor or multiples match to critical ratios of acoustic lengths inside the piping system and the speed of sound. To control the unsteady flow of a reciprocating compressor pulsation dampeners are used. They are used for a first main attenuation of the pulsation excitation for the connected piping system. Nevertheless, the rest of the attached piping system should not allow further coincidences between the pulsation frequencies and the acoustical natural frequencies.

Beside the acoustics also the structural characteristic of the piping system are designed to handle the dynamic forces due to the remaining pulsation level. Resonance should not occur either for the structural natural frequencies.

At the end both parts need to fulfil the dynamic requirements for an accurate operating behaviour.

3 Optimisation procedure

The operational vibration situation needs to be known and the structural and acoustical amplification mechanisms have to be investigated for an accurate optimisation of the vibrational behaviour. Figure 2 shows the general procedure for this task.

The approach is split in two different parts. In a first step measurement based investigations are carried out.

A modal analysis is done in this step to obtain the structural response characteristic of the plant. Ideally, this investigation is performed during shut down of the plant.

The next steps consist of vibration and pulsation measurements during operation. This is the most important part of the optimisation procedure as the operational dynamic behaviour of the plant is the reference for all further improvement activities.

Beside the metrological investigation numerical studies are employed. Finite Element (FE) models may be used for detailed structural engineering. Due to the fact that all critical structural parts are usually accessible for taking measurements, a mechanical study is often only necessary for complex piping systems. The most relevant part of numerical studies is the pulsation study. It is that important because it is difficult to measure the pulsation distribution along the whole piping. The available measuring locations may therefore not be obvious, since pulsations within a piping system are always influenced by standing waves. However, the

by: Dr.-Ing. Patrick Tetenborg, Dr.-Ing. Johann Lenz – KÖTTER Consulting Engineers GmbH & Co. KG

pulsation study gives a comprehensive overview about the pulsation distribution inside the entire piping system.

After collecting and analysing all relevant information about the system, mitigation measures can be designed. The calculations and design parameters always depend on the measure itself.

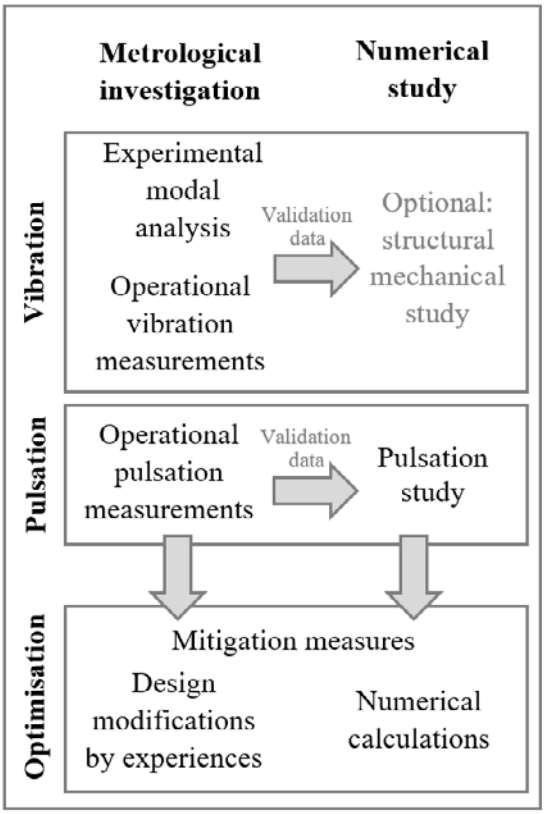

Figure 2: Procedure of a vibrational and acoustical optimisation.

4 Case study

This chapter gives a short overview on an investigated plant and the according reciprocating machinery. Two reciprocating compressors are running in a chemical process and compress gas from about 5 bar up to 65 bar in two stages. Both are four throw compressors with fixed speed and nearly constant operating conditions. A bypass line is included in the piping for rarely needed capacity reduction.

Occasionally cracks at some support structures and leakages at small bore connections occurred. Therefore, the operator wanted to carry out a vibration and acoustic optimization for a compressor in a first step. After successful optimisation the other compressor should be investigated as well.

As a small excerpt of the investigated piping system figure 3 shows the relevant measurement locations. The focused points were located on the first stage suction side. Only one measurement tap for pressure measurements was accessible (p01) in this piping area. Beside many other measurement locations for piping and compressor vibration this article deals with the three locations at two elbows and one T-junction for the bypass-line. The next chapters present the results for the optimisation of this plant section.

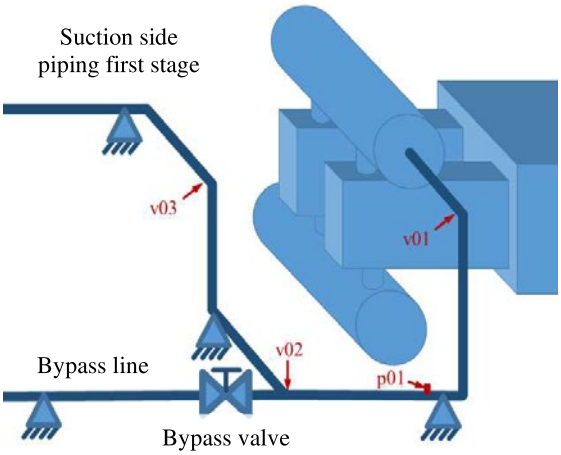

Figure 3: Relevant vibration and pulsation measurement locations on the first stage suction side piping close to the compressor.

4.1 Metrological investigation

This chapter is split in two parts. First of all, the calculation of modal parameters due to metrological investigations is presented. Afterwards, the measurement of the dynamic operational behaviour is explained. Furthermore, the assessment of the data is shown.

4.1.1 Experimental modal analysis

The experimental modal analysis yields comprehensive information on the structural design of the piping system. Usually bump tests during shut down are used for this. A special hammer with a force transducer is used to perform a local impact at the point of interest. By measuring the vibration velocity of the structure the input and also output signals for calculating a harmonic response function have been determined, see figure 4.

by: Dr.-Ing. Patrick Tetenborg, Dr.-Ing. Johann Lenz – KÖTTER Consulting Engineers GmbH & Co. KG

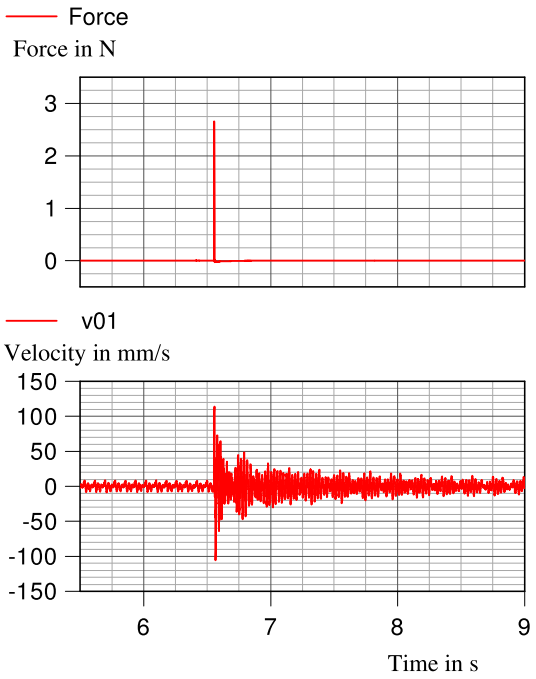

Figure 4: Time signals of force and vibration velocity during bump test.

For piping vibration the so-called "mobility" is used in common. The mobility refers to the sensitivity of a structure described by the vibration velocity on a harmonic excitation force. Thus, this gives a response characteristic quantified in (mm/s)/N.

The mobility of a structure is calculated by mathematical algorithm using spectral transformations of the measurement data. In figure 5 measured and estimated response characteristics are compared for several measurement positions. With neighbouring machines running, disruptive vibrations can interfere with the mobility calculation at some frequencies. Further analytical calculations are necessary to get more detailed information about the structure. The plot of mobility only gives information about the vibration sensitivity. Simplified modelling techniques are used to estimate the modal parameters for each natural frequency.

This tool is based on an optimisation algorithm that calculates modal parameters for the response characteristic close to obvious natural frequencies. The comparison of these analytical models with the measured response curves approves this approach. Even a disturbing operation of a neighboured machine with a permanent excitation of the natural frequency (e. g. at measuring position v03) does not affect the precision of the results. Thus, it is also possible to perform the modal analysis without a shutdown of the plant.

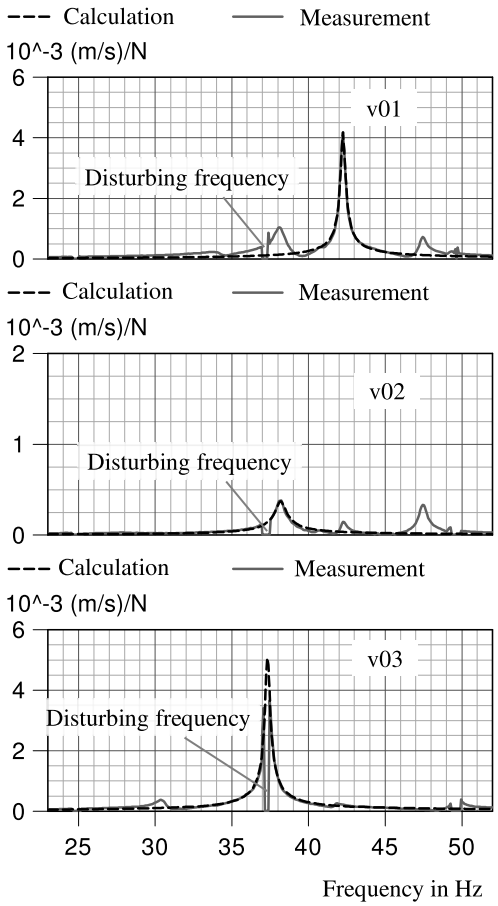

Figure 5: Measured and calculated mobility for several measurement positions.

Finally, the analytical models contain information about the modal parameters: mass m, stiffness k and damping coefficient D, see table 1. It is obvious that the weight of the bypass valve close to measurement location v02 has a massive influence on the modal mass.

Position	v01	v02	v03
f_0	42.2 Hz	38.2 Hz	37.3 Hz
D	0.3 %	0.9 %	0.4 %
m	137 kg	610 kg	105 kg
k	9.6 MN/m	35 MN/m	5.8 MN/m

Table 1: Calculated modal parameters for the obvious natural frequencies.

These data provide the opportunity to tune the numerical structural models in order to minimize the uncertainties due to the boundary conditions.

4.1.2 Operational measurements

Further necessary information for the optimisation is the operational vibration and pulsation behaviour.

The amount of measuring positions differs for every machine type and process. In case of variable

by: Dr.-Ing. Patrick Tetenborg, Dr.-Ing. Johann Lenz – KÖTTER Consulting Engineers GmbH & Co. KG

operating conditions it is recommended to install a large amount of synchronously collecting sensors. In case of nearly constant operating conditions (e. g. fixed speed compressor) it is also possible to collect vibrations and pulsations in sequence.

In this case the present compressor is a fixed speed machine. For correct phase correlations of each measurement location, a keyphasor signal was used. Figure 6 shows a typical data plot of different local pressure signals and the already referred vibration signals related to the keyphasor.

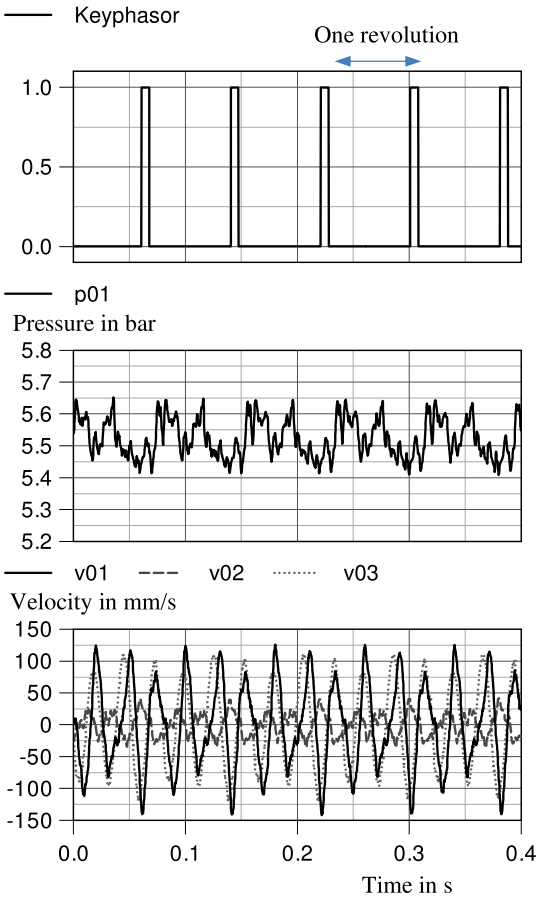

Figure 6: Keyphasor referenced time data of several pulsation and vibration measurement positions.

The whole data needed to be analysed and assessed. For the assessment of compressor vibrations the ISO 20816-8[1)] standard is typically used. The assessment of piping vibrations can also be done using this guideline. Based on our experience it is more comprehensive to perform a frequency dependent assessment of piping vibrations based on the VDI 3842 guideline[2)]. This assessment is based on a spectral analysis and refers the RMS-spectra of measured vibrations to frequency dependent guideline values, see figure 7 for this case study.

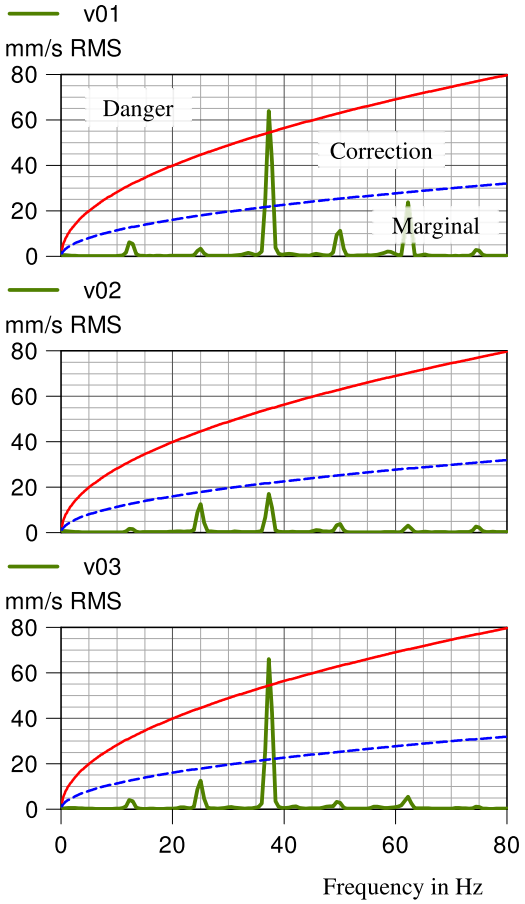

Figure 7: RMS spectra of measured vibrations referring to guideline values of VDI 3842.

For this piping system the vibration level at measuring positions v01 and v03 were within the range “Danger”, which means a mitigation of the vibrations was needed. At measurement position v02 all vibration components were within the range “marginal”. Thus, no further improvement was necessary.

The VDI guideline as well as the API 618 provides recommendations for allowable pressure pulsations as well. Due to the nature of amplified pressure pulsation in pipes an arbitrary measurement location does not match the maximum pulsation level. Nevertheless the measured data can be used to validate the numerical pulsation study.

4.2 Numerical study

Due to the extensive vibration measurements carried out, a structural numerical examination is not carried out in this case.

For the pulsation study, an acoustic one-dimensional model of the compression chamber with the adjacent gas passage, the connected pulsation dampers and the piping system was created. For numerical calculations a finite difference scheme named “Method of Characteristics” was used. The equation setup consists of mass, momentum and energy conservation for a compressible fluid.

by: Dr.-Ing. Patrick Tetenborg, Dr.-Ing. Johann Lenz – KÖTTER Consulting Engineers GmbH & Co. KG

Knowing the measured pulsation situation at position p01, the model was validated to fit the real operation conditions. Figure 8 shows the calculated numerical pulsations in comparison to the measured pulsations.

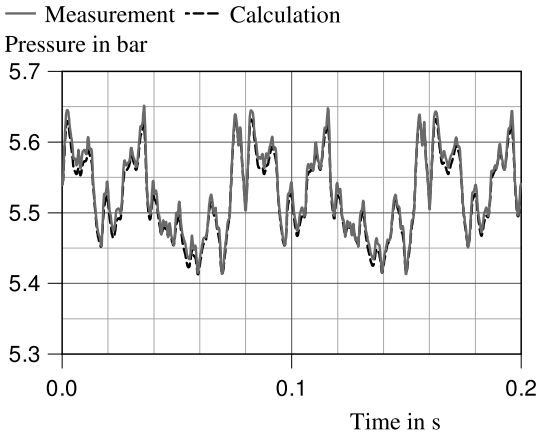

Figure 8: Time signals of measured and numerical calculated pulsations at measurement position p01.

With these well-matched results for the pulsation study, a detailed analysis of the acoustic situation within the pipes was possible. This analysis includes the localisation of the maximum pulsation level for each frequency along the piping. With the information about the piping vibrations, the focus was on the frequency of 37 Hz. In figure 9 the pulsation distribution of the piping section near to the compressor is shown for this frequency.

The local pulsation maxima and according pulsation nodes show that this frequency corresponds to a standing wave. This standing wave perfectly fits to an acoustical resonance inside the pipe section between the pulsation damper flange (acoustical open end) and the closed bypass valve (acoustical closed end). The distribution also shows that the highest pulsations occur close to the two elbows (position v01).

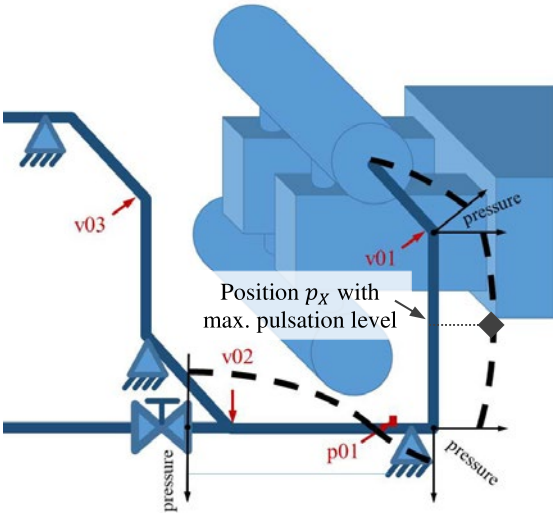

Figure 9: Pulsation distribution along the piping close to the compressor for 37 Hz.

Finally, the pulsation level of every piping section needs to be assessed. Figure 10 shows a comparison of the measured and calculated pulsation amplitudes at measurement position p01 with the relevant guideline value according to VDI 3842 / API 618. For this local position the pulsation situation was not obvious and no further action seemed to be necessary.

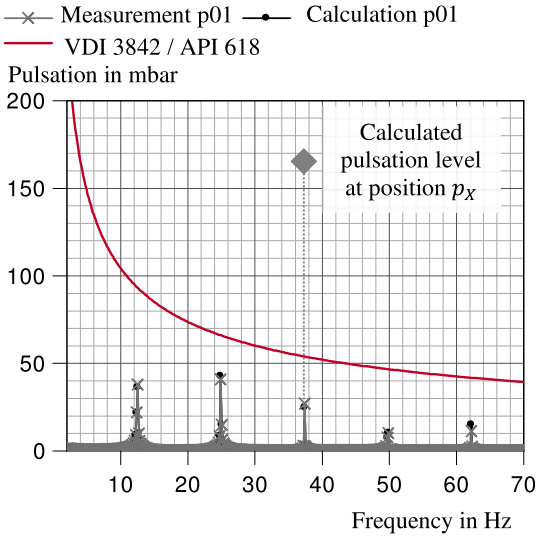

Figure 10: Amplitude spectra of pulsation level refering to guideline values of VDI 3842 / API 618.

Considering the entire pulsation distribution it becomes obvious that this assessment is incorrect. Adding only the maximum pulsation level for the position p_X shows an unacceptable pulsation situation for the suction side piping. The maximum pulsation level at 37 Hz is about 5 times higher than the measured pulsations close to a pulsation node. This example shows that an accurate pulsation assessment has to consider the pulsation distribution along the entire piping.

by: Dr.-Ing. Patrick Tetenborg, Dr.-Ing. Johann Lenz – KÖTTER Consulting Engineers GmbH & Co. KG

4.3 Optimisation measures

The combined metrological and numerical investigation revealed two main reasons for the enhanced vibration situation at measurement positions v01 and v03:

v01: acoustical resonance inside of the piping section close to the compressor

v03: structural resonance of the piping section

Both root causes are typical for reciprocating compressor systems. In figure 11 the installation positions and the measures are shown for the suction side piping system.

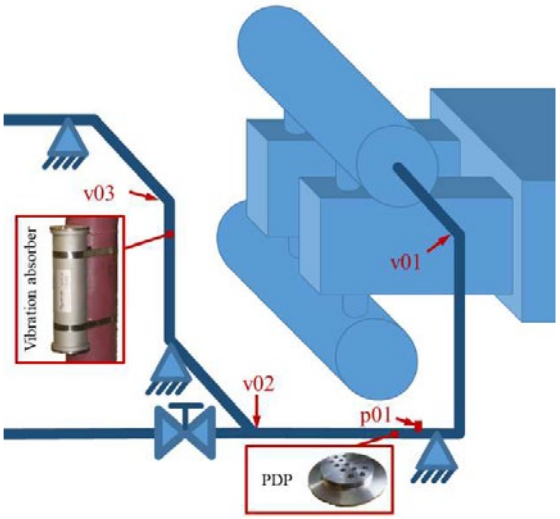

Figure 11: Installation positions of used mitigation measures.

The vibration absorber[4] has been used for eliminating the structural natural frequency. Another option for reducing vibrations was an additional support. This option has been discarded due to the short installation time line of the vibration absorber.

The pulsation reduction was achieved by an additional pulsation-damping-plate[5] (PDP) especially designed for this case. The positioning of a PDP depends on accessible flange connections. In this case a flange close to measurement position p01 was chosen. The installation position fits very well to the acoustic situation because damping plates always need to be installed close to pulsation nodes of an acoustical resonance.

After the short-term implementation of these measures, a control measurement was carried out. The overall vibration level was greatly reduced at both locations v01 and v03, see figure 12.

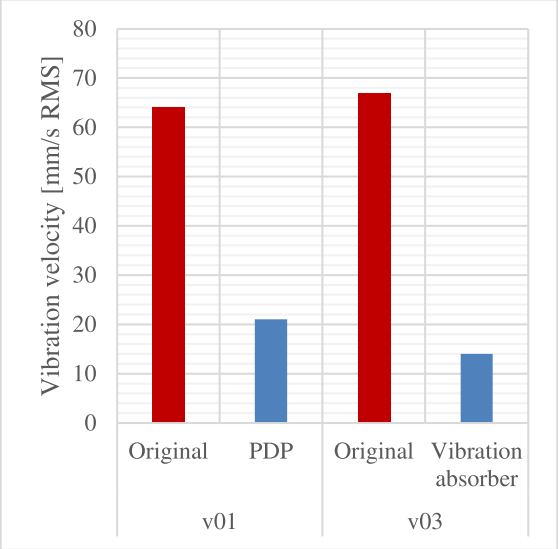

Figure 12: Comparison of vibration level before and after installation of mitigation measures.

5 Conclusion

This case study gives a brief impression of the procedure and expected benefits due to a measurement-based and theoretical optimisation of reciprocating compressor systems. The results show that modal analysis are also possible without shutdown of the investigated compressor system.

This method can be applied to any process including reciprocating compressors. Completed projects confirm the positive effects like higher availability and reduced maintenance effort and costs. Therefore, vibration and acoustic optimisations are becoming more and more relevant for the operator regarding higher efficiency and reliability of newly built and existing systems.

6 References

[1] ISO 20816-8: Mechanical vibration – Evaluation of machine vibration – Part 8: Reciprocating compressor systems. 2018-8.

[2] VDI 3842: Schwingungen in Rohrleitungs-systemen, 2004-06.

[3] API 618: Reciprocating Compressors for Petroleum, Chemical and Gas Industry Services. 5th Edition. 2007-12.

[4] Tetenborg, P. and Lenz, J.: New adjustable vibration absorber – First application on site. 11th EFRC Conference, Madrid, Spain, 2018, pages 180 – 185.

[5] N.N.: Dämpferplatte für den Einbau in Rohrleitungen, Patent Nr. 1953817, 1997.

EUROPEAN FORUM
for RECIPROCATING
COMPRESSORS

SEALING TECHNOLOGY AND EMISSIONS

206

LEADING COMPRESSOR TECHNOLOGY AND SERVICES

www.burckhardtcompression.com

Burckhardt Compression

Burckhardt Compression

Oil-free compression of hydrogen – which role plays the crosshead compressor today and in future?

by:

Thorsten Harder, Norbert Feistel, Felix Ragg
Burckhardt Compression AG
CH-8404 Winterthur, Switzerland
thorsten.harder@burckhardtcompression.com

12th EFRC CONFERENCE
August 24 – 26, 2021, Warsaw

Abstract:
An important application area of crosshead compressors for oil-free compression of hydrogen is found at refineries, where large capacities at pressures between 70 and 100 bar are required for desulphurization of petroleum products. Experience in recent years shows that a service life of up to 16,000 hours is achievable, provided that certain requirements concerning gas purity are met.
In future, oil-free compression of hydrogen with final pressures ranging between 350 bar and 500 bar will be required for storage as well as refuelling vehicles driven by fuel cells. The crosshead compressor competes with alternative concepts here. Which technological approaches are required to meet the high demands placed on dry-running friction systems, and what is the crosshead compressor's competitive ability?

by: Thorsten Harder, Norbert Feistel, Felix Ragg – Burckhardt Compression AG

1 Crosshead compressors for hydrogen compression

For many years, crosshead compressors have proven themselves successfully in a wide variety of applications for compression of hydrogen. At refineries, for example, large amounts of hydrogen are needed to convert hydrocarbons of relatively high molecular weights into low-molecular products by hydrocracking, or to de-sulphurize petroleum products by hydrogenation (hydro-desulfurization). Hydrogen in catalytic hydrocracking processes must have a pressure of 180 to 210 bar, for which purpose lubricated compressors are typically used (Figure 1).

Figure 1: Three-stage compressor for compression of 70,386 Scm/h hydrogen to a final pressure of 154 bara for a refinery application

Hydrogen for desulphurization of petroleum products must have a pressure of approximately 70 to 100 bar. Dry-running hydrogen compressors are also used for this application. Since all compression stages are double-acting, pressure differences of up to 100 bar place a high load on dry-running packings. The expected service life here is at least 8,000 hours, preferably 16,000 hours.

Hydrogen is being increasingly used for energy storage and fuel cells. Applications like power-to-gas and the use of hydrogen in CO_2-free mobility and logistics are examples of this.

Developments in recent years mean that an increasing number of solutions for hydrogen mobility and logistics are available in the market. A range of hydrogen-driven vehicles, such as forklift trucks, buses, trucks and cars, are on offer.

The incompatibility of fuel cells with even lowest quantities of oil forces the use of oil-free compressors, and the requirement for high energy density in the H_2 storage device also makes it necessary to store the hydrogen at high pressure.

The operating pressures of hydrogen tanks are specified at between 350 and 700 bar, according to the desired range per tankful and the space available for the hydrogen tanks.

1.1 Compressor technology applied

So far, it has been possible to satisfy the low level of oil-free high-pressure hydrogen required for re-fuelling and trailer filling in the initial concept studies by using robust hydraulic diaphragm compressors (Figure 2). Each compressor can compress relatively small quantities of hydrogen to high gas pressures and they are designed to operate oil-free.

1.1.1 Diaphragm compressors for small daily quantities of hydrogen

As the quantities of hydrogen required for concept studies are only small and the daily running times of diaphragm compressors are low, this makes a diaphragm compressor the ideal solution for concept studies and for projects in which smaller quantities of hydrogen are being re-fuelled each day.

The growing demand for high-pressure hydrogen for re-fuelling ever-increasing fleets of forklift trucks, trains, trucks and buses from each hydrogen tank means that larger quantities of hydrogen need to be compressed each day at filling station system pressures of between 350 and 500 bar.

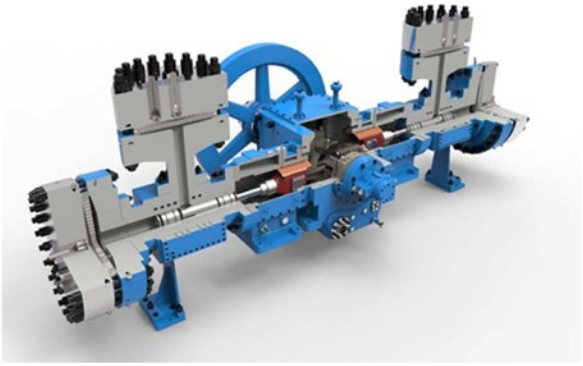

Figure 2: 2-crank dual acting diaphragm compressor

1.1.2 Oil free high-pressure piston compressors for larger daily quantities of hydrogen

As the lenticular geometry of their compression chamber puts diaphragm compressors at a disadvantage in applications with a high-volume flow rate, like trailer filling stations and fuel stations with increasingly higher mass flows compressed preference is given to reciprocating compressors with cylindrical compression chamber geometry. This means that fewer compressors are needed per hydrogen filling station. The development of robust oil-free high-pressure sealing systems with heterogeneous piston ring and packing configurations and the use of high-end ring materials allows crosshead reciprocating compressors to be used for these applications.

by: Thorsten Harder, Norbert Feistel, Felix Ragg – Burckhardt Compression AG

1.1.2.1 CAPEX advantage of reciprocating compressors

The upscaling of the hydrogen volumes to be compressed is not best realized using a diaphragm compressor as the number of diaphragm compressors needing to be installed for this purpose then also increases (e.g. six diaphragm compressors are required for a 4,000 Nm3/h H_2 filling station solution).

The space and investment required can be optimized by using oil-free high-pressure reciprocating hydrogen compressors. For a comparable 4'000-8'000 Nm3/h H_2 filling station compressor system for H_2 Bus depots or H_2 train fleets re-fuelling, e.g. six diaphragm compressors could be replaced by one reciprocating compressor.

1.1.2.2 OPEX advantages of piston compressors

In addition to the reduced space required, reduced complexity and reduced investment, the energy consumption and maintenance costs of the compressor system are also minimized.

1.1.2.3 Efficiency advantage of piston compressors

The approximately 25% lower power consumption achieved by the reciprocating compressor in comparison to a hydraulic diaphragm compressor helps those using this solution to minimize electricity costs.

This reduced power consumption results from the more efficient mechanical coupling of the piston in comparison to the hydraulic coupling of the metal membrane and the improved efficiency at partial load achieved by being able to unload the compressor valves (50% steps) and the use of clearance pockets in the crosshead reciprocating compressor.

1.1.2.4 Maintenance costs advantage of piston compressors

Maintenance costs can be minimized by using high-pressure reciprocating compressors as only one compressor needs to be maintained instead of six. The targeted maintenance interval of 12,000 hours for the reciprocating compressor is considerably higher than the typical maintenance interval for the six diaphragm compressors → 3,000–4,000 hours.

2 Challenges for sealing systems of crosshead compressors

2.1 Stability of sealing efficiency

With its low molecular mass, hydrogen imposes high requirements on the sealing elements of reciprocating compressors. Even small gaps between the sealing surfaces can lead to an unacceptably high leakage, thus necessitating premature replacement of the sealing elements. The challenges posed by oil-free compression of hydrogen are particularly evident in the piston rings' wear behaviour. Progressive loss of material caused by dry-running operation continuously enlarges the joint clearance, thus increasing the leakage flow [1].

As a result, conditions relating to capacity and / or gas temperatures quickly become unacceptable, especially during oil-free compression of hydrogen to high pressures. This can be remedied by known design measures for joint sealing, such as use of an overlapped or gas-tight joint, or a suitable combination of ring segments for a gas-tight element (Figure 3).

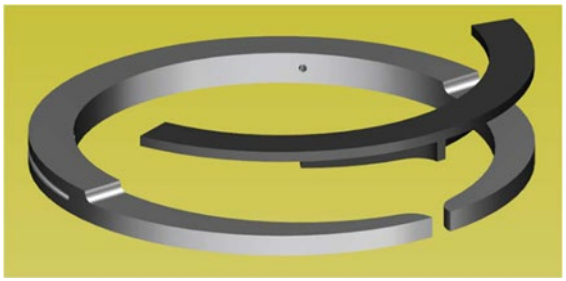

Figure 3: Piston ring with joint seal for dry-running compression of hydrogen

Admittedly, an efficient joint seal significantly improves the sealing effect and maintains it within the scope of feasible wear compensation. However, a disadvantage of such gas-tight designs is their tendency to result in a high concentration of the pressure difference on just a single sealing element at a time. In the case of the sealing elements now mostly made of plastic compounds, this can damage the joint seal to the point of fracture failure of the sealing element, depending on the material properties, the magnitude of the dynamic pressure difference and the geometric dimensions.

2.2 Purity and humidity of hydrogen

Depending on the manufacturing and purifying process, the hydrogen to be compressed might contain significant amounts of gas contamination. Experience in recent years has shown that the resultant consequences for the compressor, whether dry-running or lubricated, are not properly assessed by many operators, so that either no or only insufficient filtration technology is used, often in combination with a bypass around the filter unit.

Any particles entering the compressor have a negative influence, especially for the tribology of the dry-running sealing and rider rings and may even severely damage the counter body surfaces. Often these contaminants are manifested by ochre-coloured deposits of varying intensity inside the cylinder, on the piston as well as the sealing and rider rings (Figure 4, top and centre).

by: Thorsten Harder, Norbert Feistel, Felix Ragg – Burckhardt Compression AG

Figure 4: Ochre-coloured deposits in the compression chamber (top) and on a rider ring (centre), as well as the resultant abrasive wear in a piston ring's friction surface (bottom)

Analyses of the ochre-coloured deposits suggests an involvement of adsorbents for purifying and dehumidifying the hydrogen, as implemented in the widely-used pressure-swing adsorption (PSA) process. Iron-oxide and even aluminium-oxide particles have been found here too. Besides giving rise to abrasive wear in the friction surfaces of the sealing and rider rings, these particles can cause the counter bodies surfaces' roughness required for optimal dry running to drop below the minimum required level, to the point of producing finely polished, shiny surfaces. The inadequate roughness increases the wear rate. Practical experience has shown that the presence of such gas contamination can reduce the sealing and rider rings' service life to about a quarter of the basically possible operating period.

A further consequence of purifying by means of the PSA process is the fact that the hydrogen possessing an atmospheric dew point of -70°C or lower can be described as bone-dry, thus placing particularly high demands on the dry-running friction pairs. This significantly limits the number of usable ring materials.

3 Dry-running sealing systems for high pressures

Despite the challenges posed to sealing systems, practical experience in recent years has shown that considerable operating periods can be achieved. Given compliance with the typically moderate average piston velocities of up to 3.5 m/s for dry-running compressors, up to 16,000 hours of service life are possible for horizontal compressors with a final pressure of 80 to 120 bar. Vertical compressors operating at pressures of about 200 bar achieve at least 8,000 to 12,000 hours with the highly loaded sealing systems. In addition to the enormously important requirement for clean gas, another prerequisite for such operating periods is optimal matching between the ring material and sealing element designs, as well as a suitable combination of different designs for a sealing system.

Especially when choosing ring materials for oil-free compression of hydrogen to pressures of 200 bar, it became clear that high-temperature polymers such as PEEK or PI, which are favoured for strength reasons, do not offer the optimal solution here. Admittedly, they do not tend to creep due to the given load parameters and can therefore be used without anti-extrusion elements. However, their high stiffness quickly results in a formation of gaps and, therefore, undesirable leakage given a typically very uneven removal of material along the ring's or segment's circumference. Instead, polymer blends made of PTFE and PPS have proven to be extremely suitable dry-running materials even in very dry hydrogen. An appropriate mixture ratio supplemented with some inorganic fillers as well as a processing method matched with the plastic mixture hence results in a material with a significantly improved pressure-creep resistance as well as good flexibility compared to conventionally filled PTFE materials [4]. The strength values, which are still lower than PEEK, for example, can be counteracted by means of appropriate design measures, so that the material can be used even at final pressures above 200 bar.

In future, however, oil-free compression of hydrogen to pressures ranging between 370 bar and 500 bar will be required for storage as well as refuelling vehicles driven by fuel cells, for example. This means a further considerable increase in the

by: Thorsten Harder, Norbert Feistel, Felix Ragg – Burckhardt Compression AG

pressure load compared to the previously described applications, something which cannot be managed straight away with the common versions of dry-running friction sealing systems. Further optimization of the sealing systems and their arrangement is required here. In the case of a crosshead compressor, for example, it is advisable to use a step piston for the last two compression stages in order to at least reduce the pressure load for the most greatly burdened packing (Figure 5).

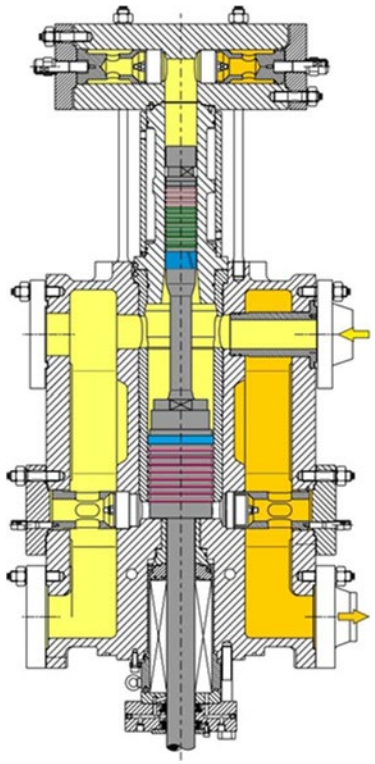

Figure 5: Step-piston version for the last two compression stages to reduce the pressure load on the most greatly burdened packing

3.1 Piston-rod sealing system

Despite the use of a step-piston design for the last two compression stages, pressure differences of up to approximately 150 to 200 bar still result for the packing exposed to the highest load, depending on the compressor design. The indirect heat dissipation via the cooling channels located in the sealing elements' chambers is especially problematic here. An optimized design is therefore used in order to minimize the friction power. Comprising eight radially arranged segments (Figure 6, bottom), this sealing element allows easy application of the pressure relief principle while achieving favourable wear compensation [2]. Up to a static pressure difference of approximately 80 bar, the segments can be realized with the PTFE/PPS polymer blend described above. In combination with the frictionless segment guide which consist of modified PEEK for such loads, a very good sealing effect is also obtained for hydrogen.

In order to avoid failure by fracture due to the dynamic component of pressure difference, the true sealing elements are preceded by several pressure-breaker rings. Very robust and not necessarily very tight designs are typically used for sealing the dynamic pressure varying between the suction and the final pressure [3]. This function is performed by a pressure-breaker element consisting of two endless rings (Figure 6, top). A spring-loaded actuator ring presses the two sealing rings in opposite directions onto the piston rod. One of the two endless rings covers about half the piston rod's circumference at a time [2]. Experience gathered during operation here shows that a sufficient number of these pressure-breaker rings can dependably protect the true sealing rings against a dynamic pressure difference of up to 120 bar. In combination with the previously described friction sealing elements, this results in a heterogeneous piston-rod sealing system which can provide reliable and effective sealing at differential pressures of up to 200 bar for the polymer-blend version (Figure 7).

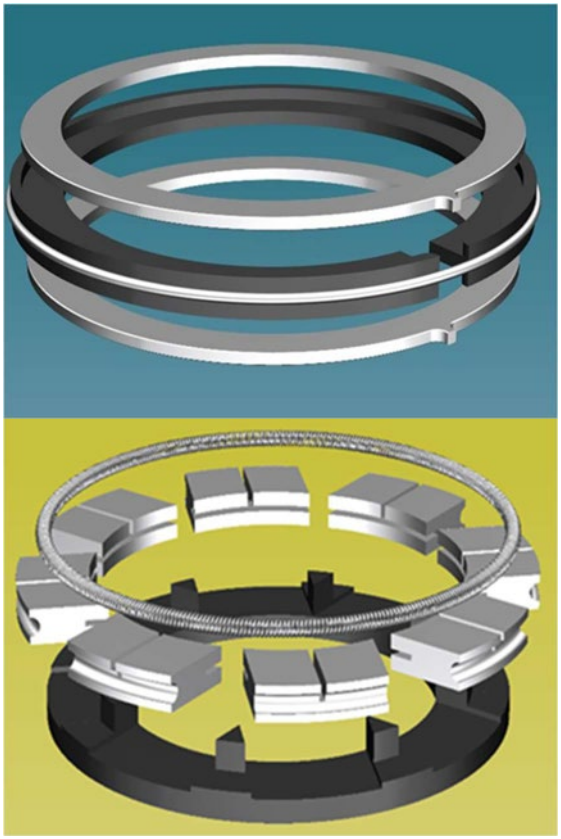

Figure 6: A sealing element consisting of eight pressure-relieved friction segments (bottom) combined with a pressure-breaker ring consisting of two endless sealing rings and an actuator ring (top)

by: Thorsten Harder, Norbert Feistel, Felix Ragg – Burckhardt Compression AG

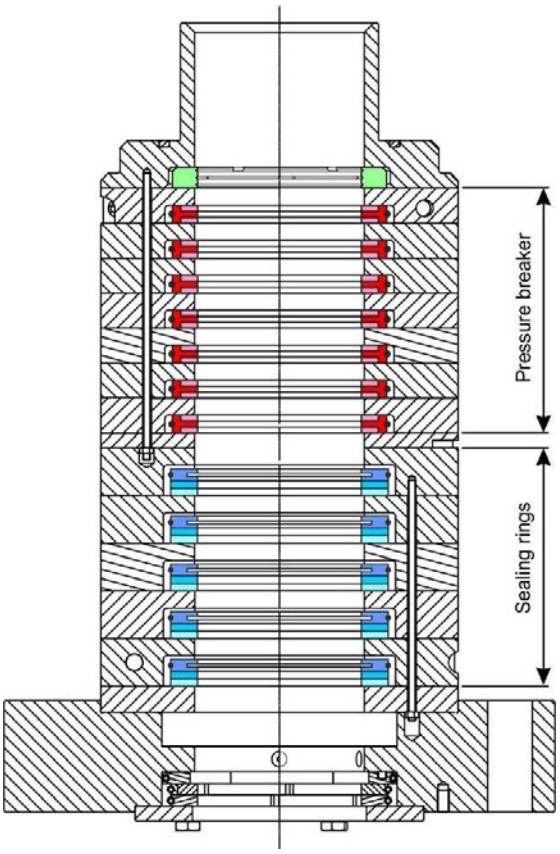

Figure 7: Heterogeneous dry-running piston-rod sealing system for high pressure loads while achieving a good sealing effect

3.2 Piston sealing system

Depending on design, pressure differences of approximately 220 to 290 bar arise for the piston-sealing system exposed to the highest load. Particular attention must be paid to the high dynamic pressure component here. However, the sealing elements must also be specially designed for the static pressure difference which can reach values of up to 120 bar.

A piston ring possessing favourable tribological properties even at very high-pressure differences can be produced by using an endless cover ring on either side of the true sealing ring. The material of the cover rings which operate primarily without friction must exhibit low thermal expansion and sufficient strength, besides having at least minimum dry-running properties. The true friction sealing element in this sandwich-like design can now be realized with an extraordinarily small axial dimension using a three-part, segmented design (Figure 8, bottom), thus minimizing the friction power. A tension spring is used for positioning the sealing surfaces on the cylinder wall and for wear compensation.

Although the armour provided by the two cover rings successfully prevents creep of the sealing-ring material and thus allows high static pressure differences, the gas-tight design also requires protection against high dynamic pressure differences. The pressure-breaker ring used here works on the same principle as that successfully applied in the packing. The main difference here involves an elastically pre-tensioned expander ring which presses the two endless sealing rings in opposite directions against the cylinder wall (Figure 8, top). Materials with sufficient strength, such as modified PEEK or bronze with solid lubricant are used for the endless pressure-breaker rings.

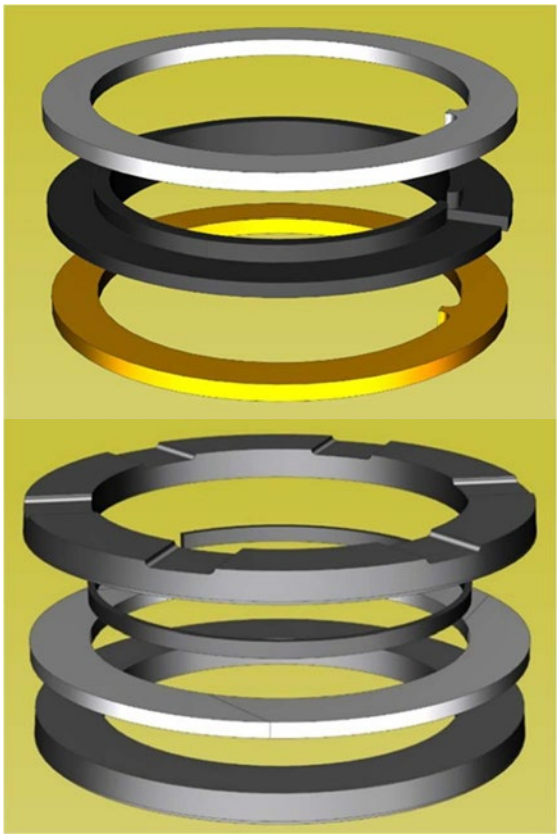

Figure 8: Piston ring with a sandwich layout (bottom) combined with a pressure-breaker ring consisting of two endless sealing rings for use in the cylinder (top)

This version of a pressure-breaker ring, delivering a high performance in the cylinder too, is now arranged in sufficient numbers between the compression chamber and the true sealing rings in a built-up piston. The piston's heterogeneous design and functional separation provide a highly resilient sealing system for dry-running compression of hydrogen to final pressures of theoretically up to 500 bar (Figure 9).

by: Thorsten Harder, Norbert Feistel, Felix Ragg – Burckhardt Compression AG

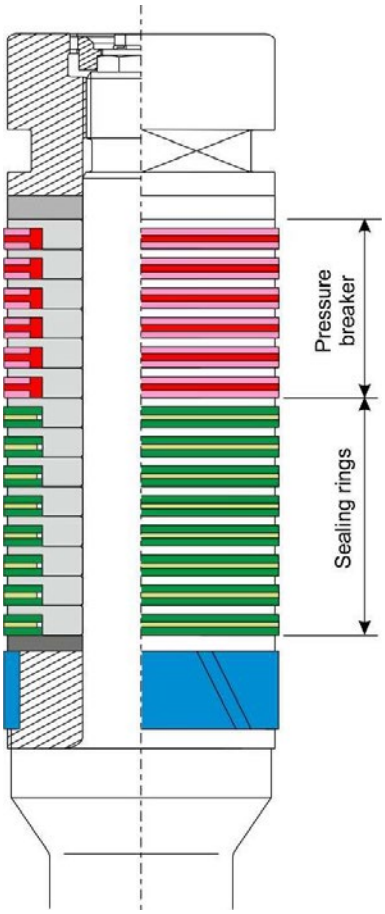

Figure 9: Heterogeneous piston sealing system for high pressure loads

4 Summary

It makes sense to implement different oil-free hydrogen compressor solutions, depending on the quantity of high-pressure hydrogen being refueled each day at the hydrogen trailer filling systems and filling stations.

For small daily quantities of high-pressure hydrogen, diaphragm compressors are the preferred solution.

If high levels of hydrogen are required, it makes sense to optimize CAPEX and OPEX costs by using crosshead reciprocating compressors with robust oil-free high-pressure piston and packing sealing systems.

The hydrogen quality/purity must be carefully taken into account while selecting the technology applied to oil-free high-pressure hydrogen compressor applications.

Notations

PTFE	Polytetrafluorethylene
PPS	Polyphenylensulfide
PEEK	Polyetheretherketone
PI	Polyimide

References

[1] Feistel, N.:
Influence of piston-ring design on the capacity of a dry-running hydrogen compressor
3rd EFRC-Conference, Vienna, Austria, 2003, 141 – 149

[2] Feistel, N.:
Performance improvement of dry-running sealing systems by optimization of wear compensation
9th EFRC-Conference, Vienna, Austria, 2014, 239 - 247

[3] Feistel, N.:
Heterogeneously designed sealing systems based on the Redura principle
COMPRESSORtech2, March 2015, pp. 44 - 48

[4] Olliges-Stadler, I.; Feistel, N.:
Persisto® 850 – a new benchmark in the compression of hydrogen and hydrocarbons
Special technical edition BCAG, 2018

A technological approach to emissions reduction: A case study at a major European refinery

by:

Paul Modern
Cook Compression
Ellesmere Port, United Kingdom
pmodern@doverprecision.com

12th EFRC CONFERENCE
August 24 – 26, 2021, Warsaw

Abstract:
Reciprocating compressor packing cases are a major source of fugitive emissions worldwide. This case study project, conducted at a major EU refinery, demonstrates a technological approach, using multiple complementary packing case and buffer gas control technologies, to reduce packing case emissions to near zero.
The paper establishes how these combined technologies resulted in a significant measured reduction in fugitive and vent flow Hydrogen gas emissions at the refinery site. Vent flow measurement data was obtained both prior to and after the installation of the upgraded designs, to verify the performance upgrade, and is shared in the paper.
The solution was applied to two separate compressors at the refinery site, compressing Hydrogen gas containing trace Hydrogen Sulphide. Discharge pressures ranged up to 200 bar. Gas emissions have a significant cost impact on operations due to loss of gas product to atmosphere, and the cost savings from the emissions reduction are also quantified within the paper.
In addition to the emissions reduction, the applied technologies significantly increased packing case component life and run time, and are included in a cost reduction analysis of the upgrade.
The paper demonstrates the significant benefits, both environmental and monetary, of applying new technologies to upgrade existing reciprocating compressor machinery.

by: Paul Modern – Cook Compression

1 Introduction

Reciprocating compressors are a major source of fugitive gas emissions worldwide. Compressor packing cases are a particular problem area due to the imperfect seal designs in standard rod packings. Rod seals are dynamics seals that must float with rod motion and self-compensate for wear. This makes them a particular design challenge.

While hydrogen (H2) gas emissions are not an issue as far as CO2 equivalency and environmental impact, release of Hydrogen gas within a refinery environment poses fundamental safety issues due to its highly flammable nature and potential to create explosive atmosphere.

At a refining site in Spain, the operator reported issues with detected gas emissions and high vent line flow from two H2 compressors used for hydrocracking duties. The operator had been tasked with improving or eliminating emissions to atmosphere in line with mandated internal policy. Unit 1 was a single stage H2 compressor with two packing cases fitted. Unit 2 was a three stage H2 compressor with a total of five packing cases fitted across all stages.

An on-site investigation was conducted to determine current packing case vent flow rates on the two compressors and establish a baseline against which to quantify potential future improvements. H2 gas monitor (sniffer) readings were obtained for the regions around the cylinder distance pieces. Additionally, a portable thermal mass flow meter was fitted in line with the vent pipework (see figure 1). In this particular facility, vent lines from multiple packing cases were combined into a single header per compressor unit that then flowed to flare. Due to the connections required and the need to keep the machines in production during testing, it was not possible to measure individual flow rates from each packing case. Average vent flow values per compressor unit were therefore the only data possible within the scope of the project.

The portable meter has a maximum scale of 25 standard cubic foot per minute (SCFM) when calibrated for H2 gas. Site measurements showed the combined packing leakage on unit 1 to be 8.89 SCFM. On unit 2, packing leakage measured 8.01 SCFM. Both readings were taken over a two-minute sample flow time.

Figure 1: On-site flow measurement and analysis using a portable thermal mass flow meter

Averaging these total flow values across the number of packings per unit produces the following flow data per packing:

Unit 1: 4.44 SCFM per packing (7.14 Nm^3/hr)

Unit 2: 1.60 SCFM per packing (2.57 Nm^3/hr)

The installed packing cases were older designs using industry-standard radial and tangent cut packing rings and a single vent cup with no purge or buffer fitted. The packings had been in operation for 8 months. In addition to gas being lost down the vent line to flare, significant gas was also being lost to the distance piece, mainly due to the absence of a buffer gas arrangement. It was not possible to accurately measure gas leakage into the distance piece during running. Gas monitor testing in the external area of the distance pieces showed measurable levels of hydrogen gas (low ppm range). For the purposes of cost analysis, we assumed 0.15x the vent flow of H2 gas as escaped gas to the distance piece.

by: Paul Modern – Cook Compression

2. Technology

The refinery site was used as a case study to see how effective a combined technology approach would be in reducing vent gas and fugitive emissions. The buffer gas will mix with the process hydrogen, so measurement at the vent for comparison after the modifications, might show an increase in gas flow. Gas sampling to determine the percentage of H2 lost to vent would therefore become necessary.

Multiple technologies are available to help reduce emissions through a packing case, but they are often applied only individually. In this case, we combined advances in ring technology, low friction buffer technology, and smart purge panel control technology incorporating vent pressure monitoring. While this is not an exhaustive list of available improvements, analysis suggested that this combination would provide a measurable improvement in the leakage rate by addressing both vent leakage and distance piece leakage.

2.1 Improved seal ring technology

Packing case rod ring seals have inherent problems in their most common form[1]. The historic industry standard has been the butt-tangent (BTR) type ring utilising a butt tangent cut ring pared with a radial cut cover ring and a radial cut backup ring (see figure 2).

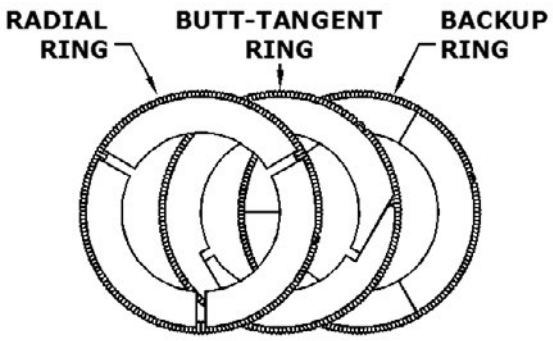

Figure 2: Butt tangent ring set

These rings are still found in a large number of packing cases worldwide. The technology works by breaking down the pressure load over multiple seal rings in the packing case. By definition, this means that each ring allows slight leakage into the adjacent cup; otherwise gas pressure would not show in the downstream packing cup positions (see figure 3).

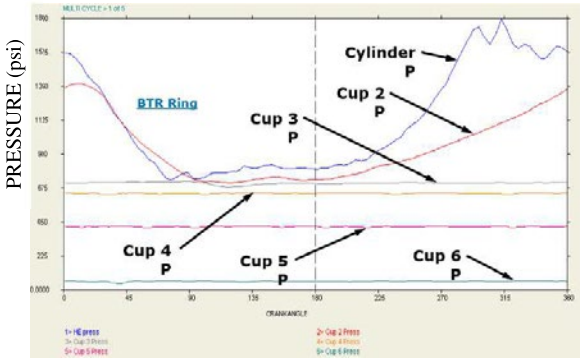

Figure 3: Breakdown of pressure across packing cups using BTR rings

The primary weakness of the BTR design is that the friction load and therefore wear rate is proportional to pressure drop across the ring set[2]. There is no mechanism in the design to offset this effect. Friction loads on the seal rings increase in proportion to the pressure within the cylinder[3].

Replacing the traditional butt-tangent type rings with low-emissions ring technology utilising solid backup rings can significantly improve sealing performance and reduce vent flow leakage. Solid ring technology uses a standard butt-tangent and radial seal pair combined with solid backup rings that have small diametric clearance over the rod (see figure 4). These backup rings are designed to 'collapse' on to the rod at elevated pressure differential and effect a tight gas seal.

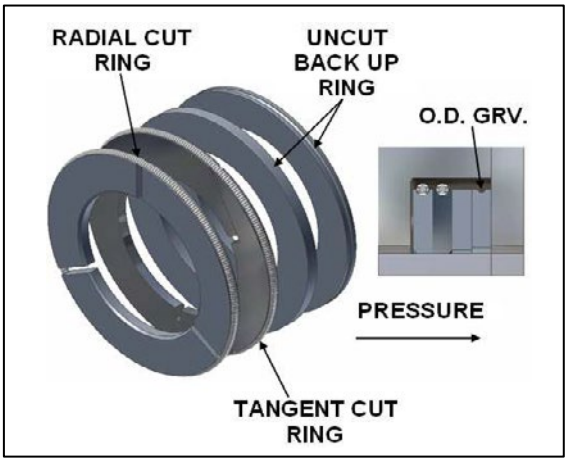

Figure 4: Solid ring BTUU design using two uncut backup rings

by: Paul Modern – Cook Compression

The two backup rings are designed with different materials and geometry in order to energise at different pressure differentials. This keeps the total ring set friction to a minimum by unloading the other rings off the piston rod. The reduced friction helps maintain a low rod temperature and extend packing ring life.

Instrumented packing case trials of solid ring technology have shown that a single ring set seals the majority of the gas pressure across cup number 2 (the first seal ring cup). (See figure 5.) This results in lower overall friction, evidenced by reduced rod temperature (see figure 6), and a significant reduction in leak rate. Since initial testing, the low-emissions ring technology has been proven in many applications worldwide.

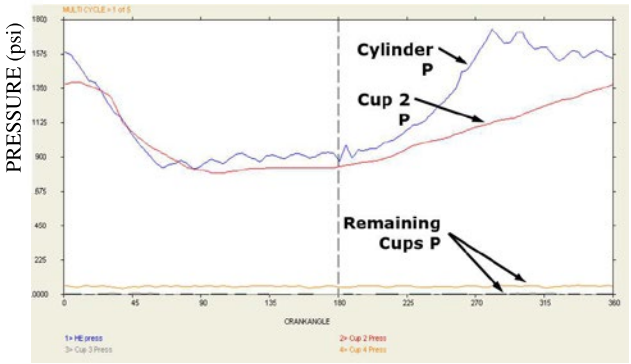

Figure 5: Breakdown of pressure using solid ring technology

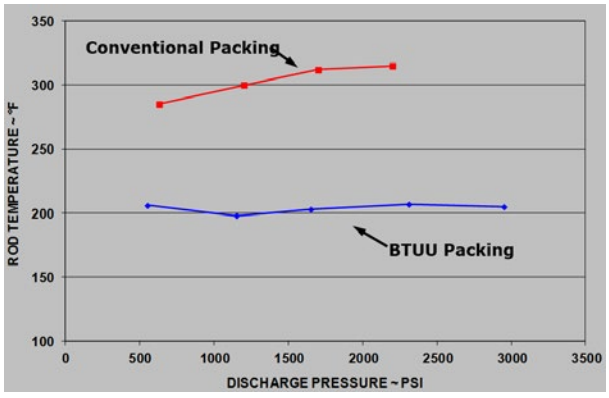

Figure 6: Reduced rod temperature using solid ring technology

For the refinery site in Spain, packing cases utilising solid ring technology were designed for both unit 1 and 2 to improve overall sealing performance. This in turn reduces process gas pressure in the region of the buffer seal rings.

2.2 Improved buffer gas technology

Buffer gas in the form of Nitrogen (N2) or other inert gas has been historically used to create an inert gas pressure barrier[4]. This prevents process gas from escaping the packing case into the distance piece. Creating a sealed chamber at the back end of the packing case with inert gas at a higher pressure than the residual process gas forces any remaining process gas into the vent line. This also compensates for any pressure pulsations resulting from compressor operation.

Traditional designs use multi-direction seal rings to contain the buffer gas in the cup. Wedge ring designs are often employed due to the low gas pressures in this region of the case and the need to side load the rings to achieve a seal on both cup faces (see figure 7). The wedge design forces the ring against adjacent cup faces.

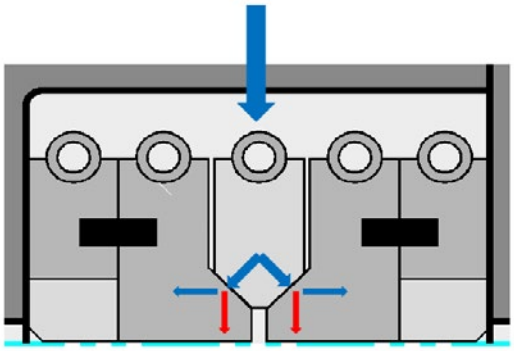

Figure 7: Wedge ring design for buffer chamber, showing the friction forces

Wedge type rings, however, create additional friction due to their strong encircling garter springs. As with any rod rings, friction is undesirable; it increases the rod temperature, which is proven to reduce seal ring efficiency and life.

On units 1 and 2 at the refinery, buffer technology was identified as the most reliable method to eliminate fugitive emissions. To avoid the problems intrinsic to wedge ring designs, the packing cases were fitted with a low-friction buffer design[5] using pressure plates to side load the seal rings in a fully contained assembly (see figure 8). The design creates a tight seal for the buffer gas while maintaining low friction and minimal heat generation.

by: Paul Modern – Cook Compression

Figure 8: Low-friction buffer assembly positioned in a packing case

To complement the buffer design, the upgrade also included a smart buffer gas control panel to monitor vent flow and vent pressure. The panel then adjusts buffer gas pressure based on the readings (see figures 9 and 10). The panel constantly monitors vent line pressure and ensures buffer gas is maintained at 1 bar higher level. That maintains sufficient buffer pressure for effective performance but limits total pressure in the system to minimize friction and therefore preserve the life of the buffer seal rings.

Figure 9: Vent monitoring and buffer gas control panel for compressor unit 1

Figure 10: Vent monitoring and buffer gas control panel for compressor unit 2

The buffer panel also monitors N2 gas usage to each individual packing case, providing an indicator for packing case seal ring condition. By monitoring and recording the N2 gas flow, it is possible to predict packing case life and extend mean time between maintenance.

3. Results

Approximately one month after the packing case upgrade installation, new data was recorded for vent flow rates. The thermal mass flow meter was calibrated for pure H2 gas. It was not possible to calibrate for an unknown mixture, so correction factors would need to be applied afterwards.

The introduction of the buffer gas, creates a mix of H2 process gas and N2 buffer gas into the vent flow. Ultimately, the concern was the leakage rate of the H2 process gas, rather than the inert N2 buffer gas.

To calculate the percentage of H2 in the vent stream, the flow of N2 into the buffer system (available via the buffer gas control panel) was compared with the overall flow at the vent position. Some N2 buffer gas will leak into the distance piece past the final buffer seal. This amount could not be measured. An assumption

by: Paul Modern – Cook Compression

of 70% N2 flow to distance piece and 30% N2 flow into the vent was made to account for this. An offset factor to account for the calibration difference between pure H2 and the known vent gas mixture was then used to determine the actual H2 flow rate at the vent header.

Measurements showed the new total H2 packing leakage on unit 1 to be 1.76 SCFM. On unit 2, the total H2 leakage measured 4.85 SCFM. Both figures adjusted for the percentage of N2 in the vent gas stream.

Averaging these new total flow values across the number of packings fitted to the compressors produces the following flow data per packing:

Unit 1: 0.88 SCFM per packing (1.42 Nm^3/hr), a reduction of 80%

Unit 2: 0.97 SCFM per packing (1.56 Nm^3/hr), a reduction of 39%

We can also now assume that fugitive emissions into the distance piece were reduced to near zero values. Gas sniffer testing provided confirmation, recording zero H2 levels in the vicinity of the packing cases. Note that previously we were obtaining H2 readings outside the distance piece, suggesting significant levels within the distance piece volume.

3.1 Cost analysis

The measured vent flow rate per packing for the original packing case designs was as follows:

Unit 1 = 4.44 SCFM per packing (7.14 Nm^3/hr)

Unit 2 = 1.60 SCFM per packing (2.57 Nm^3/hr)

H2 gas cost is variable and highly dependent on production method. For typical process H2 at the time of the initial investigation, we estimated a cost of ~$2.31/kg. One standard cubic foot of hydrogen is approximately 0.00236 kg. One normal meter cubed (Nm^3) of hydrogen is approximately 0.0899 kg. Using these figures, the cost of H2 vent gas leakage per original packing case can be estimated as follows:

Unit 1: 4.44 SCFM = 2.3 MMSCF*/year = 5,507 kg or $12,722 per packing case vent

Unit 2: 1.60 SCFM = 0.84 MMSCF/year = 1,984 kg or $4,584 per packing case vent

Combining the costs from units 1 and 2, the annual cost of hydrogen lost to vent would be $48,364. This figure does not include fugitive emissions into the distance piece, which were estimated as a further $7,000 loss. That brought the total estimated cost of lost gas to $55,364.

The vent flow rate of the H2 process gas with the upgraded packing case designs measured as follows:

Unit 1: 0.88 SCFM per packing (1.42 Nm^3/hr)

Unit 2: 0.97 SCFM per packing (1.56 Nm^3/hr)

Using the same estimated cost for H2 from the start of the project, the cost of vent leakage with the upgraded cases can be estimated as follows:

Unit 1: 0.88 SCFM = 0.46 MMSCF/year = 1,091 kg or $2,521 per packing case vent

Unit 2: 0.97 SCFM = 0.51 MMSCF/year = 1,203 kg or $2,779 per packing case vent

The combined costs of lost H2 to vent for compressor units 1 and 2 are now $18,937, creating an annual cost savings of $36,427.

In addition, gas released to atmosphere and to vent has already been compressed in the crank end of the cylinder. Therefore driver power was used to compress this gas. We can estimate the cost of the power used to compress wasted gas.

Unit 1: Absorbed power = 560 kW. Overall flow 21.0 MMSCFD* = 7,665 MMSCFY*. Lost gas flow = 2.3 MMSCFY = 0.03%. Total kWh = 4905600/yr. Lost gas flow ~ 1472 kWh ~ $88

Unit 2: Absorbed power = 2052 kW. Overall flow 13.5 MMSCFD = 4,927 MMSCFY. Lost gas flow = 0.84 MMSCFY = 0.017%. Total kWh = 17975520. Lost gas flow ~ 3055 kWh ~ $183

Given the low numbers calculated, we can consider this additional power use to be negligible and the total cost saving remains as approximately $36,000 per annum.

**MMSCFD = millions standard cubic feet per day, MMSCFY = millions standard cubic feet per year.*

by: Paul Modern – Cook Compression

4. Conclusions

A practical approach was used to quantify vent flow leakage on two H2 compressor units using older packing technology. The cost from wasted gas alone justified an upgrade. However, the upgrade had already been mandated internally for safety reasons related to fugitive H2 gas emissions into the distance pieces. The project called for a combined technology approach to reduce H2 fugitive emissions to near zero.

Implementation of upgraded packing case seal ring designs combined with a low-friction buffer design and smart buffer gas control panel successfully reduced fugitive H2 emissions to near zero rates. Vent flow of compressed product was also reduced. This was a significant site safety improvement with the additional benefit of reduced operating costs due to retention of H2 gas product. An annual product saving of more than $36K was demonstrated.

As an added benefit, monitoring of N2 gas usage by the buffer gas control system allows for condition monitoring of individual packing case seal condition, allowing for extended mean times between maintenance.

The technology applied can be directly transferred to other gas types with potential for reduction of fugitive natural gas emissions. This last point has been proven out several times at additional customer sites since the initial trial was completed.

References

[1] Investigation of the operational behaviour of dry-running piston-rod sealing systems in crosshead compressors. Prof. G.Vetter, Dr. N. Feistel, 3rd Conference of the EFRC, Vienna, 2003.

[2] Uncut Ring Technology for Compressor Packing. C.Martin, 8th Conference of the EFRC, Dusseldorf 2012.

[3] Advances in fundamental understanding of the dynamic sealing action in packing systems. Dr. T.Linder-Silwester, 5th Conference of the EFRC, Prague, 2007

[4] API 618, 5th Edition, 2007 – section 6.13.1.6.

[5] Low Friction Buffer Seals for Reciprocating Compressor Rod Packing. C.Martin, 10th Conference of the EFRC, Dusseldorf, 2016.

CPI COMPRESSOR PRODUCTS INTL
an EnPro Industries company

Proven Solutions for the Global Compression Industry™

An Improved Dynamic Rod Packing Seal and Eliminating Vent Emissions with a New Static Seal

by:

Pascal MAHIEUX
Technical Director Europe
Compressor Products International
59750 Feignies, France
pascal.mahieux@CPIcompression.com

Jonathan WHITE
Global Product Manager
Compressor Products International
59750 Feignies, France
jonathan.white@CPIcompression.com

12th EFRC CONFERENCE
August 24 – 26, 2021, Warsaw

Abstract:
Reciprocating compressor rod packing seals available today have their limits in terms of forming an effective seal. As such they are a common contributor to emissions from the main pressure packing case vent line. A new rod packing seal ring design will be presented. It has been developed to provide much improved sealing performance during operation.
Many reciprocating compressor users keep their units pressurized after they are shut down. This practice depends on the individual application, but it is most common in the upstream and midstream Natural Gas industry. This eliminates the need for blowing down the gas to atmosphere and allows the units to be ready for remote starting. Adoption of new government regulations and the reduction in regional emissions limits mean blowing down the compressor has also become a more costly and less permissible option. Traditional rod packing prevents the gas from leaking out of the compressor cylinder under dynamic conditions while it is running. However, this rod packing will leak at a higher rate in static conditions when the compressor is shut down and pressurized. Alternative packing designs have been developed that improve the static sealing performance, but they range in effectiveness and complexity of implementation. A new static packing seal design will also be presented developed specifically to improve the static sealing performance and provide ease of installation and control.

by: Pascal MAHIEUX, Jonathan WHITE – Compressor Products International

1 Introduction

The purpose of a reciprocating compressor pressure packing is to prevent leakage of gas from the cylinder to the distance piece. The packing must operate over a long period of time with little or no leakage and with the minimal amount of friction and wear. At the same time it must compensate for any wear, lateral movement of the piston rod and changes in temperature.

Reported dynamic packing emissions typically range from 0.34 to 8.5 Nm3/h (12 to 300 Scfh) for one compressor rod. In stand-by mode (cylinder pressurized) typically the leakage would be higher than during running conditions[1].

This paper presents two innovative solutions that significantly reduce leakage to the vent during dynamic operation and guarantee zero leakage of process gas to the distance piece in stand-by mode. The presented solutions are safe and economic, whilst helping safeguard the environment.

2 Historic solutions

2.1 Dynamic sealing

The principle of traditional packing is that the three cuts of the step tangent (T) cut ring lie on the axis of an equilateral triangle[2]. The ring is cut so that the segments maintain contact and generate a seal in two locations, firstly with the rod on the inside diameter and secondly at the tangential joints. As wear occurs on the inside diameter, the ring will reduce in size while continuing to seal at both locations. Clearance gaps are required between segments to allow the ring to reduce in size. Since these gaps provide a direct leak path, the step tangent ring cannot form a seal alone. To prevent leakage another, 3 segment radial (R) cut ring, is paired with the step tangent (T) cut ring. The two rings are pegged together to prevent rotation relative to one another, thereby ensuring the gaps do not align to create a leak path (see Fig. 1).

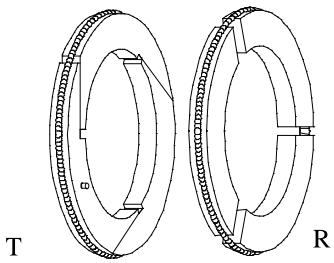

Figure 1: The basic sealing element of a mechanical packing, originally patented by A.W. France in Philadelphia, PA, founder of France Compressor Products in 1898 (which later became CPI)

An alternative to the radial/step tangent pair is the tangent to the rod ring (see Fig. 2). By eliminating the step tangent gap and the resultant stress riser, this ring is suitable for very high pressures. However, the geometry of the tangent to rod cut creates a fine point which may be at risk of damage during installation. It also provides no limit to the amount of wear, increasing the risk of ring extrusion.

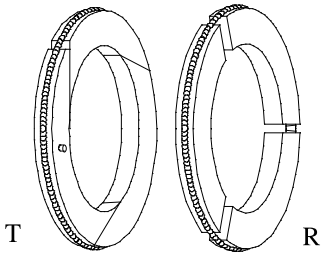

Figure 2: (T) tangent to rod / (R) radial pair element of a mechanical packing

2.2 Limits of traditional dynamic sealing solutions

Traditional radial/tangent seals leak due to their segmental design, this leakage will increase as the rings wear over time.

2.3 Static sealing

Some applications require holding pressurized gas in the compressor cylinders when the compressor is stopped. This cannot be achieved consistently with conventional compressor packings as they are intended to function under dynamic, not static conditions. In such circumstances it is necessary to incorporate a static sealing system within the packing assembly. Typically, this sealing system is activated pneumatically whenever the compressor is stopped, and de-activated when the compressor re-starts (see Fig. 3).

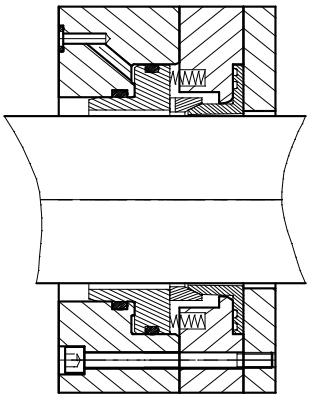

Figure 3: Typical static seal system using piston and lip seal

by: Pascal MAHIEUX, Jonathan WHITE – Compressor Products International

2.4 Limits of traditional static sealing solutions

Static seal systems (see Fig. 3) usually require a very small clearance between the piston rod and the inside diameter of the lip seal. This can lead to premature failure as the rod drops due to wear of the rider ring. It can be difficult to apply this traditional static seal in some applications due to the axial length required within the packing case. While much better than dynamic packing, this solution can leak over time.

3 New dynamic seal solution

3.1 EMISSIONGUARD TR²

The new packing is a patent pending ring design that merges the positive features of a tangent to rod ring with those of a step tangent ring, combining the two rings into one (see Fig. 4). The radial gas load is shared between the inner and outer rings resulting in: improved sealing performance, lower friction, reduced heat generation and longer running life. This design also eliminates the need for a separate radial cut ring, reducing the overall minimum length requirement.

Figure 4: Exploded view of the TR² Ring

3.2 The new packing performance tests

Acknowledging that such packing rings are designed to function dynamically, the initial development was tested under static conditions using helium at the Maestral sealing laboratory in Pierrelatte, France. The testing was undertaken in conjunction with CEA (Commissariat Energie Atomique) and with the CPI sister company Technetics Group. These tests showed the sealing performance to improve by as much as 25% compared to conventional radial/tangent ring pairs.

Further testing was undertaken using the reciprocating test compressor located in our R&D laboratory in Feignies, France (see Fig. 5). Test pressures were up to 60 Bar (870 psi) using both air or nitrogen. Linear speed ranged from 2.47 to 4.40 m/s (8.10 to 14.44 ft/s). The test rod diameter was 50 mm (1.968”).

Figure 5: R&D Test Compressor

Compared to conventional radial/tangent ring pairs, a reduction approaching 50% was observed in the dynamic leakage rate. Figure 6 illustrates test results under the following operating conditions - test gas: air, suction pressure 17 Bar (246 psi), discharge pressure 40 Bar (580 psi) piston speed 2.47m/s (8.10 ft/s).

Note: Flowmeter 0/20 N/m3h (0/706 Scfh) accuracy +/- 2% Full Scale and pressure transmitter 0/40 Bar (0/580 psi) accuracy < 1% Full Scale.

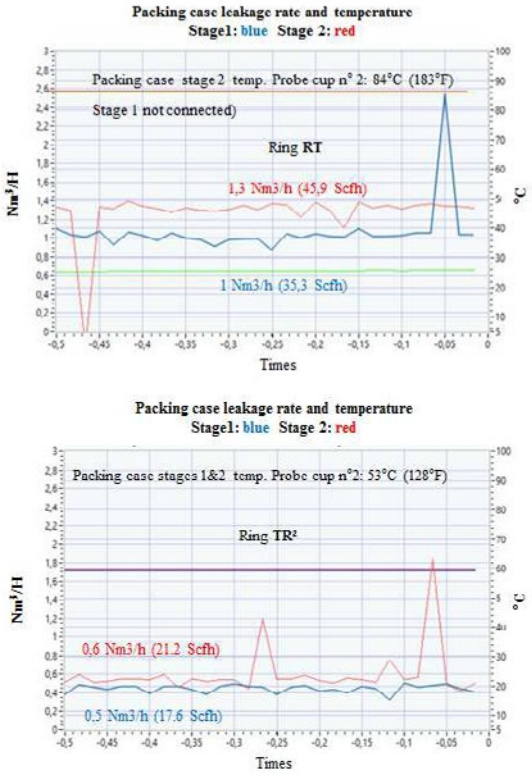

Figure 6: Screenshot from Test Compressor data acquisition software, top graph shows radial/tangent rings, bottom graph shows TR² rings with 50% leakage reduction

by: Pascal MAHIEUX, Jonathan WHITE – Compressor Products International

The improvement in both dynamic and static leakage was also seen to remain consistent throughout various states of wear on the TR² rings.

In addition, the piston rod temperature was seen to reduce by 10°C (50°F) when using TR² rings (see Fig. 7). This was the result of reduced friction due to the gas radial load being shared between the inner and outer ring the new packing.

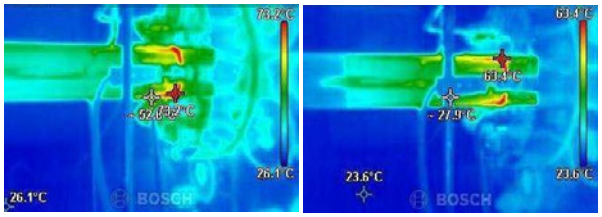

Figure 7: Dynamic piston rod temperatures 73.2°C (163.8°F) with R/T (left side image) vs 63.4°C (146.1°F) with TR² (right side image) measured using an infrared camera

The pressure drop pattern through a piston rod packing is explained in the Theory of Operation article from France Compressor Products/CPI from 1968 (re-released in 2015) (see Fig. 8).

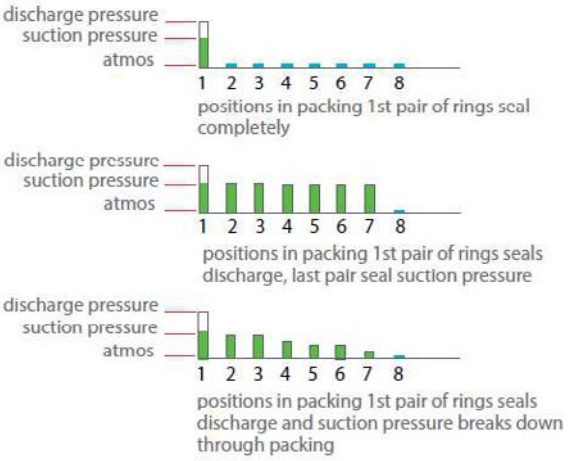

Figure 8: Pressure drop pattern through a packing

The behaviour of reciprocating compressor piston rod packing was tested by DST Raubenheimer, Shell Research limited, Thornton Research Center, UK (1989).

The methodology used by Shell Research was replicated as part of this study, analysing pressures and leak rates after individual cups throughout the packing case[3,4].

This work confirmed our previous theories and tests relating to radial/tangent ring sets. Specifically the suction pressure is sealed by the last pair of rings and the discharge pressure by the first ring pairs.

The TR² rings were seen to behave differently. Both suction and discharge pressure were sealed by the first ring (see Fig. 9).

From these results, it was concluded that the new packing forms a much more efficient seal due to the combination of the two ring styles working together to eliminate the leakage paths that exist around radial/tangent rings.

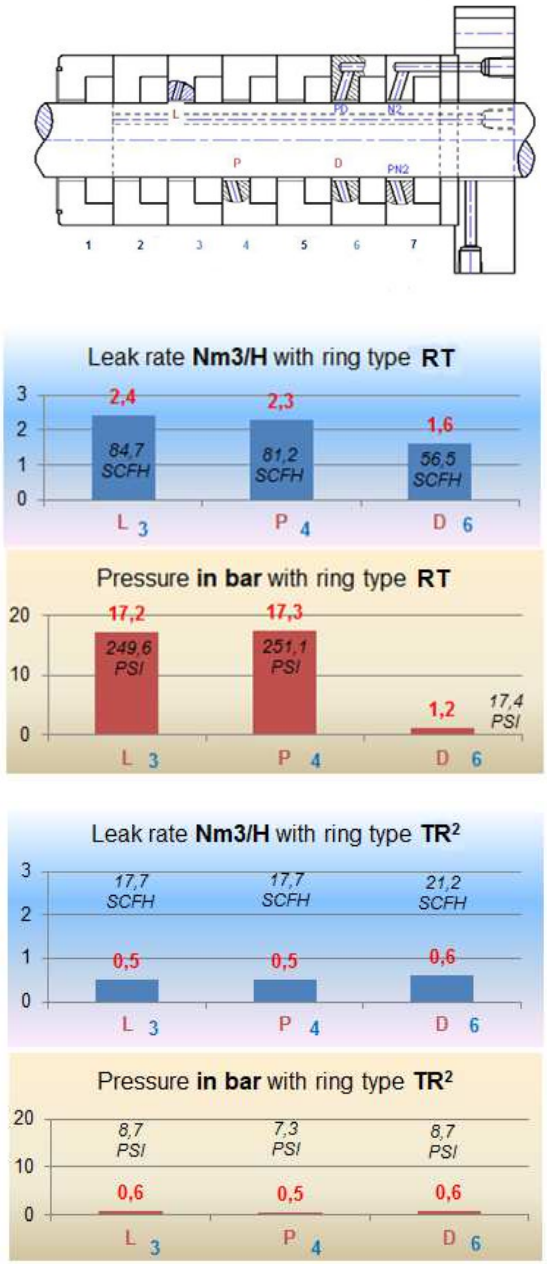

Figure 9: Pressure and leakage test results, top graph shows radial/tangent rings, bottom graph shows TR² rings

3.3 The new packing field performance results

Over the course of 3 years 50 compressors have been equipped with the new packing. These units

by: Pascal MAHIEUX, Jonathan WHITE – Compressor Products International

have demonstrated a significant improvement in sealing performance and also in running life.

Example 1: Natural gas at 60 Bar (870 psi), non-lube, equipped with TR^2 rings in CPI192 material running for more than 3 years with a vent line leak rate of 3 to 4 Nm3/h (106 to 141 Scfh). Baseline vent line leak rate was 6 to 9 Nm3/h (212 to 318 Scfh). A 21°C (70°F) reduction in the piston rod temperature was also observed.

Example 2: Supercritical CO_2 at 80 Bar (1160 psi), non-lube equipped with TR^2 rings in CPI184 material. Increase in the Mean Time Between Failure (MTBF) from 1500 hours with a vent line leakage of more than 20 Nm3/h (706 Scfh) to a running life of more than 4600 hours and a vent line leakage rate measured at 2 Nm3/h (70.6 Scfh).

4 New static seal solution

4.1 EMISSIONGUARD ES^3

The ES^3 Expandable Static Seal is the first static seal designed for both optimum sealing when the compressor is in a stationary condition and maximum reliability during dynamic operation.

The new static seal consists of a stainless steel holder, supporting an elastomer based profiled seal, fitting inside a conventional shaped cup (see Fig. 10).

The new static seal is activated using a pneumatic or hydraulic process through a connection on the flange. This enables a very efficient and reliable seal while the compressor is shut down. When de-activated while the compressor is running it provides a larger working clearance around the piston rod compared to traditional static seals.

The compact design of the new static seal allows it to be installed into the space of an existing packing cup. This eliminates the additional packing length required with historic designs.

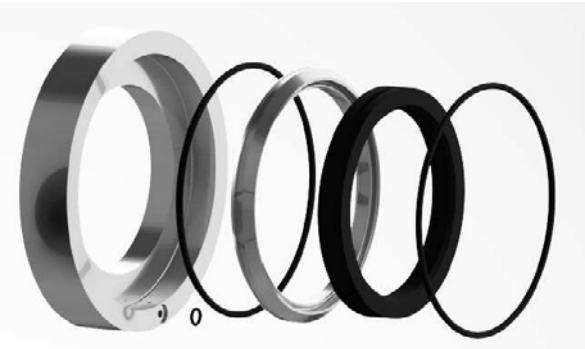

Figure 10: Exploded view of the ES^3 Seal Assembly

4.2 The new static seal development

The development of this patent pending seal was undertaken at the Maestral laboratory in conjunction with CEA and Technetics Group.

The new expandable static seal uses the proven advanced polymer technology of CEFIL'AIR® seals* which are expanded and retracted by a pneumatic or hydraulic process (see Fig. 11).

** CEFIL'AIR® inflatable seals is a registered trademark product of Technetics Group, An EnPro Industries company.*

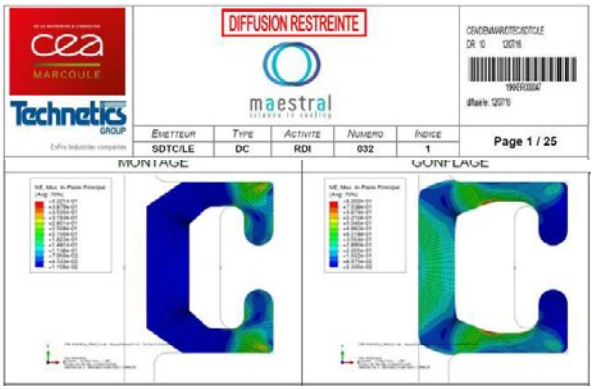

Figure 11: FEA models created as part of the testing conducted by Maestral Laboratory, left side image shows seal in free state, right side image shows seal inflated, to validate seal conformity

4.3 The new static seal performance test

CEFIL'AIR® is well known in the nuclear industry, complying with the very stringent sealing performance requirements. The Maestral laboratory testing was conducted using helium. Results showed an unprecedented level of sealing performance for the compressor industry:-

- 0.0001 Nm3/h (0 Scfh) at 50 Bar (725 psi)
- 0.0004 Nm3/h (0.0035 Scfh) at 70 Bar (1016 psi)

Compared to the typical static seal:

- 0.3 Nm3/h (10.6 Scfh) at 50 Bar (725 psi)
- 2.4 Nm3/h (84.8 Scfh) at 70 Bar (1016 psi)

Further tests were then conducted on our reciprocating test compressor. After stopping the compressor, pressure equalized in the gas closed loop at 18 Bar (261 psi). Bottled nitrogen at a pressure of 20 Bar (290 psi) was used to activate the ES^3 seal (see Fig. 12).

by: Pascal MAHIEUX, Jonathan WHITE – Compressor Products International

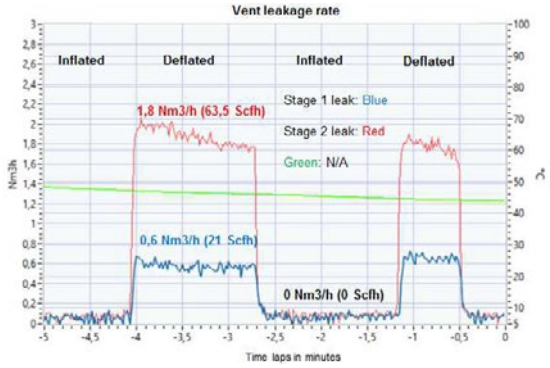

Figure 12: Screenshot from the Test Compressor data acquisition software showing no leakage when ES[3] activated

The measured leak rate out of the packing was zero. This result has proven consistent across numerous test cycles conducted throughout the last 3 years.

The volume of gas required to seal the compressor is very small. There is no nitrogen consumption when the new static seal is activated due to the CEFIL'AIR® being non porous.

The actuating nitrogen pressure required to expand and maintain the seal = cylinder static pressure + 1 Bar.

A delay between dynamic and static phases is required as it is very important to ensure that the ES[3] seal is only activated when the compressor piston rod is fully stopped.

4.4 Field results

Field tests are currently underway. Results to date are positive.

5 Summary

A new packing ring design was developed to incorporate the positive design features of traditional packing, while eliminating some of the negative features. Testing of the new packing proved them to be 50% more efficient than conventional packing rings. Due to their gas load sharing capabilities the rod temperature was reduced leading to increased lifetime. Numerous field applications have proven the new packing ring performance over the last 3 years.

A new Expandable Static Seal was developed to be more efficient, compact and durable compared to the current typical static sealing solutions. This new seal is based on an existing proven inflatable seal used in many critical applications including nuclear and aerospace. Testing of the new static seal has shown zero leakage when the compressor is stopped and pressure is held in the cylinders.

The testing conducted to date has enabled the fine tuning of the mathematical models for predicting the packing case leakage rate, while also confirming the influence of parameters such as; piston speed, gas molecular weight, gas pressure, lube or non-lube, wear, the packing ring design and quantity[5].

We will continue to conduct further tests in the near future.

References

[1] Why monitor and quantify compressor piston rod packing leakage, ACI. (2008)

[2] Mechanical packing. Design and Theory article from France Compressor Products/CPI in 1968 (re-released in 2015)

[3] The behaviour of reciprocating compressor piston rod packing. DST Raubenheimer, Shell Research limited, Thornton Research Center, UK (1989)

[4] Investigation of the operational behaviour of dry-running piston-rod sealing systems in crosshead compressors. Dr. N. Feistel, Burckhardt Compression AG, Switzerland. (2003)

[5] Gas leakage rate estimation on rod packing for reciprocating compressor, CPI, Pascal Mahieux (2007).

STASSKOL

Piston Rod Packing Solutions for Reduced Emissions

by:

Georg Flade & Marc Langela
STASSKOL GmbH
Stassfurt, Germany
Marc.langela@stasskol.de

12th EFRC CONFERENCE
August 24 – 26, 2021, Warsaw

Abstract:
Environmental protection during the actual phase of climate change is a frequent discussed topic in the public. As reciprocating compressors are important operational units at nearly every chemical plant, we also should take a closer look to this piece of equipment. So-called “recips” are quite efficient gas compression machines, but even the best system should be optimized as good as possible. Therefore, in this paper three examples will be presented, how sealing elements can be improved in order to reduce gas losses to a minimum value. These gas saving are important for environmental protection, especially at CNG and biogas applications, where Methane is compressed by reciprocating compressors. Methane plays a significant role in the climatic projections of the IPCC. Therefore, reducing leakages can be considered as an important task and beside this, it can save money and it adds reliability and trust to the reciprocating compressor system.

by: Georg Flade & Marc Langela – STASSKOL GmbH

1 Introduction

The demands on the sealing performance of piston rod seals are constantly increasing. With toxic or explosive gases, any leakage to the atmosphere must be effectively prevented. For this purpose, elaborate sealing and flushing gas systems are designed. Even with less hazardous gases, the requirements become more stringent. On the one hand, leakages can mean losses of expensive process gases, on the other hand, the energy efficiency of the compressor decreases with gas leakages. Another important fact is the impact on global warming of the important energy source methane. This gas is typically compressed in decentralized units that have no seal gas supply. Thus, solutions for reduced gas emissions are also essential in terms of climate protection.

Within the scope of this paper, different approaches for a reduction of external leakage of piston rod seals are discussed.

2 Compressed Natural Gas Solution CNGS

2.1 Sealing Lip Design

A new piston rod packing design was developed, which meets exceptional demands in sealing efficiency. Instead of using sealing ring pairs with gaps like in standard ring designs, sealing lips [1] are applied, which guarantee a higher sealing efficiency. Those sealing lips are made of special PTFE-compounds combining excellent tribological properties, high gas tightness and very good elasticity. The elasticity of the material is used to compensate the wear of the sealing lip which cannot be avoided completely in a dynamic seal. The working principle of the sealing lips is explained in figure 1.

The sealing lips are designed with initial tension. Therefore, those lips have contact to the piston rod even before the gas pressure is applied. The higher the gas pressure, the higher the additional contact forces of the sealing lips resulting in extremely high sealing efficiency. The lips are supported by anti-shear rings and backup rings made of bronze increasing the stability of the lip design which is essential for higher pressures.

Figure 1a: Design of the Sealing Lip

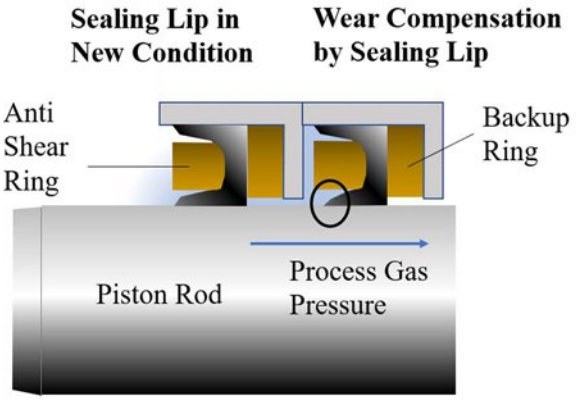

Figure 1b: Working Principle of the Sealing Lip

2.2 Compact Packing Design with Oil Wiper Seal

Due to the excellent sealing performance and gas tightness, in this CNG application no distance pieces are necessary, which are normally used as additional gas barrier to separate process gas from the atmosphere. In applications without distance piece, the oil wiper seal can be integrated in the main packing which allows a more compact compressor design.

Purpose of the oil wiper seal is to keep the oil within the crankcase. The oil which adheres to the moving piston rod is wiped off and flows back towards the crank case. In the CNGS seal, the well-proven balanced oil sealing solution (BOSS) design is applied. By using specially shaped scraping elements made of PTFE- and PEEK-compounds the efficiency of the oil wiper seal is improved. This is necessary especially for higher speeds, where the standard oil scraper made of light metal, bronze or cast iron are not working sufficiently. To further improve the efficiency of the oil wiper seal, an additional pre-scraping lip is installed. Although the whole oil wiper seal installation has shown very good results, it is not possible to make dynamic sealing absolutely oil tight. This especially refers to this compact packing design, were the installation of the main packing and the oil seal are not stroke free. Stroke free means, that the main packing and the oil wiper seal run on separate parts of the piston rod. This allows to prevent the crankcase oil completely from getting into the packing area. Here, the oil wiper seal and the main packing work partly on the same area of the piston rod. This results in a very small amount of crankcase oil getting into the main packing. As this can be tolerated in this special application, those small amounts can be used to mini-lube the sealing lips giving a higher lifetime.

by: Georg Flade & Marc Langela – STASSKOL GmbH

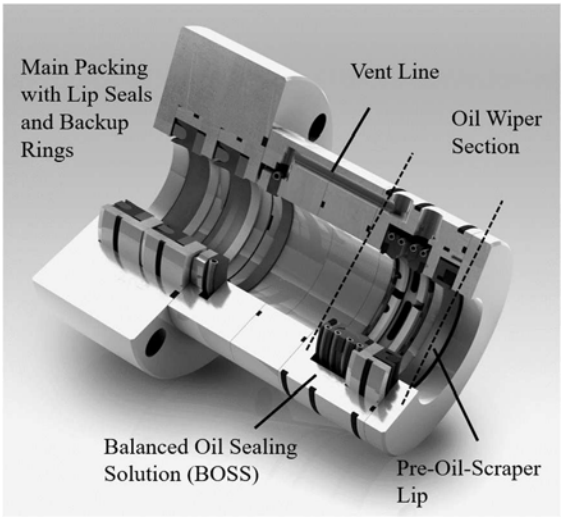

Figure 2: Complete CNGS Packing

2.3 Results in the Field

The packing has been tested on a CNG gas station compressor with end pressure of up to 250 bars. The discharge temperature was up to 155 °C. The compressor speed was 1800 rpm equivalent to 5.5 m/s. If standard ring pairs were applied here, the expected gas leakage would be several standard cubic meters per hour. The leakage of the new developed packing is several liters per hour. After 5300 h service the packings were disassembled, and the internals were inspected. The oil wiper section as well as the leakage sealing ring were in good condition. The edges of the main sealing lips were in excellent condition, but the ring material showed cracks (see figure 3).

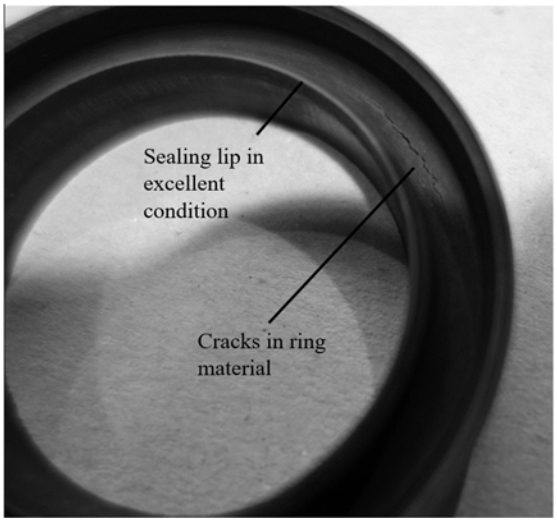

Figure 3: Main Sealing Ring after 5300 h Service

As a corrective measure the material for the sealing rings has been replaced. Now, the modified PTFE compound SK202 is used for those elements. The material SK202 is more flexible than the compound that originally was used. The average service life is 8000h running hours now. Up to now, 170 packings in 85 units have been successfully installed in the field.

3 Enhanced Sealing Performance for Standard Piston Rod Packings

3.1 Gas Tight Ring Solution GTRS

Conventional sealing ring designs have a lot of gaps, which are necessary to compensate the ring material wear [2]. Although those gaps are covered by separate cover rings, it is not possible to get those dynamic systems gastight to a 100 %. Each sealing gap represents a potential leakage path for the gas. Therefore, minimizing the gaps is the most effective way to reduce gas leakage. This design principle has been applied to the newly developed Gas Tight Ring Solution. (GTRS) The sealing ring has only a very small joint gap (ring no. 2 in figure 4), which is sealed by a cover segment. Due to the operating temperature of the seal and the high thermal expansion of the sealing material, the small gap closes completely within a short run-in phase. Thus, the sealing ring is no longer pressed against the piston rod and is therefore not subject to further wear. The very small clearance between the moving piston rod and the sealing ring is optimally covered by the 3-part tangentially cut ring (ring no. 1 in figure 4). In addition to the advantages regarding gas leakage, the design also offers advantages due to low friction as the sealing ring is not pressed against the rod by the gas pressure. This results in a low temperature development.

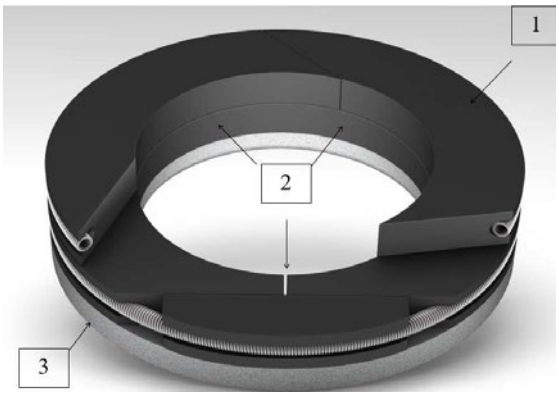

*Figure 4: GTRS-Design with tangentially cut 3-piece design (1), a **single cut** sealing ring with a single cover segment (2) and a backup ring (3)*

However, if this design is dynamically loaded and the rings start to tur, there is a risk that the sealing rings will get wear at the inner diameter. In contrast to ring designs with gaps, any increase in diameter is not compensated here. Therefore, the dynamically loaded inner rings of the packing, which are closer to the changing cylinder pressure, are designed with gaps in standard designs. Only the outer ring towards the vent-line, which seals the static suction pressure against the atmosphere, is made in the GTRS design.

by: Georg Flade & Marc Langela – STASSKOL GmbH

The last sealing element of the piston rod packing is responsible for sealing the static component of the cylinder pressure against the atmosphere, which normally causes high frictional energy as well as high wear. Especially at this position the GTRS system can benefit from the low contact forces, as the sealing ring in this arrangement (ring no. 2 in figure 4) acts like a labyrinth because of the closed gap. This keeps frictional heat at a low level.

The described GTRS-system is completed by a backup-ring to give the system an increased mechanical integrity. The system is used as standard in lubricated applications for discharge pressures above 150bar. It is also proven in dry running applications. For example, the leakage values in the application

- 100% Bone dry Hydrogen
- Discharge pressure 46 bars (g)
- Average temperature 105°C

were reduced by 80%.

3.2 Low Emission Sealing Solution LESS

3.2.1 Introduction Shut Down Seal

As described above, piston rod seals, as sealing systems of moving parts, have unavoidable leakages. In contrast, static seals can be made almost gas tight. However, there are numerous applications for reciprocating compressors in which the machine is not operational 24-7. There are long periods, when the machine is not operating but still under gas pressure. A standard piston rod seal has no diminished leakage when the machine is at a standstill. The leakage during shut down is the same as during normal compressor operation. To use the potential, that machine standstill offers in terms of freedom from leakage, piston rod seals can be combined with a shut-down seal. Typical applications for combining piston rod seals with shut down seals are compressors for natural gas storage or stand-by compressors for essential process gas machines.

3.2.2 Evolution of the Lip Seal Design

The design of a Shut Down Seal is shown in figure 5. The follower (see figure 5) distributes the pressure force of the piston and presses the sealing lip against the piston rod. The piston is activated by gas pressure. The backup ring improves the mechanical stability of the sealing lip. Since the piston rod lowers due to rider ring wear during compressor operation, it is important that the sealing lip with its follower and backup ring are radially flexible. Thus, the system can follow the piston rod.

However, improvements to the system presented were necessary. There have been failures of the shut-down seals. When assessing the failed seals, damaged sealing lips have been found (figure 6).

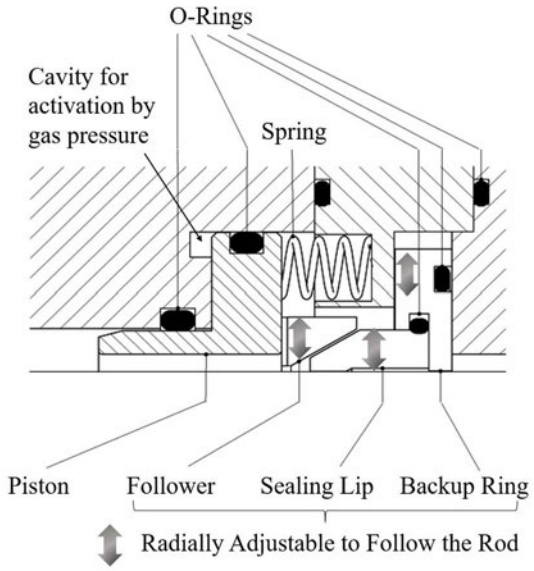

Figure 5: Original Sealing Lip Design

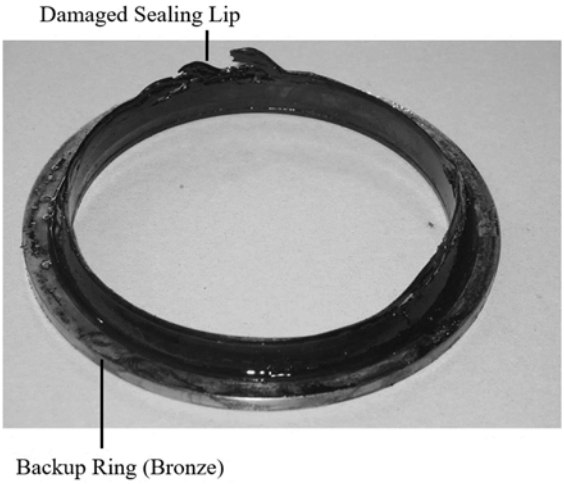

Figure 6: Damaged Sealing Lip

A root cause analysis did reveal that the follower ring was sticking to the sealing lip during the deactivation procedure of the system. The activation of the system is done by applying gas pressure at the cavity behind the piston. This pushes the piston forward into the direction of the sealing lip and moves the follower against the sealing lip to ensure a close contact between the lip and the piston rod. When the piston was deactivated (reducing pressure at the cavity), the follower ring did not follow the movement of piston, leaving the sealing lip under pressure contact with the piston rod. When the compressor was started again, the stationary lip was then destroyed by the moving rod.

As a result of the design review, the follower ring was coupled mechanically to the piston. This ensures that the piston is safely pulling the follower off the sealing lip, when the seal is deactivated. The backup ring has been reinforced to make the system suitable

by: Georg Flade & Marc Langela – STASSKOL GmbH

for higher pressures. The proven design of the LESS shut down seal is shown in figure 7.

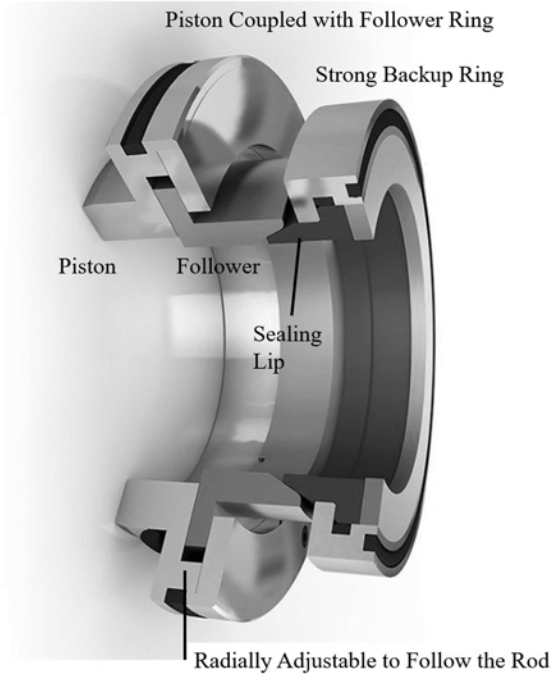

Figure 7: Updated Design of Shut-Down Seal LESS

3.2.2 Integration of the LESS in the Compressor Unit and Materials

Due to experimental results at the In-House Testbed, the activation pressure at the cavity behind the piston of the LESS shut down seal should be at least half the suction pressure of the compressor stage to ensure proper sealing. In the range of very low suction pressure, the minimum activation pressure is 3 bar. The maximum activation pressure is 50 bar for this specific design. The process gas can thus be used in a wide range to activate the shutdown seal. Diagram 1 shows the permissible range of the activation pressure.

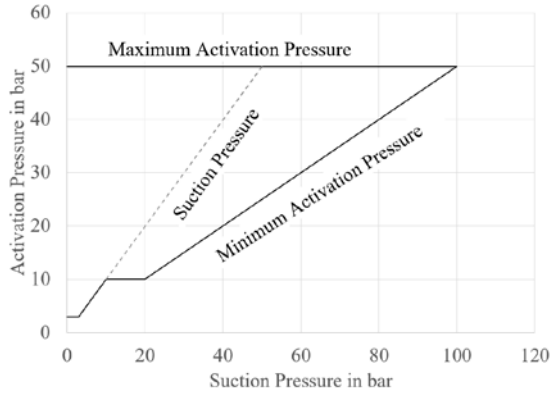

Diagram 1: Permissible Range of Activation Pressure

In order to limit the necessary activation pressure, the systems are often designed in such a way that in the case of multi-stage compressors the cylinders of the upper compressor stages are relieved to suction pressure of the 1st stage. Figure 8 shows such an exemplary P&I diagram of a two-stage compressor system.

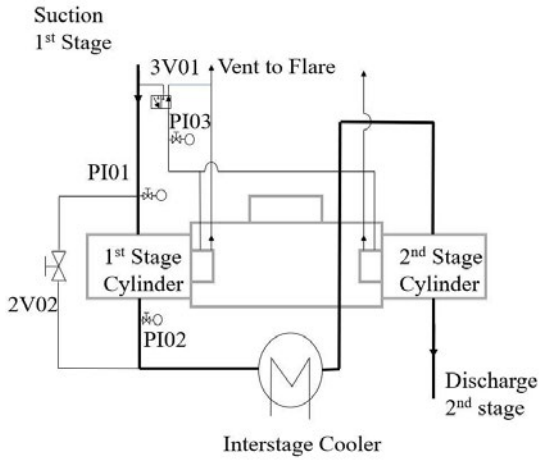

Figure 8: P&I for a 2 Stage Compressor

When selecting the material for the sealing lip, a high elongation at break is particularly important so that the sealing lip can withstand the frequent elastic deformations during activation and deactivation. In addition, sufficient mechanical stability is required to withstand the stress due to the gas pressure. The tribological properties, on the other hand, are less important since the contacting sealing surfaces are not moving against each other. Depending on the pressure range, various PTFE-based compounds are used which best meet these requirements. The follower and the backup ring are made of bronze whereas all parts without potential rod contact can be made of stainless steel.

3.2.2 Potential of Savings

The saving potential of the shutdown seals depends on the pressure range of the machine, the machine size (piston rod diameter and number of axes) and the molecular weight of the sealed gas. The decisive factor, however, is the downtime during which the compressor remains filled with process gas. The tables 1 and 2 show the saving potential for two exemplary cases.

Application	**Underground Gas Storage**	
Rod Size	140	mm
Number of Axis	5	-
Suction Pressure	70	bar
Leakage per Axis	8	Scm/h
Leakage for Compressor	40	Scm/h
% Operational time	45%	-
Standstill time	4818	h/year
Leakage	192720	Scm/year
Gas Costs	0,09	€/Scm
Savings per year	**17.344,80 €**	**per year**

Table 1: Yearly Savings for a big Underground Gas storage Compressor

by: Georg Flade & Marc Langela – STASSKOL GmbH

Application	Biogas Plant (Standard Crankcase, not Pressurized)	
Rod Size	55	mm
Number of Axis	2	-
Suction Pressure	10	bar
Leakage per Axis	2,5	Scm/h
Leakage for Compressor	5	Scm/h
% Operational time	95%	-
Standstill time	438	h/year
Leakage	2190	Scm/year
Gas Costs	0,09	€/Scm
Savings per year	**197,10 €**	**per year**

Table 2: Yearly Savings for a small Compressor on a Biogas Plant. (Not Equipped with Gastight Crankcase)

While the savings potential in natural gas storage is very high, only small savings can be expected for small compressors with little downtime under gas pressure. Therefore, it should always be assessed on a case-by-case basis, whether the investment in the shutdown seals and the associated equipment makes sense.

4 Summary

In this paper it was shown, how measures can be taken to reduce gas leakages of reciprocating compressors to a minimum value. Possible solutions are special designs of piston rod packings, special ring designs with small gaps as well as systems for static sealing when the compressor is at stand-by.

Some of these measures can be used effectively nearly at every compressor application but others must be designed to the process of the end user.

However, reducing gas losses means not only saving money during production. It improves general perception of reciprocating compressor systems and it's a good and necessary step for reducing emissions, especially for Methane applications.

Literature

[1] Peppiatt N.A. (2013) Reciprocating Lip Seals. In: Wang Q.J., Chung YW. (eds) Encyclopedia of Tribology. Springer, Boston, MA

[2] Feistel N. (2014) Performance Improvement of Dry-Running Sealing Systems by Optimization of Wear Compensation In: EFRC Proceedings, EFRC Conference, Vienna, Austria

Your Source For Gas Compression Information

Learn More At
gascompressionmagazine.com

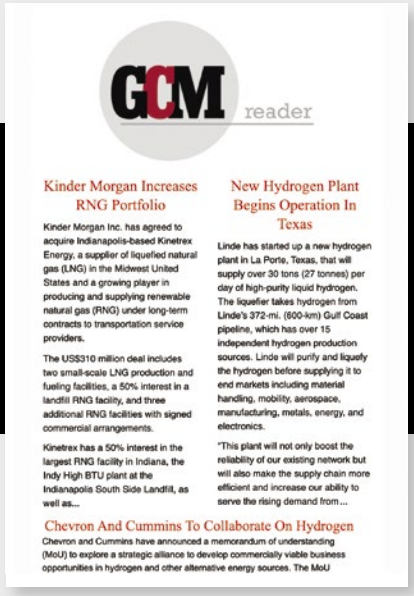

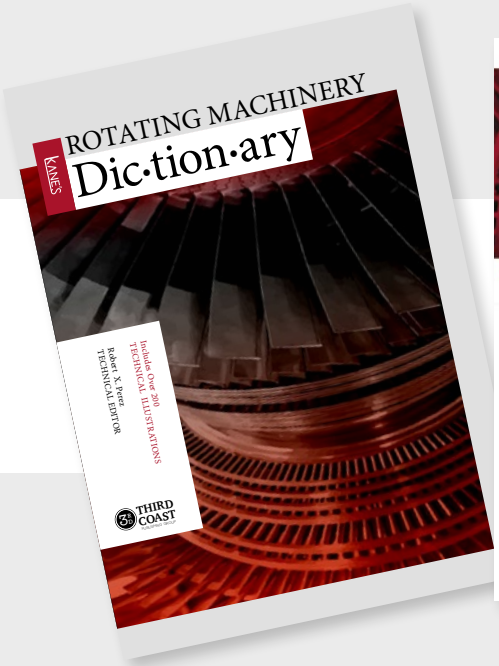

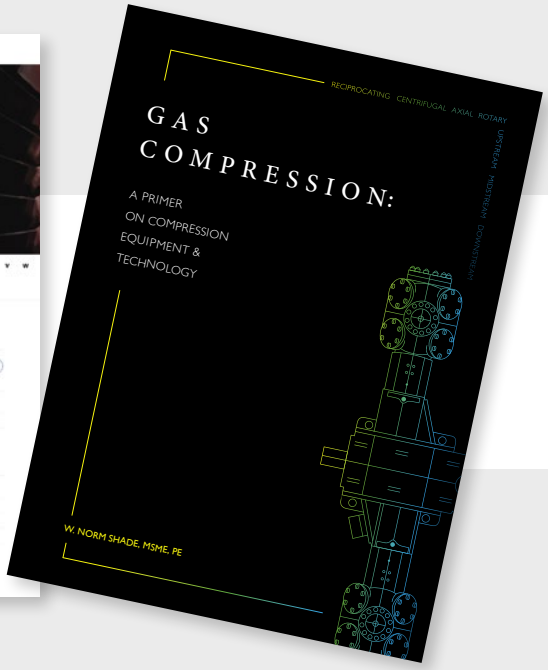

kanesdictionary.com

A comprehensive cylinder-lubrication model for reciprocating compressors

by:

Bernhard Fritz
TU Wien, Institute of Fluid Mechanics and Heat Transfer (E322)
Vienna, Austria
bernhard.fritz@hoerbiger.com

Bernhard Schleichl
TU Wien, Institute of Fluid Mechanics and Heat Transfer (E322)
Vienna, Austria
bernhard.scheichl@tuwien.ac.at

12th EFRC CONFERENCE
August 24 – 26, 2021, Warsaw

Abstract:
Cylinder lubrication is common practice in the compressor industry to significantly reduce wear and friction of the rider and piston rings. Whereas "starved" lubrication shortens the lifetime of these rings, over-lubrication adds little benefit while potentially giving rise to additional problems regarding the downstream components due to oil carryover.

Given the substantial lack of viable alternatives, it is state-of-the-art to lube compressors according to basic empirical guidelines. These disregard system-specific parameters such as clearance, piston assembly, oil viscosity, etc. and provide no guidance for an optimal lube strategy (e.g. with respect to the timing of lube injection).

This work provides a detailed look into the hydrodynamic lubrication of the rider and piston rings on an entirely rational, physical basis. Also, it sheds light on what constitutes an optimal lube strategy – something that is almost impossible to pursue by purely experimental means. Thus, a comprehensive simulation model has been developed that accounts for the mutual interactions between the oil film, the compressed gas, the piston and rider rings, the piston motion, the elastic deflection of the piston rod, and the crosshead dynamics. This model for the first time enables a detailed insight into the specific conditions of cylinder lubrication and opens a window of opportunity for a more reliable compressor operation, hence at reduced lube rates and thus maintenance costs.

by: Bernhard Fritz, Bernhard Schleichl – TU Wien, Institute of Fluid Mechanics and Heat Transfer (E322)

1 Introduction

Cylinder lubrication is a key factor in the reliable operation of reciprocating compressors with minimal downtime for maintenance: It reduces friction between rings and cylinder wall and hence extends ring lifetimes. Due to lack of alternatives, it is state-of-the-art in the compressor business to estimate optimal lube rates on the basis of quite basic empirical design formulas and charts. While over-lubrication reinforces problems with valves and components downstream of the cylinder, it is widely accepted because it avoids sudden and critical downtime due to excessive wear as a result of under-lubrication.

These empirical formulas define a lube quantity per unit time based on the total swept cylinder surface area, which in turn depends on the stroke, mean piston velocity, bore diameter, and an empirical factor which accounts for the gas type, ring material, etc. However, they do not account for system-specific parameters like clearance, piston assembly (mass, ring configuration, ring profile etc.) and oil viscosity, and give no guidance for an optimal lube strategy. A sophisticated lube strategy would take into account not only compressor-specific parameters but also the timing of oil injection, which in turn defines the position of the lube ports relatively to the piston assembly. All lube oil will finally leave the cylinder. Therefore, in steady state, the amount of lube oil supplied equals the oil consumption.

The objective of this work is to substantially deepen our insight into the mechanisms that induce oil loss from reciprocating piston compressors. This will lead to better and more precise lubrication guidelines to promote reliable and economic compressor operation – something that is almost impossible to achieve by purely experimental means. The resulting lubrication strategy should minimize the risk of oil-film rupture, while minimizing the total lube rate. Film rupture would lead to a physical contact between ring and cylinder wall, which would result in increased ring wear.

A comprehensive model has been developed that accounts for the mutual interactions between the oil film, the compressed gas, the piston rings and rider rings, the piston motion, the bending of the piston rod and the crosshead motion. It should help to specify both the best amount of oil supplied and the best timing for oil injection. The present work surveys and extends the original investigations [1].

2 Approach

Let us recall the primary task of the oil film: reducing friction. Friction between the moving surfaces is significantly reduced as long as the surface roughness R_p is smaller than the gap $h = h(x, \phi, t)$ between ring and cylinder wall, where x represents the axial direction and ϕ the azimuthal position. Hence, we need to take a close look at the ring regions to estimate how much oil it takes to ensure a certain minimum gap.

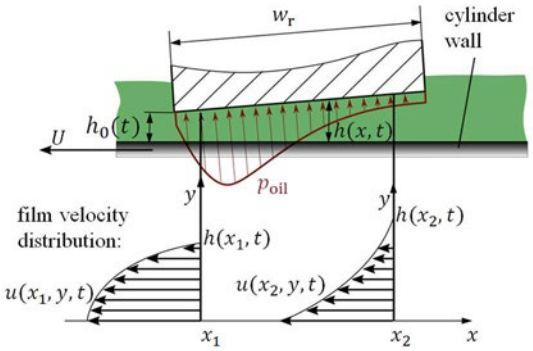

Figure 1: Pressure and velocity distributions between ring and cylinder wall

Consider an arbitrary ring cross section (Figure 1). The coordinate system moves with the piston and so the cylinder wall moves in a reciprocating fashion relative to the ring. The ring has width w_r and is separated from the moving cylinder wall by an oil film of thickness h. The ratio ϵ of the oil gap to the ring width is small, i.e. $\epsilon = h_0/w_r \ll 1$ and $\epsilon Re \ll 1$, where the Reynolds number $Re = Uh_0/\nu_f$, ν_f is the kinematic viscosity of the oil and $h_0(t)$ is the minimal gap at time t. These estimates form the prerequisites of classical lubrication theory. We therefore neglect fluid inertia and vertical pressure variations (also due to gravity) across the lubricant film. This simplifies the thin-layer approximation of the Navier–Stokes equation, resulting in a Couette–Poiseuille velocity profile:

$$u(x,y,t) = \frac{1}{\mu_f}\frac{\partial p_{oil}}{\partial x}\,(y^2 - hy) + \frac{Uy}{h(x,t)} \tag{1}$$

with the resulting volume flow per unit length:

$$\dot{V}(x,t) = \int_0^{h(x,t)} u(x,y,t)\mathrm{d}y = \\ = -\frac{h^3(x,t)}{6\mu_f}\frac{\partial p_{oil}}{\partial x} + u\frac{h(x,t)}{2}. \tag{2}$$

Using the continuity equation, this leads to the classical Reynolds equation [2] for an incompressible fluid, which takes the form

$$\frac{\partial}{\partial z}\left(\frac{h^3}{6\mu_f}\frac{\partial p_{oil}}{\partial z}\right) + \frac{\partial}{\partial x}\left(\frac{h^3}{6\mu_f}\frac{\partial p_{oil}}{\partial x}\right) = \\ = \underbrace{U\frac{\partial h}{\partial z}}_{\text{wedge}} + \underbrace{2\frac{\partial h}{\partial t}}_{\text{squeeze}}. \tag{3}$$

Equation 3 describes the time-dependent pressure distribution $p_{oil} = p_{oil}(x,t)$ within the gap, which is driven by two effects known respectively as the wedge and the squeeze. The squeeze term is driven by the vertical movement of the ring, while the

by: Bernhard Fritz, Bernhard Schleichl – TU Wien, Institute of Fluid Mechanics and Heat Transfer (E322)

ring's tilt determines the wedge effect. The force due to the pressure distribution per unit depth is:

$$F_{\mathrm{oil}}(t) = \int_0^{w_\mathrm{r}} p_{\mathrm{oil}}(x,t)\mathrm{d}x\,. \tag{4}$$

A cylinder lubrication model needs to answer, in essence, how to define a lube strategy to minimize the occurrence of asperity contacts between rings and cylinder wall. Hence, the main points which need to be covered to analyze this problem, are:

- the oil film force $F_{\mathrm{oil}}(t)$ required to avoid asperity contacts, which leads to
- the vertical ring movements and the time-dependent tilt of the rings (symmetry is assumed, lateral motions are neglected, see Sec. 2.2);
- the thickness of the oil film next to each side of the ring which is needed to calculate the amount of oil to be supplied. A sufficient oil supply is needed to create a fully flooded ring region, which in turn allows the formation of the necessary hydrodynamic pressure. (Sec. 3.1).

Step by step we will present the model details addressing the three points mentioned above. This will then lead us to a global lubrication model that allows the derivation of compressor-specific lube strategies, also by involving full computational fluid dynamics (CFD).

2.1 Oil film forces between rings and cylinder wall

A typical piston assembly usually consists of two different ring types: rider rings and piston rings (Figure 3). Both are nowadays typically made out of plastic compounds. Piston rings are exclusively designed to seal against gas pressure: Differential pressure pushes them against the cylinder wall during operation. To allow them to be placed in their retaining grooves, piston rings usually feature either a narrow gap or a multi-piece construction. This combination of material and construction makes piston rings very flexible. Deriving the required pressure force $F_{\mathrm{oil}}(\phi,t)$ and the ring deformation therefore simplifies to the description of a inertialess, flexible beam [1]. This leads to a quasi-1D problem: Inertial terms as well as gradients in circumferential directions are negligible: ϕ has become a parameter. Forces due to gas and oil

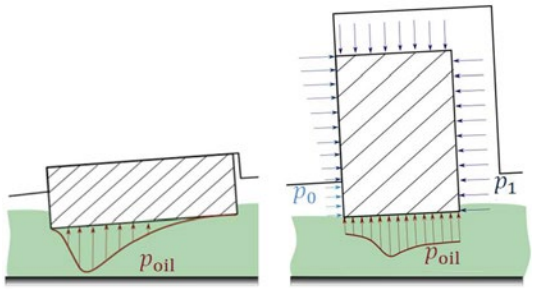

Figure 3: (left) rider ring; (right): piston ring

pressures need to be in equilibrium for all ϕ ranging from 0–π. The ring's tilt is prescribed by the piston groove, and the required F_{oil} is a function of the gas pressure.

Rider rings, on the other hand, are pressure-balanced and are seated solidly on the piston: axial slots guarantee equal pressure on both sides and prevent them from becoming "activated" by differential pressure, as piston rings are. They transmit to the piston those forces that arise in the oil film and through contact with the cylinder wall. The ring is assumed to move with the piston, so that the gap between cylinder wall and rider ring is defined solely by the piston's position and inclination as well as the deformation of the ring. The derivation of F_{oil} and the motion of the piston demand a dynamic model of the piston.

2.2 Dynamic compressor model

Describing the vertical movements of the rings, the time-dependent tilt of the rings and the required F_{oil} demand a most accurate prediction of the motion of the piston. This includes the representation of a secondary piston movement – normal to the primary direction of piston movement – due to the time-dependent piston tilt, which is a consequence of clearances around the piston and the crosshead. For simplicity, we assume symmetry and neglect any motions due to vibrations: Lateral movements or forces are neglected: Crosshead as well as piston only move axially and vertically. The resulting dynamic compressor model (Figure 2) is a lumped-element model with ideal bearings, meaning that they are assumed to have zero clearance and do not transmit a moment. It is enhanced by a 1D Ritz ansatz function describing the bending of the piston rod. All the other parts – crankshaft, connecting rod, crosshead and piston – are assumed to be rigid.

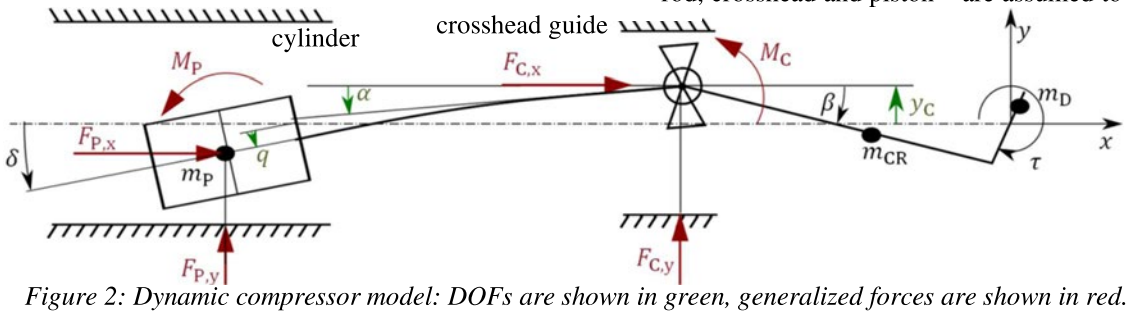

Figure 2: Dynamic compressor model: DOFs are shown in green, generalized forces are shown in red.

by: Bernhard Fritz, Bernhard Schleichl – TU Wien, Institute of Fluid Mechanics and Heat Transfer (E322)

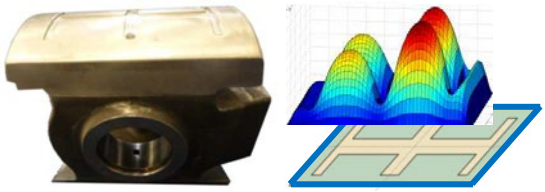

Figure 4: (left) Crosshead, and (right) the resulting pressure distribution

To describe the tilt of the piston, vertical displacements of the crosshead $y_C(t)$ and the piston $y_P(t)$ are included as degrees of freedom.

The model has three generalized degrees of freedom (DOF) according to the concept of Lagrangian mechanics and modular analysis: (i) $y_C(t)$, (ii) the tilt of the piston rod $\alpha(t)$, and (iii) $q(t)$, an approximation for the maximum vertical displacement w of the piston rod due to bending (bending length l_b). The bending line is determined using the ansatz:

$$w(\xi,t) = q(t)\,\phi(\xi)\,, \qquad \phi(\xi) = \xi^2/l_b^2\,, \qquad (5)$$

with ξ being the axial piston rod coordinate [1]. The three degrees of freedom result in three equations of motion. To close the system of equations we need to describe how the general forces and moments acting on the piston and crosshead relate to the motion of these components. This is done via two submodels representing the rider ring and the crosshead respectively. Both submodels calculate the motion-dependent pressure distributions using the Reynolds equation (3) to derive the resulting forces and moments.

2.2.1 Crosshead and rider ring submodels

The crosshead is both hydrostatically and dynamically lubricated on both its upper and lower sides, so we always have fully lubricated gaps. The 2D Reynolds equation is solved for both sides. A constant pump pressure is prescribed in the lubrication channels, while the ambient pressure is described at the fixed boundaries (Figure 3). The crosshead is assumed to be rigid, and hence the lubricated gaps are defined solely through the crosshead motion: $y_C(t)$ and $\alpha(t)$.

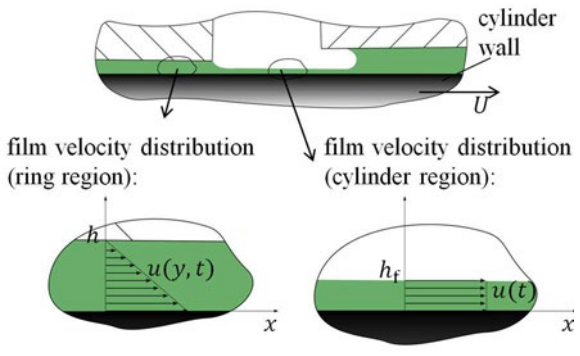

Figure 5: Interaction between two consecutive rings

The rider ring is hydrodynamically lubricated, with the lubricated gap defined by the piston movement. To solve (3), we need to prescribe the pressure at the boundaries of the fully flooded ring region.

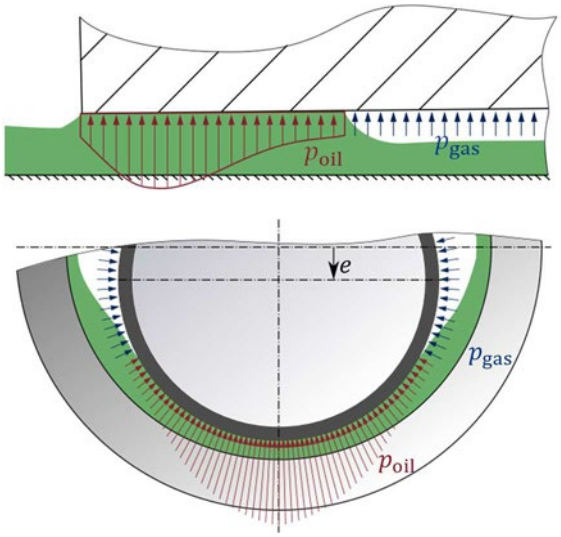

Figure 6: (top) Starved lubrication condition in the axial direction as a result of insufficient oil supply; (bottom) starved lubrication condition in the azimuthal direction due to large clearance

However, rings are not always fully flooded like in Figure 3. First, any ring can be starved of lubrication due to insufficient oil supply, resulting in shrinkage of the fully flooded ring region (Figure 6, top).

Second, the ring gap will hardly ever be fully filled with oil in the azimuthal direction (Figure 6, bottom). This is because the clearance between rider ring and cylinder wall is typically on the order of 0.1 mm (or larger due to wear), while the expected thickness of the oil film is around 0.01 mm.

This is therefore a free boundary problem: The extent of the fully flooded ring region is time-dependent, and can increase and decrease dependent on the oil film heights at its borders. Next to this region there is a passive oil film, whose pressure equals the gas pressure above the oil film. The complex region between the flooded region and the passive film we will refer to as a transition zone. To evaluate the ring's lubrication condition, we need to track these transition zones.

2.3 Two equations gas pressure model

The process of mixing in-flowing gas with the gas already in each chamber is irreversible, so we must account for both the energy balance and the mass balance. The cylinder wall is assumed to be adiabatic, and the ideal gas law is used. Above all, the process is assumed to be quasi-static, resulting in a time-dependent but uniform pressure distribution in each chamber. The mass flow across the rings and

by: Bernhard Fritz, Bernhard Schleichl – TU Wien, Institute of Fluid Mechanics and Heat Transfer (E322)

through the valves is described using the well-known Saint–Venant–Wantzel law.

2.4 Contact between rings and cylinder wall: evaluation of lubrication conditions

The Reynolds equation, which is used to calculate the pressure distribution in the fully oil-flooded gaps, is valid for ideally smooth contact surfaces. The closer the gap height is to the cylinder wall roughness, the less accurate the Reynolds equation becomes and the greater the role played by surface roughness. In the limit, when the gap height equals the surface roughness, the ring operates in the mixed lubrication regime, where the load is supported partly by the fluid film and partly by the surface asperities.

In this work we assume perfectly smooth surfaces and neglect the influence of wall roughness on the pressure distribution. The gap size is forced to remain above a certain minimum value, on the order of the cylinder surface roughness, via a basic contact model: Linear spring forces are applied to the surface of each ring. These spring forces are independent of one another and represent contact forces due to elastic deformation:

$$F_{c,k} = EA_k \frac{\mathrm{gap}_{\min} - \mathrm{gap}_k}{h}, \tag{6}$$

where A_k is a proportional section area, E is the Young's modulus and h is the height of the deforming material. Tracking the contact forces allows the introduction of the ***starving parameter St***: Its definition shall be sketched very roughly. A detailed explanation is found in [1]: for each ring, the so called wear-proportional pv load, known from the selection of materials for dry bearings [7] is calculated with zero share for vanishing contact forces and compared to the theoretical pv load of a dry-running ring over a full cycle. Hence,

$$St = \begin{cases} = 0 \ldots \text{fully hydrodynamic lubrication} \\ > 0 \ldots \text{partially mixed lubrication,} \\ = 1 \ldots \text{dry-running ring;} \end{cases} \tag{7}$$

St is important: It lets us describe the lubrication conditions of each ring with a distinctive parameter derived directly from the global lubrication model.

2.5 Free surface oil film

The film heights next to the flooded region of the ring are of great importance, since they decide whether the flooded region will grow or shrink. Film heights that are too low will lead to under-lubrication, resulting in an asperity contact between ring and cylinder wall.

2.5.1 *Oil film dynamics due to ring interaction*

Figure 5 shows two adjacent rings at rest; the cylinder wall is moving to the right. The film velocity profile between the rings corresponds to plug flow, while the velocity profile between cylinder wall and ring corresponds to a Couette flow (for simplicity we neglect the wedge and squeeze effects). The left-hand ring thus leaves a trace of oil whose height is half that of the gap. If the right-hand ring has a larger gap (as shown in *Figure* 5), its fully lubricated area will decrease and the ring will move closer to the wall.

To assess the lube situation of any particular ring it is therefore essential to take into account the interplay with other rings when calculating the film height.

2.5.2 *Oil film dynamics due to gas flow and evaporation*

Last but not least, we need to study the progression over time of the oil film height through causes apart from ring interactions. Two mechanisms which might affect the height of the oil film in the cylinder regions next to the rings are:

(1) thinning of the oil film due to evaporation; and

(2) motion of the oil film due to gas flows, gravity and capillary forces.

References [3] and [4] present oil evaporation models for piston engines. They describe the evaporation of the oil, consisting of various constituents having different vapor pressures, on the liner surface as a diffusion of oil vapor through a gas boundary layer. Oil evaporation is controlled by gas-side convection [3], and this assumption still holds for larger film heights, where diffusion inside the oil film becomes more pronounced (the Biot number increases), as expected in the cylinders of bigger compressors. Taking the figures from [3] and [4] and extrapolating to typical compressor geometries we get evaporation rates in the approximate range 10^{-3}–10^{-1} l/h, depending on compressor size. Even the upper end of this range is small compared to usual compressor lubrication rates of several liters per hour. It should also be noted that the temperatures in a typical compressor are much lower than those in an internal combustion engine, so mass transfer coefficients and hence evaporation rates will be even lower. We can therefore neglect thinning of the oil film due to evaporation.

Using basic asymptotic analysis and a CFD calculation of a compression cycle for an exemplary compressor, reference [1] shows that the shear stress is the dominant term in the Navier–Stokes equations of the gas-driven oil film, which allows us to neglect the pressure gradient. Furthermore, the maximal film velocity u_s is derived:

$$u_s = \tau_g h_f / \mu_f, \tag{8}$$

with the dynamic viscosity μ_f and the shear stress τ_g at the film surface. In addition, [1] shows that $u_s \ll U$ for typical oil film heights ($h_f < 10^{-4}$ m) in most cylinder regions. However, u_s is significantly

by: Bernhard Fritz, Bernhard Schleichl – TU Wien, Institute of Fluid Mechanics and Heat Transfer (E322)

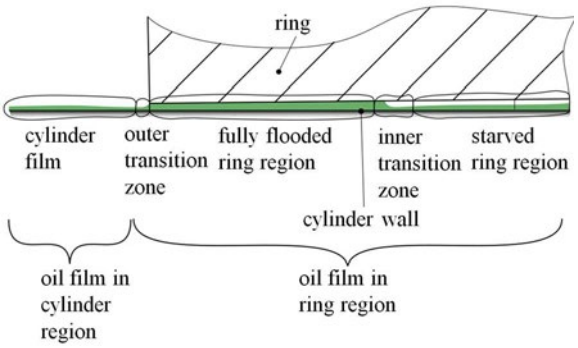

Figure 7: Definition of calculation regimes

larger only in two situations: (i) next to the valves and (ii) on the cylinder wall at higher film heights. This explains the gas-driven removal of oil next to the valves and where oil has accumulated. Additionally, capillary- and gravity-driven oil flows are shown to be negligible [1].

The arguments above confirm that we can neglect changes in oil film thickness due to evaporation, gas flow, gravity and capillary action. We therefore have time-independent oil film distribution in the cylinder regions of interest: the compression regions at the head end and the crank end, and the regions between the rings. At every time step, only the film heights of the boundary cells next to the rings need to be updated so that we can calculate the oil trace leaving each ring.

2.6 Global lubrication model

As stated at the beginning of this section, we need to take a close look at the lubrication conditions of the ring regions to estimate how much oil is required to ensure a certain minimal gap. Summarized, this requires us to:

(1) describe the time-dependent piston motion (tilt and eccentricity of piston), which requires a dynamic compressor model including accurate ring- and crosshead submodels;
(2) describe the oil supply to each ring, which requires a model which tracks the oil trace of each ring and accounts for the interplay between the rings.

We have already decided that it is reasonable to neglect gas-driven oil flow and oil evaporation.

The global lubrication model we have derived covers the above considerations. Its focus is on finding a dynamic steady state (with a periodicity of several compression cycles under rarely achievable perfect lube conditions) involving a bearable *St* number. The accumulated net-oil flow across each ring can then be evaluated. The model is computationally intensive – we can model 1–4 crank revolutions per day on a 2.7-GHz CPU – so the net oil flow must be extrapolated to get lube rates in l/day. Parameters such as ring profile, μ_f, speed and geometry and oil parameters need to be defined in accordance with steady-state conditions.

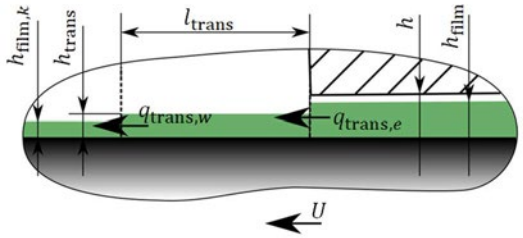

Figure 8: Schematic of the downstream outer transition zone

The simulation results provide detailed insights into cylinder lubrication conditions by describing the oil demand of each individual ring.

3 Specific model details and implementation

Oil film dynamics are modeled by dividing the calculation domain into different calculation areas which use two computational grids (see Figure 7):

- oil film in cylinder regions (CS1)
- outer transition zone
- inner transition zone
- fully flooded ring region
- starved ring region

(CS2)

CS1 is the computational grid for the cylinder region (coordinate system is at rest) and CS2 is the computational grid for the ring regions (rings have zero relative velocity). The transition zone lies between the passive oil film, which is assumed to cover the cylinder wall, and the fully flooded ring region. Its position is derived via interface tracking (see below).

3.1 Interface tracking via transition zones

Following the Volume of Fluid (VOF) method [5], the interface is tracked using the volume fraction F, which represents the ratio of the fully filled cell volume V_{oil} to the total cell volume V, and is defined for each cell k as:

$$F_k = \frac{V_{\text{oil},k}}{V_k} \,. \tag{9}$$

The evolution of F_k is derived from a mass balance for the interface cell with index k:

$$V_{\text{oil},k}^{(n)} = V_{\text{oil},k}^{(n-1)} + q_w^{(n)} - q_e^{(n)} \,, \tag{10}$$

where ${q_{e,w}}^{(n)}$ is the oil volume flowing across the east and west borders of a fully flooded ring cell at time step n. As a result:

$$F_k^{(n)} = F_k^{(n-1)} \frac{V_k^{(n-1)}}{V_k^{(n)}} + \frac{q_w^{(n)} - q_e^{(n)}}{V_k^{(n)}} \,. \tag{11}$$

by: Bernhard Fritz, Bernhard Schleichl – TU Wien, Institute of Fluid Mechanics and Heat Transfer (E322)

The numerical implementation of the transition zones will be explained using the examples shown in Figure 8 and Figure 9.

2.1 Outer transition zone

The focus in the outer transition zone lies on conservation of mass: oil must not get lost. However, slight imprecision in calculating the oil film height in the cylinder region is acceptable, so we have not examined the exact shape, growth and shrinkage of the oil menisci. Instead, the menisci are modeled as rectangular columns with constant velocity profiles – which depend on the cylinder wall velocity – at their outer edges. The name "transition zones" is chosen to emphasize this approach.

The volume flow from the ring zone to the outer transition zone depends on the oil film heights at the ring's borders: Figure 8 shows an example of a downstream transition zone. As long as the ring gap is fully flooded and the oil column can provide enough oil, the volume is defined by the velocity profile given by the Reynolds equation:

$$q_{\mathrm{trans},e} = \left(-\frac{1}{12\mu_\mathrm{f}}\frac{\partial p}{\partial x} + U\frac{h}{2}\right)\Delta t\,. \qquad (12)$$

In other cases it is defined by the height of the oil column, assuming a constant velocity:

$$q_{\mathrm{trans},e} = U h_{\mathrm{film}}\Delta t\,. \qquad (13)$$

The volume flow $q_{\mathrm{trans,w}}$ is approximated by a plug flow.

2.2 Inner transition zone

Dimensions of the meniscuses in the inner transition zones (see figure 10) are much smaller than those of typical numerical cells, whose height to length ratio is 1/100–1/10. $q_{\mathrm{film,e}}$ therefore represents an undisturbed plug flow. q_w is derived using

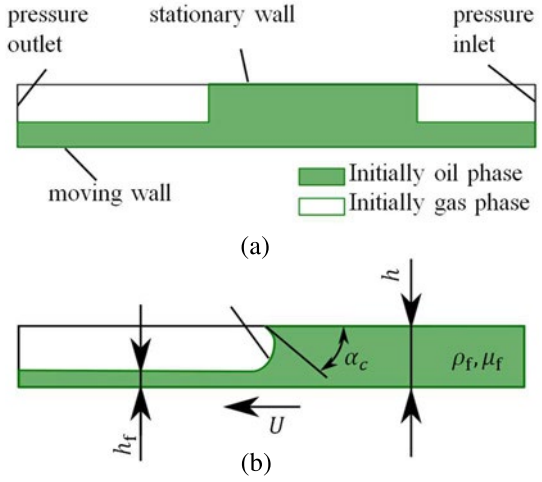

Figure 9: (a) problem definition for CFD simulation, and (b) physical quantities describing the problem

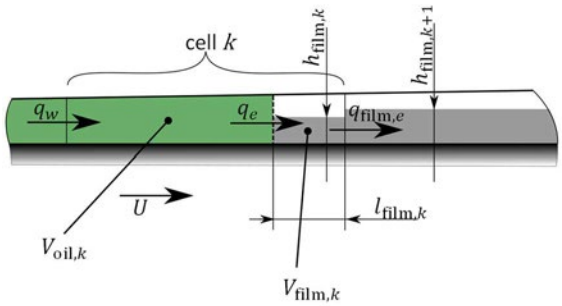

Figure 10: Schema of inner transition zone;

Equation 12, which is valid for fully lubricated gaps.

We must make a velocity-dependent distinction when defining q_e, which describes oil transport between the passive oil film and the fully flooded ring region The case of negative cylinder wall velocities is intuitively easy to describe: since our calculation show that gas convection has only little impact on the dynamics of the oil film, the latter is taken as at rest. Therefore, q_e feeding into the fully lubricated gap is governed by a uniform velocity profile.

The other case (positive cylinder wall velocity) is not as clear: What is the height of the oil film trace that the moving ring leaves behind the fully lubricated zone? We identify the following contributing physical quantities: the surface tension γ, the oil density ρ_f and dynamic viscosity μ_f, the contact angle α_c, the gap height h and the height of the oil film trace h_f. Buckingham's π theorem shows that three independent dimensionless numbers are needed to describe this problem. We choose the Reynolds number Re, the capillary number Ca and ζ, which is defined as the ratio h_f/h:

$$Re = \frac{Uh\rho_\mathrm{f}}{\mu_\mathrm{f}}, Ca = \frac{\mu_\mathrm{f}U}{\gamma}, \zeta = \frac{h_\mathrm{f}}{h}. \qquad (14)$$

Hence, the challenge is to find the function f, which describes the correlation of the numbers defined above:

$$\zeta = \mathrm{f}(Re, Ca)\,. \qquad (15)$$

This is done numerically by a CFD solution of the freely floating oil film, as sketched in Figure 9, using ANSYS FLUENT (commercial license, Re-

Table 1: physical quantities used for CFD calculations to estimate the oil film trace

physical quantity	range of calculated values
U	0.1–3.2 m/s
μ_f	0.004–0.03 Pas
ρ_f	870 kg/m^3
h	2.5×10^{-6} – 5×10^{-5} m
γ	0.04 N/m
α_c	70 degrees

by: Bernhard Fritz, Bernhard Schleichl – TU Wien, Institute of Fluid Mechanics and Heat Transfer (E322)

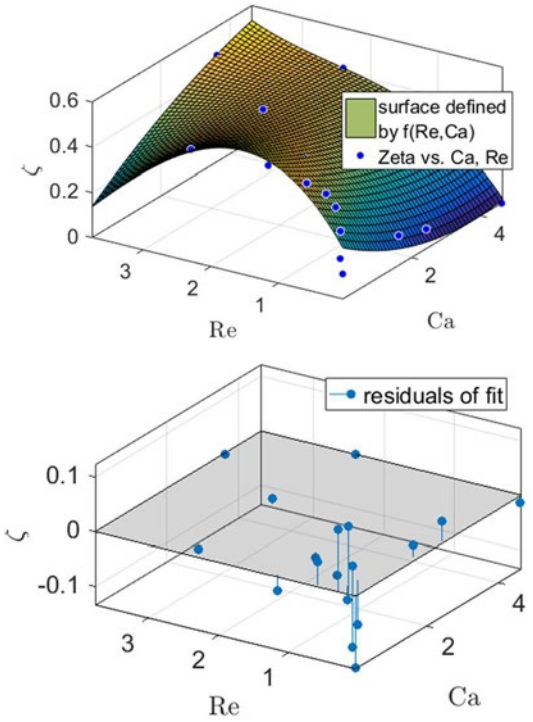

Figure 11: (top) surface representing $\zeta = f(Re, Ca)$ as calculated from CFD; (bottom) the resulting residuals

lease 14.5.7) with a range of parameters. We applied the volume of fluid (VOF) method with air as the primary phase and oil as the secondary phase. The left and right boundaries are defined as a "pressure_outlet" and a "pressure_inlet" respectively, both having the same pressure. The lower wall moves with velocity *U*. Figure 9a shows the boundary conditions, initial conditions and parameters. For each set of parameters we calculate h_f, and subsequently fit the data using the least-squares method to derive the polynomial f. Figure 11 shows the surface described by the polynomial f and the residuals for the simulated configurations; the maximum deviations are around 10%.

4 Application of Lubrication model

The global cylinder lubrication model is applied to the case of a real compressor (an ARIEL compressor), which allows to compare results with in-use lube rates, provided by state of the art guidelines.

Table 2: basic compressor data used as a test case

Compressor parameters	
speed	1000 rpm
kinematic oil viscosity	35 mm²/s (cSt)
bore	260 mm
stroke	171 mm
avg. piston speed	5.6 m/s
suction pressure	49 bar
discharge pressure	84 bar

Geometric data (basic lengths, masses, mass moments of inertia, geometry of crosshead guide, …) was kindly provided in detail by ARIEL. The basic data of this test case is shown in table 2: The machine runs with 1000 rpm, the average piston speed is 5.6 m/s. The piston is guided by one rider ring, symmetrically placed between four piston rings.

4.1 Simulation procedure

The inclination between piston ring surface and cylinder wall surface is solely defined by the piston's motion (dynamically changing) and the ring's profile (static). In case the piston rod's inclination is positive all time during operation, some ring areas will always form a divergent gap – taking an ideal, linear ring profile as an example – leading to a constant mechanical contact and hence high starving parameters *St*. Therefore, the piston rings' profiles are adapted, where the ring is in contact (corresponding to ring wear) to minimize and get realistic *St*-values. This numerical approach is motivated by run-in operation with increased lube rate, which is often done in practice for new rings.

Thus, the simulation procedure is divided into three states (see Figure 12):

1. Start with initial conditions ($h_f = \text{const} = 0.03$ mm, eccentricity $e = 0$), neglecting piston rings; the two equations gas pressure model is used in advance to estimate the pressure course next to and in between the rings. When steady compressor dynamic conditions are reached:

→ *adapt profile for piston rings, initialize oil film*

2. continue calculation with consideration of piston rings with adapted profiles until steady state is reached again;
3. continue calculation, calculate net-oil transport along rings;

→ *interpret results to derive lube strategy*

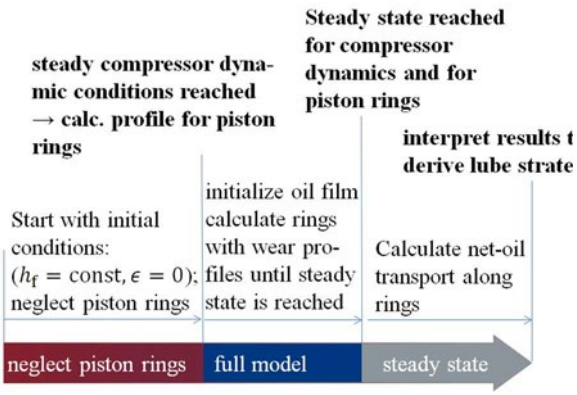

Figure 12: calculation procedure

by: Bernhard Fritz, Bernhard Schleichl – TU Wien, Institute of Fluid Mechanics and Heat Transfer (E322)

4.2 Results

The dynamic compressor model gives numerous results, like piston rod bending, piston– and crosshead eccentricities, forces (see Figure 13, which shows the traces of these results over two revolutions), clearances, moments and tilts, contact forces, etc. Let us discuss just a few of them to get an overview of the compressor's motion: We see, that the piston eccentricity is always negative: the piston is steadily guided by the bottom rider ring side with a minimal clearance ranging from 2 (approx. at tdc-position) to 16 microns (approx. at bdc-position). A minimal oil film is always preventing asperity contact leading to $St_{\text{rider}} = 0$, with an average wetting angle (angle which describes the fully flooded ring region in azimuthal direction) of approx. 40 degrees. The crosshead is moving periodically in vertical direction, also without any occurrence of asperity contacts. The minimal piston ring gaps are not plotted in this section. They range from approximately 0.6 microns to 6 microns and are considerably lower. Assuming perfectly flat surfaces, $St = 0$ for all rings.

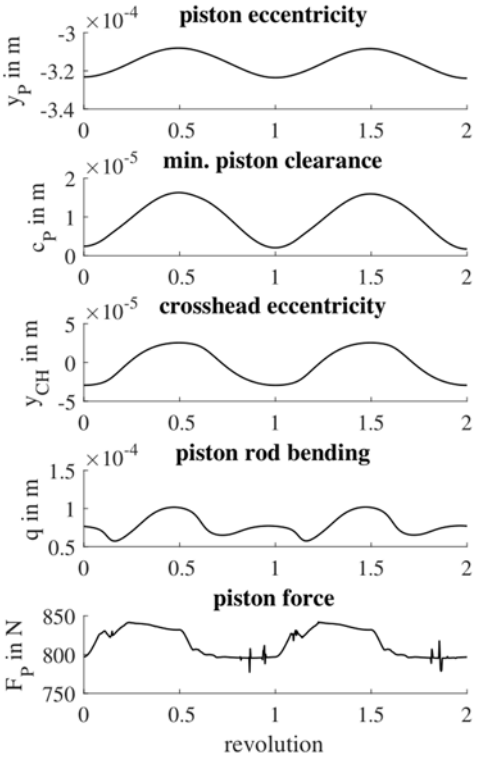

Figure 13: results of dynamical lubrication model: piston eccentricity, crosshead

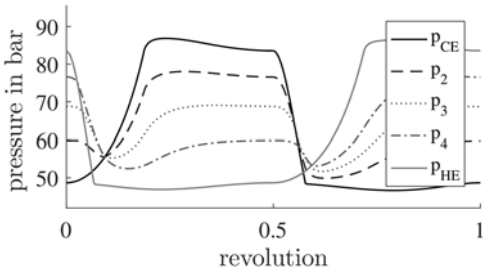

Figure 14: pressure variation next to and in between of the piston rings as a result from the two equations gas pressure model.

Table 3:net-oil flow along rings;

ring (numbering starting from left side)	net-oil flow along rings in l/day
ring 1 (piston ring)	-2.05
ring 2 (piston ring)	-1.14
ring 3 (rider ring)	-1.6
ring 4 (piston ring)	-1.16
ring 5 (piston ring)	-1.04

The strong nonlinearities of the piston force progression are due to the high dependency of pressure distribution on the gap size of the fully flooded ring regions. Small variations of eccentricity in the order of calculation accuracy cause therefore visible force peaks. This behavior is improved by choosing higher calculation tolerances. However, comparative calculations have shown negligible influence on the piston's eccentricity and on the net-oil flow. The chosen tolerances are a good compromise between calculation accuracy and calculation speed [1]. The maximal piston rod bending is in the order of a few hundreds of millimeters and affects certainly the resulting piston tilt.

The pressure variation in between and next to the piston rings is shown in Figure 14. It was calculated assuming an effective leakage area of 4 mm^2 for each ring and is mainly important for the oil pressure calculation of the piston rings.

Figure 15 shows the resulting wear profile of ring 1, plotted over the developed ring surface, which was calculated after the first calculation phase (red phase in Figure 12). It emphasizes the non-symmetry of the problem due to the non-zero tilt and eccentricity of the piston.

The evaluation of the net-oil flows along the rings

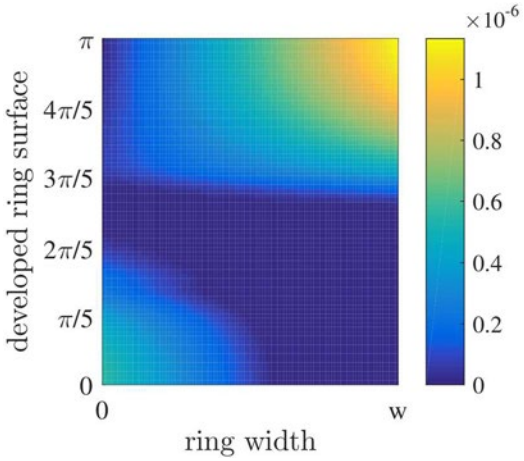

Figure 15: wear profile in m of first piston ring (from left), plotted over the developed ring surface.

by: Bernhard Fritz, Bernhard Schleichl – TU Wien, Institute of Fluid Mechanics and Heat Transfer (E322)

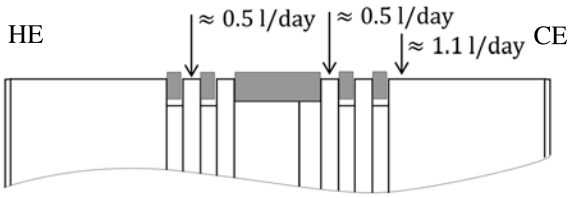

Figure 16: possible lube strategy;

is shown in table 3: there is a net-oil flow across each ring towards the left side (towards head end). The net-oil flow along the rider ring (-1.6 l/day) is about 50 % higher than the oil flow along the CE-sided piston rings. These results suggest injection of oil at three places: 50 % of the oil should be supplied at the CE side of the rings (1.1 l/day), the other half of the oil supply should be supplied at the CE sides of the rider ring and the left piston ring (see Figure 16). After a run-in phase, the resulting total lube rate of 2.1 l/day should be sufficient to allow for a reliable operation. Compared to state-of-the-art lubrication guidelines – [6] suggests a lube rate of 3.1 l/day – these results suggest a reduction of oil consumption of approx. 30 % for this specific case.

5 Summary and critical discussion

In the course of this work, a comprehensive cylinder lubrication model for reciprocating compressors was derived, which deepens the insight into the mechanisms of oil loss. The secondary piston motion is identified to be the key driver for oil consumption, the influence of evaporation and gas driven oil flow is worked out to be negligible.

This derived lubrication model allows to develop compressor specific lubrication guidelines, which go much more into detail than state of the art empirical guidelines do: By taking compressor specific parameters into account (e.g. clearances, ring profiles, moments of inertia, oil viscosity, etc.), it does not only provide an estimate for an optimal lube rate, but provides also guidance on the timing of oil injections.

In Sec. 4, the lubrication model is applied to a "real" compressor, giving a very encouraging, realistic outlook how a possible lube strategy could look like. Compared to standard empirical guideline [6] the simulation results suggest a lube oil reduction of approx. 30 %.

However, lacking empirical proof yet, this model needs to be verified experimentally. Above all, some aspects are not covered yet or show room for improvement: For instance, oil consumption due to oil mist is not covered at all, assuming ideal lube conditions. Oil mist possibly forms in the course of oil injection. Another possibility is the inertial driven formation of oil mist. If oil accumulates on any piston region and forms a large droplet, the piston acceleration can force a detachment of the oil droplet. Keep in mind that such formations of oil droplets do not necessarily lead to an increase of oil consumption, since the oil drops might reattach at the cylinder wall. Above all, they are a result of over lubrication and might be avoided anyhow.

The lube conditions discussed above lead to $St = 0$. Reducing the lube rate does not necessarily lead to $St > 0$: On the one hand, various ring wear profiles could lead to lower net-oil flows. On the other hand, in case of rider rings, a reduction of lube rate would result in lower wetting angles, hence smaller fully flooded ring regions. However, they might still allow for pressure distributions, which are high enough to avoid asperity contacts.

The results also suggest that generally, an increase of lube rates does not necessarily improve the lube condition of every ring, and hence the compressors reliability: In this test case, for example, increasing the lube rate on the right side of the rings would not improve the lube conditions of the rider ring, since the piston rings in between would serve as an oil barrier. Then again, generally, lube conditions could even be improved despite lower lube rates, but with better timing.

The presented results emphasize that this newly developed lubrication model could effectively be used to derive lubrication strategies for reciprocating compressors resulting in significantly reduced oil consumption and increased compressor reliability.

References

[1] B. Fritz, Development of a comprehensive cylinder lubrication model for reciprocating piston compressors to minimize oil consumption. PhD thesis, TU Wien, 2019.
[2] O. Reynolds. On the theory of lubrication and its application to Mr. Beauchamp Tower's experiments, including an experimental determination of the viscosity of olive oil. Proceedings of the Royal Society of London, 40:191–203, Jan. 1886.
[3] E. Yilmaz. Sources and characteristics of oil consumption in a spark-ignition engine. PhD thesis, Massachusetts Institute of Technology. Dept. of Mechanical Engineering, 1970.
[4] L. Liu. Modeling the performance of the piston ring-pack with consideration of non-axisymmetric characteristics of the power cylinder system in internal combustion engines. PhD thesis, Massachusetts Institute of Technology, 2005.
[5] C. W. Hirt and B. D. Nichols. Volume of fluid (vof) method for the dynamics of free boundaries. Journal of Computational Physics, 39(1):201–225, 1981.
[6] P. C. Hanlon. Compressor Handbook. McGraw-Hill. 2001
[7] B. Bhushan. Introduction to Tribology. John Wiley & Sons, 2013

Early work supporting future conductive sealing rings to reduce piston rod temperature and wear

by:

Cyril Wentzel
inventor
Wentzel Dynamics, The Netherlands
cyril@wentzeldynamics.com

Marc Langela
head of research
Stasskol GmbH, Germany
marc.langela@stasskol.de

12th EFRC CONFERENCE
August 24 – 26, 2021, Warsaw

Abstract:
Sealing ring wear can be improved by increasing heat transport away from the frictional interface. Over the past decades, efforts have looked at ways to increase heat transport through the rod itself, arguably with success in an EFRC sponsored project and manufacturers now can choose to implement this measure. A novel way to achieve heat transport from the friction interface was sought in a special sealing ring optimised for heat transport. The EFRC R&D group has endorsed this approach by executing a phased feasibility study on novel conductive ring concepts. The present paper reports on work in progress concerning a measurement campaign to quantify heat generation and flow paths. For the project, with the acronym IRINCO, detailed transient measurements were made of rod and ring temperature to quantify the heat flow from the friction interface and to develop an appropriate numerical calculation model to support the evaluation of ideas. It is shown that simplified heat generation models and assumptions seem totally inadequate to explain the observed transient heating, suggesting more complex mechanisms and a transient behaviour. Unique transient measurements with sealing ring mounted sensors allow monitoring the sealing ring temperature itself, showing high sensitivity to tribologically relevant phenomena. Work in this area is an ongoing topic in the EFRC R&D working group.

by: Cyril Wentzel – Wentzel Dynamics; Marc Langela – Stasskol GmbH, Germany

1. Introduction

1.1 Lower temperatures cause less seal wear

Sealing ring wear is one of the important contributing factors for short maintenance time intervals for dry running recip applications. It has long been acknowledged that improved cooling of the piston rod could remedy this situation.

Over the past decades, efforts have looked at ways to increase heat transport through the rod itself, arguably with success and manufacturers now can choose to implement this measure.

A novel way to achieve heat transport from the friction interface was sought in special sealing ring concepts optimised for heat transport. The EFRC R&D group has endorsed this approach by executing a phased feasibility study. The present paper reports on work in progress concerning a measurement campaign to quantify heat generation and flow paths, rather than on ring concepts.

1.2 EFRC Project IRINCO

For the project, with the acronym IRINCO (Improve RINg COncept), detailed transient measurements were made of rod and ring temperature to quantify the heat flow from the friction interface. Such measurements are aimed at a better understanding of the heat flow problem involving heat flow from the frictional interface towards cooler areas of the machine mainly through the following flow paths:

- the piston rod, towards:
  - the crosshead
  - ambient atmosphere in the distance piece
  - the piston (if piston temperature is low enough)
- gas, sealing rings and support rings to the sealing housing
- to the leakage gas

1.3 State of the art

Several publications have outlined methods to compute in detail the physics of the interaction of a sealing ring on a rod under reciprocating motion. For example, Silvester[1] describes in detail the elements of such a multiphysics method, involving mechanical behaviour, heat flow and gas flow dynamics, along with tribological empirical laws for wear and gas pressure intrusion in the frictional interface.

As an illustration for the several types of cooling channel architecture, the publication[2] by Feistel et al. is well known (Figure 1) in the industry. Its main message is that - since heat transfer path through the gas has high resistance, the main driver of the cooling channel design is reliability rather than high heat transfer.

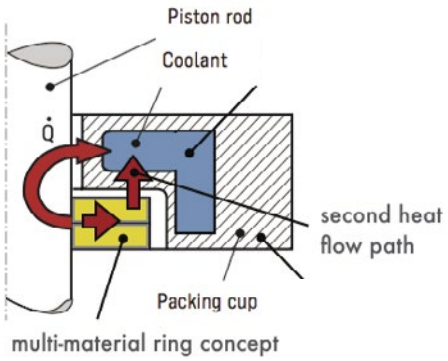

Figure 1 Illustration of the targeted principle of opening up a second heat flow path to the packing cup (adjusted illustration from ref. 2).

The concept of heat partitioning is central to the evaluation of new ideas for conductive rings. It is the phenomenon of asymmetric heat flow from a frictional interface when the temperatures and conductivity on both sides of a multi-material assembly are different. The topic has been studied in classical literature as a theoretical case of Hertzian contact of sliding interfaces[3].

Analytical solutions for simplified problems provide relationships for such heat flow and temperature distribution as a function of the ratio of conductivity values alfa besides the Péclet number accounting for velocity of the friction interface.

Modern computational methods allow the problem to be approached using a suitable thermo-mechanical numerical model, e.g. based on an ALE (Arbitrary Lagrangian Euler) formulation with a transient scheme tracking the heat flow and temperature solution, with an assumption of temperature continuity across the interface.

However, none of these references was seen to provide sufficient base for reliably solving the basic question how heat conductivity enhancement of the ring would influence the actual equilibrium temperature in a reciprocating configuration. Also for this reason, the first emphasis was to generate detailed experimental data which could be used for validating numerical tools. Building on this, the initial exploration of any novel concept can be better grounded.

Literature data on experimental investigation is sparse. Whereas a previous EFRC investigation[4] by Thomas did address temperature reduction, the focus was on the piston rod internal conductivity enhancement towards the crosshead and not on the ring-housing heat flow path.

As mentioned, the current approach relies on transient rather than equilibrium measurements. This requires extensive instrumentation of the reciprocating piston rod. There appear to be four ways of providing the diagnostic architecture: 1) telemetry, 2) contact-less pyrometry surface measurement, 3) signal wire chain and 4) free floating wire bridging.

by: Cyril Wentzel – Wentzel Dynamics; Marc Langela – Stasskol GmbH, Germany

The initial assessment was that the reliability and accuracy requirement demanded a robust contact sensor (e.g. thermocouple or thermistor) based measurement rather than pyrometry, given the challenges like the high reflectivity piston rod. There are similar concerns for its self-lubricating polymer contaminated surface conditions.

Whereas method 3) was applied in ‚test rig alfa' of a previous EFRC research by TU Dresden[4], an alternative was sought to avoid integration difficulties on the available test machine.

Interestingly, the fourth method was applied in the automotive world where a similar challenge exists for investigating combustion engines. As an example, Hamzehei[5] mentions the extensive use of thermocouples (TC) in measuring piston rod and piston temperatures. Transfer of these signals relied on the TC wire itself, with bridging of the wire to the stationary engine carter wall and electronics, i.e. amplifiers and data acquisition. Apparently, the selected TC wires were able to survive such harsh environments and large amplitude motion - be it for limited time requirement.

It was decided to also employ TC instrumentation on the piston rod in phase 1 and if necessary to implement a telemetry solution in a later stage of the research.

1.4 Heat input estimation

For comparing the observed thermal behaviour to a model, we apply a simplified model with boundary conditions for temperature and thermal mass and heat input at a fixed mid-stroke position.

The most elementary heat input q [W/m²] can be based on contact pressure p_c, mean velocity V and friction coefficient μ as by

$$q = \mu p_c V \quad (1)$$

Now the difficulty here is that the contact pressure is not homogenous across the friction interface in either circumferential or axial direction (Figure 2). Whereas sophisticated methods can be deployed (e.g. ref.6) to allow for both interface gas pressure intrusion and contact pressure of a non-rigid seal element, we will for the present purposes denote their combined effect by a single multiplication factor f to result in an effective heat input q_e as in:

$$q_e = f\ \mu p_c V \quad (2)$$

We will use this factor to adjust the nominal heat input quantity from (1) to a level in a model that will roughly reproduce and can be compared to the observed warming. In the most simple case, such a factor would be constant, but there are no good grounds to expect such an empirical convenience.

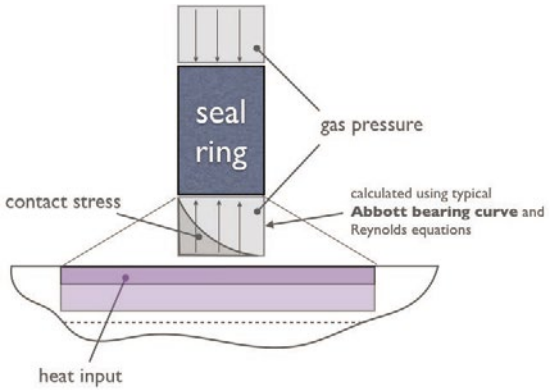

Figure 2: Cross sectional schematic of radial forces acting on sealing ring and (simplified) computational heat input projection along the stroke length of the piston rod. Note the mechanical simplification for segmented ring which has no axial symmetry.

1.5 Scope and purpose

A good quantification of heat flows in a representative configuration of ring and rod under reciprocating motion is required before a concept study can be done into modification of these flows to lower the interface temperature significantly.

Detailed measurements on a representative research compressor configuration are intended to quantify these heat flows and allow adjusting a calculation model to the use in exploring new concepts.

The results of such measurements are described in this paper. It concerns the first exploratory phase, testing the idea to employ the transient heating behaviour to quantify the absolute and relative heat fluxes. The use of transient heating is justified by the idea that it is less sensitive to the exact knowledge of unknown heat transfer coefficients as would be required for equilibrium analysis.

The overall project also aims to develop an appropriate numerical calculation model to support the evaluation of novel ideas. A relatively simple model is reported in the present paper, although more sophisticated models can be applied.

2. Test set-up

2.1 Test requirements

A number of requirements can be specified for generating the required transient data.

- First and foremost, the test machine should allow accessibility for cost effective diagnostics including temperature and pressure in both adjacent moving and stationary parts.
- The equipment should preferably run in the medium pressure range (e.g. 50 bar), generating sufficient frictional heat input resulting in relatively fast transient heating.
- Preferably, the complexities associated with recip pressure (from constant to variable pressure) and ring configuration (single ring, multiple rings, non-overlapping stationary ring input) should be

by: Cyril Wentzel – Wentzel Dynamics; Marc Langela – Stasskol GmbH, Germany

adjustable, allowing to start with low complexity and then gradually introducing further complex elements.

- Full instrumentation on leakage gas and (controllable) cooling flow.

2.2 Test machine description

The test machine (Figure 3, top) is a NEA built dedicated packing test device which is essentially a semi-functional compressor enabling the control of compression parameters and extensive diagnostics. For the present purposes, these diagnostics were extended to the piston rod however. The machine runs at 623 rpm, resulting in an average speed of 2.7 m/sec with a 130 mm stroke.

The suction pressure was set at 30 bar. A special piston without piston rings was used to avoid gas compression and therefore to apply a constant static pressure to simplify the test for phase one.

Within the pressure packing only one sealing ring was used, with the leakage gas sealing rings outside of the direct contact area on the rod (Figure 3, bottom). The sealing ring used was a standard commercially available segmented ring made from a PTFE/PPS/carbon-fiber type grade (SK802). Bronze support rings were applied. A planform view of the sealing ring is visible in Figure 5.

It should be noted that the piston rod is hollow and extends out of the machine (tail rod configuration), facilitating access to inside-rod measurements.

The piston rod was an existing one with an extensive usage history, justifying the assumption that a tribological transfer layer would be present already from the beginning of the test. This is relevant because the tribological conditions are much dependent on the presence of such a layer. Transient measurements should account for this difficulty, in contrast to equilibrium measurements where it is part of the equilibrium process.

To provide the pressurised 30 bar „suction gas", a separate compressor is used. At the time of phase 1 testing, the fixed programming of the equipment imposed the undesirable but normally required purging cycles. In a follow-up phase to this research, this restriction will have been removed.

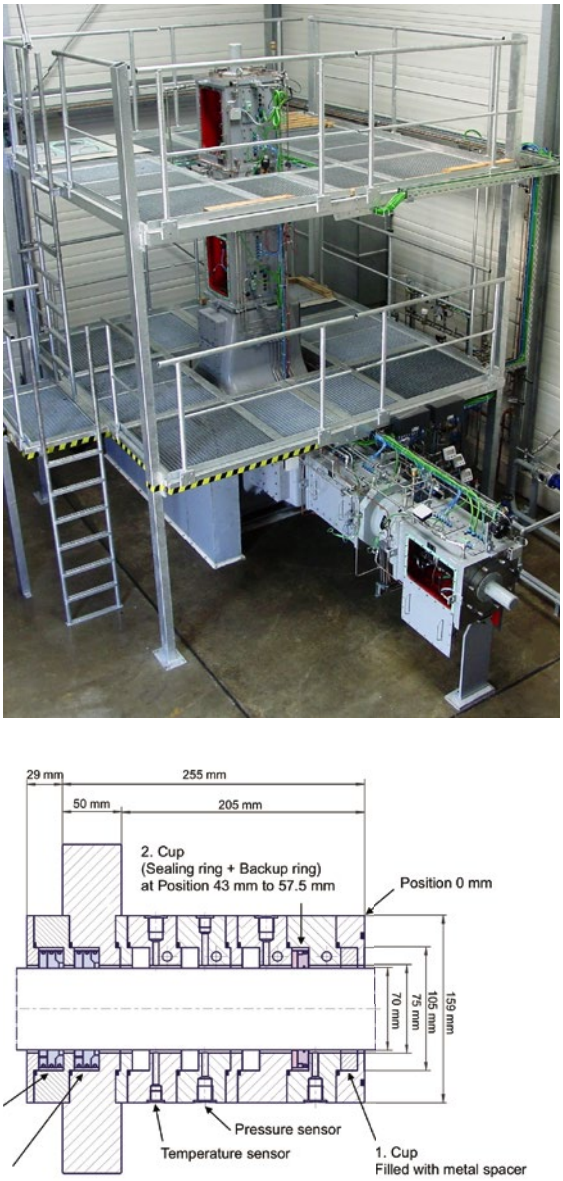

Figure 3: Test machine and high pressure packing housing with single sealing ring. The actual test section is the right hand side (red) section.
Single sealing ring with backup ring against ~30 bar (right) and 2 leakage gas rings (0.5 bar) (right).

2.3 Instrumentation

Many relevant parameters were recorded by default, such as temperatures and pressures at relevant locations, as well as leakage rates. A data acquisition system allows the recording of peaks in time, was well as time resolved detail measurements during cycles.

For the desired transient thermal behaviour, additional temperature recordings were made within the ring and inside the piston rod. Figure 4 shows a scheme of the packing cup with the connections for the instrumentation.

The ring temperature measurement requirement was to measure within 0.5 mm of the actual friction interface, with minimum alteration of the local conductivity and hence temperature distribution.

by: Cyril Wentzel – Wentzel Dynamics; Marc Langela – Stasskol GmbH, Germany

This measurement allows also observations relating to the heat partitioning mentioned in 1.3 above.

Based on a detailed model of the thermocouple wire, junction, radial borehole and thermosetting adhesive used, a computational assessment of the TC sensing indicated that temperature field distortion would indeed be very small. Figure 5 shows an impression of the installed sensing wire, where measures were also taken to suppress ring rotation and secure gas pressure tightness for the wire feed-through connector.

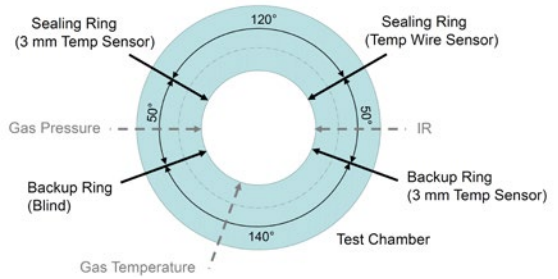

Figure 4: Axial view of several sealing ring and support ring sensor positions.

It is noteworthy to mention that the conventional TC sensors have significant thermal inertia, heat capacity and also distort the temperature field due to their bulky conductivity path, so are not suitable for the most interesting (transient) measurements. Thin wire TC was therefore used throughout for the ring and the piston rod. A laser weld joining the wire ends made it possible to have a well-defined location of the hot junction, hence a truly local temperature measurement relative to steep spatial gradients which occur in transient heating in low conductivity materials.

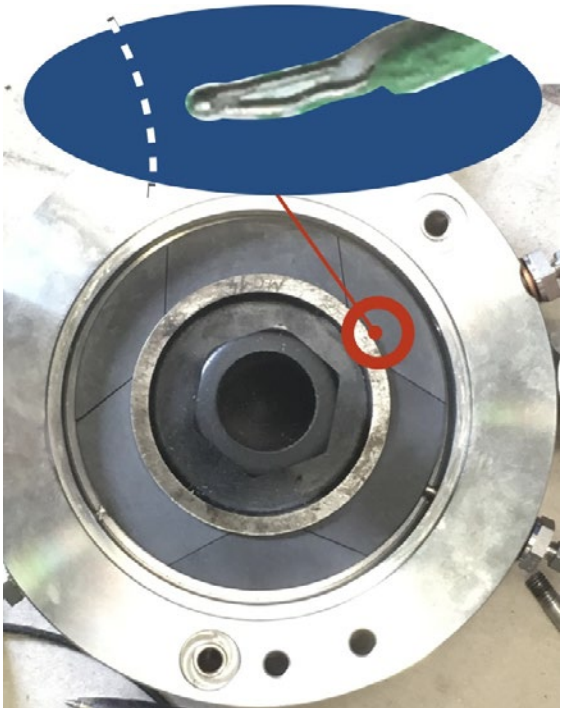

Figure 5: Close-up of thermocouple thin wire hot junction embedded in sealing ring segment close to frictional interface; segmented sealing visible in cup fitted around an assembly caliber.

The piston rod inside was equipped with two TC wires with a surface mounting to the inside of the 70 mm outer diameter, 50 mm inner diameter rod. Both mono filament and multi filament wire constructions were tested to find out which one gave the better fatigue life. For bridging to the stationary mounting, flexible transition spring supports were used. Experimentation with adjustment of the position and tension yielded a position where dynamic swings seemed to be minimum as estimated by amplitude and reaction force.

The temperature at the tail rod end (right hand side in Figure 3, top) was also measured with a view to providing a well-defined thermal boundary condition in a simulation model.

Finally, it is mentioned that the other sealing and support ring temperature sensors consist of 3 mm diameter rods which slide in radial bore holes of slightly higher diameter. These are also visible in Figure 5. It should be expected that they give a temperature indication only due to absence of good, well-defined thermal contact and other reasons as well.

2.4 Test procedure

After selection of the test type, the special design piston with a pressure relieved rider ring and without piston rings (in this case for approximating constant pressure) was mounted and the assembly of instrumented piston rod and pressure packing was installed.

Starting from an ambient condition with equal temperature distribution, the machine was initially switched on, however without applying gas pressure, but already activating data acquisition.

Starting with an air filled cylinder, the gas pressure was applied with Nitrogen gas and the actual test was started. The behaviour was carefully monitored and the machine program allowed for a continuous measurement span of 15 minutes before a the first of three gas purging cycle took place. This involves rapid unloading followed by gradual re-pressurisation. Specific runs often extended over several such cycles. Also pressurisation was removed entirely with either running or stopped machine to allow the temperature distribution to even out.

Since the tail end of the piston rod was supported by a dry running bearing, its heat input would distort the measurements for longer running times if left unaltered. Therefore, cold nitrogen gas was fed to this bearing, in part of the test runs, in order to suppress the temperature to below 45ºC.

For promoting well-defined boundary conditions for transient heating, the cooling system for the packing housing was switched off throughout all runs.

by: Cyril Wentzel – Wentzel Dynamics; Marc Langela – Stasskol GmbH, Germany

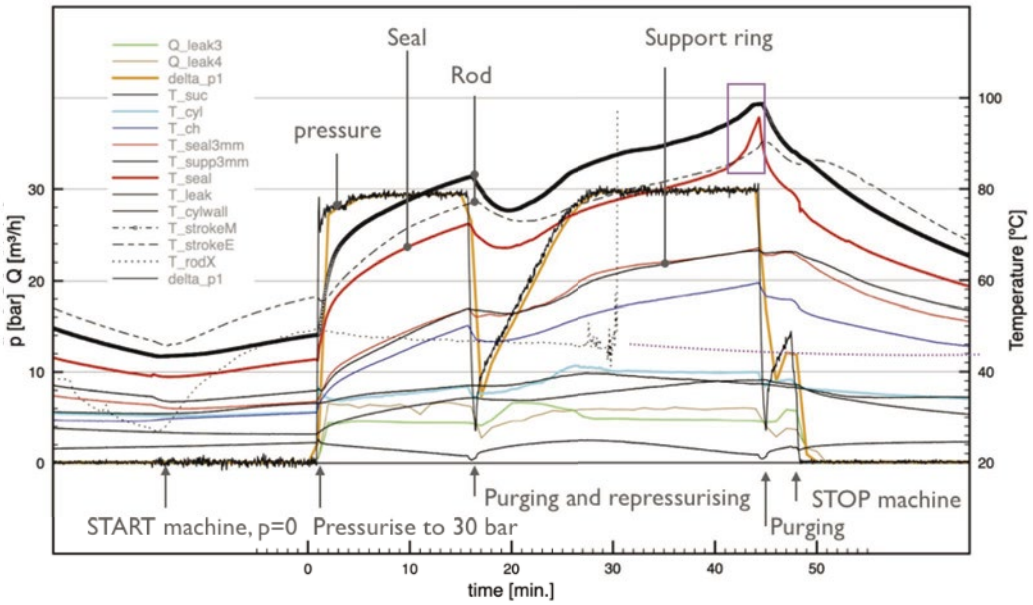

Figure 6: Typical overall result, highlighting rod and seal temperature increase as a function of time under two pressurisation cycles and one purge interruption.

3. Results of phase 1 experiments

Several runs were performed. Due to complexities caused by the purging cycle and regular TC wire failures, often a pause was applied or a short period of unloaded operation to allow temperatures to settle.

The results are discussed on the basis of one specific run (Run 4) which is very much typical of the overall results.

In Figure 6, the left part shows multiple machine temperatures settling from a previous run. Then, after running for 15 minutes, the pressure is switched on at t = 0, activating the heat input by the sealing ring sliding friction. The most rapid temperature increase is seen in the rod mid-stroke position, followed by the end-stroke position. The seal near-interface measurement – the red curve in Figure 6 – does follow this heating with a roughly 10º lower level than the average of the rod inside.

Temperature indications from the support ring sensors are some 20º lower than the maximum ring temperature during this initial heating where temperatures stay below 100ºC.

Leakage rates remained reasonably flat at roughly 5 [m³/h] which is not an abnormal value considering single ring operation.

One example of a failure of the TC wire is visible in Figure 6 at t=30 minutes, where the dashed line indicates the temperature of the rod tail end. The dotted line represents a tentative extrapolation to insignificantly low temperature of 42ºC.

The second pressurisation is applied more gradually, taking between 10 and 15 minutes to complete. Accordingly, the more gradually increasing heat input translates to a more gradual transition from cooling of the piston rod seal section to warming.

The heating continues at 30 bar with slightly lower rates and after 10 minutes into the second cycle, there is a clear sudden increase in heating at the interface, visible in the deflection upward in the red curve (indicated by the rectangle). That this is not an instrumental anomaly, is apparent from the fact that also such a deflection occurs simultaneously in the piston rod temperatures. Here it is seen that the direct access to the friction interface of the thin wire sensor in the sealing ring provides a sensitive means to detect any change in the tribological conditions.

This remarkable and somewhat intriguing event is interrupted however by the pressure drop of the last purging cycle and the machine was stopped, disabling any further investigation. The surface condition of the sealing ring was visually inspected and it seemed that the wear layer separating the surface from the TC tip was still intact, so this possibility was eliminated as a potential cause.

4. Comparison to Simple model calculations

4.1 Numerical analysis model

An overview of the FEM model used to analyse the transient temperature increase as a function of ring heat input is obtained from Figure 7 which also shows a temperature distribution field at t=900 s.

Heat input into the model has been addressed in paragraph 1.4, with parameter **f** governing the effective heat flux into the interface. The reciprocating motion in this model is accounted for by setting the temperature at the ring surface equal

by: Cyril Wentzel – Wentzel Dynamics; Marc Langela – Stasskol GmbH, Germany

to the spatial average of the temperature along the stroke on the piston rod surface (Figure 2).

For transient behaviour, the heat flux into the model was based on the measured pressure difference across the packing, i.e. the pressure profile which follows the purging cycle.

Further model assumptions concern several temperature boundary conditions on the rod which were prescribed where available. The value for the heat transfer coefficient from the rod to the surrounding air was set at a representative educated guess value of 200 W/m²K. Future measurements will provide more precise values.

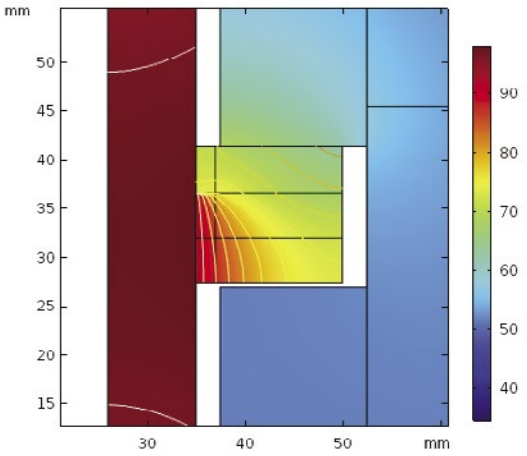

Figure 7: 2D computational model of sealing and support ring, showing part of the cup (right) and piston rod wall (left); temperature distribution in ºC as an example, with enhanced ring conductivity after 15 minutes heat input.

4.2 Comparison of experiment and simple model results

Interpretation of the measured result is made easier by comparing the heating curves to those computed using the model for transient heating.

Figure 8 presents the comparison.

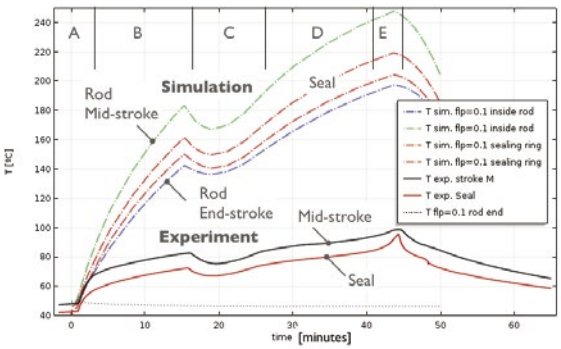

Figure 8: Comparison of 50 minute Run4 results to computed results for effective heat load parameter f=0.1.

It is seen that for the selected value of **f** = 0.1, only the first part of the curve (the first few minutes in part A) correspond in terms of slope. The next parts with pressurised condition, B and D, show a large and gradually increasing discrepancy between computed warming and recorded temperature increase.

Assuming that no errors were made with either the measurements or the computation, there can be only one conclusion restricted to the temperature range below 100ºC. Generally it is clear that the assumptions of the simple model are inadequate. Leakage flow (typically 5m³/h) effects were also neglected. Apparently, the factor **f** could become a complex function of time while at the same time it should become much smaller than 0.1, which itself is already quite a small value. But this is merely a tentative semi-empirical approach. More information is required.

It therefore becomes even more relevant to investigate longer runs. This is both because the results should be reproduced again and the sudden increase in part E points at increased heat input, which could be related to persistent wear-in phenomena.

One other explanation of the discrepancy could involve heat loss from the rod to the ambient air. Whether this could have such a strong influence is doubtful however. It was already foreseen to apply heat flux measurements to the rod in a follow-up phase of the research project; this will provide additional information on a more accurate range of heat transfer to the air, while also enabling equilibrium type of measurements.

There could also be the possibility that the observed discrepancy is related to the freshness of the sealing ring. Even though the results shown were from a run preceded by several other runs, the accumulated running time was far less than what would be considered a normal wear-in time.

The complexities encountered in the present work confirm the soundness of eliminating other complicating factors such as variable pressure for the first phase of the project. With longer measuring times as a first priority, seeming anomalies such as the sudden warming (E) can be studied and reproducible results for transient heating can be achieved. This however does require the following modifications to the test:

- telemetry for temperature signals on the rod should enable longer running times;
- with telemetry in place, equilibrium measurements become a possibility;
- for better tuning of the computational analysis model, heat flux measurements on the piston rod will be very useful

The latter point involves additional diagnostics which should also be connected to the telemetry system. Such additional capability will enable assessment of the requirements for a computational model suitable for better interpretation and determination of heat flux.

In any case, the instrumented sealing ring has proven to be a successful way to measure the near-

by: Cyril Wentzel – Wentzel Dynamics; Marc Langela – Stasskol GmbH, Germany

interface temperature, creating a highly sensitive sensor for directly accessing the tribological behaviour in a complex machine environment.

5. Conclusions and outlook

5.1 Conclusions

The first phase results of an EFRC pre-competitive research project was presented. Whereas the (IRINCO) project itself aims to explore new ways to lower the sealing interface temperature by modification of the ring, extensive and detailed measurements are first made to ground the new ideas in reliable insights into heat flow in the conventional configuration where sealing rings have intrinsically poor heat conductivity.

The available equipment has proven to be well suited to investigate the heat flux distribution. The initial idea to use transient heating did provide interesting results which still have to be better understood.

The diagnostics challenge involved both unique temperature measurement in the sealing ring itself as well as temperature measurements in the moving rod. Wired transmission of the temperature signals proved partially successful, with lifetime being in the order of 15 or 30 minutes or so. The temperature sensor integrated in the sealing ring appeared to function to the best of expectations.

From the 15 minutes results at low temperature (below 100ºC near the interface), it was concluded that there are different and more complex mechanisms at work than those which are modeled. This is because there is a large difference between the actual warming curves and those from the simple model, occurring after a two minutes window in which there is reasonable agreement between the two, assuming a 10% effective heat flow (factor **f**, refer to equation (2)).

In the light of investigating these complexities, it was a fortunate choice to apply constant pressure to the rings in phase 1 of the present work.

In any case, the notion which is sometimes found in the literature that sealing ring heat input is in the order of the ‚nominal' heat input q following equation 1 is seen to be incorrect.

5.2 Recommendations

Improvements which should be made to the test system for follow up work involve elimination of the machine purge cycles, adoption of telemetry for piston rod TC sensors and also heat flux measurement on the rod.

With these extensions in place, it will be possible to make heat flux estimations based on transient heating as well as longer equilibrium measurements and compare the two.

5.3 Outlook

Based on the improvements as recommended, a next step can be made by applying cyclic pressures to the ring (by installing normal piston rings). This should yield a set of consistent heat flux data.

With both the improved heat flux estimation and the improved model in place, evaluation can be made of the alternative ring concepts that are generated in the IRINCO project in the course of 2021.

6 Acknowledgements

We would like to express our appreciation to the members of the EFRC R&D working group for enabling this work and granting permission to publish part of it.

We also express appreciations to the reviewers for their thorough and valuable work.

References

1. Lindner-Silwester, T. (2007): „Advances in fundamental understanding of the dynamic sealing action in packing systems". 5th Conference of the EFRC, Prague.
2. Heat dissipation from piston rod sealing systems – different concepts with consideration of the API-618." Dr. Norbert Feistel, Dr. Georg Samland, Besim Fejzuli, Burckhardt Compression.
3. Kennedy, F.E. (2013): „Frictional heat generation, partitioning and dissipation in dry tribological contacts", in Encyclopedia of Tribology
4. Thomas (née Hammer), C. (2013): Innenkühlung der Kolbenstange von trockenlaufenden Kolben-verdichtern. Dissertation. Technische Universität Dresden
5. Hamzehei , M. (2006): „Determination of Piston and Cylinder Head Temperature Distribution in a 4-Cylinder Gasoline Engine at Actual Process", Proceedings of the 4th WSEAS Int. Conf. on heat transfer, thermal engineering and environment, Elounda, Greece, (pp153-158)
6. Kaufmann, Lindner-Silwester. (2018): "New insight into the wear of packing rings: model, calculation, experiment", EFRC conference.

NOTES

NOTES

NOTES

NOTES

Promoter

European Forum for Reciprocating Compressors e. V.
c/o Technische Universität Dresden
01062 Dresden, Germany
Telefon: +49 (351) 463-32815
E-Mail: contact@recip.org
www.recip.org

Layout

Sanja Kaltenbrunner-Jelic, sanja.at e.U., 1160 Vienna, Austria

Druck

Druck.at, 2544 Leobersdorf, Austria

ISBN 978-3-200-07873-4

WWW.RECIP.ORG